

IMAGE QUALITY  
OF  
MEDICAL X-RAY SYSTEMS

PIETER JOHANNES 'T HOEN





# IMAGE QUALITY OF MEDICAL X-RAY SYSTEMS



C10046  
99102

VERVALLEN

P1629  
4243

PROEFSCHRIFT TER VERKRIJGING VAN DE  
GRAAD VAN DOCTOR IN DE TECHNISCHE WE-  
TENSCHAPPEN AAN DE TECHNISCHE HOGE-  
SCHOOL DELFT, OP GEZAG VAN DE RECTOR  
MAGNIFICUS, VOOR EEN COMMISSIE AANGE-  
WEZEN DOOR HET COLLEGE VAN DEKANEN  
TE VERDEDIGEN OP WOENSDAG 1 OKTOBER  
1980 TE 16.00 UUR DOOR

PIETER JOHANNES 'T HOEN

NATUURKUNDIG INGENIEUR  
GEBOREN TE DEN HELDER

1629 4243

BIBLIOTHEEK TU Delft  
P 1629 4243



C

469910



**Dit proefschrift is goedgekeurd door de promotoren  
prof. dr. ir. J. Davidse en prof. dr. M.A. Bouman**

## CONTENTS

page

1. INTRODUCTION .....	1
1.1 The image .....	2
1.2 Image properties .....	2
1.3 The subjective image quality criterion .....	3
1.4 Problems to be solved .....	4
1.4.1 Physical aspects .....	4
1.4.2 Visual aspects .....	5
2. VISUAL RESOLUTION .....	5
2.1 Introduction .....	5
2.2 Working model of the visual system .....	6
2.2.1 Signal processing .....	7
2.2.2 Noise processing .....	17
2.3 Measuring set-up .....	20
2.3.1 Viewing conditions .....	20
2.3.2 Apparatus .....	22
2.3.3 Psychometry .....	25
2.3.4 Contrast measurements .....	28
2.4 Spatial effects .....	31
2.4.1 Measurements on the influence of the unsharpness .....	31
2.4.1.1 Method .....	31
2.4.1.2 Predictions .....	31
2.4.1.3 Measurements on disks .....	34
2.4.1.4 Measurements on bars .....	41
2.4.1.5 Influence of the monitor luminance .....	45
2.4.1.6 Conclusion .....	46
2.4.2 Measurements on the influence of the object size .....	48
2.4.2.1 Method .....	48
2.4.2.2 Measurements on disks .....	50
2.4.2.3 Measurements on bars .....	52
2.4.2.4 Conclusion .....	54
2.4.3 Analysis of results in the literature .....	54
2.4.3.1 The visibility of simulated lung lesions .....	54
2.4.3.2 The visibility of Gaussian and rectangular bars .....	59
2.4.4 Measurements on the visibility of the unsharpness .....	61
2.4.4.1 Absolute threshold unsharpness .....	62
2.4.4.1.1 Method .....	63
2.4.4.1.2 Results .....	64
2.4.4.2 Threshold unsharpness-increment .....	65
2.4.4.2.1 Method .....	65
2.4.4.2.2 Results .....	66
2.4.4.3 Conclusion .....	71

2.4.5 Correlation with the contrast sensitivity function of the visual system	72
2.4.5.1 Introduction	72
2.4.5.2 Spatial contrast sensitivity	74
2.4.5.2.1 Signal processing	75
2.4.5.2.2 Visual system strategy	79
2.4.5.2.3 Conclusion	80
2.4.5.3 Application	83
2.4.5.3.1 Sine-wave and square-wave sensitivity	83
2.4.5.3.2 Moving gratings	84
2.4.5.3.3 Adaptation effects	85
2.4.5.4 Conclusion, discussion	86
2.5 Noise effects	88
2.5.1 Dynamic noise	88
2.5.1.1 Influence of the noise intensity	89
2.5.1.2 Influence of the gamma	92
2.5.1.2.1 Franken's measurements	92
2.5.1.2.2 Van Meeteren's measurements	95
2.5.1.3 The noise-equivalent aperture of the visual system	96
2.5.1.3.1 Physical measurement	97
2.5.1.3.2 Psychophysical measurement	102
2.5.1.4 Influence of the viewing distance	108
2.5.2 Static noise	110
2.5.2.1 Noise intensity measurement	111
2.5.2.2 Influence of the viewing distance	112
2.6 Conclusion	114
2.6.1 Object processing	114
2.6.2 Noise processing	118
2.6.2.1 Dynamic noise	118
2.6.2.2 Static noise	122
2.6.3 Discussion	123
2.6.4 Operational model of the visual resolution	132
3. OBJECT RESOLUTION	135
3.1 Introduction	135
3.2 Moving objects	141
3.2.1 Shadow image MTF, focal-spot choice	141
3.2.1.1 Maximization of the modulation transfer	147
3.2.1.2 Maximization of the peak contrast gradient	153
3.2.2 Choice of the geometric magnification, influence of the image receptor MTF	155
3.2.2.1 Mathematical formulation	156
3.2.2.2 Influence of the object-to-image receptor distance	159



3.2.3	Influence of the focal spot-to-image receptor distance	163
3.2.4	Nomograms	164
3.2.4.1	Optimum focal-spot size	164
3.2.4.2	Non-optimum focal-spot size	164
3.2.4.3	Object position	167
3.2.4.4	X-ray system MTF quality	167
3.2.4.5	Application	169
3.2.5	Conclusion	171
3.3	Stationary objects	172
3.3.1	Choice of the focal spot	172
3.3.2	Choice of the geometric magnification	173
3.3.2.1	Mathematical formulation	173
3.3.2.2	Influence of the object-to-image receptor distance	176
3.3.3	Influence of the focal spot-to-image receptor distance	179
3.3.4	Nomograms	179
3.3.4.1	Influence of the focal-spot size	180
3.3.4.2	Object position	180
3.3.4.3	X-ray system MTF quality	181
3.4	Focal-spot intensity distribution	184
3.4.1	Moving objects	186
3.4.1.1	Optimum focal-spot size	186
3.4.1.1.1	Homogeneous and camel-back distribution	189
3.4.1.1.2	Gaussian distribution	190
3.4.1.1.3	Falling intensity distribution	191
3.4.1.2	Influence of the image receptor	193
3.4.1.3	The system line-spread function	194
3.4.2	Stationary objects	197
4.	THE IMAGE CONTRAST	198
4.1	Scattered radiation	198
4.1.1	Introduction	198
4.1.2	Definition of characteristic parameters	201
4.1.3	Measuring arrangement	202
4.1.4	Contrast improvement factor	206
4.1.5	The relative intensity	211
4.1.6	The selectivity of geometric magnification	214
4.1.7	Conclusion	214
4.2	Absorption contrast	214
4.2.1	Introduction	214
4.2.2	Measuring arrangement	215
4.2.3	Contrast measurements	219
4.2.4	Attenuation measurements	222

5. QUANTITATIVE ANALYSIS OF MEDICAL X-RAY SYSTEMS	225
5.1 Object resolution	226
5.1.1 Stationary objects	227
5.1.1.1 Medical data and results	228
5.1.1.2 Conclusion	232
5.1.2 Moving objects	238
5.1.2.1 Influence of geometric magnification	239
5.1.2.2 Focal-spot choice	241
5.1.2.3 Influence of the image receptor	243
5.1.3 Focal-spot intensity distribution	245
5.1.3.1 Stationary objects	245
5.1.3.2 Moving objects	245
5.1.3.3 Discussion	247
5.2 Visual resolution	248
5.2.1 The relation between object resolution and visual resolution	249
5.2.1.1 Coupling of the visual system to the X-ray system	250
5.2.1.2 Point, line and edge spread function imaging	255
5.2.1.3 Estimation of the maximum contrast gradient	257
5.2.1.4 Variation of the position of the object	260
5.2.1.4.1 Nomograms	260
5.2.1.4.2 Mathematical formulation	263
5.2.1.5 Variation of the focal spot-to-image receptor distance	266
5.2.1.5.1 Stationary objects, fixed focus	267
5.2.1.5.2 Stationary objects, fixed exposure time	267
5.2.1.5.3 Moving objects, optimum focus size	268
5.2.1.6 Variation of the focal-spot size	269
5.2.1.7 Variation of the visual system MTF in the image receptor input plane	270
5.2.1.7.1 Noiseless and static noisy systems	271
5.2.1.7.2 Dominant dynamic X-ray noise	271
5.2.1.8 Variation of the image receptor	271
5.2.1.8.1 Variation of the unsharpness	272
5.2.1.8.2 Comparison of different receptors	273
5.2.1.9 Advantages of varying the viewing conditions	274
5.2.2 Application to stationary object imaging	274
5.2.2.1 Magnification	275
5.2.2.2 Image receptor	276
5.2.2.3 Focal spot and focal-spot intensity distribution	277
5.2.2.4 Focal spot-to-image receptor distance	278
5.2.2.5 Conclusion	279
5.2.3 Application to moving object imaging	280
5.2.3.1 Introduction	280
5.2.3.2 Characteristic parameters	282
5.2.3.3 Choice of the X-ray tube	283

5.2.3.4	Magnification	285
5.2.3.5	Image receptor	285
5.2.3.6	Conclusion	286
5.2.4	Influence of the X-ray beam quality	287
5.2.4.1	Introduction	287
5.2.4.2	Stationary objects	289
5.2.4.3	Moving objects	290
5.2.4.4	Conclusion	291
5.2.5	Influence of the scattered radiation	291
5.2.5.1	Introduction	291
5.2.5.2	Moving objects	292
5.2.5.3	Stationary objects	296
5.2.5.4	Conclusion	298
5.2.6	The dose administered to the patient	299
5.2.6.1	Introduction	299
5.2.6.2	Fluoroscopy	300
5.2.6.3	Geometric magnification	300
5.2.6.4	Beam quality	301
Appendix	I Theoretical threshold contrast curve for disks	303
	II Noise-equivalent aperture	305
	III Luminance distribution measurement on the monitor	307
	IV The influence of scattered radiation on the optimum modulation transfer function of an X-ray system	310
	V Photomultiplier amplifier/divider	312
	VI Remarks on computerized tomography	316
Summary		Su
Samenvatting		S
References		R
Symbols		Sy
Curriculum Vitae		





## 1. INTRODUCTION

The quality of images made by medical X-ray systems is of interest both for the user and for the developer of such systems.

This thesis deals firstly with the development of subjective criteria and secondly gives a comprehensive physical description of imaging. Finally, some present X-ray systems are analysed by combining these two areas of work.

This research is an extension of the rich history of the Philips' concern in this field.

Much credit must be given to Bouwers (1931, 1934), who analysed the interdependence of the movement and the X-ray source unsharpness, to Burger and van Dijk (1936), who described many psychovisual phenomena, and to Burger, Combée and v.d. Tuuk (1946), who analysed the geometric magnification technique.

Further, the analysis of the image intensifying technique by Tol, Oosterkamp and Proper (1955) should be mentioned. Oosterkamp and Albrecht (1959), following a suggestion by v. Alphen, introduced the modulation transfer function concept to describe the unsharpness. A description of the noise has been given by Albrecht and Proper (1965). A systematic approach to the optimization of the system as a whole was started by Albrecht and Oosterkamp as early as 1962, and by Kühn in 1964/1965. Botden should be mentioned for his unremitting efforts to promote the technical application of the modulation transfer function. Franken must be given credit for starting in 1973 an investigation into the perception of X-ray television images.

Although many practical results have been obtained by the investigators mentioned, a more realistic model for the imaging will be of advantage for the following reasons. (i) It has been assumed that the noise is integrated over the detail area, and that the visual system unsharpness has no influence. This is a good technical definition, but it leads to an unrealistic relation between the threshold contrast and the diameter of disks. (ii) It has been stated without proof that dynamic (X-ray television) and static (radiograph) noise is handled equally by the visual system. (iii) It has not been possible to predict the influence of the unsharpness on the threshold contrast, i.e. to establish the relation between the threshold contrast and the modulation transfer function. (iv) Although the modulation transfer function gives a correct description of the unsharpness, it has proved difficult to handle the functions and to estimate the relative influence of components.

The present study relates to the above subjects (i) to and inclusive (iv) which have not been dealt with elsewhere. The analysis is confined to conventional X-ray systems, which means that computerized tomography imaging is excluded. However, because of the great interest of the latter technique, a brief analysis is given in an appendix. The developed subjective criteria — whose validity is not restricted to conventional X-ray imaging — are applied.

## 1.1 The image

The primary or shadow image is made (fig. 1.1.1) with a wide beam of X-rays which traverses the patient. The inhomogeneous attenuation of the X-rays in the patient induces a spatial intensity-modulation of the beam. The intensity profiles are converted by an image receptor which provides the observer with an intensity modulated picture. The spatial luminance distribution of this picture reflects the attenuation properties of the object.

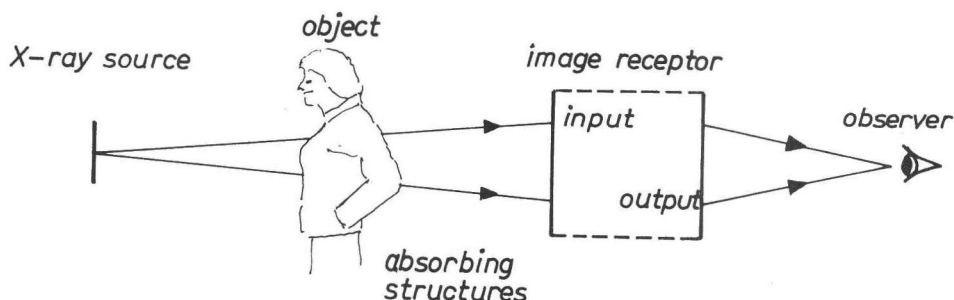


Fig. 1.1.1.  
Medical X-ray system

## 1.2 Image properties

Unlike the subjective properties, the physical properties can relatively easily be described. The physical properties are the unsharpness, the contrast and the noise. Unsharpness is introduced by the finite dimensions of the X-ray source, the limited resolution of the image receptor, and the movement, if any, of the object. The contrast is the fractional luminance increment or decrement in relation to the local mean luminance. It corresponds to the differential absorption of structures. By noise is meant visible noise, i.e. stochastic spatial and/or temporal variations of the luminance. This noise is due to the quantum character of the X-ray beam and to noise introduced by the image receptor. As to the latter, the grainy structure of the image receptor is always involved. Static noise occurs when the image is stored on film. Dynamic noise occurs in fluoroscopy, i.e. when the image is presented on a TV monitor by means of an image intensifier coupled to a TV camera. The electrical noise of this system is then involved as well. (Other fluoroscopic systems, i.e. with a direct view of the image intensifier or of an intensifying screen, are hardly used and will therefore not be dealt with in this study). Dynamic noise also occurs in cine fluorography, i.e. when the image intensifier output is filmed, and in video fluorography, i.e. when the TV signal is stored on magnetic tape.

The subjective properties are correlated with e.g. the confidence level of the

information extracted from the image, the viewing time needed to reach a conclusion about the pathology, the fatiguing effect of reading the images, the appreciation by the viewer, and so on. These properties cannot easily be described, and it is virtually impossible to find a quantitative correlation between them and physical properties.

### 1.3 The subjective image quality criterion

The diagnostic quality depends at least on the visibility of structures, and this criterion has therefore been chosen. The visibility is expressed in terms of the visual threshold contrast.

To be in line with earlier X-ray research and the practice of general psychophysical research, simple isolated structures like disks, bars and edges have been chosen as objects. Correlation with anatomical objects is nevertheless retained: disks resemble gallstones, calcifications and the like. Bloodvessels, stomachwall striations and bone structures can be described as bars, whereas edges correspond to coarse patterns like a tumour mass-outline. These structures are of course not isolated, but are embedded in an inhomogeneous environment. It will be shown that this structure 'noise' (it is not a stochastic phenomenon — the term 'noise' is to be understood here as a masking effect) does not impair the description of the visibility found for a dynamic or static noisy background.

It has generally been shown that the threshold contrast increases with unsharpness (Bronkhorst, 1927; Chantraine, 1933a, b; Burger and v. Dijk, 1936; Middleton, 1937; Newell and Garneau, 1951; Tuddenham, 1957; O'Brien, 1958). A few exceptions exist; one is found in Kruithof's work (1950). In his view, the threshold contrast is not affected by an unsharpness less than roughly 7', and goes asymptotically to a higher level as the unsharpness increases. The absence of any effect for small unsharpness is also found by Middleton. It can be explained by the predominant unsharpness of the visual system as such. The trend for greater unsharpness, however, cannot be explained. In view of all the other results — and our results — there must be something wrong. This has also been concluded by O'Brien (1958), who does not give any reason, however. We may think of the correction that Kruithof had to apply for the contrast of the unsharp disk. This correction is of the order of 20%; its value is related to the unsharpness applied. The unsharp objects were obtained by defocusing a lens system, which however introduced an uncertainty as to the contrast at the edge of the object — and this is of course crucial.

The greater the unsharpness, the smaller is the unaffected area of the object. If the image only consists of penumbra, then 'the visibility of such an object is doubtful', as Burger et al. (1946) have stated. Many others (Schober, 1935; Büchner, 1954; Evers and Schober, 1955; Feddema and Botden, 1965) apply this criterion.

But a quantitative evaluation of the influence of the unsharpness is lacking. We will further show that the visual size of the object, i.e. the viewing distance, is involved as well.

The visibility of structures also depends on the noise in the image. Its masking effect depends on the intensity and the unsharpness of the noise. Both effects will be studied, especially in relation to the viewing distance, which can be easily varied by the observer.

## 1.4 Problems to be solved

### 1.4.1 Physical aspects

'Unsharpness' and 'resolution' are themselves subjective criteria, so they cannot be used for a physical description of the system. The spatial spread of information is unambiguously described however by the optical transfer function (OTF) of the system. The OTF consists partly of the modulation transfer function (MTF), which describes the modulation transfer of sinusoidal gratings. Further, the phase transfer function  $\phi(\nu)$  describes the phase shift per frequency. As  $\phi(\nu)$  has a simple shape for practical systems, it has become common practice to use the term MTF alone as a characterizer. We shall follow that practice in this thesis, although in the case, for example, of an asymmetrical focal spot intensity distribution (sec. 3.4) the phase transfer must be taken into account as well. A prerequisite for the existence of the OTF is the linearity of the imaging system. An X-ray system does not meet this requirement, unless only small signal excursions are applied. This is generally the case for the threshold visibility condition.

In optimizing the system MTF, the following two problems have to be dealt with:

- (i) For moving objects, the X-ray source dimensions (hence its loadability) must be optimized in relation to the movement distortion.
- (ii) The position of the object between the source and the image receptor must be chosen with due regard to its antagonistic effect on the effective image receptor MTF and the X-ray source (and movement) MTF.

The *contrast* depends on the differential absorption of structures, hence on the energy spectrum of the X-ray beam.

This spectrum depends primarily on the X-ray tube high voltage, but also on the applied filtration, i.e. on the absorption of the materials in the beam. It is therefore not so easy to predict the contrast of structures, especially since the spectral response of the image receptor is also involved. It was decided therefore to measure the contrast directly as delivered by the image receptor. The same strategy has been followed to estimate the influence of scattered radiation. Spatial information is not retained by this radiation. The result is a more or less uniform increase of the background luminance, so the contrast is decreased. The effective intensity of scattered radiation also depends on the X-ray spectrum. The position of the object is



involved as well, which makes it even more difficult to predict the influence of this adverse effect.

The *noise* should be described in physical terms which can be correlated with its visual effect. The physical description is very difficult, and it is not at all sure whether after all a comprehensive correlation with the visual effects can be established. We have therefore opted for the pragmatic approach, and will study the relevance of the noise intensity in terms of the X-ray exposure rate at the input of the image intensifier. Further the smoothing effect caused by the unsharpness of the imaging system will be analysed.

#### 1.4.2 Visual aspects

The threshold contrast of isolated objects must be known as a function of the size of the object, the MTF of the imaging system, and the background luminance. These investigations must be done for different types of backgrounds, i.e. for dynamic noise, static noise and an apparently noise-free background.

We shall try to establish a relatively simple analytical/optical model of the visual system, so as to facilitate an analytical description of the whole system, including the observer.

In this perception research practical situations will be simulated, i.e. free search pattern, binocular viewing, no artificial pupils, unlimited viewing time, no head fixation, and a luminance like that in X-ray rooms.

## 2. VISUAL RESOLUTION

### 2.1 Introduction

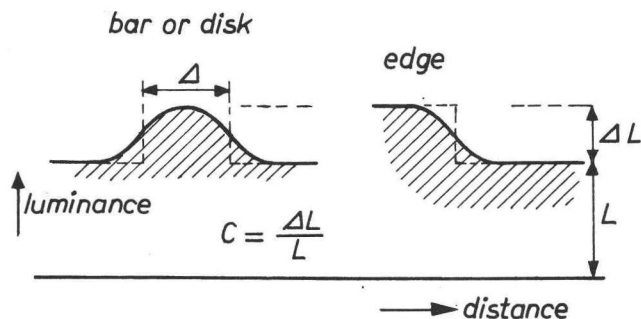


Fig. 2.1.1.  
Definition of contrast  $C$

The unsharpness of the imaging system causes a rounding of the edges of objects, as illustrated in fig. 2.1.1. This makes it difficult to define the contrast,  $C$ , and the size,  $\Delta$ , of the object. To circumvent this problem the contrast and size will be defined with respect to the originally sharp object, unless otherwise stated. As indicated in the figure, the contrast equals the fractional luminance decrement or increment,  $\Delta L/L$ .

As far as the spatial processing is involved, increment contrasts are equivalent to decrement contrasts (Blackwell, 1946). The threshold contrast,  $C_T$ , is defined as the contrast for which the object is just visible. This 'just visible' criterion must of course be specified.

The threshold contrast depends on the background luminance, on the noise in the background and the object, and on the size and the unsharpness of the object. The spatial effects, i.e. the two latter parameters, will be dealt with first (secs. 2.4.1, 2.4.2 and 2.4.3). The noise effects will be studied in sec. 2.5.

There are already many models for the prediction of the threshold contrast. Eleven relevant models will be discussed in sec. 2.6.3. These models are based on combinations of assumptions such as: (i) the threshold is noise-limited or signal-limited, (ii) the noise-sampling is size-independent or size-dependent, (iii) the visual system is perfectly sharp or has an inherent unsharpness, (iv) size-tuned detection takes place or the object is detected by a single channel. Up to now, however, the visual mechanisms underlying this behaviour are unclear (Gelade et al., 1974). Sec. 2.2 presents our working hypothesis for the visual system, which does give at least a good description of the perceptual phenomena in our field. The actual way in which the visual system works has not been established, but an analysis of all the results obtained and data from the literature (sec. 2.6) suggest that some basic processes have been described.

The interesting confrontation of this model with the sensitivity of the visual system for sinusoidal gratings is discussed in sec. 2.4.5. One is tempted to argue that this sensitivity is closely related to the MTF description of X-ray systems.

It is further interesting to determine the visibility of the unsharpness as such. These experiments are described in sec. 2.4.4.

## 2.2 Working model of the visual system

Three working hypotheses must be established: (i) one regarding the signal (or object) processing by the visual system, (ii) one concerning noise processing, and (iii) one referring to the relationship between noise and signal processing. Every proposal as to the third subject tends to be speculative, because in most of the experiments reported so far the signal and the noise were altered simultaneously. Delicate measurements are needed to separate the two effects. For the time being,

therefore, we are bound to assume that the noise and signal processing are independent of each other. The validity of this assumption is discussed in sec. 2.6.3. The next two sections deal with the working model of the visual system for signal and noise processing.

### 2.2.1 Signal processing

The model is based on the visibility of sharp disks as a function of their size, as measured by Blackwell, part III (1946). (Blackwell's own explanation is discussed in sec. 2.6.3, model A).

The viewing conditions resemble ours, i.e. free search allowed, the position of the disk to be viewed is known, a fairly long viewing time (15 seconds was adequate), binocular viewing, no viewing aids. The stimulus configuration is given in fig. 2.2.1.

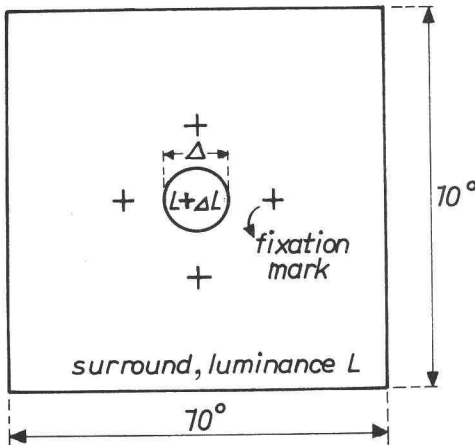


Fig. 2.2.1.  
Stimulus configuration for Blackwell's (1946) measurements.

A sharp and brighter circular spot of diameter  $\Delta$  with increment luminance  $\Delta L$  is projected onto a background having a luminance  $L$  and sides corresponding to  $10^\circ$  of visual angle. Four fixation marks are located at roughly  $2^\circ$  from the edges of the target. The thresholds were reliably determined, both physically and visually. Approximately 90000 observations were made by a group of seven observers.

A typical  $C-\Delta$  curve, giving the relation between the disk size and the threshold contrast, is shown in fig. 2.2.2. The background luminance is  $34 \text{ cd/m}^2$ , which is comparable with that in our situation. Since the threshold for small disks is inversely proportional to the diameter squared, the integrated intensity is crucial in this region. For large disks, the threshold contrast is independent of the diameter. Hence, as the parameters are plotted on a logarithmic scale, the curve approaches an asymptote with a slope  $-2$  for small disks, and zero slope for large disks.

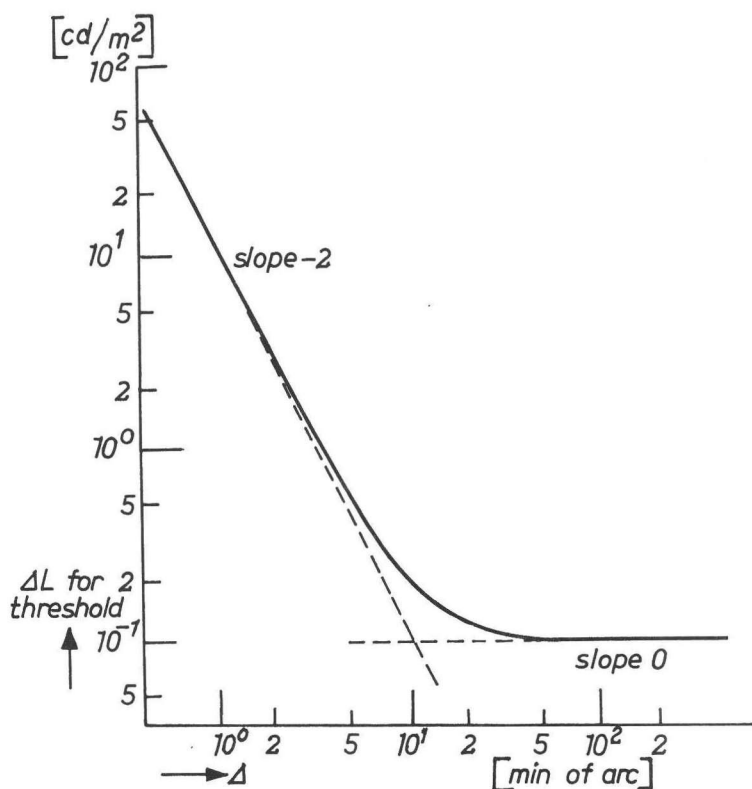


Fig. 2.2.2

Threshold luminance increment of disks as a function of the diameter; background luminance  $34\ cd/m^2$  (borrowed from Blackwell, 1946)

Similar curves have been found by many others (e.g. by Tol et al., 1955). We have chosen Blackwell's results for analysis because they are very well documented, and because more observational data were available.

It is noteworthy that the typical behaviour of the threshold contrast as a function of size has its counterparts in the imaging by an unsharp optical system (fig. 2.2.3). The image of a small object has the shape of the point-spread function (PSF) irrespective of its size. As to the intensity of the PSF, it is only the integrated intensity of the object that counts. For the homogeneous disks studied, the integrated intensity is directly proportional to the diameter squared. For large objects edge-spread function (ESF) imaging takes place. The image parameters at the edge are independent of the size of the object. Consequently we might conceive of the visual system as being an unsharp optical system. This is only a speculation, and so too is our choice of the criterion for visibility.



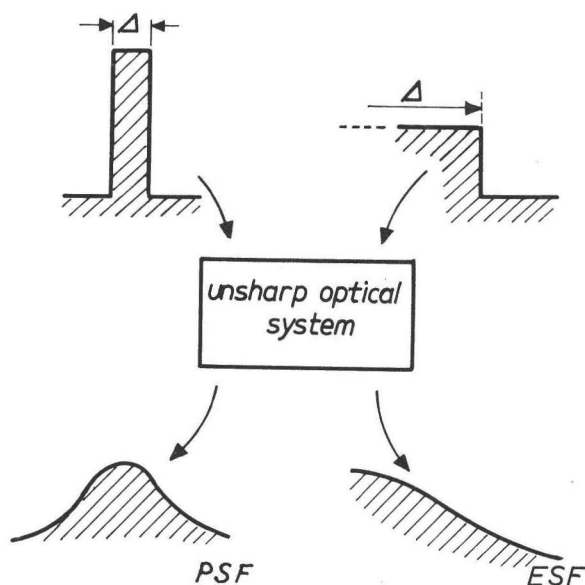


Fig. 2.2.3  
Imaging by an unsharp optical system

It will lead however to a good description of the visual phenomena, found by Blackwell for sharp disks and established from our experiments on sharp and unsharp disks and bars.

A criterion for visibility must be chosen in order to find a quantitative relation between size and visibility. Since, as stated, with either small or large disks the image shape is independent of the size of the disk, any criterion could be applicable here; no conclusions should be drawn, therefore, about the validity of a model on the basis of good results in these regions. Consequently the critical region corresponds to the intermediate size of disks. But the model can still be wrong even if good results are obtained, because there are three degrees of freedom, i.e. the unsharpness of the system, the detection criterion and the noise processing.

The criterion should take into account the high sensitivity of the visual system for temporal and spatial changes in the scene. In fact, spatial changes are transformed to temporal ones by virtue of the eye movements. The characteristics of the involuntary eye movements are given in table 2.2.1 (Ditchburn, 1955; HeckemueLLer, 1965; Steinman et al., 1973).

TABLE 2.2.1: Characteristics of involuntary eye movements

type	amplitude	velocity	time course
tremor	5 – 30''	$20^{\circ} \cdot s^{-1}$	30 – 100 Hz
microsaccades	2 – 10'	$1 - 10^{\circ} \cdot s^{-1}$	irregular intervals, i.e. 0.03 – 5 s
drift	5 – 10'	$1^{\circ} \cdot s^{-1}$	—

The excursions are generally substantially larger than the size of the smallest receptive unit for foveal vision, the cone. The mean cone diameter is roughly 18'' (Jones and Higgins, 1947).

The eye movements need not be the sole factor governing the spatial/temporal gradient. The retina itself may make a spatial derivative by reason of its built-in network: lateral inhibition takes place (Cornsweet, 1970).

Ultimately, perception is impossible without eye movements, as is shown by 'stabilized retinal image' experiments (Heckenmueller, 1965; Ditchburn and Fender, 1955): the image fades away after a few seconds. The temporal derivative of the stimulus does indeed play an important role. If the light is interrupted, brightness is estimated to be higher (sometimes by a factor of 100, Ditchburn and Fender, 1955). This may be due to the unusually large temporal gradient at an interruption compared with the normal-vision situation.

Further evidence in support of the great sensitivity of the visual system to changes in intensity is provided by measurements on the discharge of impulses in optical nerve fibres (Hartline, 1940). Relatively large responses are elicited if the light changes in intensity. Cortical cells, too, are highly sensitive to such stimuli. Hubel and Wiesel (1962) explored the activity of cortical cells of the cat. They showed that such a cell fires best if a characteristic stimulus is imaged on a certain section of the retina. By definition this section is called the 'cortical receptive field'. Its shape can be simple (edge, disk etc.) or complex. The animal was paralysed, so that the retinal image was fixed. The authors remark that 'moving stimuli were more effective than stationary ones'. Such a moving form is normally present by virtue of the eye movements.

In conclusion, as a working model of the visual system, we assume that the threshold contrast is inversely proportional to the *maximum spatial contrast gradient* of the image. This image is thought to be the output of the unsharp optical system which represents the imaging by the visual system. Anticipating the confrontation of this model with other models of the visual system, it can be said that the following characteristics are important:

- the model can deal with unsharp stimuli as occur in X-ray imaging;
- knowledge of the stimulus configuration is not needed (which may not be the case in models based on size-tuned receptive field detection): the position of the maximum gradient automatically follows from the stimulus.

The unsharpness of the model of the visual system can now be quantified by means of a fit with the measured C-Δ curves. The unsharpness is described in terms of an MTF of the general form

$$\text{MTF}_v = e^{-\beta \cdot [\nu^\gamma]} \quad (2.2.1.1)$$

where

$\text{MTF}_v$  is the visual system MTF,  
 $\nu$  is the spatial frequency in periods per degree,  
 $\beta$  and  $\gamma$  are the fitting parameters,  $\beta$  being expressed in degrees.

For  $\gamma = 1$ , the shape of the MTF is exponential, for  $\gamma = 2$  the MTF is Gaussian. For the small contrast under consideration the visual system can be treated as being linear (Hay, 1976), so the MTF concept holds. Further, as the spatial extension of the objects is small (a few degrees), the imaging is assumed to be isotropic.

The predicted and measured C-Δ curves are compared below.

For the mathematics concerning the predicted curve, see Appendix I.

The contrast distribution of the image in the output plane of the visual system is described by  $C_s(r_v)$ , where  $r_v$  is the radial distance in degrees ('v' stands for visual). The following proportionality is applicable to this case:

$$C_s(r_v) \sim \Delta \cdot \int_0^\infty e^{-\beta \cdot [\nu^\gamma]} \cdot J_1(\pi \nu \Delta) \cdot J_0(2\pi \nu r_v) d\nu \quad (2.2.1.2)$$

For the contrast gradient,  $\frac{d}{d r_v} C_s(r_v)$  we may write:

$$\frac{d C_s(r_v)}{d r_v} \sim \Delta \cdot \int_0^\infty \nu \cdot e^{-\beta \cdot [\nu^\gamma]} \cdot J_1(\pi \nu \Delta) \cdot J_1(2\pi \nu r_v) d\nu \quad (2.2.1.3)$$

The inverse of the maximum contrast gradient is given in a normalized form in fig. 2.2.4. To facilitate comparisons the diameter  $\Delta$  is expressed in units of the full width at half the maximum (FWHM) of the point-spread function corresponding to the proposed MTF.

Only the result for  $\gamma = 1$ , i.e. an exponentially shaped MTF, is given, because this

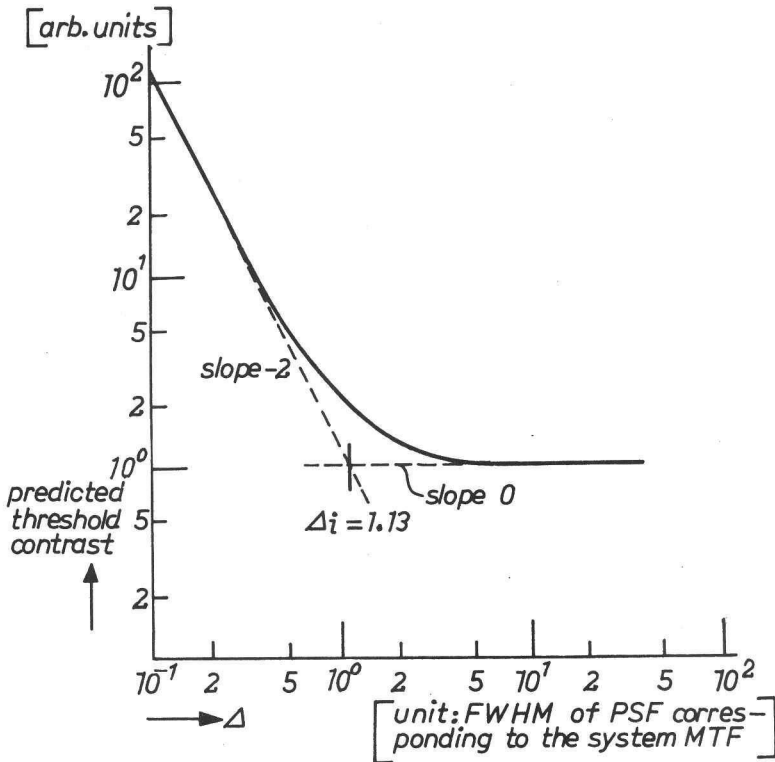


Fig. 2.2.4.

*Predicted shape of the threshold contrast curve, exponentially shaped MTF of the visual system.*

leads to a relatively simple MTF and a reasonable fit with the experiments. The asymptotes for small and large disks intersect at  $\Delta = 1.13$  FWHM. The disk size at the intersection is denoted by  $\Delta_i$ . The value of  $\beta$  can now easily be found, because

$$\text{FWHM} = 0.24 \beta, \quad (2.2.1.4)$$

and therefore

$$\beta = 3.62 \Delta_i \quad (2.2.1.5a)$$

For bars we find by means of an analogous procedure:

$$\beta = 4.07 \Delta_i \quad (2.2.1.5b)$$

The results of Blackwell's measurements (1946) are compared with the predicted curves for ambient luminances from 0.34 to 3400 cd/m<sup>2</sup> in figs. 2.2.5 – 2.2.9.

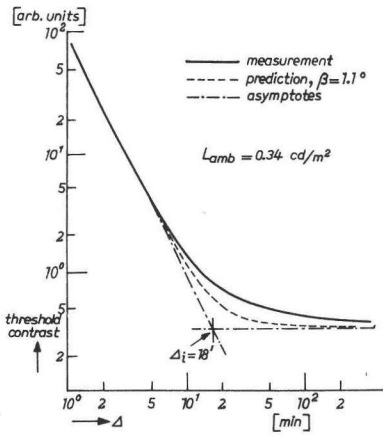


Fig. 2.2.5

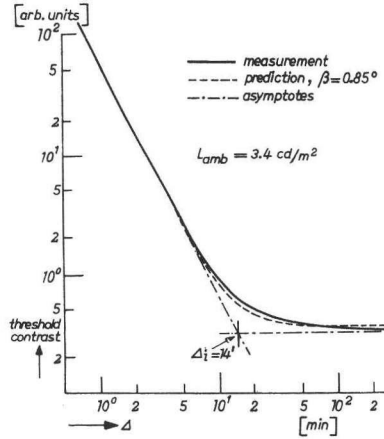


Fig. 2.2.6

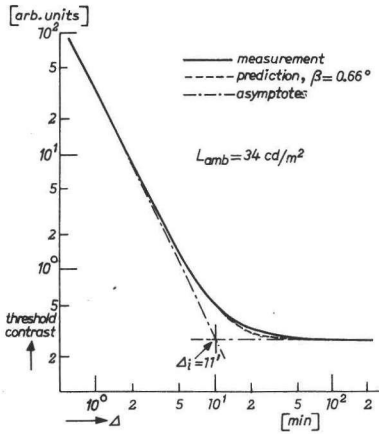


Fig. 2.2.7

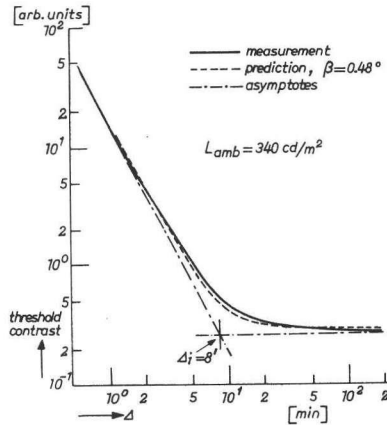


Fig. 2.2.8

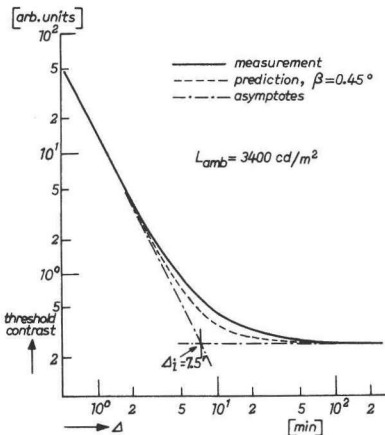


Fig. 2.2.9

Fig. 2.2.5 – 2.2.9

Measured (Blackwell, 1946) and predicted (this work) C- $\Delta$  curve; ambient luminance  $0.34 \text{ cd/m}^2$ – $3400 \text{ cd/m}^2$

The fit is reasonable (misfit 0.1 log unit) for the medium ambient luminances. Both for the largest and the smallest luminance the fit is only indicative. At the lower end this discrepancy may be due to the application of parafoveal scanning instead of foveal scanning. The medium luminances, however, are practical for normal X-ray viewing. The residual misfit in this region is too small to be considered in this stage of research.

The inferred values of  $\Delta_i$  and  $\beta$  are given in table 2.2.2. per ambient luminance. The value of  $\beta$  as a function of the luminance is shown in fig. 2.2.10. The expected trend emerges, i.e. the visual system is 'sharper' for larger luminances. The value of  $\beta$  only accounts for the position of the C- $\Delta$  curve in relation to the size axis. In addition, the threshold contrast will be lower for higher ambient luminances.

TABLE 2.2.2: MTF data for the visual system model

ambient luminance [cd · m <sup>-2</sup> ]	$\Delta_i$ [min.]	$\beta$ [deg.]
0.34	18	1.1
3.4	14	0.85
34	11	0.66
340	8	0.48
3400	7.5	0.45

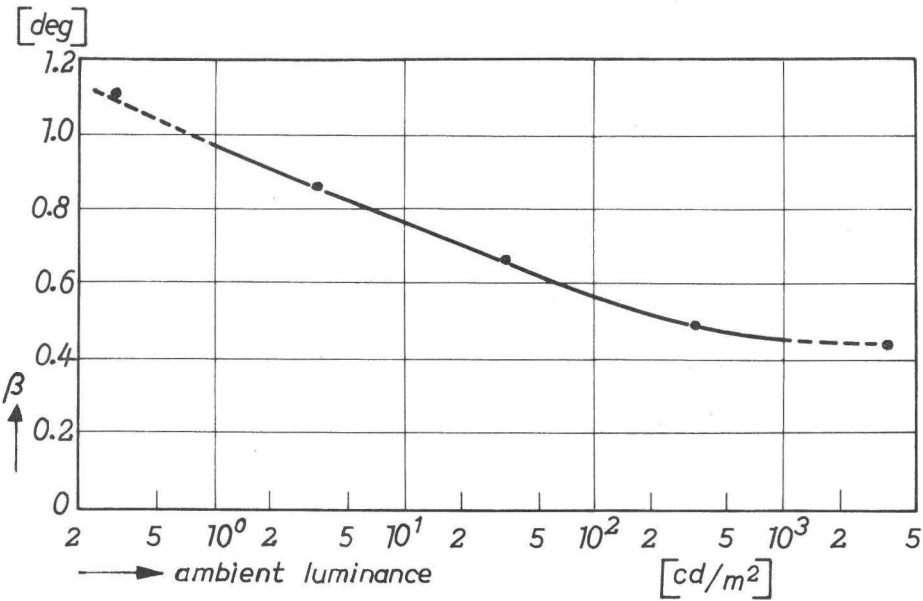


Fig. 2.2.10.  
Visual system MTF-parameter  $\beta$  as a function of the ambient luminance.



The rate of change of  $\beta$  is not large, however, in view of the wide range of luminances applied. Under practical luminance conditions, therefore, the spatial contrast processing does not change very much.

The principles of the model and the layout of the practical situation are illustrated by fig. 2.2.11. The luminance is denoted by  $L$ , the luminance increment by  $\Delta L$ , the contrast by  $C$ , the distance by  $r$ . Dimensional scaling takes place in nearly all the parts of the imaging chain, so the absolute value of  $r$  will change.

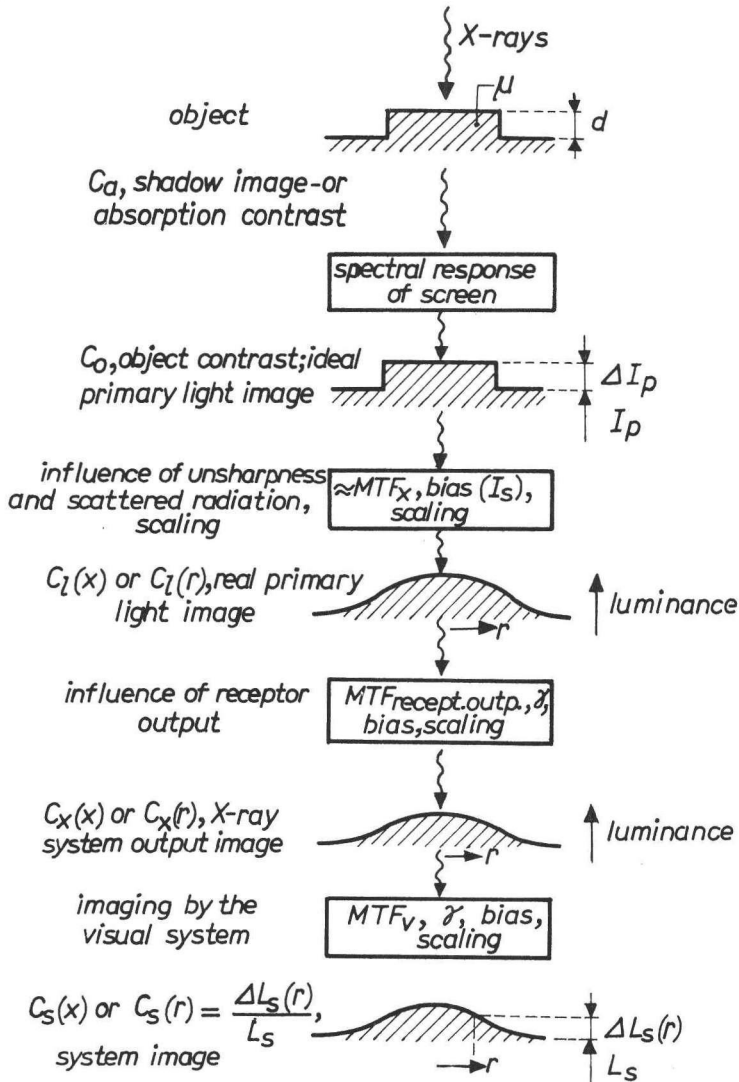


Fig. 2.2.11

Implementation of the visual system model in practical imaging

The following definitions are given:

- $C_a$  : shadow image or absorption contrast; since only small contrasts are involved, its value is proportional to  $\mu \cdot d$ , where  $\mu$  is the linear attenuation coefficient and  $d$  is the thickness of the object.
- $C_o$  : the shadow image is transformed to a light image by the intensifying screen or the image intensifier. The X-ray spectrum and the spectral response of the screens are of significance. The resulting contrast is measured and expressed in terms of  $\Delta I_p / I_p$ , where  $I_p$  is the light intensity corresponding to the X-ray intensity. The contrast of the primary light image thus defined is the object contrast  $C_o$ , i.e. neither the unsharpness of the X-ray system nor the biasing caused by scattered radiation, denoted by  $I_s$ , plays a role.
- $C_1(r)$  : the real primary light image  $C_1(r)$  is obtained by introducing the unsharpness of the X-ray system and the scattered radiation, so that a luminance distribution results.
- $C_x(r)$  : the  $C_x(r)$  distribution describes the final image made by the X-ray system. This will either be that on the film in the viewbox or that on the monitor screen. The extra unsharpness has already been included in the X-ray system MTF of the former step. This is allowed, although a non-linear operation is carried out. As we are dealing, however, with small deviations from a background level, the system can be considered as quasi-linear. The small excursion non-linearity is denoted by  $\gamma$ . Bias, i.e. a low-frequency drop can occur as well.
- $C_s(r)$  : the final step is the introduction of the visual system, modelled as an optical system with an MTF<sub>v</sub>. Of course biasing and a gamma may occur as well as scaling.

The resultant distribution  $C_s(r)$  is then scanned on the maximum gradient, and the proposal is that the threshold contrast is inversely proportional to the ultimate maximum contrast gradient:

$$C_T \sim \frac{1}{\left. \frac{d C_s(r)}{dr} \right|_{\max}} \quad (2.2.1.6)$$

This model of the visual system is valid for the prediction of the threshold contrast of sharp disks. We will examine its applicability to the perception of unsharp disks also (sec. 2.4.1). The independence of the noise processing is checked by applying different noisy backgrounds. C- $\Delta$  curves are also measured (sec. 2.4.2), to find out which visual system MTF must be taken in the experiments.

To widen the scope of the model the investigations are also done for bars. It is not

self-evident that bars are to be handled in the same way. The visual system may make use of the signal correlation along the bar.

Further, our results are compared with findings reported in the literature (sec. 2.4.3), both as to the visibility of unsharp isolated objects, and as to the visibility of gratings (2.4.5). This last topic is interesting because this is another method that can be used to measure the modulation transfer of the visual system. Its transfer ratio is defined as the reciprocal of the threshold modulation of the grating. The corresponding MTF is quite contrary to our proposal. Further, subjective quality criteria are often based on grating visibility, i.e. a part of a grating is imaged by a system.

Finally, the visibility of the unsharpness as such is investigated (sec. 2.4.4). It is of interest to know whether properties of supra-threshold objects are seen by the same method as the visibility of the object as a whole.

### *2.2.2 Noise processing*

The noise in X-ray system images is often due primarily to the quantum character of the X-ray flux. The noise is static if the image is stored on film. The noise is dynamic if an image-intensifier/TV combination or an image-intensifier/cine-camera combination is used. Image receptor noise can also occur, i.e. due to the graininess of the sensitive layers, or resulting from the electrical circuits in the TV. We have carried out many experiments for situations where dynamic noise is dominant, i.e. where the image receptor noise can be neglected. The results are interesting because this noise may be visually processed in much the same way as the invisible and dynamic photon noise in normal scenery. Further, the application of fluoroscopy will be more important in view of the recent advent of high resolution image intensifiers.

A model for the noise processing cannot be easily established. The mathematics involved is complex because of the statistical nature of the phenomenon. Further, it is unclear which signal is extracted by the retinal and higher order elements. The different character of static and dynamic noise also makes it unlikely that one model will describe both phenomena. Owing to the framing of the TV system, the dynamic noise on the TV monitor is supplied in the form of pulses. The repetition rate is 50 Hz, which is so high that fusion occurs and no flicker is perceived. A fast 'Plumbicon' camera is used, so there is hardly any correlation between successive frames. Consequently stabilized retinal image conditions exist, because the extent of eye movement is rather small between frames (a medium excursion of 7" in 20 ms is given by Riggs et al., (1954)). We may state, then, that the temporal gradients are mainly induced by the characteristics of the TV system. This is in contrast with the perception of static noise, for which eye movements considerably mediate the temporal gradients.

Several models of noise processing have nevertheless been developed. They generally assume that the noise is integrated over a surface, and that the effective noise is correlated with the statistical variation in the number of events. Thus, in the case of X-ray fluoroscopy, the noise signal is inversely proportional to the square root of the number of X-ray quanta absorbed per unit surface and unit time. This relation has indeed been confirmed by investigations of threshold contrast with the assumption that the relevant stimulus signal is the contrast (Coltman, 1954; Kühl, 1965; van Meeteren, 1973). However, there are too many degrees of freedom to allow any conclusive decision to be reached about the way in which the visual system actually works: the integration surface may or may not be correlated with the size of the object, and different ways are conceivable in which the spatial processing of the stimulus may take place. It is further relevant that the implicit assumption is made that statistical events are counted. The counting probability, however, is correlated with both the intensity (e.g. the number of photons) and the spatial density of the events. The interesting experiments reported by van Meeteren (1973) in this area are discussed in sec. 2.5.1.2.2.

The 'signal-to-noise ratio' concept must also be mentioned. According to de Vries (1943) and Rose (1948) it is assumed that the perceived contrast must be equal to a few times the perceived statistical variation of the noise to render the stimulus visible. The inferred values of the so defined signal-to-noise ratio lie between 0.13 (Morgan, 1965) and 5 (Rose, 1948). This large range is not surprising because two unknowns are combined, i.e. the perceived signal and the perceived noise. There is further the problem that one must know the 'integration time' of the visual system in order to evaluate the noise. One generally assumes this time to be 'the well-known integration time of 0.2 s', without any reference, however. Others refer to the work of Rose (1948) who compared *static* noisy images with *dynamic* noisy images – which method itself is subject to all the deficiencies mentioned so far. Taking into account previous work, he concludes that 'the effective storage time may be anywhere between the physical storage time of 0.2 s and the actual observation time of 1 s'. This uncertainty is partly due to the inconsistency of his quotations. Blondel and Rey (1911) investigated the threshold visibility of point-like flashes on a dark background – this is not the situation in fluoroscopy. Langmuir and Westendorp (1931) also used point sources at very low background luminances. Rose further states that the data of Cobb and Moss (1928) match the data of Connor and Ganoung (1935). There is poor correspondence, however, between the data (see Connor and Ganoung, fig. 4), and the exposure times were 0.17 s and 3 s respectively (and not the cited 1 s for Connor and Ganoung, Rose, page 207).

In view of the methodological problems involved in the direct investigation of the integration time of the visual system, such a conception will perhaps not apply to practical situations. Firstly, the observation time can only accurately be defined by flashing the stimulus, but the switching of the stimulus then introduces enhanced responses. This means that the sensitivity to transients is measured, but

this need not be correlated with the integration of apparently continuously presented noise. The effect of transients can be reduced by presenting sinusoidal temporal stimuli. In that case, however, the predictability of the stimulus must be taken into account, whereas the actual noise is scarcely predictable. Secondly, the stimulus must also be accurately defined by using an isolated object. In noise, however, many different stimuli are present simultaneously. Therefore the effects of 'metaccontrast' (Weiner, 1935; Cohn and Lasley, 1975; Growney, 1976) will be present: the apparent brightness of the stimulus depends on its environment, i.e. on the intensity distribution and time course.

In conclusion we may state that the temporal and spatial processing of the noise are as yet unknown. We will nevertheless try to relate the spatial processing to our model of the visual system, i.e. an unsharp optical system. The unsharpness leads to a smoothing of the noise. The same effect would occur if the noise in the image plane were spatially integrated by an aperture and subsequently measured. This 'noise equivalent aperture' was introduced by Schade (1954, 1964). It is denoted by  $A_{eq}$ , and its value is directly related to the MTF of the imaging system. For isotropic systems (v. Leunen and Pennings, 1973) we have:

$$A_{eq} = \frac{1}{\int_0^{\infty} 2\pi \nu \text{MTF}(\nu)^2 d\nu} \quad (2.2.2.1)$$

Thus, the  $A_{eq}$  value is indeed inversely related to the MTF quality of the system. (In eq. 2.2.2.1 an isotropic two-dimensional geometry is assumed. Generally, formulas for a uni-dimensional geometry are used, which leads however to false results — see Appendix II.)

We will investigate (sec. 2.5.1.3) whether this noise-equivalent aperture concept holds good, as Morgan (1965) assumed it did. The experiments will be carried out by varying the unsharpness of the noise on the monitor screen, either by defocusing the image intensifier or by interchanging X-ray and electrical noise. This latter noise has a very different spatial character. Apart from other effects (no correlation between lines, electrical filtering) the image intensifier and optics are not involved in the imaging, so this noise is much sharper.

We will further investigate the influence of the noise intensity (sec. 2.5.1.1), the gamma of the TV system (sec. 2.5.1.2), and the viewing distance (sec. 2.5.1.4).

Static noise is investigated in sec. 2.5.2.

## 2.3 Measuring set-up

### 2.3.1 Viewing conditions

The viewing conditions are chosen so as to simulate practical X-ray conditions.

The stimulus is centrally depicted on the monitor (type EL8119) screen. The monitor field is 300 mm high and 380 mm wide (fig. 2.3.1).

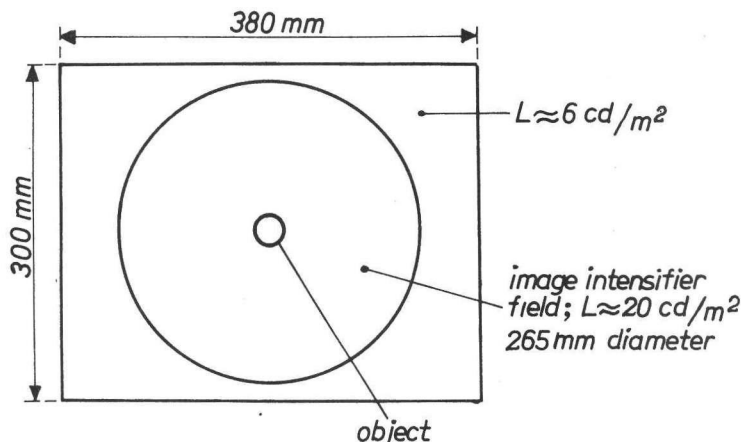


Fig. 2.3.1  
Stimulus configuration

A brighter circular field with a diameter of 265 mm corresponds to the image intensifier input screen. The luminance of this field is roughly  $20 \text{ cd/m}^2$ , the surroundings have a luminance of  $6 \text{ cd/m}^2$ . The central field luminance is continuously measured by means of a spot meter (Asahi Pentax III) to which a digital read-out is coupled.

Both the observer and the monitor are situated in a dimly lit room,  $1.8 \times 3.8 \text{ m}$ . The ambient luminance is adjusted to roughly  $5 \text{ cd/m}^2$  by means of two floodlights behind the observer. The experimenters are outside this room: only auditive contact is possible.

The observer is seated in a chair with head-rest. The head-rest does not affect the movement of the head, it only serves as an aid to fixate the viewing distance.

Binocular viewing without artificial pupils is used. The observer is free to search the screen for the presence of the object. In retrospect, the observers reported that their strategy was to move to and fro across the expected borderline. This strategy

apparently favours visibility: if the observers were asked to fixate on the centre of the object, the threshold contrast could be up to 50% higher.

No strict time limit was set. If the object was clearly supra-threshold, the observer's response came immediately. In the near-threshold situation the observation time did not exceed about 5 seconds. This procedure introduced a variation of an important parameter, i.e. the observation time. Such uncertainties as to a parameter value should be avoided. We tried to improve our experiments by presenting the object for a preset time but we had to abandon this method, because the perception differed too much from that in the continuous presentation, as was revealed by the following experiment. When the observer felt he was ready, he pushed a button, after which the object was presented for a preset number of TV frames. If the pulse time was short (0.2 s), a flash was perceived. The spatial extension of the percept did not resemble the object; it could be any shape within the borders. Further, the threshold contrast was independent of the edge unsharpness. We therefore concluded that spatial effects cannot be built up in such a short time. If the pulse time was relatively long (2 s) temporal effects occurred, associated with the rise and decay of the pulse. A flash could then clearly be perceived, whereas for the rest the object could be at subthreshold. The variation in the results was much greater than for the continuous presentation. This may be due to fluctuations in the observer's attention despite the arrangement by which the observer set the moment of presentation.

Different viewing distances were used, ranging from 400 to 6400 mm. The brighter field of the monitor then subtends  $37^\circ$  and  $2^\circ 30'$  respectively.

Two observers ('t H. and v.d.L.) were continuously available during the two and a half years of experiments. One out of four observers (S., v.d.T., v.G., T.) joined the group temporarily. Anomalous results were sometimes obtained by S.; his results will be used with reserve.

In general every threshold contrast was measured by three observers. The symbols used in the graphs per observer are given in table 2.3.1.

**TABLE 2.3.1: Symbols per observer**

observer	symbol
't H	•
vdL	+
vdT	x
S	o
vG	□
T	◇

### 2.3.2 Apparatus

A versatile set-up is obtained when the object and the background can be varied independently. To this end (fig. 2.3.2) the signals of two TV chains are mixed, one for the object and one for the background. The objects are artificially made by means of an optical bench, so the difficult fabrication of X-ray phantoms is avoided. The object channel gives a relatively noise-free image.

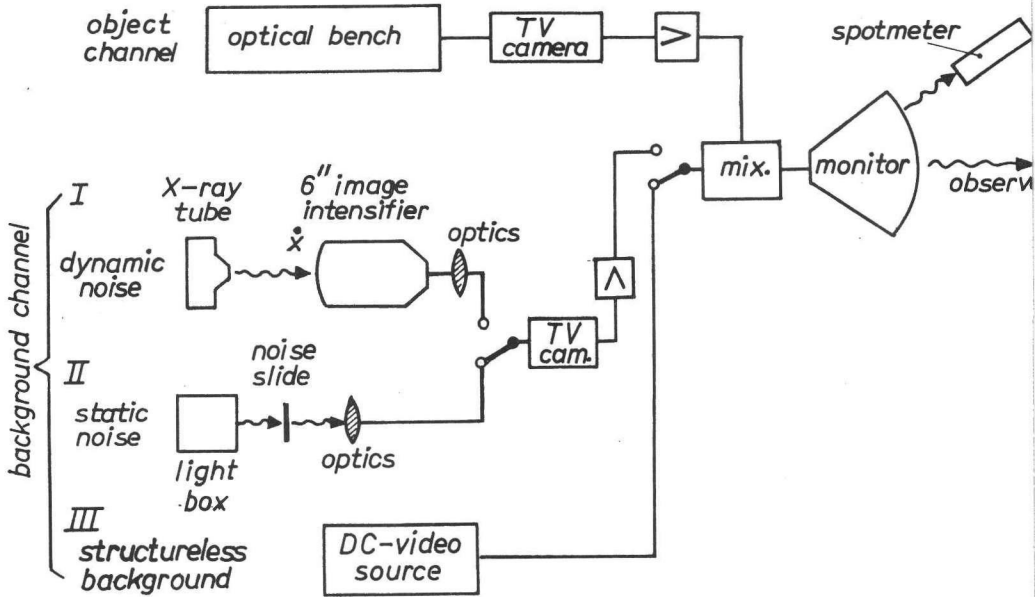


Fig. 2.3.2  
Overview of experimental set-up

This set-up implies additive noise. However, in X-ray systems the noise is multiplicative, i.e. the X-ray intensity and hence the noise depends on the absorption by the object. In our situations, however, the object has little influence on the noise. In the threshold condition the contrast is of the order of 1%. In the analysis of the visibility of the unsharpness (sec. 2.4.4), the typical contrast is only 5%.

The background signal corresponds to dynamic noise, static noise or to a structureless background. These measuring set-ups are denoted by I, II or III.

#### Set-up I:

This set-up corresponds to fluoroscopy. An X-ray tube (Rotalix 21944/00) irradiates a 6" image intensifier (type OB110). The optical system (tandem 0.88/58 and 0.75/50) relays the 19 mm output image to a 'Plumbicon' TV camera (type



XG 5030/10). The X-ray exposure rate  $\dot{X}$  (unit  $\mu\text{R/s}$ ) at the input screen of the image intensifier governs the intensity of the dynamic noise. Practical exposure rates are in the range from 40 to 120  $\mu\text{R/s}$ . The smaller exposure rate corresponds to very prominent noise. The noise for the larger rate is still clearly visible. The TV chain is of the type XG 7105, the mixer type is LDH 4001/00. The automatic gain control of the TV chain ensures that the monitor luminance is constant within 1%.

#### Set-up II:

This situation simulates the viewing of radiographs with frozen noise. The light-box illuminates a noise slide, which is seen via an optical system (type Rayxar E65/0.75, De Oude Delft) by the TV camera. The slide was a picture of the output screen of the image intensifier.

#### Set-up III:

This corresponds to the ideal situation for which no apparent noise is present in the image. A DC video signal is made by the blanking mixer type PM 5572.

#### Object channel:

The object channel simulates practical X-ray systems as to their imaging properties, i.e. disks, edges and bars can be imaged with different size, contrast and sharpness. The TV camera (type XG 5030/10) also contains a Plumbicon tube.

The optical bench (fig. 2.3.3) consists essentially of an adjustable light source and a ground glass on which the object is imaged. The object is either a slit or a circular diaphragm, placed between the source and the ground glass. The unsharpness of the image seen by the TV camera is governed by the size of the source and the position of the object. What is in fact important is the size of the source in the plane of the ground glass. The parameter  $s$  denotes the visual angle corresponding to the source as depicted on the monitor screen.

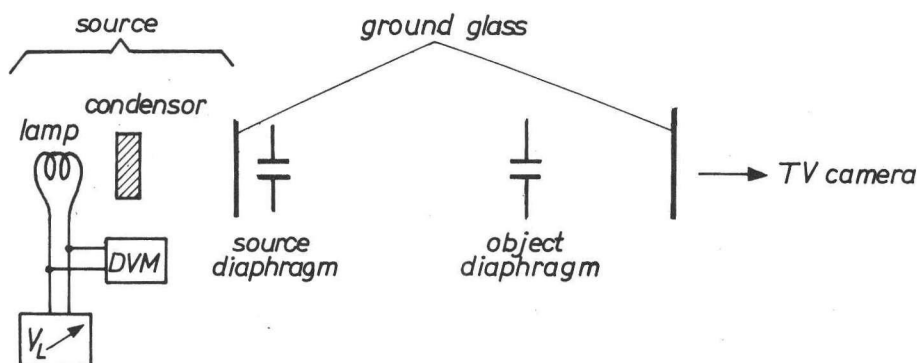


Fig. 2.3.3.  
Optical bench set-up.

The source consists of an aperture placed close to another ground glass, which is evenly illuminated by a lamp/condensor system. The lamp voltage  $V_L$  controls the contrast of the image.

The situation for bars differs from that for disks, because the first objects should be infinitely long to exclude edge-effects. This is of course impossible, so a set-up is made to ascertain that the ends of the bar do not serve as a clue to its presence. This is secured by giving the ends a very gradual slope. These slopes are in any case much smaller than the slopes at the sides, in which we are interested. For comparison, practical longitudinal and transversal luminance profiles are given in fig. 2.3.4. The largest practical length of the bar corresponds to  $4^\circ$  for a viewing distance of 400 mm. We have demonstrated that this is already long for the visual system by measuring the influence of lengths of this order on the threshold contrast.

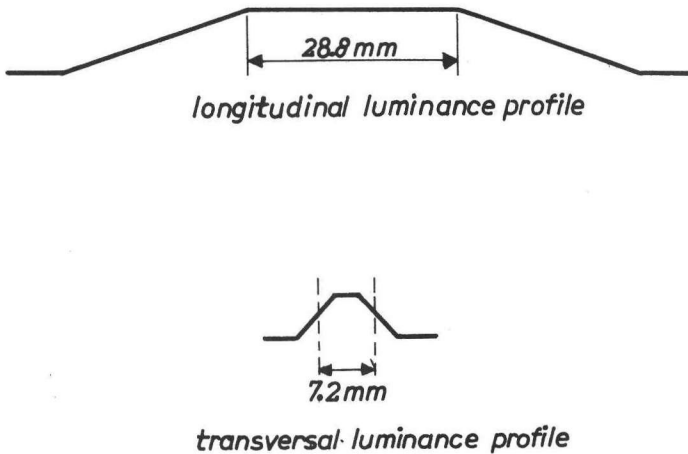


Fig. 2.3.4.

*Typical luminance profiles on the monitor screen, for bars.*

An  $11.4^\circ$  sharp bar served as the reference for three shorter bars of  $5.7^\circ$ ,  $3.8^\circ$  and  $1.9^\circ$  length. The threshold contrast relative to the one for the largest bar is 1.11, 1.20 and 1.30 respectively (result from one observer, 't H, who measured once). Furthermore the influence of a parameter variation can be reliably measured by keeping the length constant during a session.

The optical bench for bars is shown in fig. 2.3.5. The source and object are represented by vernier callipers. The length of the bar is oriented vertically on the monitor screen. The unsharp longitudinal luminance profile is obtained by means of a long source (8 mm), and a diaphragm with a diameter of 10 mm midway between the ground glasses.

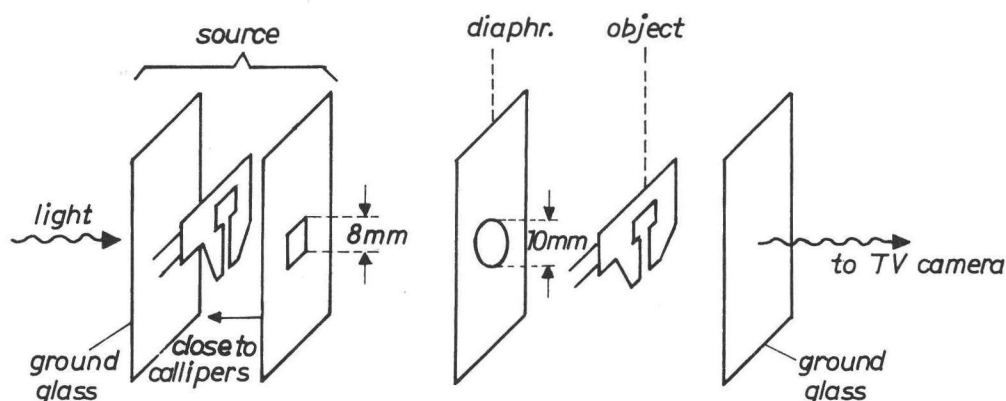


Fig. 2.3.5

*Optical bench for bars.*

The image on the ground glass is seen by the TV camera via a fixed-focus lens (type Projar 1:5.1/300, Isco Göttingen) and a zoom lens (type F.28-112 mm, Angenieux).

The directional effects of the radiation emitted by the ground glass can be neglected, as the aperture of the fixed-focus lens is small ( $12^\circ$  with respect to the ground glass). The zoom lens permits quick scaling of the optical bench parameters. The smallest and often applied magnification factor between the monitor screen and the ground glass is 2.4.

#### Monitor setting:

The appearance of the background and the object can be changed at will with the brightness and contrast controls. Furthermore, the monitor is a highly non-linear element (gamma between 0.1 and 10). During the experiments the monitor setting was fixed so as to give the system an overall gamma of roughly 2. This was proved by Franken et al. (1973b) to be an 'optimum' adjustment for our conditions (ambient luminance  $5 \text{ cd/m}^2$ , X-ray exposure rate  $40\text{--}160 \mu\text{R/s}$ ), for the appearance of a skull phantom. 'Optimum' is placed between inverted commas because no quality criterion could be given: the observers (11) were free to set their own criterion.

#### 2.3.3 Psychometry

Preliminary measurements of the threshold contrast showed that one threshold could be reliably measured, but also that the performance of the observers was liable to temporal shifts (50% shift is possible); the threshold contrast could vary during the day or even within an hour. This may be due to fatigue, or to a change in confidence level. Hence the influence of a parameter value can only be assessed

either by performing many experiments and by applying statistical methods or by presenting the different situations simultaneously. We decided on the latter course by applying only two parameter values in the same session. The two situations are presented alternately. This prevents biasing of the observers, so that a good comparison is possible. A difference in the threshold contrast of a few percent can thus be reliably detected. This would be a time-consuming affair with statistical methods.

The results of the experiments are recorded on-line, (fig. 2.3.6) by means of an X-Y recorder (type PM 8120). The lamp voltage, which is a measure of the contrast, is entered horizontally. The information 'situation 1' or 'situation 2' is retained by coupling the Y-position to it. This is done either manually or by means of micro-switches on the optical bench.

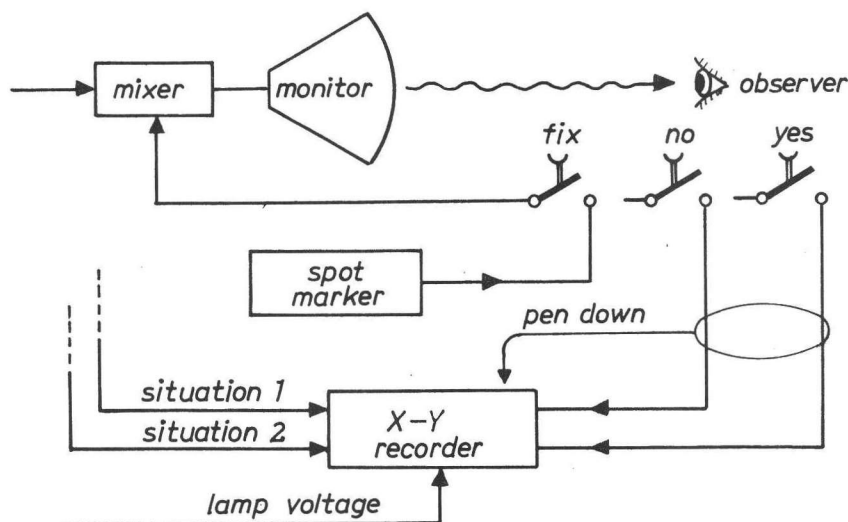


Fig. 2.3.6.  
*Psychometric method.*

The information 'object seen' or 'object invisible' is retained by actuation of the 'yes' or 'no' button. The corresponding 'yes' and 'no' voltages are coupled to the Y-axis. The actuation of the buttons is further coupled to the 'pen-down' switch of the recorder. A typical result of a session is shown in fig. 2.3.7. The yes and no signals result in two overlapping rows of dots. The threshold or uncertainty region is an inherent part to the situation. A typical range is 10% in the threshold contrast, but much smaller values also occur. More measurements do not lead to any shrinking of this region. A session lasting 15 minutes is reasonable: a shorter duration leads to worse statistics, while a longer time may cause temporal shifts in the observer's performance to become more prominent.

A difference in threshold can now easily be detected by eye, especially since the overlaps are generally of the same kind.

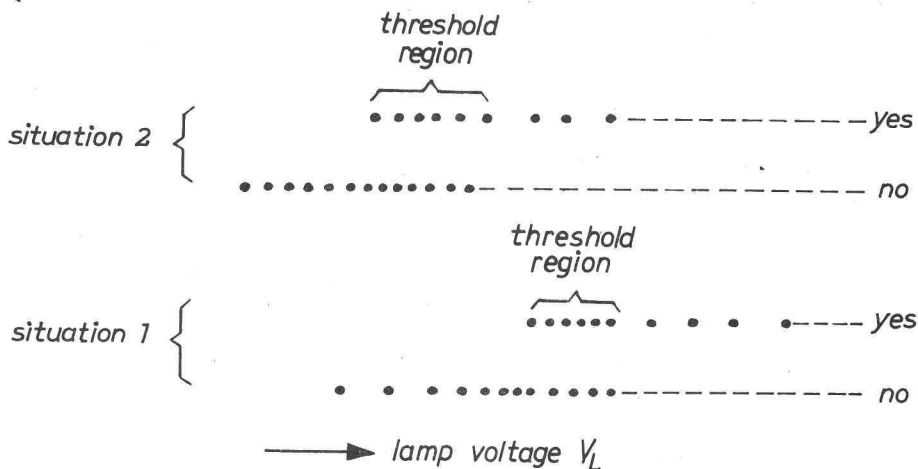


Fig. 2.3.7

*Typical observer responses*

The lamp voltage is first coarsely varied to find the threshold region. The voltage for this region is varied in finer steps. No prescribed strategy is used; it is left to the experimenter to delineate the borders of the region as well as possible. The decision time of the observer is a clue for this purpose: the time is longer (up to  $\approx 5$  seconds) for near-threshold contrast than for clearly supra- or subthreshold contrasts.

This procedure had to be extended when static noisy backgrounds were applied. Although at first sight the noise may not be prominent, difficulties are nevertheless encountered with threshold measurements. During the scrutiny of the monitor screen for the object, subjective regularities in the noise patterns interfere. In any case the object, once seen, shows irregularly shaped edges. As a consequence contrast thresholds cannot be reliably measured, unless different static noises are used for each response of the observer. This situation is approximated by a different shift and rotation of the slide after each response. It is inherent to dynamic noise that different noises are presented. The perception in dynamic noise is also different, i.e. relatively sharp borders can be perceived in the threshold condition. This may be due to the possibility of filling-in the object border temporally.

The interesting feature, the threshold contrast ratio, can be reliably calculated because its value is fairly insensitive to the experimental criterion for the threshold. Either the smallest or the largest lamp voltage corresponding to the uncertainty region can be used. A ratio is involved, so deviations cancel out to some extent. Generally, the smaller lamp voltage was used.

When the uncertainty regions could not be clearly delineated, the experiment was stopped and repeated after a period of rest or on another day. Peculiar results were sometimes obtained. Large shifts (50%) in the threshold contrast ratio were occasionally found, especially if a very unsharp object and a sharp object were compared. This must be due to problems with the criterion setting of the observer. In addition, fatigue and motivation certainly play a role. The repeated judgement of the presence of a barely visible object in noise is an awkward task. Shifts in the threshold contrast ratio were easily detected with our psychometric method. Although it would be interesting to analyse the causes of these shifts, we confined ourselves to repeated measurements with two or three observers so as to obtain a mean threshold contrast ratio. The instability of the individual performances, however, (in particular as regards the criterion for visibility) implies that only a rough confirmation of visual system models can be obtained.

The shape and position of the object are known by the observer so as to make the uncertainty region as small as possible. The shape is made known by presenting from time to time a clearly suprathreshold object. The 'yes' points thus obtained do not contain information, of course. The position is known by virtue of a fixation spot which the observer can recall whenever he wishes by depressing a knob marked 'fix' (fig. 2.3.6). The spot is dim and the observer is instructed to use it sparingly, so as to avoid induction effects. The fixation spot must be absent when the observer makes his decision as to the visibility of the object.

#### *2.3.4 Contrast measurements*

Since the monitor luminance is vignettted, a contrast distribution is involved. This applies to the physical measurement, and also to the visual system. It could be deduced, however, from the following considerations, that the near surroundings of the object are used as the reference level.

The luminance distribution for the middle horizontal line is given in fig. 2.3.8. The threshold of a disk of 44' diameter was measured with and without an absorbing filter covering the left half of the X-ray beam, in a dynamic noisy background (set-up I). This edge evoked a clearly visible darker left-half on the monitor screen (luminance  $\approx$  10% smaller, see fig. 2.3.8). The viewing distance was 400 mm. The presence of this dark field did not alter the threshold contrast for a distance of 15 mm between the border of the disk and the edge. This distance corresponds to  $2^\circ$ ; data from literature (Thomas et al., 1968; Kulikowski and King-Smith, 1973; Gelade et al., 1974; Cohn and Lasley, 1975) indicate that spatial interference sets in only at even smaller distances of about 20 – 100'. As a consequence the contrast is measured at the central position of the object. For objects of the order of centimetres, however, this central contrast is only an approximation. The local contrast at the edges — which is relevant in our view — is then non-iso-

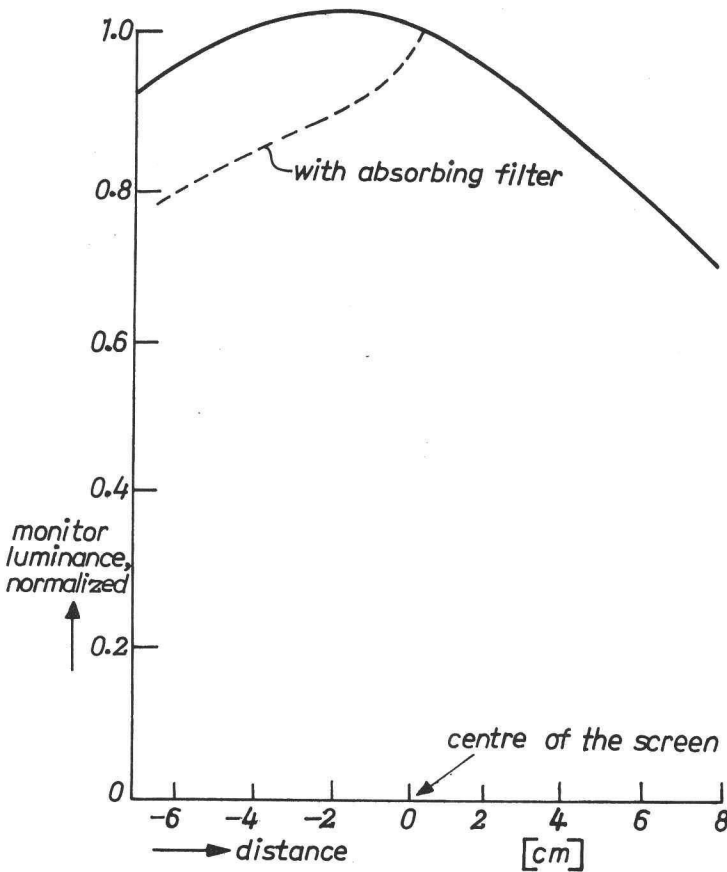


Fig. 2.3.8  
Vignetted monitor luminance; horizontal mid-line.

tropic. This is confirmed in retrospect, as specific sections of such edges are more prominent. This effect does not impair the validity of experiments if objects with the same size and the same position are compared. In our experiments the same position was always carefully retained. Keeping the size invariable is in principle impossible when investigating the C- $\Delta$  curve, but it is roughly achieved in the crucial experiments on the influence of the unsharpness on the visibility.

The monitor luminance  $L_{\text{mon}}$  is of the order of  $20 \text{ cd/m}^2$ . The  $L_{\text{mon}}$  may differ between successive sessions. The measurements are comparable, however, as the threshold contrast proved to be a certain fraction of the background luminance (Weber's law). We measured the  $C_T$  for a  $3^\circ 23'$  disk using two pairs of background luminances: 20 and 19, and 20 and  $17 \text{ cd/m}^2$ . The X-ray exposure rate was  $43 \mu\text{R/s}$ .

No significant shift in the threshold contrast could be measured. Further the influence of the unsharpness proved to be practically independent of the monitor luminance (sec. 2.4.1.5).

Because of the non-linearity of the lamp output as a function of the lamp voltage, and in view of the uncertainty of the gamma of the TV system, we measured the luminance contrast as a function of the lamp voltage after each session. The measurements were carried out with the spot meter, fixated on the centre of the object. The object was made large enough to fill completely the sensitive field of the spotmeter ( $1^\circ$ ), so that the initial contrast of the sharp object was measured in accordance with the definition.

Low threshold contrasts are involved (0.3 – 3%) which implies that the monitor can be regarded as linear as far as the object is concerned. The assessment of the lower contrasts is improved by applying neutral density filters during the experiment, placed between the condensor and the ground glass. The contrasts were measured without the filter.

A typical luminance contrast curve is given in fig. 2.3.9. The lamp voltage is plotted horizontally. The measuring error and the instability of the monitor luminance

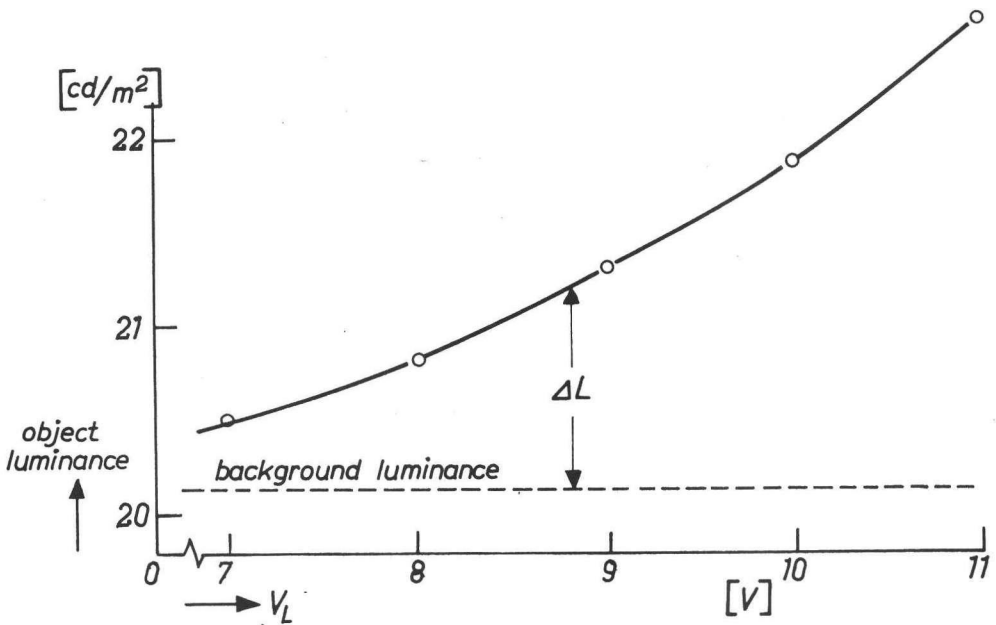


Fig. 2.3.9  
Typical luminance-contrast curve.



result in an error of about 1%. This leads to rather large errors in the absolute threshold for the smaller contrast. The ratio of the threshold contrast for two situations can nevertheless reliably be measured, because the errors are then cancelled out to some extent. The effect of the measuring errors is also reduced by drawing a smooth curve through the measuring points. A conventional estimate of the error in the contrast ratio is 5%.

## 2.4 Spatial effects

### 2.4.1 *Measurements on the influence of the unsharpness*

#### 2.4.1.1 Method

A relatively sharp object and an unsharp object of the same size were presented alternately. The sharp object was made by placing a circular diaphragm or the vernier callipers as close as possible to the ground glass. The unsharp object was made by situating the object somewhere between the ground glasses (usually mid-way) and by choosing a source of appropriate size. The actual size of the unsharp diaphragm or callipers was smaller, so as to cancel out the effect of the geometric magnification.

The sharp and the unsharp object could be quickly shifted into their positions. The choice of the object was coupled to the X-Y recorder by means of microswitches.

Different backgrounds were used, i.e. dynamic noise, static noise and a structureless background. The practical range of dynamic noise corresponds to an exposure rate of 40 up to 120  $\mu\text{R/s}$ . To cover the whole range, the measurements on disks were made with 40  $\mu\text{R/s}$  noise. One control measurement was done in 160  $\mu\text{R/s}$  noise. The situations were interchanged for the bar experiments.

#### 2.4.1.2 Predictions

The predicted threshold contrast ratio equals the inverse of the calculated maximum contrast gradient ratio for objects with the same contrast. Computer programs were written for calculating the intensity distribution of bars and disks. The calculations were done in the Fourier domain, hence in terms of the spatial frequency content of the object and of the spatial frequency modulation transfer.

In principle there is one unknown in this calculation, i.e. the modulation transfer of the visual system. To be consistent with the correct predictions of the Blackwell curves, an exponentially shaped MTF,  $\text{MTF}_v = e^{-\beta\nu}$  is applied.. The value of  $\beta$  can only be estimated to be in the range of from 0.6 to 0.8 (fig. 2.2.10), dependent on the relevant adaptation luminance: either the ambient or the monitor luminance is crucial.

The spatial frequency content of a disk is proportional to  $J_1(\pi\nu\Delta)/\nu$ , that of a bar is proportional to  $\sin(\pi\nu\Delta)/\nu$ . The diameter or the width is denoted by  $\Delta$ . The same expressions apply to the modulation transfer corresponding to a source diameter or width equal to  $s$ . The MTF of the appropriate TV system including the imaging ground glass is assessed by scanning an edge intensity distribution on the monitor screen. The MTF can be approximated by

$$\text{MTF} = e^{-(2.55 \nu)^{1.55}} \quad (2.4.1.1)$$

with the spatial frequency  $\nu$  in cycles per millimetre on the monitor screen. This MTF is comparable with the result of measurements done by Franken et al. (1973a) for such systems. The TV system can further be considered as isotropic, as was concluded from the equivalence of a vertical and a horizontal edge intensity distribution. Since for practical situations the threshold contrast is not primarily governed by the TV MTF, the approximations mentioned are allowed. The measurements on edge intensity distributions are discussed in detail, however, in Appendix III because a derivative of the apparatus will also be used for the noise measurements, and because some interesting instrumental features are incorporated.

Typical MTFs and the influence of the viewing distance are illustrated in figs. 2.4.1.1 and 2.4.1.2. The MTFs of the TV chain, of the source with a diameter of  $80'$ , and of the visual system with  $\beta = 0.8^\circ$  are given in fig. 2.4.1.1. for a viewing

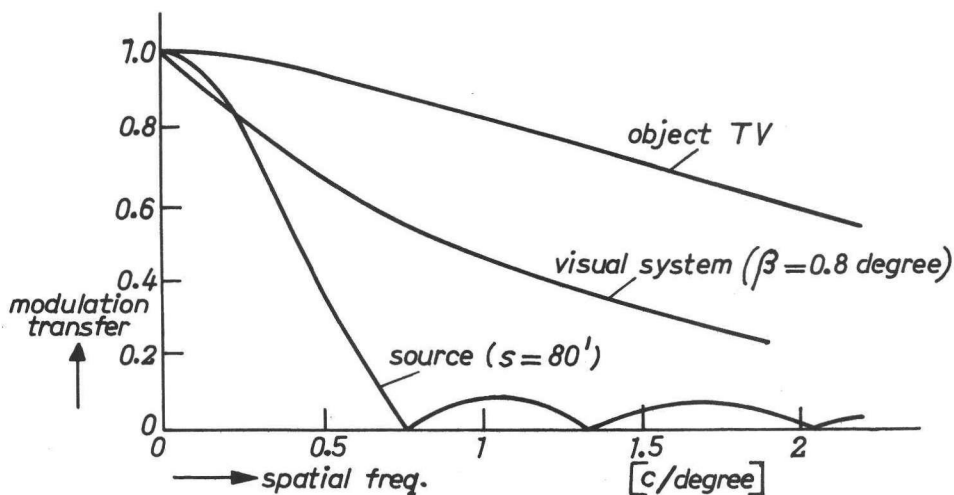


Fig. 2.4.1.1.

Typical MTFs for a viewing distance of 400 mm, source diameter on the monitor screen  $\approx 80'$  (9.2 mm).

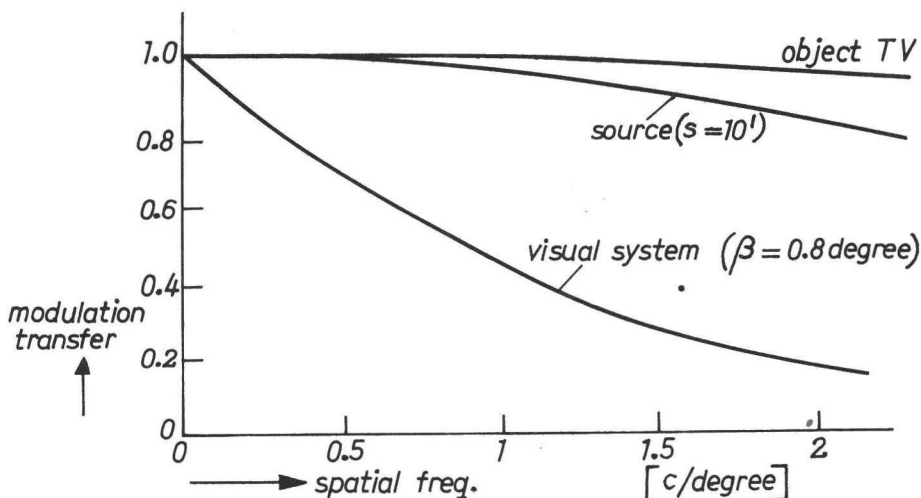


Fig. 2.4.1.2

Typical MTFs for a viewing distance of 3200 mm, source diameter on the monitor screen  $\approx 10'$  (9.2 mm).

distance of 400 mm. The spatial frequency is in periods per degree. The TV MTF is best, the source MTF is the worst one. The influence of this MTF is reduced, however, because the MTF of the visual system must also be taken into account. If the viewing distance is increased, the relative influence of the unsharpness on the monitor screen will be further reduced. This is indeed indicated in fig. 2.4.1.2, where the MTFs are given for a viewing distance of 3200 mm (which is rather large compared with the distances in practical situations).

The inherent unsharpness of the visual system will smooth the influence of the system unsharpness. This is shown in fig. 2.4.1.3, which gives the resulting edge intensity distributions of a sharp and an unsharp object. The predicted threshold contrast ratio for the sharp and the unsharp object corresponding to the MTFs already given, is depicted in fig. 2.4.1.4 as a function of  $\beta$  of the visual system. The  $C_T$  ratio is entered on the right vertical axis, the maximum contrast gradients for a unity contrast object are plotted along the left axis. The larger the value of  $\beta$ , the more the  $C_T$  ratio tends to unity.

This latter curve, denoted by 'ratio', does not strongly depend on  $\beta$ . No great importance can therefore be attached to a value of  $\beta$  as inferred from one measured threshold contrast ratio. A few measured ratios are included as examples. The large variation in the measured ratios is primarily due — in our view — to shifts in observer criteria. Most of the measurements cluster reasonably around  $\beta = 0.8^\circ$  or  $\beta = 1^\circ$ , but the result of S is outside the tolerable range.

The best correspondence between predictions and measurements is obtained with

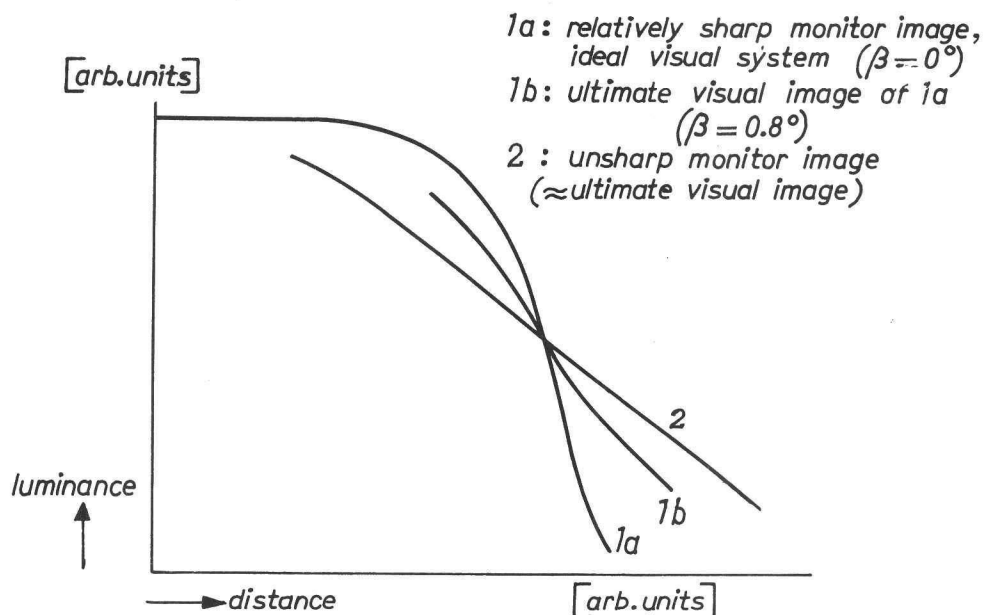


Fig. 2.4.1.3

Edge intensity-distribution for the sharp and the unsharp image corresponding to fig. 2.4.1.1 (viewing distance 400 mm)

$\beta = 1^\circ$ , for the whole range of viewing conditions, disk sizes and unsharpnesses. This result was obtained afterwards, but for convenience it will be used beforehand to analyse the measurements. This will be done by plotting the results in log-log graphs. The measured ratio is entered horizontally on a line corresponding to the predicted CT ratio, which is plotted vertically (fig. 2.4.1.5). A larger CT ratio corresponds to a greater unsharpness of the unsharp object. Clustering of the measured points around the line  $y = x$  indicates a good correspondence. The use of log-units makes easy comparison of relative deviations possible.

### 2.4.1.3. Measurements on disks.

#### Dynamic noise

First, measurements were carried out for the shorter viewing distance of 400 mm. This almost impracticably short distance was chosen to make the influence of the unsharpness more prominent, and to allow the use of relatively small disks so as to minimize the effect of the spatial inhomogeneity of the monitor screen.

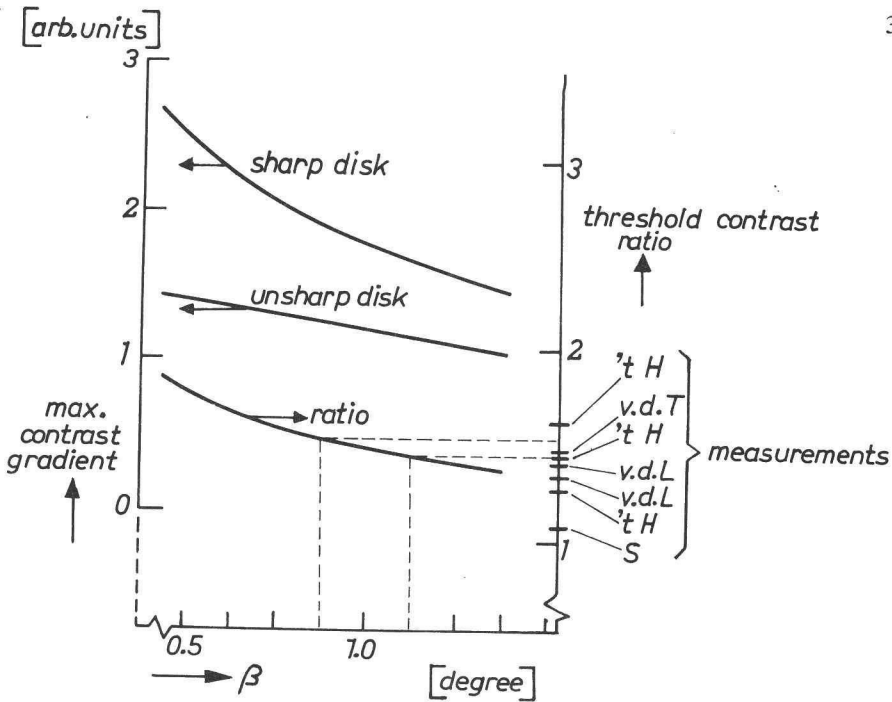


*Fig. 2.4.1.4*

*Predicted and measured threshold contrast ratio; 2°55' disk, 80' source, viewing distance 400 mm.*

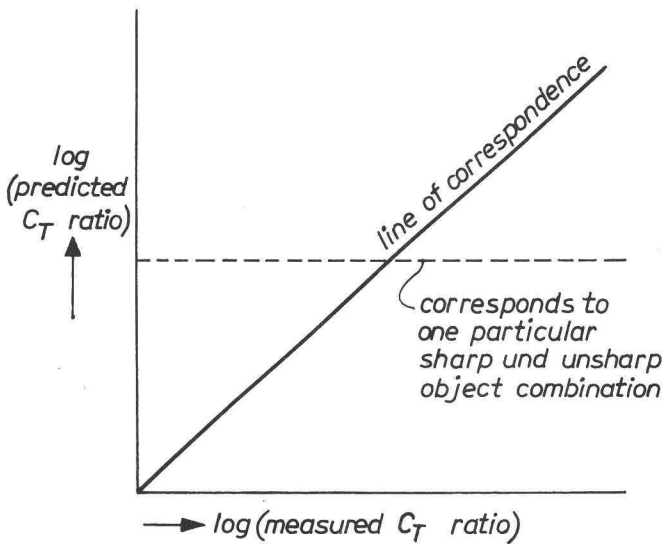


*Fig. 2.4.1.5*

*Graphical confrontation of measurements with theory.*

The experimental conditions are given in table 2.4.1.1; the results are depicted in fig. 2.4.1.6. The experiments are numbered for easy reference. The control measurement number 2 was done with  $\dot{X} = 160 \mu\text{R/s}$ .

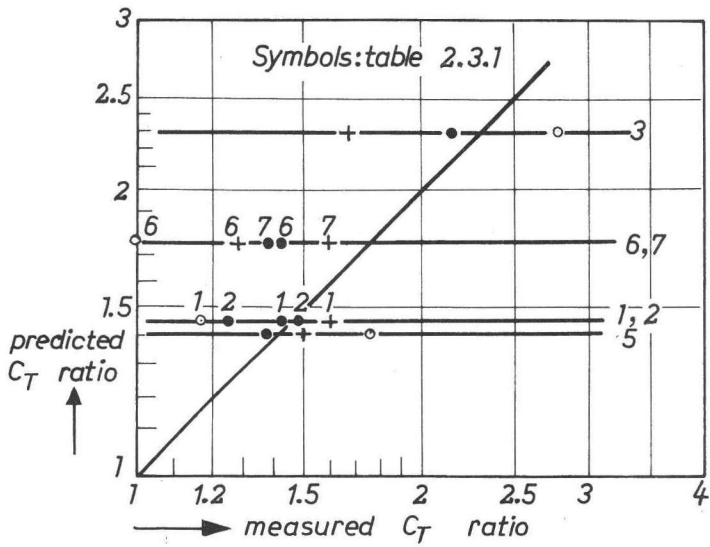


Fig. 2.4.1.6.  
Experiments on disks,  $vd = 400 \text{ mm}$  (table 2.4.1.1).

TABLE 2.4.1.1: Experiments on disks,  $vd = 400 \text{ mm}$

no.	date	vd [mm]	$\dot{X} [\mu\text{R/s}]$	$\Delta$	s
5	17-10-75	400	40	$1^\circ 8'$	$1^\circ 8'$
1	15-09-75			$2^\circ 55'$	$1^\circ 20'$
7	20-10-75			$2^\circ 4'$	$2^\circ 20'$
6	07-01-76			$2^\circ 4'$	$2^\circ 20'$
3	15-09-75		40	$4^\circ 35'$	$4^\circ$
2	08-03-76	400	160	$2^\circ 55'$	$1^\circ 20'$

The following remarks can be made:

- As these were the first experiments, very good correspondence, if any, was not to be expected. Even so, the expected behaviour shows up more or less. An important conclusion is that even for the very large unsharpness introduced, the influence on the threshold contrast is relatively small.
- To obtain a considerable threshold contrast ratio, the unsharpness must be large. Ultimately a triangular intensity distribution may result on the

monitor screen (nos. 5, 6, 7 and 3), which means that very different objects are compared. This may account for the relatively large scatter in the results.

- (iii) In the threshold condition hardly any judgement can be given of the degree of unsharpness. This is bound to be the case, as the perception of structure in the object would require a better spatial resolution. However, the noise speckles are easily seen in the objects because of — in our view — their high temporal contrast gradient. In developing our model of the visual system, we attached great value to the ultimate temporal contrast gradient, either induced by eye movements or externally imposed by the TV framing.
- (iv) The results of S (6, 5) are anomalous. These results will therefore be used with reserve.
- (v) A difference in object processing for different noises ( $40 \mu\text{R/s}$ , 1;  $160 \mu\text{R/s}$ , 2) cannot be reliably deduced.

The unsharpnesses introduced so far are large. Smaller values can easily be obtained by increasing the viewing distance. This was done for experiment no. 3, using distances of 400, 1600 and 3200 mm. The same object and source sizes were used, so the influence of the distance can be reliably measured.

The conditions are given in table 2.4.1.2, and the results are depicted in fig. 2.4.1.7.

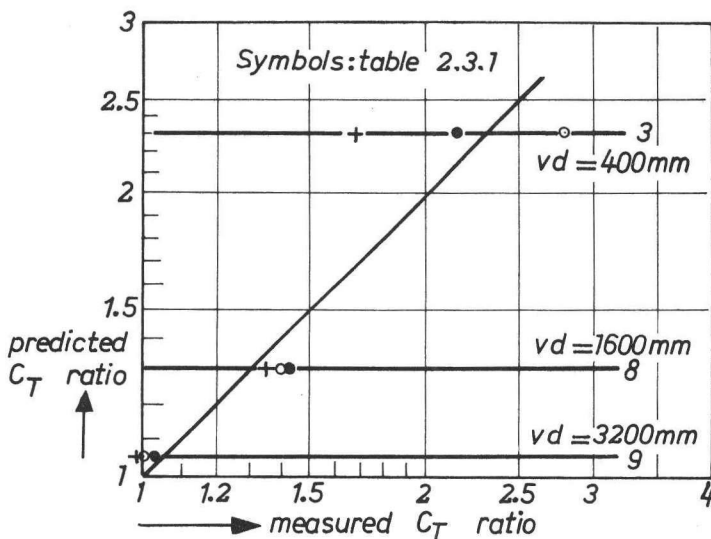


Fig. 2.4.1.7

Experiments on disks, different viewing distances (table 2.4.1.2)

TABLE 2.4.1.2: Experiments on disks, different viewing distances

no.	date	vd [mm]	$\dot{X}$ [ $\mu$ R/s]	$\Delta$	s
3	15-09-75	400	40	4°35'	4°
8	22-10-75	1600	40	1°8'	1°
9	23-10-75	3200	40	34'	30'

The expected reduction of the influence of the unsharpness at greater distances is quantitatively confirmed. The unsharpness on the monitor screen is therefore of no value for assessing the subjective quality. This point would not be stressed if so many authors had not taken only the imaging system into account. The smaller difference in unsharpness (8) leads to more consistent results. The  $C_T$  ratio for the largest distance could not be reliably established to differ from unity.

The considerable variation in the measurements could also be due to the interference of the TV lines. These are clearly visible at a viewing distance of 400 mm. This argument is perhaps invalidated by the fact that the interference may be the same because two objects with the same size are used. For confirmation we performed a series of experiments for the more practical viewing distance of 800 mm. At this distance the noise is less troublesome and the TV lines interfere only to a small extent. The measuring conditions are given in table 2.4.1.3, the results are depicted in graph 2.4.1.8.

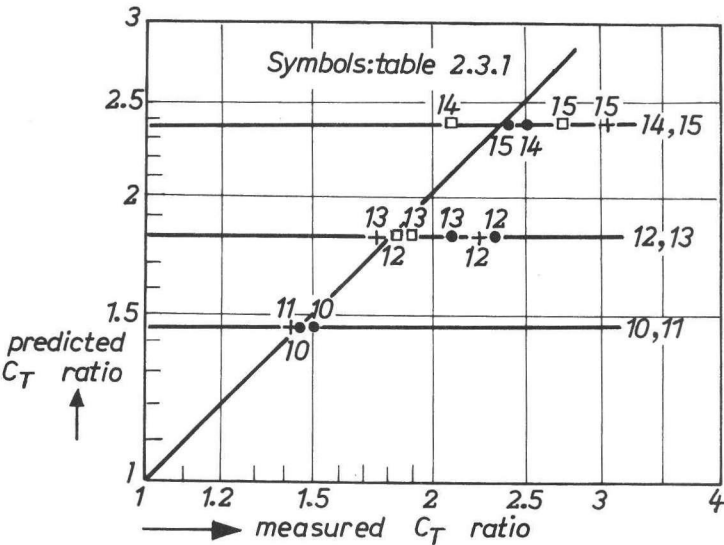


Fig. 2.4.1.8  
Experiments on disks,  $vd = 800$  mm (table 2.4.1.3).



TABLE 2.4.1.3: Experiments on disks,  $vd = 800$  mm

no.	date	vd [mm]	$\dot{X}$ [ $\mu\text{R/s}$ ]	$\Delta$	s
10	07-01-77	800	40	$2^\circ 55'$	$1^\circ 20'$
11	10-01-77			$2^\circ 55'$	$1^\circ 20'$
12	11-01-77			$2^\circ 4'$	$2^\circ 20'$
13	12-01-77			$2^\circ 4'$	$2^\circ 20'$
14	12-01-77			$4^\circ 35'$	$4^\circ$
15	13-01-77	800	40	$4^\circ 35'$	$4^\circ$

The results of the measurements are indeed found to cluster better around the predictions than in the 400 mm situation.

Since many measurements were done for the same situations, the mean values can also be calculated. This was done for observers 't H and vd L. The following measurements are grouped together: 1, 2, 10 and 11; 6, 7, 12 and 13; 3, 14 and 15. The results are given in fig. 2.4.1.9, and show a satisfactory correspondence for different unsharpnesses. The number of measurements is given in brackets.

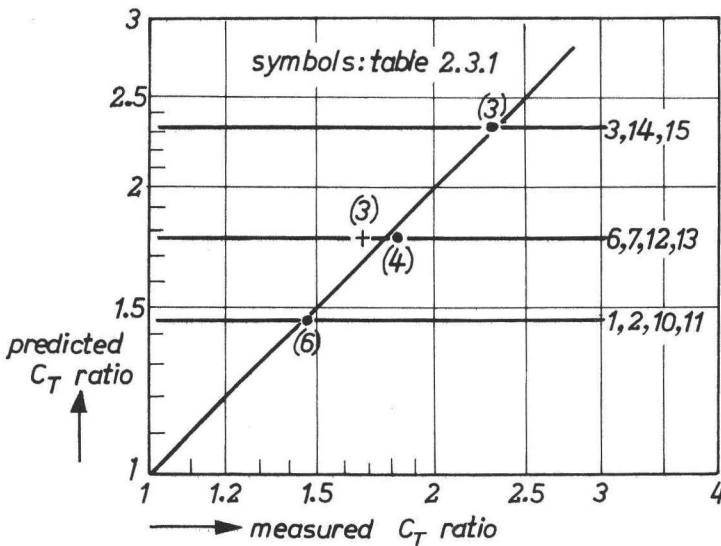


Fig. 2.4.1.9  
Average value of measurements on disks.

#### Static noise

Experimental set-up II was used. Two typical static noises were applied, i.e. one which resembled the noise corresponding to a radiograph made with Philips' Universal

intensifying screens, and one which corresponds to the noise in a 70 mm negative film made from the image intensifier output. The first will be denoted by 'large-size noise', the second by '70 mm noise'. The large-size noise was obtained by depicting a negative film made from the intensifier output-screen by a 35 mm camera. The sensitivity of the X-ray system/ photocamera was varied and appropriate contrast and brightness settings of the TV chain were chosen, while comparing the monitor screen with a standard film on a view box. The 70 mm noise was obtained by depicting a section of a 70 mm film, which was exposed in accordance with appropriate X-ray system settings, i.e.  $80 \mu\text{R}$  at the image intensifier input screen for a tube high voltage of 40 kV. The density of the film was 0.55. The 70 mm radiograph was made with a 9" image intensifier, so it can be deduced that a viewing distance of 1600 mm to the monitor corresponds to the practical viewing distance of 500 mm if the 70 mm film were seen with the naked eye.

The experimental conditions are given in table 2.4.1.4, the results are depicted in graph 2.4.1.10.

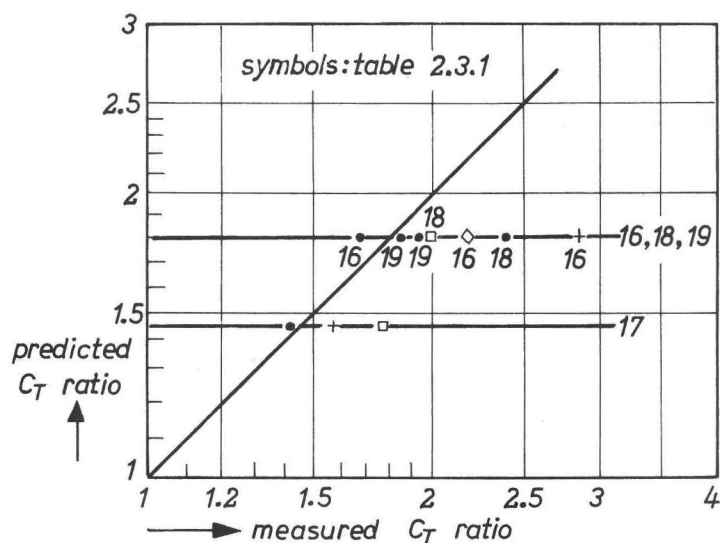


Fig. 2.4.1.10

Measurements on disks, static noise background (table 2.4.1.4).



TABLE 2.4.1.5: Experiments on bars,  $vd = 400$  mm

no.	date	vd [mm]	$\dot{X}$ [ $\mu R/s$ ]	$\Delta$	s
5	20-05-76	400	160	62'	20'
8	18-08-76		160	1° 43'	20
6b	24-05-76		160	2° 45'	20'
6	21-05-76		160	{ 62'	20'
				{ 62'	41'
12	25-08-76		40	{ 62'	20'
				{ 62'	41'
10	23-08-76		160	62'	41'
11	23-08-76		40	62'	41'
3	13-05-76	400	160	41'	41'

The following remarks can be made:

- (i) In general the measured  $C_T$  ratios tend to be too small, especially if the unsharpness is large (triangular luminance distribution with measurement 3). We cannot account for this phenomenon; perhaps the criterion is less strict for such a very unsharp object.
- (ii) The same unsharpness is introduced for different object sizes, i.e.  $\Delta = 62'$ ,  $1^\circ 43'$ ,  $2^\circ 45'$  in experiments 5, 8 and 6b. The measured threshold contrast ratio is indeed independent of the size of these large objects.
- (iii) Two unsharp objects are compared in experiments 6 and 12. The influence of the intrinsic unsharpness of the TV system is then reduced, so more reliable measurements are possible. The results are encouraging.
- (iv) The influence of different noisy backgrounds is investigated in experiments 10 and 11, and 6 and 12. Our hypothesis as to the invariability of the signal processing is confirmed within the experimental error.
- (v) The measurements are difficult, and this difficulty may explain some anomalous results (8, 'tH and vdT; 12, 'tH).

The measurements with greater viewing distances lead to the same conclusions as for disks. The experimental conditions are given in table 2.4.1.6, the results are depicted in fig. 2.4.1.12. The same objects on the screen were presented in experiments 10, 2 and 7. The reduction in the  $C_T$  ratio at larger viewing distances is indeed found.

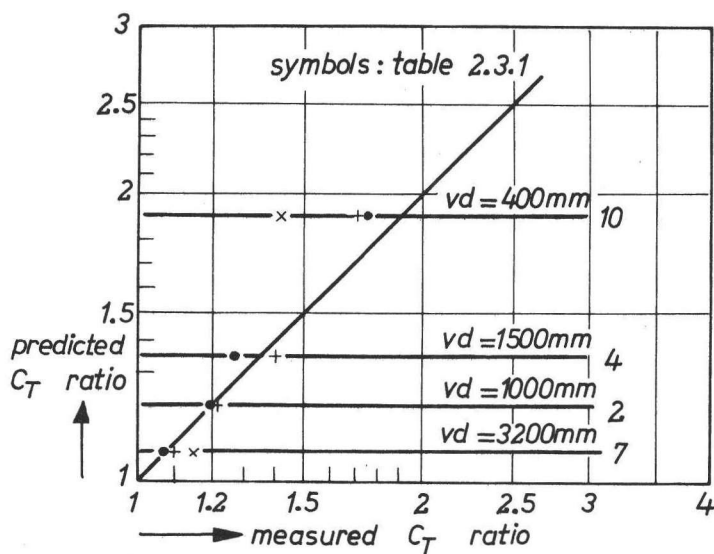


Fig. 2.4.1.12.

Experiments on bars, different viewing distances (table 2.4.1.6).

TABLE 2.4.1.6: Experiments on bars, different viewing distance

no.	date	vd [mm]	$\dot{X}$ [ $\mu\text{R/s}$ ]	$\Delta$	s
10	23-08-76	400	160	62'	41'
4	18-05-76	1500		33'	22'
2	10-05-76	1000		25'	16'
7	18-08-76	3200	160	7.2'	5.1'

The sometimes large discrepancies at a viewing distance of 400 mm may be due to the interference of the TV lines. Some experiments (table 2.4.1.7) were therefore repeated with the larger viewing distance of 800 mm. The same amount of angular unsharpness was introduced with experiments 14, 15 and 16 as with experiments 10, 5 and 3.

TABLE 2.4.1.7: Experiments on bars, vd = 800 mm

no.	date	vd [mm]	$\dot{X}$ [ $\mu\text{R/s}$ ]	$\Delta$	s
15	02-02-77	800	160	62'	20'
13	25-01-77			1°43'	30'
14	27-01-77			62'	40'
16	03-02-77	800	160	41'	41'

The measured ratios (fig. 2.4.1.13) are indeed observed to cluster better around the expected values.

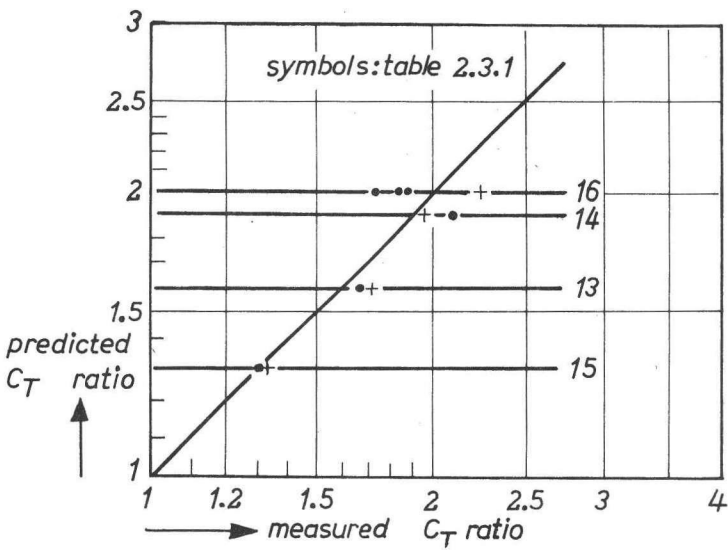


Fig. 2.4.1.13.  
Measurements on bars,  $vd = 800\text{ mm}$  (table 2.4.1.7).

Static noise background and homogeneous background  
The experimental set-ups II and III (fig. 2.3.2) were used. The experimental conditions were chosen so as to cover the smaller  $C_T$  ratio range, as the experiments on disks in static noise involved larger ratios. The conditions are given in table 2.4.1.8. The satisfactory results are depicted in fig. 2.4.1.14.

TABLE 2.4.1.8: Experiments on bars, static noise background and homogeneous background

no.	date	vd [mm]	noise	$\Delta$	s
17	23-09-76	1600	{ large	15'	10'
18	01-10-76			15'	10'
20	21-09-76		{ no	15'	5'
19	30-09-76	1600		15'	10'

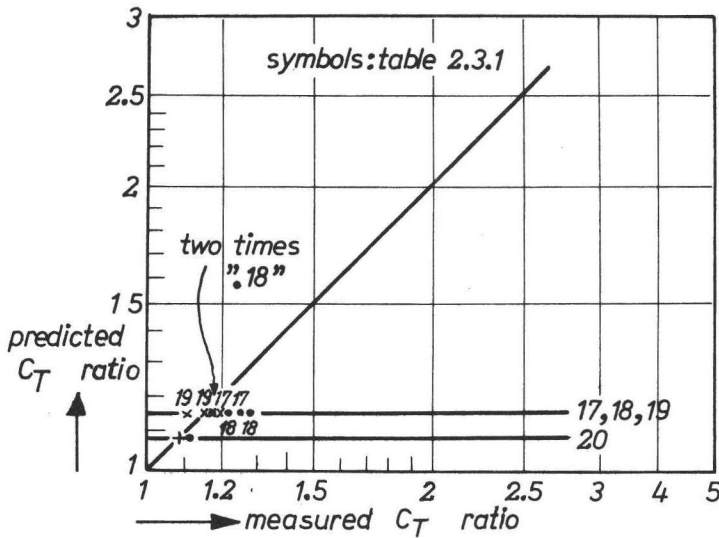


Fig. 2.4.1.14

Measurements on bars, static noise and structureless background (table 2.4.1.8).

#### 2.4.1.5 Influence of the monitor luminance

The influence of the practical range of monitor luminances on the signal processing by the visual system should be small, as the value of  $\beta$  of the visual system MTF does not change rapidly with luminance (fig. 2.2.10). This was confirmed within experimental error by experiments on disks for the substantially larger monitor luminance of  $35 \text{ cd/m}^2$ . Observer 'tH made three measurements for two different unsharpnesses (fig. 2.4.1.15). The experimental conditions are given in table 2.4.1.9.

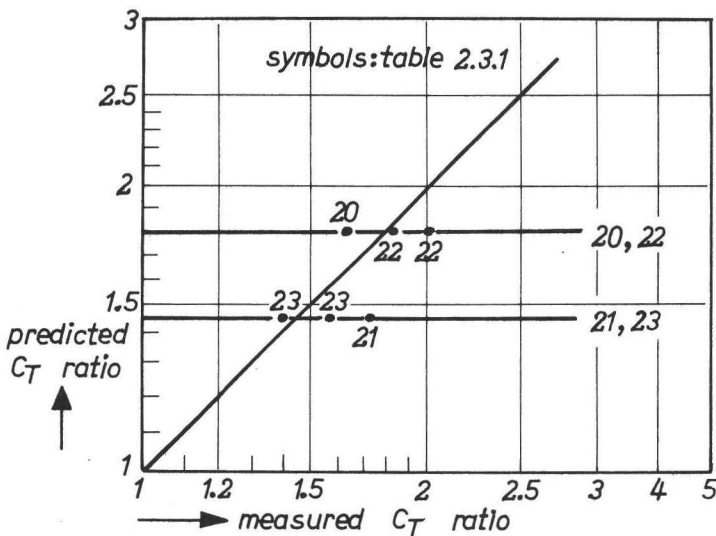


Fig. 2.4.1.15

Measurements on disks, larger monitor luminance ( $35 \text{ cd/m}^2$ , table 2.4.1.9).

TABLE 2.4.1.9: Experiments on disks, larger monitor luminance

no.	date	vd [mm]	$\dot{X}$ [ $\mu$ R/s]	$\Delta$	s
21	19-04-77	800	40	} 2° 55'	1° 20'
23	20-04-77				
20	19-04-77			} 2° 4'	2° 20'
22	20-04-77	800	40		

2.4.1.6 Conclusion

The perception of objects at threshold proves to be a difficult task. Large variances in the threshold contrast ratios occur, and even anomalous results have been obtained both at the higher and the lower end of the  $C_T$  ratio scale. So a conclusion as to the value of  $\beta$  of the visual system MTF can only be drawn on the basis of many experiments. The mean value of a number of experiments then indicates that  $\beta$  is approximately equal to 1 degree. All the experimental results cluster around the prediction corresponding to this value, as can be seen in figures 2.4.1.16 and 2.4.1.17. The data points are given, irrespective of the different conditions, for disks and bars.

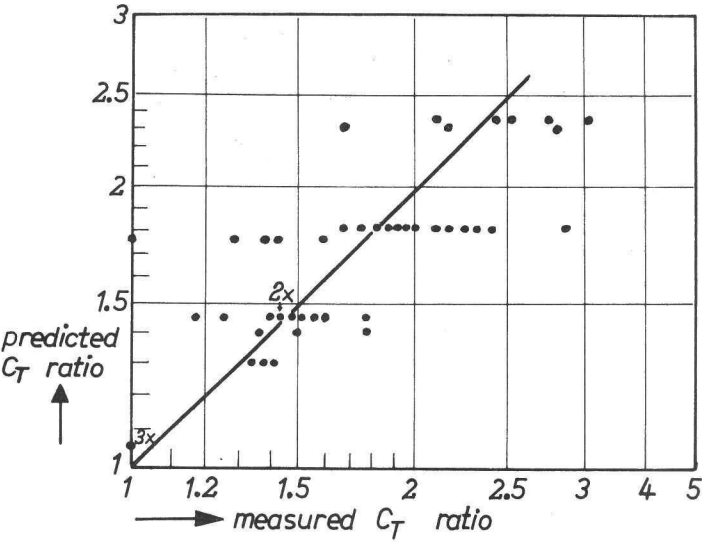


Fig. 2.4.1.16  
Survey of experiments on disks



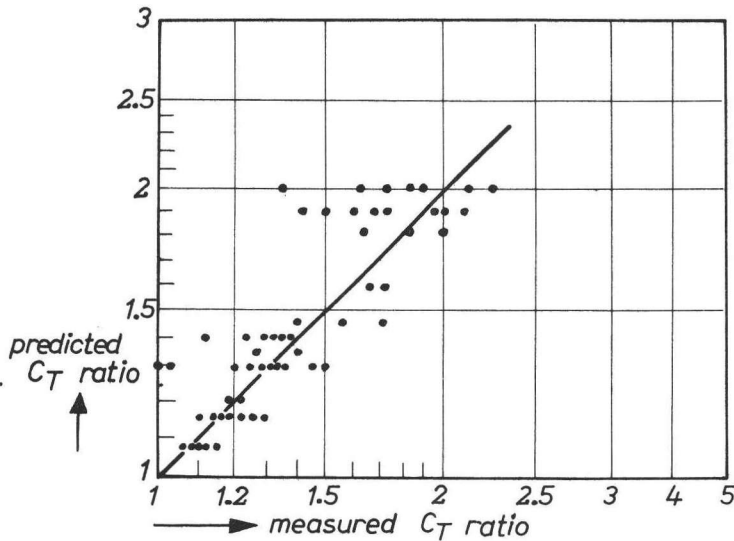


Fig. 2.4.1.17  
Survey of experiments on bars.

Within the variations of individual observers, we conclude that:

- (i) Bars and disks are processed in the same way, i.e. the maximum contrast gradient is decisive.
- (ii) This object processing does not depend on the kind of noise, i.e. it is irrespective of whether it is 40 or 160  $\mu\text{R/s}$  dynamic noise, dynamic noise or static noise (fluorographic noise or screens/large size film) or whether the background is structureless. The same conclusion was drawn by Chesters and Hay (1976b) for disks in a homogeneous and static noisy background. Strictly speaking, this statement has not been proved for bars in static noise, as this noise does not dominate at the viewing distance concerned (1600 mm; see sec. 2.5.2.1). We cannot, however, conceive of a mechanism that would make the perception of bars in dominant static noise an exceptional case, especially since the general effects of static noise (an irregular border of the object at threshold) were still perceived.
- (iii) The processing is invariant with the viewing distance. This parameter therefore is crucial in determining the ultimate influence of unsharpness on the monitor screen.

The validity of the maximum contrast gradient model has thus been confirmed. Its independence on the noise processing has only been demonstrated for objects of equal size. The influence of size will be investigated in the next section.

### 2.4.2 *Measurements on the influence of the object size*

Another method of measuring the value of  $\beta$  of the visual system model MTF is to assess C- $\Delta$  curves, i.e. by measuring the threshold contrast of sharp disks and bars as a function of their size. Our model predicts that the C- $\Delta$  curve for disks on a homogeneous background corresponds to a value of  $\beta$  of about 1 degree. Any confirmation in this respect does not prove the reality of the model, because the model is based on a fitting of C- $\Delta$  curves. It would prove, however, the consistency of the model, the more so because the value of  $\beta$  found, i.e. 1 degree, is rather large for the luminance concerned (a value of 0.8 degree would do better; see fig. 2.2.10). As regards the C- $\Delta$  curve for noisy backgrounds it is generally believed that photon noise, i.e. the noise caused by the quantum character of light, is equivalent to dynamic X-ray noise (Sturm and Morgan, 1949), so the shape of the C- $\Delta$  curve should be independent of the background. This need not be the case, however, as the processing of the visible, coarse X-ray noise may differ from that of the invisible photon noise. It is further not self-evident that the C- $\Delta$  curve for bars can be described with the same model of the visual system, because use may be made of the spatial correlation of such a long object.

As we were unable to find in the literature any firm confirmation of the equivalence of noisy backgrounds as regards the visibility of isolated objects, we decided to do relevant experiments using our sensitive apparatus. C- $\Delta$  curves were measured for bars and disks on a structureless and a dynamic noisy background. Owing to lack of time only one experiment was performed for static noise (sec. 2.5.2.2).

#### 2.4.2.1 *Method*

The threshold-contrast curve is made up of many measuring points. This implies problems of temporal shift in observer performance. This difficulty can be overcome either by making many measurements per point and calculating the mean value (Blackwell, 1946) or by reducing the observation time drastically. In the latter method many detail sizes and contrasts are presented simultaneously (e.g. the phantom described by Burger et al., 1946). The method of Franken et al. (1973c) is a mixture of these methods in that three observers measure simultaneously and that the different sizes are presented in a single object. The contrasts, however, are presented consecutively. This method is discussed here in more detail because some of the results of these measurements will be used in this and other sections. The test objects are placed in front of the image intensifier. They consist of perspex plates on which disks of different diameters are glued. The configuration of the disks is shown in fig. 2.4.2.1. All the disks on one plate have the same X-ray absorption contrast. The plates with different contrasts can be presented in arbitrary order by means of a changer. The viewing distance is 2100 mm (7 times the picture height),

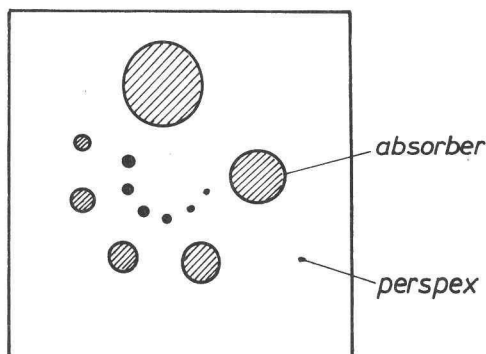


Fig. 2.4.2.1.

*X-ray phantom of Franken (1973c)*

the total viewing time is reasonably short, i.e. about half an hour. The reliability of the measurements on the larger disks (i.e. for smaller contrasts) is worse for two reasons. First, limited use, if any, can be made of the predictability of the pattern. This means that nothing is seen, or only a few disks. It seldom happens that only the very first disk is seen. Second, the large disks are situated at the periphery of the monitor. This means that interference with other structures may occur.

Moverover, these disks are somewhat deformed and unsharper.

Contrary to our method (see below) high primary contrasts can easily be made, so smaller disks can be investigated.

With our apparatus the Blackwell method would be too time-consuming, and the method of Burger or Franken is impossible. We therefore measured the shape of the C- $\Delta$  curve by alternately presenting objects of two different sizes and by measuring the threshold contrast ratio. The temporal variation of the observer is eliminated in this way. The C- $\Delta$  curve is then built up consecutively by investigating adjacent sets of two sizes. Deviations accumulate in this method, but the shape of a part of the curve can be measured quickly and reliably.

The aim should be to obtain in the background a noise equivalent to the noise for the measurements on the unsharpness. This equivalence cannot be retained because the required contrast is not feasible for the smaller disks in the  $40 \mu\text{R/s}$  noise.

Further, the viewing distance must be increased to make small disks (in angular width) without interference with the TV lines: the line distance is 4' at a viewing distance of 400 mm. A different viewing distance also implies another effective noise (sec. 2.5.1.4). Nevertheless we can state that the noise intensities are comparable in their dominance, i.e. a reduction of the exposure rate leads to an increase of the threshold contrast (see sec. 2.5.1.1).

In general only the measurements of observer 'tH are given because his results so far are representative ( $\beta = 1$  degree, see fig. 2.4.1.9). Occasionally, however, the results of the other observers are also discussed.

#### 2.4.2.2 Measurements on disks.

##### Dynamic noise.

The experimental conditions are given in table 2.4.2.1. For the larger disks the smallest viewing distance is chosen to avoid prominent monitor inhomogeneities. Unlike the measurements on the influence of the unsharpness, the edge of the object is situated at different positions on the screen. For the smaller disks larger viewing distances are used to avoid different influences of the line structure of the monitor screen for the two objects (see sec. 2.5.1.4).

**TABLE 2.4.2.1: C- $\Delta$  curve for disks in dynamic noise**

no.	date	vd [mm]	$\dot{X}$ [ $\mu$ R/s]	$\Delta_1/\Delta_2$
1a	23-10-75	400	40	2° 54' / 4° 24'
1b	23-10-75	400	40	1° 33' / 2° 45'
8	18-01-77	1600	120	31' / 1° 33'
9	18-01-77	3200		21' / 31'
10	20-01-77			12' / 21'
12	21-01-77			15' / 20'
13	21-01-77			15' / 20'
14	21-01-77			12' / 15'
11	20-01-77	3200		7.5' / 12'
16	21-01-77	6000	120	4' / 6'

The measured results are compared with the predicted C- $\Delta$  curve for  $\beta = 1$  degree in fig. 2.4.2.2. The results for disks over 31' and smaller than 6' are satisfactory. The anomalous result for 1a might be due to the inhomogeneity of the monitor screen.

The measurements in the asymptotic ranges of the C- $\Delta$  curve contain only rough information on the value of  $\beta$ . More precise information therefore has to be extracted from the measurements in the transition region. There is perhaps a tendency for these results (13, 10, 11) to show a too low threshold contrast ratio. In other words the objects are too large in relation to the proposed unsharpness of the visual system. This may be checked by comparing the results with a prediction based on  $\beta = 0.5$  degree (fig. 2.4.2.3). However, some measurements show a good correspondence, others do not. Since this may be due to the poor statistics, we decided to make repeated measurements of the critical threshold contrast ratio for a 12'/20' combination.

The mean value of the  $C_T$  ratio of eight measurements by 'tH (1.30, 1.35, 1.07, 1.12, 1.30, 1.30, 1.20, 1.21) equals 1.23 with a standard deviation of 0.14. The

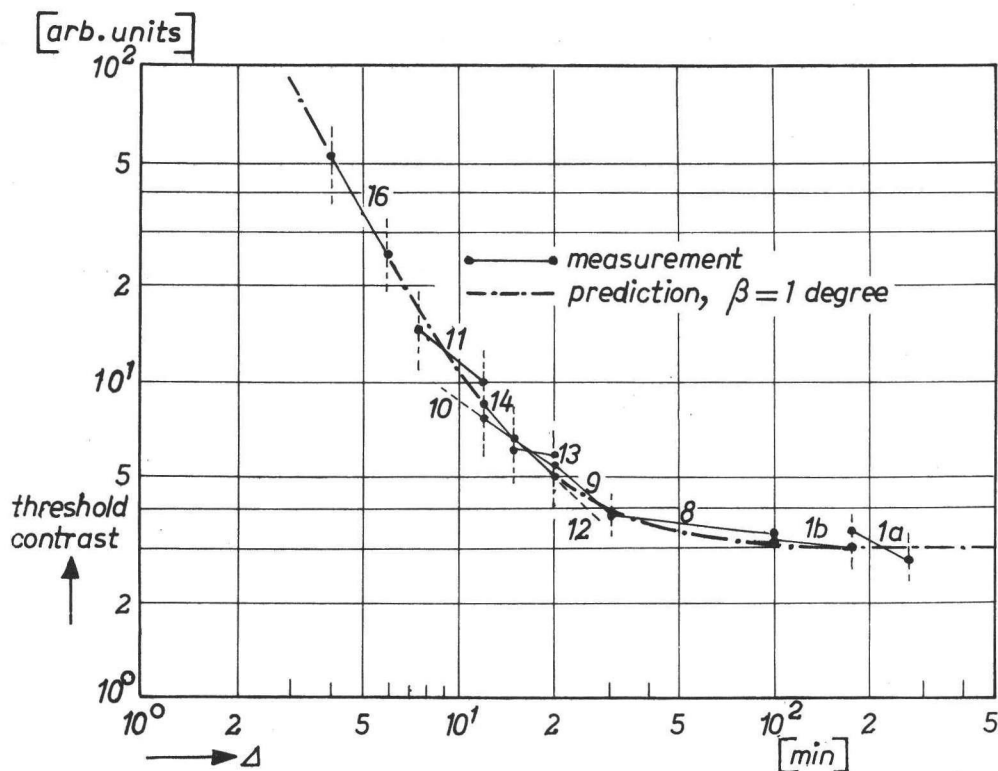


Fig. 2.4.2.2.

Predicted  $C\text{-}\Delta$  curve for disks and measurements, dynamic-noise background;  
 $\beta = 1^\circ$  (table 2.4.2.1).

mean value corresponds to the expectation for  $\beta = 0.5$  degree (fig. 2.4.2.3). The expected value for  $\beta = 1$  degree is 1.72. This is significantly larger ( $\approx 3$  times the standard deviation) than the measured result, so the value of  $\beta$  for the influence of the size differs from the one for the influence of the unsharpness.

#### Homogeneous background.

A homogeneous background was obtained with set-up III (fig. 2.3.2). The  $C\text{-}\Delta$  curve as a whole was not measured, only the critical sizes 12' and 21' (experiment 10) were presented. The mean  $C_T$  ratio of four measurements of 'tH (1.60, 1.65, 1.90, 2.20) was found to equal 1.84 with a standard deviation of 0.28. This ratio is well within the range for the prediction for  $\beta = 1$  degree, i.e. 1.72. This is even more true if the measurement of vG and vdL are included (1.53 and 1.43). The mean value equals 1.72, then.

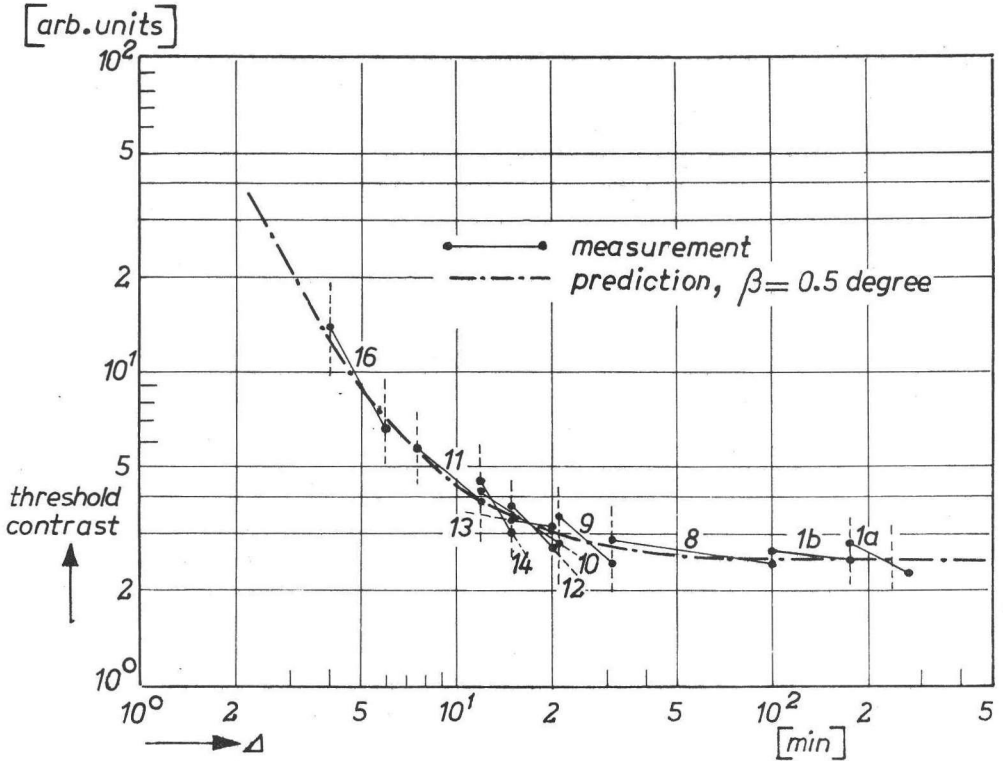


Fig. 2.4.2.3.

*Predicted C- $\Delta$  curve for disks and measurements, dynamic-noise background;  $\beta = 0.5^\circ$  (table 2.4.2.1).*

For the homogeneous background, then, the validity of the visual system model is retained, i.e.  $\beta = 1$  degree in all situations.

Results of Franken et al. (1973c).

Franken's results show the same threshold contrast dependence on the size, at least for disks with diameters in the range of 1.5 to 6 minutes of arc.

#### 2.4.2.3. Measurements on bars.

Dynamic noise.

Preliminary measurements on the C- $\Delta$  curve showed that the value of  $\beta$  for bars in noise might also be equal to 0.5 degree instead of 1 degree. The predicted C- $\Delta$  curve for  $\beta = 0.5$  degree is given in fig. 2.4.2.4. Consequently, the contrast ratio for the critical widths 8' and 16' was measured repeatedly.

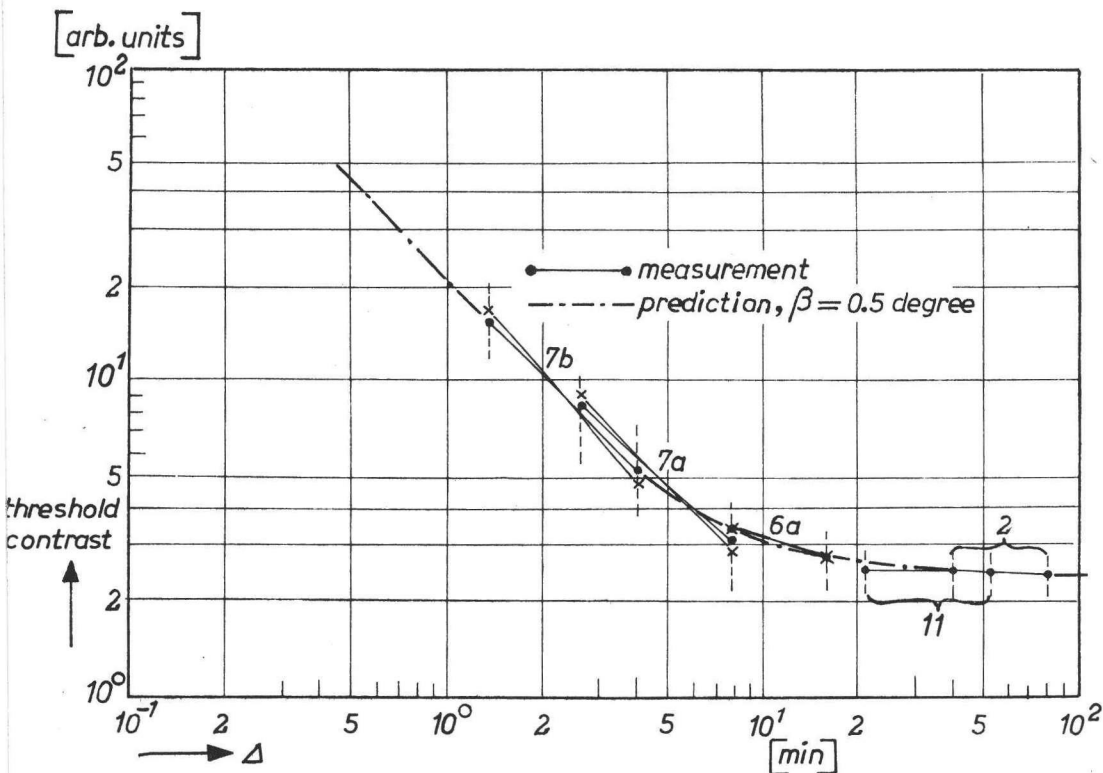


Fig. 2.4.2.4.

Predicted  $C$ - $\Delta$  curve for bars and measurements, dynamic-noise background;  
 $\beta = 0.5^\circ$  (table 2.4.2.2).

The mean of eleven measurements by 'tH (1.21, 1.41, 1.23, 1.05, 1.11, 1.20, 1.22, 1.42, 1.65, 1.19, 1.19) equals 1.26 with a standard deviation of 0.19. The predicted ratio for  $\beta = 0.5$  degree equals 1.23, so we might state that the  $C$ - $\Delta$  curve for disks and bars in noise is described with the same model of the visual system. The results of vdL are 1.23, 1.13, 1.18 and 1.00, the result of vdT equals 1.22. The mean of all the measurements equals 1.23, which is much smaller than the expected ratio with  $\beta = 1$  degree, i.e. a ratio of 1.60.

The conditions for the measurements so far are in accordance with experiment 6a in table 2.4.2.2 below. This table also gives the conditions for the other measurements on the  $C$ - $\Delta$  curve. The results are entered in fig. 2.4.2.4 and show satisfactory agreement. The length, 1, of the bar is also entered in the table. It is inevitably

smaller for smaller bars, because these had to be made by increasing the viewing distance: very small bars cannot be reliably adjusted with the optical bench. The C-Δ curve as a whole might therefore be wrong, but the shape of parts of the curve is correctly measured. We will see later, in the implementation of the model into practical systems, that only this latter aspect is of importance.

TABLE 2.4.2.2: C-Δ curve for bars in dynamic noise

no.	date	vd [mm]	$\dot{X}$ [ $\mu$ R/s]	$\Delta_1/\Delta_2$	l
2	08-06-76	400	160	40' / 1°20'	4°
11	26-04-77	800	120	21' / 53'	2°
6a	03-11-76	1600		8' / 16'	1°40'
7a	04-11-76	1600		2.7' / 8'	1°40'
7b	04-11-76	3200	120	1.33' / 4'	50'

Homogeneous background.

As the mean value of the threshold contrast ratio of 'tH (1.07, 1.30, 1.19, 1.23) for the 8'/16' combination (exp. 6a) equals 1.20 with a standard deviation of 0.16, we are sure that β for the structureless background is not equal to 1 degree. We may further state that the C-Δ curve in this situation is reasonably well described by setting β = 0.5 degree.

2.4.2.4 Conclusion

The model of the visual system is confirmed as far as the influence of the unsharpness of disks and bars and of the size of disks on a homogeneous background is concerned. No confirmation was found for the influence of the size of bars and disks in a noisy background. A discussion of these results and the extension of the model to static noisy backgrounds must await further experiments taken from the literature (sec. 2.4.3). For the discussion see sec. 2.6.

2.4.3 Analysis of results in the literature

Some authors have done experiments on the visibility of sharp and unsharp isolated objects simply to obtain practical rules of thumb or to investigate other models of the visual system. Their results can also be used in this work as a further quantitative check on our model of the visual system.

2.4.3.1 The visibility of simulated lung lesions

The paper by Hemmingsson, Jung and Lönnerholm (1975) entitled "Perception of simulated lesions in the lung" is very interesting because a lung radiograph is used as



the background. In their case the practical static noise and anatomical noise are present — a situation we were not able to investigate. Further, they used practical viewing conditions, the radiographs being examined on a viewbox (Rolloskop, Siemens-Elema). They investigated the influence of the viewing distance (300, 1000 or 3000 mm) and the influence of the unsharpness of the lesions on their threshold contrast. The lesions were simulated by disks with different unsharpness, made by exposing a film/intensifying screens combination (Curix RP1L, Agfa Gevaert; Saphir, Siemens; the same combination was used for the radiographs) on which cylindrical and conical methylmethacrylate objects (fig. 2.4.3.1) were placed. Different contrasts were obtained by applying different exposure times.

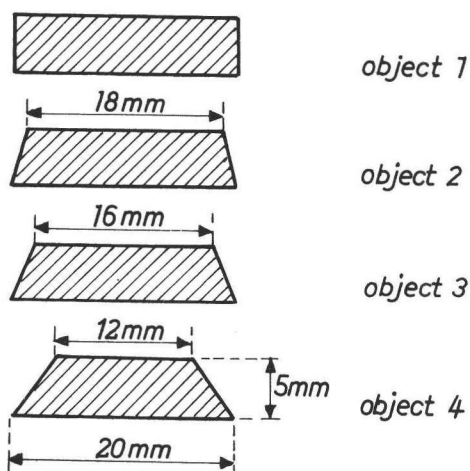


Fig. 2.4.3.1.

*Objects to simulate lung lesions (Hemmingsson et al., 1975).*

These object-films and radiographs were superposed and viewed by the observer. Only one object was present in any of six lung areas, and none was present outside these areas. The distance between the objects was always greater than 4 cm, i.e. the angular distance was at least  $45^\circ$  ( $vd = 3000$  mm). Consequently the objects did not interfere perceptually (see sec. 2.3.4). The viewing time was not restricted.

The density differences rendering the four objects visible with 50 per cent probability are given in table 2.4.3.1. The objects are numbered in increasing order of unsharpness (see also fig. 2.4.3.1). The angular size of the objects is also entered in the table. This size is smaller the larger the unsharpness, owing to the manner in which the unsharpness is introduced.

The requisite density differences are plotted in fig. 2.4.3.2.

TABLE 2.4.3.1: Density difference for 50% visibility of simulated lung lesions

object no.	vd [mm]	$\Delta$	density difference for visibility
1	300	$3^{\circ}53'$	0.024
	1000	$1^{\circ}10'$	0.026
	3000	$23.4'$	0.039
2	300	$3^{\circ}48'$	0.030
	1000	$1^{\circ}84'$	0.026
	3000	$22.8'$	0.035
3	300	$3^{\circ}28'$	0.033
	1000	$1^{\circ}2.5'$	0.027
	3000	$20.8'$	0.040
4	300	$3^{\circ}$	0.059
	1000	$54'$	0.045
	3000	$18'$	0.053

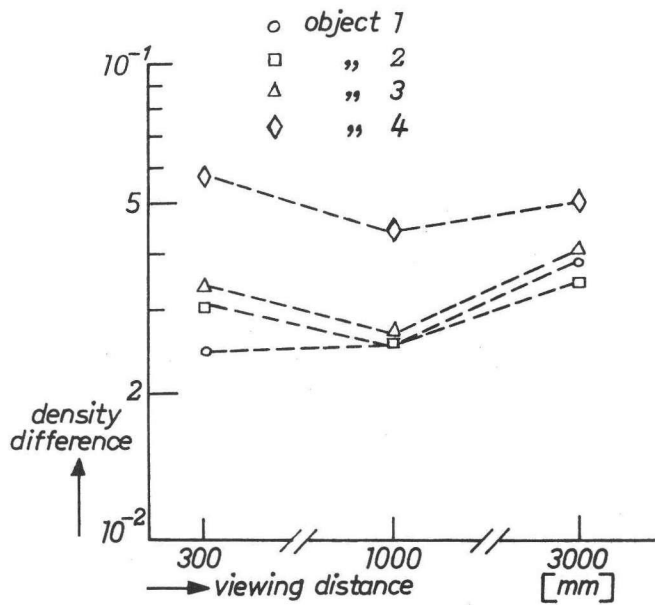


Fig. 2.4.3.2.  
Density difference for 50% probability of detection (table 2.4.3.1, Hemmingsson et al., 1975).

Three conclusions are drawn:

- (i) the greater the unsharpness, the larger is the required density difference;
- (ii) the influence of the viewing distance is relatively small for the sharp objects;
- (iii) a larger viewing distance favours the visibility of unsharp objects.

These trends can be quantitatively understood with the aid of our model of the visual system. The inverse of the maximum contrast gradients is given in fig. 2.4.3.3, together with the measured density differences. The calculated values are shifted vertically for the best fit by eye. The shift is applied to all results simultaneously, so that the influence of the viewing distance is retained. The fit is best for  $\beta$  of the visual system MTF equal to 0.8 degree – which is comparable to the value we found (1 degree). The authors do not quote the ambient luminance level, but this will also be comparable with that in our situation as the viewbox was masked except for the radiograph, and no other lighting was applied.

On the object unsharpness entered into our computer program, the authors state that 'the density gradients across the borders of the three tapered objects - - - - are

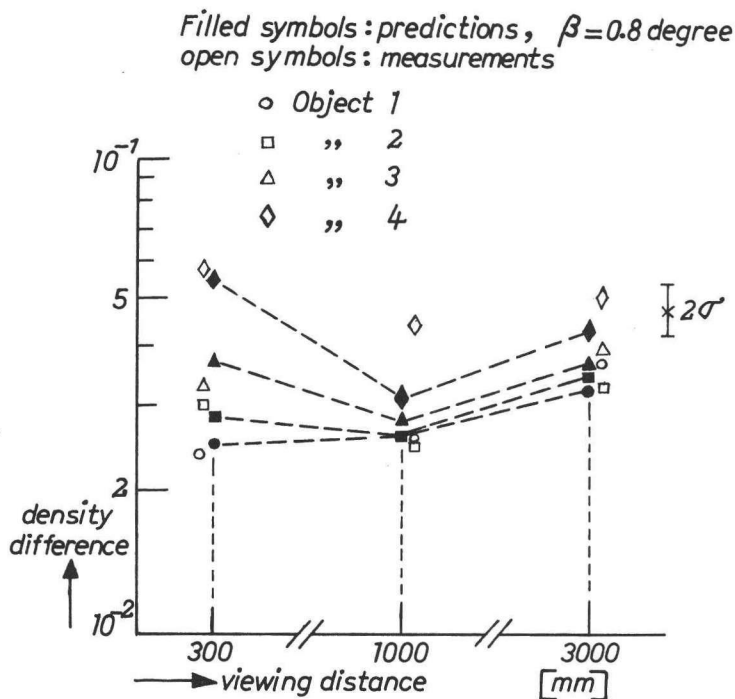


Fig. 2.4.3.3.

Measured (Hemmingsson et al., 1975) and predicted (this work) density difference for 50% probability of detection. Standard error  $\sigma$ .

----- close copies of the objects themselves'. Apparently, the influence of the screens/film system is negligible. For the straight cylinder an anomalous result was then obtained, because 'the density gradient had a width of 0.8 mm due to geometric distortion'. Now the geometry during radiography could only lead to an unsharpness of 0.025 mm, so the unsharpness must be due to the screens. Their unsharpness, however, is of the order of tenths of a millimetre. Besides, the corresponding density gradient should not be linear but S-shaped. This implies that errors may have been made in the microdensitometry. The slit aperture might have been larger than the quoted 0.2 x 2 mm. Consequently we disregarded the geometric unsharpness; the screen unsharpness is thought to be comparable with that of Philips' Universal screens ( $MTF(\nu) = e^{-0.38\nu}$ ,  $\nu$  in periods per mm).

#### Explanation of the findings.

In view of the relatively large standard error, the correspondence between predictions and measurements is surprisingly good. This holds especially for the shortest viewing distance, at which the influence of the unsharpness is prominent. At this distance the objects are so large ( $\Delta > 3^\circ$ ) that size effects do not play a role (see fig. 2.4.2.2). The same holds for the middle viewing distance. Since the influence of the unsharpness is also much smaller, all the calculated values cluster. The influence of the unsharpness is negligible at the larger distance, although here the size effect starts to be significant.

The influence of the viewing distance as such is also correctly predicted. For the sharp object no. 1 only a small size effect occurs. For the unsharper objects, the reduced effective unsharpness initially benefits visibility; at the greater distances the visibility deteriorates owing to the reduced angular size. This beneficial effect of increasing the viewing distance for the perception of large unsharp objects has already been mentioned by Newell and Garneau (1951) and Tuddenham (1957). Minification (as in image intensifier fluorography) would then be of advantage.

Only one substantial deviation could be found, i.e. for object 4 at a viewing distance of 1000 mm. The predicted required density difference is too low. No explanation could be found for this effect. An experimental check was performed by measuring the threshold contrast for this object at different viewing distances. Our results correspond well with our prediction, so no mistake was made in the computer program. The main difference between the measurements is the background: we use a background without anatomical structures. We cannot conceive of any mechanism that would obscure this particular object so disproportionately.

We conclude that generally the model of the visual system for the prediction of the visibility of single objects is also valid if a real anatomical structure is used as the background. In view of the value of  $\beta$ , 0.8 degree, it may be stated that this background acts as a structureless background.

### 2.4.3.2 The visibility of Gaussian and rectangular bars

The work of Shapley (1974) is interesting because the threshold contrasts of sharp and Gaussian-shaped bars are compared. In addition the relation with the visibility of sinusoidal gratings, i.e. a repetition of 'bars', is investigated. A theoretical approach to the prediction of the contrast sensitivity for gratings (see sec. 2.4.5) on the basis of our model of the visual system leads to the equation

$$\text{SGSF}(\nu) \sim \nu e^{-\beta \nu} \quad (2.4.3.1)$$

where SGSF stands for the spatial grating sensitivity function. Its value equals the reciprocal of the threshold modulation of the grating. In the literature it is called the 'contrast sensitivity function'. It is striking that the SGSF for one of the observers, RMS, is described 'for calculational convenience' by equation 2.4.3.1. It can be deduced, then, that  $\beta$  equals 13'. We will examine below whether we can use this value of  $\beta$  to predict the measured C- $\Delta$  curves for sharp and Gaussian-shaped bars. In sec. 2.6.1 we will investigate whether this rather small value of  $\beta$  fits with other data.

The bars were oriented vertically and centrally on a circular screen with a diameter of  $5.5^\circ$ . The luminance of the screen was  $100 \text{ cd/m}^2$ . Binocular viewing was used. The subject was instructed to set his threshold under free inspection. The contrast thresholds were determined by adjustment and had a standard error of 5 percent. The test pattern was displayed continuously on the screen.

This experiment differs from ours in that the luminance of the screen is much larger. This may account for the smaller value of  $\beta$  (we found  $\beta = 0.5^\circ - 1^\circ$  for  $L = 20 \text{ cd/m}^2$ ). Secondly, the psychometry is also different — the consequences will be discussed where necessary.

The measured threshold contrasts of the sharp bars for observer RMS are given in fig. 2.4.3.4. The results of observer FWC are not given because they do not deviate significantly. The predicted C- $\Delta$  curve for  $\beta = 13'$  is also given. There is a very good correspondence between measurements and predictions. The threshold contrast for Gaussian bars is given in fig. 2.4.3.5 as a function of their effective width (a sharp bar with this width and the same contrast would envelop the same area as the Gaussian bar). For small bars the threshold contrast decreases with size, whereas for large bars an increase sets in owing to the increasing unsharpness. The position of the minimum threshold decisively determines the value of  $\beta$ ; the asymptotic branches of the curve do not contain information in this respect. The prediction for  $\beta = 13'$  (fig. 2.4.3.5) shows a minimum at a size that is too small. The value of  $\beta$  should therefore be larger to fit the measurements better. The value of  $\beta$  will be made twice as large, because we found this same ratio in our research: we described the influence of the unsharpness with  $\beta = 60'$ , whereas we described the influence of the size by taking  $\beta = 30'$ .

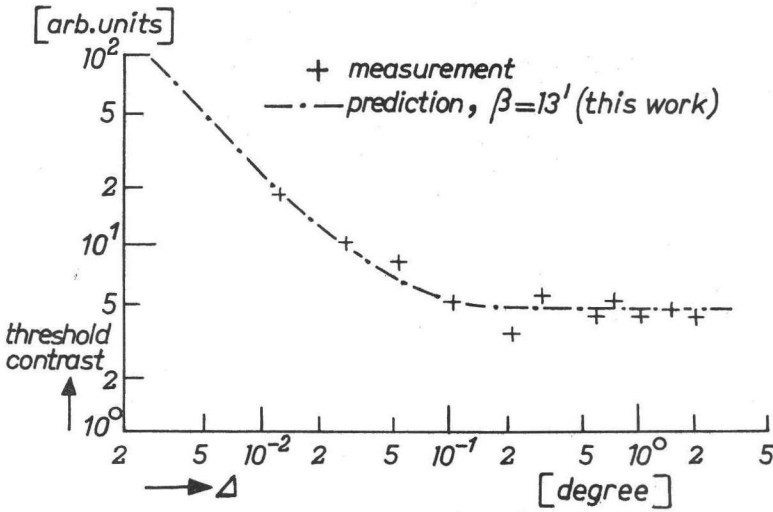


Fig. 2.4.3.4.

*C- $\Delta$  curve for sharp bars, observer RMS (Shapley, 1974).*

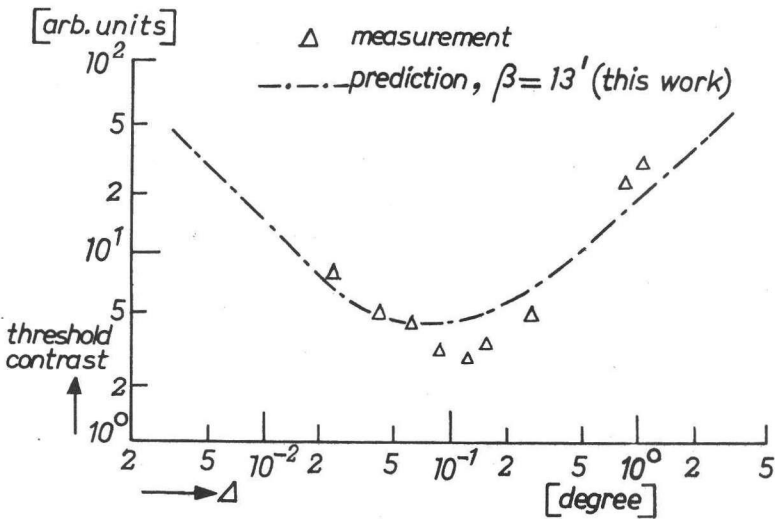


Fig. 2.4.3.5.

*C- $\Delta$  curve for Gaussian bars, observer RMS (Shapley, 1974).*

The prediction for the Gaussian bar relative to the sharp bar is now obtained in two steps. The size effect is described with  $\beta = 13'$ , whereas the corresponding relative increase in threshold contrast due to the unsharpness is described with  $\beta = 26'$ . The resulting comparison between predictions and measurements is given in fig. 2.4.3.6. A reasonable fit is obtained.

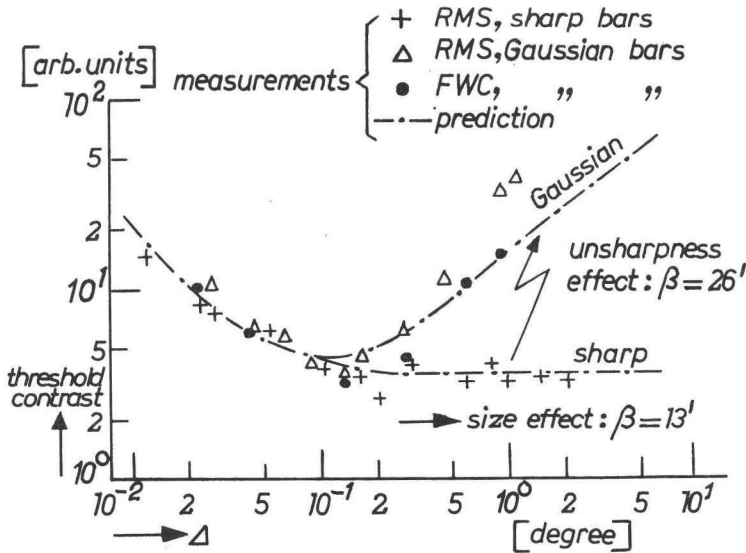


Fig. 2.4.3.6.

Measured (Shapley, 1974) and predicted (this work)  $C-\Delta$  curves for sharp and Gaussian bars.

The discrepancies may be ascribed to the following causes:

- (i) The ratio between the thresholds for the different bars was not reliably measured, because the measurements were carried out consecutively.
- (ii) In our view, the adjustment of the threshold contrast by the *observer* is subject to large variations. We tried it with our experimental set-up, but threshold variations of 100% occurred.

#### 2.4.4 Measurements on the visibility of the unsharpness

As stated before, the unsharpness — or in other words the luminance distribution of the object — is hardly perceived in the threshold condition. The only information obtained then is the presence of the object. Nevertheless the visibility of the unsharpness as such is worth investigating because the unsharpness impression will also play a role in the judgement of the image quality. Besides it is believed that perceptible differences in unsharpness need not lead to correspondingly large influences on the threshold contrast (Higgins and Jones, 1952; Schober, 1953). This would imply that the threshold unsharpness increment is a more sensitive criterion for X-ray system optimization. A few pilot experiments will be carried out to investigate the absolute and the incremental threshold by comparing a supra-threshold unsharp object with either a relatively sharp or an unsharp object.

No reliable quantitative data on these effects have yet been published, and many authors only give descriptions or data for the unsharpness in the viewed plane. The

influence of the viewing distance should however be taken into account, since the permissible unsharpness may be larger for a larger distance.

#### Absolute threshold unsharpness.

Some authors claim 0.3 mm to be the critical value for the unsharpness, but without mentioning the viewing distance (Zimmer, 1952; v.d. Plaats, 1952). Only Schober (1953) gives an angular width of 2', i.e. 0.17 mm at a viewing distance of 300 mm.

#### Threshold unsharpness-increment.

The basic experiments have been carried out by Warren (1937, 1940) and by Klasens (1946). They visually compared an object of known and simple unsharpness with one that had a compound unsharpness, i.e. corresponding to more than one source of unsharpness. Their aim was to find empirical formulae to predict the effective unsharpness corresponding to such a compound unsharpness. In this sense leaving the influence of the viewing distance out of account is not so detrimental, as a reference stimulus is used. A conclusion as to the increment threshold unsharpness, however, is doubtful. This may account for the discrepancy between e.g. Klasens (1946) and Chantraine (1930). The sources of unsharpness were not the same, but their conclusions are so different that one can indeed speak of a discrepancy. The first author states that unsharpnesses smaller than one-third of the main unsharpness cannot be perceived in the final result. The latter author states that an increment of one-fifth of the initial unsharpness leads to a noticeably worse impression.

#### Influence of the contrast.

The degree of visibility of the object as such has an influence on the judgement of the unsharpness. In fact, for near-threshold contrast, the reference object may be visible whereas the unsharper object is not. For higher contrasts there is no consensus of opinion in the literature. Warren (1937) could not find any difference when contrasts according to density differences of 0.1, 0.2 and 0.8 were applied. Bronkhorst (1927) states that the perceived unsharpness is smaller for larger contrasts. This conclusion is also adopted by Meiler (1955), Evers and Schober (1956) and by Rossmann and Seeman (1961), without experimental proof, however. Finally, Higgins and Jones (1952) explicitly state that the influence of the contrast is unknown. The problem with higher contrast is further that the non-linearity (e.g.  $\gamma$  of the film) can play a role. This may occur in our experiments on the absolute threshold unsharpness in oral radiography (sec. 2.4.4.1). The conclusions can nevertheless be used, because practical contrasts have been chosen. Fortunately, the results fit well with those for the threshold unsharpness increment (sec. 2.4.4.2), for which the ultimate contrast was only 5%.

#### 2.4.4.1 Absolute threshold unsharpness.

The measured results have been extracted from our pilot study on the image quality of oral radiographs. Since these are generally made on non-screen film, favourably sharp and relatively noise-free images can be made.



Questions arose with respect to the influence of the focal spot size of the X-ray tube on the image quality. One of the aspects is the influence of the corresponding unsharpness.

2.4.4.1.1. *Method.* The production and physical measurements of the radiographs were performed by Timmer and den Boer of the Medical Systems Division. The X-ray set-up is depicted in fig. 2.4.4.1. Different edge unsharpnesses of a square phantom ( $8 \times 8 \text{ mm}^2$ ) are achieved by choosing the larger or the smaller focal spot of the X-ray tube and/or by changing the phantom-film distance, denoted by  $o$ . The focus-to-film distance is denoted by  $f_r$ , and equals 315 mm. The X-ray tube has a nominal spot size of 1.2 and 2.0 mm, so the effective sizes, denoted by  $f$ , are taken to be 1.8 and 3.0 mm (see sec. 3.2.1). The films are of the type DuPont Super Dozahn,  $30 \times 40 \text{ mm}^2$ . The tube high voltage is 50 kV, a 4 mm Al filter is used.

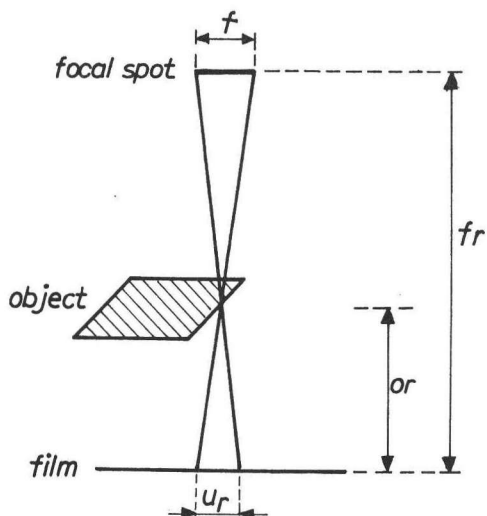


*Fig. 2.4.4.1.*  
*X-ray set-up for oral phantom radiographs.*

The radiograph data are given in table 2.4.4.1, in increasing order of unsharpness, denoted by  $u_r$ . Here  $u_r$  is defined as  $f \cdot \text{or} / (f_r - \text{or})$  (fig. 3.1.1a).

The object and background densities are different, but these small changes in contrast does in our view not affect the unsharpness impression (see sec. 2.4.4.2). Film densities were measured with a Joyce-Loebel MK III CS densitometer.

The radiographs are judged in pairs to determine whether there is any difference in unsharpness. Three responses are possible, i.e. 'yes', 'no' and 'not certain'. The

TABLE 2.4.4.1: Oral phantom radiograph data

no.	$u_r$ [mm]	f [mm]	or [mm]	density	
				object	background
6	0.06	1.8	10	0.39	0.55
5	0.10	3.0	10	0.35	0.55
2	0.12	1.8	20	0.34	0.47
3	0.26	1.8	40	0.31	0.46
1	0.32	3.0	20	0.31	0.46
4	0.44	3.0	40	0.36	0.51

radiographs are presented in random order to two or three observers ('tH, vdL, vdT). The number of observers and measurements are small, hence at best trends can be decided upon. The viewing conditions are chosen so as to cover practical situations: free-roaming eye, no artificial pupils, no time limit set.

Condition I : the observer is seated in the dimly-lit room as described in sec. 2.3.1. The viewing distance is 500 mm. The pairs of film are mounted on a viewing box. Their separation is 95 mm, the bright field amounts to  $90 \times 400 \text{ mm}^2$ . The illumination of the eye is practically entirely due to the viewing box and has a value of about 10 lux. Three observers measured twice.

Condition II : in condition I stray light might unfavourably interfere. Further, the luminance level might be too low and the viewing distance too large. So in condition II, the distance is reduced to 250 mm. The viewing box is masked by black paper, except for the rectangle in which the films were placed. The room is lit by outdoor light, the illuminance at the eye is about 500 lux. Two observers measured once.

2.4.4.1.2 *Results.* The number of correct and false responses is given in table 2.4.4.2 for comparison with situations 5 and 6. For each condition the increment angular unsharpness, denoted by  $\Delta u$ , is given in minutes of arc. This can be regarded as the absolute increment unsharpness, as the edges 5 and 6 cannot be discerned from an ideally sharp edge. Physically, a difference in unsharpness was always present, so if no difference was reported, this response was judged as "false".

TABLE 2.4.4.2: Response in unsharpness measurements, oral radiography

combination	condition I			condition II		
	$\Delta u$ [min]	correct	false	$\Delta u$ [min]	correct	false
5-2	0.02	3	3	0.03		2
6-5	0.03		6	0.05		2
6-2	0.04	4	2	0.08	1	1
5-3	1.1	3	3	2.2	1	1
6-3	1.4	1	5	2.8	2	
5-1	1.5	5	1	3.0		2
6-1	1.8	3	3	3.6	1	1
5-4	2.4	5	1	4.8	2	
6-4	2.6	6		5.2	2	

Guessing does play a role, as can be seen from the responses to the first four combinations. Since the number of experiments is small, conclusions should be drawn with some caution. The material suggests in any case that an unsharpness increase over say 2 to 3 minutes has a good chance of being perceived. No different performance between condition I and II can be established.

#### 2.4.4.2 Threshold unsharpness-increment

The reference stimulus is a 31 mm sharp disk on the TV monitor screen. The unsharpness introduced by the TV system is perceived at viewing distances smaller than say 2000 mm. The reference stimulus is therefore itself unsharp, and the threshold unsharpness-increment can be measured for this situation. The same apparatus as for the threshold contrast measurements was used, so the influence of the noise level and the contrast can easily be investigated.

We will try to apply our model of the visual system to the phenomena with the increment threshold unsharpness as well. It will be shown that a larger increment unsharpness is allowed for a larger viewing distance. This would indeed confirm the idea that the visual system has its own unsharpness, which has a greater influence at larger distances.

**2.4.4.2.1 Method.** The experimental set-up I (fig. 2.3.2) is used with a few modifications. The reference object is a relatively sharp disk with a diameter of 31 mm; the corresponding diaphragm is situated as close as possible to the TV ground glass. The unsharper disk is imaged about 50 mm above the sharp one on the monitor screen by choosing one of a set of diaphragms situated between the two ground glasses. This distance is large enough ( $> \approx 50'$ , see sec. 2.3.4) to exclude visual

interaction between the stimuli. The size of the unsharper disks is made the same by choosing the correct size of the diaphragms, which are magnified according to the position between the ground glasses. The unsharpness values corresponding to the diaphragms are given in table 2.4.4.3 for the two viewing distances of 1600 and 3200 mm, in terms of the source diameters as seen on the monitor screen.

The objects are numbered for easy reference.

**TABLE 2.4.4.3: Unsharpnesses of disks on the monitor**

number	unsharpness [min]	
	vd = 1600 mm	vd = 3200 mm
1	11.6	5.8
2	8.6	4.3
3	7.5	3.8
4	6.2	3.1
5	4.7	2.4
6	3.2	1.6
7	2.1	1.0

In general, ten measurements were made per pair of disks. The pairs were randomly chosen by the experimenter. The observer pushed the 'yes' or 'no' button, to indicate whether a difference was perceived or not. The responses were stored on the XY-recorder. The X-scale was divided into four or five sections, in each of which the responses were accumulated by choosing a disk-pair and shifting the pen of the recorder (by hand) accordingly.

The responses are given below as a percentage of detection.

An unsharpness difference was always present, no blanks were presented. The upper disk was always the unsharper one. The observer was of course not informed of the unsharpness introduced.

**2.4.4.2.2. Results.** A few pilot experiments were done to investigate the influence of the noise of the background and the contrast of the objects. For the noise, the pairs were presented ten times at 1600 mm in a background corresponding to either 30 or 60  $\mu\text{R/s}$ , resulting in prominent noisy, and also prominently different backgrounds. The percentage of detection is given in table 2.4.4.4 for observers 'tH and vdT. No significant difference could be found.

The 50% probability of seeing corresponds to unsharpnesses between 3.2 and 4.7 minutes of arc. Comparable results were obtained for an exposure rate of 200  $\mu\text{R/s}$ , which was chosen for all the subsequent measurements. For the contrast the pairs were presented with a contrast of 2.5, 5 and 15 times the threshold contrast (which

TABLE 2.4.4.4 Percentage of detection for different noise levels

	Unsharpness [min]							
	6.2		4.7		3.2		2.1	
$\dot{X}$ [ $\mu\text{R/s}$ ]	30	60	30	60	30	60	30	60
't H	90	100	60	50	20	30	0	0
vdT	100	100	90	80	40	30	0	0

was of the order of 1%). The results are given in table 2.4.4.5, for observers vdT and 'tH. In one session, two contrast levels were presented, i.e. 2.5 and 5 times for the first, and 5 and 15 times for the second session.

TABLE 2.4.4.5: Percentage of detection for different contrasts

	Unsharpness [min]											
	6.2			4.7			3.2			2.1		
$C/C_T$	2.5	5	15	2.5	5	15	2.5	5	15	2.5	5	15
'tH	80	100		30	20		30	40		0	0	
vdT		100	100		80	80		80	0		0	0
	60	100		20	80		40	80		20	0	
		80	100		40	80		40	20		0	0

Only five measurements per pair were done, which may account for the rather large variations between the results for five times the threshold contrast in different sessions. Again the 50% probability of detection is between 3.2' and 4.7' unsharpness. In comparing the results on one row of the table – for which the smallest performance shift should be present – no difference between the 5 and 15 times threshold contrast can be reliably discerned. Large increases occur, as well as decreases of the percentage of detection. The results may indicate that the number of correct decisions is smaller for the smallest contrast. This trend was to be expected, because the difficulty of detecting the object as such will become dominant. In principle, in the near-threshold region, the unsharper object will not be seen at all. To study this effect in more detail, the pair corresponding to the 4.7' unsharpness was presented for different contrasts, starting with the threshold contrast. The yes and no responses are given in fig. 2.4.4.2.

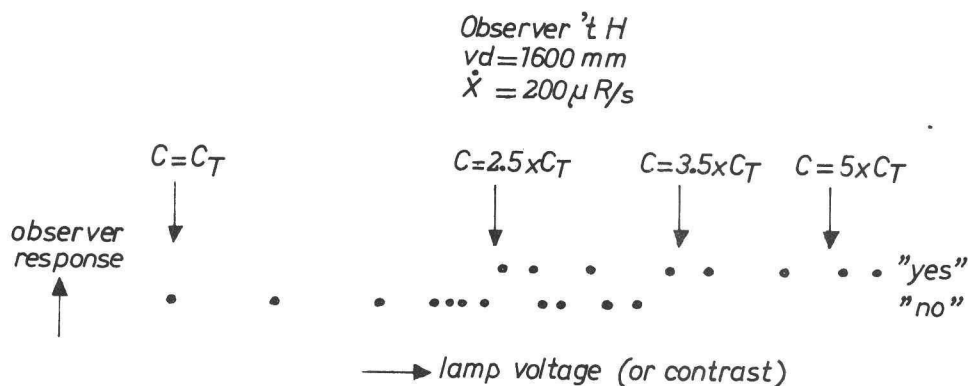


Fig. 2.4.4.2.

Visibility of 4.7' unsharpness as a function of the contrast

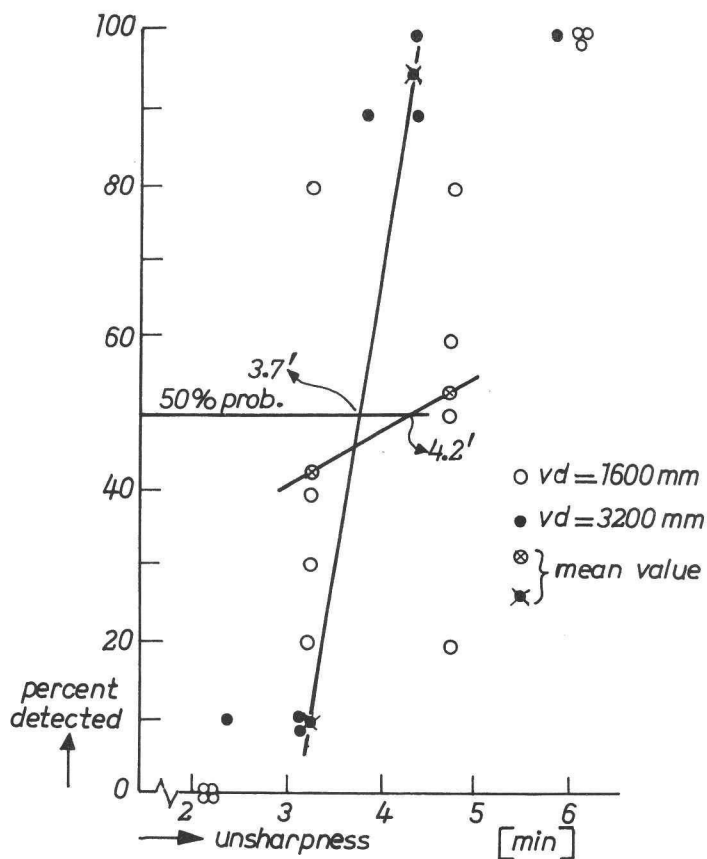


Fig. 2.4.4.3.

Percentage of detection of the unsharpness for two viewing distances; observer 'tH.

From threshold up to about 2.5 times the threshold contrast, no difference could be perceived. For contrasts over  $\approx 3.5$  times the threshold, the unsharpness difference was always perceived. As we could not find any difference between the 5 and the 15 times threshold contrast situations, we took in the subsequent experiments a contrast of 5 times the threshold. Any effect of the contrast is then small, and the imaging can still be regarded as linear.

The influence of the viewing distance was studied by using two distances, i.e. 1600 and 3200 mm. The percentages of detection for the measurements (10 per pair) are given as a function of the unsharpness in fig. 2.4.4.3 for 'tH, and in fig. 2.4.4.4 for vdT. The mean values per viewing distance were also determined. The 50% probability of detection can therefore be more reliably found by interpolation. The corresponding unsharpnesses are given in table 2.4.4.6.

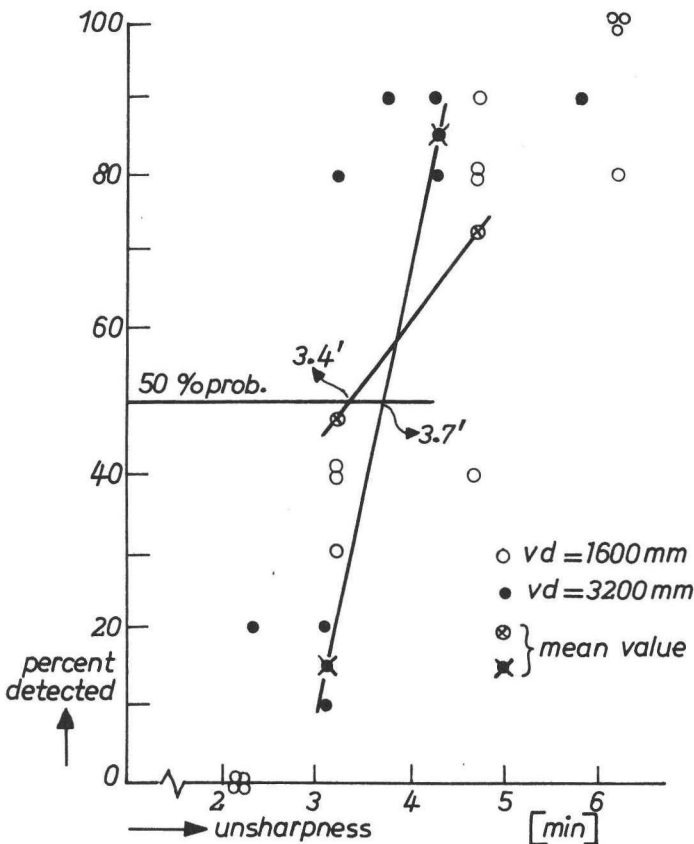


Fig. 2.4.4.4.  
Percentage of detection of the unsharpness for two viewing distances; observer vdT.

TABLE 2.4.4.6: Unsharpness for 50% detection probability

observer	unsharpness [min]	
	vd = 1600 mm	vd = 3200 mm
tH	4.2	3.7
vdT	3.4	3.7

We conclude that the angular unsharpness is of the same order of magnitude for the two distances, so that the permissible unsharpness on the screen can be larger the larger the viewing distance. Consequently it is pointless to stipulate a permissible X-ray system unsharpness without defining the viewing distance as well.

Correlation with the modulation transfer function and the maximum contrast gradient

It is interesting to correlate the measured threshold unsharpness-increment with the MTF of the TV system used, and with the MTF of the proposed model of the visual system. The subjective sensitivity for changes of the X-ray system MTF in practical conditions can be studied in this way. The TV-MTF and the one corresponding to an unsharpness with 50% detection probability are given for observer 'tH in fig. 2.4.4.5.

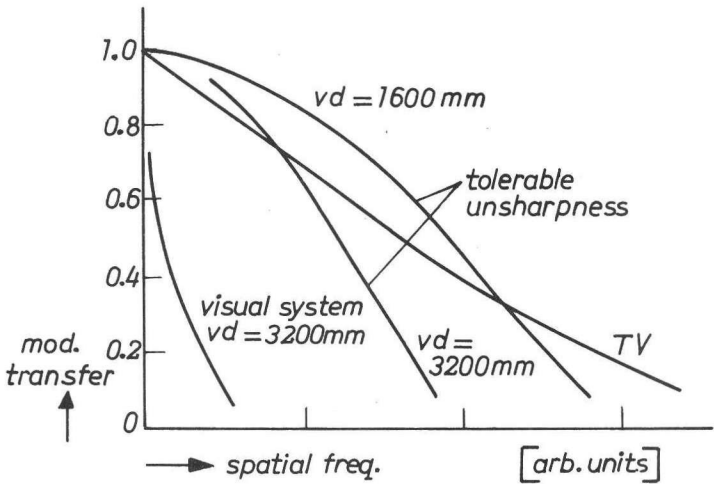


Fig. 2.4.4.5.  
Comparison of MTF qualities as to the visibility of an unsharpness increment.



Apparently, the unsharpness can be of the same order of magnitude as the TV unsharpness for the smaller viewing distance. At the greater distance of 3200 mm, the tolerable drop in MTF quality is correspondingly larger.

To predict the corresponding change in the threshold contrast, the maximum contrast gradient for the whole system must be known. For this purpose, the proposed MTF of the visual system model is also indicated in fig. 2.4.4.5. This MTF is by far the worst link in the chain, so we expect that a tolerable unsharpness will have only a small effect on the threshold visibility. To investigate this further, we calculated the maximum contrast gradients for each unsharp object. The percentage decrease relative to the maximum gradient for the sharp object was plotted as in figs. 2.4.4.3 and 2.4.4.4. It turned out that an unsharpness increment corresponding to a 3% decrease of the maximum contrast gradient is certainly detected. The decrements for 50% probability of detection are likewise obtained by interpolation. The values are given in table 2.4.4.7.

**TABLE 2.4.4.7: Decrease of maximum contrast gradient for 50% detection probability of the corresponding unsharpness increment.**

observer	percentage decrease	
	vd = 1600 mm	vd = 3200 mm
'tH	2.0	1.8
vdT	1.4	1.8

As the threshold contrast is inversely proportional to the maximum contrast gradient, we conclude that a tolerable unsharpness increment would lead to a very small increase of the threshold contrast. So the visibility of the unsharpness is indeed a more sensitive criterion for the image quality. We doubt whether this criterion can be made operational at this stage of the investigation. It is encouraging that the maximum contrast gradient decrease is virtually independent of the viewing distance, so a unifying theory is possible. This calculated independence can be found, however, for a large range of values of  $\beta$  of the visual system with correspondingly larger (smaller  $\beta$ ) or smaller (larger  $\beta$ ) values of the critical percentage decrease of the gradient.

#### 2.4.4.3 Conclusion

As a suggestion for further study it is worth verifying the validity of the statement that a tolerable unsharpness (increment) corresponds to say 2 to 4 minutes of arc. We deduced this for practical systems, and it can also be deduced from the literature. According to this criterion the unsharpness of the relatively

sharp object on the TV monitor should be perceptible for the shorter viewing distance of 1600 mm, and should lie below threshold for the larger viewing distance of 3200 mm. These predictions indeed prove to be true if the object border is compared with the perfectly sharp border of a piece of tape stuck on the screen. For the smaller distance, then, we are allowed to speak in terms of the threshold unsharpness-increment. For the larger distance, the situation resembles the absolute threshold unsharpness situation.

In any case we conclude that a tolerable unsharpness increment would lead to only a very small increase of the threshold contrast. This means that the visibility of the object as such is a less sensitive criterion than the visibility of the unsharpness of supra-threshold objects.

It should be emphasized that the foregoing remarks refer to the imaging of edges. The smallest presented object subtended 33' (viewing distance 3200 mm). The situation for smaller objects may be different.

For a discussion of these results in connection with our other investigations, see sec. 2.6.1 'Object processing'.

#### *2.4.5 Correlation with the contrast sensitivity function of the visual system*

##### **2.4.5.1 Introduction**

It is common practice in optics and electronics, for instance, to describe the response of linear and stationary systems in terms of their modulation transfer function, i.e. by their response to spatial or temporal sinusoidal signals. The response to any signal can then be conveniently calculated with the aid of Fourier theory.

Many workers have tried to extend this method to the visual system. The stimuli used for the measurement of the transfer functions fall into at least four categories:

- (i) stationary spatial gratings,
- (ii) empty fields whose luminance varies sinusoidally with time,
- (iii) moving spatial gratings, and
- (iv) spatial gratings whose modulation varies with time (e.g. sinusoidal, on/off or alternating modulation).

The threshold modulation of the grating is measured. The inverse of the threshold modulation as a function of frequency is referred to as the spatial or temporal contrast sensitivity function.

Many difficulties arise, however:

- (i) The modulation transfer cannot be measured directly, because we do not know the perceived signal. We must therefore resort to some standard (verbal) output of the observer, e.g. 'grating seen'.

- (ii) In doing so, we implicitly assume, but do not prove, that the modulation is the crucial signal.
- (iii) We further assume that the system is stationary as to its detection criterion. Adaptation, however, and changes in the confidence level take place.
- (iv) In comparing modulation thresholds at different frequencies, we assume that signals of the same kind (whatever they may be) are measured. The visual system may however adopt different strategies for different situations.
- (v) The differentiation between stationary and temporal stimuli is fictitious because eye movements occur. The image on the retina is therefore never at rest, but moves rather irregularly with respect to speed, direction and shift.
- (vi) Only for not too large modulations may the system be regarded as linear.

Despite these difficulties, one measures threshold modulation functions all the same. There are only qualitative explanations. We shall try, however, to predict the shape of the functions quantitatively. For the reasons mentioned above, we abandon the terminology 'modulation transfer function of the visual system' or 'modulation sensitivity' and the like.

We prefer to introduce the term 'spatial grating sensitivity function' (SGSF).

The shape will be quantified on the basis of our model of the visual system. Thus, instead of assuming the modulation to be the crucial signal, we assume that the gradient of the signal is decisive. This may account for the low-frequency drop in sensitivity found for both spatial and temporal gratings. Models of the visual system which are based on a Fourier handling of signals, with the SGSF as the MTF of the visual system, give wrong results in this very region (Campbell and Robson, 1968). Our model may be invalid for high frequencies because no mechanism can be conceived that measures the contrast gradient for very small spatial or temporal distances. Nevertheless this part of the SGSF is also studied in order to investigate whether an MTF concept is valid. Further, many visual tests of the quality of imaging systems are based on the visibility of such spatial frequency gratings.

As we are interested in the spatial resolution in radiographic imaging, spatial gratings will be investigated in particular. No experiments were done — only data from literature are used. Standard data do not exist, unfortunately, because the above mentioned difficulties play a role. This involves the influence of a lot of parameters and conditions, viz.

- (i) the viewing distance;
- (ii) the luminance;
- (iii) the size and shape (circular, rectangular) and the edge sharpness of the test field;
- (iv) spectral distribution of the light;
- (v) duration and the time course (e.g. fast-on/slow-off in pulsed presentation of spatial gratings) of the stimulus;

- (vi) pupil size (natural or artificial);
- (vii) use of one eye or both eyes;
- (viii) use of correcting lenses, with or without paralyzation of the accommodation;
- (ix) free roaming vs fixating eye;
- (x) the detection criteria;
- (xi) the psychometric method.

#### 2.4.5.2. Spatial contrast sensitivity.

A typical grating sensitivity function according to Campbell and Robson (1968) is given in figure 2.4.5.1. The spatial frequency in cycles per degree,  $\nu$ , is entered on the x-axis. The contrast sensitivity, being the reciprocal of the threshold modulation of the grating, is plotted along the y-axis. The system sensitivity seems to exhibit a bandpass characteristic. There is a sharp decline at the high frequency end, and a less prominent fall-off for the low frequencies. There are many qualitative explanations for this behaviour. We shall first develop our own thoughts, and relate our model to other proposals later on (see sec. 2.4.5.4).

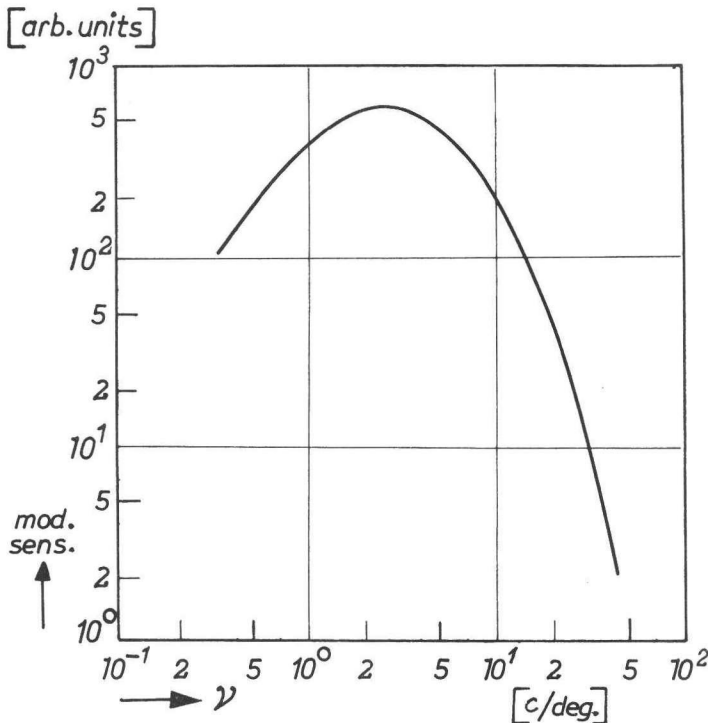


Fig. 2.4.5.1.  
Typical spatial grating sensitivity function (Campbell and Robson, 1968, fig. 2,  
500 cd/m<sup>2</sup>)

We shall compare our predictions with Campbell's measurements, as his experimental conditions are comparable with ours, i.e.

- (i) The grating can be considered stationary.

It was presented for 1000 ms, so that transient phenomena are not important. Both Tynan and Sekuler (1974) and Nachmias (1967) found the typical sensitivity functions for presentation times of 512 and 500 ms respectively. Sachs et al. (1971) stated that the change from 180 ms to 760 ms 'did not significantly affect their results'. Kulikowski (1971a) used 1000 ms and found almost no difference with the stationary presentation.

- (ii) The test field is likely to be so large that a sufficient number of periods will be present for the low spatial frequency gratings. The test field subtended  $10^\circ$ , implying reliable results for  $\nu \geq 0.4$  c/deg. Campbell claims that 'contrast thresholds are significantly raised if less than four cycles of the grating are visible'. A smaller number has the effect of a) shifting the maximum of the sensitivity function to higher frequencies, and b) reducing the lower spatial frequency sensitivity. These trends are confirmed by many authors, although there is no consensus of opinion regarding the critical number of periods. No influence was found by Hoekstra et al. (1974) for 10 periods. This number is given as 9 by Pollehn and Roehrig (1970), (for  $\nu = 1.5$  c/deg.), 7 according to Coltman and Anderson (1960), and 3 is claimed by McCan et al. (1974). On the other hand Campbell does not say what is meant by a 'considerable increase'.
- (iii) We shall check our prediction by comparing the modulation threshold for sine-wave and square-wave gratings.

Campbell reliably measured these thresholds simultaneously by presenting the different gratings alternately, thus avoiding shifts in sensitivity and confidence level, etc..

Only one eye was used, equipped with an artificial pupil of 2.5 mm diameter. Refractive errors were corrected for within 0.25 D. These measures at the eye-level may have small influence, as the subsequent retina-neural system is by far the worst part of the chain (Van Nes and Bouman, 1967; Campbell and Green, 1965; Westheimer, 1960).

We shall develop our prediction of the SGSF by assuming that basic signal processing takes place. The basic signal can be extracted, in principle, from one period of a grating. Further, we think that the visual system develops strategies to use the periodicity of the grating.

**2.4.5.2.1 Signal processing.** In our view the basic signal corresponds to the maximum gradient as measured by the visual system, i.e. to the gradients at the zero-crossings of the sine-wave. The modulation threshold is thus inversely proportional to this maximum gradient, so that we can write for the SGSF:

$$\text{SGSF}(\nu) \sim \nu e^{-\beta \nu} \quad (2.4.5.1)$$

if we assume — as confirmed earlier — that the visual system MTF can be described by  $e^{-\beta \nu}$ . This SGSF is depicted in fig. 2.4.5.2, which indeed shows the typical shape.

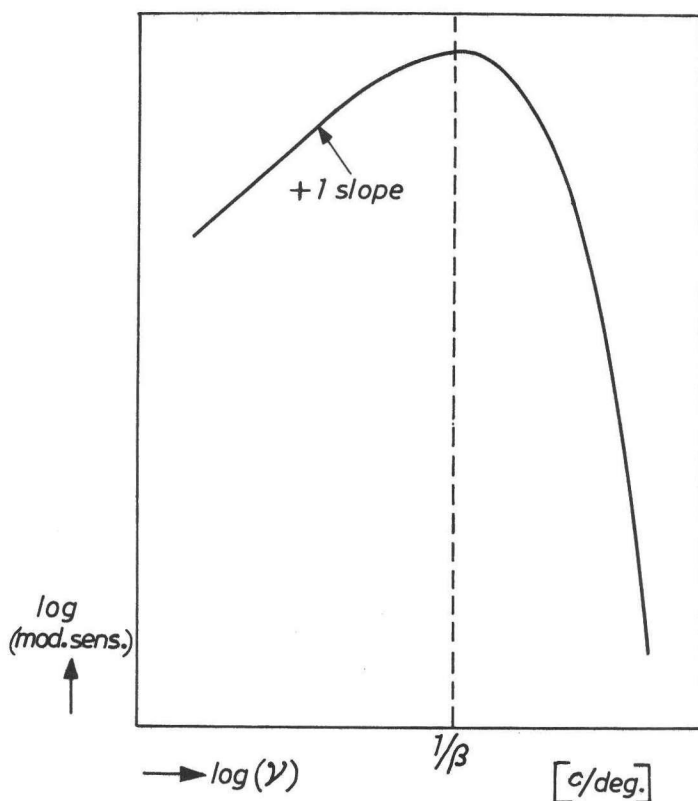


Fig. 2.4.5.2.

Predicted SGSF for  $\text{MTF}_\nu = e^{-\beta \nu}$

The maximum is situated at  $\nu = 1/\beta$ . For the low frequency region the modulation transfer approaches unity, but the gradient diminishes in proportion to  $\nu$ . We expect a slope +1 on log-log scales, which has indeed been measured by many authors (De Palma and Lowry, 1962; van Nes and Bouman, 1967; Campbell and Robson, 1968; Kulikowski and Tolhurst, 1973; Breitmeyer and Julesz, 1975). There is a rapid high-frequency fall-off.

A comparison of our prediction with measurements from Campbell and Robson (1968, fig. 4) is illustrated by fig. 2.4.5.3, for a luminance of  $500 \text{ cd/m}^2$  and  $0.05 \text{ cd/m}^2$ . Considering the very simple model used, the predicted curves fit well.

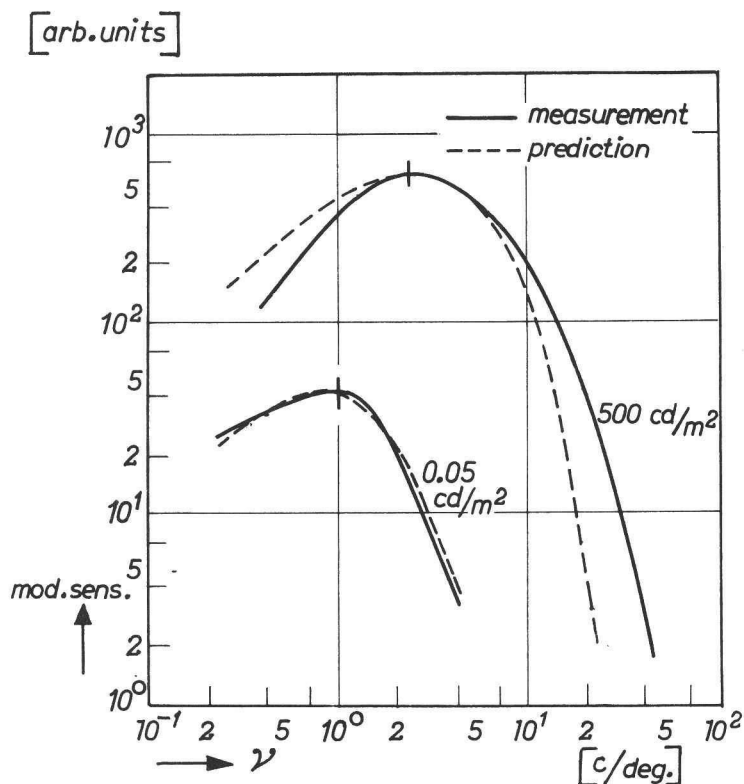


Fig. 2.4.5.3.

*Predicted and measured (Campbell and Robson, 1968, fig. 4) SGSF.*

This may also hold quantitatively. For the high luminance we expect  $\beta$  to be about  $0.5^\circ$ , and the low luminance  $\beta$  is about equal to one degree (fig. 2.2.10). The maxima of the curves are indeed situated at  $\nu \approx 2$  and  $\nu \approx 1$  c/deg. This correspondence should be treated with reserve. For the model to fit well, the  $\beta$  values for bars should be used. These values are smaller than those for disks. Further, large ranges of peak-sensitivity spatial frequencies (2 – 7 c/deg.) are found in the literature, so individual differences and experimental conditions may play a role. In any case, we can conclude again that a large step in adaptation luminance (4 decades) leads to a small shift in spatial processing (see fig. 2.2.10).

Significant deviations occur in the low and the high frequency regions. For the low frequency region the predicted sensitivity is too high, whereas the reverse is true for the high frequency region. These deviations are found by many authors. (There are exceptions, however. For example Pollehn and Roehrig (1970) found the predicted steep high frequency fall-off, but the reason must be of instrumental origin, as the modulation transfer of the TV system is insufficient.)

We think that these deviations can be partially explained by assuming a spatial-frequency dependent strategy of the visual system for extracting the information from basic signals. Again, one should be careful in applying such corrections. The measurements of Shapley (1974) are perfectly described with the SGSF according to eq. 2.4.5.1.

If our concept is true, then a satisfactory fit at the high frequency region can also be obtained by using another visual system MTF. Only the transfer for the high frequencies need be altered. Hence the imaging of isolated objects is not altered to a large extent, as then the *weighted* sum of the object spatial frequencies comes into play. The effect of different MTFs on the SGSF is shown in fig. 2.4.5.4. The MTF has a slower fall-off for  $\nu \geq 3/\beta$ , owing to the coefficient  $h$  being smaller than unity:

$$\text{MTF}_V(\nu) = e^{(3h-3)} \cdot e^{-\beta h \nu}, \nu \geq 3/\beta \quad (2.4.5.2)$$

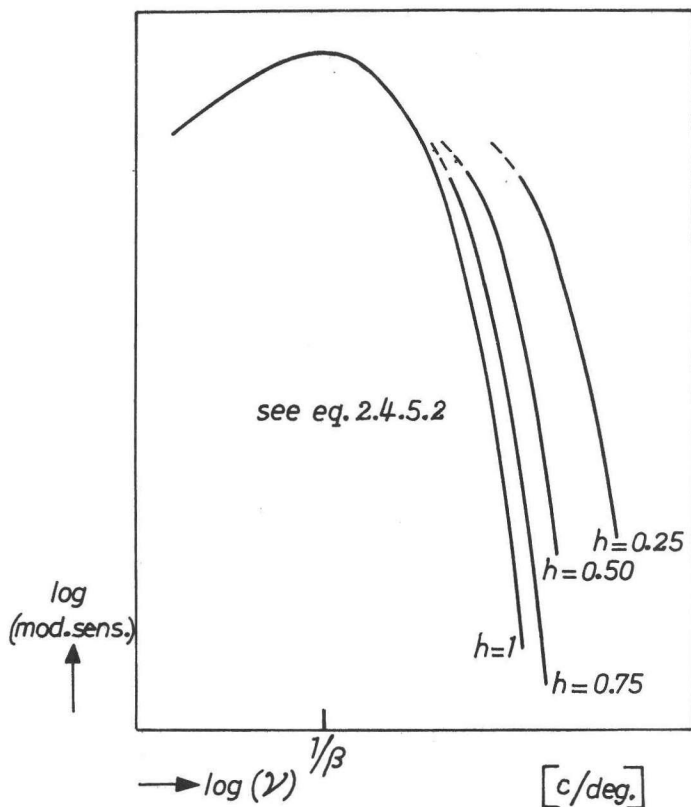


Fig. 2.4.5.4

Effect of a change of the high frequency end of the visual system MTF on the predicted SGSF.



The shift from  $h = 1$  to for instance  $h = 0.5$  has a marked effect on the SGSF, but the effect on the imaging of an isolated detail is indeed small. If the width of a bar is of the order of the line spread function width, then the change in  $h$  mentioned above leads to an increase in the maximum contrast gradient of about 5%. Our experiments on bars and disks are therefore primarily suited for investigating the low spatial frequency response of the visual system. The measurements on gratings are very sensitive to the individual high frequency response.

**2.4.5.2.2 Visual system strategy.** A fundamentally different solution for the discrepancies may be found in our proposed strategy of the visual system to make use of the periodicity of the signal. Since a number of periods are available, probability summation may take place. On the other hand, the sensitive aperture of the visual system may vary with the spatial frequency.

**Probability summation.**

This is suggested for instance by Nachmias (1968) to explain the threshold contrast difference for sine-wave and two-bars stimuli, and by van Meeteren and Vos (1972). Suppose that the visual system is capable of summing up the signals present in a certain spatial field. If pure summation were carried out then a higher frequency would correspond to more periods, thus for SGSF ( $\nu$ ) we should write:

$$\text{GSF}(\nu) = \nu^2 \cdot e^{-\beta \nu} \quad (2.4.5.3)$$

However, we expect the system to be noise-limited, so a higher frequency leads to smaller sampling areas and correspondingly smaller signal-to-noise ratios per measuring point. Another reason for the exponent in eq. 2.4.5.3 to be smaller than 2 is the impossibility of pure summation. It is remarkable that Kelly (1977) applies a theoretical contrast sensitivity function of exactly the same shape, though on different grounds.

The predicted ideal SGSF is given in fig. 2.4.5.5. The peak sensitivity shifts to  $\nu = 2/\beta$ . The gradient for the low-spatial frequency region is +2 on log-log scales. In certain situations there is good agreement between prediction and measurement (see the result of Breitmeyer and Julesz (1975), also depicted in figure 2.4.5.5). Generally, however, only a limited part of the curve, if any, shows a +2 slope. We shall discuss this in detail in the next section.

**Sensitive aperture of the visual system.**

From the literature we arrive at the idea that the visual system strategy varies with the spatial frequency under consideration. Kulikowski and Tolhurst (1973) state that extra eye movements are necessary for the perception of low spatial frequency gratings. De Palma and Lowry (1962) suggest that 'the judgement of the very coarse pattern is influenced by spatial contour', while Hoekstra et al. (1974) suggest that

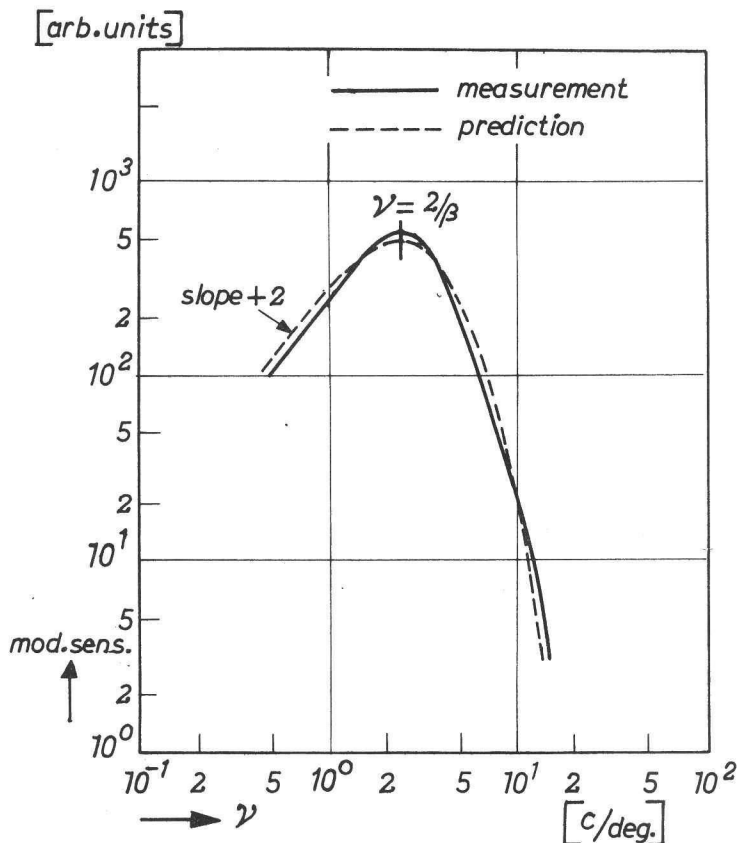


Fig. 2.4.5.5.

*Predicted SGSF if summation of signals occurs. Measured results from Breitmeyer and Julesz (1975), fig. 2.*

‘for some frequency, which is lower than 0.5 c/deg., the maximal luminance gradient is going to be the limiting factor . . .’. Thus for low frequency gratings no probability summation takes place, but one single period is analysed.

For higher frequencies the concept of an invariant sensitive field size may also be invalid. Campbell and Green (1965) state that ‘at higher frequencies (i.e. higher than 35 – 40 c/deg) the perception of the pattern is confined more and more to the central region of the fovea’. This may be due to the fact that the visual acuity decreases with greater excentricity of the image. Thus the higher the frequency, the smaller the section of the retina involved.

**2.4.5.2.3. Conclusion.** We tentatively conclude that the perception of gratings of not too high a frequency ( $\nu < 10$  c/deg.) is performed by deriving basic signals, i.e.

maximum spatial contrast gradients, and by applying strategies to make use of the periodicity (if any) of the signal. At low frequencies, contour detection is carried out. At higher frequencies an (imperfect) summation of basic signals takes place. At first an invariant field size is used, at higher frequencies the sensitive aperture of the visual system shrinks.

For the lower spatial frequencies this statement is confirmed by some papers. The expected gradual transition from a slope +1 to a slope +2 indeed takes place (Kulikowski and Tolhurst, 1973 — see also fig. 2.4.5.6; Patel, 1966; Breitmeyer and Julesz, 1975).

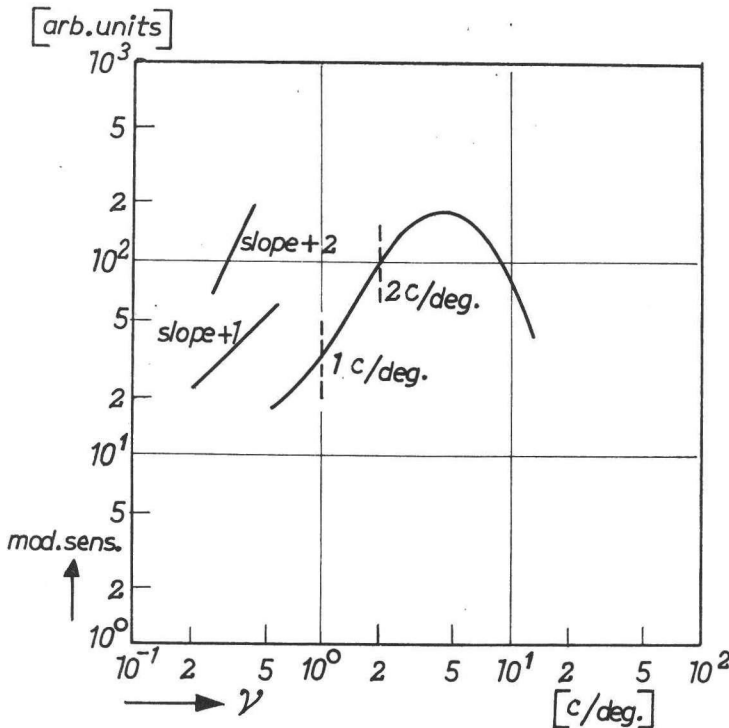


Fig. 2.4.5.6.  
Typical slopes of the SGSF, according to Kulikowski and Tolhurst (1973), fig. 3.

The systematic deviations between the predictions and the measurements, like those of Campbell and Robson (1968) — see fig. 2.4.5.3 — may also be ascribed to probability summation. The curves have been fitted at the peak sensitivity frequency, with the corresponding number of periods used. For lower frequencies, fewer periods are available to the visual system, so the predicted sensitivity is too high. It is tempting to state that the reverse is equally true for the high frequency end,

which would then explain the too small predicted sensitivity. There are too many uncertainties, however, about the MTF, the strategy and the sensitive aperture of the visual system in this region.

Support for our ideas can also be found in their application (see next section) and in the sensitivity of the visual system to temporal signals. Temporal and spatial contrast gradients are equivalent in our view. This implies that the flicker sensitivity function (FSF) should show the same shape as the SGSF. This has indeed been pointed out by many authors, for instance by Robson (1966). A typical FSF is given in fig. 2.4.5.7. It is borrowed from Kelly (1961) who applied a large structureless circular field ( $60^\circ$  diameter). Spatial effects are absent, as the signal in the retina is then shift-invariant, so that the effects of pure temporal variations can be studied. The shape of the FSF indeed corresponds to that of the SGSF.

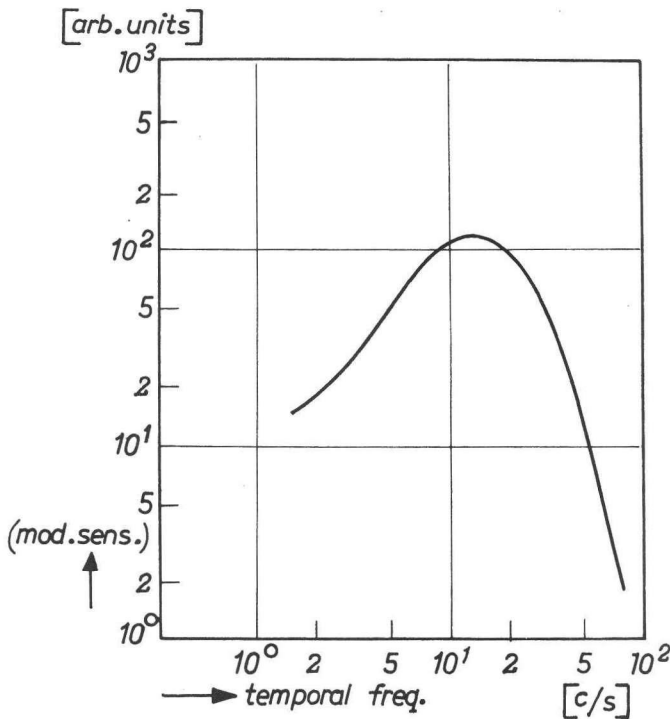


Fig. 2.4.5.7.  
FSF measured by Kelly (1961), fig. 4.

Further, good correlation could be found with the work of Shapley (1974; see sec. 2.4.3.2) for the sensitivity to spatial gratings and to isolated bars.

### 2.4.5.3 Application

2.4.5.3.1. *Sine-wave and square-wave sensitivity.* We will use the results of Campbell and Robson (1968) because they reliably measured the relative sensitivities by presenting the different gratings alternately. The results are depicted in fig. 2.4.5.8.

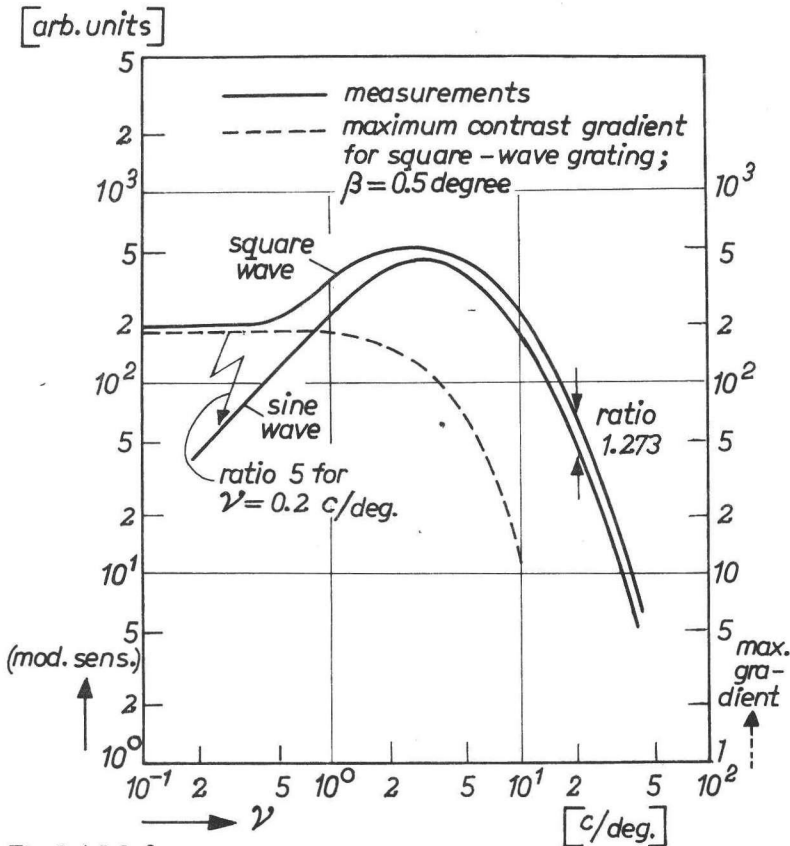


Fig. 2.4.5.8.

Square-wave and sine-wave SGSF.

Measurements from Campbell and Robson (1968), fig. 4.

Low spatial frequencies.

The sensitivity for the square-wave does not depend on the frequency. In our view this is due to the invariance of the spatial luminance gradient in this region. This gradient has been calculated for  $\beta = 0.5$  degree, the one which corresponds to the SGSF for sine-waves, and is also given in the figure. As the sensitivity grows for  $\nu > 0.4$  c/degree, probability summation apparently sets in beyond this frequency.

The predicted sensitivity ratio at  $\nu = 0.2$  c/degree is 7.2 while a ratio of 5 has been measured. Taking into account the different experimental conditions and the limited number of observers, we may state that this is a relatively small discrepancy. The following points may further account for the discrepancy:

- (i) non-linearity of the visual system: the ratio between the gradients is large.
- (ii) blurredness of the square-wave due to instrumental imperfections. Campbell states that '... (with) frequencies of more than 10 c/cm on the screen it was noted that there was a significant decrease in contrast due to limitations of the cathode ray tube'. If the 'significant decrease' is 50%, then the predicted ratio changes from 7.2 to 6.5.
- (iii) the uncertainty in the value of  $\beta$ , as deduced from the SGSF (see the discussion in sec. 2.4.5.2).

High spatial frequencies.

The maximum gradient ratio is indeed 1.273, according to the larger fundamental-frequency amplitude of the square-wave.

In this region, a prediction on the basis of the maximum modulation (as Campbell makes) is equally good, but completely fails to predict the low frequency character. In fact, many models would do at high frequencies, but the critical region is the low frequency end. A parallel can be drawn with the prediction of C- $\Delta$  curves. Many models are possible for small objects, but the critical region is situated at larger objects.

2.4.5.3.2. *Moving gratings.* Tolhurst (1973) applied drifting spatial gratings. For a drift of 5 c/s he found an increase in the sensitivity for frequencies less than 7 c/degree. We ascribe this to the increased temporal or effective spatial gradient.

If  $v_v$  denotes the mean eye velocity, and  $v_d$  is the drift velocity (units deg/s and c/s), then we may write for the predicted sensitivity ratio for stationary and drifting gratings:

$$\text{sensitivity ratio} = 1 + \frac{v_d}{\nu \cdot v_v} \quad (2.4.5.4)$$

This ratio is given in fig. 2.4.5.9 as a function of  $\nu$  together with a few measured results, for  $v_v$  equal to 2.5, 3.0 and 3.5 deg/s. The curve for  $v_v = 3.0$  deg/s fits reasonably well, except at the lowest spatial frequency. We can now also imagine why the drift (but also the mode of presentation, on-off or alternating, see Kuliowski (1971a)) has no influence for high frequency gratings: the temporal gradients evoked by the visual system dominate.

The proposed velocities for the eye movements are not uncommon for micro-saccades (see Zuber and Stark, 1965; Yarbush, 1967; we assume an amplitude of 2 to 10 minutes of arc).

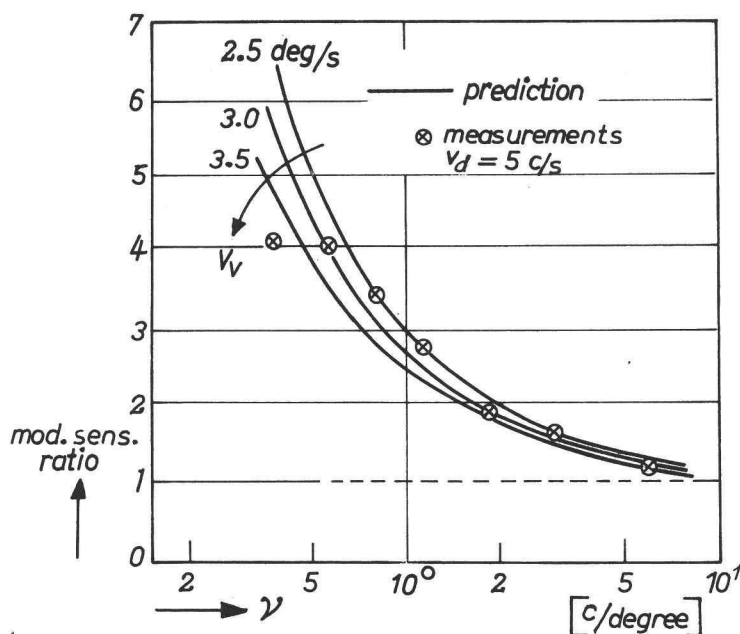


Fig. 2.4.5.9.

Modulation sensitivity ratio for moving and stationary gratings. Measurements from Tolhurst (1973), fig. 1.

2.4.5.3.3. *Adaptation effects.* Blakemore and Campbell (1969) presented a supra-threshold grating prior to the threshold measurement. They found adaptation effects, as they called them:

- (i) a temporary rise in contrast threshold sets in, limited to a band of frequencies centered at the relatively high adaptation frequency.
- (ii) for lower adaptation frequencies, the peak of the effect stays at 3 c/deg.
- (iii) for medium frequencies the bandwidth of the effect is just over an octave at half amplitude. For higher frequencies ( $> 20$  c/deg) the bandwidth is narrower.

Unlike these authors, who introduced 'channels' specifically sensitive to a narrow band of frequencies, we may assign the first two effects to two adaptation phenomena: signal, but also strategy adaptation takes place.

Strategy adaptation:

If the grating is clearly visible, probability summation is not needed. Hence the sensitive field size is reduced, and the attention is focused on, say, one period. As a consequence, the threshold contrast is elevated.

For low-spatial frequency gratings we deduced the strategy that one single period is analysed. Hence adaptation to such gratings has only effects for gratings where otherwise probability summation would play a role. As a consequence the adaptation effect is situated at a higher frequency.

#### 2.4.5.4 Conclusion, discussion

We propose that a grating sensitivity function cannot be regarded as being the *modulation transfer function of the visual system*. In doing so, we would (i) omit the effect of different strategies for such repetitive stimuli, (ii) implicitly state that the modulation is the crucial signal, whereas we think that the maximum contrast gradient is decisive, and (iii) lack some statement as to the phase transfer function of the visual system. Campbell and Robson (1968) nevertheless applied the sensitivity functions for the threshold prediction of different gratings. Their prediction is only correct for high spatial frequencies ( $\nu > 10$  c/deg). In this region the maximum contrast gradient and modulation criterion are equivalent, however, and the visual system strategy presumably does not change rapidly. The illegitimate use of the SGSF as the MTF of the visual system may be the basis for such remarks as made by van Meeteren (1973, page 25) that 'It is not clear how to extend this relation (= visibility of isolated objects) to sine wave gratings'. We were nevertheless able to find for our proposed MTF of the visual system a good correspondence between the SGSF and the C- $\Delta$  curve for bars (Shapley, 1974; see sec. 2.4.3.2).

As to the *models of the visual system*, we consequently abandon the one of Campbell and Robson (1968) who argue that 'the envelope of the contrast sensitivity functions of all the channels would be the contrast-sensitivity function of the visual system'. A 'channel' selects specific information from the stimulus. In this case the channel is sensitive to a narrow band of spatial frequencies.

It is a modern trend to introduce 'channels' for all kinds of psychophysical phenomena (size, orientation, shape, movement, flicker etc.). This trend is stimulated by physiological research, showing that many kinds of specific channels exist in the visual system. But neither a quantitative nor a qualitative explanation of the experimental findings is given by the introduction of channels. In this context, 'transient' and 'sustained' channels are worth mentioning. They are introduced to describe the threshold perception of *flickering spatial gratings*.

Three thresholds should be discerned, as Kulikowski and Tolhurst (1973) pointed out: for flicker detection, for pattern recognition and for the detection of the stimulus. The corresponding sensitivities (fig. 2.4.5.10) behave differently as a function of the spatial frequency. Thus Kulikowski introduced the 'transient channel' for the perception of flicker, and the 'sustained channel' for the perception of the grating. Many authors relate these channels to the Y- and X receptive fields of retinal ganglion cells, as found by Enroth-Cugell and Robson (1966). We think that the distinction between stationary and temporally modulated gratings is



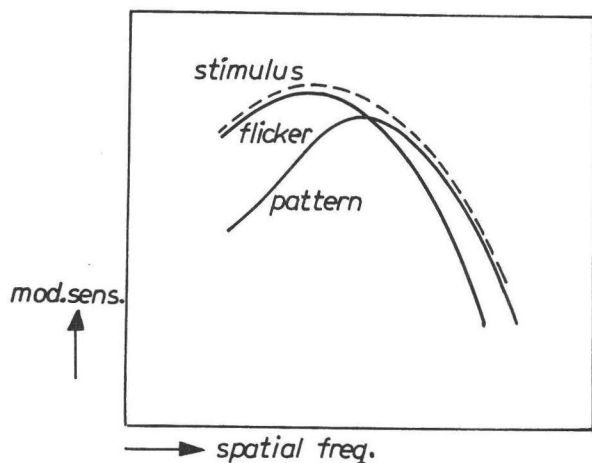


Fig. 2.4.5.10

*Typical sensitivity functions for a temporally modulated spatial grating (Kulikowski and Tolhurst, 1973).*

fictitious. Eye movements play a role, as Kulikowski (1971b) and Kelly (1977) showed, and both cells respond (non-linearly) to temporal variations. We suggest that again the temporal gradient is decisive. Our clue is the perceptual phenomena mentioned (Kulikowski and Tolhurst, 1973):

- *low spatial frequencies*: the pattern recognition sensitivity is smaller than the flicker sensitivity. This is caused by the enhanced temporal gradient if the grating is modulated in time. In the latter situation, eye movements no longer primarily mediate the generation of temporal gradients.  
As a consequence the spatial information is lost and no grating is perceived.
- *high spatial frequencies*: the lateral shift of the finely structured retinal image evokes large temporal gradients. Hence the additional temporal modulation has only a small effect and the grating is seen, whereas the flicker is not perceived.

The same argumentation can be applied to the perceptual phenomena for moving gratings, as reported by Tolhurst (1973).

Many authors (e.g. De Palma and Lowry, 1962; Levinson, 1964; Robson, 1966) ascribe the *drop in sensitivity for low spatial frequency* gratings to the typical structure of simple receptive fields: an excitatory central part surrounded by an inhibitory region. Coarser patterns stimulate both regions and a lower sensitivity results. This reasoning contradicts itself since receptive fields have different sizes (see e.g. Hubel and Wiesel, (1962), for cortical fields) which can be tuned to low spatial frequencies as well. A different time course of the response of the inhibitory

region and its counterpart has been assumed to explain a number of phenomena (Levinson, 1964; Tynan and Sekuler, 1974; Breitmeyer and Julesz, 1975). Kulikowski and Tolhurst (1973) showed, however, that temporal modulation (3.5 c/s) does *not* affect the shape of the pattern recognition sensitivity function. According to Hoekstra et al. (1974) the low frequency sensitivity drop is caused by the shrinking number of periods in the image. But van Meeteren and Vos (1972) used a very large field ( $17^\circ \times 11^\circ$ ) and they also report the drop in sensitivity.

As to the *use of gratings for a subjective test* on the quality of for instance X-ray systems, one generally measures the frequency corresponding to the just visible grating, for a given modulation. We refer to this frequency as the threshold frequency. The following remarks can be made:

- (i) since a fairly large portion of the image should be used, the anisotropy of the imaging may interfere.
- (ii) since the method yields only one point of the MTF of the system, the correlation with practical objects, i.e. isolated objects instead of a grating, cannot be made.
- (iii) We define the sensitivity of the method as the relative variation of the threshold frequency divided by the relative variation of the modulation of the grating. This sensitivity is governed by the inverse of the gradient of the SGSF curve. As this gradient is very small at the peak of the curve, an almost impractical range of the threshold frequency can be found for a low-modulation grating (Rosenbruch, 1959). The peaked shape of the SGSF curve may further imply ambiguous results, as both a low and a high threshold frequency can be found per modulation.

## 2.5 Noise effects

The problems to be solved in conceiving a model of the visual system for its noise processing are discussed in sec. 2.2.2. It is unlikely that one model will apply to both static and dynamic noise, so both situations will be studied separately (sec. 2.5.1 and 2.5.2). The measurements on dynamic noise to determine its masking effect on the visibility of bars and disks refer to the influence of the noise source intensity (sec. 2.5.1.1), the influence of the gamma of the TV system (sec. 2.5.1.2), and the relation with the unsharpness of the noise (sec. 2.5.1.3). The value of these parameters could not be varied for static noise. The effect of the viewing distance is studied for both noises in sections 2.5.1.4 and 2.5.2.2.

### 2.5.1 Dynamic noise

The noise consists of more or less random flashes of light on the monitor screen. The flashes are spatially correlated by the unsharpness of the imaging system. In addition, temporal integration takes place by the TV system, whose integration

time is about 20 ms (a Plubicon camera is used). A physical description of such noise cannot easily be given. The influence of a few parameters, however, can be described without much difficulty. To this end, the speck density and the speck intensity are introduced. (These terms are borrowed from van Meeteren, 1973). A 'speck' is not so simple to define; perhaps the best description is 'a countable event'. We can state, however, that the speck density, i.e. the number of events per unit of space and time, is directly proportional to the X-ray exposure rate at the image intensifier input screen. If we think in units of angular space, then the speck density is proportional to the square of the viewing distance. The speck intensity is defined in terms of the number of photons per speck entering the observer's eye. The intensity is proportional to the amplification factor of the image intensifier/TV system. The speck intensity in terms of the energy impinging on the observer's pupil is inversely proportional to the viewing distance squared.

The influence of the gamma, i.e. of the small signal amplification of the TV system, can be described for our systems, because the speck density is generally so high that a continuous background is perceived with fluctuations on it. The amplitude of the fluctuating component — however it is described — is proportional to the gamma.

#### 2.5.1.1 Influence of the noise intensity.

The threshold contrast of disks and bars will be measured as a function of the X-ray exposure rate, for a given X-ray beam quality. It is generally stated (e.g. Coltman, 1954; Kühl, 1965; van Meeteren, 1973) that the threshold contrast is inversely proportional to the square root of the speck density, i.e. to the square root of the X-ray exposure rate. A prerequisite is that the other noise sources (including the internal noise of the visual system) are of secondary importance. We will check the dominance of the X-ray noise by measuring the influence of the noise source intensity on the threshold contrast of objects.

#### Method.

Measuring set-up I (fig. 2.3.2) was used. The threshold contrast of an object was measured for two different noisy backgrounds by presenting the backgrounds alternately. Two exposure rates were chosen by using two apertures of the optical diaphragm in front of the TV camera (fig. 2.5.1.1). Automatic control of the TV chain ensures (i) that the signal current of the camera remains the same by adjusting the X-ray tube current and (ii) that the monitor luminance does not change during the experiments.

The electrical noise in the image can be neglected because the signal current is large ( $\approx 175$  nA; see Franken et al., 1973c).

The threshold contrast ratios were measured for a series of exposure rates so as to

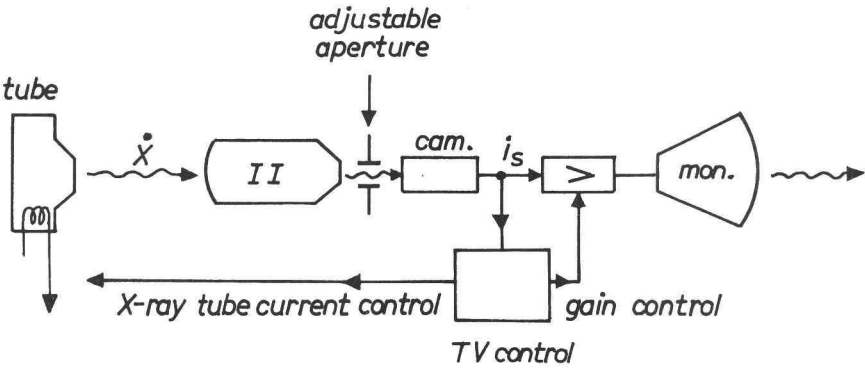


Fig. 2.5.1.1.  
Set-up for X-ray exposure-rate variation.

scan the range between  $\approx 30$  and  $500 \mu\text{R/s}$ . Practical exposure rates range from 30 to  $120 \mu\text{R/s}$ . The larger the exposure rate, the finer is the structure of the noise. Three observers made one measurement each ('tH, vdL, vdT').

Results for disks.

The threshold contrast of a 4' disk at a viewing distance of 3200 mm is given in figure 2.5.1.2 as a function of the exposure rate (at 60 kV tube voltage). As can be seen,  $C_T$  is indeed inversely proportional to the square root of the exposure rate

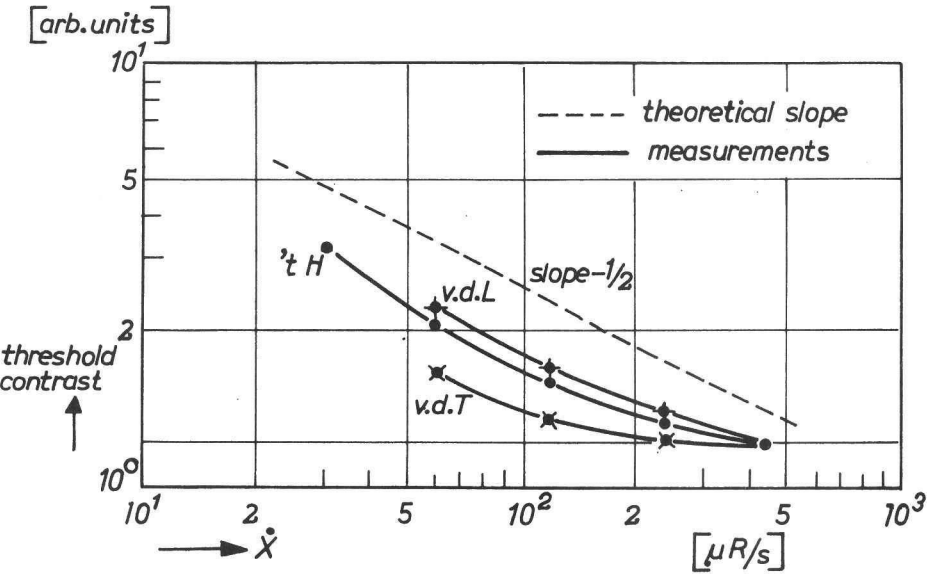


Fig. 2.5.1.2.  
Threshold contrast of 4' disk as a function of the X-ray exposure rate; viewing distance 3200 mm.

if  $\dot{X} < \approx 120 \mu\text{R/s}$ . For higher exposure rates other noise sources tend to dominate. The difference between the observers results from the normalization of the threshold contrast with respect to the value for the highest rate ( $480 \mu\text{R/s}$ ). Comparable results were obtained with a  $1^\circ$  disk at the same viewing distance, for  $\dot{X}$  equal to 30 and  $60 \mu\text{R/s}$  (three observers). 'tH obtained analogous contrast ratios at a shorter viewing distance (400 mm) for a  $32'$  disk,  $\dot{X}$  30 –  $120 \mu\text{R/s}$ .

Results for bars.

An  $8'$  bar was observed at a distance of 1600 mm. The relative threshold contrasts are given in figure 2.5.1.3 for  $\dot{X}$  ranging from 40 to  $400 \mu\text{R/s}$ . The same trend as for disks is shown. The dependence on  $\dot{X}$  brakes down at larger exposure rates, as the noise is more prominent at this shorter viewing distance.

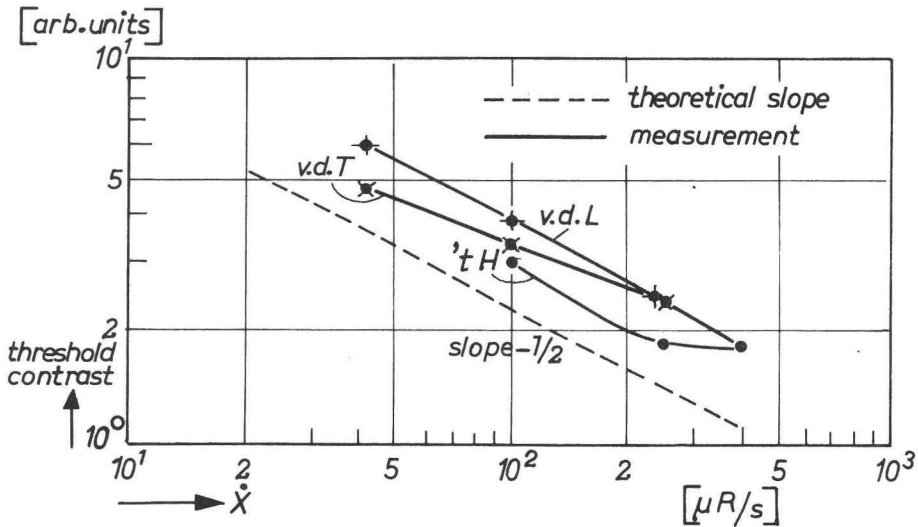


Fig. 2.5.1.3.

Threshold contrast of  $8'$  bar as a function of the X-ray exposure rate; viewing distance 1600 mm.

Conclusion.

We conclude that the X-ray noise dominates at practical exposure rates. The invariance of our model of the visual system to the kind of background (40 or  $160 \mu\text{R/s}$  background, or a structureless background) is therefore not the result of the noise being negligible.

Further, the threshold contrast is found to be inversely proportional to the square root of the speck-density, i.e. to the number of events. Apparently the speck intensity has no effect, although the constancy of the monitor luminance implies that the intensity is inversely proportional to the speck density.

### 2.5.1.2 Influence of the gamma

The gamma of an imaging system describes its non-linearity; the gamma can be seen as the small-signal amplification factor.

We made no measurements on the gamma, but the results of Franken et al. (1973d) and of van Meeteren (1973) will be analysed. Franken used the same equipment as we did, so his results can be used. Van Meeteren investigated the visibility of gratings in dynamic noise, as a function of the speck density and the speck intensity. The variation of the speck intensity for the same density is comparable with the variation of the gamma. There is one fundamental difference between the experiments, however. With the TV system, measures were taken to keep the monitor luminance at the same level. In van Meeteren's experiment, the luminance of the screen is directly proportional to the speck intensity and the speck density.

**2.5.1.2.1 Franken's measurements.** The psychometry is discussed in sec. 2.4.2.1. The monitor luminance is  $22.5 \text{ cd/m}^2$ , which is comparable with our situation ( $\approx 20 \text{ cd/m}^2$ ). The viewing distance is 2100 mm. The gamma is defined as:

$$\gamma_x = \frac{d(\log L_{\text{mon}})}{d(\log \dot{X})} \quad (2.5.1)$$

$L_{\text{mon}}$  denotes the image receptor output (i.e. the monitor screen) luminance. The gamma was measured by plotting  $L_{\text{mon}}$  and  $\dot{X}$  on log-log scales, and measuring the slope of these curves. The gamma depends intricately on the video amplification (contrast control), the video bias (brightness control), the cut-off voltage of the monitor tube and the ambient luminance. It is nevertheless possible to choose appropriate contrast and brightness settings of the monitor so as to secure a constant monitor luminance for different gammas, at a given X-ray exposure rate.

The gamma influences both the object contrast and the noise. At the low contrast involved, the object contrast is directly proportional to the gamma. The same may be said of the masking effect of the noise. The noise is perceived as small deviations from the mean luminance level; the amplitude of this deviation is equally amplified by the gamma. Therefore the influence of the gamma on the threshold contrast at the input of the image intensifier should be absent. The measured results only partially satisfy this requirement. Typical results are given in fig. 2.5.1.4, for exposure rates of 6.25, 12.5, 25, 100 and 200  $\mu\text{R/s}$ . The gamma is set out horizontally, the inverse of the input contrast of a 30' disk is entered on the vertical axis. Only for relatively large values of the gamma does it hold good that the input threshold contrast does not change. For small gamma values the threshold input contrast turns out to be inversely proportional to the gamma.

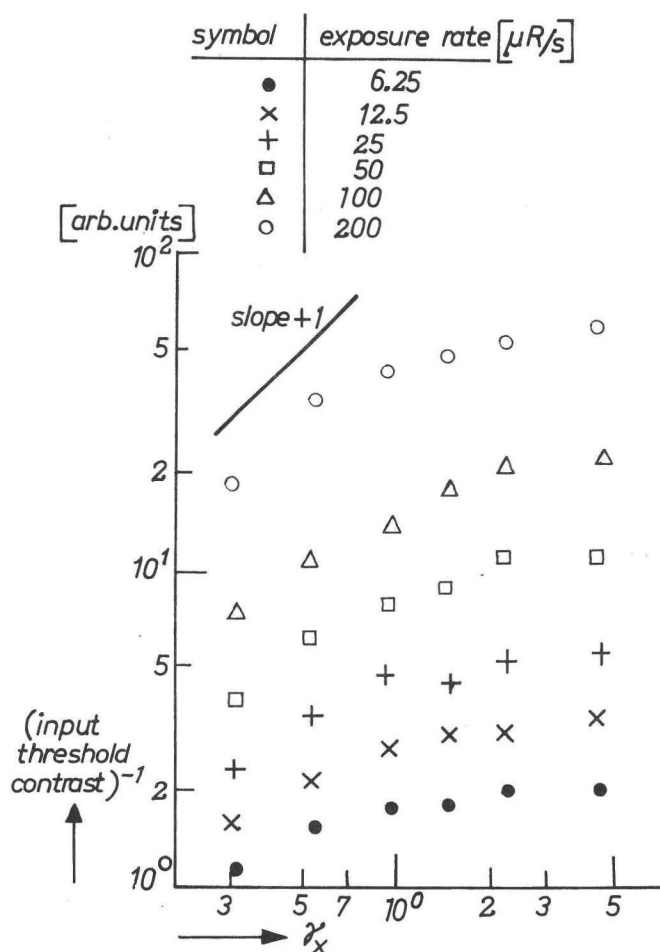


Fig. 2.5.1.4.

Input threshold contrast as a function of the gamma  $\gamma_x$  of the TV system, 30' disk (Franken et al., 1973d).

We explain these findings as follows. The noise is less prominent the smaller the value of the gamma. For small values of gamma, then, no external noise sources are effective, only the photon noise and the internal noise of the visual system mask the disks. Consequently the influence of the gamma on the noise is absent, and the output threshold contrast is invariant with the gamma. It is very relevant in this respect that the noise itself is reported to be visible only at gamma values larger than about 0.5. At large gamma values the gamma does in fact influence the noise and the contrast equally.

In terms of speck density and speck intensity, we may state that the masking effect of the clearly visible noise as a function of the gamma is governed by the speck intensity, as the speck density is constant for a given exposure rate. The statistical variation of the speck intensity is proportional to the value of gamma. At low gammas, this variation is below other fluctuations. As the relative statistical variation is also inversely proportional to the square root of the exposure rate, we expect the invariability of the input threshold contrast to set in at smaller gammas when the exposure rate is lower. This trend can indeed be perceived in fig. 2.5.1.4. This is more clearly seen in fig. 2.5.1.5, where the results are set out as a function of the value of  $\gamma_x/\sqrt{\dot{X}}$ . An additional vertical shift is applied to the data of fig. 2.5.1.4.

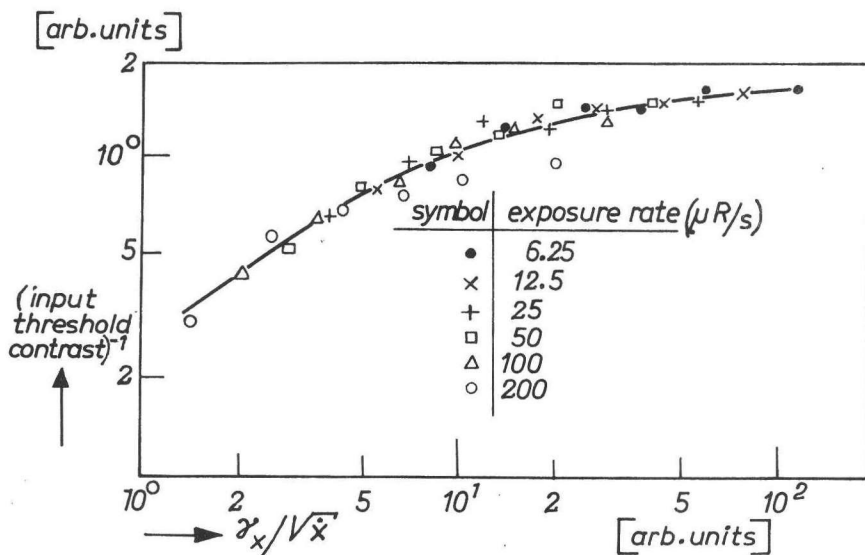


Fig. 2.5.1.5.

Predicted (this work) threshold contrast as a function of the masking effect of the X-ray noise, 30' disk.

Only the results for  $\dot{X} = 200 \mu R/s$  are not lying on the mother curve. This may be due to the fact that the electrical noise is not negligible in this situation. The measurements on the influence of the exposure rate (sec. 2.5.1.1) point to this fact, i.e. the noise corresponding to an X-ray exposure rate of  $200 \mu R/s$  is already comparable with other noise sources.

Apparently, the relative statistical variation of the speck intensity is one of the aspects which governs the masking effect of dominant external noise. This conclusion will be compared with the one of van Meeteren in the next section.



Comparable results were obtained by Franken for 15' and 6' disks, so the conclusions given above are valid for the practical range of disk diameters.

**2.5.1.2.2 Van Meeteren's measurements (1973).** The threshold modulation of a sine wave grating of 4.5 periods per degree, subtending  $3^\circ \times 3^\circ$ , was measured as a function of the speck intensity for a given speck density. The field was foveally fixated. Although his experimental conditions differ substantially from ours (one eye with artificial pupil used, grating instead of isolated object, detection of the orientation of the grating), the *relative* influence of one parameter like the speck intensity can nevertheless be studied.

Typical results are given in fig. 2.5.1.6 for a speck density of 18.2, 2.2 and 0.18 specks per sec per min.<sup>2</sup> of arc. For the explanation of these curves, van Meeteren attaches great value to the visibility of the specks, whereas we think in terms of the statistical variation of the speck intensity. In the former view, the increasing contrast sensitivity with increasing speck intensity is explained by an increase of the detection probability of specks. At higher intensities all specks are detected, and therefore the contrast sensitivity levels off. No explanation can be given for the trend that the levelling-off sets in at higher speck intensities for lower speck densities.

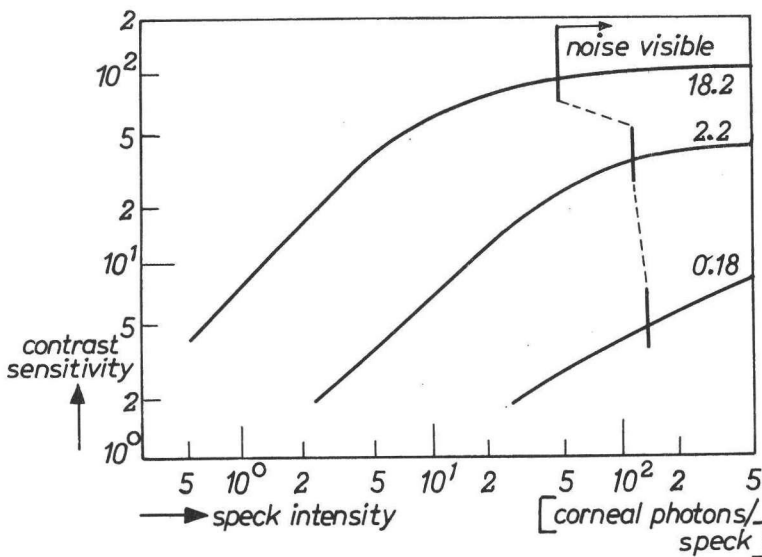


Fig. 2.5.1.6.

Contrast sensitivity as a function of the speck intensity, with speck density (specks per second per min. of arc squared) as parameter (van Meeteren, 1973, fig. 10).

This reasoning would invalidate our explanation of Franken's results. For high values of gamma all specks would be detected, so the noise would be independent of the gamma. Consequently, the input threshold contrast would be lower the higher the value of gamma. On the contrary, it will be shown below that our explanation can also be applied to the results of van Meeteren. In this connection, due account must be taken of the fact that the luminance level is linearly related not only to the speck intensity but also to the speck density.

We stated that for dominant external noise the relative variance of the speck intensity governs the masking effect of the noise. The specks are made by counting light photons and amplifying the corresponding electrical signal. Hence the relative variance of the speck intensity is independent of the intensity, and so is the noise. The modulation of the grating is equally independent of the speck intensity, so a levelling of the contrast sensitivity is obtained at high speck intensity. It is a prerequisite that the speck noise be prominent. This has indeed been measured (fig. 2.5.1.6); the smallest speck intensities for which the image can just be distinguished from a normal, smooth image are situated at the transition region of the curves for the higher speck densities (see below for low speck density). For low intensities the photon noise dominates, and the specks are not counted as such. A higher speck intensity entails then a higher photon density and less photon noise, so that the contrast sensitivity increases.

As to the influence of the speck density, the following remarks may be helpful in further research. The screen luminance is smaller, the smaller the speck density. Accordingly photon noise is larger, so that the speck noise intensity must be larger to become dominant, as has indeed been measured. For very low speck densities we imagine that problems arise with the signal processing by the visual system. For the grating to be detected, specks as such must be detected. But also a correlation must be made between the counted results in different positions. The chance of making such a correlation is of course small if the number of specks per unit surface is small. This may explain the fact that the screen luminance is not the sole determinant of the contrast sensitivity. (See van Meeteren, 1973; fig. 15; after all it is questionable whether the *physical* screen luminance is decisive. The perceived luminance of speck images may be different because of the higher temporal gradients associated with the pulsed presentation.) At low densities, the sensitivity is smaller than that for normal vision at the same adaptation level. The contrast sensitivity for speck images can also be higher than that for normal vision. This has been explained by stating that the quantum efficiency of the retina is higher when the light is clustered in specks (Bouman and Koenderink, 1972). This phenomenon cannot easily be reconciled with the reported lower sensitivity.

### 2.5.1.3 The noise-equivalent aperture of the visual system

A number of models of the visual system assume that the noise is integrated over a

certain surface. This can be (i) the object surface (Rose, 1948), or (ii) a surface correlated with the unsharpness of the whole imaging system, i.e. the noise-equivalent aperture (Morgan, 1965). The unsharpness leads to a smoothing of the noise: the same effect would occur if the noise were spatially integrated by an aperture. The surface can also be (iii) a combination of the object and the noise-equivalent aperture, as introduced by Schade (1964).

The first view leads to unrealistic C- $\Delta$  curves (see sec. 2.6.3, model B and phenomena 2a and 2b; the threshold contrast is governed by the statistics in the number of events within the object, so as to render  $C_T$  inversely proportional to  $\Delta$ . This is only the case, however, for about a factor of 2 in diameter), whereas the latter proposal is mathematically and psychophysically incorrect the way Schade (1964) introduced it (sec. 2.6.3, model C). We will therefore investigate the validity of the second view.

The noise-equivalent aperture, denoted by  $A_{eq}$ , is given by:

$$A_{eq} = [2\pi \int_0^{\infty} \nu \text{MTF}(\nu)^2 d\nu]^{-1} \quad (2.5.2)$$

One method that can be used to investigate its validity is to change the MTF of the system in a known manner, and check whether the threshold contrast is indeed inversely proportional to the square root of  $A_{eq}$ . If it is, then there still remains the uncertainty as to the MTF of the visual system to be substituted.

We try out our proposed MTF, i.e.  $\text{MTF}_v(\nu) = e^{-\beta\nu}$ , in experiments described in sec. 2.5.1.3.2. The unsharpness of the noise is varied by defocusing the image intensifier.

The unsharpness of the noise can also be varied by displaying either dominant X-ray noise or dominant electrical noise on the monitor screen. The intensities of the noises can be adjusted so as to obtain visually equivalent noises, i.e. the same C- $\Delta$  curve results. The noises should then also be equivalent for any model of the visual system. Subsequent physical measurements on the noises (sec. 2.5.1.3.1) may thus indicate the validity of the  $A_{eq}$  concept of the visual system.

**2.5.1.3.1 Physical measurement.** In the  $A_{eq}$  concept, the visual system can be described as sampling the noise in space and time. If the noise is measured with an apparatus which performs the same action, then more quantitative insight into the visual system can be obtained. A measurement on noise is of less value if a visual reference for comparison is lacking. This problem can be avoided by comparing the results measured on noises which differ as to their spatial frequency content, yet have the same masking effect on the perception of disks. The noises are physically different, but they should be equivalent for the visual system.

To this end threshold contrast curves were measured in X-ray noise and electrical noise. The electrical noise on the monitor screen is much sharper because the MTF of the image intensifier, optics and TV camera target is not involved. The higher spatial frequency character is further accentuated — but only along a TV line — by the bandpass character of the noise as produced by the camera amplifier. The noise intensities were varied such that the same C- $\Delta$  curves resulted. These noises should give the same output when scanned with the  $A_{eq}$  of the visual system.

#### Psychophysical method.

As two C- $\Delta$  curves must be measured in a short time we used Franken's method (see sec. 2.4.2.1).

The slightly changed measuring set-up I is depicted in fig. 2.5.1.7. The medical objects are simulated by the test object consisting of perspex plates provided with X-ray absorbing disks of different diameter  $\Delta$ . The test object is placed near the input screen of the intensifier, so that the source unsharpness is negligible. The optical system between the intensifier and the TV camera is provided with an iris diaphragm, by means of which the signal current  $i_s$  of the camera and hence the electrical signal-to-noise ratio can be varied. The variation of the monitor luminance is minimized by the TV AGC (Automatic Gain Control).

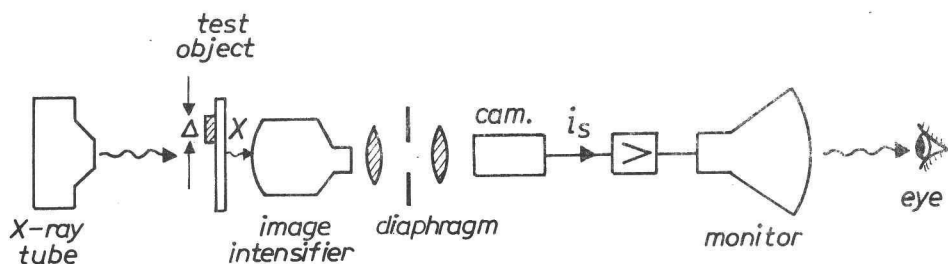


Fig. 2.5.1.7.

*Measuring set-up for investigating C- $\Delta$  curves for X-ray and electrical noise.*

The tube current was adjusted to get an exposure rate of  $43 \mu\text{R/s}$ . The diaphragm was opened to adjust a signal current of 200 nA, rendering the electrical noise negligible. The viewing distance was 400 mm. Two observers ('tH, vdL) made one measurement each.

Subsequently a C- $\Delta$  curve with electrical noise was measured. The exposure rate was increased to  $2500 \mu\text{R/s}$ , making the X-ray noise negligible. The electrical noise intensity on the screen was varied by adjusting the optical diaphragm. The C- $\Delta$  curve corresponding to an  $i_s$  of 10 nA showed good correspondence (fig. 2.5.1.8) with the one for the X-ray noise. The measured deviation between the observers is given by the horizontal line segments. These are rather large, which may be due to the limited number of observations and to the large diameter- and contrast steps.

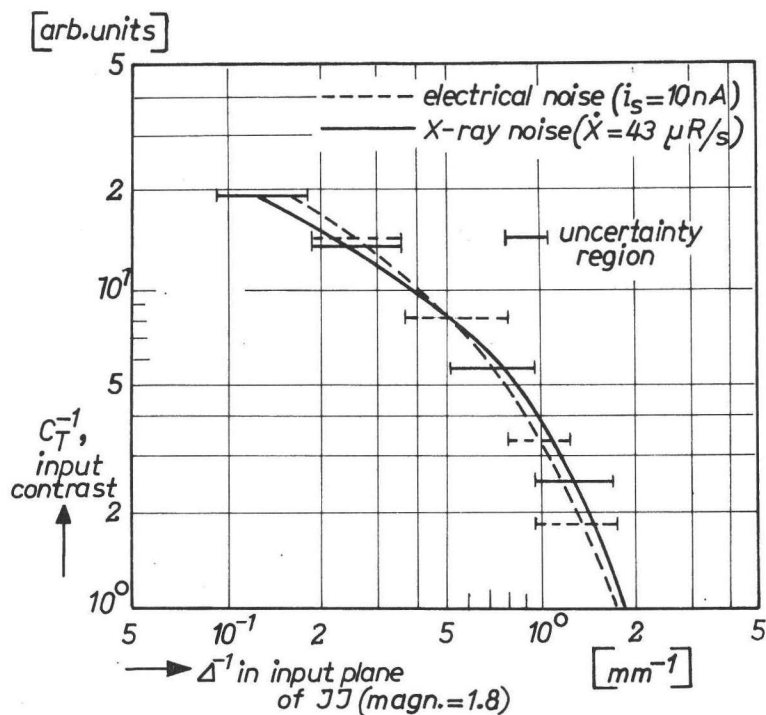


Fig. 2.5.1.8.

$C$ - $\Delta$  curve for X-ray and electrical noise.

#### Physical method.

The apparatus used to simulate an integration in time and space is a modification of the one described in Appendix III. The set-up is given in fig. 2.5.1.9. By means of the lens and the diaphragm, a part of the monitor screen is seen by the photo-multiplier PM (type 153 AVP). In this way an integration in space is performed. Every 20 ms or, if only one line is seen, every 40 ms, the scanning beam of the monitor generates a light pulse, which is converted by the PM to an electrical signal. The decay time of the light is roughly  $20 \mu\text{s}$ . This means that the duty cycle of the signal is very low, implying a poor signal-to-noise ratio. The ratio is improved by a sample-and-hold circuit (Brookdeal type 415). The signal is sampled and integrated when the pulse is present, and held at the measured value until the next pulse arrives. The gate is triggered via a video selector (made in our laboratory), whose window is adjusted to the corresponding integration surface on the monitor. The integration time is simulated by filtering the hold signal with an RC circuit, with time constant  $\tau$ . The samples are stored by a 400 channel analyser (type PW 4400). The signal is read every  $\tau$  seconds by opening the analyser gate via a free running oscillator. The luminance of the monitor is checked using a spotmeter connected to a digital voltmeter.

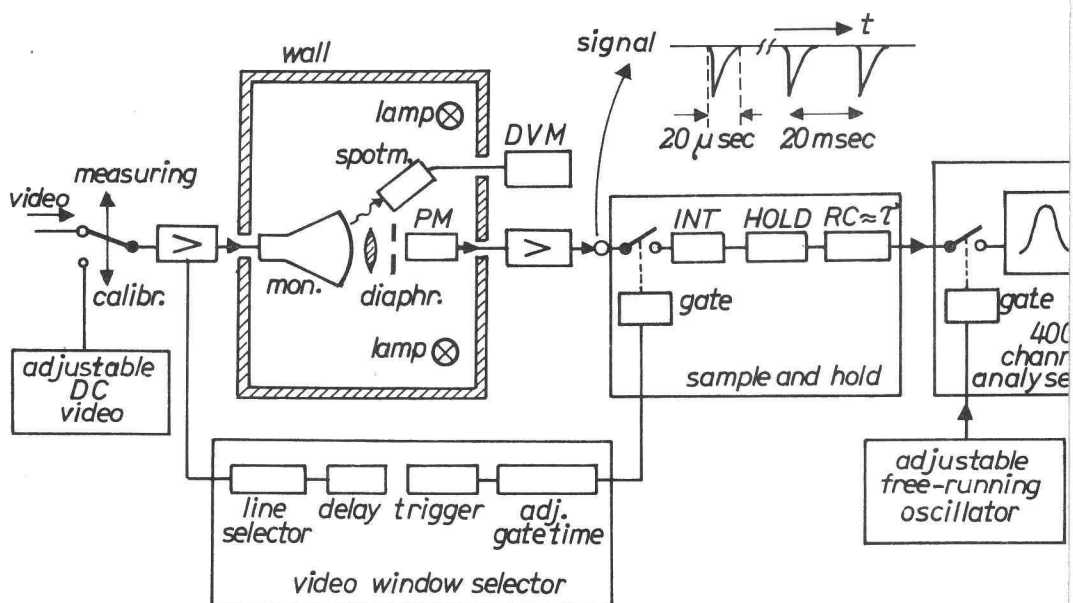


Fig. 2.5.1.9.

Noise measurement on the monitor screen.

We performed a series of noise measurements under the two noise conditions described. The integrating surface was a square with side  $d$  between 0.2 and 2.0 mm (or at 400 mm, between  $1'25''$  and  $17'$  visual angle). The integration time was varied between 10 and 300 msec. Only one TV frame was repeatedly measured. The square was laid symmetrically, in a vertical sense, on the lines of the frame (the width of the lines and their separation was roughly 0.4 mm). The samples were stored in the 400 channel analyser, giving a probability curve with a mean pulse intensity. After having stored a statistically sufficient number of counts, the half-width of the probability curve at half maximum, FWHM, was estimated. Finally, the pulse height axis of the channel analyser was calibrated by applying a constant video signal. The value of the photometer reading was applied to the corresponding channel. In this way the standard deviation FWHM was calculated in units 'mV of photometer reading'.

The standard deviations are given in fig. 2.5.1.10 as a function of the side of the integrating square, with the integration time as parameter. The full curve gives the X-ray noise situation. The dotted curve corresponds to the electrical noise. The measuring errors are rather large. Some error indication is given (10 – 20%) in the figure. The errors are mainly due to the DC shifts of the luminance level, which have the same effect on the photomultiplier signal as the noise signal. (A modification of the apparatus circumvents this problem, but owing to lack of time only

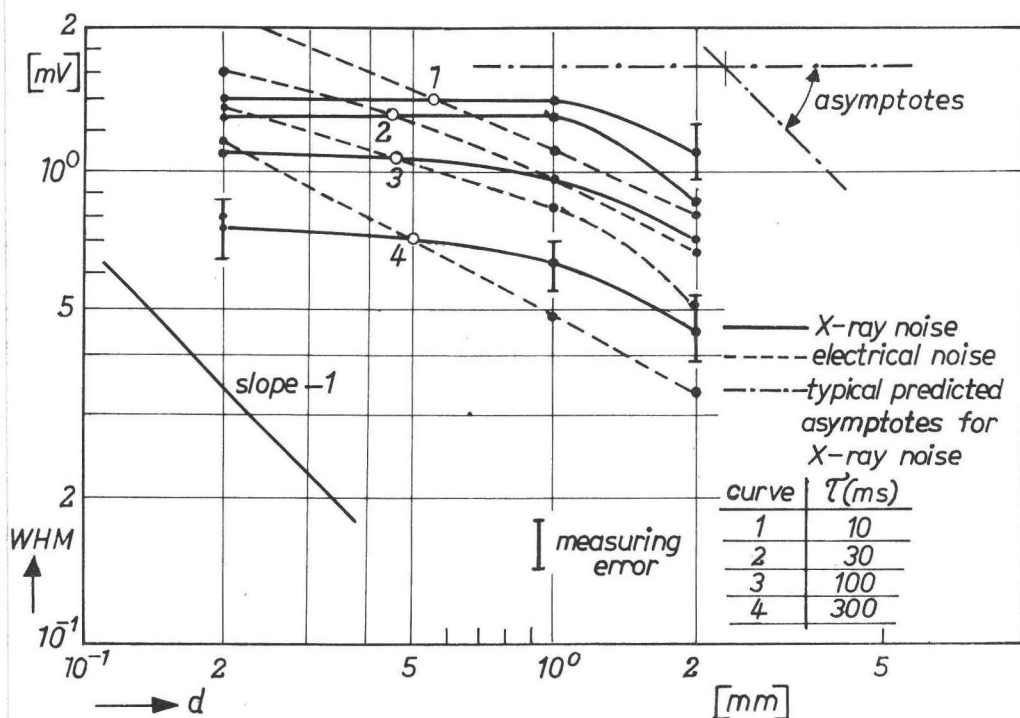


Fig. 2.5.1.10.

Measured noise as a function of the width of the integrating rectangle;  $\tau$  is parameter.

a few measurements could be made. Any DC shift over periods longer than about 40 ms is eliminated by storing the difference of the hold signal of two successive frames. The signal of the first frame is fed to a second sample-and-hold circuit, and is held there long enough to make comparison with the signal of the first hold circuit from the second frame possible.) The elimination of this shift (see the remark between brackets) reduced the error considerably, so we can conclude that the influence of line jitter and photomultiplier noise is small.

The curves show more or less the expected behaviour. If the integrating surface is small in relation to the unsharpness of the system, only the unsharpness defines the noise. The reverse is true if the surface is relatively large, implying a mere integration over this surface. In terms of spatial modulation transfer functions it can be stated in other words: the noise integrating properties are defined by the MTF, the MTF of the sampling aperture included. In the case of a small aperture, its MTF has practically no influence. The reverse is true if the aperture is large, which means that its MTF is the worst in the chain.

### X-ray noise

For small values of the side of the square  $d$ , and at least for integration times shorter than  $\approx 300$  msec, the sampling aperture has indeed hardly any influence on the noise. For large values of  $d$ , a mere integration over the surface is expected, implying a curve with a slope  $-1$  on log-log scales. The measurements indicate such a behaviour, at least for small values of the integration time.

The point of intersection of the asymptotes for small and large integrating surfaces should occur at  $d = 2.3$  mm, as can be deduced from the MTF measured by Franken et al. (1973d). The measurements are not in contradiction with this, although an ultimate test could not be performed, the noise of the measuring equipment becoming dominant with larger apertures. Nevertheless we may state that the noise-equivalent aperture concept at least gives good indications about the physical description of the noise on the monitor screen.

### Electrical noise

As stated, the electrical noise is much sharper than X-ray noise. Mere integration over the sampling aperture occurs therefore at smaller surfaces than in the X-ray noise situation. The dotted curves in fig. 2.5.1.10 show indeed a larger slope, roughly  $-1$ , than the corresponding X-ray noise curves.

A closer look at fig. 2.5.1.10 shows that the perceptually equivalent X-ray noise and electrical noise are physically equivalent if they are scanned with an integrating surface of  $0.5$  mm squared. This holds in fact for all the integrating times, as the noise samples per frame are independent of each other. (A Plumbicon tube is used. The FWHM is shown to be inversely proportional to the square root of the integration time if  $\tau > \approx 20$  ms. So the integration time, i.e. the number of frames, affects the two noises equally.) Such an aperture at a viewing distance of  $400$  mm subtends  $16$  minutes of arc squared, which is small in relation to the aperture corresponding to our proposed MTF of the visual system. Despite the large measuring errors, this conclusion in comparative terms can confidently be drawn, as the measured aperture is much smaller. A discussion and conclusion must await the general discussion in sec. 2.6.2.1.

#### 2.5.1.3.2 Psychophysical measurement

##### Method and calculations

Measuring set-up I (fig. 2.3.2) was used. The unsharpness of the noise was varied without changing the object, by changing the focusing voltage of the image intensifier. The modulation transfer function of the total chain for different voltages (fig. 2.5.1.11) has been given by Franken et al. (1973d). His notations will be used for easy reference, i.e. condition 1 corresponds to the sharpest system, system 3 is unsharper while condition 4 represents the most unsharp system used. The relative increase in the threshold contrast of an object is reliably measured by presenting two unsharpness values alternately. The measured threshold contrast ratio should be inversely proportional to the square root of the noise-equivalent aperture ratio. The MTF of the visual system to be entered in equation 2.5.2 is given by  $\text{MTF}_v(\nu) = e^{-\beta \nu}$ , with  $\beta$  of the order of  $1$  degree.



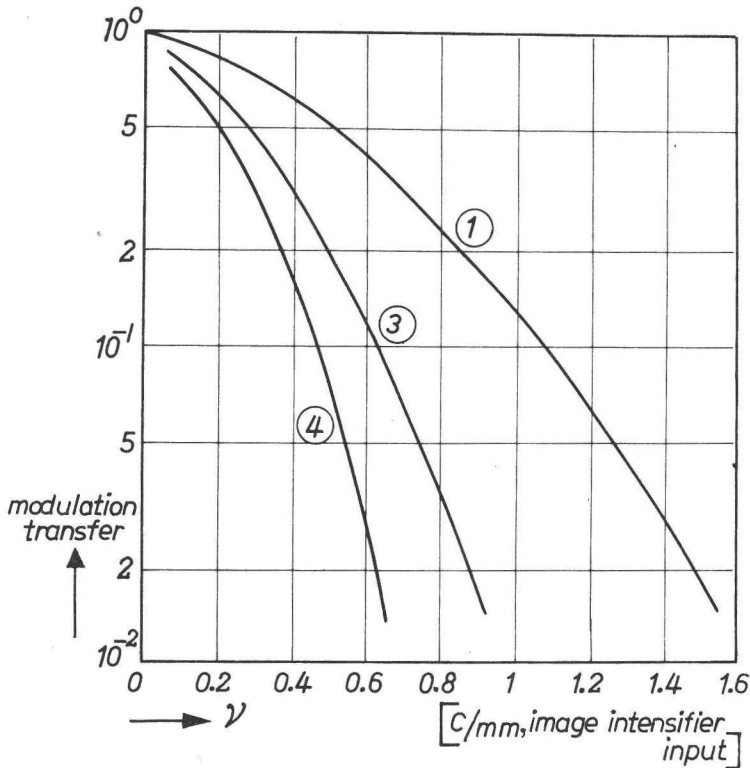


Fig. 2.5.1.11.  
System MTFs governing the unsharpness of the X-ray noise.

Measurements were performed for conditions 1 and 3 at a viewing distance of 400 mm, and for conditions 1 and 3 and 1 and 4 at a viewing distance of 1600 mm.

The calculated noise-equivalent aperture values and the predicted threshold contrast ratios are given in figures 2.5.1.12 and 2.5.1.13 as a function of the value of  $\beta$ . For  $\beta = 0$  an ideally sharp visual system is considered and a relatively large contrast ratio is expected. Apparently, the supposed unsharpness of the visual system reduces the predicted ratio considerably. This holds especially for the larger viewing distance. In other words, the MTF of the visual system is the worst link in the chain. This is once more illustrated by figures 2.5.1.14 and 2.5.1.15, which give the MTFs that govern the imaging in the conditions applied.

#### Results for disks.

First, measurements were carried out at the shorter viewing distance of 400 mm, as the influence of any change in the properties of the TV system should then be more prominent.

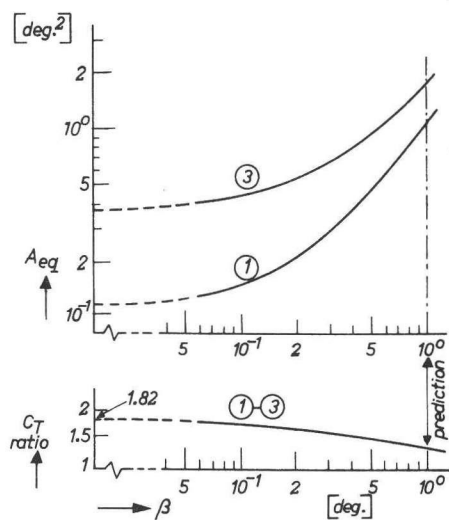


Fig. 2.5.1.12

$A_{eq}$  and the predicted  $C_T$  ratio for the conditions 1 and 3; viewing distance 400 mm.

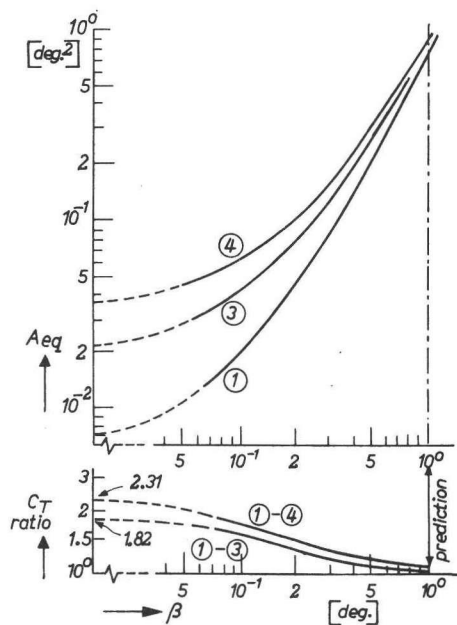


Fig. 2.5.1.13.

$A_{eq}$  and the predicted  $C_T$  ratio for the conditions 1 – 3 and 1 – 4; viewing distance 1600 mm.

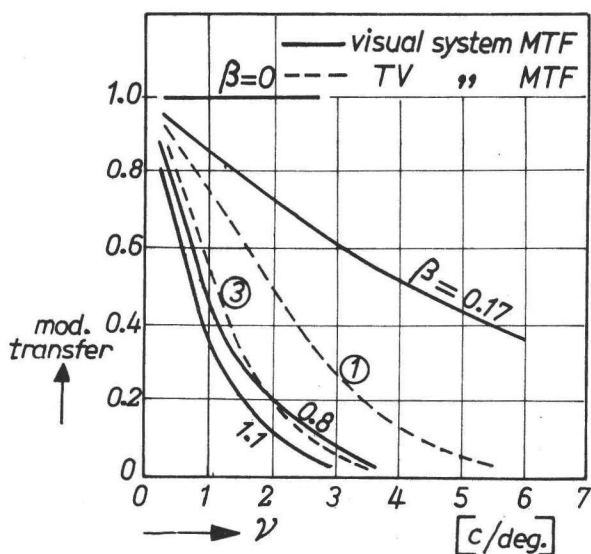


Fig. 2.5.1.14.

MTFs for imaging at a viewing distance of 400 mm, different visual system MTFs.

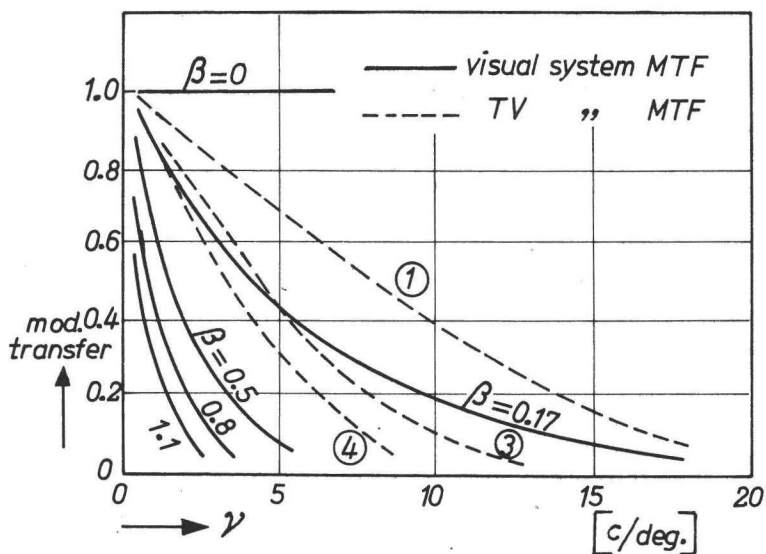


Fig. 2.5.1.15.

MTFs for imaging at a viewing distance of 1600 mm, different visual system MTFs.

Threshold contrast ratios were measured for conditions 1 and 3, by four observers: 'tH, vdL, vdT and S. Three disk diameters were considered, namely 21', 1°33' and 4°35', on a prominent noisy background corresponding to an exposure rate of 43 or 60  $\mu\text{R/s}$ . The measured ratios are closer to unity than expected for all the observers. A typical result is given in fig. 2.5.1.16 for 'tH, disk diameter 1°33', exposure rate 60  $\mu\text{R/s}$ , conditions 1 and 3. The threshold lamp voltages are 10.75V (sharp noise) and 10.65V (unsharp noise), corresponding to a threshold contrast of 6 and 5.5%. Their ratio is 1.09, while the predicted ratio is 1.30. The lamp voltage corresponding to this prediction is also entered on the X-axis, showing even better the discrepancy between theory and practice. We cannot conclude, however, that the noise-equivalent aperture concept is invalid, as the clearly visible TV lines may also play a role. We therefore decided to do experiments at the more practical viewing distance of 1600 mm.

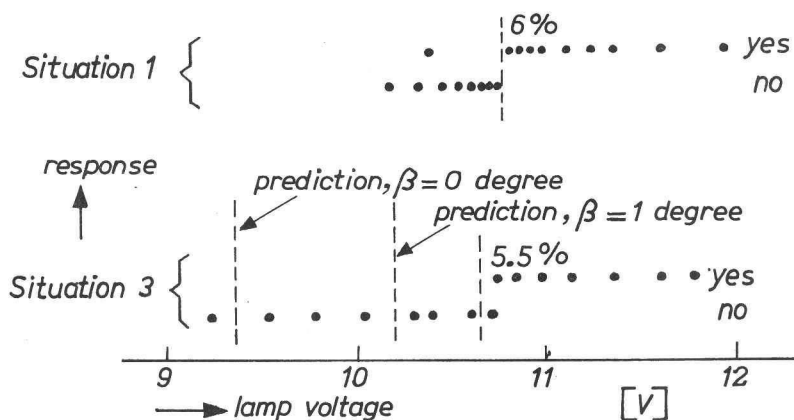


Fig. 2.5.1.16.

*Influence of noise unsharpness for 'tH, 1°33' disk, 400 mm viewing distance.*

The predicted contrast ratio for situations 1 and 3 is now 1.08. To obtain more reliable results we chose conditions 1 and 4 — for which the predicted ratio is larger, i.e. 1.12 — although the noise in situation 3 is already unusually unsharp.

Measurements were performed by three observers on a 15' and a 41' disk. The results are given as raw data (fig. 2.5.1.17 and fig. 2.5.1.18), i.e. the 'yes' and 'no' signals of the observers as (i) the threshold contrast ratio is small, and (ii) the spread in the measurements is sometimes large. But trends can easily be perceived in this way. The predicted lamp voltages are also entered, based on the threshold contrast ratio 1.12. The following remarks can be made:

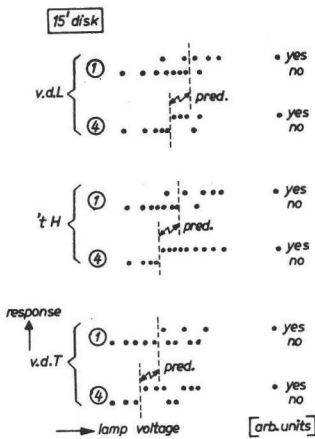


Fig. 2.5.1.17

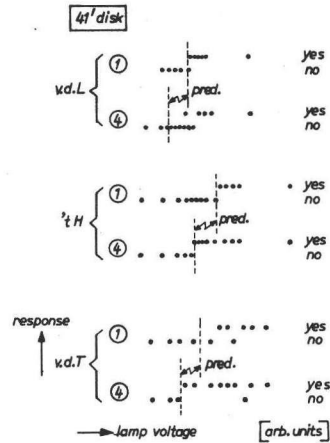


Fig. 2.5.1.18

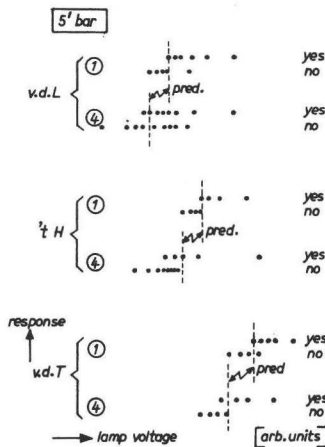


Fig. 2.5.1.19

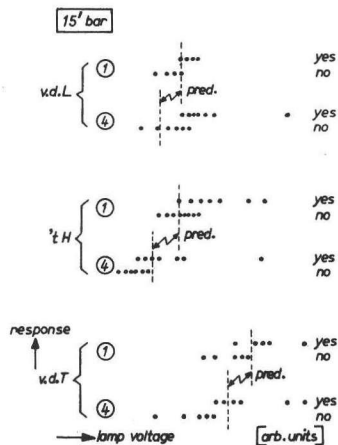


Fig. 2.5.1.20

Fig. 2.5.1.17 – 2.5.1.20

Observers' response for sharp ( ① ) and unsharp ( ④ ) noise, 15' and 41' disk, 5' and 15' bar.

- (i) The masking effect of the unsharp noise is indeed smaller. Observer vdL, 41' disk, did not measure any difference, however.
- (ii) The measured threshold contrast ratios are quantitatively correct for 'tH and vdL, 15' disk, and 'tH, 41' disk.
- (iii) There is uncertainty as to the validity of the prediction for vdT, 15' disk, and vdT, 41' disk.
- (iv) The predicted ratio is too small for vdT, 15' disk, and too large for vdL, 41' disk.

Generally, we may state that apparently the noise-equivalent aperture concept provides an approximate quantitative prediction of the influence of the unsharpness of the noise on its masking effect at not too small distances, if our proposed MTF of the visual system is applied. Further, we conclude that the unsharpness of the noise has little influence in practical situations.

#### Results for bars.

Measurements were carried out for a 5' and a 15' bar (figs. 2.5.1.19 and 2.5.1.20). There is no reason to amend the general conclusion of the previous section for disks, although the results for the 15' bar may be equivocal. Both too large threshold contrast ratios (vdT and tH) and too small a ratio (vdL) were measured. The results for the 5' bar are satisfactory.

For a comparison of the conclusions reached so far with the other results, see sec. 2.6.2.1.

#### 2.5.1.4 Influence of the viewing distance.

An increase of the viewing distance at which a noise image is observed implies:

- (i) a relatively sharper imaging system;
- (ii) an increase of the speck density related to the eye. The speck density is directly proportional to  $vd$  squared;
- (iii) a corresponding decrease of the speck intensity. The statistical relative variation of the speck intensity does not change, however;
- (iv) the angular width of the object decreases.

Many parameters thus vary at a time. This is undesirable but inevitable. The angular width of the object can be corrected however. In this way the influence of the noise proper can be studied. The two main ideas as to the masking effect of the noise lead to the same conclusion, i.e. that the threshold contrast is inversely proportional to the viewing distance. With the noise-equivalent aperture concept, the influence of the distance on the relative unsharpness of the imaging system can be neglected. So the  $A_{eq}$  is proportional to the viewing distance squared. The classical theory states that the number of events per object surface is crucial: this number is also proportional to the viewing distance squared. Our addition as to the influence of the relative statistical variation is ineffective because this value is invariant with the distance. As regards the influence of the angular unsharpness of the objects, we predict a negligible influence at the distances concerned ( $vd \geq 1600$  mm).

The influence of the TV line structure and the effects of different accommodation of the eye are studied by presenting the objects on a noiseless background also. The threshold contrast is then expected to be invariant.

#### Psychometry.

The relative influence of the viewing distance can be reliably measured by presenting the two distances alternately. This has already been proposed by Morgan (1969),

who used however one monitor for each distance. In his experiments, this necessitated different contrast and brightness settings to obtain the same luminance. As this influenced the gamma, his results on the noise intensity as a function of the viewing distance are suspect. We however used the *same* imaging system by situating two mirrors (fig. 2.5.1.21) such that the virtual images of the monitor screen were at the distances desired. The angular size of the object was corrected by choosing appropriate objects on the optical bench. The angular size of the screen was also made the same by means of a black paper mask on the mirror nearest to the observer. Without this mask, a darker after-image of the previously fixated more distant monitor was perceived. Two practical viewing distances were applied, i.e. 1600 and 3200 mm.

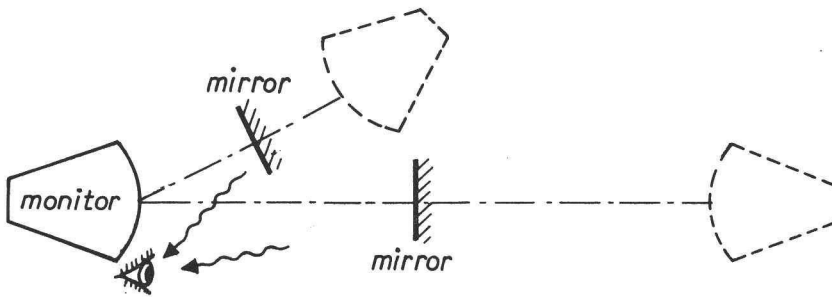


Fig. 2.5.1.21.

*Set-up for simultaneous application of two viewing distances.*

#### Influence of the TV line structure.

The TV lines may play a role for the smaller disks, as then the built-in image structure in the vertical sense may interfere. The bars are long in the vertical direction, so no influence is to be expected then.

To investigate this so as to be sure of studying the influence of the noise proper, the experiments were first carried out for a homogeneous background (set-up III). The results and measuring conditions are given in table 2.5.1.

**TABLE 2.5.1: Influence of the viewing distance, structureless background**

no.	date	$\Delta$ [min]		C <sub>T</sub> ratio, 1600–3200 mm				
		disk	bar	'tH	vdL	T	vG	mean
3	08-03-77	30'		1.10	1.00	1.00		1.00
5	08-03-77	15'		1.13	1.20	1.30		1.21
7	18-03-77	7.5'		2.46	1.93		2.00	2.13
6	09-03-77		7.5'	1.00		1.30		1.15

It can be deduced that the invariance of the threshold contrast with the viewing distance is less true the smaller the disk. The 7.5' disk corresponds to about 7 lines at the shorter viewing distance. The percept corresponds to this line effect: the 7.5' disk has an irregular structure at 1600 mm viewing distance, whereas it is perceived as a disk at 3200 mm. The influence for the 7.5' bar is indeed still small.

The results for the smaller disks should be handled with reserve. In retrospect, the observers reported great difficulty in assessing the presence of the disk at the smaller distance. The background itself did not give any clue as to the accommodation required. Perhaps this may be the reason why the object seemed to be situated in front of instead of on the screen. Accommodation was slightly easier after the introduction of an edge on the monitor screen.

Nevertheless we may state that an increase in the number of lines, as is planned for high definition TV systems, may be useful for the imaging of small objects.

### Results.

The results and conditions are given in table 2.5.2. The X-ray noise corresponds to an exposure rate of  $40 \mu\text{R/s}$ , so that the noise dominates. Measurements on the 7.5' disk were not performed because factors other than noise (line structure) may not be negligible.

**TABLE 2.5.2: Influence of the viewing distance, dynamic noise background**

no.	date	$\Delta$ [min]		CT ratio, 1600–3200 mm			
		disk	bar	tH	vdL	vdT	vG
—	26-03-76	15'		1.80		2.20	
—	30-03-76	15'				2.07	
23	13-04-77	30'		2.4/2.3			2.00
—	13-10-76		5'	2.20	2.50	1.65	

The measured CT ratios indeed cluster around a value of 2, so that the predictions as to the influence of the viewing distance are confirmed as true. The difference between the influence of the distance for the noise and for the no-noise situation is striking.

#### 2.5.2 Static noise

As discussed in sec. 2.4.1.3, we were able to reproduce two kinds of static noise on the monitor screen by means of set-up II: either 'large-size noise' or '70 mm noise'. The 70 mm noise corresponds to a picture made by a 70 mm camera of the image intensifier output in practical conditions. A viewing distance of 1600 mm to



the monitor screen corresponds to a normal viewing distance of about 500 mm to the 70 mm film on the viewing box. The conditions for the large-size film are less clear. Its equivalence with the large-size noise was adjusted at  $vd = 400$  mm. We can state, however, that the two noises are visible at the distances applied (400, 800, 1600, 3200 and 6400 mm), at least if the noise is shifted somewhat. In any case, the object at threshold suffers from the typical effects of static noise, i.e. its outline is irregular.

Before doing experiments on the influence of the viewing distance, we measured the noise intensity so as to find out whether the noise dominates. This is also important for the relevance of the conclusions as to the influence of the unsharpness of the objects in a static noisy background (sections 2.4.1.3 and 2.4.1.4).

### 2.5.2.1 Noise intensity measurement

Set-ups II and III (fig. 2.3.2) were used alternately for the same disk, i.e. the  $C_T$  ratio was measured for a static noisy and a homogeneous background. The monitor luminance was made the same by a careful preadjustment of the appropriate TV mixers. The threshold contrast ratios for the large-size noise are given in table 2.5.3.

**TABLE 2.5.3: Noise intensity measurement, large-size noise**

no.	date	vd [mm]	$\Delta$	$C_T$ ratio		
				tH	vdL	vdT
14	01-04-77	1600	30'	1.22	1.23	1.04
18c	06-04-77	1600	1° 2'	1.10		
21	07-04-77	1600	1° 2'	1.67		
18b	06-04-77	800	2° 4'	2.10		
21	07-04-77	800	2° 4'	2.54		

We conclude that the influence of the noise is small at the larger distance of 1600 mm. At the shorter distance this influence is substantial. The measurements on the influence of the unsharpness of the disks (table 2.4.1.4) were therefore carried out in dominant static noise, unlike the case with the measurements on bars (table 2.4.1.8).

The data of the measurements on disks in the 70 mm noise are given in table 2.5.4. Larger viewing distances were used to investigate small objects without interfering with the line structure of the TV system.

TABLE 2.5.4: Noise intensity measurements, 70 mm noise

no.	date	vd [mm]	$\Delta$	C <sub>T</sub> ratio			
				tH	vdL	vdT	vG
12	29-03-77	6400	3.75'	2.42	2.30	2.64	2.20
		3200	7.5'	2.98	1.91	2.04	
15	01-04-77	3200	30'	2.14	2.20	1.85	
				2.06			
22	07-04-77	3200	30'	2.31			
17a	05-04-77	800	2°4'	3.10			

These data suggest that the 70 mm noise dominates at all the applicable viewing distances (800 mm corresponds to 250 mm viewing distance to a viewing box). It may also be noticed that the noise influence is roughly independent of the disk size and of the viewing distance. The same shape of the C- $\Delta$  curve should therefore be found for different static noise intensities. This has indeed been confirmed by Chesters and Hay (1977a). Furthermore, unlike the dynamic X-ray noise situation, the viewing distance may have no influence.

### 2.5.2.2 Influence of the viewing distance

In general the viewing distances 1600 and 3200 mm were presented alternately. In this way a direct comparison with the dynamic noise situation was obtained.

Further, practical 70 mm viewing conditions were simulated. To investigate small objects without interference with the TV line structure, the distances 3200 and 6400 mm were also used.

For the large-size noise the viewing distance is expected to have hardly any influence, as the noise has little effect on the threshold contrast (table 2.5.3). This expectation was confirmed by experiments. The measuring conditions and results are given in table 2.5.5. The mean C<sub>T</sub> ratio for the homogeneous background is also given.

Except for the 15' disk, the C<sub>T</sub> ratios in noise reflect the ratio measured without noise. A reasonable correspondence is found for the 7.5' disk and bar, so that the large ratios found for the 7.5' disk should not be attributed to noise effects.

The results of the measurements given so far are not critical, as the masking effect of the noise is small. The experiments on 70 mm noise (table 2.5.6) are more illuminating in this respect. The distances were 3200 and 6400 mm. Only disks were investigated.

**TABLE 2.5.5: Influence of the viewing distance, (1600/3200 mm), large-size static noise**

no.	date	$\Delta$ [min]		$C_T$ ratio, noise				mean $C_T$ ratio, hom.
		disk	bar	'tH	vdL	T	vG	
2	04-03-77	30'		1.00	1.00	1.13		1.00
4	04-03-77	15'		1.83	1.47	1.76		1.21
7	18-03-77	7.5'		2.38				
8	18-03-77	7.5'		2.20	1.65		2.05	2.13
9	10-03-77		7.5'	1.25	1.25	1.46		1.15

**TABLE 2.5.6: Influence of the viewing distance, (3200/6400 mm), 70 mm static noise**

no.	date	$\Delta$	$C_T$ ratio		
			'tH	vdL	vG
10	24-03-77	7.5'	1.30	0.86	1.32
16	01-04-77	30'	1.00	0.54	0.85

The result of vdL seems anomalous. As to the other results it can be concluded that the masking effect of the noise does not depend on the viewing distance, although the masking effect as such is considerable (table 2.5.4). There is perhaps a slight tendency for the masking effect to be smaller for smaller distances.

The influence of the viewing distance (3200/6400 mm) was also studied without correction for the angular size of the disk. A 3.75' and a 7.5' disk are thus compared. As the influence of the noise is the same, effectively a part of the C- $\Delta$  curve for disks in static noise was measured. The  $C_T$  ratios are 3.4 ('tH), 2.0 (vdL) and 1.8 (vG). The mean value of 2.4 corresponds to a value of  $\beta$  equal to 26', which is close to the range of  $\beta$  measured so far (30' - 1°).

We cannot state that static noise is processed differently from dynamic noise. There may be a unifying principle which causes the masking effect of dynamic noise to be inversely proportional to the distance, whereas the influence of the distance is nil for static noise.

## 2.6 Conclusion

In this section we will analyse the results of the experiments in relation to each other, and formulate general conclusions (sections 2.6.1 and 2.6.2). In sec. 2.6.3 our ideas will be confronted with other models of visual processing. Finally, in sec. 2.6.4, an operational model of the visual system will be developed for application in medical X-ray systems.

Generally, we may be allowed to deal separately with object processing and noise processing because at least our measurements deal with one aspect at a time. There may be mutual influences, of course. For instance, in the investigation of the influence of the unsharpness one may argue that the unsharper disk corresponds to a smaller noise-integrating aperture, if any. These effects will be discussed in sec. 2.6.2.1.

### 2.6.1 Object processing

The value of  $\beta$

For the value of  $\beta$  of the visual system MTF, the following conflicting results have been obtained:

- (i) The effect of the unsharpness of disks and bars on their threshold contrast for largely different backgrounds, viewing distances and object sizes is described with  $\beta$  equal to 1 degree.
- (ii) The threshold contrast of disks as a function of their size is described with  $\beta$  equal to 1 degree for a homogeneous background; for a dynamic noisy background  $\beta$  equals 0.5 degree.
- (iii) The threshold contrast of bars as a function of their size is described with  $\beta$  equal to 0.5 degree for a homogeneous and a dynamic noisy background.

The first result convinces us that the basic object processing can indeed be described with  $\beta$  equal to 1 degree, in view of the large range of parameter values used and the fact that the size of the object was not altered in the experiments. This value of  $\beta$  is comparable with the values which we have deduced from Blackwell's measurements (1946). The same holds for our measurements on the C- $\Delta$  curve for disks on a homogeneous background, and for the measurements in comparable conditions reported by Hemmingsson, Jung and Lönnerholm (1975), sec. 2.4.3.1.

Thus, although the basic processing is described, the final outcome of the analysis by the visual system may depend on additional factors. This must be the case in the second result, which implies that the threshold contrast of medium-sized disks ( $12'/20'$ ) increases less rapidly with decreasing size for a noisy background than for

a homogeneous background. No explanation can be given, although one might think of a better spatial correlation of the coarse X-ray noise at the smaller distances involved. A noise speck subtends a few minutes. The percept might support this view: all observers reported that the 12' disk was 'unexpectedly bright' compared with the 20' disk, and compared with the homogeneous background situation. It seemed as if the speck density in the disk was larger than elsewhere.

As for the third result, the threshold contrast of medium-sized bars increases less rapidly with decreasing size than in the disk situation. This is true of the dynamic noisy background, for which the same arguments can be used as for the C- $\Delta$  curve of disks in noise. But it also holds for a homogeneous background. An explanation for the discrepancy may be found in the different character of the object. It is known that the visual system is very sensitive to lines. Integration but also interpolation (vernier acuity) and extrapolation is easily performed. These effects may facilitate the perception of bars if the two edges are so close that lines are perceived. This percept indeed sets in at a width of about 8', which is in the critical region for the assessment of  $\beta$ . As to the spatial correlation effects, Foley-Fisher (1977) commented along more or less independent lines on his finding of an optimum linewidth for vernier acuity. Improved acuity corresponds to a spatial summation process which is limited to the central part of the fovea. 'Such regions are between 10 and 20 min arc in diameter'.

This analysis stresses once more that our model of the visual system does not necessarily represent its actual working method, although the data on the influence of the unsharpness strongly suggest that at least the basic signal is extracted in the way proposed. Here we encounter the same problem as with the explanation of the sensitivity for gratings. The basic signal processing, but also the higher order effects (e.g. anticipation) should be taken into account. In any case, our model gives good quantitative predictions for low frequency gratings, which may be looked at as consisting of separate bars.

### Influence of the luminance

Our experimental set-up did not enable us to vary the adaptation level considerably. A small variation was applied ( $20 \text{ cd/m}^2 - 35 \text{ cd/m}^2$ ), and no shift in the value of  $\beta$  could be measured. This is in correspondence with the expectation, because the value of  $\beta$  does not strongly depend on the adaptation luminance (fig. 2.2.10). Our measured value of  $\beta$  is given once more in fig. 2.6.1 in relation to the values deduced from Blackwell's measurements. The uncertainty as to the adaptation level (either  $5 \text{ cd/m}^2$  from the environment, or  $20 \text{ cd/m}^2$  from the monitor screen) is indicated. The uncertainty in the value of  $\beta$  as deduced from the measurements on the C- $\Delta$  curve is indicated by standard deviations. Such analysis is difficult for our measurements on the influence of the unsharpness. At least the largest value of  $\beta$  indicated (75') would still fit the experimental results.

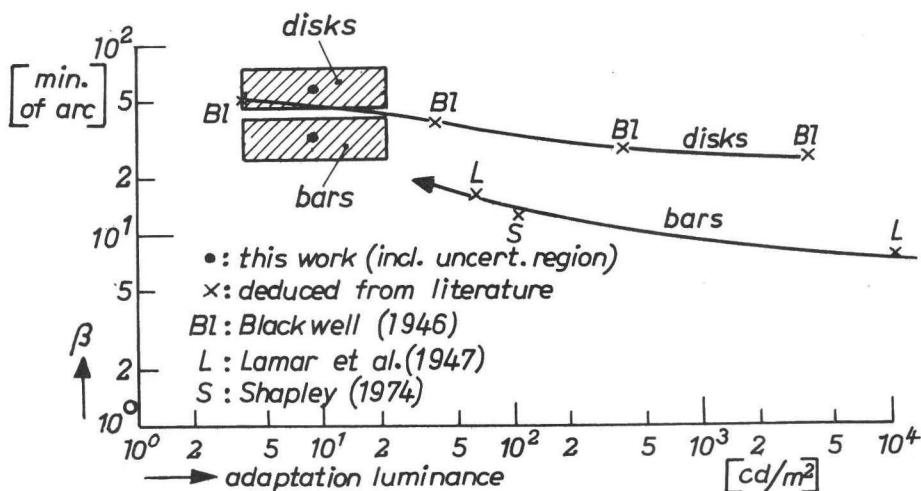


Fig. 2.6.1.

The value of  $\beta$  of the visual system MTF as a function of the adaptation luminance.

The measured values of  $\beta$  fit reasonably well. The discrepancy, if any, can be attributed to statistical and systematic deviations as only two observers were continuously available, whereas the Blackwell data are based on the mean of seven observers (and 90,000 observations). There is further the uncertainty in the fitting of the Blackwell C- $\Delta$  curves.

Measurements on the influence of the size of bars were only performed at the monitor luminance of  $20 \text{ cd/m}^2$ . A few data from the literature are however available to extend the range of adaptation luminance. We concluded from the work of Shapley (1974) that  $\beta$  is  $13'$  for an adaptation luminance of  $100 \text{ cd/m}^2$ . Lamar et al. (1947) measured the threshold contrast of bars at  $60 \text{ cd/m}^2$  and  $10,000 \text{ cd/m}^2$ . We deduce from their measurements on sufficiently long bars ( $\approx 100'$ ) that the value of  $\beta$  is  $17'$  and  $8.7'$  respectively. These values cannot be deduced very reliably, as only three fitting points are available per C- $\Delta$  curve (fig. 2.6.2). Nevertheless the values fit reasonably well with the other values — see fig. 2.6.1. The curves for bars and disks show the same behaviour, which is reassuring.

As to the influence of the unsharpness, we tentatively propose to describe this with a value of  $\beta$  equal to the one for the C- $\Delta$  curve for disks on a homogeneous background. This gave good results in our situation. As for the influence of the size of bars, the value of  $\beta$  should be halved. This gave good results in our experiments, and also for the prediction of the visibility of Gaussian bars (Shapley, 1974).

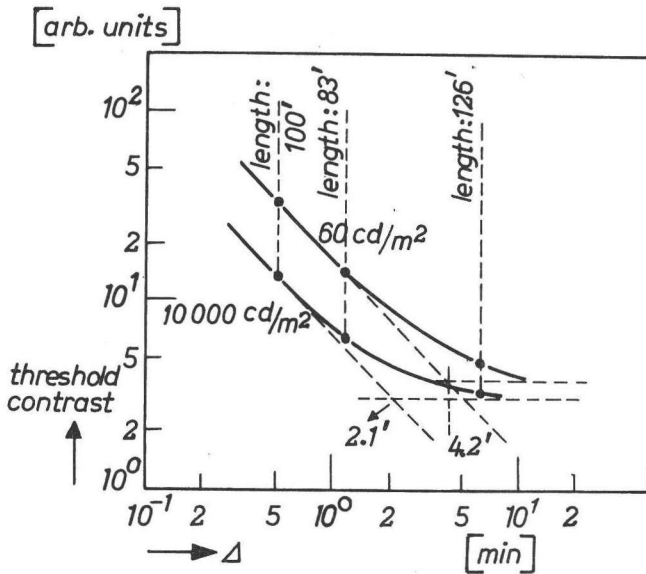


Fig. 2.6.2.

*C- $\Delta$  curves for bars, according to Lamar et al. (1947)*

### Threshold and supra-threshold vision

The analysis of the threshold unsharpness-increment taught that this unsharpness would lead to only a very small increase of the threshold contrast. Hence the visibility of the unsharpness of supra-threshold objects is a more sensitive criterion than the visibility of the object. This holds for the parameter unsharpness. The reverse is true if the contrast is to be investigated. The visibility of the unsharpness is rather insensitive to the contrast applied, whereas the visibility of the object is primarily governed by the contrast.

The discrepancy between threshold and supra-threshold vision can be fictitious, because the same decision scheme may be applied by the visual system. In the threshold task, the maximum contrast gradient is compared with a built-in or measured (external noise!) criterion level. Contrasts of the order of a few per cent are then needed. We found the same order of percentage decrease in maximum contrast gradient in assessing the smallest perceptible increase of the unsharpness. The signals, i.e. the maximum gradients, are clearly above threshold, their difference is fed to the decision centre and compared with the same criterion level. This reasoning remains speculative, of course, as explorative calculations show that consistent predictions of the threshold unsharpness can also be obtained with other choices of the visual system MTF (i.e. other values of  $\beta$ ).

### Shape of the visual system MTF

Within our model of the visual system an exponential shape gives good predictions in a wide range of situations. Only the low frequency part is of importance, as we have calculated that the predictions are rather insensitive to the higher frequency part (modulation transfer  $< 5\%$ ,  $\nu > 3/\beta$ ).

An exponentially shaped MTF is assumed, so the modulation transfer is smaller the higher the frequency. For the low spatial frequencies this behaviour is in contrast with that suggested by many authors on the basis of the visibility of gratings: their MTF increases with frequency. We have argued, however, that it is not allowed to call the contrast sensitivity function the MTF of the visual system. Further, the low frequency drop is consistent with our model of the visual system: the maximum contrast gradient should be taken into account, which is proportional to the spatial frequency. So the threshold modulation of low-frequency gratings will indeed be inversely proportional to the frequency.

### 2.6.2 Noise processing

#### 2.6.2.1 Dynamic noise

A model for noise processing should also state whether the masking effect of the noise is object-dependent or not. The validity of such a statement can perhaps never be proved, because the same fundamental problem is involved as with the assessment of the signal-to-noise ratio: the statement as to the noise depends on the assumption for the object processing and vice versa. To facilitate the development of a noise model, the measurements for which the object was not altered are treated first. Secondly, the object variations, i.e. the variation of the unsharpness and size, are also taken into account. The experiments on the unsharpness of the noise are also discussed in this section, because unsharper noise may correspond to object-dependent different noise processing.

#### No object variation.

A plausible explanation of a number of phenomena could be conceived by thinking in terms of the retinal speck density and the relative statistical variation of the speck intensity. The threshold contrast, then, is inversely proportional to the square root of the speck density, and directly proportional to the relative statistical variation of the speck intensity. The first relation corresponds to the statistics in a number of events, the second relation corresponds to the statistics in the signal going with each event. We cannot give a proper definition of an 'event' or a 'speck' for our complex and unsharp imaging system. We may state, however, that the speck density is proportional to the X-ray exposure rate. The speck intensity is proportional to the amplification of the X-ray TV chain. The relative statistical variation, however, mainly depends on the statistics of the X-ray absorption in the image intensifier screen (Albrecht and Oosterkamp, 1962).



Within certain limits, therefore, the amplification does not influence the masking effect of X-ray noise, unless the amplification is so small that only the naturally occurring photon noise is present. Nevertheless the proposed model of the noise processing could also be applicable to photon noise. The speck density should be replaced by the photon density on the retina, whereas the relative statistical variation of the speck intensity is represented by the variation of the energy deposited per photon. This retinal efficiency may depend on the adaptation level, i.e. on the photon density, but the main trend will indeed be that the threshold contrast is inversely proportional to the square root of the adaptation luminance if the internal noise of the visual system can be neglected (i.e. if the adaptation luminance is smaller than about  $0.3 \text{ cd/m}^2$ ; see Blackwell, 1946). For practical luminances the threshold contrast is independent of the adaptation luminance (Weber-Fechner law), so that the internal noise can then be considered as the sole determinant of the noise level.

*X-ray exposure rate.* The threshold contrast is inversely proportional to the square root of the X-ray exposure rate. This corresponds to the direct proportionality of the speck density with the X-ray exposure rate. The relative variation of the speck intensity did not change, although the amplification was adjusted to keep the monitor luminance level constant. At large exposure rates other noise sources tend to dominate and the threshold contrast levels off.

*Viewing distance.* The threshold contrast is inversely proportional to the viewing distance, as the retinal speck density is proportional to the viewing distance squared and as the relative variation of the speck intensity does not change. For the latter, the variation of the viewing distance is equivalent to a variation of the amplification factor of the TV chain. The noise unsharpness is varied as well, but this has only negligible effects (see below).

*Gamma.* As the relative variation of the speck intensity is proportional to the gamma of the TV system, we deduced the intensity of the noise to be proportional to the gamma. This is only true if the external noise dominates, i.e. if the X-ray exposure rate is not too high.

This enabled us to explain the results of Franken et al. (1973d) for a large range of gammas and exposure rates, and the results of van Meeteren (1973) who varied both the speck intensity and the adaptation luminance.

#### Object variation.

The C- $\Delta$  curve for disks in photon noise can be completely predicted by stating that the noise is integrated over a fixed aperture. The size of this aperture is unimportant in this respect. The same holds for the experiments on the X-ray exposure rate, the viewing distance and the gamma of the TV system. Any model based on the integration of statistical events over a certain area would correctly predict the results.

If the noise-equivalent aperture is introduced, then the influence of the unsharpness of the noise can be roughly predicted. At least it must be concluded that the influence is small, in other words that the unsharpness of the visual system dominates.

This was also concluded from the measurements on the influence of the unsharpness of the object.

The value of  $\beta$  of the visual system MTF is one degree for the situations mentioned. For the C- $\Delta$  curve of disks in X-ray noise, however, a value of  $\beta$  equal to 0.5 degree fits better. Since the basic object processing can be described by  $\beta$  equal to one degree for all noises and unsharpnesses, we must conclude that the processing of X-ray noise differs from the processing of photon noise. In fact, the X-ray noise processing may be object-dependent in the sense that the spatial correlation of the X-ray noise in medium-sized disks ( $\approx 10'$ ) is better than for larger disks. This may also occur for bars, although here the complicating effect of another object shape also plays a role. This may account for the fact that the C- $\Delta$  curve for bars in photon noise must also be described by  $\beta$  equal to 0.5 degree.

Other explanations of the findings can easily be given, because the conclusions as to the noise and object processing are mutually dependent. One may for instance think of noise integration over the noise-equivalent aperture, whereas the object acts as the sampling aperture. This resembles the physical method described in sec. 2.5.1.3.1, i.e. the sampling of a given noise by an adjustable aperture. For visual system models, it corresponds to a mixture of the model given by de Vries (1943) and Rose (1948) who assumed that an ideally sharp visual system integrates the noise over the object, and Morgan's concept (1965). The latter postulated an unsharp visual system, and assumed the noise to be integrated over the noise-equivalent aperture.

In this mixture of models, the blurring of an object may lead to a smaller sampling aperture of the noise. This corresponds to another effective noise if the diameter of the object is large compared with the noise-equivalent aperture of the total system. The signal-to-noise ratio does not depend on the size of small objects. The applied ranges of the sharp/unsharp disks and bars are given in fig. 2.6.3 for the proposed visual system MTF in terms of the product  $\Delta \cdot R$ . Here  $R$  denotes the appropriate spatial frequency which corresponds to a modulation transfer of 1 per cent. The influence of  $\Delta$  on the noise is represented by the ratio  $\pi\Delta^2/(4 A_{eq})$ , plotted along the y-axis. The curve has been borrowed from van Leunen and Pennings (1973). A slope of +2 on log-log scales indicates the dominance of the noise-equivalent aperture, and objects in this region are looked upon as small.

The objects are small to medium-sized so that the influence, if any, of the blurring of the object on the effective noise is absent or small. Thus this model is consistent in this respect.

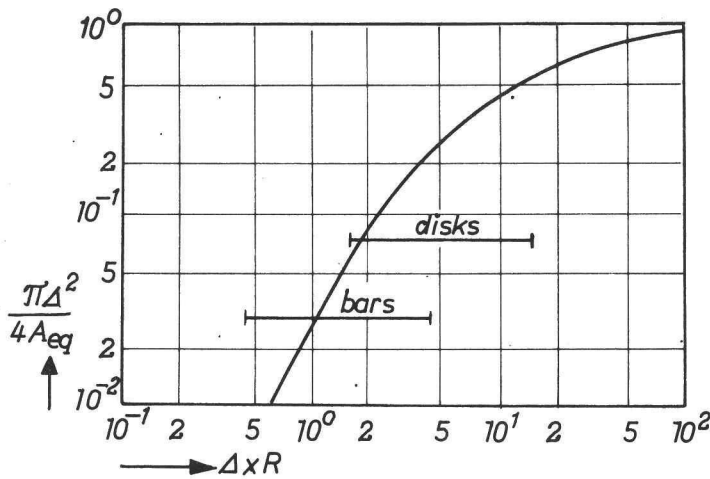


Fig. 2.6.3.

*Widths of objects investigated in relation to the noise-equivalent aperture.*

Up till now, we cannot arrive at any reliable conclusion with respect to the validity of the noise integration area of the visual system. The  $A_{eq}$  concept indicates a good prediction at the larger viewing distance of 1600 mm, but the ultimate effect of a practical unsharpness variation of the noise is so small as to be hardly measurable. There is further the result of the physical measurement of the  $A_{eq}$  value by means of simulating the visual system to determine its sampling action in time and space. This  $A_{eq}$  value is of the order of 19 min. of arc<sup>2</sup>, whereas the  $A_{eq}$  value on the basis of the deduced visual system MTF equals 2300 min. of arc<sup>2</sup>. Can these two data be reconciled?

It is striking that the smaller  $A_{eq}$  value may well correspond to that of the eye optics and the retina. If we assume again an exponentially shaped MTF, then a value of  $\beta$  of  $0.09^\circ$  corresponds to the wanted  $A_{eq}$  value. The PSF has a FWHM of  $1'20''$ . The MTF is plotted in fig. 2.6.4, together with a representative MTF for the eye optics (van Meeteren, 1974). We can perhaps dispense with an attempt to explain the discrepancy, in view of the uncertainty in the data. Any discrepancy can easily be attributed to light-spread in the retina. If this spread has a FWHM of  $1'$  then the two MTFs fit perfectly. Such a spread over a few cone diameters (the mean cone diameter is  $18''$ , Jones and Higgins (1947)) is not unlikely. This means that the cones received the same signal for the X-ray and electrical noise which were equivalent with respect to their masking effect. As a consequence the idea emerges that the basic signal assessment is done by the cones, but that higher-order signal processing takes place which minimizes the effect of the noise. This reduction of the effective noise can be performed in many ways, and the quantitative correspondence between the predicted and measured  $C_T$  ratio for differently unsharp noises might be accidental. In any case, it implies a rather coarse sampling.

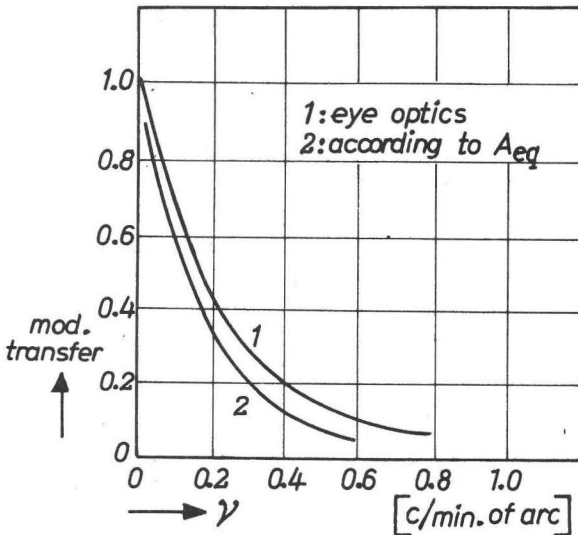


Fig. 2.6.4.

MTF of the eye optics (van Meeteren, 1974) and the MTF corresponding to the physically measured  $A_{eq}$  (this work)

This may be in contrast with the visual resolution of noise: the specks can be distinguished and the introduction of unsharpness is also perceived. We should bear in mind, however, that the noise is at supra-threshold, for which other rules may apply. Furthermore, in the presentation of noise specks, high temporal gradients are involved, for which the visual system is very sensitive.

Whatever method is chosen to describe the influence of the noise unsharpness, its influence appears to be independent of the type and size of the object: a 41' and 15' disk and a 15' and 5' bar did not give fundamentally different results. This is confirmed by measurements reported by Hay (1976) on 20', 4' and 2' sinusoidal bars.

#### 2.6.2.2 Static noise

The appearance of static noise differs considerably from that of dynamic noise. This can be attributed to the fact that the retinal temporal variations of dynamic noise are mainly determined by the pulsed presentation of the TV system, whereas for static noise the eye movements induce temporal gradients. Further, the object at threshold in static noise appears with an irregular shape and intensity distribution. In dynamic noise, the proper shape is ultimately perceived. In static noise the irregular appearance of the object begins at quite small noise intensities, i.e. at intensities that hardly increase the threshold contrast.

These substantial differences make it plausible that the influence of the viewing distance is quite different in the case of static noise: the threshold contrast does not depend on the viewing distance in practical ranges of distances. This conclusion may be supported by the results on the threshold visibility of simulated lung lesions as a function of the viewing distance (sec. 2.4.3.1). Good predictions could be obtained without taking into account the effect, if any, of the viewing distance on the masking efficiency of the noise. It is however possible that there was hardly any noise.

Our material suggests that the influence of the noise intensity does not depend on the size of the object. Accordingly, the same shape of the C- $\Delta$  curve should be found irrespective of the static noise intensity. Only one measurement was done for one noise intensity, and the value of  $\beta$  deduced indeed points to such a conclusion. Two results from literature confirm this statement. Both Chesters and Hay (1977a) and Franken et al. (1975) applied large ranges of noise intensities, including the no-noise situation (Chesters and Hay) and found roughly the same shape of the C- $\Delta$  curves for disks. So we will set our value of  $\beta$  equal to 1 degree for disks, in order to predict the C- $\Delta$  curves in static noise. No measurements on bars are known as yet. Owing to a lack of clues to other mechanisms, we will set our value of  $\beta$  equal to 0.5 degree for the C- $\Delta$  curves of bars.

The unsharpness of the noise proper was not varied. The measurements reported by Chesters and Hay (1977b), who varied the unsharpness of static noise over large ranges, point to an object dependence of the unsharpness: the shape of the C- $\Delta$  curve changes for  $\Delta > 10'$ . This result, however, cannot easily be implemented.

The unsharpness of the noise was of course varied in the experiments on the influence of the viewing distance. We found no influence of the viewing distance. This has important practical implications, but no conclusion as to the static noise processing can be drawn because more than one parameter was varied at the same time.

### 2.6.3 Discussion

Although numerous models of the visual system have been devised, relatively little attention has been paid to the influence of the unsharpness of the object. Further, the masking effect of external noise has generally not been dealt with. It is very useful to confront our model with other models so as to gain some idea of their relative predictive power. This will be done by analysing a number of perceptual phenomena. We will further investigate whether our model lines up with the historical development.

#### Models of the visual system

Two main streams of object-processing models can be distinguished: (i) In the

*single channel* models all the information converges upon one neural summing point. (ii) In the *multiple channel* models, each object is detected by specific, size-tuned sensitive regions. There are also two main schools of thought as regards noise processing: (i) the noise is integrated over the *surface of the object*, or (ii) the noise is integrated over the *noise-equivalent aperture*.

The investigation of all possible models is complicated, because mixtures of these four schools of thought have also been conceived. Further the number of models can be extended at will by postulating different unsharpnesses of the visual system. We are constrained to confine ourselves here to eleven more or less representative models. The models are mentioned in chronological order.

**A** Graham et al. (1939); Kincaid, Blackwell and Kristofferson (1960).

*Object processing*: single channel model. The photoreceptor excitation converges upon a neural summing point. For symmetrical objects this summing point is located at the centre. The element contribution function describes the response of a receptor as a function of the distance to the summing point. This function decreases monotonically with increasing distance. The photoreceptor response is logarithmic according to Graham et al.; according to Kincaid et al. it is linear.

*Noise processing*: not mentioned.

**B** De Vries (1943); Rose (1948).

*Object processing*: in fact a multiple channel model, although it was not formulated in that way. The visual system is ideally sharp, hence a perfect image is made of all objects.

*Noise processing*: the statistical variation of the photon flux limits the object visibility. The photon flux is accumulated over the object surface. The crucial signal is the contrast, which is compared with the relative statistical variation of the noise.

**C** Schade (1954, 1964); Morgan (1965).

*Object processing*: single channel model. The unsharpness of the visual system corresponds to the contrast sensitivity function for gratings. The maximum contrast or modulation is the crucial signal.

*Noise processing*: the external noise is integrated over the noise-equivalent aperture corresponding to the proposed MTF (Morgan). Schade's rather arbitrary criterion will not be taken into account here. Schade states that the noise is integrated over the sum of the object surface and the noise-equivalent aperture. No experimental evidence is given to support this assumption, however. The mathematical treatment is in any case invalid, as the equations used (1964, eq. 7) (i) only hold for Gaussian-shaped MTFs, but the Fourier transform of an isolated object is generally not Gaussian, and (ii) they refer to one-dimensional objects whereas in general two-dimensional objects are imaged.

**D Thomas (1970).**

*Object processing:* multiple channel model. It is based on physiological studies (e.g. Hubel and Wiesel (1962)), which show that neurones exist that are sensitive to specific objects. The portion of the visual field to which the neuron responds is called the receptive field. The element contribution function consists of a positive central region and a negative outer region. These excitatory and inhibitory regions cause the neuron response to be size-tuned. When a particular stimulus is presented it is examined by many fields; in the threshold condition only the fitting neuron will respond sufficiently.

*Noise processing:* not mentioned.

**E<sub>1</sub> Bagrash (1973).**

*Object processing:* mixture of single and multiple channel processing. The responses of small edge detectors (Tolhurst, 1972) are pooled by a mechanism like A.

*Noise processing:* not mentioned.

**E<sub>2</sub> Bagrash (1973).**

*Object processing:* multiple channel model. The responses of small edge detectors are pooled by a mechanism like D.

*Noise processing:* not mentioned.

**F Gelade et al. (1974).**

*Object processing:* single channel model. The element contribution facilitates edge detection, i.e. a bi-phasic function is assumed. The pooling centre is situated at the edge.

*Noise processing:* not mentioned.

**G Hay and Chesters (1977).**

*Object processing:* multiple channel model. The object signal is integrated over the object as enlarged by the unsharpness of the visual system. From the fitting of predictions and measurements it is concluded that the unsharpness can be described by a PSF with an 'effective diameter' (comparable to a noise-equivalent aperture) of 3.8 min. of arc (Chesters and Hay, 1976).

*Noise processing:* the noise is integrated over the same modified object surface.

**H<sub>1</sub> This work.**

*Object processing:* single channel model. The object signal is modified by the unsharpness of the visual system. Contrary to other models, the signal is the maximum contrast gradient. The FWHM of the corresponding PSF is of the order of 12 min. of arc.

*Noise processing:* the noise is integrated over the noise-equivalent aperture corresponding to the postulated unsharpness. The masking effect of the noise is inversely proportional to the square root of the number of specks in the aperture, and directly proportional to the relative statistical variation of the intensity per speck.

**H<sub>2</sub>** This work.

*Object processing:* see H<sub>1</sub>.

*Noise processing:* see H<sub>1</sub>; the blurred object acts as the sampling aperture.

**H<sub>3</sub>** This work.

*Object processing:* see H<sub>1</sub>.

*Noise processing:* the noise is integrated over a fixed angular aperture of whatever size.

The object processing of our model could equally well be described by the reversed order of steps. Thus, first the spatial gradient of the object signal is established, and next a spatial integration according to our visual system MTF is made. This model is perhaps more plausible, as we argued that the retina may in fact produce the derivative of the signal by built-in circuitry or by virtue of eye movements. In this set-up our model comes close to that of Bagrash (E<sub>1</sub>) as the proposed edge detectors respond best to contrast gradients.

Our model is essentially a single channel model, but the principal response is different: neither a linear nor a logarithmic response is supposed; what is decisive is the spatial/temporal derivative. As to the multiple channel models, one may argue that the size-tuned receptive fields may also be capable of measuring the spatial derivative by moving the field over the object, or by using the signal from the inhibitory region on account of the unsharpness.

Finally, a spatial derivative could also be measured by the bi-phasic element contribution of Gelade (F). In fact, then, there need not be any contradiction with other models although their working method is generally not formulated in terms of measuring derivatives.

With respect to the noise processing, we remark that the size of the noise-equivalent aperture is much greater than that used by Hay (G). Even so, our model H<sub>2</sub> comes close to Hay's model in concept. Our A<sub>eq</sub> is also much larger than that published by Schade and Morgan (C), because they enter the contrast sensitivity for gratings as the MTF of the visual system.

### Perceptive phenomena

The following phenomena in the perception of isolated objects will be used to investigate the validity of the models of the visual system. The phenomena are numbered for easy reference.

The first three phenomena are related to the threshold contrast as a function of the size as found by many authors and confirmed by our experiments:



1. The larger the width of the object, the smaller is the threshold contrast.
- 2a For small widths, the threshold contrast is inversely proportional to the diameter squared (disks) or to the width (bars).
- 2b For large widths, the threshold contrast is independent of the width.

The next three phenomena are related to the influence of the unsharpness of the objects:

- 3 Flanking of a bar by subthreshold bars leads to an increase of the threshold contrast (Gelade et al., 1974).
- 4 The increase of the threshold as a function of the position of the subliminal bars depends on the width of the central bar (Gelade et al., 1974).
- 5 The unsharpness of the object has less effect on the threshold contrast the larger the viewing distance (this work).

The following three data have been borrowed from adaptation experiments by Bagrash (1973). The functioning of the visual system is investigated by presenting specific supra-threshold stimuli, followed by measurements of their influence on the threshold contrast of the same or other stimuli. The idea is that the adaptation leads to less sensitivity for specific aspects of the threshold stimuli:

- 6a Adaptation to a disk increases the threshold contrast of the corresponding disk; no effect is measured for considerably smaller and larger disks.
- 6b Adaptation to an annulus at the edge of the disk (i.e. the outer diameters coincide) increases the threshold contrast of the disk.
- 6c Adaptation annuli produce an effect which is out of proportion to their area. A greater effect is obtained by adding area at the edge of the adaptation stimuli than by adding area at the centre.

The next six experimental data have mainly been borrowed from this work. They deal with phenomena in external noise:

- 7 The C- $\Delta$  curve for disks in external noise differs from the one for photon noise.
- 8 The influence of the unsharpness of the object does not depend on the kind of noise (dynamic, static, photon noise).
- 9 The threshold contrast is inversely proportional to the square root of the X-ray exposure rate (as found by many others). The threshold contrast of disks and bars in dominating dynamic noise is inversely proportional to the viewing distance, provided the same angular dimension of the object has been chosen.
- 10 The masking effect of the dynamic noise is proportional to the gamma of the imaging system, as we inferred from the results of Franken (sec. 2.5.1.2.1).
- 11 The masking effect of the dynamic noise is inversely proportional to the

square root of the noise-equivalent aperture. In practical systems, the influence is negligible.

- 12 The masking effect of the noise as a function of its unsharpness is independent of the size of the object.

Validity of the models

The predictions derived from the models are compared with the perceptual results in table 2.6.1. The indication ‘+’ corresponds to a good prediction or the potential to give a good prediction. The ‘-’ indicates a false prediction, and the questionmark stands for uncertainty as to the validity of the prediction.

TABLE 2.6.1: Validity of visual system models

perc. experiment		model										
		A	B	C	D	E <sub>1</sub>	E <sub>2</sub>	F	G	H <sub>1</sub>	H <sub>2</sub>	H <sub>3</sub>
photon noise	1	+	+	+	?	+	?	?	+	+	+	+
	2a	+	-	+	+	+	+	?	+	+	+	+
	2b	+	-	+	?	+	?	+	-	+	-	+
	3	-	-	-	+	+	+	+	?	+	?	+
	4	+	+	+	?	+	?	-	?	+	?	+
	5	+	+	+	?	+	?	-	?	+	?	+
	6a	-	-	-	+	+	+	-	+	+	+	+
	6b	+	+	+	+	+	+	+	+	+	+	+
	6c	-	-	-	-	+	+	+	-	+	+	+
	7		?	-					?	-	?	-
external noise	8		-	+					-	+	?	+
	9		+	+					+	+	+	+
	10		+	+					+	+	+	+
	11		?	-					?	+	?	?
	12		-	+					-	+	-	+

The justification of the results is given below for each phenomenon.

Phenomenon 1:

- + : A, C, E<sub>1</sub>, H<sub>1</sub>, H<sub>2</sub>, H<sub>3</sub> ; the single channel model implies less signal for smaller objects.
- + : B, G; a smaller object goes with a potentially larger effective noise.
- ? : E<sub>2</sub>, F; the sensitivity of different-sized tuned channels is unknown.
- ? : D; the implementation of the edge detector is unknown, especially for smaller objects.

## Phenomenon 2a:

- + : A, G,  $H_1$ ,  $H_2$ ,  $H_3$  ; good correspondence is obtained
- + : C,  $E_1$  ; good correspondence is possible.
- ? : F ; see phenomenon 1.
- : B ; as only the noise fluctuation is of importance, the threshold contrast should be inversely proportional to the square root of the surface of the object, i.e. inversely proportional to the diameter of disks or the square root of the width of bars.
- + : D,  $E_2$  ; good correspondence is possible if the objects are smaller than the minimum size of tuned fields.

## Phenomenon 2b:

- + : A,  $H_1$ ,  $H_3$  ; good correspondence is obtained.
  - + : C,  $E_1$  ; good correspondence can be obtained.
  - : G ; the model breaks down for disk sizes over 30'.
- The noise- and signal integration predicts an ever decreasing threshold contrast.
- ? : D,  $E_2$  ; see phenomenon 1.
  - :  $H_2$  ; the noise integration predicts an ever decreasing threshold contrast.
  - + : F ; edge detection predicts such a behaviour.
  - : B ; see phenomenon 2a.

## Phenomenon 3:

- : A, C ; integration of more signal takes place, so a lower contrast would be needed.
- : B ; integration of more noise takes place, so a lower contrast would be needed.
- + :  $H_1$ ,  $H_3$  ; good predictions demonstrated.
- + : D,  $E_2$  ; the subthreshold stimuli give rise to inhibiting responses, so the threshold contrast should be higher.
- + :  $E_1$ , F ; edge detectors respond less to unsharper edges.
- ? : G ; more noise is integrated, but there is also more inhibiting response.
- ? :  $H_2$  ; the contrast gradient is smaller, but the noise is integrated over a larger surface.

## Phenomena 4 and 5:

- + :  $H_1$ ,  $H_3$  ; proved correspondence.
- ? : G,  $H_2$  ; see phenomenon 3.
- ? : D,  $E_2$  ; would imply different sensitivity distributions for different sizes.
- + : A, C,  $E_1$  ; the use of an element contribution function implies an object-size dependence.
- + : B ; the relative increase in noise-integrating area is of importance.
- : F ; the edge detector response does not depend on the size of the object.

## Phenomenon 6a:

- : A, B, C, F; the adaptation effect is non-selective.
- + : D, E<sub>1</sub>, E<sub>2</sub>, G; the multiple channel models predict this effect.
- + : H<sub>1</sub>, H<sub>2</sub>, H<sub>3</sub>; if the model is understood as the derivation of spatial gradients and the subsequent pooling of the information, then good correspondence may be obtained.

## Phenomenon 6b:

- + : A, C, D, E<sub>1</sub>, E<sub>2</sub>, F; these models do not exclude the adaptation effect of any stimuli within the object.
- + : B, G; the noise is integrated over a smaller area.
- + : H<sub>1</sub>, H<sub>2</sub>, H<sub>3</sub>; see phenomenon 6a.

## Phenomenon 6c:

- : A, C; the reverse would be expected for the element contribution function used.
- : B, D, G; no particular importance is attached to the edges by these multi-channel models.
- + : E<sub>1</sub>, E<sub>2</sub>, F, H<sub>1</sub>, H<sub>2</sub>, H<sub>3</sub>; the use of edge detectors or the derivation of spatial gradients indicates such effects.

## Phenomenon 7:

- : C, H<sub>1</sub>, H<sub>3</sub>; the noise-integrating aperture is fixed, so the C-Δ curve shape should be independent of the noise.
- ? : B, G, H<sub>2</sub>; since the noise-integrating aperture depends on the object, the unsharpness of the noise may play a role.

## Phenomenon 8:

- + : C, H<sub>1</sub>, H<sub>3</sub>; noise and object are processed independently.
- : B, G; the noise integrating aperture depends on the object, hence on the unsharpness of the object and of the noise.
- ? : H<sub>2</sub>; no decision can be made, see sec. 2.6.2.1. 'Object variation'.

## Phenomenon 9:

Every model predicts such a behaviour. The models C, G and H use integrating surfaces which depend on the unsharpness, so a prerequisite is that the imaging system unsharpness can be neglected for the different viewing distances.

## Phenomenon 10:

A higher gamma indicates a proportionally larger speck intensity variation, so each model predicts such a behaviour.

## Phenomenon 11:

- + :  $H_1$  ; proved correspondence;
- : C; the applied  $A_{eq}$  value is much smaller, so a larger influence of the unsharpness would be predicted.
- ? : G,  $H_2$  ; the object size also plays a role, so uncertainty exists (for  $H_2$ , see sec. 2.6.2.1, 'Object variation'.
- ? : B; the visual system is ideally sharp, so the influence of the noise unsharpness is potentially large. For large objects, however, the influence will be small.
- ? :  $H_3$  ; no statement is given as to the size of the aperture.

## Phenomenon 12:

- + : C,  $H_1$ ,  $H_3$  ; this is a fundamental property of these models.
- : B,  $H_2$ , G; the influence of the noise is size-dependent, and so is the influence of the unsharpness of the noise.

## Conclusion

No model predicts all the phenomena correctly. If only the object processing is considered, the best scores are made by the single-channel edge-detector pooling model of Bagrash ( $E_1$ , 1973) and by our models  $H_1$  and  $H_3$ . The Bagrash model, however, gives only qualitative predictions, whereas our model gives good quantitative predictions for a large range of practical situations. Moreover, our model takes the external noise into account as well, which is often crucial for X-ray imaging.

The first model on object processing (A, Graham et al., 1939) cannot correctly take into account the unsharpness of objects. The first model, which also includes the noise processing (B, de Vries, 1943; Rose, 1948), predicts unrealistic threshold contrast curves, whereas the size of objects is a very important aspect in many applications. The models based on size tuning may be physiologically correct, but only qualitative explanations can be given. Further, the noise is generally not taken into account. Hay and Chesters must be given credit for applying the multiple channel model in combination with an unsharp visual system and in combination with external and internal noise. But their model breaks down for disks with a diameter larger than about  $30^\circ$ , i.e. 4.5 mm at 500 mm viewing distance — which evidently hampers the application to X-ray imaging.

The model of Campbell et al. (1968, 1969) has not been mentioned so far as it does not primarily aims at the perception of isolated objects like disks, but at gratings. The visual system is thought of as being equipped with channels, each sensitive to a specific band of spatial frequencies. The outputs of these channels are pooled by a threshold device. The critical signal is the maximum modulation, i.e. the difference between the maximum and the minimum response. Good predictions could be obtained for the visibility of a 'single bar', i.e. a half-cycle of a sines, with widths

smaller than about 6'. The perceptual phenomena 1 and 2a are therefore correctly predicted, but the important perception of large bars (2b) could not be handled. Besides, we stated before that predictions for small objects do not prove much about the validity of a model. The phenomena related to the unsharpness of objects (3, 4 and 5) cannot be handled because the objects are large. The adaptation effects (6a, 6b, 6c) refer to disks, whereas Campbell investigated a one dimensional situation only. Further, the noise is not mentioned. Phenomena 7 to 12 are therefore beyond the scope of Campbell's work.

2.6.4 Operational model of the visual system

Object processing

To simplify the fitting of the visual system in the X-ray system, preferably only one value of  $\beta$  should be used. At first sight this seems impossible as different values of  $\beta$  had to be used in different situations. We shall analyse these situations and see whether a compromise is possible.

If only small and large objects are considered, then no problems exist because the relation between the threshold contrast and the size does not depend on the value of  $\beta$ . So a value of  $\beta$  equal to 1 degree can be chosen to describe the influence of the unsharpness properly. This holds for any background, whether noisy or homogeneous.

The correct description of the C- $\Delta$  curves is of prime importance if medium-sized objects are considered. Values of 0.5 and 1 degree should therefore be applied, whereas the influence of the unsharpness must be described by  $\beta$  equal to 1 degree.

The required values of  $\beta$  are summarized in table 2.6.2.

TABLE 2.6.2: Values of  $\beta$  per visual task (n.i. = not of interest)

object		background/task					
		dynamic noise		static noise		structureless	
		C- $\Delta$	MTF	C- $\Delta$	MTF	C- $\Delta$	MTF
large	} disk	n.i.	1°	n.i.	1°	n.i.	1°
small							
medium	disk	0.5°	1°	0.5°	1°	1 °	1°
-----		-----		-----		-----	
large	} bar	n.i.	1°	n.i.	1°	n.i.	1°
small							
medium	bar	0.5°	1°	0.5°	1°	0.5°	1°

A structureless background seldom occurs. Furthermore, since the effects of size variation are much more prominent in practical systems than unsharpness variations (see section 5.2), a value of  $\beta$  equal to 0.5 degree will generally be applied.

The predictions as regards the effect of the unsharpness of disks then correspond to about the maximum effect found instead of to the mean effect. This may be concluded from fig. 2.4.1.4, which gives the predicted effect as a function of  $\beta$ , and the measured results (fig. 2.4.1.16). The effect of the unsharpness of bars will be overestimated though not to a large extent (compare fig. 2.4.1.17: such large  $C_T$  ratios are not present).

## Noise processing

### — Magnification factors:

The masking effect of a dynamic noisy background is inversely proportional to the operative visual angle. This angle is governed by the viewing distance, the use of optical aids and the scaling which is applied by the image receptor of the X-ray system. To take the visual angle into account, an image plane must be the reference.

The operative magnification factors are thus  $M_a$  ('a' stands for angular; unit: degree/mm),  $M_o$  ('o' stands for optical) and  $M_r$  ('r' stands for receptor).

The masking effect of practical static noises does not depend on the applied magnification.

### — Noise intensity:

The masking effect is inversely proportional to the square root of the exposure rate  $\dot{X}$  (dynamic noise, fluoroscopy) or the exposure per image (dominant static noise, radiography, Franken et al. 1975). The latter parameter value is proportional to the product of the X-ray tube current and the irradiation time, denoted by  $Q$ .

### — Gamma:

The effect could not be studied for static noise (although, if one deals with dominant static noise, it can be deduced from the work of Chesters and Hay (1977a) and of Reichmann (1974) that the masking effect of static noise is proportional to  $\gamma$ ). The masking effect of dominant dynamic noise has been shown to be linearly proportional to the gamma,  $\gamma_x$  (eq. 2.5.1).

### — Unsharpness:

For dynamic noise and practical viewing distances the influence of the unsharpness of the noise can be described by means of the noise-equivalent aperture. A value of  $\beta$  equal to 1 degree must be used, but no large deviations are introduced if the proposed value of 0.5 degree is applied (see fig. 2.5.1.13): the effect, if any, is small.

No measurements could be done for static noise. The results for different viewing distances suggest that the influence for practical ranges of unsharpness is small or even absent.

Mathematical formulation for the threshold contrast of disks and bars, based on the conclusions in section 2.6.

- Homogeneous background:

The influence of the noise is absent, so the threshold contrast (eq. 2.2.1.6) is given by:

$$C_T \sim \frac{1}{\left. \frac{d C_s(r)}{dr} \right|_{\max}} \quad (2.6.1)$$

The influence of the magnification factors is contained in the luminance intensity distribution  $L_s(r)$  as far as the object processing is concerned. The value of  $\beta$  of the visual system MTF equals 1 degree.

- Static noise background:

Here  $C_T$  is given by:

$$C_T \sim \frac{1}{\sqrt{Q}} \cdot \frac{1}{\left. \frac{d C_s(r)}{dr} \right|_{\max}} \quad (2.6.2)$$

The influence of the gamma cannot be taken into account. The influence of the magnification factors on the noise is absent. The value of  $\beta$  equals 0.5 degree.

- Dynamic noise background:

The threshold contrast is given by

$$C_T \sim \frac{\gamma_x \cdot M_r \cdot M_o \cdot M_a}{\sqrt{\bar{X} \cdot A_{eq}}} \cdot \frac{1}{\left. \frac{d C_s(r)}{dr} \right|_{\max}} \quad (2.6.3)$$

The value of  $\beta$  equals 0.5 degree.



### 3. OBJECT RESOLUTION

#### 3.1 Introduction

This chapter deals with the spatial spread of information as caused by the imperfection of the imaging by the X-ray system. The visual system is not taken into account, so the term 'object resolution' is chosen. We will use the term 'unsharpness' for the spread of information, although its definition is as yet unclear. The unsharpness is caused by the finite X-ray source size, the movement of the object and the imperfection of the image receptor.

Firstly, the object resolution will be described and optimized for a given image receptor and required energy per radiograph, for radiography of both moving and stationary objects. The fluoroscopy of stationary objects is consequently described as well. This analysis encompasses the influence of the X-ray source size and the position of the object. Secondly, this analysis will be extended to take into account the influence of different image receptors as well.

The description of the object resolution is only a first step towards a complete description of the imaging. After its establishment, the parameters which influence the contrast of the image will also be taken into account, i.e. the X-ray beam quality (sec. 5.2.4) and the scattered radiation (sec. 5.2.5). The corresponding effects on the contrast are to be measured (sec. 4.1 and 4.2). For the time being, however, the X-ray tube high voltage has the value chosen in practice, and an anti-scatter grid is always applied. (The relation between the object resolution and the position of the object if no grid is used is rather complex; the analysis is given in Appendix IV.)

The imaging of X-ray systems is anisotropic. We shall describe the object resolution for the worst case direction, but the description can easily be extended to other directions as well.

#### Unsharpness

The term unsharpness has generally been used to denote the spatial spread of the image of an edge. Such an edge spread function (ESF) is given in fig. 3.1.1a for a homogeneous X-ray source and an ideal image receptor. A linear intensity distribution results. There are at least three reasons why this method could not lead to a complete, comprehensive description of the unsharpness of a system: (i) The definition of the spatial spread is liable to be arbitrary if the edge spread intensity distribution is non-linear. This is the case if the unsharpness of an intensifying screen is to be described: the edge spread function has an S-shape (fig. 3.1.1b). This problem also occurs if the X-ray source has a non-homogeneous intensity distribution. (ii) The combination of unsharpnesses leads in general to a non-linear spread, so the same difficulties arise. (iii) The correlation with the perception of the image cannot easily be obtained.

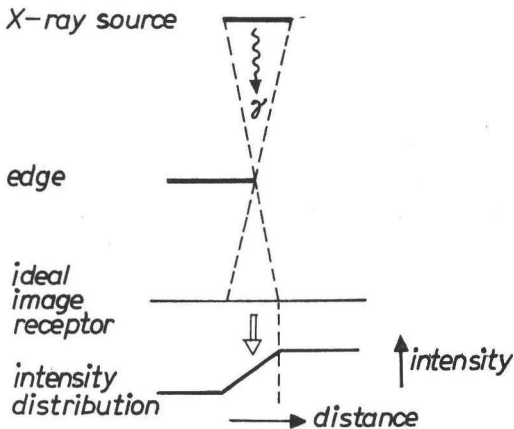


Fig. 3.1.1a. X-ray source unsharpness

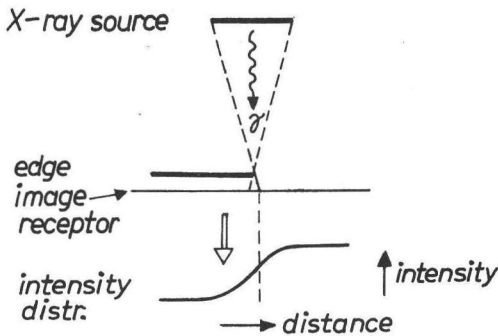


Fig. 3.1.1b. Image receptor unsharpness

Fig. 3.1.1.

*Edge spread functions.*

re. (i): The screen unsharpness is simply described by a single value, e.g. 0.3 mm by Bouwers (1931), Burger et al., (1946); v.d. Plaats (1952) and Feddema and Botden (1963).

Other definitions that do not take perceptive criteria into account are based on the area enclosed by the edge spread function (Nitka, 1938; Nemet et al., 1946), on its maximum gradient (Morgan, 1949), on the 0.065 and 0.935 relative intensity points (Meiler, 1955) or the 0.10 and 0.90 relative intensity points (Meiler, 1963), or erroneously a Gaussian spread is assumed (Spiegler and Norman, 1973). A few definitions are based on perceptive phenomena. Chantraine (1933b), Bouwers and Ooster-

kamp (1936) and Klasens (1946) made a comparison with a known unsharpness. The latter deduced the 0.16 and 0.84 relative-intensity points as being crucial. Finally, Higgins and Jones (1952) established the order of perceived sharpness on the basis of the 'acuity', which is a measure of the means of the square of the density gradient of the edge spread function between the points with 'just perceptible gradient'.

- re. (ii): At first, a number of authors (Bouwers, 1931, 1934; Wilsey, 1933; Bouwers and Oosterkamp, 1936; v.d. Tuuk, 1938) simply added up unsharpnesses, although Bronkhorst pointed out as early as 1927 that the total unsharpness is less than the sum of the factors. This has to do with the resulting S-shaped intensity distribution of an edge image. Other definitions have been given on the basis of a visual comparison of resulting images. Newell (1938) compared the images of thin cylinders for combinations of movement and X-ray source unsharpness. Nemet et al. (1946) compared the areas enclosed by edge spread functions, whereas Morgan (1949) investigated the maximum gradient. These methods point indeed to a total unsharpness which is smaller than expected. The equations found read

$$u_t = \sqrt[n]{\sum u^n} \quad (3.1.1)$$

in which  $u_t$  is the total unsharpness, and  $u$  represents an unsharpness factor. For  $n$ , values between 2 and 3 have been deduced. Equations of the same kind were found by Warren (1937, 1940) and Klasens (1946).

- re. (iii): Only a few authors (Warren, 1937; Klasens, 1946; Higgins and Jones, 1952) have investigated the perceptive consequences. The phenomena were above threshold, so a correlation with threshold criteria cannot be assessed. Further, operational definitions could only be obtained for a particular situation. As to the non-perceptive definitions, many authors (including Tuddenham, 1957 and Rossmann and Seemann, 1961) postulated that the maximum density or intensity gradient is of importance. Higgins and Jones (1952) explicitly state, however, that the maximum gradient is not indicative of the perceived unsharpness.

In conclusion, we may state that a surprising number of criteria exist. Since only suprathreshold phenomena have been investigated for the perceptive aspects, the relation with the threshold contrast is unclear. Although operational definitions have been found for particular situations, an overall view cannot be obtained in this way.

### The MTF concept

The situation with respect to the physical description of unsharpness has been definitely improved by applying the Fourier concept, as introduced by Coltman (1954b). The spatial spread is then analysed in terms of its spatial frequency content. The resulting spatial modulation transfer function (MTF) describes the modulation transfer of sinusoidal gratings by the system. The Fourier analysis of any object suffices to reconstruct its image in an analytical manner.

Although the description of X-ray systems is then complete, it is laborious and difficult because *functions* must be handled. Efforts have therefore been made to combine the advantages of the unsharpness description and the MTF description by assigning a single number to each MTF. These methods are generally not based on perceptive criteria. In any case, the criteria are not generally applicable, because either the shape of the MTF is not taken into account, or only specific shapes are considered. The following single-number criteria for the MTF quality have been used:

- (i) It is stated that the visual system is capable of just perceiving a grating with a few per cent modulation. Thus the spatial frequency for 4% modulation transfer is used by Fenner and Stahnke (1966), by Pfeiler and Linke (1972) and by Haendle and Horbaschek (1976). The 5% criterion is used by Feleus and Vijverberg (1970). These criteria are wrong in four respects:
  - (a) The MTF describes the modulation *transfer* whereas the visibility of a grating is governed by the absolute modulation.
  - (b) The *shape* of the MTF is not taken into account.
  - (c) The visibility of gratings is only weakly correlated with the visibility of *anatomical* (single) objects.
  - (d) If the criterion were correct, then the absolute value would still be wrong because gratings with a much smaller modulation can still be seen (Campbell and Robson, 1968).
- (ii) The spatial frequency for zero modulation is used (Hollander et al., 1972; Stargardt and Angerstein, 1975). The same criticism as under (i) is applicable, added to which is the fact that the MTF of an image receptor asymptotically approaches the zero value. This criterion is therefore not generally applicable.
- (iii) The shape information is retained by giving the modulation for a few spatial frequencies. No decision can be made, however, if MTFs with different shapes are to be compared (Fenner and Stahnke, 1966; Hale and Mishkin, 1969; Gajewski and Kuhn, 1970 and 1972; Doi and Sayanagi, 1970; Rao et al., 1973).

- (iv) The information on shape and spatial-frequency range is implicitly retained by taking the noise-equivalent aperture or the like (Spiegler and Norman, 1973; Wagner et al., 1974). The system MTF quality is then given by equation 3.1.1. with  $n = 2$ . Every 'unsharpness factor' has an appropriate weighting factor. This criterion is based on the central limit theorem in the sense that the cascading of a sufficient number of MTF components leads to a Gaussian-shaped MTF. This may be true for some imaging systems, but not for the X-ray system:
  - (a) The number of components should be 'sufficiently large' (Papoulis, 1968, page 79). The practical number is four at most, however, and two components or even one component can play a dominant role. In the case of two components (X-ray source and movement) a triangular line spread function may occur, so the corresponding MTF deviates greatly from a Gaussian one.
  - (b) The component MTF qualities should be 'reasonably concentrated' around the mean quality (Papoulis, 1965, page 267). It is not explained what is meant by 'reasonable', but the MTF qualities of the X-ray system components can differ so much as to certainly invalidate the stated prerequisite.

#### This work

We will also use the MTF concept for the description of the object resolution. The analysis of X-ray systems as a whole is made easier by analysing its components separately, and by developing pragmatic and dedicated MTF descriptions for sub-systems and the system as a whole. A set of newly defined characteristic numbers for the balance between the MTF quality of the components greatly facilitates this task. A number of approximations and limitations are needed, of course. They will be justified now or later on if appropriate.

We will aim at a system MTF for which the spatial frequency for all modulation transfer values is as large as possible. The corresponding images will be better, whatever they may be. This criterion cannot be satisfied for the optimization of the object position; instead of the MTFs, the corresponding images will then be examined. In fact, the MTF is only a description of the system, whereas the images are crucial.

In optimizing the object resolution, two main problems are to be dealt with:

- (i) For the imaging of moving objects, the movement unsharpness and the X-ray source unsharpness are inversely related via the X-ray tube loadability. This means that an *optimum X-ray source size* may exist. This will be studied in sec. 3.2.1. The optimum size also depends on the intensity distribution of the X-ray source, because the specific heat load of the X-ray tube depends on it. This will be studied in sec. 3.4.

- (ii) All the MTFs are defined in the object plane, to make comparison with object dimensions possible. This implies that any variation in the position of the object will have an antagonistic effect on the MTF of the X-ray source and the image receptor. The corresponding influence of the *geometric magnification* will be studied in sec. 3.2.2 for moving objects and in sec. 3.3.2 for stationary objects.
- re. (i): The optimization schemes on the basis of the unsharpness are of course beset with the faults inherent in this concept. Further the ideas as to the loadabilities of X-ray tubes as a function of the size of the X-ray source may differ. Consequently, the optimum source size corresponds to a range of balances between the size unsharpness of the X-ray source,  $u_f$ , and the movement unsharpness,  $u_m$ , i.e.  $u_f = u_m$  (Bouwers and Oosterkamp, 1936; Chérigé, 1972),  $u_f = \sqrt{2} \cdot u_m$  (Newell, 1938), and  $u_f = 2u_m$  (Bouwers, 1931; v.d. Tuuk, 1938). Bouwers should be credited for the insight that the movement and the source unsharpness should be of the same order for the optimum, and that this optimum is rather smooth. The same conclusion is to be found in this work, but "Bouwers' work is not just duplicated; the optimization is carried out analytically for present-day standards and concepts. The results can further easily be implemented. A complete description in terms of MTFs was obtained by Albrecht and Oosterkamp (1962). They found a similar expression for the shadow image MTF as our equation 3.2.18, for the low-frequency end. The remaining analyses are at best computer programs to calculate resulting MTFs for a given parameter set (Feddemma et al., 1969; Feleus and Vijverberg, 1970; Gajewski and Kuhn, 1970 and 1972; Rao et al. 1973; Stargardt and Angerstein, 1975). Insight into the problem cannot easily be obtained in this way.
- re. (ii): The consequences of geometric magnification can only be assessed in practical use, that is to say by viewing the enlarged image. As two aspects are then varied at the same time, i.e. the unsharpness and the size, a systematic investigation of for instance the factors that influence the unsharpness is not possible. Therefore we will first investigate the resolution in the object plane. The criterion borrowed from the unsharpness concept was worded by Burger et al. (1946), who stated that the visibility of an object is 'doubtful' if the unsharpness equals the size of the object. Several authors have used this criterion (Schober, 1953; Büchner, 1954; Feddemma and Botden, 1965). Apart from being based on the doubtful concept of the unsharpness, its perceptive validity has not been proved. Furthermore the unsharpness is calculated in the image plane.

The criteria based on the MTF concept have already been discussed. They are invalid for assessing the image quality, especially if differently shaped MTFs are to be compared. This is generally the case when the geometric magnification is varied: the shape of the source MTF differs from that of the image receptor MTF.

On the basis of Bouwers' criterion, that 'all errors should be of the same order of magnitude', one may argue that the image receptor unsharpness – whatever that may be – should be of the order of the other unsharpness factors. Evers and Schober (1955) and Dünisch et al. (1971) used this criterion, but we will show that it is invalid as far as geometric magnification variation is concerned.

### 3.2 Moving objects

Two parameters are varied to optimize the object resolution, namely the size of the X-ray source, hence the loadability of the X-ray tube, and the object position. We will first define the optimum source size for a given object position, and show that it is dependent on this position. Secondly, we shall seek the optimum object position. For every position, the corresponding optimum source is chosen. In this way the absolute optimum is reached in two steps.

The system MTF is the product of three MTFs:

$$\text{MTF}_x(\nu) = \text{MTF}_f(\nu) \cdot \text{MTF}_m(\nu) \cdot \text{MTF}_r(\nu) \quad (3.2.1)$$

where  $\nu$  is the spatial frequency in the object plane,  $x$  stands for the X-ray system,  $f$  denotes the X-ray source,  $m$  refers to the movement and  $r$  relates to the image receptor. The product of  $\text{MTF}_f$  and  $\text{MTF}_m$  governs the shadow image MTF,  $\text{MTF}_a$ :

$$\text{MTF}_a(\nu) = \text{MTF}_f(\nu) \cdot \text{MTF}_m(\nu) \quad (3.2.2)$$

Mathematically speaking, the  $\text{MTF}_x$  is optimized by first optimizing the  $\text{MTF}_a$  for a given object position by varying the source size. The optimum size depends on the object position and so does the  $\text{MTF}_r$ . So the next step is to optimize  $\text{MTF}_x$  by varying the object position.

#### 3.2.1 Shadow image MTF, focal-spot choice

To optimize the shadow image  $\text{MTF}_a$ , analytical expressions are needed for its constituent terms, i.e.  $\text{MTF}_f$  and  $\text{MTF}_m$ . Fortunately, both MTFs can be approximated by a  $\sin(x)/x$  function. In other words, the corresponding line spread functions (LSF) can be approximated by rectangular distributions.

### X-ray source MTF

The X-ray source is the focal spot of a rotating anode X-ray tube. The cathode-anode configuration of the tube is given in figures 3.2.1a and 3.2.1b. The number of revolutions per second is  $n$ , and  $\bar{r}$  is the mean focal track radius. A line focus is projected on the anode by the electrons emitted by a helix of tungsten wire,

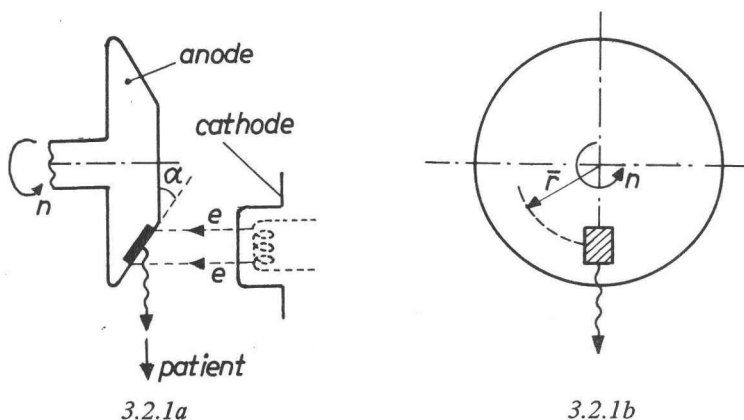


Fig. 3.2.1.

*Anode-cathode configuration of a rotating anode X-ray tube.*

placed in a slot which serves as an electronic lens system. The focus is optically seen as — more or less — a square with a typical intensity distribution: a 'camel-back' in the anode-tangential direction, a bell-shaped distribution in the direction of the radius. So the MTF of the focal spot is non-isotropic. The use of a line focus and the corresponding anode angle  $\alpha$  implies further that the MTF is also anaplanatic. We will investigate, however, the imaging of small, isolated objects so that the influence of the anaplasia will be small. The central ray of the X-ray beam will be considered, i.e. the line perpendicular to the centre of the image receptor, because this corresponds to an important region in many applications. In any case, the theories to be developed can fairly easily be extended to other directions.

As regards the anisotropy, we will investigate the worst case condition, i.e. the camel-back distribution direction. This is also the interesting situation if other focal-spot intensity distributions are to be dealt with. This will be done in sec. 3.4. This analysis can in principle also be applied to the focal-spot optimization in any other direction.

Owing to the fact that an intensity distribution is concerned, it is not easy to



characterize a focus by its width. To solve this problem we introduce an 'effective focus width'  $f$ . Its value is defined as the width of a homogeneous intensity distribution, with more or less the same modulation transfer function as the real focus. The MTF of such an effective focus has a  $\sin(x)/x$  shape:

$$\text{MTF}_f(\nu) = \left| \frac{\sin(\pi\nu f)}{\pi\nu f} \right| \quad (3.2.3)$$

where  $\nu$  is the spatial frequency in the focus plane.

Comparison of this  $\sin(x)/x$  function with real MTFs (fig. 3.2.2) shows that an approximation is reasonable for frequencies smaller than and including the first zero modulation transfer frequency. The situation for higher frequencies is not so important, as the generally known rule that 'for an optimum, errors must be of the same order of magnitude' will prove to hold in this situation. Beyond that frequency, then, the combination of  $\text{MTF}_m$  and  $\text{MTF}_f$  gives only small (a few percent) modulation. This small modulation has even less effect if the image receptor MTF is also taken into account.

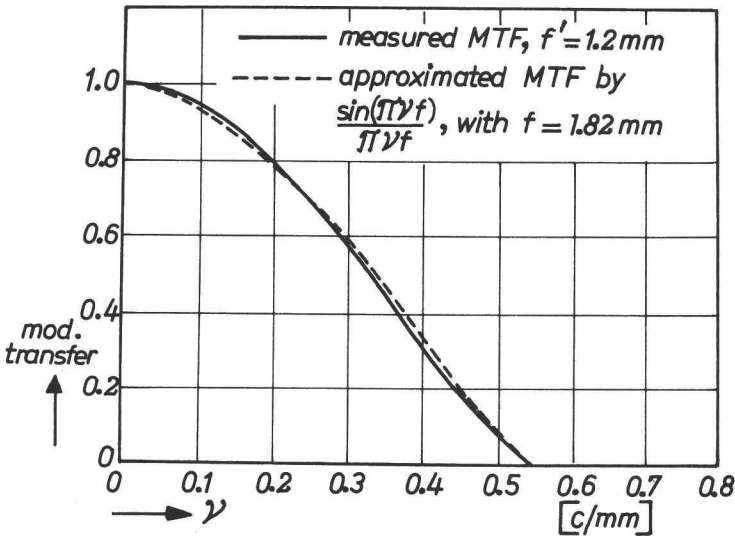


Fig. 3.2.2.

Measured (Timmer, 1972) and approximated (this work) MTF for commercially available 1.2 mm focus, 'camel-back' distribution

The work of Rao and Bates (1970) also indicates that such an approximation is allowed. This is confirmed for the Philips' foci with a nominal size, denoted by  $f'$ , equal to 0.3, 0.6, 1.2 and 1.5 mm. A typical example is given in fig. 3.2.2 for the

1.2 mm focus. It turns out that the effective width is about 1.5 times as large as the nominal width:

$$f \approx 1.5 f' \quad (3.2.4)$$

Due to geometrical considerations, the corresponding unsharpness in the object plane is smaller than the effective focal-spot size just defined. The reduction factor is  $or/fr$  (fig. 3.2.3), where  $or$  is the object-to-image receptor distance, and  $fr$  is the focal spot-to-image receptor distance. For  $MTF_f$  we can thus write:

$$MTF_f(\nu) = \left| \frac{\sin(\pi \nu f \cdot \frac{or}{fr})}{\pi \nu f \cdot \frac{or}{fr}} \right| \quad (3.2.5)$$

where  $\nu$  is the spatial frequency in the object plane.

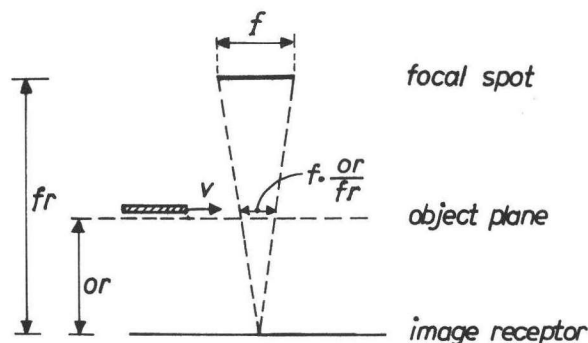


Fig. 3.2.3.  
X-ray system geometry

### Movement MTF

In fig. 3.2.3, a moving edge is drawn with a time-dependent velocity  $v$ . It will be shown below that the imaging of such an object can be regarded as linear, which means that an MTF exists. The object velocity has either a small or a large, relatively constant, value: during the filling of the organ the velocity is low for a comparatively long time, for a short time the organ is emptied with high velocity. Preliminary calculations show that in general the exposure time is so short ( $< 0.1$  sec.) that  $v$  and the X-ray production per unit time can be assumed constant. (This latter point has to do with typical X-ray tube properties.)

The movement MTF can thus be written as:

$$\text{MTF}_m(\nu) = \left| \frac{\sin(\pi\nu v \cdot t)}{\pi\nu v \cdot t} \right| \quad (3.2.6)$$

where  $t$  is the exposure time.

The exposure time can be expressed in terms of the focal spot size  $f$ . The exposure time equals the ratio of the required energy per exposure and the short-time loadability  $P$  (unit kW) of the tube. The required energy equals the product of the milliamperere-seconds product (mAs product) denoted by  $Q$  and the high voltage  $U$  (unit kV) on the tube.

These values per object to be imaged are given in so-called exposure tables for a given focus-to-image receptor distance. These reference data will be denoted by the subscript  $p$  (from 'patient'). The  $Q$  value can be calculated for any other  $f$  value from the inverse square law. The short-time ( $t \leq 0.1$  s) loadability  $P$  is in general given by:

$$P = c_{th} \cdot \frac{f^{1.5} \sqrt{2\pi\tau \cdot n}}{\sin \alpha} \quad (3.2.7)$$

where  $c_{th}$  (unit kW/mm<sup>2</sup>) is a characteristic parameter of the anode material and focus intensity distribution. The proportionality with  $f^{1.5}$  is typical of rotating anode tubes, as has been deduced by Oosterkamp (1939). It stems from the fact that a limit is set to the temperature rise of the anode after its passage through the electron beam. The temperature rise is approximately proportional to the square root of the time spent in heating, i.e. inversely proportional to  $f^{0.5} (2\pi\tau \cdot n)^{0.5}$ . The proportionality with the radial length of the focus is further expressed by the factor  $f/\sin\alpha$ . Both the establishment of a relationship as mentioned and the choice of the value of  $c_{th}$  can be discussed because (i) subjective criteria are involved (the maximum temperature rise influences the *expected* lifetime of the X-ray tube) and (ii) for small focal spots ( $\leq 0.3$  mm) the relationship for the temperature rise no longer holds, as lateral diffusion of heat is no longer negligible. We shall nevertheless use the relationship mentioned, to be in line with the X-ray tube manufacturer (Möller, 1973). If practical, small focal spots are included as well, the loadability is predicted within 10%; this deviation is not excessive in view of the other uncertainties involved. The same holds for experimental errors (especially for the psychophysical experiments). Furthermore, although we shall have to deal with large *ranges* of parameter values, only two focal spots are applicable per X-ray tube.

In this section only the focal-spot size is varied, and therefore eq. 3.2.7 can be simplified by introducing the characteristic X-ray tube parameter  $c_f$  (unit kW/mm<sup>3/2</sup>):

$$P = c_f \cdot f^{1.5} \quad (3.2.8)$$

For the product  $v \cdot t$  we can thus write:

$$v \cdot t = v \cdot \frac{Q_p \cdot U_p \cdot (fr/fr_p)^2}{c_f \cdot f^{1.5}} \quad (3.2.9)$$

The parameters  $v$ ,  $Q_p$ ,  $U_p$  and  $fr_p$  serve as patient characteristic parameters. Their influence can conveniently be described by introducing the number  $c_{p,m}$  (unit kW/mm):

$$c_{p,m} = \frac{v \cdot Q_p \cdot U_p}{fr_p^2} \quad (3.2.10)$$

The ratio of  $c_{p,m}$  and  $c_f$  characterizes the intrinsic absorption image properties for the application concerned. This ratio is therefore denoted by  $c_{a,m}$  (unit  $\text{mm}^{1/2}$ ), and the product  $v \cdot t$  is thus given by

$$v \cdot t = c_{a,m} \cdot \frac{fr^2}{f^{1.5}} \quad (3.2.11)$$

#### Shadow image MTF

Combination of eqs. 3.2.5, 3.2.6 and 3.2.11 now gives the shadow image MTF. The resulting equations can be greatly simplified by introducing the parameters  $u_f$  and  $u_m$  for the effective focal-spot size and the translation of the object:

$$u_f = f \cdot \frac{\text{or}}{fr} \quad (3.2.12)$$

$$u_m = c_{a,m} \cdot \frac{fr^2}{f^{1.5}} \quad (3.2.13)$$

These might be called 'unsharpness factors' in the old-fashioned sense. For  $\text{MTF}_a$  we can now write

$$\text{MTF}_a(\nu) = \left| \frac{\sin(\pi\nu u_f)}{\pi\nu u_f} \cdot \frac{\sin(\pi\nu u_m)}{\pi\nu u_m} \right| \quad (3.2.14)$$

The maximization of  $\nu_{a,z}$  (fig. 3.2.4), the spatial frequency for a modulation transfer  $z$  of the absorption image MTF, will now be carried out with three different methods (sections 3.2.1.1, 3.2.1.2): (i) analytically, to obtain insight into the

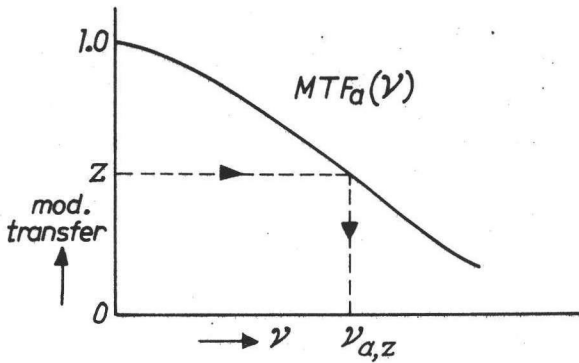


Fig. 3.2.4.  
Definition of  $v_{a,z}$

problem; (ii) by means of a computer program to derive the exact solution; and (iii) by calculating the LSFs to correlate the result with images.

### 3.2.1.1. Maximization of the modulation transfer

The dependence of the spatial frequency for a modulation  $z$  on the focal spot size is implicitly given by eq. 3.2.14. Further simplification of this expression is needed to solve the problem analytically. This simplification is obtained by describing the  $\sin(x)/x$  function by a parabola and a straight line (fig. 3.2.5):

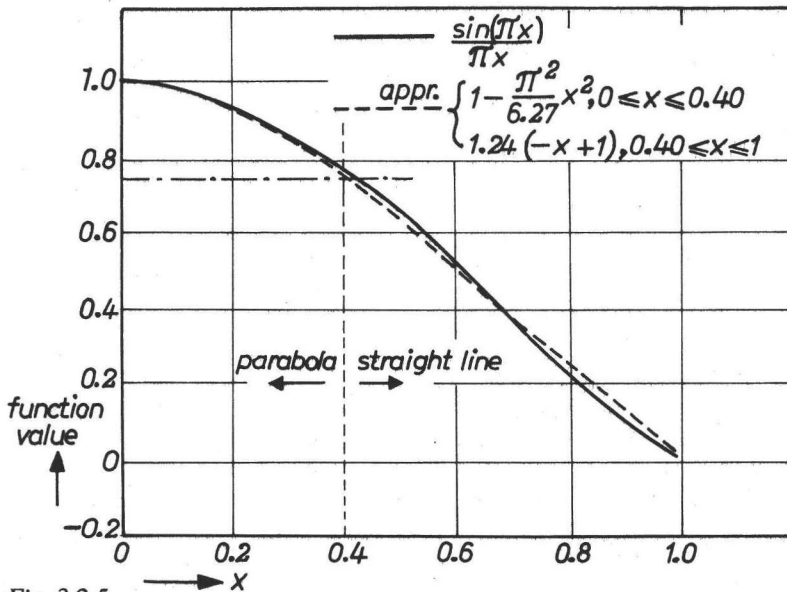


Fig. 3.2.5.  
Approximation of  $\sin(\pi x)/(\pi x)$  by polynomials.

$$\frac{\sin(\pi x)}{\pi x} \approx 1 - \frac{\pi^2}{6.27} x^2, \quad 0 \leq x \leq 0.4 \quad (3.2.15)$$

$$\frac{\sin(\pi x)}{\pi x} \approx 1.24(1 - x), \quad 0.4 \leq x \leq 1 \quad (3.2.16)$$

The parabolic approximation has already been applied by Albrecht and Oosterkamp (1962).

Parabolic region.

For the appropriate spatial frequency range, eq. 3.2.14 reads

$$\text{MTF}_a(\nu) \approx \left(1 - \frac{\pi^2}{6.27} \nu^2 u_f^2\right) \cdot \left(1 - \frac{\pi^2}{6.27} \nu^2 u_m^2\right) \quad (3.2.17)$$

As both  $\nu \cdot u_f$  and  $\nu \cdot u_m$  are smaller than 0.4, the value of  $\nu_{a,z}$  can be approximated by

$$\nu_{a,z} \approx \sqrt{\frac{6.27}{\pi^2}} \cdot \sqrt{1-z} \cdot \frac{1}{\sqrt{u_f^2 + u_m^2}} \quad (3.2.18)$$

The value of  $\nu_{a,z}$  can thus be maximized by minimizing the sum of the unsharpness factors squared. This approach is analogous to former analyses, as discussed in sec. 3.1 under the heading 'Unsharpness', re. (ii). Substitution of the appropriate values of  $u_f$  and  $u_m$  (eqs. 3.2.12 and 3.2.13) and variation of the focal-spot size gives the following optimum size  $f_{\text{opt}}$ :

$$f_{\text{opt}} = 1.08 \frac{c_{a,m}^{2/s} \cdot fr^{6/s}}{or^{2/s}} \quad (3.2.19)$$

The corresponding maximum value of  $\nu_{a,z}$  reads:

$$\nu_{a,z|\text{max}} = 0.59 \sqrt{1-z} \cdot \frac{1}{c_{a,m}^{2/s} \cdot fr^{1/s} \cdot or^{3/s}} \quad (3.2.20)$$

In this optimum situation  $u_f$  is 1.22 times as large as  $u_m$ , so that they are indeed 'of the same order of magnitude'.

Straight line region.

For this spatial frequency range, eq. 3.2.14 reads:

$$\text{MTF}_a(\nu) \approx 1.24^2 (1 - \nu \cdot u_f) \cdot (1 - \nu \cdot u_m) \quad (3.2.21)$$

For  $\nu_{a,z}$  it therefore holds that:

$$u_f \cdot u_m \cdot \nu_{a,z}^2 - (u_f + u_m) \nu_{a,z} + \left(1 - \frac{z}{1.52}\right) \approx 0 \quad (3.2.22)$$

This quadratic equation has two roots, of which only the smaller root is of interest. Consequently we have

$$\nu_{a,z} = \frac{u_f + u_m - \sqrt{(u_f + u_m)^2 - 4 \left(1 - \frac{z}{1.52}\right) u_f \cdot u_m}}{2 u_f \cdot u_m} \quad (3.2.23)$$

This frequency must be maximized by varying the focal-spot size. This must be done with the aid of a computer, except if  $z$  equals zero. For zero modulation depth the worse MTF is decisive, implying equal MTFs for the optimum condition.

The analysis is facilitated by the introduction of the balance factor  $b_a$  between  $u_f$  and  $u_m$ :

$$b_a = \frac{u_f}{u_m} \quad (3.2.24)$$

The focal-spot size variation can now also be expressed in a variation of the balance factor. For  $u_f$  and  $u_m$  (substitute eq. 3.2.12 and eq. 3.2.13 into eq. 3.2.24, and substitute the focus size as a function of  $b_a$  into eqs. 3.2.12 and 3.2.13) we can therefore write:

$$u_f = c_{a,m}^{2/5} \cdot fr^{1/5} \cdot or^{3/5} \cdot b_a^{2/5} \quad (3.2.25)$$

$$u_m = c_{a,m}^{2/5} \cdot fr^{1/5} \cdot or^{3/5} \cdot b_a^{-3/5} \quad (3.2.26)$$

These values can be substituted into eq. 3.2.23, resulting in

$$\nu_{a,z} = \frac{1}{c_{a,m}^{2/5} \cdot fr^{1/5} \cdot or^{3/5}} \cdot \left\{ \frac{1}{2} b_a^{1/5} (b_a^{2/5} + b_a^{-3/5} - \sqrt{(b_a^{2/5} + b_a^{-3/5})^2 - 4 \left(1 - \frac{z}{1.52}\right) b_a^{-1/5}}) \right\} \quad (3.2.27)$$

As the term between braces depends only on  $z$ , the same analytic structure as for the parabolic region (eq. 3.2.20) is obtained.

The optimum value of the balance factor  $b_a$  is given in fig. 3.2.6, for the whole range of modulation transfer ratios  $z$ . These values are obtained by means of a numerical solution of the exact expression 3.2.14. In the parabolic region  $b_a$  indeed equals 1.22, whereas in the straight-line region the difference with the solution according to eq. 3.2.27 can hardly be made visible. Our  $\sin(x)/x$  approximation is therefore allowed. Fig. 3.2.6 shows that the unsharpness factors are indeed of the same order of magnitude.

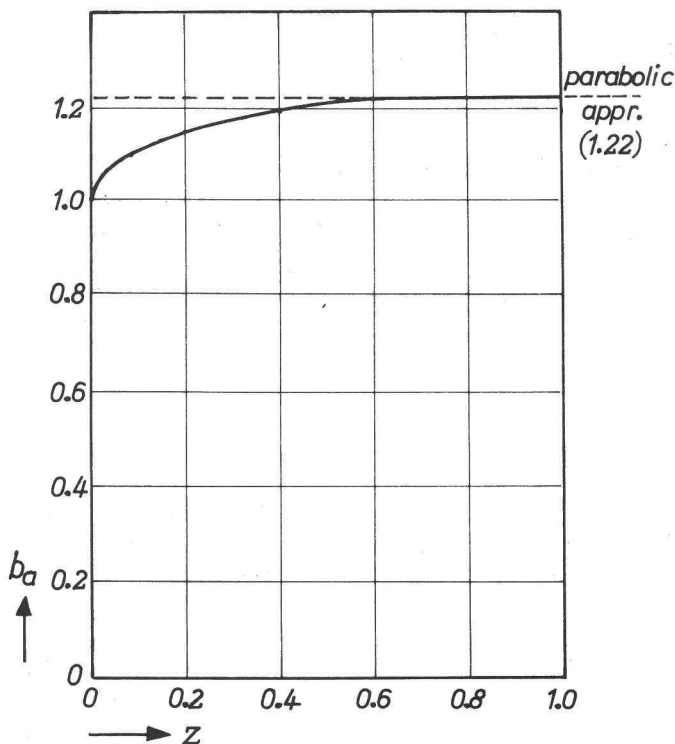


Fig. 3.2.6.

Optimum shadow image balance factor  $b_a$  as a function of the modulation transfer  $z$ .

### Conclusion

The maximum spatial frequency for a given modulation transfer,  $\nu_{a,z|\max}$ , apparently depends on the product  $c_{a,m}^{2/5} \cdot fr^{1/5} \cdot or^{3/5}$  (eqs. 3.2.20 and 3.2.27) and on  $z$ . The dependence on  $z$  can be described by the function  $f(z)$ , depicted in fig. 3.2.7 and implicitly given by

$$\nu_{a,z|\max} = f(z) \cdot \frac{1}{c_{a,m}^{2/5} \cdot fr^{1/5} \cdot or^{3/5}} \quad (3.2.28)$$



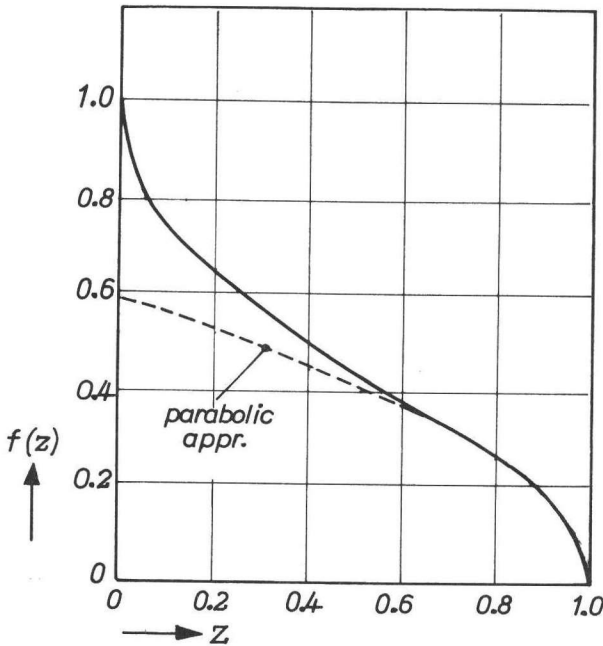


Fig. 3.2.7.  
The proportionality factor  $f(z)$ .

For the parabolic region,  $f(z) = 0.59 \sqrt{1-z}$  (eq. 3.2.20). For the straight line region eq. 3.2.27 must be applied with the optimum value of  $b_a$ . This maximum frequency is obtained with a focal-spot size which is also dependent on  $z$ :

$$f_{\text{opt}} = b_a^{2/5}(z)|_{\text{opt}} \cdot \frac{c_{a,m}^{2/5} \cdot f_r^{6/5}}{o r^{2/5}} \quad (3.2.29)$$

The modulation transfer is thus involved as well, which implies the optimization of the focal-spot size in relation to patient properties like object frequency-spectra and contrasts. To circumvent the inherent problems, we will investigate whether the modulation dependence can be cancelled by choosing just one  $b_a$  value. To achieve this, insight into the smoothness of the optima is desired. This is obtained by calculating  $\nu_{a,z}$  for non-optimum conditions. The results are given in fig. 3.2.8 for  $z$  equal to 0, 0.2, 0.6 and 0.8, as a function of  $b_f$ . This is the ratio between the actual and the optimum focal-spot size for  $z = 0$ . It is clear that for the parabolic region the maximum  $\nu$  is reached with a larger optimum focus.

Further, it can be seen that both for too great and too small focus sizes  $\nu$  is smaller, due to too much geometrical blurring or too much movement blurring, as the case may be. Concerning the smoothness of the optima, it can be stated that the optimum is smoother the greater the value of  $z$ . This is more distinctly shown in

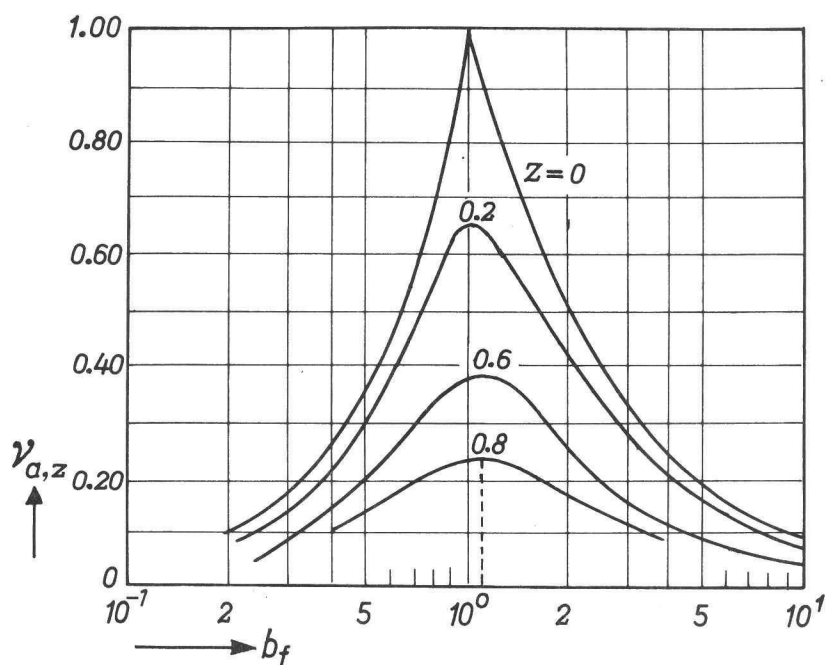


Fig. 3.2.8. The influence of the non-optimum focus size on the spatial frequency for modulation transfer  $z$ .

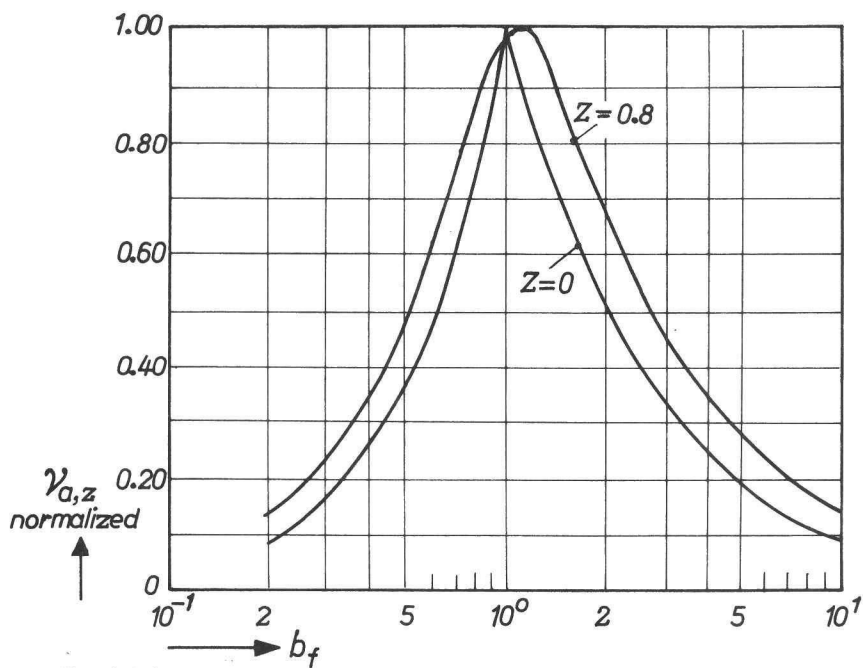


Fig. 3.2.9  
Smoothness of the optima of  $v_{a,z}$ , for large and small  $z$

fig. 3.2.9, where the frequencies are normalized to the maximum frequency for the value of  $z$  concerned, for  $z = 0$  and  $z = 0.8$ . We conclude, then, that the modulation transfer dependence can practically be cancelled by optimizing the focal spot size for the most critical situation, i.e. for zero modulation transfer. This criterion leads to only small deviations in  $\nu_{a,z}$  if  $z \neq 0$  ( $\approx 1\%$  if  $z = 0.8$ ). Because the proportionality factor  $f(z)$  is hardly influenced by this choice, the following set of equations describes the optimum conditions:

$$\nu_{a,z|opt} = f(z) \cdot \frac{1}{c_{a,m}^{2/5} \cdot fr^{1/5} \cdot or^{3/5}} \quad (3.2.30)$$

$$f_{opt} = \frac{c_{a,m}^{2/5} \cdot fr^{6/5}}{or^{2/5}} \quad (3.2.31)$$

corresponding to  $b_a = 1$  or  $u_f = u_m$ . The resulting  $MTF_a$  has a  $\sin(x)/x$ -squared shape. Instead of  $\nu_{a,z|max}$  the name  $\nu_{a,z|opt}$  is used because, strictly speaking, the maximum value is not represented by eq. 3.2.30. For convenience,  $\nu_{a,z|opt}$  will be called in the following  $\nu_{opt}$ . With respect to the parameters of the equation, the following can be said:

- (i) The influence of the focus-to-image receptor distance on the  $MTF_a$  quality is small. A large distance need not therefore be detrimental, although a much larger focal-spot size and loadability is required.
- (ii) The influence of the object-to-image receptor distance is relatively large; a small distance is advantageous. A correspondingly larger focal-spot size must be chosen.

In the limit, the object should be placed on the image receptor but this is of course not practicable. Eq. 3.2.30 predicts then that the  $MTF_a$  is unity, which is obtained by an infinite focal-spot size (eq. 3.2.31): both the  $u_f$  and the  $u_m$  are indeed zero.

- (iii) As regards the absorption-image characteristic parameter: a smaller  $c_{a,m}$  value favourably influences the  $MTF_a$  quality and tube loadability. With respect to the factors which build up  $c_{a,m}$  we note (a) that the influence of the focal track speed is small (power  $1/5$ ), (b) that the weight of the anode angle is larger (power  $2/5$ ), and (c) that the weight of the  $Q$  value also corresponds to a power  $2/5$ .

### 3.2.1.2 Maximization of the peak contrast gradient

A practical way to assess the effect of the choice of the focal-spot size is to investigate the corresponding images. In each image the whole spatial frequency spectrum is involved so we expect a smoothing out of the effect, if any.

The practical image chosen is the edge. The edge image quality is closely related to the maximum contrast gradient, as has been shown in our research on the visibility of edges. This maximum gradient is directly proportional to the peak contrast of the line spread function (the LSF can be regarded as the derivative of the ESF). It therefore suffices to calculate this peak contrast.

In general terms, the LSF intensity is given by

$$\text{LSF}(x) = \int_{-\infty}^{+\infty} \text{OTF}(\nu) \cdot e^{2\pi j\nu x} d\nu \quad (3.2.32)$$

where  $\text{OTF}(\nu)$  is the optical transfer function, and  $x$  denotes the distance. The OTF can be written as

$$\text{OTF}(\nu) = \text{MTF}(\nu) \cdot e^{j \cdot \varphi(\nu)} \quad (3.2.33)$$

where  $\varphi(\nu)$  represents the phase transfer function. The LSF is real, so it holds that

$$\text{OTF}(\nu) = \text{OTF}(-\nu)^* \quad (3.2.34)$$

Hence, the  $\text{LSF}(x)$  can be written as

$$\text{LSF}(x) = 2 \int_0^{\infty} \text{MTF}(\nu) \cdot \cos(2\pi\nu x + \varphi(\nu)) d\nu \quad (3.2.35)$$

Equation 3.2.35 is used to maximize the contrast of the LSF corresponding to the shadow image OTF (cf. eq. 3.2.14). This maximization is carried out by varying the focus size by the factor  $b_f$ , so that

$$u_f \sim b_f \quad (3.2.36a)$$

and

$$u_m \sim b_f^{-3/2} \quad (3.2.36b)$$

As the shape of the LSF indicates that the maximum contrast will be found at  $x = 0$ , the maximum contrast gradient of the edge image is proportional to  $\text{LSF}_a(0)$ :

$$\text{LSF}_a(0) = 2 \int_0^{\infty} \frac{\sin(\pi\nu b_f)}{\pi\nu b_f} \cdot \frac{\sin(\pi\nu b_f^{-3/2})}{\pi\nu b_f^{-3/2}} d\nu \quad (3.2.37)$$

The normalized  $LSF_a(o)$  value is given in fig. 3.2.10 as a function of  $b_f$ . The maximum is indeed found for  $b_f$  about unity, i.e. the distortion factors  $u_f$  and  $u_m$  are about equal. (In fact, the best value of  $b_f$  is so close to unity that it cannot be indicated in the figure).

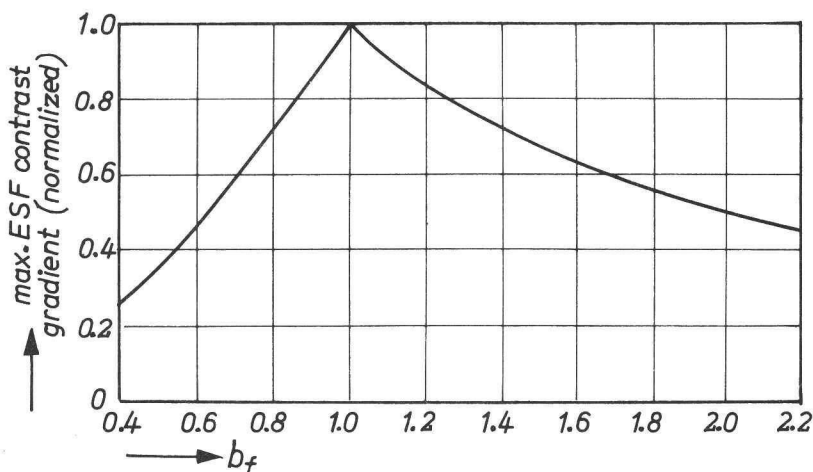


Fig. 3.2.10.

*Influence of the non-optimum focus size on the maximum ESF contrast gradient.*

The figure shows again that a too large focal spot is less detrimental than a too small one. This corresponds to the relatively large influence of the focal-spot size on the movement unsharpness.

### 3.2.2 Choice of the geometric magnification, influence of the image receptor MTF

The divergence of the X-ray beam indicates that the objects are depicted enlarged on the image receptor input screen. This reduces the influence of the unsharpness of the image receptor. Translated to the object plane, the image receptor MTF is correspondingly better. Mathematically, a scaling of the frequency axis is applied with the factor  $M_g$ , the geometric magnification factor. Its value ranges between unity and infinity (object close to the image receptor or close to the focal spot), which is not a convenient range for calculations. Furthermore an indication of the corresponding object position is not directly obtained. To circumvent these problems, the normalized object position characterizer  $\eta$  is introduced. Its value equals  $o/fr$ , so it ranges between zero and unity. The magnification is given by

$$M_g = \frac{1}{1 - \eta} \quad (3.2.38)$$

As the variation of  $\eta$  has antagonistic effects on the shadow image and image receptor MTF, the problem now is to optimize  $MTF_x$ :

$$MTF_x(\nu) = MTF_a(\nu) \cdot MTF_r(\nu) \quad (3.2.39)$$

The optimum focus size will be chosen for every  $\eta$ ; the  $MTF_a$  is then implicitly given by eq. 3.2.30.

### 3.2.2.1 Mathematical formulation

To arrive at a convenient analytical expression for  $MTF_x$ , the image receptor MTF should also be described mathematically. An exponentially shaped MTF will be chosen because the present day MTFs are reasonably described then, as has been verified by e.g. Harms and Zeilinger (1977) and Rao and Fatouros (1978). The corresponding LSF has the Lorentzian shape (Johnson, 1973), i.e.  $LSF(x) \approx 1/(1+c \cdot x^2)$ .

Later on it will be shown that the shape of the MTF is of minor importance as far as the optimization of the object position is concerned. The  $MTF_r$  is thus sufficiently characterized by any reasonable combination of the spatial frequency and the modulation transfer. We shall choose the modulation transfer 0.5, because the measurement of the MTF in this range is relatively simple. Further, the MTF is approximated best by a fitting in the mid-frequency range. The corresponding spatial frequency is formally written as  $\nu_{r,z=0.5}^r$ ; the superscript denotes that the receptor plane is chosen, the subscripts denote that the image receptor is involved and that the modulation transfer equals 0.5. For convenience, the term  $\nu_{rec}$  will be used as the characteristic parameter of the intrinsic resolution.

The  $MTF_a$  in the optimum situation is given by a  $\sin(x)/x$ -squared function, so that we can write

$$MTF_x(\nu) = e^{-\frac{0.693(1-\eta)}{\nu_{rec}} \cdot \nu} \cdot \left| \frac{\sin(\pi \nu u_f)}{\pi \nu u_f} \right|^2 \quad (3.2.40)$$

The  $u_f$  value can also be expressed in terms of  $\eta$ , by substituting  $\eta$  into eq. 3.2.25, and stating that  $b_a$  equals unity for the optimum. The  $MTF_x$  then reads

$$MTF_x(\nu) = e^{-\frac{0.693(1-\eta)}{\nu_{rec}} \cdot \nu} \cdot \left| \frac{\sin(\pi \nu c_{a,m}^{2/5} \cdot fr^{4/5} \cdot \eta^{3/5})}{\pi \nu c_{a,m}^{2/5} \cdot fr^{4/5} \cdot \eta^{3/5}} \right|^2 \quad (3.2.41)$$

Further simplification is apparently needed to obtain insight into the problem. We achieve this by describing  $MTF_X(\nu)$  in terms of the balance between  $MTF_r$  and  $MTF_a$ , instead of in terms of their absolute values. When this is done the terms  $\nu_{rec}$ ,  $c_{a,m}$  and  $fr$  are brought together into a new, dimensionless X-ray system characteristic parameter  $c_{x,m}$  ('m' stands for moving objects). To this end the object position  $\eta_{x,m}$  is defined, for which the  $MTF_a$  and  $MTF_r$  coincide at a modulation 0.5 (fig. 3.2.11).

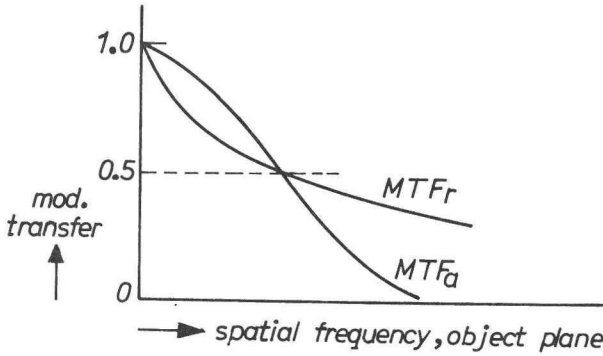


Fig. 3.2.11.

Definition of the  $\eta_{x,m}$  condition.

The value 0.5 is chosen just for convenience, although one might argue that the two MTFs indeed balance. Therefore the  $\eta_{x,m}$  condition will also be denoted as 'the equality of MTFs' condition.

The  $\eta_{x,m}$  value is uniquely defined by  $c_{x,m}$ , as follows.

For the  $\eta_{x,m}$  condition we may write

$$\nu_{opt,z=0.5} = \frac{\nu_{rec}}{1 - \eta_{x,m}} \quad (3.2.42)$$

According to the definition of  $\eta_{x,m}$ , we have

$$\frac{1 - \eta_{x,m}}{\eta_{x,m}^{3/5}} = \frac{c_{a,m}^{2/5} \cdot fr^{4/5} \cdot \nu_{rec}}{0.442} \quad (3.2.43)$$

The right-hand side of eq. 3.2.43 is replaced by  $c_{x,m}$ , so by definition

$$c_{x,m} = \frac{c_{a,m}^{2/5} \cdot fr^{4/5} \cdot \nu_{rec}}{0.442} \quad (3.2.44)$$

All the relevant X-ray system data are combined in this dimensionless parameter  $c_{x,m}$ , i.e. object data, X-ray tube data, geometry data and image receptor data. The object-to-image receptor distance is of course not involved.

All the information contained in  $c_{x,m}$  is also present in the  $\eta_{x,m}$  parameter, via eq. 3.2.43. The value of  $\eta_{x,m}$  is given in relation to the  $c_{x,m}$  value in fig. 3.2.12. The larger  $c_{x,m}$ , the smaller  $\eta_{x,m}$ . This can be understood by considering the factors determining  $c_{x,m}$ , and their influence on the  $MTF_a$  and  $MTF_r$ . For example, a large  $c_{a,m}$  corresponds to a relatively poor  $MTF_a$ . A large  $\nu_{rec}$  corresponds to a relatively good  $MTF_r$ . For both conditions the magnification must indeed be relatively small to achieve equality of the two MTFs.

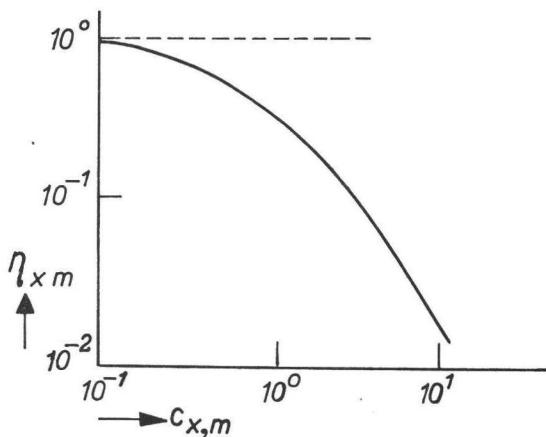


Fig. 3.2.12.

Object position for equality of  $MTF_a$  and  $MTF_r$  as a function of  $c_{x,m}$

Equation 3.2.41 can now be written in a normalized form with respect to frequency. The shape of  $MTF_x$  is then given by

$$e^{-\frac{1-\eta}{1-\eta_{x,m}} \cdot \nu} \cdot \left| \frac{\sin\left(\frac{0.442}{0.693} \pi \left(\frac{\eta}{\eta_{x,m}}\right)^{3/5} \nu\right)}{\frac{0.442}{0.693} \pi \left(\frac{\eta}{\eta_{x,m}}\right)^{3/5} \nu} \right|^2 \quad (3.2.45)$$

In the derivation of  $c_{x,m}$  it is a prerequisite that its terms are independent on the object-to-image receptor distance. This is not completely true for the Q value contained in the parameter  $c_{a,m}$ . This value depends on the effective intensity of scattered radiation (see sec. 4.1), which is smaller the larger the value of  $\nu$ . The effect is negligible if an anti-scatter grid is used — which has been the case in the calculations so far. If it is not used, then the discussion in Appendix IV shows that the main conclusions of this section remain valid.



### 3.2.2.2 Influence of the object-to-image receptor distance

The antagonistic influence of  $\eta$  is mathematically expressed as the application of a scaling factor to the appropriate  $\nu$ -axis. The scaling factor (fig. 3.2.13) is  $1/\eta^{3/5}$  for  $MTF_a$  and  $1/(1-\eta)$  for  $MTF_r$ .

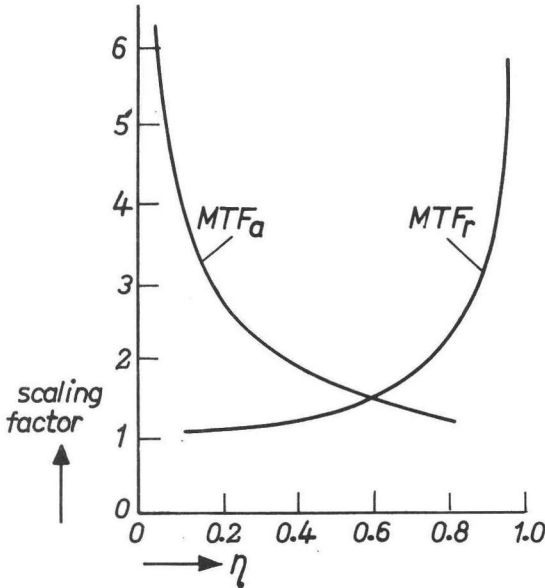


Fig. 3.2.13.

*Spatial frequency-axis scaling factor as a function of the object position.*

As a first attempt, and bearing the equality law of unsharpnesses in mind, the optimum  $\eta$  value might correspond to the  $\eta_{x,m}$  value defined before. By varying  $\eta$ , with  $\eta_{x,m}$  as starting value, we can conclude whether the equality situation is best.

If another  $\eta$  is chosen, then the system MTF will change in accordance with the changes of its two constituents, i.e.  $MTF_a$  and  $MTF_r$ . An insight into the influence of these changes can be obtained by considering the gradient of the curves giving the scaling factor of the frequency axis as a function of the ratio  $\eta$ , with  $\eta_{x,m}$  as starting point. For ratios larger than  $\approx 0.6$ , the gradient for the image receptor situation is large compared with that for the shadow image MTF. The reverse is true if  $\eta$  is smaller than  $\approx 0.4$ . For values in between, the gradients are more or less balanced. Thus, if the starting value  $\eta_{x,m}$  is large, a still larger ratio  $\eta$  gives a better  $MTF_r$ , and has a relatively small influence on  $MTF_a$ . The geometric magnification should therefore be as large as possible for the best system MTF. The reverse holds

if  $\eta_{x,m}$  is small. There is of course an intermediate range of  $\eta_{x,m}$  for which the influences of changes of  $MTF_r$  and  $MTF_d$  more or less cancel out.

These expectations materialize in the corresponding system MTFs. In figs. 3.2.14, 3.2.15, 3.2.16 and 3.2.17 system MTFs are plotted with  $\eta$  as parameter, for a small (0.2), medium (0.4, 0.525) and a large (0.7)  $\eta_{x,m}$  value. For certain ranges of  $\eta_{x,m}$  the equality law for the unsharpness does not hold: the smallest  $\eta$  is best for the small  $\eta_{x,m}$  value, whereas the largest value is best for the large value of  $\eta_{x,m}$ .

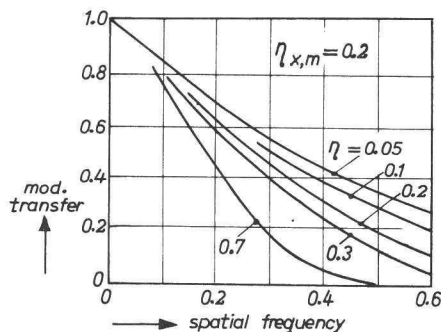


Fig. 3.2.14

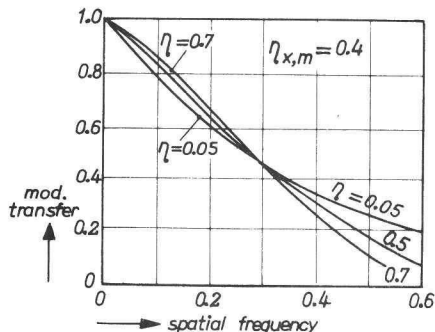


Fig. 3.2.15

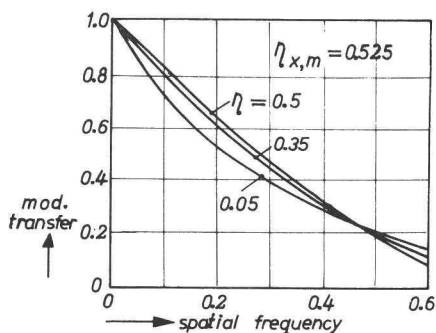


Fig. 3.2.16

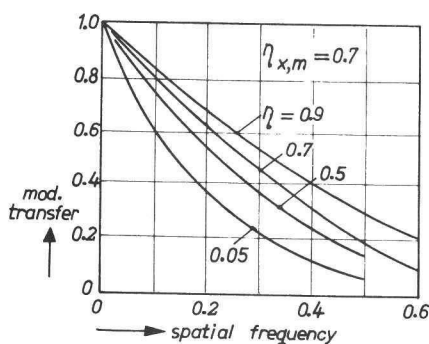


Fig. 3.2.17

Fig. 3.2.14 – 3.2.17.

System MTF with  $\eta$  as parameter,  $\eta_{x,m}$  equal to 0.2, 0.4, 0.525 and 0.7.

This holds for all spatial frequencies, so any object will indeed be imaged sharper if the smaller or the larger  $\eta$  value, as the case may be, is chosen. For the intermediate value of  $\eta_{x,m}$  no such simple conclusion can be drawn. The shape of the  $MTF_x$  changes with  $\eta$  in such a way that it depends on the spatial frequency region whether the modulation transfer will be better or not. There would be no problem, of course, if a sinusoidal grating were imaged. But this is not the case, so we should

resort to the image which corresponds to the MTF under investigation. In this way the effects of different MTFs are visualized, so that a direct correlation with practice is obtained.

As outlined already in sec. 3.2.1.2, the corresponding line spread functions give relevant information, as their peak contrast is directly proportional to the maximum contrast gradient of the edge image. The LSF as such is also relevant. It corresponds to the image of small, long structures (e.g. a blood vessel), so apart from the peak contrast, two other criteria should be taken into account: (i) the contrast gradient of the LSF should be high so as to favour its visibility, (ii) its spatial extension should be small to resolve closely packed structures. Due to physical reasons these criteria are favourably correlated in the sense that a high peak value generally corresponds to a large gradient and to a small spatial extension.

The LSFs corresponding to the MTFs of figures 3.2.14 – 3.2.17 are given in figures 3.2.18 – 3.2.21. The analysis proceeds as follows:

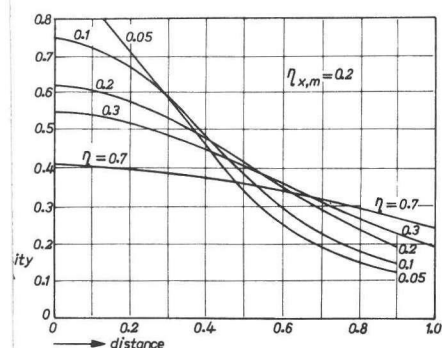


Fig. 3.2.18

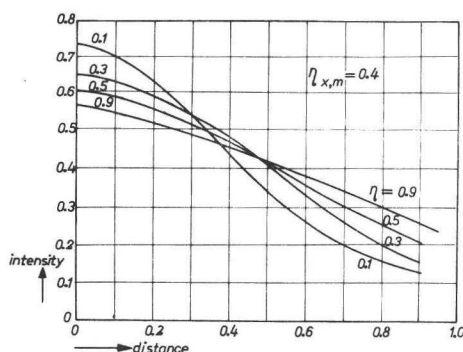


Fig. 3.2.19

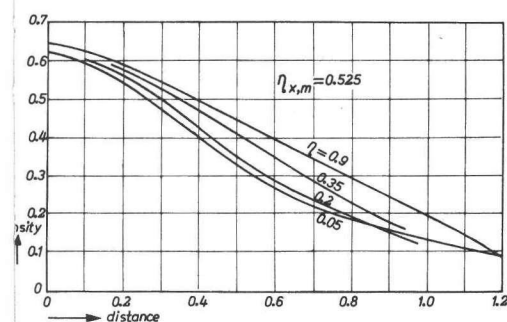


Fig. 3.2.20

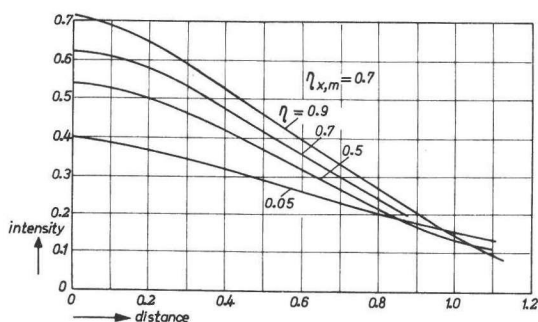


Fig. 3.2.21

Fig. 3.2.18 – 3.2.21.

System LSF with  $\eta$  as parameter,  $\eta_{x,m}$  equal to 0.2, 0.4, 0.525 and 0.7.

- $\eta_{x,m} = 0.2$  : The MTFs indicate that  $\eta$  should be as small as possible. This conclusion is also valid for the LSFs: the LSF has a larger peak value and gradient for smaller  $\eta$ .
- $\eta_{x,m} = 0.4$  : Investigation of the MTFs gives no definite answer. On the basis of the LSFs, however, we conclude that  $\eta$  should be as small as possible.
- $\eta_{x,m} = 0.525$  : No definite answer is obtained on the basis of the MTFs, nor on the basis of the LSFs.  
The peak value of the LSF is independent of  $\eta$ , but the maximum gradient is slightly larger for small  $\eta$ . For large  $\eta$ , however, the spatial extension is smaller, and therefore no unambiguous conclusion can be drawn. The spatial extension is reduced for larger  $\eta$ , because then the shadow image LSF dominates, which has a triangular shape (for the optimum situation, i.e. where movement MTF and focal spot MTF are equal, the convolution of two equal rectangular LSFs is involved; see also sec. 3.4). The image receptor LSF is more extended, its intensity is zero at infinity only.
- $\eta_{x,m} = 0.7$  : No problem arises as to the LSF and the MTF system description:  $\eta$  should be as large as possible.

With this LSF concept we have obtained a sharper criterion for the usefulness of geometric magnification. A detailed analysis shows that geometric magnification is of advantage only if  $\eta_{x,m} > \approx 0.5$ .

Though good image quality predictions are possible on the basis of LSFs, their description is rather complicated because a convolution is involved. A criterion on the basis of MTFs (a multiplication is involved) would therefore be of advantage. Comparison between the MTFs and the corresponding LSFs shows that the larger the spatial frequency for the modulation transfer 0.25, the better the LSF. This is adstrued by figures 3.2.22, 3.2.23 and 3.2.24 for  $\eta_{x,m}$  equal to 0.2, 0.4 and 0.7. The peak contrast of the LSF and the  $\nu_{x,z=0.25}$  value show the same behaviour as a function of  $\eta$ . It is further indicative that no decision could be made on the basis of the MTFs nor on the LSFs for  $\eta_{x,m} = 0.525$  (figs. 3.2.16, 3.2.20). In fact, the MTFs cross at a modulation transfer equal to 0.25.

For comparison, the full width at half maximum (FWHM) of the LSF and a measure of the conventional unsharpness (the square root of the sum of the FWHM of the shadow image and image receptor LSF squared) are also given in the figures. If  $\eta_{x,m}$  is small or medium (figs. 3.2.22, 3.2.23) any criterion will do. If  $\eta_{x,m}$  is large (3.2.24), the usefulness of the FWHM and of the unsharpness is limited. On

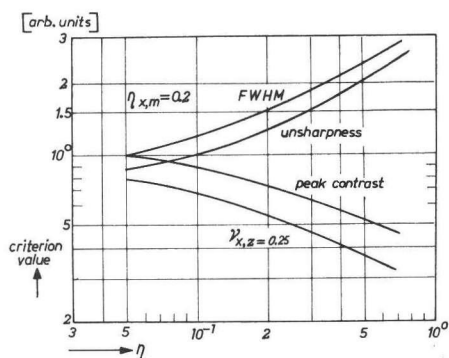


Fig. 3.2.22

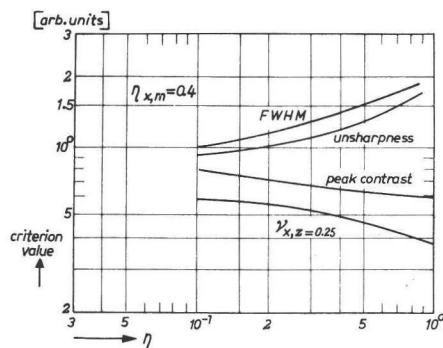


Fig. 3.2.23

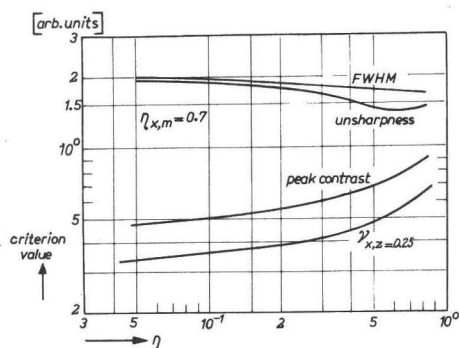


Fig. 3.2.24

Fig. 3.2.22 – 3.2.24.  
Comparison of system LSF and MTF  
criteria as a function of  $\eta$ ,  $\eta_{x,m}$  equal  
to 0.2, 0.4 and 0.7

the basis of the unsharpness an optimum is mistakenly suggested at rather large values of  $\eta$ . We shall choose the  $\nu_{x,z}=0.25$  criterion, i.e. an MTF criterion. We then stay in line with our description of the visual system, and also with the current description of X-ray systems.

### 3.2.3 Influence of the focal spot-to-image receptor distance

The best object resolution is obtained if the focal spot-to-image receptor distance is chosen as small as feasible. Both the shadow image and the image receptor MTF improve at smaller distances. The latter factor benefits from the favourable effect of an increased geometric magnification. For the  $MTF_a$ , the effect of the smaller energy per exposure outweighs the unfavourable effect of the geometric magnification (eq. 3.2.30): the  $MTF_a$  improves in inverse proportion to  $fr^{1/5}$ .

More attention will be paid to this topic in sec. 5.2.1.5.

### 3.2.4 Nomograms

The analytical description of the system MTF is complete and already gives an impression of the relative importance of the parameters involved. Graphs can be more illustrating, however. They can further serve to obviate the laborious quantitative implementation of the equations. For this purpose four nomograms have been developed:

- (i) for the choice of the optimum focal-spot size,
- (ii) for the effect of a non-optimum focal-spot size,
- (iii) for the effect of the object position,
- (iv) for the assessment of the MTF quality of the X-ray system as a whole.

In the latter three nomograms, the  $\nu_{x,z=0.25}$  spatial frequency will be chosen as the criterion. Its use is valid for situations (iii) and (iv). For small deviations from the optimum, it will also hold for situation (ii). For large deviations, the  $\sin(x)/x$ -squared shaped  $MTF_a$  reduces to a  $\sin(x)/x$ -shaped one. This resembles stationary object imaging (sec. 3.3) for which it will be shown that the  $\nu_{x,z=0.25}$  criterion also holds.

#### 3.2.4.1 Optimum focal-spot size

The optimum focal-spot size depends on  $f_r$ ,  $o_r$  and  $c_{a,m}$  (eq. 3.2.31). As  $\eta = o_r/f_r$ , we can equally state that the optimum size depends on  $f_r$ ,  $\eta$  and  $c_{a,m}$ . The value of  $c_{a,m}$  is given by the ratio of  $c_{p,m}$  (eq. 3.2.10) and  $c_f$  (eq. 3.2.8), so exposure table data and the tube characteristic parameter are involved. The fig. 3.2.25 is based on the analytical interrelation mentioned. The lower x-axis gives the  $c_{a,m}$  value, the upper x-axis gives the nominal optimum focus size  $f_{opt}$ . Once the parameters  $f_r$  and  $\eta$  are chosen, the focus size is found by following the lines as indicated by LMNP. A small  $\eta$  and a large  $f_r$  indicate a larger focal-spot size.

#### 3.2.4.2 Non-optimum focal-spot size

The choice of the focal-spot size will generally be a compromise because (i) the demands corresponding to a range of parameter values (e.g. object velocities) cannot be met simultaneously; (ii) there is a limited choice of spot sizes available; and (iii) one is forced to use too small a focus if the required optimum size corresponds to a rating over 200 kW (which is the maximum in present tube technology), or if the high voltage generator or the mains restrict the maximum power. The influence of a non-optimum choice should therefore be investigated.

The deterioration of the  $MTF_x$  quality is prominent when the  $MTF_a$  dominates. To investigate this further, the balance factor  $b_x$  is defined for the balance between the optimum  $MTF_a$  and  $MTF_r$ . Its value equals the ratio (fig. 3.2.26) between the spatial frequencies at a modulation transfer 0.5 for  $MTF_a$  and  $MTF_r$ . Thus, if  $b_x$  is small the choice of the focal spot size is relatively critical.

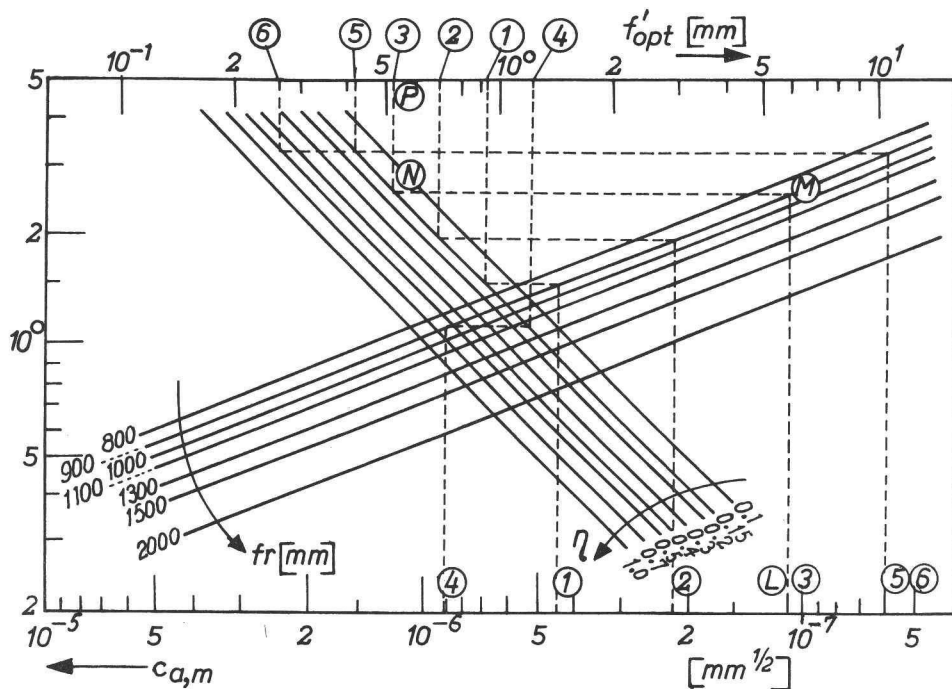


Fig. 3.2.25.  
Nomogram for optimum focus-size determination.

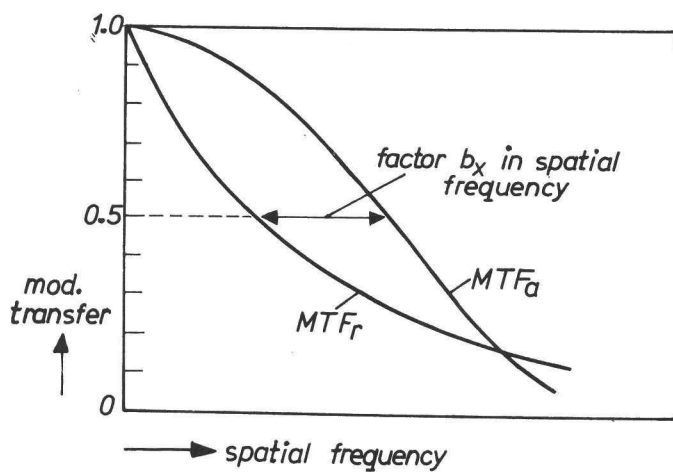


Fig. 3.2.26.  
Definition of  $b_x$ .

As a starting point, the optimum focal spot situation has been chosen. This implies that the value of  $b_x$  is completely determined by  $\eta$  and  $\eta_{x,m}$  (fig. 3.2.27). The smaller  $\eta$  and the larger  $\eta_{x,m}$  the larger will be the value of  $b_x$  because these situations imply a relatively good shadow image MTF. The analytical expression for  $b_x$  reads:

$$b_x = \frac{1-\eta}{1-\eta_{x,m}} \cdot \left( \frac{\eta_{x,m}}{\eta} \right)^{3/5} \quad (3.2.46)$$

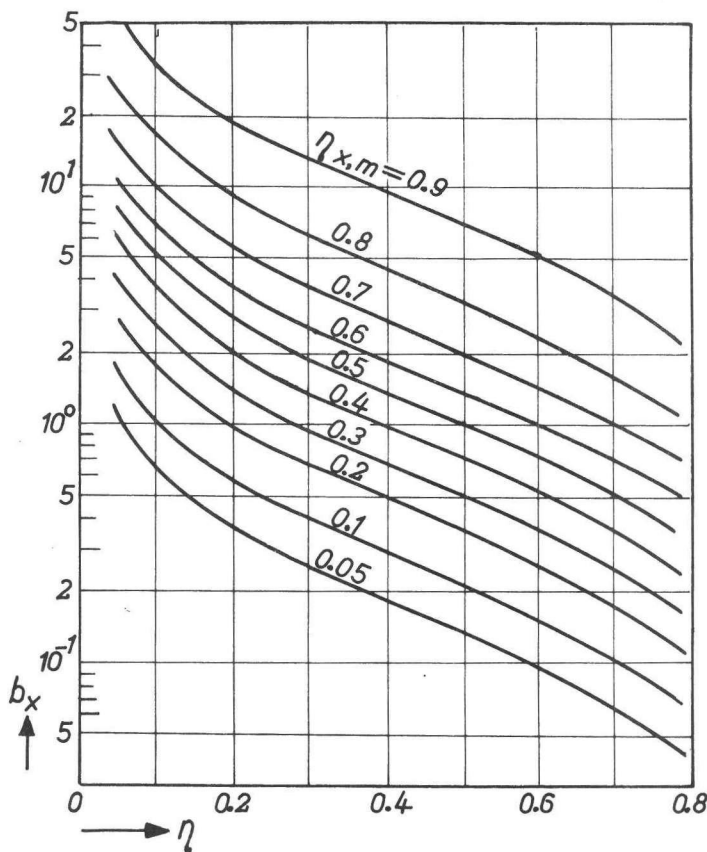


Fig. 3.2.27.

$b_x$  as a function of  $\eta$ , with  $\eta_{x,m}$  as parameter.

The reduction of the MTF quality in terms of the  $\nu_{x,z=0.25}$  spatial frequency is given in fig. 3.2.28 as a function of  $b_f$ , the ratio between the actual and optimum focus size, with  $b_x$  as parameter. If  $b_x$  is large, say 4, then even large deviations from the optimum give only a small reduction in MTF quality, as is to be expected.



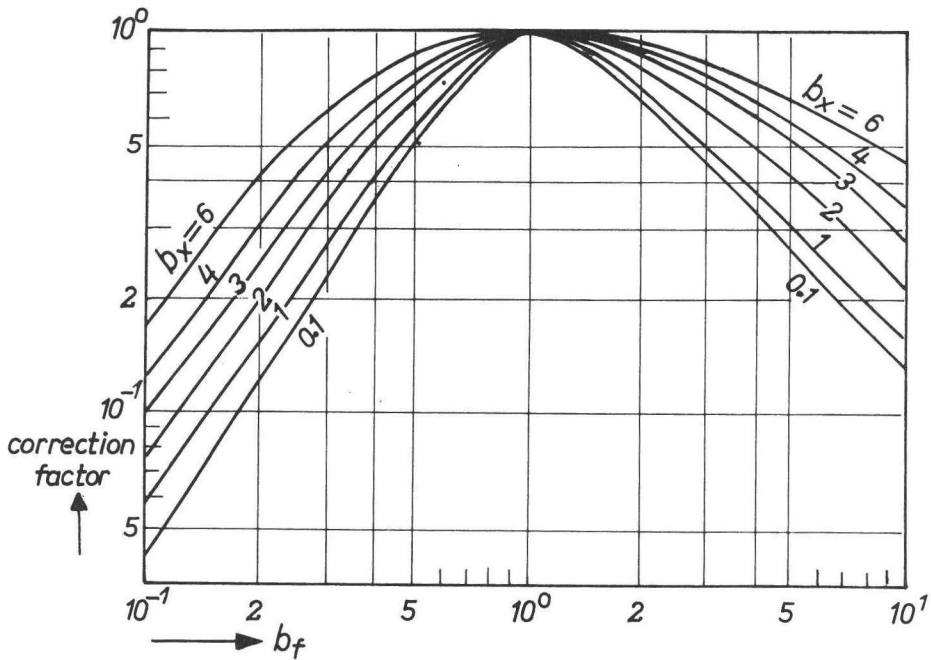


Fig. 3.2.28.

Correction factor on  $\nu_{x,z=0.25}$  if a non-optimum focus size is chosen; parameter  $b_x$ .

### 3.2.4.3 Object position

The starting point is the  $\eta_{x,m}$  position, i.e.  $\eta = \eta_{x,m}$ . If  $\eta$  differs from  $\eta_{x,m}$ , then the  $\nu_{x,z=0.25}$  value will be worse or better than the initial value, depending on the ratio  $\eta/\eta_{x,m}$  and the absolute value of  $\eta_{x,m}$ . The correction factor on  $\nu_{x,z=0.25}$  is given in fig. 3.2.29 as a function of  $\eta$ , with  $\eta_{x,m}$  as parameter. The figure shows once more that (i) for  $\eta_{x,m} < \approx 0.5$ ,  $\eta$  should be as small as possible, and (ii)  $\eta$  should be as large as possible for  $\eta_{x,m} > \approx 0.5$ .

### 3.2.4.4 X-ray system MTF quality

A complete analysis is obtained by varying the image receptor and the focal spot-to-image receptor distance as well. As the latter analysis is rather complicated, its variation is not considered here (see further sec. 5.2.1.5). As regards the image receptor, both its intrinsic resolution and the X-ray sensitivity are involved. Consequently a different MTF balance is obtained because of the change in  $MTF_r$  quality, and also because of a different optimum spot size.

Firstly, the  $\eta_{x,m}$  or equality of MTFs situation will be considered. By definition  $\nu_{x,z=0.25}$  must equal  $\nu_{opt,z=0.25}$ . Further, as  $\eta = \eta_{x,m}$ , we can write for  $\nu_{x,z=0.25}$ :

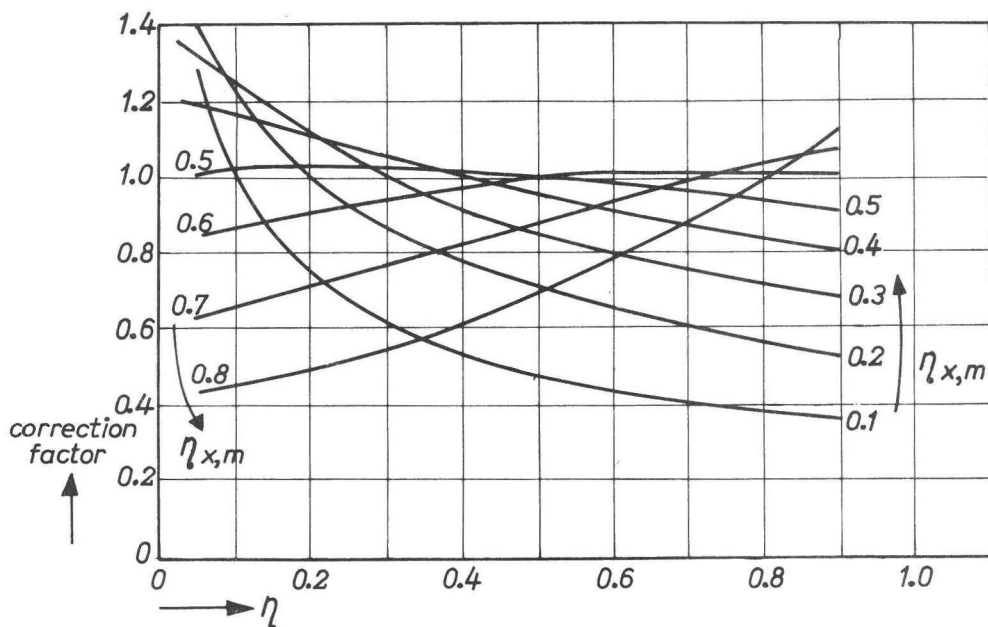


Fig. 3.2.29.

Correction factor on  $\nu_{x,z=0.25}$  as a function of  $\eta$ ,  $\eta_{x,m}$  as parameter.

$$\nu_{x,z=0.25} \sim \frac{1}{c_{a,m}^{2/5} \cdot \eta_{x,m}^{3/5}} \quad (3.2.47)$$

Any change in  $c_{a,m}$  influences  $\nu_{x,z=0.25}$  in two ways. There is a direct influence via  $c_{a,m}$ , but also an indirect one because  $\eta_{x,m}$  depends on  $c_{a,m}$  via  $c_{x,m}$ . A change in the intrinsic resolution of the image receptor only influences  $\eta_{x,m}$ .

The nomogram is given in fig. 3.2.30. It is built up as follows:

- The correlation between  $c_{x,m}$  and  $\eta_{x,m}$  is given by curve AB.  $c_{x,m}$  is on the y-axis,  $\eta_{x,m}$  is on the lower x-axis.
- The  $\nu_{x,z=0.25}$  value is on the upper x-axis. A change in  $\nu_{rec}$  influences this frequency in proportion to the corresponding change in  $\eta_{x,m}^{3/5}$ . This is achieved by reflecting the  $\eta_{x,m}$  value via a line with gradient  $-3/5$  (CD) and a line with gradient 1 (EF). As an example the line GHJK is drawn for  $\eta_{x,m} = 0.25$ .
- The influence of the  $\eta$  value is accounted for by the application of a correction factor on the function value of the line with gradient  $-3/5$ . Four curves are drawn, for  $\eta = 0.1, 0.15, 0.3$  and  $0.5$ . These curves cross at  $\eta_{x,m} \approx 0.5$ . If  $\eta$  is

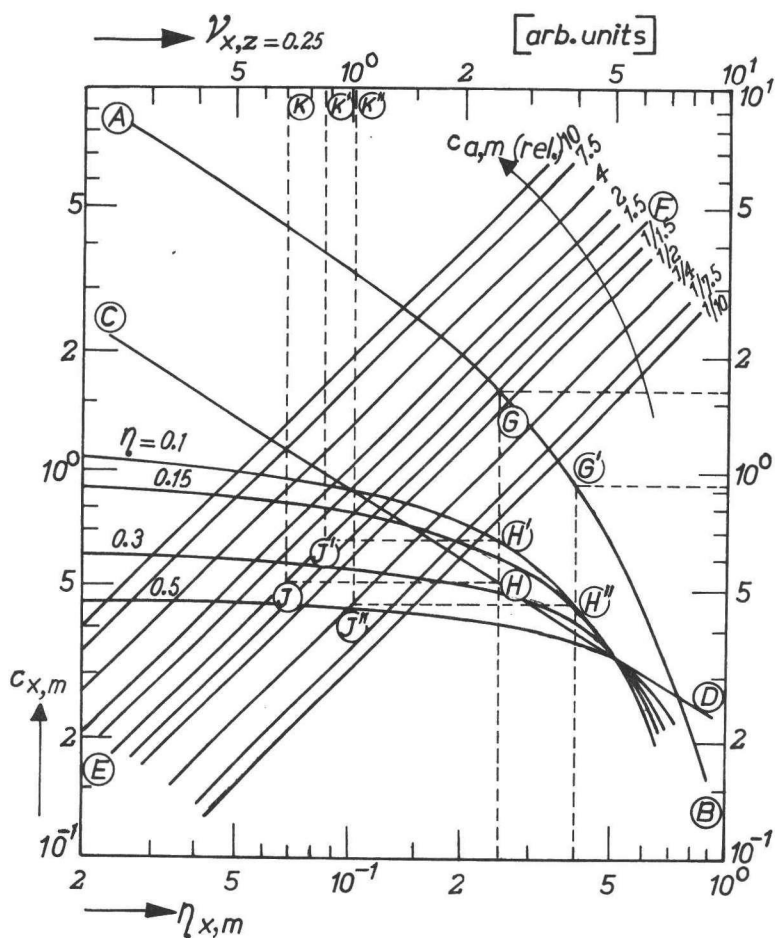


Fig. 3.2.30.

Nomogram for the system MTF quality, moving objects.

e.g. 0.1, then the lines GHJK for  $\eta_{x,m} = 0.25$  will be GH'J'K', where the spatial frequency for K' is, of course, larger than for K.

- d. If  $c_{a,m}$  is varied, then  $\nu_{x,z=0.25}$  varies in proportion to  $c_{a,m}^{-2/5}$ . This is introduced by translating the line with gradient 1 (EF) according to this factor. Hence a set of parallel lines is obtained, for which  $c_{a,m}$  is equal to 1/10 to 10 times the original value. If now the  $c_{a,m}$  value were 1/4 of the original,  $c_{x,m}$  would be smaller by a factor of  $4^{2/5}$ , and the line GH'J'K' would become line G'H''J''K''.

### 3.2.4.5 Application

As an example, the imaging of a slow moving part ( $v = 5$  mm/sec) of the

stomach has been investigated. The outcome of the following analysis is borrowed from sec. 5.1.2, to which reference is also made for the underlying data. The  $f_r$  value is 900 mm. Four film/screens combinations are compared, numbered 1 to 4 in table 3.2.1 below. The rare-earth intensifying screens are assumed to be four times as sensitive as the universal screens; the intrinsic resolution in terms of MTF is the same. (These data reflect the tendency for these new screens.) A 9" image intensifier system is also used, numbered 5 and 6. For the latter system, two  $\eta$  values are applied, i.e. 0.15 and 0.5 (the minimum and maximum practical value), because geometric magnification will prove to have advantages.

The  $\nu_{x,z}=0.25$ , the optimum focus sizes and the other relevant parameter values are given in the table. The lines 1 to 6 in fig. 3.2.31 and fig. 3.2.25 indicate how the MTF quality and the focal-spot size are obtained.

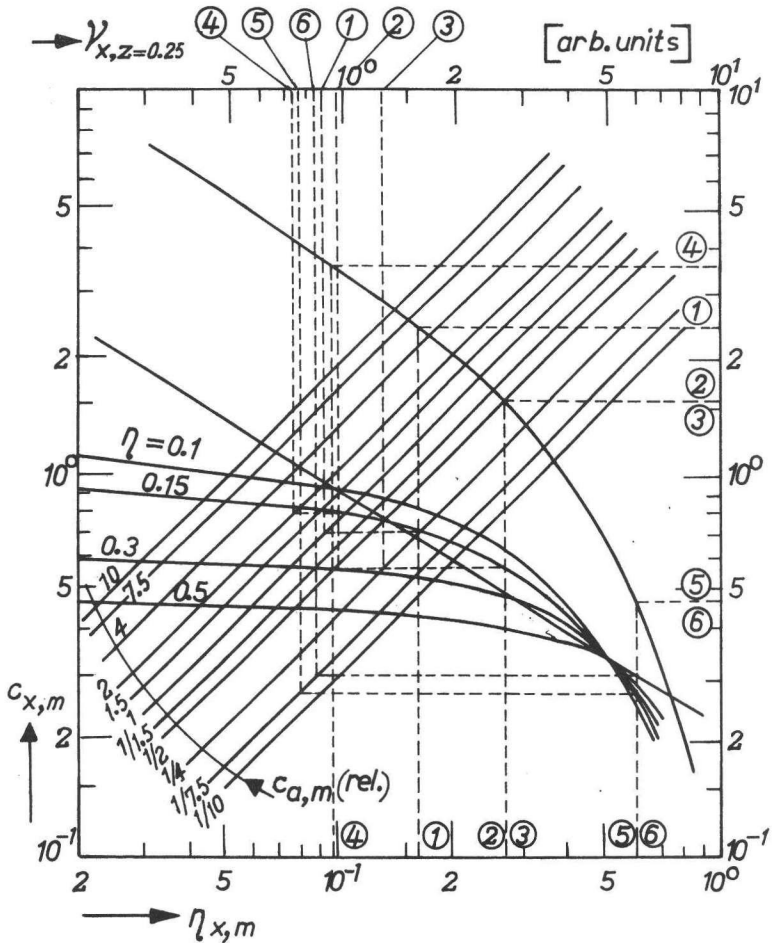


Fig. 3.2.31.  
System MTF quality for stomach radiography, different image receptors.

The optimum focus size is smallest for the most sensitive system, the 9" image intensifier. The MTF quality, however, is best for the rare-earth screens, which are less sensitive but have a higher intrinsic resolution.

**TABLE 3.2.1: Comparison of six radiographic systems for the imaging of the stomach**

no.	receptor	$\eta$	$\eta_{x,m}$	$c_{a,m} \cdot 10^6$ [mm <sup>1/2</sup> ]	$\nu_{x,z=0.25}$ [mm <sup>-1</sup> ,norm]	$f'_{opt}$ [mm]
1	univ. screens	0.15	0.16	0.45	1.00	0.93
2	fast screens	0.15	0.27	0.22	1.06	0.70
3	rare-earth scr.	0.15	0.27	0.11	1.36	0.52
4	hi.def.screens	0.15	0.10	0.90	0.83	1.25
5	OB128/9"	0.15	0.60	0.06	0.84	0.42
6	OB128/9"	0.50	0.60	0.06	0.94	0.26

Since  $\eta_{x,m}$  is large for the image intensifier technique under investigation, the application of geometric magnification is indeed useful. The consequences for the dose to the patient – which will be inherently larger – will be discussed in sec. 5.2.6.

To illustrate the influence of the non-optimum focus size, a 1.5 mm focal-spot size is combined with the fast intensifying screens/film combination. The focal spot is too large by a factor of 2.1 (so  $b_f = 2.1$ ). The balance factor  $b_x$  is not small, being 1.5 (fig. 3.2.27,  $\eta = 0.15$  and  $\eta_{x,m} = 0.27$ ), so the reduction factor for the system MTF quality is 0.75 (fig. 3.2.28).

### 3.2.5 Conclusion

In optimizing the object resolution of radiographic systems for the imaging of moving objects, the following directives apply:

1. If the shadow-image MTF dominates, that is if  $\eta > \eta_{x,m}$ , an increase in intrinsic resolution of the image receptor is of less value, as is indicated in fig. 3.2.30. The  $\eta$  curves approach a constant value for small  $\eta_{x,m}$  values. An increase in shadow image quality (e.g. by the application of a more sensitive image receptor) is then of value for the same reason.  
If the image receptor distortion dominates, that is if  $\eta < \approx 2 \cdot \eta_{x,m}$ , attention should be paid to the image receptor resolution. The choice of the focus size, or of any parameter determining the shadow image distortion, is not critical in this situation.

2. Although parameter values like  $c_{a,m}$  can vary considerably, the change in MTF quality may be small, because
  - generally, the sensitivity and intrinsic resolution of image receptors are related. Hence, an improved shadow image MTF (higher sensitivity) is associated with a worse image receptor MTF;
  - the parameters affect only a part of the imaging system, hence the relative influence on the final image quality is reduced.
3. From fig. 3.2.28 we conclude that too large a focus size is less unfavourable than a too small one. The movement MTF deteriorates more in the latter situation than does the geometric MTF in the former (loadability  $\sim f^{1.5}$ ).
4. The value of  $\eta_{x,m}$  that gives the object position for equality of the shadow image and the image receptor MTF, serves as an indication for the optimum object situation. If  $\eta_{x,m} < \approx 0.5$ , then the object should be as close as possible to the image receptor. If  $\eta_{x,m} > \approx 0.5$ , then geometric magnification has advantages.
5. It turns out that the unsharpness factors must indeed be 'of the same order of magnitude' for the optimization of the shadow image MTF, by varying the focal-spot size. This statement is not valid for the optimization of the system MTF obtained by varying the object position.

### 3.3 Stationary objects

#### 3.3.1 Choice of the focal spot

The optimum focal-spot size cannot be regarded as a limiting case for the imaging of moving objects. One would conclude that for zero object velocity the optimum focal-spot size is also zero, and the shadow image quality is ideal. This is mathematically correct, but the exposure time would be infinitely long.

Another criterion must therefore be applied namely that the optimum focus size corresponds to a short-time loadability such that a reasonably short exposure time is just obtained. The chance of voluntary or involuntary movements is then reduced to an acceptable level. To be in line with practice, the permissible exposure times were provided by Mrs. Feddema (1976) of the Applications Department of Philips. Unlike the moving object situation, then, the exposure time is given beforehand. Correspondingly, it will be denoted by  $t_p$ . In many applications an exposure time of the order of 0.1 s or shorter is required, so the focal-spot size/short-time loadability relationship (eq. 3.2.7) can be applied. Consequently, for  $t_p$  we can write

$$t_p = \frac{Q_p \cdot U_p \cdot (f_r/f_p)^2}{c_f \cdot f_{opt}^{1.5}} \quad (3.3.1)$$

If the patient characteristic parameter for stationary objects,  $c_{p,st}$  (unit kW/mm<sup>2</sup>), is defined as

$$c_{p,st} = \frac{Q_p \cdot U_p}{t_p \cdot f_r^2}, \quad (3.3.2)$$

we can write for  $f_{opt}$

$$f_{opt}^{1.5} = \frac{c_{p,st}}{c_f} \cdot f_r^2 \quad (3.3.3)$$

Analogous to the moving objects situation the absorption image characteristic parameter  $c_{a,st}$  (unit mm<sup>-1/2</sup>) is defined as

$$c_{a,st} = \frac{c_{p,st}}{c_f} \quad (3.3.4)$$

so that the optimum focus size is given by

$$f_{opt} = c_{a,st}^{2/3} \cdot f_r^{4/3} \quad (3.3.5)$$

In the same way as for the moving object, we will consider the worst case situation, i.e. the direction corresponding to the camel-back distribution of the focus. Only the perpendicular central ray of the X-ray beam is considered.

For the moving objects, the focal spot MTF could be described by a  $\sin(x)/x$  function because the movement MTF considerably damps the transfer of higher spatial frequency gratings, for which the approximation would not be correct. This damping is also caused by the image receptor MTF. It will be shown in sec. 5.1.1 that, generally, the  $MTF_r$  dominates. So the focal-spot MTF can again be approximated by a  $\sin(x)/x$  function according to eq. 3.2.5.

### 3.3.2 Choice of the geometric magnification

In the optimization of the object position the same problem exists as with moving objects. The scaling factor of the spatial frequency axis of  $MTF_a$  is different, but the behaviour as a function of the object position is the same.

#### 3.3.2.1 Mathematical formulation

Since the  $MTF_x$  is the product of  $MTF_r$  and  $MTF_a$ , we can write for  $MTF_x$  (eq. 3.2.40)

$$\text{MTF}_x(\nu) = e^{-\frac{0.693(1-\eta)}{\nu_{\text{rec}}} \cdot \nu} \cdot \left| \frac{\sin(\pi \nu u_f)}{\pi \nu u_f} \right| \quad (3.3.6)$$

The  $u_f$  value is given by eq. 3.2.12. (Again, the influence of the scattered radiation is not taken into account, as an anti-scatter grid is used — see Appendix IV). The  $u_f$  is simply expressed in terms of  $\eta$ ,  $c_{a,\text{st}}$  and  $\text{fr}$  by combining eq. 3.2.12 and eq. 3.3.5. Expression 3.3.6 can thus be written in characteristic parameters as follows:

$$\text{MTF}_x(\nu) = e^{-\frac{0.693(1-\eta)}{\nu_{\text{rec}}} \cdot \nu} \cdot \left| \frac{\sin(\pi \nu c_{a,\text{st}}^{2/3} \cdot \text{fr}^{4/3} \cdot \eta)}{\pi \nu c_{a,\text{st}}^{2/3} \cdot \text{fr}^{4/3} \cdot \eta} \right| \quad (3.3.7)$$

Further simplification is obtained by introducing the object position  $\eta_{x,\text{st}}$  for the balance of  $\text{MTF}_a$  and  $\text{MTF}_r$ . The  $\eta_{x,\text{st}}$  value is uniquely defined by  $\nu_{\text{rec}}$ ,  $c_{a,\text{st}}$  and  $\text{fr}$ . For the  $\eta_{x,\text{st}}$  condition we have

$$\nu_{\text{opt},z=0.5} = \frac{\nu_{\text{rec}}}{1 - \eta_{x,\text{st}}} \quad (3.3.8)$$

so that for  $\eta_{x,\text{st}}$  we can write

$$\eta_{x,\text{st}} = \frac{1}{1 + c_{a,\text{st}}^{2/3} \cdot \text{fr}^{4/3} \cdot \nu_{\text{rec}}/0.603} \quad (3.3.9)$$

Analogously we define the dimensionless X-ray system characteristic parameter  $c_{x,\text{st}}$  as follows:

$$c_{x,\text{st}} = \frac{c_{a,\text{st}}^{2/3} \cdot \text{fr}^{4/3} \cdot \nu_{\text{rec}}}{0.603} \quad (3.3.10)$$

The derivation of the characterizers  $c_{p,\text{st}}$ ,  $c_{a,\text{st}}$  and  $c_{x,\text{st}}$  is based on the focus size/loadability relation of X-ray tubes. This relation breaks down for small loadabilities ( $\approx 10$  kW) and for exposure times longer than 0.1 s. In these situations, a focal-spot size must be chosen pragmatically. The analysis of the object position is still valid, of course, and an  $\eta_{x,\text{st}}$  value also exists. In eq. 3.3.9 the actual focal-spot size must be introduced, i.e.

$$\eta_{x,\text{st}} = \frac{1}{1 + f \cdot \nu_{\text{rec}}/0.603} \quad (3.3.11)$$



and for  $c_{x,st}$  we have

$$c_{x,st} = \frac{f \cdot \nu_{rec}}{0.603} \quad (3.3.12)$$

The  $\eta_{x,st}$  value is given as a function of  $c_{x,st}$  in fig. 3.3.1.

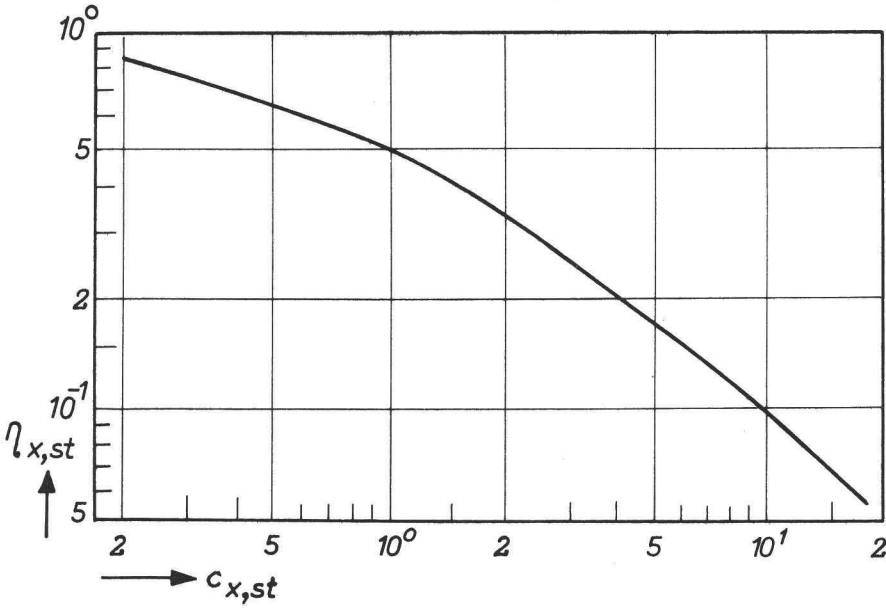


Fig. 3.3.1.

Object position  $\eta_{x,st}$  for equality of  $MTF_a$  and  $MTF_r$ , stationary objects

Equation 3.3.12 clearly shows that  $c_{x,st}$  indeed deals with the balance between the focal spot and image receptor unsharpness.

The shape of  $MTF_x$  (eq. 3.3.7) can now be given in a normalized form in terms of  $\eta$  and  $\eta_{x,st}$ :

$$e^{-\frac{1-\eta}{(1-\eta_{x,st})} \cdot \nu} \cdot \left| \frac{\sin \left( \frac{0.603}{0.693} \pi \frac{\eta}{\eta_{x,st}} \nu \right)}{\frac{0.603}{0.693} \pi \frac{\eta}{\eta_{x,st}} \nu} \right| \quad (3.3.13)$$

### 3.3.2.2 Influence of the object-to-image receptor distance

For the influence of the object-to-image receptor distance variation on  $MTF_a$  and  $MTF_r$ , the same argumentation as for the moving object situation holds. The scaling factor for the appropriate  $\nu$ -axis is  $1/\eta$  for  $MTF_a$  and again  $1/(1-\eta)$  for  $MTF_r$ .

For large values of  $\eta_{x,st}$  there will therefore be a tendency to increase the  $\eta$  value to improve  $MTF_x$ . The reverse is true for small values of  $\eta_{x,st}$ . For intermediate values the same problems concerning the MTF quality will occur, as the MTFs cross for different  $\eta$  values. These expectations are confirmed in practical cases. The system MTFs according to eq. 3.3.13 are given for different object positions for a small, medium and large value of  $\eta_{x,st}$  in figures 3.3.2 ( $\eta_{x,st} = 0.1$ ), 3.3.3 ( $\eta_{x,st} =$

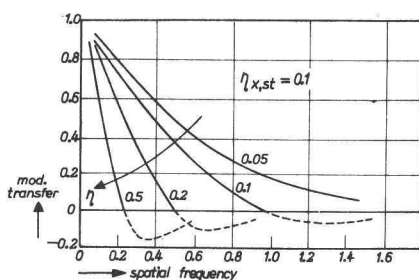


Fig. 3.3.2

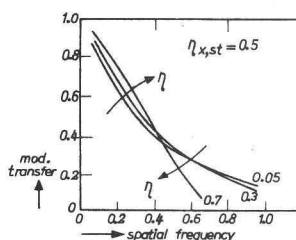


Fig. 3.3.3.

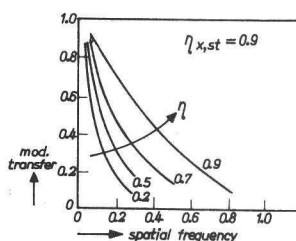


Fig. 3.3.4

Fig. 3.3.2 – 3.3.4.

System MTF with  $\eta$  as parameter,  $\eta_{x,st}$  equal to 0.1, 0.5 and 0.9

0.5) and 3.3.4 ( $\eta_{X,st} = 0.9$ ). The best  $MTF_X$  is obtained with the smallest  $\eta$  for the small value of  $\eta_{X,st}$  (fig. 3.3.2). The reverse is true for the large  $\eta_{X,st}$  situation (fig. 3.3.4). For the intermediate values of  $\eta_{X,st}$ , the investigation of the corresponding LSFs should give the criterion for the choice of  $\eta$ .

The conclusions for small and large values of  $\eta_{X,st}$  are confirmed by this analysis. The LSFs are given in fig. 3.3.5 ( $\eta_{X,st} = 0.1$ ) and fig. 3.3.6 ( $\eta_{X,st} = 0.9$ ) for different  $\eta$ . For these situations, the three criteria are favourably correlated in the sense that a high peak value corresponds to a large gradient and to a small spatial extension. This correlation vanishes if the  $MTF_a$  and  $MTF_r$  quality are of the same order of magnitude for a relatively large range of  $\eta$ , i.e. for intermediate values of  $\eta_{X,st}$ . The shapes of the two constituent LSFs are substantially different (a rectangular shape and a Lorentzian, i.e. a  $1/(1+x^2)$  shape, are involved), and so is the system LSF. (This problem was not met with moving objects because the LSF shapes are more related; the optimum  $MTF_a$  corresponds then to an LSF of triangular shape.) This is illustrated by fig. 3.3.7, which gives system LSFs for  $\eta_{X,st} = 0.7$ .

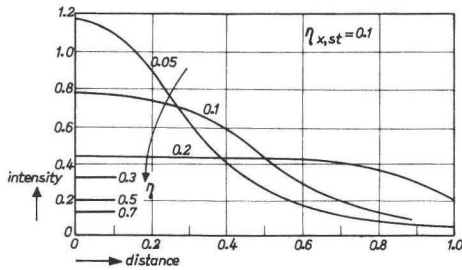


Fig. 3.3.5.

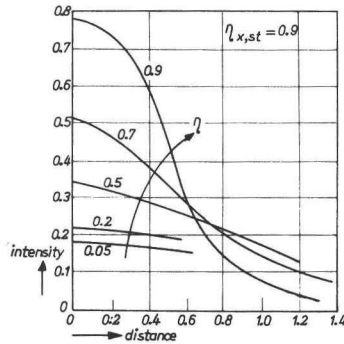


Fig. 3.3.6

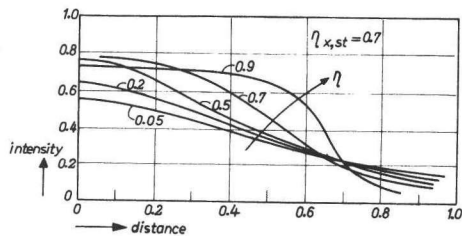


Fig. 3.3.7

Fig. 3.3.5 – 3.3.7  
System LSF with  $\eta$  as parameter,  
 $\eta_{X,st}$  equal to 0.1, 0.9 and 0.7.

The peak value for  $\eta = 0.5$  is roughly equal to the one for  $\eta = 0.7$ . The latter LSF, however, shows a larger gradient, and is therefore considered to be better.

An edge is often the crucial object to be imaged. Its visibility is governed by the maximum gradient of the ESF, which is proportional to the peak value of the LSF. So we can state that the latter parameter provides a legitimate criterion. Since the peak value proves to be positively correlated with  $\nu_{x,z=0.25}$ , the spatial frequency which is imaged with a modulation transfer 0.25, a convenient description on the basis of MTFs is possible. A few examples of this correlation are given in fig. 3.3.8, 3.3.9 and 3.3.10, which show the peak contrast, the  $\nu_{x,z=0.25}$  value, and also the FWHM of the system LSF and the 'unsharpness' of the system (square root of the sum of the FWHMs squared) as a function of  $\eta$  for  $\eta_{x,st}$  equal to 0.1, 0.5 and 0.9.

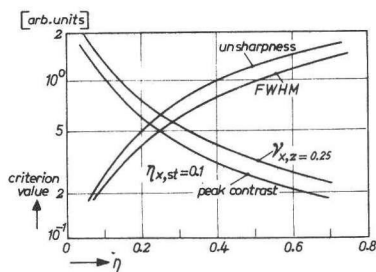


Fig. 3.3.8

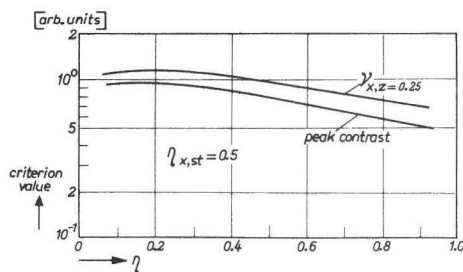


Fig. 3.3.9

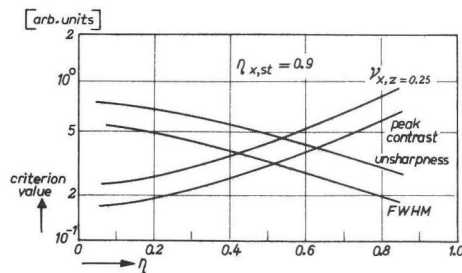


Fig. 3.3.10

Fig. 3.3.8 – 3.3.10  
Comparison of system LSF and MTF  
criteria as a function of  $\eta$ ,  $\eta_{x,st}$  equal  
to 0.1, 0.5 and 0.9.

Each of these criteria will do. Further, the choice of  $\eta$  is not critical for  $\eta_{x,st} = 0.5$  (fig. 3.3.9). This appears to be the case for  $\eta_{x,st}$  in the range of about 0.45 to about 0.7. For the larger values in this range, the shape problem of the LSFs occurs, as mentioned before. As the practical  $\eta_{x,st}$  values are generally smaller than 0.7, we conclude that the  $\nu_{x,z=0.25}$  criterion will not lead to large errors in practice.

We conclude, then, that (i) for  $\eta_{x,st}$  smaller than about 0.45, the smallest  $\eta$  is best;

(ii) for  $\eta_{x,st}$  larger than 0.7, the largest  $\eta$  is best; (iii) for  $0.45 < \eta_{x,st} < 0.7$ , the choice of  $\eta$  is not critical.

The largest value of  $\eta_{x,st}$  for which geometric magnification should not be applied equals 0.45. This enables us to calculate the corresponding critical focal-spot sizes for practical image receptors. The  $\nu_{rec}$  values of a number of generally used image receptors (ch. 5) are given in table 3.3.1, together with the critical focal-spot sizes.

**TABLE 3.3.1: Maximum focal-spot size for which geometric magnification is of advantage**

image receptor	$\nu_{rec}$ [c/mm]	critical focal-spot size $f'$ [mm]
film	8.00	0.06
universal screens/film	1.83	0.26
fast screens/film	1.39	0.35
9" } image	0.66	0.75
6" } intensifier +	0.91	0.54
5" } optics + film	0.75	0.66
6" image intensifier/TV system	0.50	1.00

### 3.3.3 Influence of the focal spot-to-image receptor distance

From a reasoning analogous to that for the imaging of moving objects it is concluded that a small  $fr$  distance favours the object resolution. If the optimum focal-spot size is chosen for each  $fr$  distance, then we can write for  $u_f$  (eq. 3.2.12 and eq. 3.3.5)

$$u_f = c_{a,st}^{2/3} \cdot or \cdot fr^{1/3} \quad (3.3.14)$$

The  $MTF_a$  quality is thus inversely proportional to  $fr^{1/3}$ . Further, a smaller  $fr$  corresponds also to a larger geometric magnification factor, and hence to a better image receptor MTF in the object plane.

For a further quantitative analysis see sec. 5.2.1.5.

### 3.3.4 Nomograms

The derivation of nomograms is less intricate than for the imaging of moving objects, because the shadow image MTF is characterized by one term, i.e. the focal spot MTF. It is therefore possible to apply the focal-spot size as a characterizer instead of a parameter like  $c_{a,m}$  or  $c_{a,st}$ .

Three nomograms will be developed:

- (i) for the influence of the focal-spot size,
- (ii) for the effect of the object position,
- (iii) for the assessment of the MTF quality of the X-ray system as a whole.

In all situations, the  $\nu_{a,z=0.25}$  spatial frequency is chosen as the criterion. Its use is valid because  $\sin(x)/x$  shaped and exponentially shaped MTFs are compared.

#### 3.3.4.1 Influence of the focal-spot size

The choice of the focal-spot size is important if the corresponding MTF dominates. The balance between the shadow image and image receptor MTF is described in terms of the factor  $b_x$  (fig. 3.2.26), i.e. the ratio between the spatial frequencies at a modulation transfer 0.5, for  $MTF_a$  and  $MTF_r$ . A large value of  $b_x$  indicates a small influence of the focal-spot size, and consequently a relatively large influence of the image receptor MTF.

The value of  $b_x$  is uniquely defined by the values of  $\eta$  and  $\eta_{x,st}$ . We write

$$b_x = \frac{1 - \eta}{1 - \eta_{x,st}} \cdot \frac{\eta_{x,st}}{\eta} \quad (3.3.15)$$

The corresponding value of  $b_x$  is given in fig. 3.3.11. The smaller  $\eta$  and the larger  $\eta_{x,st}$  the larger will be the value of  $b_x$ , because this indicates a dominance of the image receptor MTF.

The correction factor for  $\nu_{x,z=0.25}$  as a function of the change of the focus size is given in fig. 3.3.12. The change is expressed in terms of the parameter  $b_f$ , although the reference focus size can be a non-optimum one. A smaller focus size corresponds to a better  $MTF_x$  quality (if moving objects were investigated, the  $MTF_x$  quality would deteriorate due to the increase of the exposure time). The influence is smaller the larger the value of  $b_x$ , as expected. If  $b_x$  equals 4, for instance, then the choice of a less sensitive but better resolving image receptor will improve the system MTF quality. The focal spot must then be larger to obtain the same exposure time, but this does not lead to a dramatic deterioration of the MTF quality.

#### 3.3.4.2 Object position

The starting point is the  $\eta_{x,st}$  position, i.e.  $\eta = \eta_{x,st}$ . A different  $\eta$  value will lead to a better or worse  $\nu_{x,z=0.25}$  value, depending on the relative and absolute value of  $\eta_{x,st}$ . The correction factor on  $\nu_{x,z=0.25}$  is given in fig. 3.3.13 as a function of  $\eta$ , with  $\eta_{x,st}$  as parameter. The general tendencies as governed by the  $\eta_{x,st}$  value are clearly perceived.

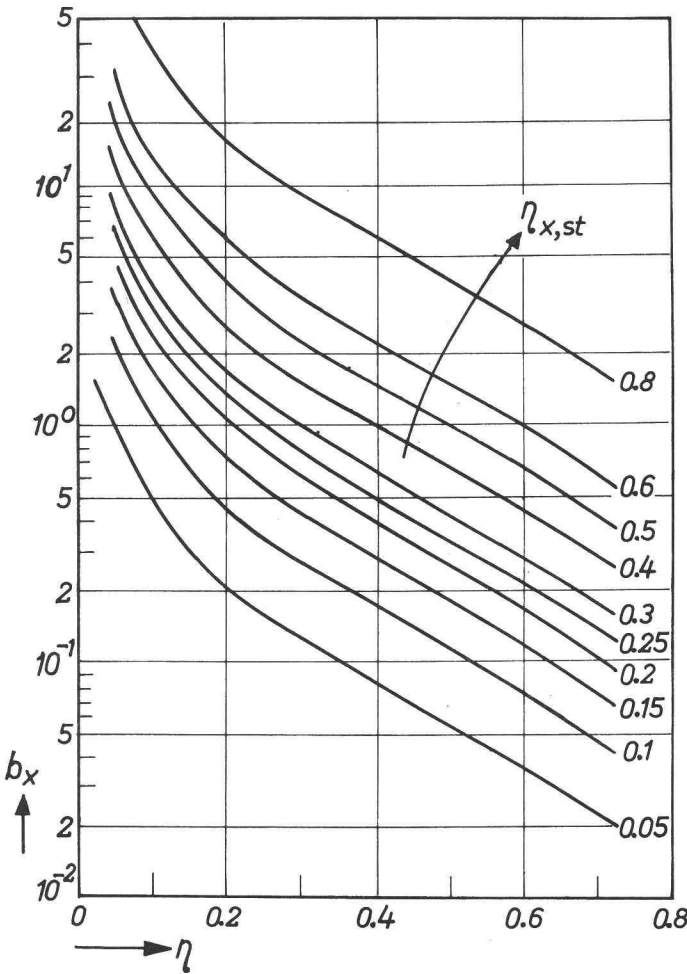


Fig. 3.3.11.  
Value of  $b_x$  as a function of  $\eta$ ,  $\eta_{x,st}$  as parameter.

### 3.3.4.3 X-ray system MTF quality

The influence of the image receptor choice, the focal-spot size and the object position are combined in the nomogram in fig. 3.3.14. The nomogram is built up as follows:

- The correlation between the image receptor, the focal-spot choice and  $\eta_{x,st}$  is given by curve AB. The product  $f \cdot \nu_{rec}$  is entered on the right y-axis, the  $\eta_{x,st}$  value is entered on the lower axis.
- The  $\nu_{x,z=0.25}$  is on the upper x-axis. Its value is inversely proportional to  $\eta_{x,st}$  if this object position is chosen. Hence the  $\eta_{x,st}$  value is reflected about a line with gradient  $-1$  (CD) and  $+1$  (EF). As an example, the line GHJK has been drawn for  $\eta_{x,st} = 0.2$ .

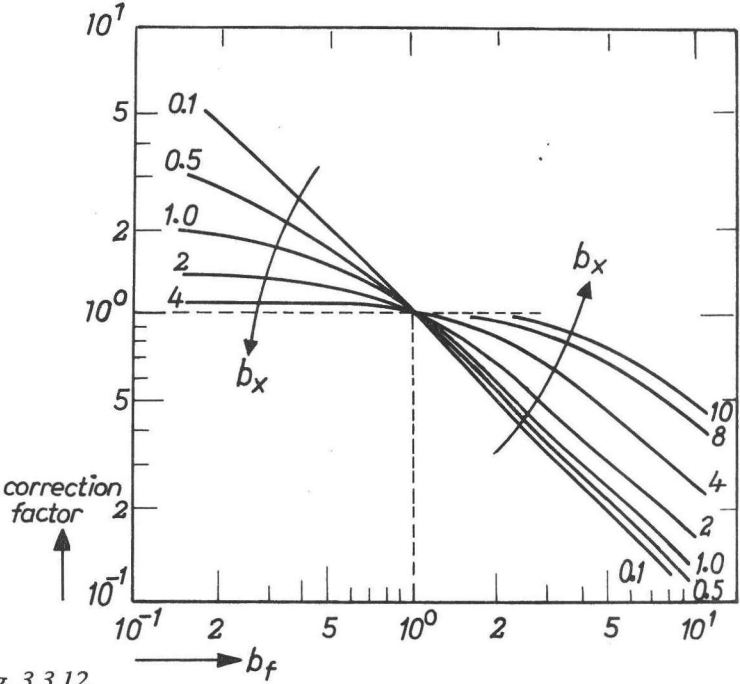


Fig. 3.3.12.  
Correction factor on  $v_{x,z}=0.25$  as a function of the change of the focus size.

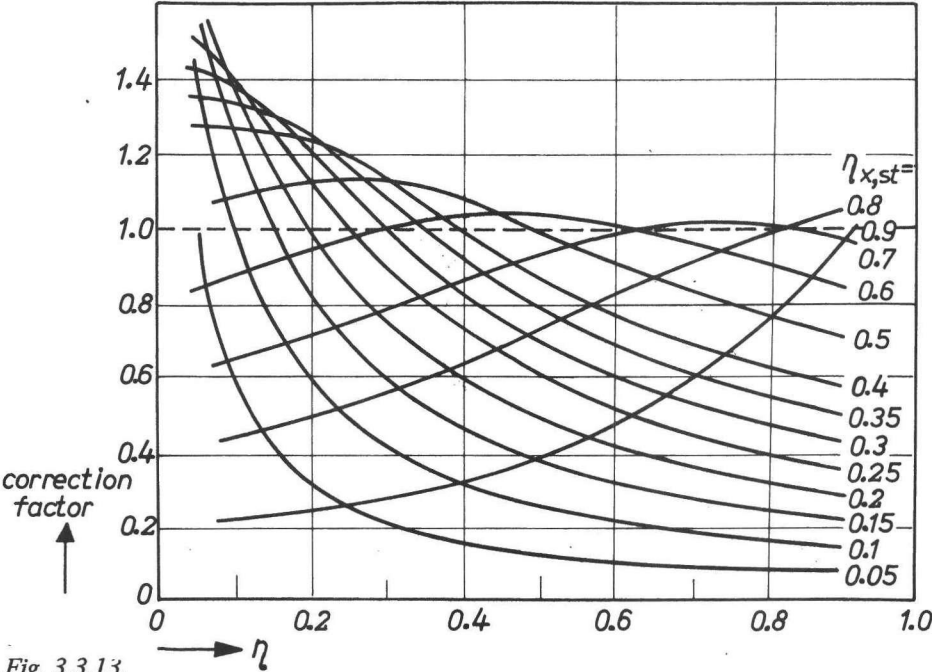


Fig. 3.3.13.  
Correction factor on  $v_{x,z}=0.25$  as a function of  $\eta$ ,  $\eta_{x,st}$  as parameter.



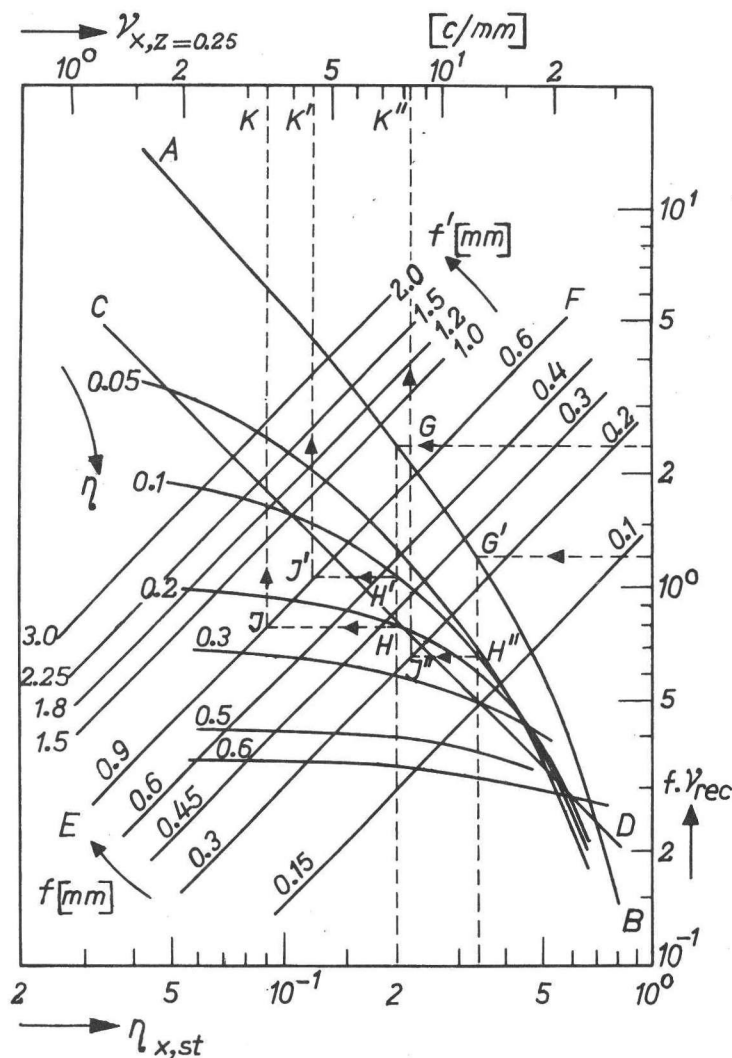


Fig. 3.3.14.

Nomogram for the system MTF quality, stationary objects.

- c. The influence of  $\eta$  is accounted for by the application of a correction factor to the function value of the line with gradient  $-1$ , which corresponds to the  $\eta_{x,st}$  situation. Curves are drawn for  $\eta = 0.05, 0.1, 0.2, 0.3, 0.5$  and  $0.6$ . If  $\eta = 0.1$ , then the line GHJK becomes GH'J'K'. The spatial frequency for K' is of course higher.

- d. The influence of the focal-spot size is accounted for by introducing a set of lines parallel to the line EF, for sizes from 0.1 mm to 2 mm. The change in  $\nu_{x,z=0.25}$  is inversely proportional to  $f$ . The absolute value of  $\nu_{x,z=0.25}$  is read off, as  $f = 0.9$  mm corresponds with line EF.

If we now used a 0.3 mm focus instead of the 0.9 mm one, the the line GH'J'K' would become G'H''J''K''. The MTF quality improves correspondingly. The associated  $\eta_{x,st}$  value is of course larger.

### 3.4 Focal-spot intensity distribution

As mentioned before (sec. 3.2.1), the X-ray source is a line source on a rotating anode. Its intensity distribution corresponds to the spatial intensity distribution of the cross-section of the electron beam impinging on the anode. The distribution in the direction of the focal track on the anode is of interest for two reasons. Firstly, the MTF of the focus and its corresponding imaging properties depend on it. In fact, the preceding sections dealt with the imaging by a camel-back intensity-distribution. Secondly, for a given overall focal-spot width, the short time loadability of the X-ray tube depends on the distribution, and so does the movement MTF. This corresponds to the fact that the heat balance of each anode element depends on the time course of the energy applied to it, which is governed by the spatial intensity distribution mentioned.

Consequently, the influence on the imaging of moving objects is of interest (sec. 3.4.1), particularly because other distributions than the camel-back can give a higher loadability. A different intensity distribution may invalidate the optimization schemes used so far. This is investigated in sec. 3.4.1.1.

The image receptor LSF will mask the effect of the intensity distribution to some extent. This will be studied for moving objects (sec. 3.4.1.2) and for stationary objects (sec. 3.4.2). The latter situation is less complicated because the loadability is not directly involved. Less attention is therefore paid to this class of systems.

A new system-characterizing number will be introduced analogous to the  $\eta_x$  parameter, which enables us to assess the sensitivity of the X-ray system imaging for the focal-spot intensity distribution.

As before the quality criterion will be the peak value of the line spread function, instead of a criterion based on the MTFs, for two reasons. On the one hand, the MTF may only partly describe the imaging because the phase transfer function must explicitly be dealt with as well. This occurs for the asymmetric intensity distributions. On the other hand, differently shaped MTFs must be compared.

By reason of the sometimes intricate phase transfer function, the LSF cannot always easily be obtained by means of the Fourier method (eq. 3.2.32). The LSF

will therefore be calculated by means of the convolution of the constituent LSFs. The result corresponds to the image of a small blood vessel. A computer program has been written to calculate the shadow image intensity distribution as a function of (fig. 3.4.1) 1) the focal-spot size, 2) its intensity distribution, 3) the vessel diameter  $\Delta$ , 4) the linear attenuation coefficient  $\mu$ , 5) the displacement of the vessel,  $u_m$ , and 6) the geometry of the system (focus-image receptor and object-image receptor distance,  $f_r$  and  $o_r$ ). All the following calculations are carried out for the central axis projection, although the program is capable of dealing with oblique projections. The  $\mu$ -value is chosen arbitrarily, with the restriction that the maximum contrast is a few percent, so as to ensure a linear system.

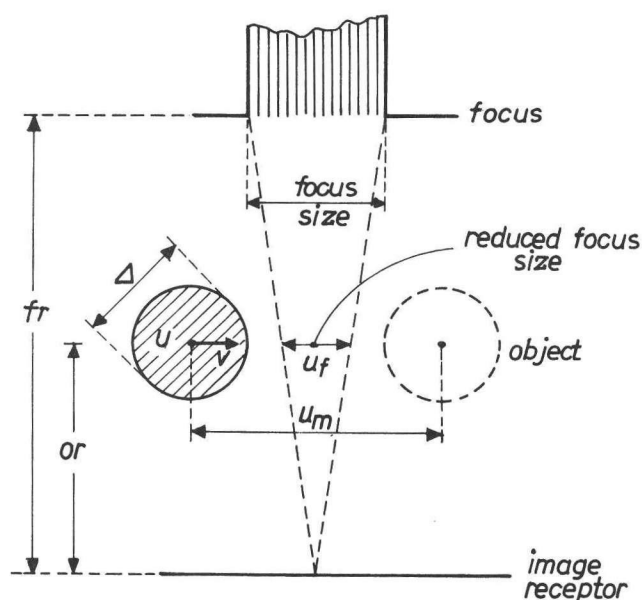


Fig. 3.4.1.  
Geometry for the imaging of a blood vessel.

We found that an LSF image is made if the vessel diameter is smaller than one quarter of the larger of  $u_m$  or the equivalent focal-spot size  $u_f$ . And indicative result is given in fig. 3.4.2, for the homogeneous intensity distribution and the optimum condition  $u_f = u_m$ . The shadow image LSF is a triangle, which is indeed approximated if  $\Delta = 0.25u_f$ .

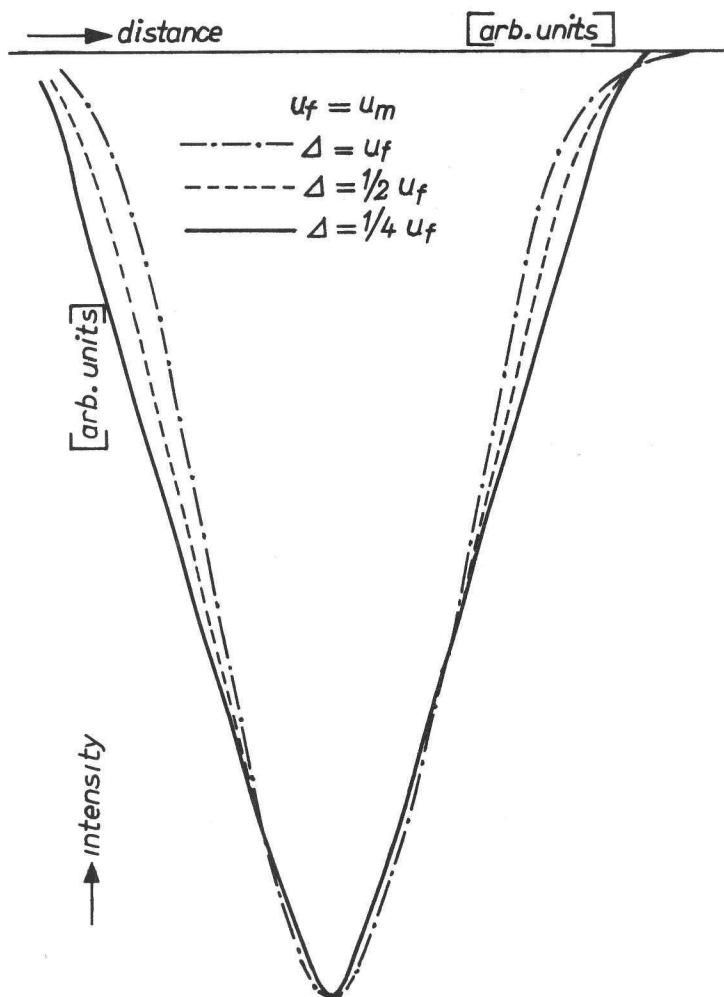


Fig. 3.4.2.

Normalized shadow image of relatively small blood-vessels.

### 3.4.1 Moving objects

#### 3.4.1.1 Optimum focal-spot size

In the reports of Marschall (1973) and Marschall and Möller (1973) a number of foci with different intensity distributions are dealt with. The foci have equal short-time loadability (100 kW) and equal loss of anode material of the focal track. The following four representative distributions are chosen for comparison (fig. 3.4.3):

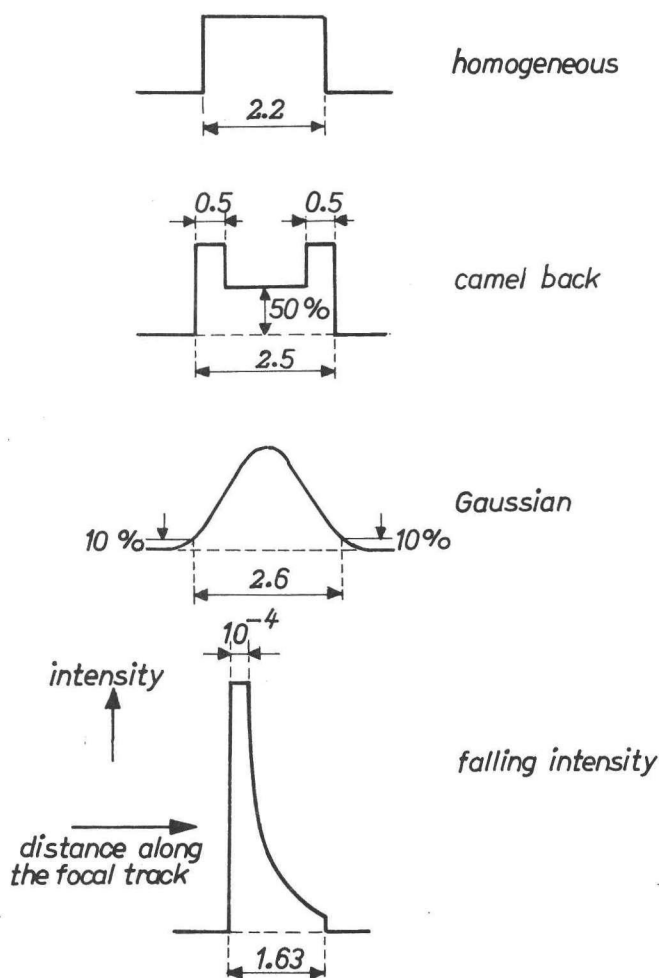


Fig. 3.4.3.  
100 kW focal-spot intensity distributions (dimensions in mm).

- a homogeneous distribution;
- a camel-back distribution, representing the present X-ray tube situation;
- A Gaussian-shaped distribution, which matches good loadability with small induced spatial distortion (Fenner et al., 1972);
- a falling intensity distribution, as suggested by Oosterkamp (1974). The distribution has a leading edge of infinite intensity (for practical reasons, the initial intensity is thought to be finite and constant; see fig. 3.4.3). The intensity decreases in proportion to the inverse square root of the distance covered by a point of the focal track in the electron beam. This focus represents the highly asymmetric type with high loadability but with perhaps a worse spatial resolution.

As the focus size and loadability are related, the focus size can be adjusted so as to obtain the least possible shadow image distortion. As, however, a focus intensity *distribution* occurs, a focus size can only be specified by definition. The focus size will be determined on the basis of the MTF, depicted in fig. 3.4.4. Both the Gaussian and the falling intensity focus have a pronounced high spatial-frequency end. A  $180^\circ$  phase shift occurs at the zero transfer for the homogeneous and camel-back focus. This may lead to black-white reversal ('spurious resolution'). The Gaussian focus does not give rise to any phase shift, while the falling intensity focus corresponds to a rather intricate and irregular shift.

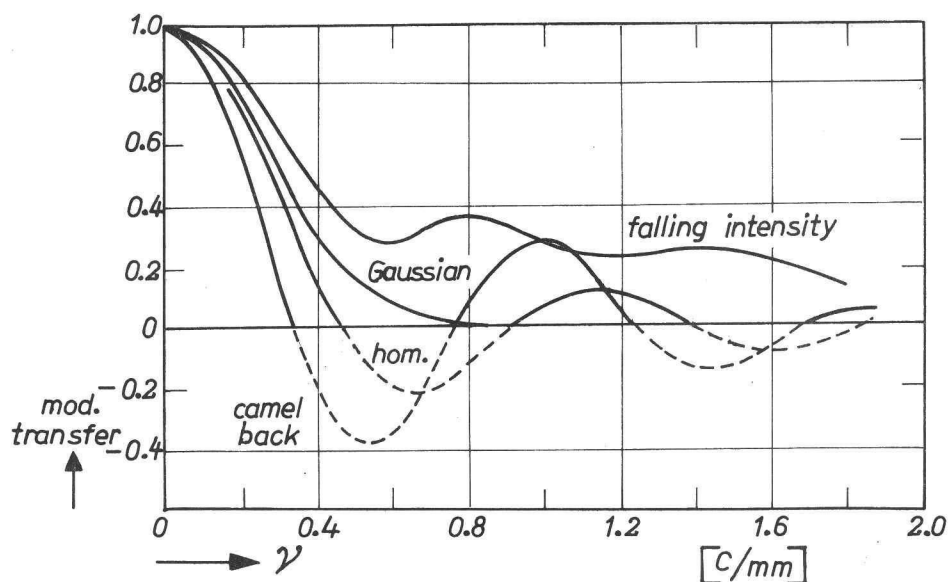


Fig. 3.4.4.

MTF of foci with different intensity distribution (the  $180^\circ$  phase-shifted parts are drawn dotted).

In the next three sections a relationship for the optimum size per distribution is obtained. Fortunately, the effect of the intensity distribution is considerably smoothed by the movement LSF, so the outcome of the optimization is not very sensitive to the quality criterion chosen. The smoothing by the movement is illustrated by fig. 3.4.5, which gives the LSF for the prominent asymmetric falling intensity distribution for different  $u_f$  and  $u_m$  combinations. If  $u_m$  is relatively small ( $u_m = 1/8 u_f$ ), the focus intensity distribution is present in the image. If  $u_m$  is large this is not the case. For the best shadow image LSF, we may intuitively state that  $u_f$  and  $u_m$  are of the same order of magnitude. It turns out, then, that the intensity distribution is already considerably masked. The  $u_f$  must of course specifically be defined for this distribution (sec. 3.4.1.1.3).

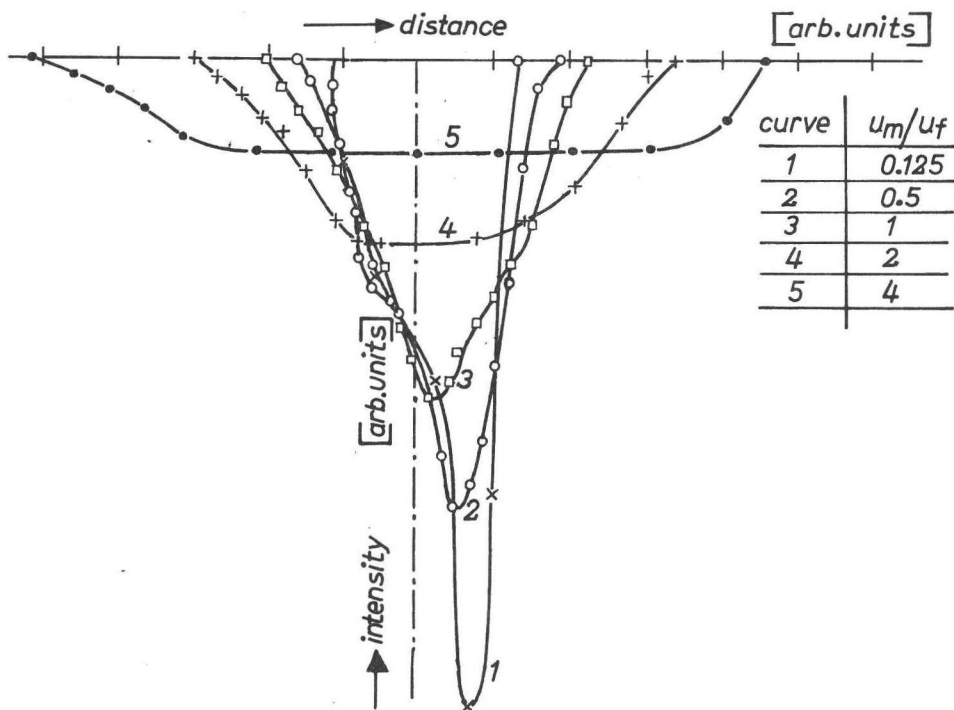


Fig. 3.4.5.

*Masking of the intensity distribution by the movement; falling intensity distribution.*

For the loadability of the tube as a function of the focal-spot size, we will use the same relation (eq. 3.2.7) as for the camel-back distribution. It represents an overall characteristic of rotating anode X-ray tubes, which will not vary substantially with the distribution. In any case, it holds for a homogeneous distribution, and it appears to give a good indication of the camel-back distribution.

**3.4.1.1.1 Homogeneous and camel-back distribution.** It has been shown in sec. 3.2.1 that the camel-back distribution can be approximated by a homogeneous one, with a corresponding MTF which has the same first zero modulation-transfer frequency. The homogeneous distribution can therefore be considered as representative. Both the maximization of the peak LSF contrast (sec. 3.2.1.2) and the optimization of the shadow image modulation transfer lead to the conclusion that the movement and focal-spot unsharpness factor should be of the same order of magnitude. In fact, the condition  $u_f = u_m$  is best. Fig. 3.2.10 applies to this optimization.

3.4.1.1.2 *Gaussian distribution.* The MTF is once more given in fig. 3.4.6. The effective focus size is now defined as the size of the homogeneous focus with an MTF that coincides at a modulation ratio of 0.5. Hence  $f = 2$  mm, which is smaller than the 10% width (2.6 mm). As a first attempt at finding the optimum, we again put  $u_f = u_m$ , where  $u_f$  is calculated on the basis of the effective focus width. Variation of the focal-spot size and a calculation of the peak LSF contrast may prove whether this equality situation is best.

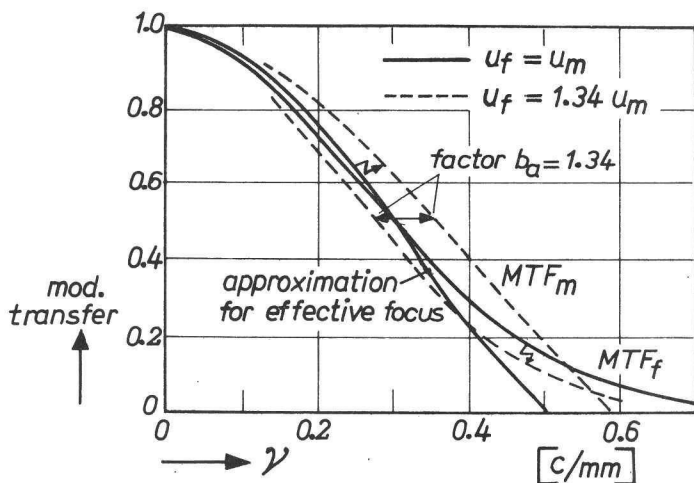


Fig. 3.4.6.

Definition of the effective focus size for the Gaussian distribution; optimum MTFs for  $b_a = 1.34$ .

The focus OTF is written as:

$$\text{OTF}_f(\nu) = e^{-b_f^2 \cdot 7.7 \nu^2} \quad (3.4.1)$$

The movement OTF is written as:

$$\text{OTF}_m(\nu) = \frac{\sin(2\pi\nu/b_f^{1.5})}{2\pi\nu/b_f^{1.5}} \quad (3.4.2)$$

The peak LSF contrast will be situated at the centre, so the peak contrast is given by

$$\text{LSF}_a(o) \sim \int_0^\infty \frac{\sin(2\pi\nu/b_f^{1.5})}{2\pi\nu/b_f^{1.5}} \cdot e^{-b_f^2 \cdot 7.7 \nu^2} d\nu \quad (3.4.3)$$



The normalized value of the integral is given in fig. 3.4.7, together with the homogeneous distribution situation. As the maximum value occurs at  $b_f = 1.12$ , the focus size must be chosen larger than for the equality condition. The reason can be found in the high frequency end of the focus MTF, which indicates that the choice of a larger focus has a less detrimental effect. The optimum in fig. 3.4.7 is less sharply peaked for the same reason.

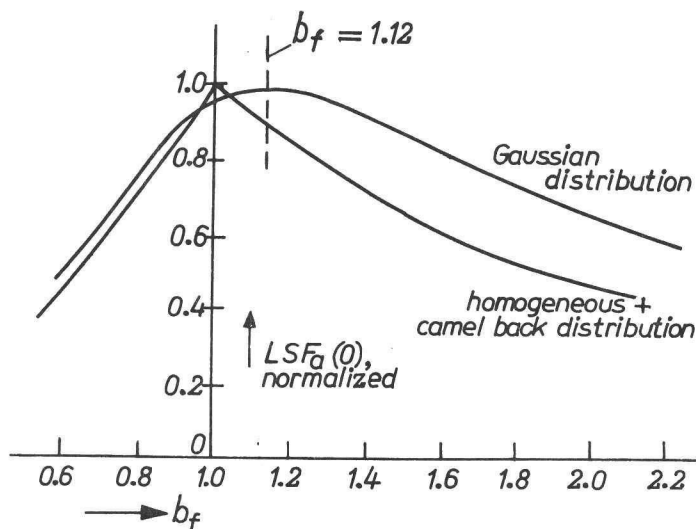


Fig. 3.4.7.

*Influence of the focus size on the maximum ESF contrast gradient, for different focal spot intensity distributions.*

The  $MTF_f$  and  $MTF_m$  for the optimum situation are given in fig. 3.4.6, showing the non-equality of MTFs. The ratio  $b_a = \frac{u_f}{u_m}$  (eqs. 3.2.2.4, 3.2.12 and 3.2.13) equals  $1.12^{2.5} = 1.33$ . In principle one cannot speak about 'non-equality of MTFs', because differently shaped MTFs are compared. Further, the focal-spot size definition was chosen rather arbitrarily.

**3.4.1.1.3 Falling intensity distribution.** The MTF of the 100 kW focus is given in fig. 3.4.8. The high frequency end of the MTF is even more pronounced, and therefore we expect the same tendencies as for the Gaussian distribution. The effective focus size  $f$  is defined accordingly, so  $f = 1.61$  mm. As a starting point for finding the optimum we again put  $u_f = u_m$ , so  $b_a = b_f = 1$  (fig. 3.4.8, drawn curve).

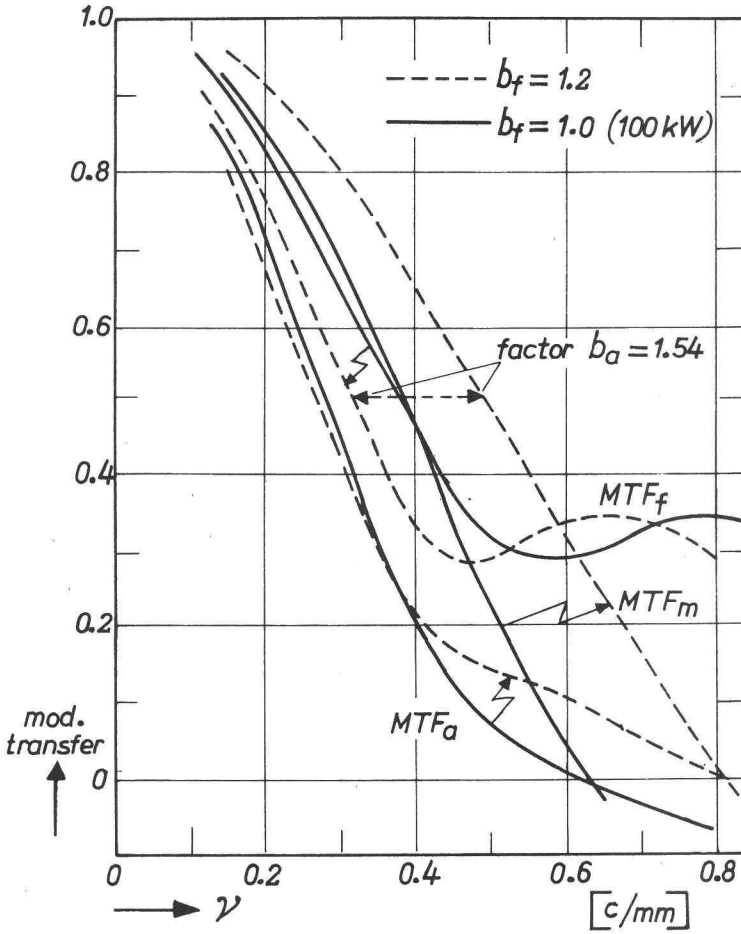


Fig. 3.4.8.  
MTFs as a function of focus size; falling intensity distribution.

The position of the maximum contrast of the LSF is not known, because the focus intensity distribution is asymmetric. In varying the focus size ( $b_f$  value), then, the complete LSF must be calculated. The results are given in fig. 3.4.9. The maximum contrast corresponds to a rather large focus ( $b_f = 1.8$ ), but in this situation the shape of the intensity distribution also stands out clearly ( $u_m < u_f$ ). A good compromise seems to be case 3, with  $b_f = 1.2$ . The corresponding MTFs are also shown in fig. 3.4.8. For the optimum situation the ratio  $b_a$  will therefore be  $1.2^{2.5} = 1.54$ .

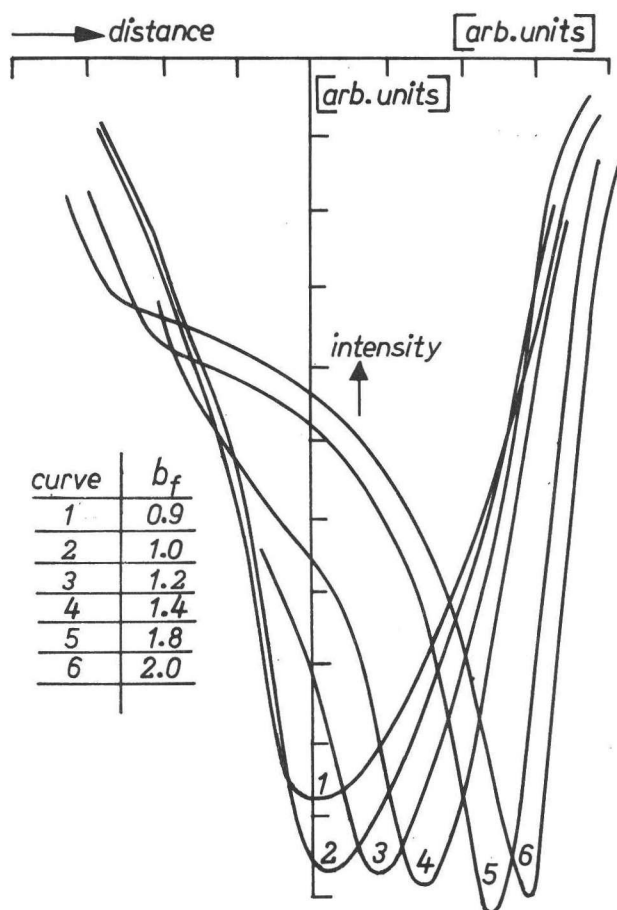


Fig. 3.4.9.

$LSF_a$  as a function of the focus size; falling intensity distribution.

### 3.4.1.2 Influence of the image receptor

Like the movement unsharpness, the limited spatial resolution of the image receptor will also smooth the effect of the intensity distribution in the final image. The smoothing effect depends completely on the balance between the LSF of the shadow image and the image receptor in the object plane. In the following, only the optimum shadow image LSF will be considered for the homogeneous/camel-back intensity distribution, so as to make reference to the present systems possible.

The previously defined balance factor for this purpose, i.e. the  $\eta_{x,m}$  position for equality of MTFs, can of course be used. But the corresponding masking effect of

the image receptor LSF is small, because its FWHM is 50% smaller than the FWHM of the shadow image LSF (for a homogeneous/camel-back intensity distribution). We therefore decided to define a new characteristic object position for which the FWHMs are equal. This position is denoted by  $\eta_{eq}$ ; in words it is described as 'the equality of LSFs' position.

The value of  $\eta_{eq}$  can be calculated with  $\eta_{x,m}$  as the starting point. The  $\eta_{eq}$  value will be smaller than  $\eta_{x,m}$ , because the image receptor LSF must become worse whereas the LSF<sub>f</sub> must improve. If the MTFs are equal, then the width of the image receptor LSF is smaller by a factor of 2. We can therefore conclude that for equality of LSFs the ratio  $b_x$  between the spatial frequencies where the modulation transfer is 0.5 must also be equal to 2.

The ratio between  $\eta_{x,m}$  and  $\eta_{eq}$  can thus be calculated, bearing in mind that the choice of a particular value of  $\eta$  corresponds to a scaling factor of the  $\nu$ -axis of  $1/\eta^{3/5}$  for MTF<sub>a</sub> and  $1/(1-\eta)$  for MTF<sub>r</sub>. For  $\eta_{eq}$  we may therefore write

$$\frac{1 - \eta_{x,m}}{1 - \eta_{eq}} = 2 \left( \frac{\eta_{x,m}}{\eta_{eq}} \right)^{3/5} \quad (3.4.4)$$

This ratio and the  $\eta_{eq}$  value are given in fig. 3.4.10. For small values of  $\eta_{x,m}$  the ratio approximates  $2^{5/3} = 3.17$ . For large values, the ratio tends to unity.

If now  $\eta$  is much smaller than  $\eta_{eq}$ , then the LSF of the image receptor dominates and the influence of the shadow image will be small, quite apart from the influence of the intensity distribution on the system LSF. The reverse is true if  $\eta \gg \eta_{eq}$ .

### 3.4.1.3 The system line-spread function

The influence of the choice of the intensity distribution is calculated by assuming an arbitrary movement MTF for a given loadability and intensity distribution, and by calculating the corresponding optimum focal-spot size for each distribution. The resulting system LSF is calculated for two situations, i.e. for an ideal image receptor and for the  $\eta_{eq}$  situation. In this way the relative influence of the distribution can be assessed. In principle there is no need to quantify the movement MTF. To elucidate the procedure, however, the starting point is taken as the Gaussian 100 kW focal spot, and the MTF<sub>m</sub> is characterized by  $u_m = 2$  mm (fig. 3.4.6, drawn lines). As outlined in sec. 3.4.1.1.2, the optimum 10% width equals  $1.12 \times 2.61 = 2.91$  mm, the short-time loadability  $P$  equals  $100 \times 1.12^{1.5} = 119$  kW. The corresponding data for the falling intensity distribution are derived from sec. 3.4.1.1.3. The optimum sizes for the camel-back and homogeneous distributions are calculated with the method described in sec. 3.2.1.

The optimum conditions are summarized in table 3.4.1. The loadability is larger the larger the specific energy (unit kW/mm<sup>2</sup>) of the focus. So if one wants to take

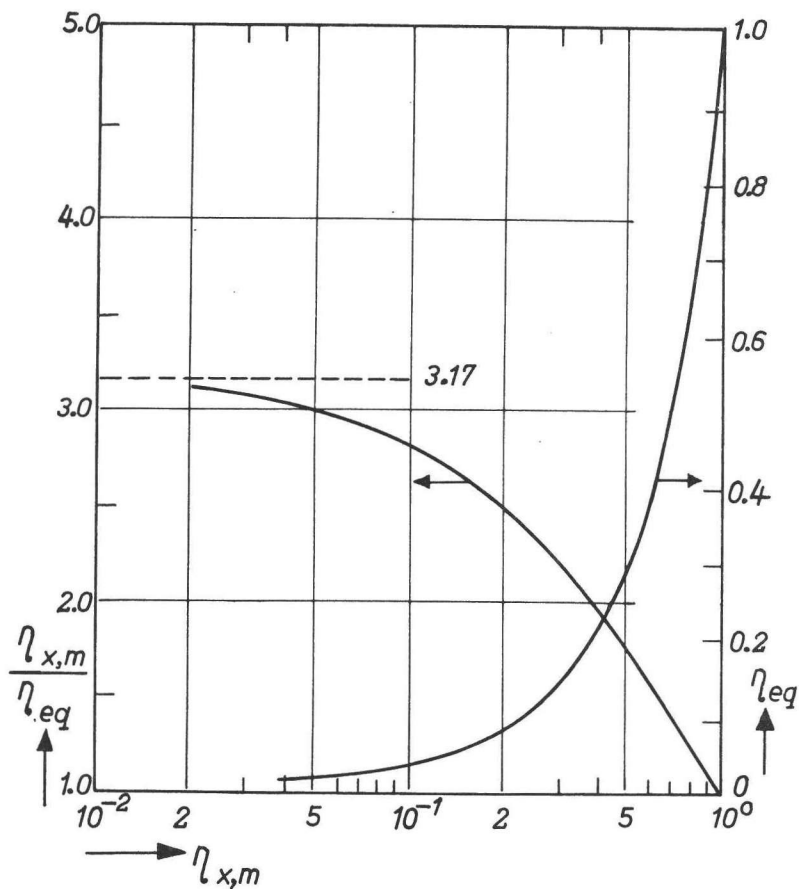


Fig. 3.4.10.  
 $\eta_{eq}$  as a function of  $\eta_{x,m}$ .

TABLE 3.4.1: Optimum focus sizes and short-time loadabilities

intensity distribution	optimum focus size [mm]	$u_m$ [mm]	loadability [kW]	
			abs.	rel.
camel-back	2.12 { eff.	2.12	78	1.00
homogeneous	2.54 { value	2.54	94	1.20
Gaussian	2.91 : 10% value	1.69	119	1.53
falling intensity	2.14 : width	1.35	148	1.90

full advantage of a better intensity distribution, higher short-time loadabilities will be needed. If for instance an optimum situation is obtained for a camel-back distribution, then a better distribution with the same loadability corresponds to a better focus MTF in relation to the movement MTF. The focal-spot size must therefore be chosen larger to obtain the new optimum. The loadability is correspondingly higher, and the movement MTF is improved.

The shadow image LSFs for the optimum situations are given in fig. 3.4.11. These LSFs correspond also to the system LSF for an ideal image receptor. The camel-back distribution gives the worst, the falling intensity distribution gives the best LSF. In both situations the distribution as such is not very apparent. In the case of equality of LSFs, the  $\eta_{eq}$  situation, the same tendencies show up, although the differences are smaller, of course. The intensity distribution as such is almost

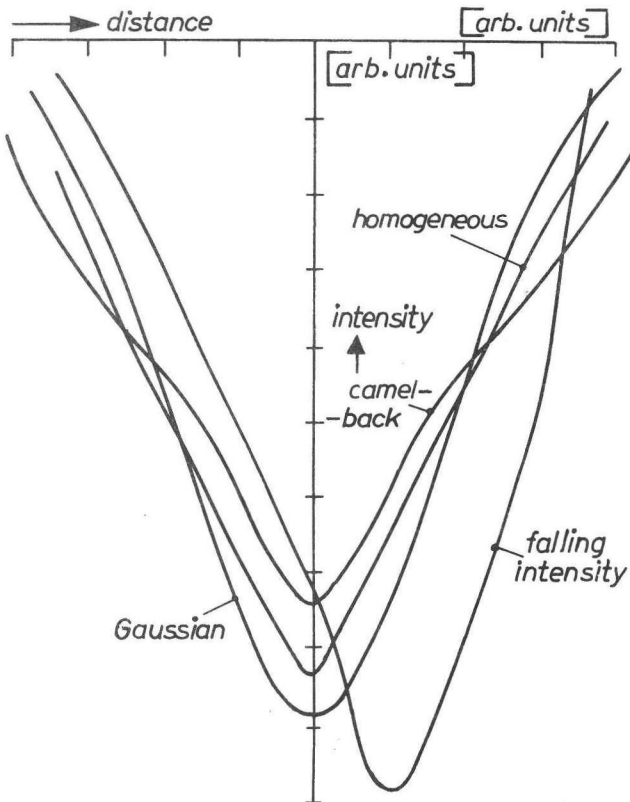


Fig. 3.4.11.

System LSF for different focus intensity distributions; ideal image receptor/optimum focus size.

completely masked, so that graphs of the system LSFs would not give extra information. The maximum LSF contrasts are given in table 3.4.2 for the ideal receptor and the  $\eta_{eq}$  situation, normalized to the Gaussian situation. The Gaussian situation is chosen as the starting point (i) to situate the reference in the mid-range of the possibilities, and (ii) because one is generally interested in this distribution as the successor of the camel-back distribution.

**TABLE 3.4.2: Maximum LSF<sub>x</sub> contrast for different focal-spot intensity distributions**

intensity distribution	ideal image receptor	equality of LSFs ( $\eta_{eq}$ )
camel-back	83%	88%
homogeneous	95%	96%
Gaussian	100%	100%
falling intensity	111%	102%

It appears that the change from a camel-back to a homogeneous distribution is a relatively large step forward. The advantages in going further to a Gaussian distribution are smaller. The improvement with respect to the present situation can be up to 17%. The use of a falling intensity distribution gives only small improvements for the  $\eta_{eq}$  situation. If the image receptor LSF can be neglected, then relatively large improvements are obtained. The maximum contrast can be up to 30% larger than with the present foci.

### 3.4.2 Stationary objects

As stated before, less attention is paid to the stationary object situation because generally the image receptor LSF dominates. Consequently, only the camel-back intensity distribution is investigated as this is currently used. The representative distribution is given in fig. 3.4.3. The system balance factor  $b_x$  is readily available for this simple system, because the movement MTF is not involved. If  $b_x$  is large, then the image receptor LSF dominates, and a considerable smoothing of the intensity distribution will occur. Since a zero value of  $b_x$  corresponds to an ideal image receptor, the distribution completely describes the system LSF.

To quantify these trends, the system LSFs have been calculated for a number of  $b_x$  values (fig. 3.4.12). It is indeed found that if the image receptor is relatively good ( $b_x = 0.05$ ) hardly any smoothing occurs. For the  $b_x = 1$ , i.e. the  $\eta_{x,st}$  situation, a considerable amount of smoothing takes place. If the image receptor unsharpness dominates ( $b_x > 1$ ) no irregularities in the LSF are present.

We will use  $b_x = 1$  as the critical value for stationary object imaging in sec. 5.1.3.1.

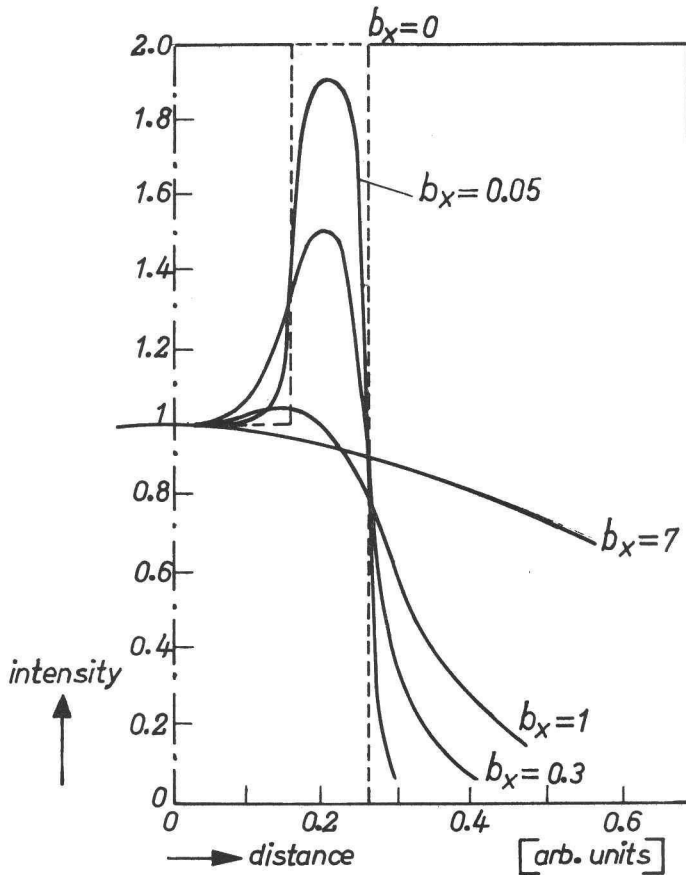


Fig. 3.4.12.

$LSF_x$  for camel-back focus intensity distribution and different image receptor LSF.

#### 4. THE IMAGE CONTRAST

##### 4.1 Scattered radiation

###### 4.1.1 Introduction

In fig. 4.1.1 a schematic presentation is given of a medical X-ray system. The primary beam impinges on the object, in which X-rays are absorbed and scattered. The remainder of the primary beam is correlated with the shadow image, and the scattered radiation acts as a veiling glare. This glare is not homogeneous, as the scattered radiation intensity is up to 30% smaller at the borders of the object (Nemet et al., 1953). As before, however, we shall confine ourselves to the central



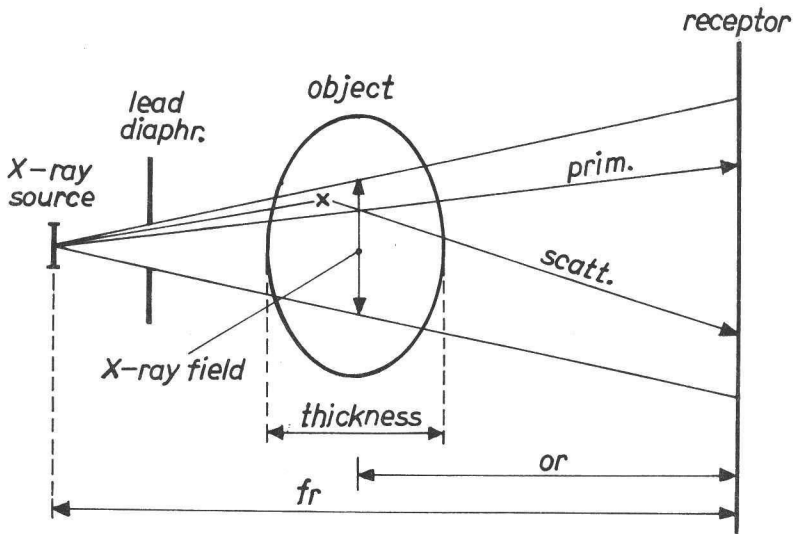


Fig. 4.1.1.  
Scattered radiation in X-ray systems.

region. Object information is retained in the scattered radiation. For radiography this information cannot be used, however, because of lack of spatial definition: the scattered radiation involves the superposition of the images of all the scatterers in the irradiated volume. An image can only be built up by investigating small volumes of tissue, i.e. by the application of a collimated source and detector (Lale, 1959).

The contrast reduction by scattered radiation can partly be overcome by using the fact that the object itself is the source of scattered radiation. This implies that the angle of incidence is relatively large. Thus, an X-ray absorbing grid of lead slats preferentially absorbs the scattered radiation. Another method consists in removing the source, i.e. the object away from the image receptor. This is called the air-gap technique, as introduced by Groedel in about 1925. The first technique (grid) has been extensively investigated by Hondius Boldingh (1964). Such an elaborate analysis of the air-gap technique does not exist, although many results have already been obtained by Nemet et al., (1953). In addition it is general practice (Feddemma and Botden, 1965; Hale and Mishkin, 1969) to use a fixed X-ray beam aperture; as a result the irradiated object volume decreases with increasing geometric magnification. This greatly exaggerates the beneficial effect of the air-gap technique, at the expense of the depicted object area (the X-ray field, fig. 4.1.1). We, on the contrary, will keep the irradiated object area constant, because we are interested in imaging an object irrespective of the geometric magnification. This approach was also adopted by Rao et al. (1973, Part I).

The air-gap technique is also interesting because of the consequences for the object resolution already described (ch. 3). In sec. 5.2.5, the contrast effect and the 'unsharpness' effect will be confronted for practical systems. The selective absorption of scattered radiation also leads to an increase of the exposure time. This affects the patient-characterizing number  $c_p$ , and consequently the shadow image MTF as a function of the geometric magnification. This effect is studied in Appendix IV.

The effective scattered radiation intensity depends on a large number of parameters in an intricate way. Some parameter values also depend on the X-ray energy, so a convolution with the X-ray spectrum is involved. This hampers a quantitative, predictive analysis. We have therefore chosen the pragmatic approach of *measuring* the intensities as a function of

- the X-ray beam quality
- the choice of the image receptor (universal or fast  $\text{CaWO}_4$  Philips' intensifying screens, or a 6" CsJ OB110 image intensifier. Films without intensifying screens will not be investigated because in practice they have only a very limited range of applications);
- the object thickness and object area;
- the geometric magnification;
- the application of a grid.

To include the spectral response of the image receptor as well, the intensities will be defined in terms of the corresponding light intensity ( $C_1(r)$ ) of the real primary light image in fig. 2.2.11.

The potential benefits of the air-gap technique can be estimated by applying the inverse-square law for the primary radiation intensity at the object and the scattered radiation intensity at the image receptor. For a small irradiated volume in the central beam the induced source intensity of scattered radiation will be proportional to  $1/(fr - or)^2$ . The scattered radiation intensity at the image receptor is reduced by a factor  $or^2$ , so the intensity at the receptor is proportional to

$$\frac{1}{(fr - or)^2 \cdot or^2} \quad (4.1.1)$$

This relation is given in fig. 4.1.2 as a function of  $\eta = or/fr$ . This may also indicate the trend for practical systems. A substantial reduction in scattered radiation seems possible. Further, an optimum may exist for object positions mid-way between the source and the receptor. If the object is shifted further away, then the induced source intensity increases unfavourably fast. These phenomena have already been found by Seemann (1938).

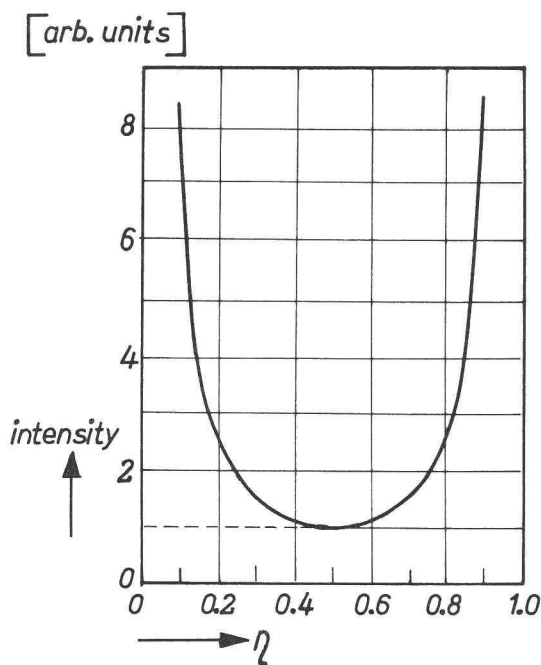


Fig. 4.1.2.  
Estimated intensity of scattered radiation.

#### 4.1.2 Definition of characteristic parameters

Analogous to the mathematical description of the contrast improvement by grids (Hondius Boldingh, 1964) the following characteristic parameters can be defined: the Bucky factor  $B$ , the contrast improvement factor  $K$ , the selectivity  $\Sigma$ , and the relative intensity of scattered radiation  $a$ . Their value can be calculated with the aid of the intensity of the primary and scattered radiation on the receptor if no magnification is applied (intensities  $I_p$  and  $I_s$  respectively), and for magnification (intensities  $I_p'$  and  $I_s'$ ). In practice, a magnification equal to unity is not feasible. The value  $I_s$  is therefore represented by  $I_s'$  for small values of  $m$ , i.e.  $m = 50$  mm. Unlike the grid situation,  $I_p = I_p'$ , so

$$K = B = \frac{I_p + I_s}{I_p + I_s'} \quad (4.1.2)$$

The Bucky factor equals the factor by which the X-ray tube load per radiograph must be increased. Further,

$$\Sigma = \frac{I_s}{I_s'} \quad (4.1.3)$$

and

$$a = \frac{I_s}{I_p} \quad (4.1.4)$$

According to this definition, 'a' is only defined for the non-magnified situation. However, we will use 'a' as a symbol for the relative intensity of scattered radiation, and so generally we put  $a = I_s/I_p$ .

### 4.1.3 Measuring arrangement

The measuring arrangement (fig. 4.1.3) consisted of an X-ray source, a beam-limiting lead diaphragm, an artificial object (phantom), and a receptor to measure the light normally reaching the film.

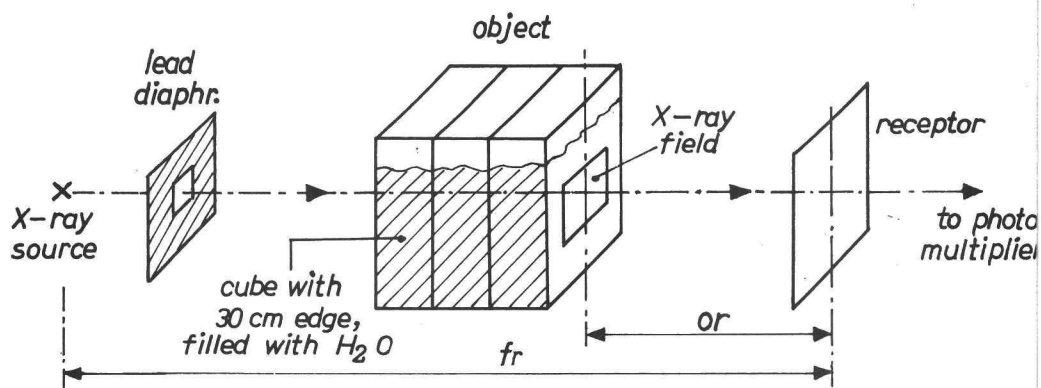


Fig. 4.1.3.

*Arrangement for the measurement of the scattered radiation intensity.*

The arrangement had the properties of generally used X-ray systems:

- Primary X-ray source: a type 21944/00 Rotalix X-ray tube (inherent filter 2 mm Al) and a Medio 50 power control.
- Practical X-ray beam quality, i.e. an additional filter of 2 mm Al was employed. The peak value of the high voltage on the tube was 60 or 110 kV, and the tube current was 1 to 3 mA. The ripple on the real primary light intensity was about 20% top-top for 1 mA tube current, and about 80% for 3 mA. In the latter case a full-wave rectified high voltage situation was thus approximated, whereas in the former situation the conditions for a 6 or 12 pulse X-ray generator were simulated. The higher tube current had to be used only for the thickest phantom so as to obtain a reasonable signal. In any case, the effect of the X-ray beam quality proved to be small, so less attention was paid to the high voltage ripple.

- c. Object: a water phantom was built to simulate the medical object. It consisted of a cube with two partitions so as to obtain a water thickness of 100 mm (skull), 200 mm (lung) or 300 mm (stomach). The water surface perpendicular to the central X-ray beam had an area of  $30 \times 30 \text{ cm}^2$ . The X-ray field corresponded to the surface nearest to the receptor, a choice generally in accordance with medical practice.
- d. Source-receptor distance: a commonly used  $r$  value of 1000 mm was chosen.
- e. The minimum object-receptor distance was 50 mm, which is a practical value.
- f. Object area: three sets of interchangeable lead diaphragms were used to irradiate object areas of  $6.5 \times 6.5 \text{ cm}^2$ ,  $14.3 \times 14.3 \text{ cm}^2$ , and  $21.5 \times 21.5 \text{ cm}^2$  for or values up to 600 mm (so the maximum magnification was 2.5). These fields correspond to commonly used receptor sizes, i.e. 6" image intensifier, and  $24 \times 24 \text{ cm}^2$  and  $43 \times 43 \text{ cm}^2$  film.
- g. Receptor: a 6" image intensifier (CsJ input screen) or a universal or high-sensitive intensifying screen were used. (In practice a front and a back screen are employed, but the screens are identical.)

### Receptor

The receptor/photomultiplier (PM) arrangements are given in fig. 4.1.4a and fig. 4.1.4b for the screen and the image intensifier situation. The intensifying screen is provided with a lead diaphragm so as to irradiate a disk with a diameter of 35 mm. This is sufficiently small compared with the smallest X-ray field, so no edge effects occur. A lead-glass disk is placed between the screen and the PM cathode to absorb X-rays which otherwise would lead to spurious PM signals. A lead shield around the PM is also used. A sufficiently small section of the image intensifier output screen (fig. 4.1.4b) is seen by the PM via a collimator (diam. = 1 mm, length 3 mm). The PM is of the 153 AVP type.

The fluctuating component of the PM signal, which is due to the ripple of the tube high-voltage and to the noise caused by the stochastic flow of X-ray quanta, was suppressed by an RC filter with  $\tau = 1 \text{ s}$ . The DC component was measured with a digital voltmeter, type PM 2422.

It proved necessary to continuously monitor and adjust the X-ray tube current during the measurements. Its variation could be kept lower than 1%.

After all the relevant parameters were adjusted, the object was placed at the minimum distance from the receptor. The PM signal was measured for this and other distances.

The non-linearity of the PM is probably smaller than 3%. In fact, the uncertainties in the applied geometrical factors are the main cause of the uncertainty as regards the linearity, which was measured as follows. With a fixed X-ray tube setting (60 kV and 0.2 mA) the tube was placed at several distances from the receptor

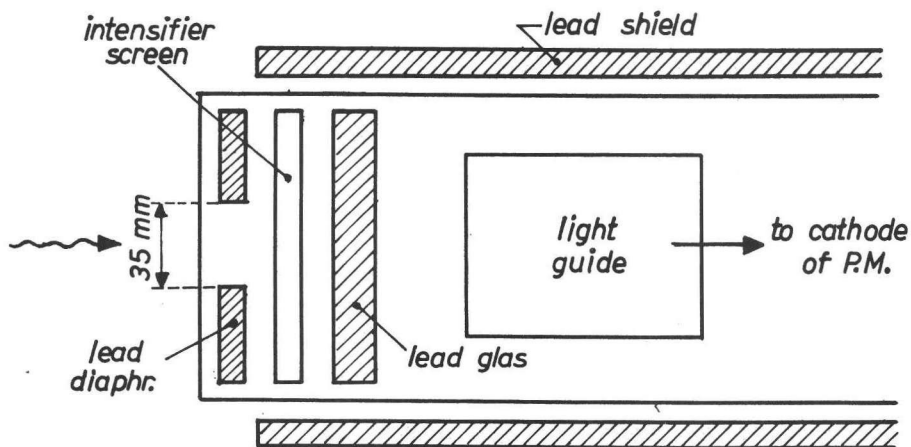


Fig. 4.1.4a Intensifying screen

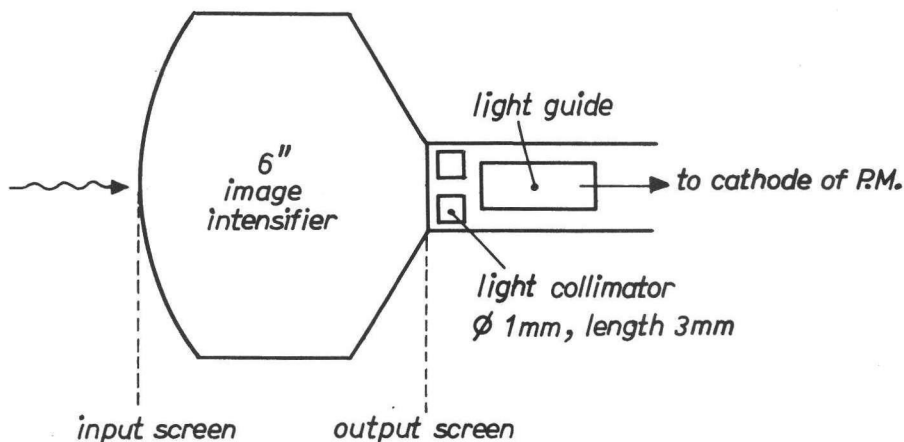


Fig. 4.1.4b Image intensifier

Fig. 4.1.4a/b

Image receptor/P.M. combination.

(universal screen). No object was present. In this way the X-ray exposure rate on the detector varies in a known way and the X-ray beam quality does not change.

#### Measuring errors

Analysis of the measurements shows that the errors in the measured curves are mainly caused by variations of three kinds:

- a. Variation of X-ray tube current. This variation does not exceed 1%.
- b. Variation of the object area, introduced by dimensional errors in the set of lead diaphragms. The relative error is between 2% (for the largest area,  $21.5 \times 21.5 \text{ cm}^2$ ) and 6% (for the  $6.5 \times 6.5 \text{ cm}^2$  area). The influence of these errors on the PM signal can be found with the aid of fig. 4.1.9 'Influence of field area'. It turns out that the error in the PM signal does not exceed 4% (small field, small or), and is at least 1% (large field, large or).
- c. Variation of the object-receptor distance. These errors are at a maximum for small distances, and play hardly any role at larger distances (flat minimum of PM signal, fig. 4.1.5). The error in the distance does not exceed 2% (or = 50 mm, error  $\pm 1 \text{ mm}$ ), which implies an error in the PM signal of 4% at the most (the influence of  $f_o$  must be squared, eq. 4.1.1).

Variation of the tube high-voltage may also occur. This cannot easily be measured. The linearity check may indicate that this variation is of minor importance.

Recapitulating, the relative probable errors do not exceed 9%, and are at least 2%.

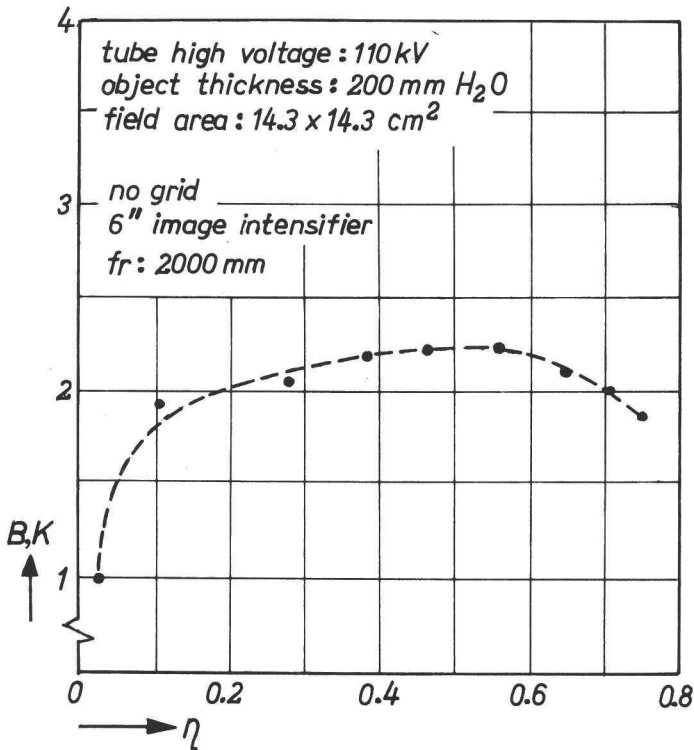


Fig. 4.1.5  
Influence of large geometric magnification factor.

#### 4.1.4 Contrast improvement factor

Due to the large number and range of the parameters that determine the effect of X-ray scattering, only a rough typical indication of the influence of each parameter can be given here. PM signals are given in 'V of D.V.M. reading', or given as the inverse of this value, normalized to the signal measured for the minimum object receptor distance (50 mm). This normalized inverse value is equal to the Bucky factor and the contrast improvement factor.

The object-receptor distance is also given in a normalized form, i.e. in units of  $\eta$ . The parameter values are given in the figures.

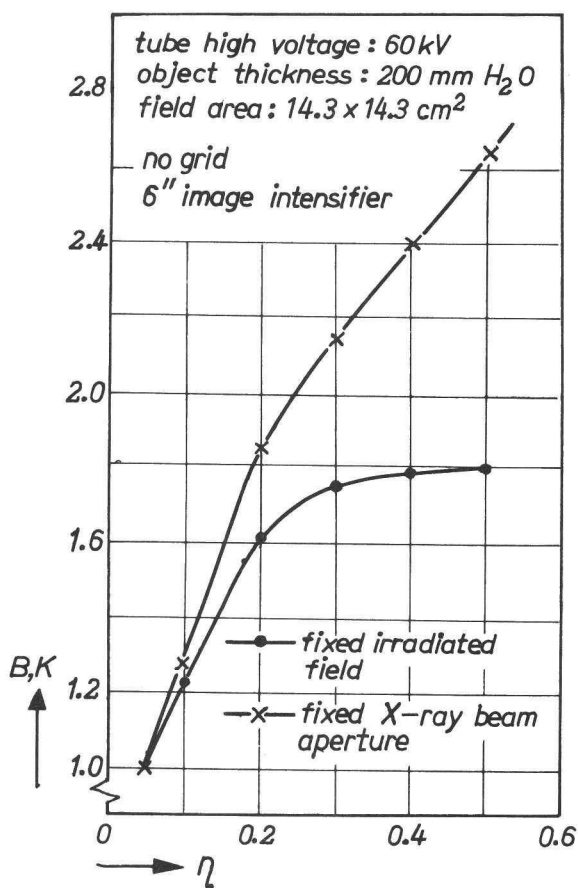


Fig. 4.1.6

Comparison of fixed field and fixed beam-aperture situation.



### Influence of large geometric magnification factor

As pointed out in the introduction, the scattered radiation intensity at the receptor decreases with increasing object-receptor distance. At relatively large distances, however, the intensity becomes higher again. This is shown in fig. 4.1.5, for  $\eta$  values larger than 0.5. The fr distance was 2000 mm to attain these larger  $\eta$  values with the set of lead diaphragms available.

### Fixed object area vs. fixed X-ray beam aperture

As stated in the introduction, the beneficial effect of geometric magnification is exaggerated if a fixed beam-aperture is used. A comparison of the contrast improvement factors (fig. 4.1.6) indeed shows such a behaviour.

### Influence of receptor choice

Differences in X-ray spectral sensitivity determine the influence on the PM signal. The results are shown in fig. 4.1.7 where a universal and a highly sensitive screen, and a 6" image intensifier are compared. The influence of the receptor choice is small.

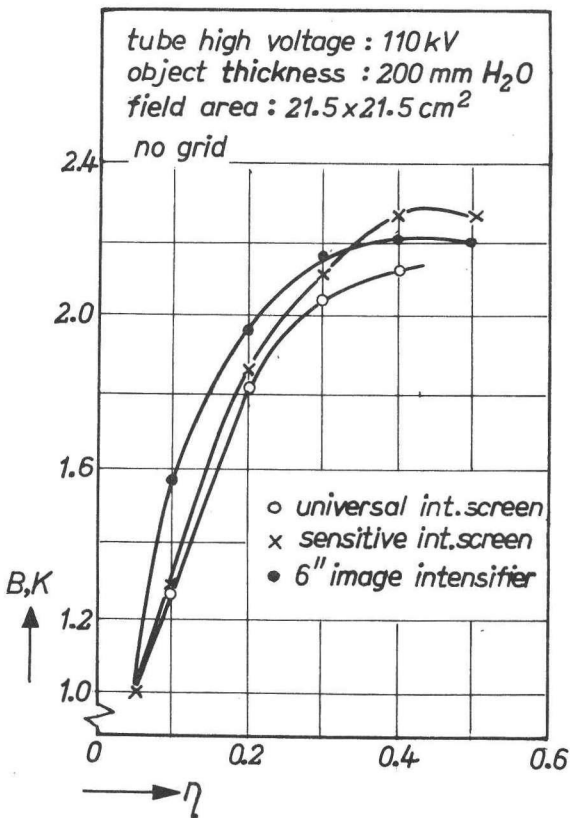


Fig. 4.1.7  
Influence of the image receptor choice.

### Influence of beam quality

The interactions between X-rays and matter are determined by the scattering and absorption coefficients. Since these coefficients, and the sensitivity of the receptors, depend on the energy of the applied X-rays, a dependence of the PM signal on the tube high voltage can be expected.

This influence is relatively small, as is shown in fig. 4.1.8. Generally, the relative intensity of scattered radiation is greater at higher tube voltages.

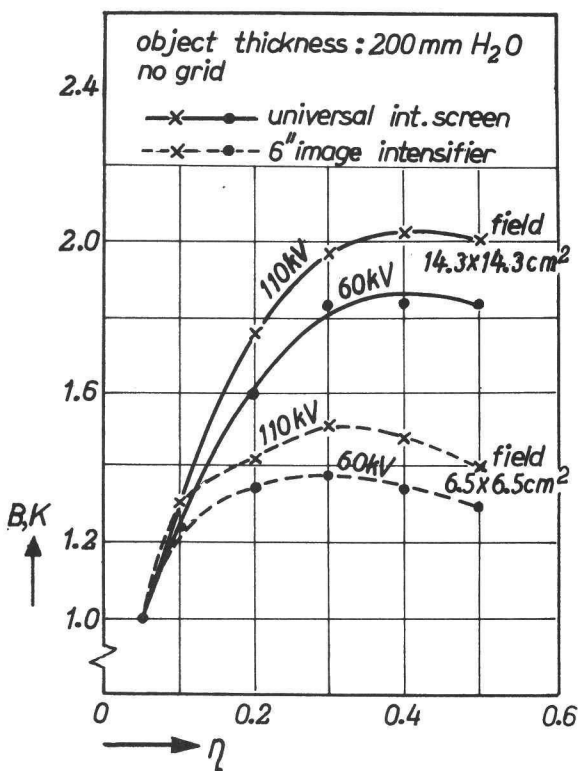


Fig. 4.1.8.  
Influence of the tube high voltage.

### Influence of irradiated object area

An increase of the object area gives rise to an increase in scattering volume. This corresponds to a larger scattering intensity; a larger PM signal therefore can be expected. This behaviour is shown in fig. 4.1.9, where the PM signal is given as a function of the object area. We may say that:

- the scattered radiation intensity is roughly proportional to the irradiated object area, and
- even at large object-receptor distances the scattering has a considerable influence.

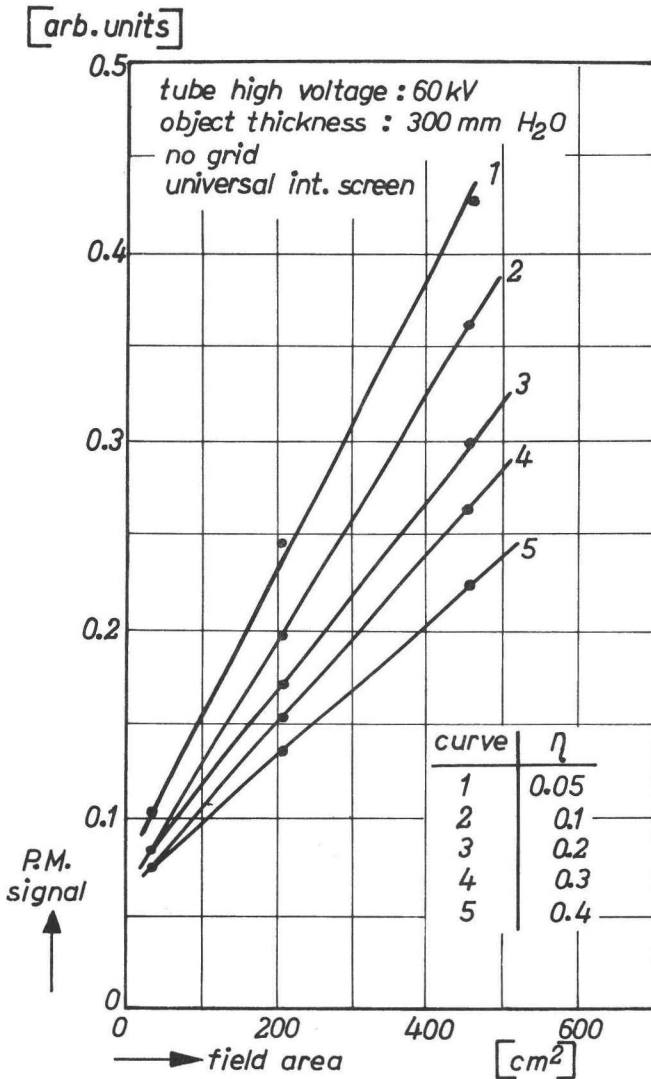


Fig. 4.1.9.  
Influence of field area.

#### Influence of the object thickness

If the object is thicker, more scattering takes place. Therefore we expect a larger increase of the B and K value for larger thicknesses. This is indeed true, as indicated in figure 4.1.10. Different magnification factors and object areas are considered. The curves tend to unity for zero thickness, as should be the case. The curves peak at a thickness of about 200 mm: for larger thicknesses a smaller Bucky factor has

been measured. This can be understood by bearing in mind that a part of the 300 mm phantom is situated at  $\eta$  values of 0.4 or larger, where a further reduction of effective scattered radiation does not take place.

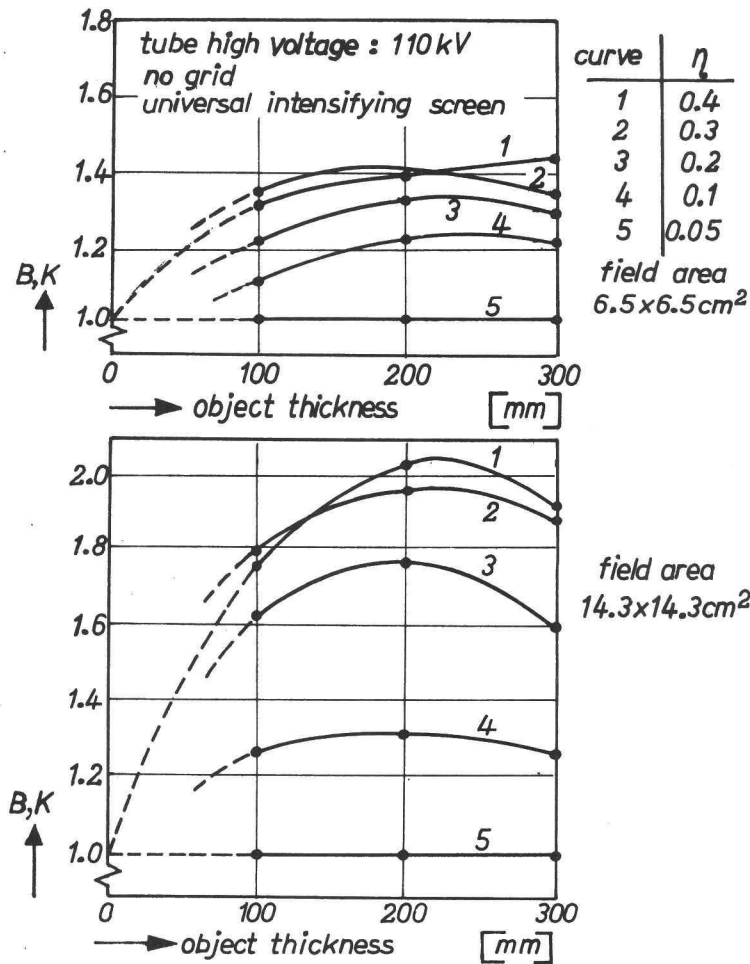


Fig. 4.1.10.  
Influence of object thickness.

**Influence of anti-scatter grid**

A grid considerably reduces the effective scattered radiation intensity. This is shown in fig. 4.1.11, where the influence of a grid is given for two irradiated object areas. Further, it can be seen that even if a grid is applied, a small geometric magnification is advantageous.

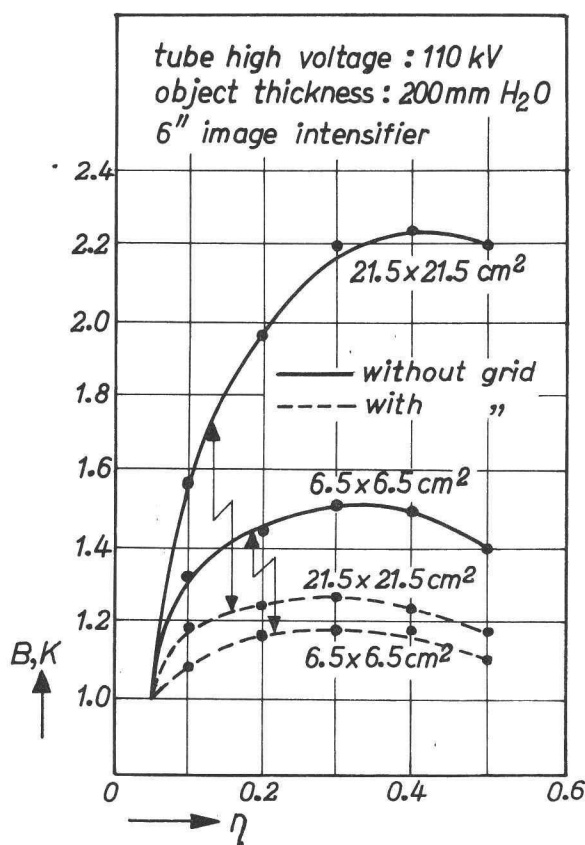


Fig. 4.1.11.  
Influence of anti-scatter grid.

#### 4.1.5 The relative intensity

The relative intensity 'a' of the scattered radiation is defined as  $a = I_s'/I_p$ . The values of  $I_s'$  and  $I_p$  can be deduced from graphs like fig. 4.1.9, in which the relation with the field area is given. Extrapolation of the curves to zero area gives the intensity of the primary beam  $I_p$ .  $I_s'$  can then be found by subtracting this  $I_p$  value from the measured PM signals. The  $I_p$  value is generally measured by applying a small X-ray field, but in our set-up such an extra measurement is not needed.

This is carried out graphically in figures 4.1.12, 4.1.13 and 4.1.14 for the three object thicknesses and the relevant object-receptor distances, as a function of the irradiated object area. The same procedure has been applied for the grid situation (fig. 4.1.15).

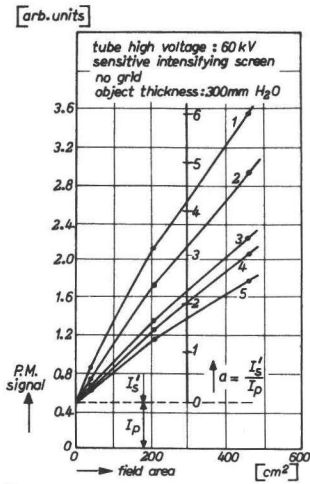


Fig. 4.1.12

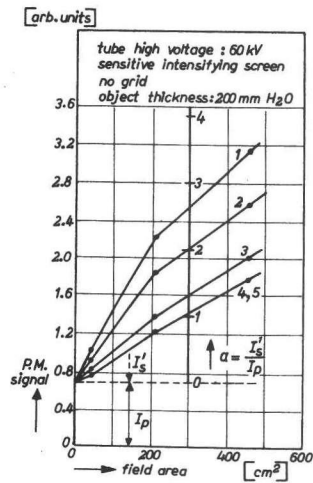


Fig. 4.1.3

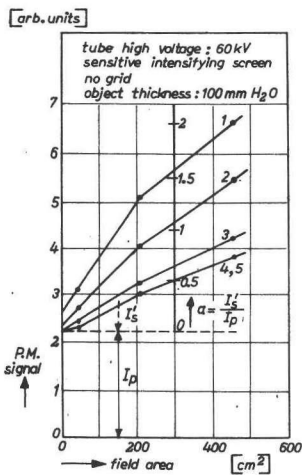


Fig. 4.1.14

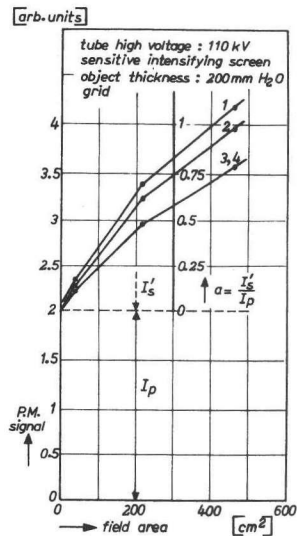


Fig. 4.1.15

Fig. 4.1.12 – 4.1.15

Relative intensity of scattered radiation; object thickness 100, 200 and 300 mm  $\text{H}_2\text{O}$ , without grid, and 200 mm  $\text{H}_2\text{O}$  with grid; curve 1 :  $\eta = 0.05$ ; 2 :  $\eta = 0.1$ ; 3 :  $\eta = 0.2$ ; 4 :  $\eta = 0.3$ ; 5 :  $\eta = 0.4$ .

The maximum value of 'a' is about 6, its value for thin objects (100 mm) is generally smaller than 2. If a grid is used, 'a' is usually smaller than 1. To review the influence of the object thickness, the relative intensity of the scattered radiation is once more given for the universal intensifying screen situation in fig. 4.1.16, as a function of the object thickness, irradiated object area and or value. The relative intensity is roughly proportional to the object thickness. The curves tend to zero for zero thickness, which should of course be the case.

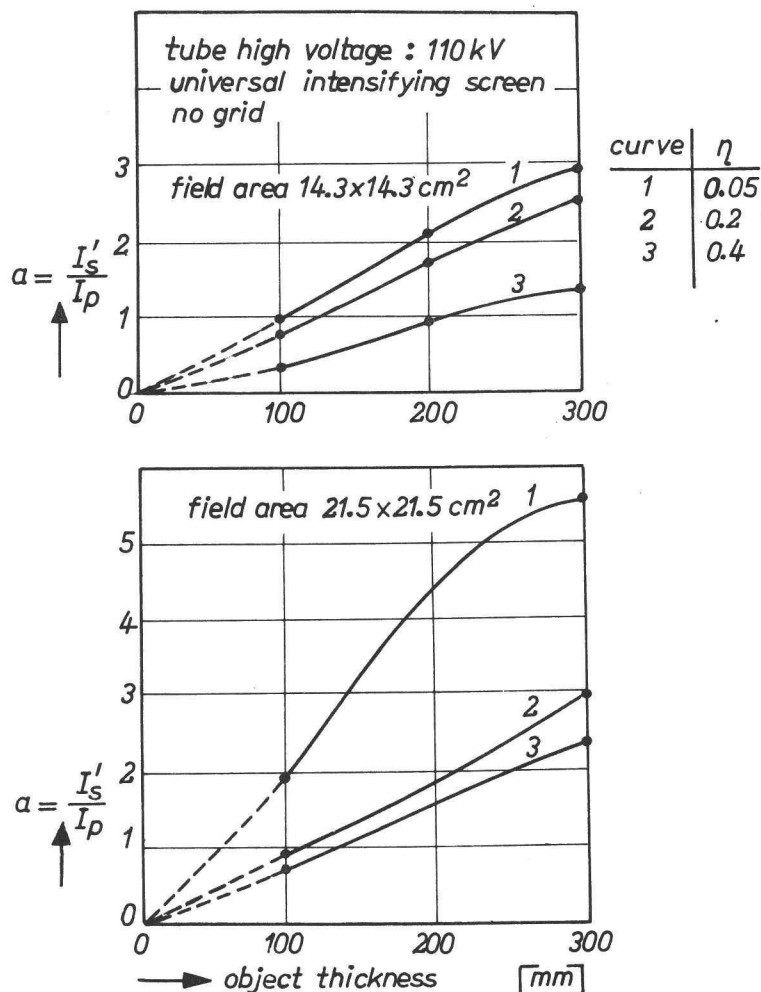


Fig. 4.1.16.

Relative intensity of scattered radiation as a function of the object thickness.

#### 4.1.6 *The selectivity of geometric magnification*

Comparison of the  $a$ -values for small and large values of  $\eta$  in figures 4.1.12, 4.1.13 and 4.1.14 shows that the selectivity is roughly between 2 and 4 if no grid is used. The selectivity is larger for smaller object thickness and for smaller field areas. The selectivity of a grid is of the same order of magnitude. For the smallest  $\eta$  value (curve 1 in figs. 4.1.13 and 4.1.15) and comparable parameter values (200 mm  $H_2O$  thickness) the use of the grid reduces the  $a$ -value by a factor of 3.

#### 4.1.7 *Conclusion*

Geometric magnification is a valuable tool for reducing the influence of scattered radiation. This is only true if the object-receptor/source-receptor distance ratio is not too large. The optimum ratio is roughly 0.4 – 0.6, for which the Bucky factor and the contrast improvement factor have a value of about 2.

The relative intensity of scattered radiation compared to the primary radiation intensity is roughly proportional to the irradiated volume of the object. The X-ray beam quality and the choice of the image receptor have relatively little influence. The maximum relative intensity is about 6, while its value in the case of an anti-scatter grid is generally smaller than unity.

The selectivity of the magnification technique lies between  $\approx 2$  and  $\approx 4$ . If in addition a grid is used, the selectivity is smaller than  $\approx 1.3$ .

A grid intercepts a considerable amount of the scattered radiation. It may be advantageous, however, to apply a slight magnification in addition (ratio object-receptor/source-receptor distance 0.3 for 110 kV tube high voltage).

### 4.2 **Absorption contrast**

#### 4.2.1 *Introduction*

The X-ray absorption contrast of the soft tissues is generally too small to yield useful radiographs. (The situation is of course different in computerized tomography; see Appendix VI.) For this reason contrast media are administered to the patient. Solutions based on barium are used for the digestive tract, whereas iodine is used for images of the blood circulation system, the lymphatic and the nervous system. In general, the lower the X-ray tube voltage (or X-ray beam quality), the larger the resulting absorption contrast. On the other hand the X-ray attenuation by the patient is greater, so the exposure time can become unfavourably long. The latter behaviour is described by the so-called  $p$  factor: the light output of the screen is proportional to the tube high voltage to the power  $p$ . The value of  $p$  is also voltage dependent in the sense that the larger the value of  $U$ , the smaller  $p$  will be.



There may thus be an optimum tube voltage. As the number of parameters is large and it has not yet proved possible to predict the visual consequences, the pragmatic approach has been adopted up till now.

The perceptual analysis can now be carried out, so that only a knowledge of the absorption contrast is lacking.

A theoretical approach is difficult for the reasons mentioned in the analysis of the scattered radiation intensity: it involves a convolution of the X-ray spectrum of the tube with the energy-dependent attenuation of the materials in the beam, and with the response of the image receptor. It was decided, therefore, to measure the object contrast  $C_0$  (fig. 2.2.11), i.e. the light contrast as delivered by the image receptor. We are interested in small contrasts, i.e. the non-linearity of the subsequent film need not be taken into account.

As mentioned, small contrasts are involved. As we further want to investigate the (perhaps small) change of the contrast, the instability of the X-ray production by medical systems — which must be used to simulate practical spectra — poses a problem. This cannot be circumvented by applying a larger contrast, say 20%, because then self-absorption occurs. One should thus resort to a reference measurement of the X-ray intensity. This can be done by using film and by measuring the density *difference* of an object (Oosterkamp, 1939; Ter-Pogossian, 1956), or by using an image intensifier/TV chain and by measuring the difference in video amplitude (Lantz and Strid, 1973). We have devised a versatile instrument which combines the simplicity of the first method with the real-time character of the second. Two photomultipliers are used; one provides the reference, i.e. a signal proportional to the momentary X-ray output, the other measures the transmitted intensity through the contrast medium. The normalization is carried out by a divider circuit. The remaining effective variation is of the order of a few per mille so the contrast — which is of the order of 10% — can be assessed with a relative error of a few per cent.

Only the iodine contrasts were measured; the similarity of the mass attenuation coefficient of barium and iodine (Oosterkamp, 1961) indicates that the results may be valid for barium as well. Either a Philips' Universal screen or a screen on the basis of rare-earth technology ( $\text{BaFCl} : \text{Eu}^{2+}$ , type Azuray of Philips) was used.

The measuring arrangement is described in sec. 4.2.2. The contrast measurements are discussed in sec. 4.2.3, and the measurement of the attenuation is dealt with in sec. 4.2.4. The implementation of the data with respect to the choice of the tube high voltage is discussed in sec. 5.2.4.

#### 4.2.2 *Measuring arrangement*

The light-intensity normally impinging on the film is measured with and without the iodine solution in the beam. The contrast can be deduced from the ratio of the intensities.

The X-rays traverse a certain water thickness, so as to simulate the patient.

### Apparatus

The arrangement is shown in fig. 4.2.1. A Rotalix tube type 21944/00 (inherent filter 2 mm Al) and a Medio 50 power control are used. Like in practice, the tube is equipped with a 2 mm Al additional filter. A practical anti-scatter grid (ratio 7, 24 strips per cm) can be placed in the beams. The PMs are of the 150 AVP type, each equipped with one of the screens mentioned (see further fig. 4.1.4a). The central beam is used to measure the iodine contrast. The X-ray field is  $1\text{ cm}^2$  at most, so the contribution of the scattered radiation is less than 1% (fig. 4.1.9; maximum water thickness 200 mm,  $\eta$  about 0.4). The reference beam traverses the same water thickness in a reservoir of  $7.5 \times 24\text{ cm}^2$ . The lead diaphragm in front of the reference PM also has an area of  $1\text{ cm}^2$ . To prevent interference from scattered radiation, lead sheets are placed as indicated.

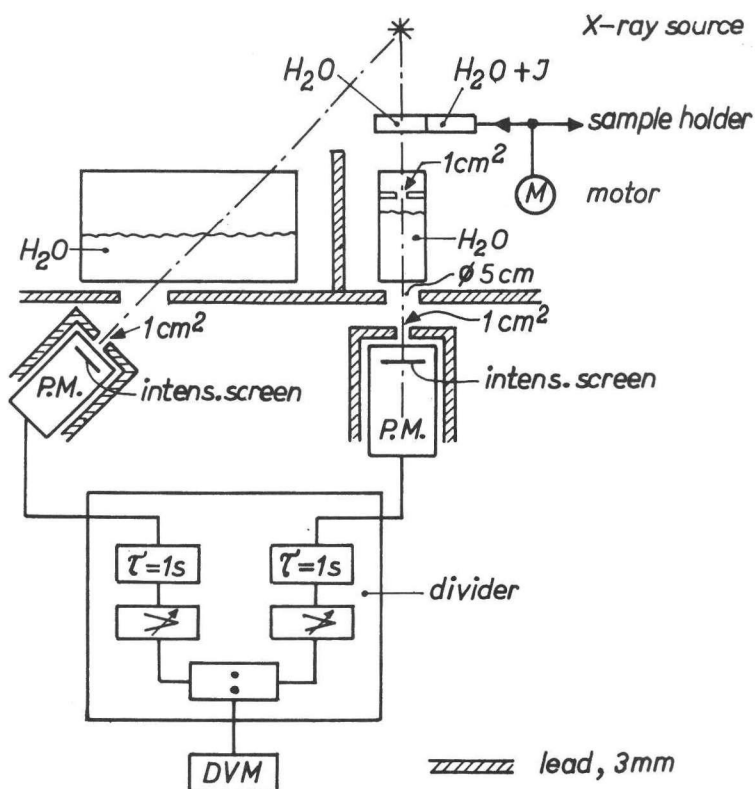


Fig. 4.2.1.

Arrangement for the object contrast measurement.

The iodine solution is made by diluting the generally used 65% Angiografin (Schering) solution with water. The solution is contained in one compartment of a sample holder. The other compartment contains water to serve as the reference as far as the water attenuation is concerned. The compartments are 10 mm thick in the clear and have a surface of  $4 \times 4 \text{ cm}^2$ . The sample holder can quickly ( $\approx 2 \text{ s}$ ) be shifted in the beam by a motor drive, thus minimizing residual temporal variations of the apparatus. The sample compartments are equal within 0.3% as far as the water attenuation is concerned. The water reservoirs are made of perspex with a thickness of 3 mm.

The divider circuit was our own make. It is described in Appendix V. It consists essentially of an analog divider type AD 426L (Analog Devices), and two amplifiers with adjustable gain. The output is fed to a DVM type PM 2422. The short-term signal fluctuations (X-ray noise, ripple of the X-ray output) are damped by RC circuits with a time constant of 1 s. The divider substantially reduces the effects of X-ray tube variations. A variation of the tube current by a factor of 4 ( $0.5 \rightarrow 2 \text{ mA}$ ) introduces a variation of the divided result of only 5%. A shift in the tube high voltage from 60 to 80 kV introduces a decrease of the result of only 2%.

### Procedure

An X-ray tube current of 1 mA was chosen for all voltages. The resulting light output ripple was about 20% peak-to-peak, so 6 and 12 pulse X-ray generator radiography was simulated. In any case, this short-term temporal variation in beam quality and the limited accuracy of the voltage setting are of less importance for the contrast measurements, because the contrast is found to vary slowly with the voltage. The voltages were selected with the dial of the generator. According to Proper's method (1975) the actual tube voltages deviate only a few percent. The following values were chosen: 50, 55, 60, 65, 70, 80, 90, 100 and 110 kV. More steps at the lower voltages were chosen because (i) the contrast is then relatively strongly dependent on the choice of the phantom thickness, and (ii) the relative errors in these results are larger than elsewhere (more attenuation). Three phantom thicknesses were used, i.e. 80 mm water, 130 and 180 mm water. Together with the 9 mm perspex and the 10 mm water in the sample holder, about 100, 150 and 200 mm water thickness was simulated, corresponding to skull, lung and stomach radiography. A thicker phantom may be needed for simulating the abdomen, but then the X-ray intensity is unfavourably low in our set-up. As a matter of fact, however, the contrast behaviour will be shown to be relatively independent of the phantom thickness in this region.

To investigate the response of the receptors to the initial X-ray spectrum, measurements were also carried out without the phantom. There was then only 10 mm water and 6 mm perspex in the beam. For convenience it is denoted by the 16 mm  $\text{H}_2\text{O}$  situation.

The result obtained by division is still prone to statistical variations. These can be as

small as a few per mille for the large PM signals, i.e. for small water thicknesses and/or high voltages. Up to about 2% variation can occur for the small signals. To obtain some averaging, the divided result was observed for a few seconds and a mean value was decided upon. The sample holder was then shifted to the other position and the same procedure was followed. The contrast was calculated from these two results. This procedure was repeated three ( $U > 65$  kV) or five times. The average contrast is entered in the figures. The error is taken to be one half of the interval between the largest and the smallest result.

The actual PM signal was also noted with a view to investigating the p factor.

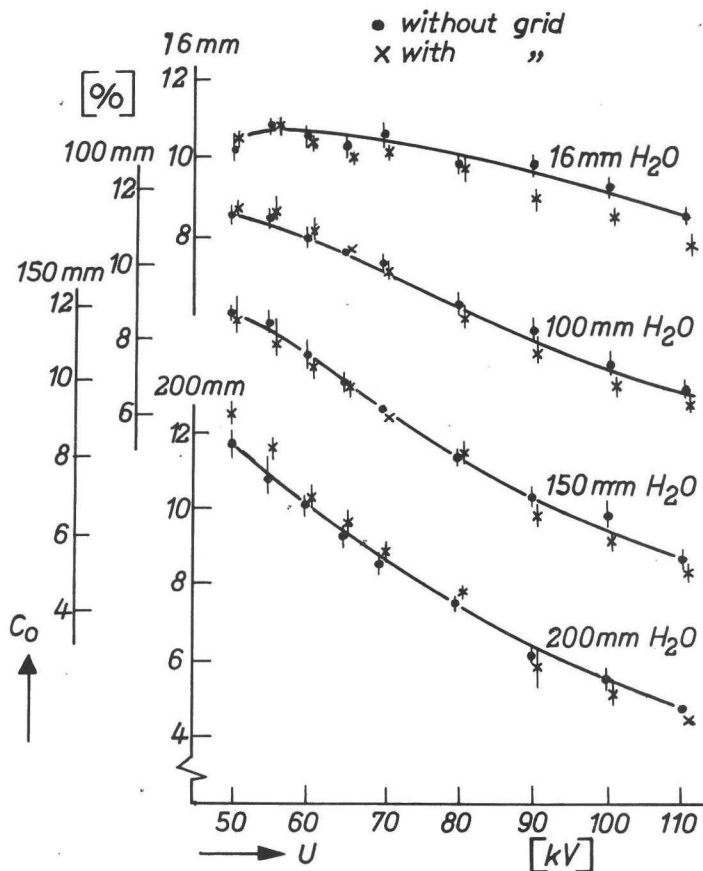


Fig. 4.2.2.

Object contrast of an iodine solution with a universal intensifying screen as receptor, with and without grid.

### 4.2.3 Contrast measurements

The measured contrast  $C_0$  is given for the universal intensifying screen in fig. 4.2.2. The deduced ranges of the results are also indicated. It appears that the presence of a grid does not lead to substantially different contrasts, especially if rare-earth intensifying screens are applied. For convenience, then, only the no-grid situation will be considered further. (For a few situations there may be a difference between the grid and the no-grid situation, e.g. for  $U = 50$  kV, 200 mm  $H_2O$ . These are interesting points for future calculations on the absorption contrast.)

The contrast is indeed smaller at higher voltages, for practical phantom thicknesses. For the no-phantom situation (16 mm  $H_2O$ ) a perhaps significant *decrease* occurs in going from 60 to 50 kV. The relative behaviour of the contrast is more clearly shown in fig. 4.2.3. The rate of decrease with higher voltages is smaller the thinner the phantom. The same tendencies are found if rare-earth screens are used (fig. 4.2.4). The contrasts for the two screens are compared in fig. 4.2.5. The rare-earth screen generally give lower contrasts. In the mid-voltage range and for practical patient thicknesses this can amount to about 10%. The reduction is smaller both for high and low voltages.

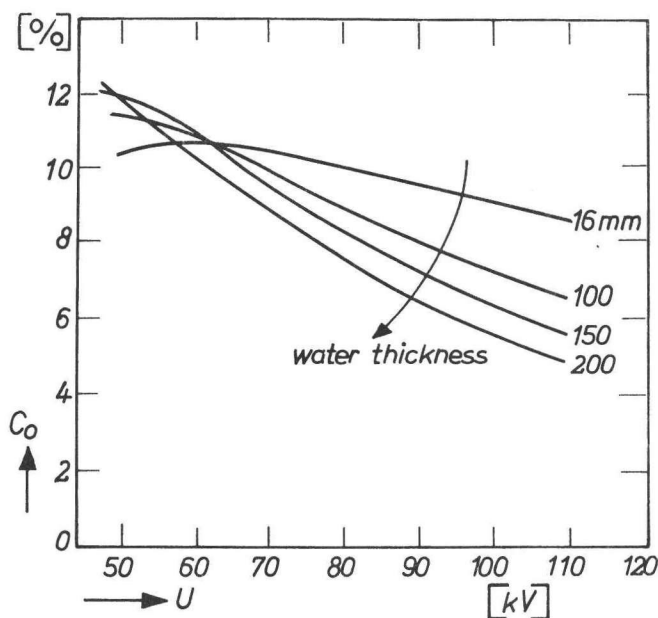


Fig. 4.2.3

Object contrast of an iodine solution; universal intensifying screen, no grid.

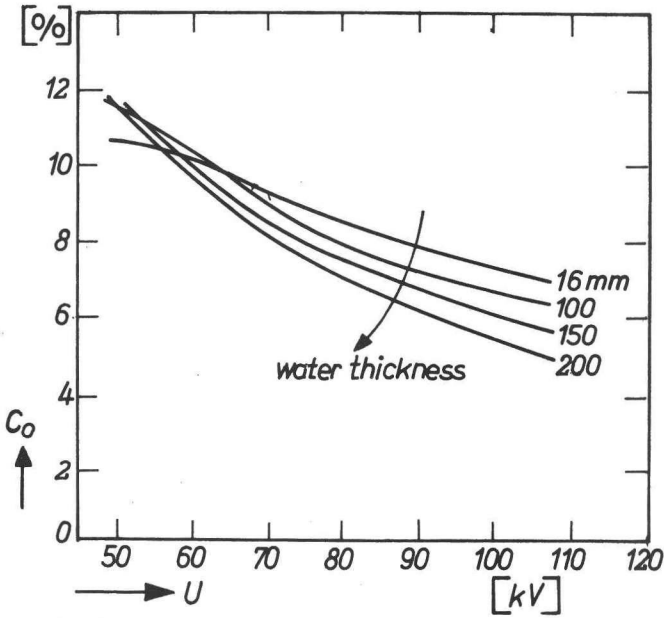


Fig. 4.2.4.  
Object contrast of an iodine solution; rare-earth intensifying screen, no grid.

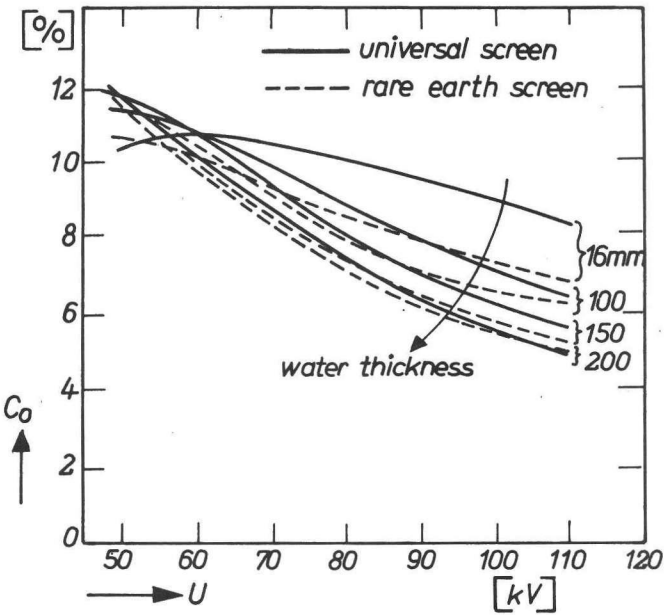


Fig. 4.2.5.  
Comparison of iodine contrast with universal and rare-earth intensifying screen.

The contrast curves resemble a hyperbolic shape. This may enable us to formulate a rule-of-thumb for the contrast. To investigate this further, the measured results are drawn on log-log scales. The results for the universal screen (fig. 4.2.6) can be approximated by straight lines for voltages not lower than 60 kV, i.e. for the practical range. The gradients, denoted as  $\gamma_c$  ('c' for contrast), are also indicated. Apparently we have

$$C_o \sim U^{\gamma_c} \quad (4.2.1)$$

with  $\gamma_c$  about minus unity for a mean patient thickness. This is comparable with the value of 0.75 found by Oosterkamp (1939) for the 'Philite' contrast, a material whose characteristics are close to those of water. This kind of approximation is even better allowed (lowest voltage 50 kV) for the rare-earth screen (fig. 4.2.7). The resulting  $\gamma_c$  values show the same trend as a function of the object thickness (see table 4.2.1). Therefore, in view of the measuring errors and the fitting by eye of the straight lines, we may state that for medium object thickness (150 mm H<sub>2</sub>O) and for voltages over and including 60 kV, the small-range iodine contrast is inversely proportional to the tube high voltage.

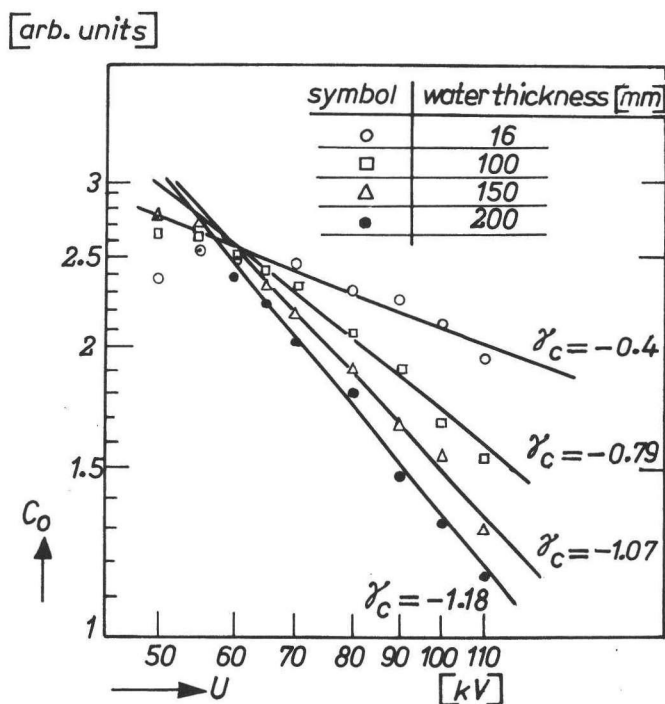


Fig. 4.2.6.

$\gamma_c$  for iodine contrast and universal intensifying screen; no grid.

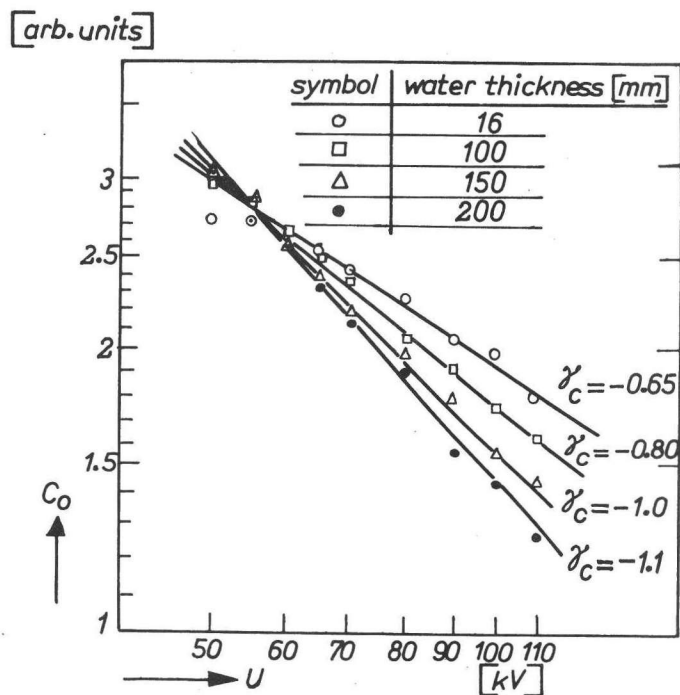


Fig. 4.2.7.  
 $\gamma_c$  for iodine contrast and rare-earth intensifying screen; no grid.

TABLE 4.2.1  $\gamma_c$  per object thickness

object thickness [mm]	$\gamma_c$	
	CaWO <sub>4</sub> screen	BaFCl : Eu <sup>2+</sup> screen
100	-0.79	-0.80
150	-1.07	-1.00
200	-1.18	-1.10

4.2.4 Attenuation measurements

Universal screen

The intensity of the light produced by the universal screen as a function of the tube high voltage is given in fig. 4.2.8, normalized to the 70 kV situation. The PM signal is entered without any correction because the PM proved to respond linearly to light over at least three decades. As the curves for 150 and 200 mm water thickness almost



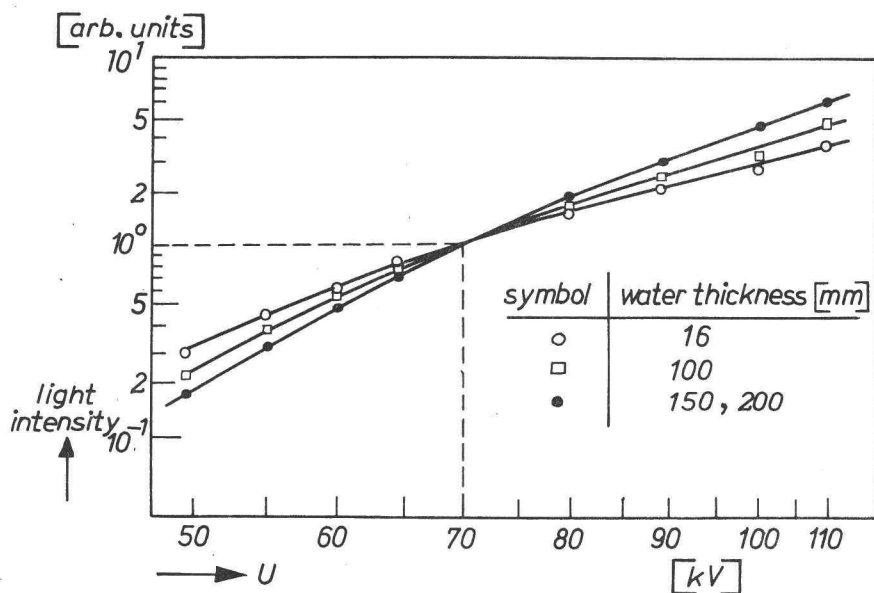


Fig. 4.2.8.

*Light intensity as a function of the tube high voltage; universal intensifying screen.*

coincide, only one curve is drawn. The increase of the light output is smaller at higher tube high-voltages and smaller water thickness. The same curves were found when the grid was present.

The  $p$  factor cannot reliably be obtained with our method, primarily because the errors in the voltage settings are too large. This caused no problem in the contrast measurements, because the contrast curve as a function of the voltage is smooth. But the  $p$  factor depends strongly on the errors in the voltage. If for instance the real difference between the 65 and the 70 kV setting were 6 kV – which can easily be the case – then the  $p$  factor for 150 mm water thickness should be 2.9 instead of 3.5. The calculated  $p$  factors must therefore be looked upon with reserve. They are given in fig. 4.2.9, which shows indeed a large variation and sometimes (perhaps) anomalous results. We could say that the largest  $p$  factor is about 6, for  $U = 50$  kV. It is 4 at about 70 kV, and about 3.5 at 110 kV.

#### Rare-earth screen

There is a stronger influence of the high voltage (fig. 4.2.10) as compared with the universal screen situation. For the 200 mm water thickness the light intensity is increased by a factor of about 90 in going from 50 kV to 110 kV; for a universal screen this factor equals about 40.

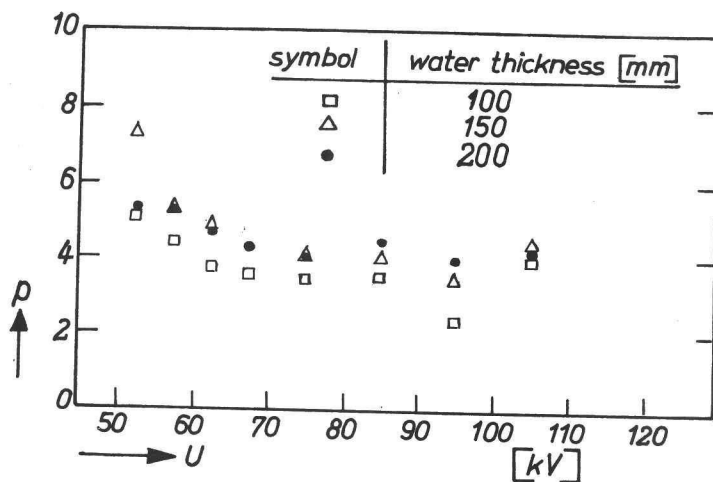


Fig. 4.2.9.

$p$  factor as a function of the tube high voltage; universal screen, grid applied.

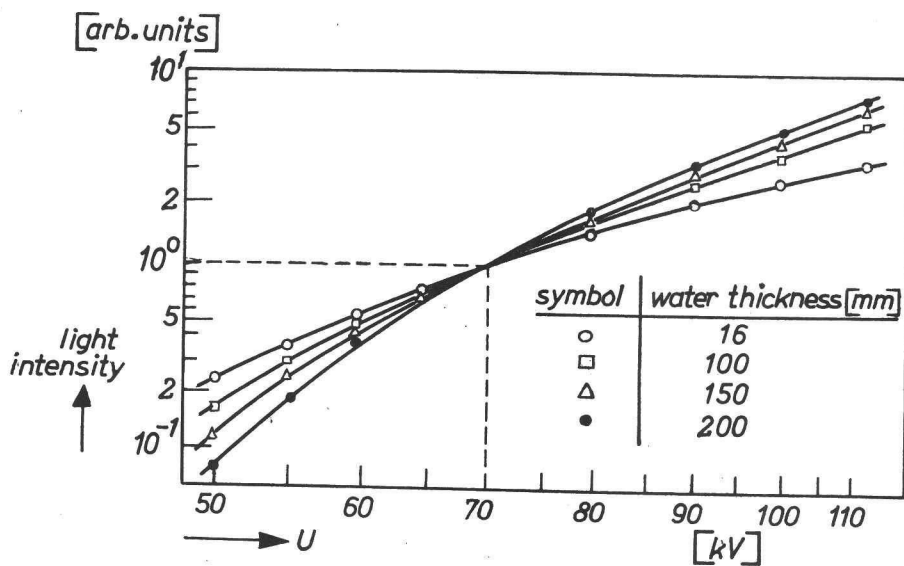


Fig. 4.2.10.

Light intensity as a function of the tube high voltage; rare-earth intensifying screen.

## 5. QUANTITATIVE ANALYSIS OF MEDICAL X-RAY SYSTEMS

A quantitative analysis will be carried out by substituting the relevant parameter values for a number of medical techniques involving the imaging of moving and stationary objects, the use of noisy and noiseless images, and for different viewing conditions. As a starting point, the present standard conditions will be used, (i) to provide the patient- and other characteristic parameters, (ii) to investigate whether trends towards improvements can be discerned, and (iii) to investigate the relative importance of the choice of parameters like the focal-spot size etc.

Medical technique data have been borrowed from the Philips' table 'Exposure data for 6- and 12 pulse apparatus', or were obtained via personal communication with employees of the Medical Systems Division (MSD) of Philips.

The MTFs of most of the image receptors (fig. 5.1) have been borrowed from Mr. Timmer (1973). The intrinsic resolution,  $\nu_{\text{rec}}$ , and the sensitivity relative to the universal screens/film combination are given in table 5.1.

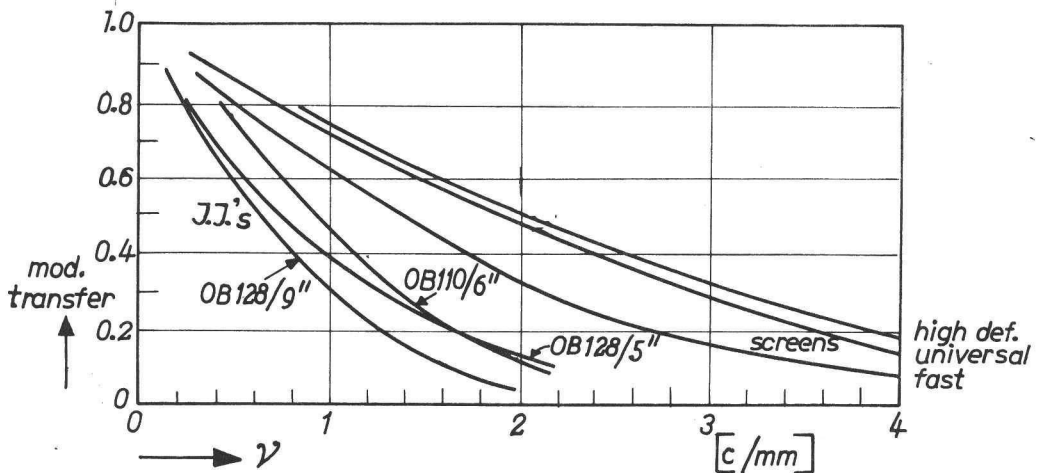


Fig. 5.1.  
MTF of screens/film and image intensifier/optics/film combinations.

There is uncertainty as to the  $\nu_{\text{rec}}$  value of film. The given value is based on the work of Morgan et al. (1964), but measurements at MSD indicate a substantially smaller value ( $\approx 8$  c/mm). Both values are however so large as to give the same results in the analysis of the imaging of stationary objects (sec. 5.1.1). The  $\nu_{\text{rec}}$  value for a 6" image intensifier/TV system has been borrowed from Franken et al. (1973a). The relative sensitivities of conventional intensifying screens are according to Stieve (1967). The value for the new screens based on rare-earth phosphors can be deduced from the manufacturers' leaflets. Of course larger and smaller relative

TABLE 5.1: Image receptor data

image receptor	$\nu_{\text{rec}}[\text{c/mm}]$	rel. sensitivity
universal screens	1.83	1
high definition screens	1.94	0.5
fast screens	1.39	2
rare-earth screens	1.83	4
non-screen film	20	?
9", OB128 } image intensifier	0.66	7.5
5", OB128 } + optics	0.75	2.3
6", OB110 } + 70 mm film	0.91	3.3
6" image intensifier/TV system	0.50	—

sensitivities are possible (up to eight is stated), but a factor of 4 is considered a reasonable mean value. Their  $\nu_{\text{rec}}$  value equals the one for universal screens. The relative sensitivity for the 9" image intensifier 70 mm filming is a compromise between the values 5 to 10 mentioned in personal communications, and the values 4 (Feddemma et al., 1969) and 10 (Elmer, 1967; Gajewski and Kuhn, 1970; Pfeiler and Linke, 1972; Stieve, 1972) and 15 (Elmer, 1967). No definite value can be given because the sensitivity of image intensifiers is continuously adjustable, and the adverse effect of the resulting noise in the image is partly a matter of personal taste. The sensitivity for the 6" and 5" image intensifiers was calculated from the 9" data by taking the reduced input screen area into account. A relative sensitivity for the fluoroscopic situation is not applicable.

The 100 kW focus of the generally used Super Rotalix tube XF 2056/00, 12° anode angle, has been chosen for the calculation of the X-ray tube characteristic parameter  $cf$ . The effective focal spot-size equals 2.25 mm, so  $cf$  equals (eq. 3.2.8)  $29.6 \text{ kW/mm}^{3/2}$ .

Section 5.1 deals with the object resolution. In sec. 5.2 the visual resolution is investigated by means of a mathematical and nomogrammmical description of the X-ray system including the visual system. In the subsequent sections we investigate the imaging of stationary and moving objects, the influence of the X-ray beam quality, and the scattered radiation. Finally (sec. 5.2.6), the consequences for the dose administered to the patient are analysed.

## 5.1 Object resolution

The imaging of stationary objects is discussed in sec. 5.1.1. Section 5.1.2 is devoted to the imaging of moving objects, and sec. 5.1.3 deals with the influence of the focal-spot intensity distribution.

### 5.1.1 Stationary objects

We shall examine the resolution obtained with a number of medical techniques, grouped into eight categories:

- (i) radiography of the skull,
- (ii) radiography of the trunk,
- (iii) radiography of upper extremities,
- (iv) radiography of lower extremities,
- (v) radiography of kidneys and gall-bladder,
- (vi) cerebral and abdominal angiography,
- (vii) mammography,
- (viii) fluoroscopy.

The optimum focal-spot size and the short-time loadability, the  $\eta, \eta_{x,st}, b_x$  and the  $\nu_{x,z=0.25}$  value (the measure of the object resolution) are calculated for each technique. As a starting point, the current standard conditions will be used. Most of the data on the maximum permissible exposure time, the image receptor choice and the geometry were provided by Mrs. Feddema (1976) of the Application Department; the data on angiographic procedures are due to Knibbe (1976).

Mammography and fluoroscopy are dealt with separately because of their special nature.

The influence of the focal-spot size on the image quality is analysed on the basis of the  $\eta_{x,st}$  and  $b_x$  values. Only general conclusions can be drawn because the visual system is not yet involved. The choice of a particular non-optimum focal spot must be weighed with the properties of the visual system; this also applies to the influence of the focal spot-to-image receptor distance, the image receptor and the focal-spot intensity distribution. These analyses are discussed in sec. 5.2.

The standard conditions are (unless otherwise stated):

- (i)  $f$  equals 1000 mm.
- (ii) the nominal focal spot is such that the maximum permissible exposure time is just obtained. This size is denoted by  $f_{opt}$  ('opt' stands for optimum). The optimum size is calculated on the premise that the short-time loadability ( $P$ ) is proportional to the focus size to the power of 1.5. This relation breaks down for focal-spot sizes smaller than roughly 0.3 mm, and for exposure times over a few tenths of a second. In these situations, the calculated optimum sizes are indicative only.
- (iii) a universal screens/film combination is used.
- (iv) the object-to-image receptor distance, or, is either given in the tables or can be derived from the  $os$  (the object to skin distance) and the image receptor to skin distance. This distance is zero for contact film; for the skull stand the distance is 45 mm and it equals 80 mm if a bucky is used.

## 5.1.1.1 Medical data and results

The medical data and calculated results are given in tables per category, if applicable. The  $\eta$ ,  $\eta_{X,st}$  and  $b_X$  values are given in figures 5.1.1 and 5.1.2 for all the techniques. The techniques are numbered for easy reference.

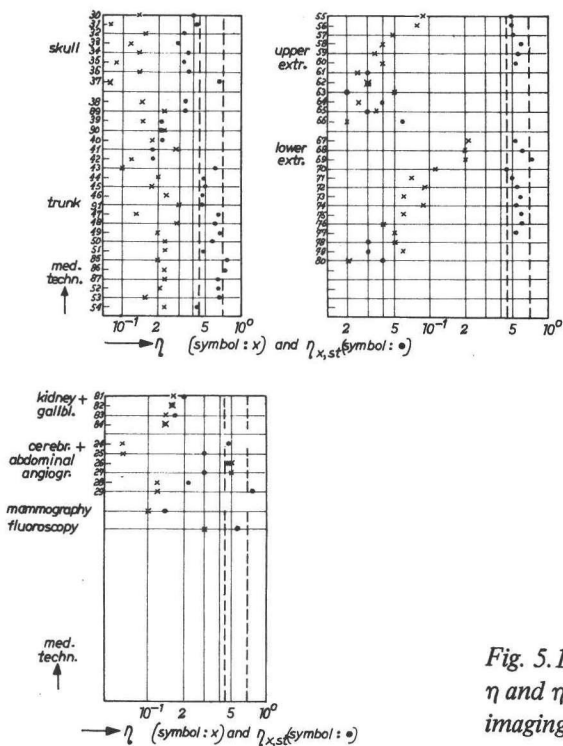


Fig. 5.1.1.  
 $\eta$  and  $\eta_{X,st}$  for stationary object imaging

## Mammography

As the exposure time may be a few seconds, a different approach is adopted for this technique. A 0.8 mm focal spot (effective) is used. High-definition non-screen film is applied. It can be inferred that  $\eta_{X,st}$  equals 0.14. The  $\eta$  value is about 0.10 for a focal spot-to-image receptor distance equal to 500 mm. Since the value of  $b_X$  is about 1.5, the choice both of the image receptor and of the focal-spot size is of importance. The trend to reduce the dose by the use of screens will lead to smaller focal spots, but the inevitably larger decrease of the image receptor MTF will lead to a worse object resolution (cf. table 5.1 and fig. 3.3.14 for  $\eta_{X,st} = 0.14$ ). As  $\eta_{X,st}$  is smaller than 0.45, geometric magnification is not recommended.

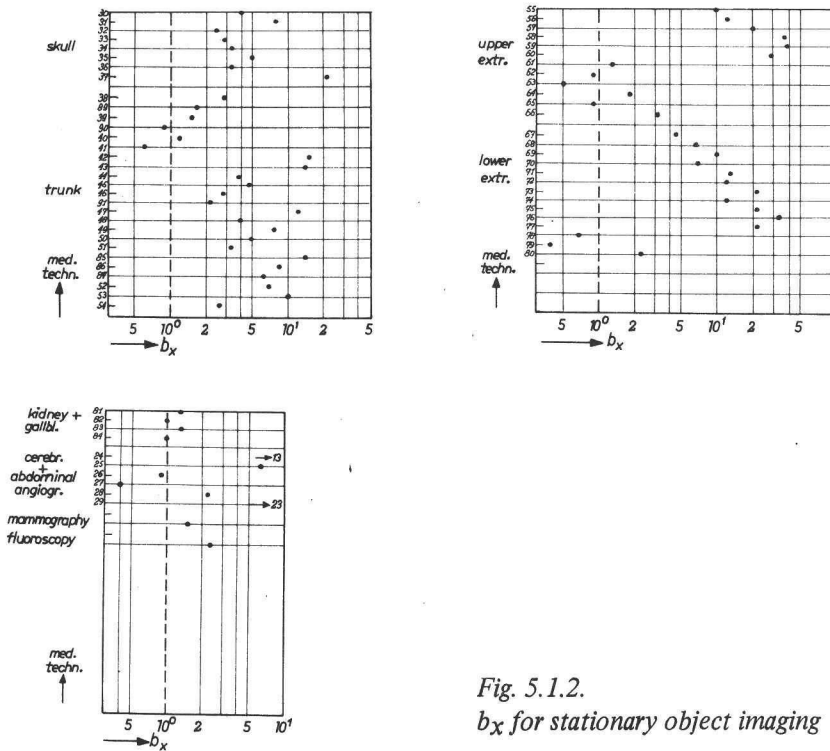


Fig. 5.1.2.  
 $b_x$  for stationary object imaging

### Fluoroscopy

The noise in the image is primarily governed by the continuous loadability of the tube, which does not depend on the focal-spot size. Calculation of an optimum size is therefore out of the question. We can nevertheless investigate the influence of the focal-spot size and other parameters by choosing a proper reference condition. We assume a 0.6 mm focal spot and a 6" image intensifier/TV system. The value of  $\eta$  equals 0.3, the value of  $\eta_{X,st}$  equals 0.57. As the value of  $b_x$  is 2.3, the beneficial effect of a sharper image receptor will be larger than the effect of a smaller focal spot. As  $\eta_{X,st}$  is larger than 0.45 but smaller than 0.7, the influence of geometric magnification will be small.

TABLE 5.1.1: Radiographic data of skull <sup>1)</sup>

no.	description	U <sub>p</sub> [kV]	Q <sub>p</sub> [mAs]	os [mm]	f <sub>opt</sub> [mm]	P [kW]	t <sub>p</sub> [s]	$\nu_{x,z=0.25}$ [c/mm]
30	survey p-a	75	80	100	0.33	10	0.3	3.9
31	survey lat.	65	80	40	0.30	8.8		3.9
32	survey axial	85	90	120	0.45	16		3.6
33	nasal access. sinusses	70	130	80	0.54	22		3.5
34	petrous bone	65	120	100	0.39	13		3.8
35	mastoid	65	140	50	0.43	15		3.8
36	optic foramen	56	120	100	0.39	13		3.8
37	lower jaw, obl.	65	15	40	0.11	2	0.3	4.0

<sup>1)</sup> film to skin distance is 45 mm.

TABLE 5.1.2: Radiographic data of trunk <sup>1)</sup>

no.	description	U <sub>p</sub> [kV]	Q <sub>p</sub> [mAs]	os [mm]	f <sub>opt</sub> [mm]	P [kW]	t <sub>p</sub> [s]	$\nu_{x,z=0.25}$ [c/mm]
38	ribs 1-7 a-p	60	25	70	0.43	15	0.1	3.6
89	ribs 1-7 a-p <sup>3)</sup>	60	25	70	0.43	15		3.3
39	ribs 8-12 a-p	65	60	70	0.81	39		2.8
90	ribs 8-12 a-p <sup>3)</sup>	65	60	70	0.81	39		2.2
40	sternum obl.	60	65	100	0.81	39		2.6
41	sternum lat.	60	90	200	1.00	55	0.1	1.6
42	clavicle p-a	60	15	40	0.10	2	0.5	4.1
43	scapula a-p	60	25	20	0.15	3		4.0
44	scapula lat.	60	50	120	0.23	6		4.1
45	cervical spine a-p	60	45	100	0.22	6	0.5	4.2
46	cervical spine obl.	60	25 <sup>4)</sup>	160	0.25	7	0.1 <sup>2)</sup>	4.0
91	cervical spine lat.	60	25 <sup>4)</sup>	220	0.25	7	0.1 <sup>2)</sup>	3.9
47	dorsal spine a-p	65	70	50	0.12	2	2.0	4.2
48	dorsal spine lat.	70	80	210	0.14	3		4.6
49	lumbar spine a-p	70	60	120	0.12	2		4.6
50	lumbar spine obl.	75	85	150	0.15	3		4.4
51	lumbar spine lat.	80	150	150	0.23	6		4.1
85	lumbar spine a-p	125	30 <sup>5)</sup>	120	0.06	1		4.5
86	lumbar spine obl.	125	50 <sup>5)</sup>	150	0.10	1.4		4.6
87	lumbar spine lat.	125	80 <sup>5)</sup>	150	0.12	2		4.6
52	pelvis+hips	65	70	130	0.12	2		4.5
53	sacrum a-p	70	60	80	0.12	2		4.3
54	sacrum lat.	80	200	80	0.28	8	2.0	3.9



- 1) film to skin distance is 80 mm
- 2) shorter time in view of less immobilization
- 3) larger or distance (160 mm) for sick patients
- 4) at fr = 1500 mm, without grid
- 5) at fr = 1500 mm, with a higher tube voltage than in technique 49, 50 and 51.

TABLE 5.1.3: Radiographic data of upper extremities <sup>1)</sup>

no.	description	U <sub>p</sub> [kV]	Q <sub>p</sub> [mAs]	os [mm]	f <sub>opt</sub> [mm]	P [kW]	t <sub>p</sub> [s]	$\nu_{x,z=0.25}$ [c/mm]
55	shoulder a-p	55	10	90	0.22	5.6	0.1	4.0
56	shoulder axial	55	10	80	0.22	5.6		3.9
57	humerus a-p/lat.	50	10	50	0.21	5.1		3.8
58	elbow a-p/lat.	50	6	40	0.15	3.0		3.8
59	lower arm a-p	45	8	35	0.16	3.6		3.8
60	lower arm lat.	45	10	40	0.19	4.6		3.8
61	wrist a-p	50	50 <sup>2)</sup>	25	0.60	2.5		24
62	wrist obl.	50	65 <sup>2)</sup>	30	0.71	33		19
63	wrist lat.	50	80 <sup>2)</sup>	50	0.82	40		11
64	hand a-p	50	30 <sup>2)</sup>	25	0.43	15		29
65	hand obl.	50	50 <sup>2)</sup>	35	0.60	25		20
66	fingers a-p/lat.	50	20 <sup>2)</sup>	20	0.33	10	0.1	35

- 1) close contact between skin and film assumed.
- 2) non-screen film.

TABLE 5.1.4: Radiographic data of lower extremities <sup>1)</sup>

no.	description	U <sub>p</sub> [kV]	Q <sub>p</sub> [mAs]	os [mm]	f <sub>opt</sub> [mm]	P [kW]	t <sub>p</sub> [s]	$\nu_{x,z=0.25}$ [c/mm]
67	hip joint a-p	65	65	130	0.18	4.3	1.0	4.3
68	hip joint lat.	65	40	200	0.13	2.6	1.0	4.4
69	femur a-p/lat.	65	20	130	0.10	1.3	1.0	4.6
70	knee a-p	55	13	110	0.26	7.2	0.1	4.0
71	knee lat.	55	10	70	0.22	5.6		3.9
72	lower leg a-p	55	8	90	0.19	4.5		4.0
73	lower leg lat.	55	6	60	0.16	3.3		3.9
74	ankle a-p	55	8	90	0.19	4.5		4.0
75	ankle lat.	55	6	60	0.16	3.3		3.9
76	heel-bone lat.	55	6	40	0.16	3.3		3.8
77	heel-bone axial	55	8	50	0.19	4.5		3.8
78	foot p-a	50	45 <sup>2)</sup>	50	0.56	23		16
79	foot obl.	50	65 <sup>2)</sup>	65	0.71	33		10
80	toes a-p/lat.	50	30 <sup>2)</sup>	20	0.43	15	0.1	32

- 1) close contact between film and skin except for 67 and 69, for which a bucky is used.
- 2) non-screen film.

TABLE 5.1.5: Radiographic data of kidney and gall-bladder <sup>1)</sup>

no.	description	U <sub>p</sub> [kV]	Q <sub>p</sub> [mAs]	os [mm]	f <sub>opt</sub> [mm]	P [kW]	t <sub>p</sub> [s]	ν <sub>x,z=0.25</sub> [c/mm]
81	kidneys survey	65	70	80	0.89	46	0.1	2.6
82	kidneys detail	65	50 <sup>2)</sup>	80	1.10	67	0.1	2.2
83	gall-bladder survey	60	100	60	1.10	61	0.1	2.5
84	gall-bladder detail	60	65 <sup>2)</sup>	60	1.30	80	0.1	2.2

- 1) a bucky is used; film to skin distance 80 mm.
- 2) at an fr distance of 700 mm.

TABLE 5.1.6: Cerebral and abdominal angiography data

no.	description	U <sub>p</sub> [kV]	Q <sub>p</sub> [mAs]	or [mm]	f <sub>opt</sub> [mm]	P [kW]	t <sub>p</sub> [s]	ν <sub>x,z=0.25</sub> [c/mm]
24	cerebral angiogr.	70	45	65	0.24	6.4	0.50 <sup>3)</sup>	3.9
25	cerebral angiogr.	70	45	65	0.51	20	0.16 <sup>3)</sup>	3.7
26	cerebral angiogr.	70	45	500 <sup>1)</sup>	0.24	6.4	0.50 <sup>3)</sup>	3.4
27	cerebral angiogr.	70	45	500 <sup>1)</sup>	0.51	20	0.16 <sup>3)</sup>	1.8
28	abdominal angiogr.	60	45	120	0.73	34	0.08	3.2
29 <sup>2)</sup>	abdominal angiogr.	60	6 <sup>2)</sup>	120	0.19	4.6	0.08	1.5

- 1) cerebral angiography is also planned with a geometric magnification factor of 2.
- 2) abdominal angiography is also carried out with a 9" image intensifier.
- 3) difference in exposure time indicated by the film changer.

5.1.1.2 Conclusion.

Geometric magnification

The critical values of  $\eta_{x,st}$ , i.e. 0.45 and 0.7, are also drawn in figure 5.1.1. For  $\eta_{x,st}$  values in this range, the influence of different  $\eta$  is small. For  $\eta_{x,st}$  values smaller than 0.45 geometric magnification is not recommended, whereas for  $\eta_{x,st}$  values larger than 0.7 it will give a better object resolution. As the  $\eta_{x,st}$  values are generally smaller than 0.7, geometric magnification is not recommended. A few exceptions exist. For technique 85/86 (lumbar spine) a

relatively small focus can be applied because high voltage technique is chosen and the permissible exposure time is long. A small focus can also be used for technique 69 (femur a-p/lat.) and technique 29. In the latter case a highly sensitive and relatively unsharp 9" image intensifier is used.

#### Image receptor choice

The values of  $b_x$  are given in figure 5.1.2. As  $b_x > 1$ , it can be concluded that the image receptor MTF dominates, so that a sharper receptor will be of advantage. The rare-earth technology might be used here for developing sharper screens with about the same sensitivity. A number of exceptions can be found, for which the focus and receptor MTF are more or less balanced, i.e. for which  $b_x$  is about unity: (i) techniques 90, 40 and 41 (trunk), (ii) kidney and gall-bladder radiography, (iii) cerebral angiography with geometric magnification (26, 27) for the longer exposure time of 0.5 s and (iv) the non-screen film techniques 61 – 65 and 78 and 79.

#### Focal-spot size

The conclusions for the image receptor choice can be applied in a reversed sense: as far as the system MTF is concerned, the choice of the spot size is not critical. As a consequence, the choice is primarily governed by the permissible exposure time. Extra attention must nevertheless be paid when  $b_x$  is of the order of unity. The ultimate choice is summarized per medical technique in table 5.1.13. The decision is made on the basis of the analysis with tables 5.1.7 – 5.1.12. They give per medical technique the change in per cent of  $\nu_{x,z=0.25}$  for different appropriate foci out of the range 0.15, 0.3, 0.6, 1.2 and 1.5 mm, relative to the optimum focus situation. This analysis is of direct interest for the development of systems. The optimum focal-spot size is also entered, together with the resulting exposure time per focus in seconds. The percentage change of  $\nu_{x,z=0.25}$  is denoted by  $\Delta\nu$ . Positive values of  $\Delta\nu$  occur for the perhaps intolerably longer exposure times ( $f' < f_{opt}$ ).

**TABLE 5.1.7: Focal-spot influence, skull radiography**

		$f'$ [mm]							
no.	$f_{opt}$	0.15		0.30		0.60		1.2	
	[mm]	$\Delta\nu$ [%]	t [s]	$\Delta\nu$ [%]	t [s]	$\Delta\nu$ [%]	t [s]	$\Delta\nu$ [%]	t [s]
30	0.33	+ 8	1.0	+ 1	0.30	-16	0.12	-42	0.04
31	0.30	+ 2	0.8	0	0.30	- 7	0.10	-24	0.04
32	0.45	+20	1.5	+ 9	0.50	-11	0.20	-41	0.07
33	0.54	+17	2.1	+12	0.70	- 3	0.26	-30	0.09
34	0.39	+12	1.2	+ 5	0.40	-12	0.15	-40	0.05
35	0.43	+ 6	1.4	+ 3	0.50	- 5	0.18	-25	0.06
36	0.39	+12	1.2	+ 5	0.40	-12	0.15	-40	0.06
37	0.11	- 0.3	0.2	- 2.3	0.07	- 9	0.02	-26	0.01

### Focal spot choice

The optimum value ranges from 0.11 to 0.54 mm. From table 5.1.7 we learn, however, that all the techniques can be carried out with a 0.3/0.6 mm X-ray tube: the value of  $b_x$  (fig. 5.1.2) is large, so that the choice of the focal spot is not critical. The 0.15 mm focal spot would require too long an exposure time. The 1.2 mm focal spot is so large that a considerable reduction of the object resolution would result, despite the large  $b_x$  value.

TABLE 5.1.8: Focal-spot influence, trunk radiography

no.	$f_{opt}$ [mm]	$f^* \text{ [mm]}$							
		0.15		0.30		0.60		1.2	
		$\Delta\nu$ [%]	t [s]	$\Delta\nu$ [%]	t [s]	$\Delta\nu$ [%]	t [s]	$\Delta\nu$ [%]	t [s]
38	0.43	+ 15	0.5	+ 8	0.2	-11	0.06	-40	0.02
89	0.43	+ 35	0.5	+ 16	0.2	-18	0.06	-51	0.02
39	0.81	+ 50	1.2	+ 39	0.4	+15	0.15	-22	0.05
90	0.81	+100	1.2	+ 72	0.4	+22	0.15	-27	0.05
40	0.81	+ 67	1.2	+ 52	0.4	+18	0.15	-24	0.05
41	1.00	+181	1.7	+126	0.6	+50	0.21	-14	0.08
42	0.10	0	0.3	- 5	0.1	-17	0.04	-39	0.01
43	0.15	0	0.5	- 3	0.2	-12	0.06	-32	0.02
44	0.23	+ 6	0.9	- 6	0.3	-30	0.12	-56	0.04
45	0.22	+ 1	0.6	- 13	0.2	-37	0.07	-62	0.02
46	0.25	+ 11	0.2	- 6	0.08	-34	0.03	-61	0.01
91	0.25	+ 17	0.2	- 8	0.08	-41	0.03	-67	0.01
47	0.12	- 1	1.4	- 5	0.5	-19	0.18	-42	0.06
48	0.14	- 1	1.8	- 22	0.6	-49	0.22	-71	0.08
49	0.12	- 2	1.3	- 13	0.5	-34	0.20	-60	0.06
50	0.15	0	2.0	- 14	0.7	-40	0.25	-63	0.09
51	0.23	+ 8	3.8	- 7	1.3	-34	0.50	-60	0.17
85	0.06	- 3	0.5	- 14	0.2	-36	0.07	-60	0.02
86	0.10	- 4	0.9	- 18	0.3	-41	0.11	-65	0.04
87	0.12	- 2	1.4	- 16	0.5	-40	0.18	-65	0.06
52	0.12	- 2	1.4	- 14	0.5	-36	0.18	-61	0.06
53	0.12	- 11	1.3	- 8	0.5	-26	0.17	-50	0.06
54	0.28	+ 14	5.1	- 2	1.8	-30	0.60	-58	0.22

### Focal spot choice

For a few techniques (89, 39–41, fig. 5.1.2)  $b_x \approx 1$ , and therefore the choice of the focal spot can be critical. This is seen e.g. for technique 41.

All techniques can be carried out with a 0.3/0.6 mm X-ray tube, with the exception

of technique 41. Here a 1.2 mm focus would do better. A number of techniques (42, 43, 45, 47, 48, 49, 50, 85, 86–53) could also be done with a smaller focal spot, e.g. 0.15 mm.

The  $\nu_{x,z}=0.25$  value when a 0.3 mm focus is used is considerably smaller for a few techniques only: 48, 86 and 87.

TABLE 5.1.9: Focal-spot influence, radiography of the upper extremities

		$f^* \text{ [mm]}$							
no.	$f_{\text{opt}}$	0.15		0.30		0.60		1.2	
	[mm]	$\Delta\nu$ [%]	t [s]	$\Delta\nu$ [%]	t [s]	$\Delta\nu$ [%]	t [s]	$\Delta\nu$ [%]	t [s]
55	0.22	0	0.11	– 3	0.04	–14	0.02	–36	0.005
56	0.22	0	0.11	– 3	0.04	–12	0.01	–31	0.005
57	0.21	0	0.16	0	0.06	– 3	0.02	–11	0.007
58	0.15	0	0.10	0	0.03	– 2	0.01	– 8	0.004
59	0.16	0	0.11	0	0.04	– 2	0.01	– 6	0.005
60	0.19	0	0.14	0	0.05	– 2	0.02	– 8	0.010
61 <sup>1)</sup>	0.60	+ 58	0.80	+ 38	0.28	0	0.10	–39	0.040
62 <sup>1)</sup>	0.71	+ 97	1.00	+ 64	0.36	+13	0.13	–34	0.040
63 <sup>1)</sup>	0.82	+200	1.30	+116	0.45	+30	0.16	–29	0.060
64 <sup>1)</sup>	0.43	+ 32	0.50	+ 15	0.17	–17	0.06	–50	0.020
65 <sup>1)</sup>	0.60	+ 89	0.80	+ 52	0.28	0	0.10	–43	0.030
66 <sup>1)</sup>	0.33	+ 12	0.30	+ 2	0.11	–21	0.04	–49	0.020

<sup>1)</sup> non-screen film is used.

### Focal spot choice

The choice of the focal spot is critical for the non-screen film techniques, because its MTF then dominates. The corresponding values of  $b_x$  (fig. 5.1.2) are small.

The table shows that a 0.6 mm focal spot will do for all the techniques, although the exposure time is perhaps too long for technique 63.

The resolution will be better with a 0.3 mm focus for techniques 55 and 56.

TABLE 5.1.10: Focal-spot influence, radiography of the lower extremities

		f' [mm]							
no.	f <sub>opt</sub> [mm]	0.15		0.30		0.60		1.2	
		$\Delta\nu$ [%]	t [s]	$\Delta\nu$ [%]	t [s]	$\Delta\nu$ [%]	t [s]	$\Delta\nu$ [%]	t [s]
67	0.18	+ 2	1.30	− 10	0.50	−34	0.17	−60	0.060
68	0.13	− 1	0.80	− 12	0.30	−34	0.10	−60	0.040
69	0.10	− 4	0.40	− 15	0.15	−37	0.05	−62	0.020
70	0.26	+ 2	0.23	− 1	0.08	−12	0.03	−34	0.010
71	0.22	0	0.17	− 1	0.06	− 6	0.02	−19	0.010
72	0.19	0	0.14	− 2	0.05	− 9	0.02	−18	0.010
73	0.16	0	0.50	− 1	0.04	− 4	0.01	−15	0.005
74	0.19	0	0.14	− 2	0.05	− 9	0.02	−27	0.006
75	0.16	0	0.10	− 1	0.04	− 4	0.01	−15	0.005
76	0.16	0	0.10	0	0.04	− 2	0.01	− 8	0.005
77	0.19	0	0.14	0	0.05	− 3	0.02	−11	0.006
78	0.56	+117	0.71	+ 56	0.25	− 6	0.09	−48	0.030
79	0.71	+205	1.00	+103	0.36	+17	0.13	−38	0.040
80	0.43	+ 22	0.47	+ 11	0.17	−14	0.06	−45	0.020

Focal spot choice

A 0.3/0.6 mm X-ray tube will do.

The 0.3 mm focus can be used for techniques 67–77. The exposure time is not too short for techniques 67, 68 and 69, as the 1.0 second exposure is permitted, but a shorter time is preferred. The exposure time is slightly too long for technique 79, 0.6 mm focus, but the gain in object resolution is considerable.

TABLE 5.1.11: Focal-spot influence, radiography of the kidney and gall-bladder

		f' [mm]							
no.	f <sub>opt</sub> [mm]	0.30		0.60		1.2		1.5	
		$\Delta\nu$ [%]	t [s]	$\Delta\nu$ [%]	t [s]	$\Delta\nu$ [%]	t [s]	$\Delta\nu$ [%]	t [s]
81	0.89	+52	0.5	+23	0.18	−18	0.06	−30	0.04
82	1.10	+80	0.7	+46	0.26	− 3	0.10	−18	0.07
83	1.10	+59	0.7	+34	0.24	− 7	0.08	−20	0.06
84	1.30	+80	0.9	+52	0.30	+ 5	0.11	−10	0.08

### Focal spot choice

Since the values of  $b_x$  (fig. 5.1.2) are close to unity, the choice of the focal spot is critical. This is shown by table 5.1.11: a smaller focal spot leads to a considerably better object resolution. In view of the permissible exposure time, the 1.2 mm focal spot will give good results.

**TABLE 5.1.12: Focal-spot influence, cerebral and abdominal angiography**

no.	$f_{opt}$ [mm]	$f'$ [mm]							
		0.15		0.30		0.60		1.2	
		$\Delta\nu$ [%]	t[s]	$\Delta\nu$ [%]	t[s]	$\Delta\nu$ [%]	t[s]	$\Delta\nu$ [%]	t[s]
24	0.24	0	1.0	0	0.35	- 5	0.12	-17	0.040
25	0.51	+ 4		+ 3		- 2		-14	
26	0.24	+ 35		-16		-53		-76	
27	0.51	+152	1.0	+57	0.35	-13	0.12	-55	0.040
28	0.73	+ 27	0.8	+22	0.30	+ 7	0.11	-22	0.040
29	0.19	0	0.1	0	0.04	- 3	0.01	-10	0.005

### Focal spot choice

Especially in the geometric magnification techniques (26, 27), the influence of the focus choice is considerable ( $b_x < 1$ , fig. 5.1.2). A 0.3/0.6 mm X-ray tube will do for this purpose, and can also be used for the other techniques. The choice is of course not critical for the image intensifier system (techn. 29), due to its low intrinsic resolution ( $b_x = 23$ ).

### Conclusion

The required loadabilities, sizes and exposure times are summarized in table 5.1.13. It can be inferred that a three-focus tube with a 0.3, 0.6 and 1.2 mm focus would do for all purposes. The corresponding loadabilities are 10, 25 and 80 kW.

**TABLE 5.1.13: Summary of focal-spot sizes,  $f_r = 1000$  mm**

technique	foci [mm]	loadability [kW]	t [s]
skull	0.3/0.6	10/25	0.3
trunk	0.3/0.6	10/25	0.1/0.5/2
upper extremities	0.3/0.6	10/25	0.1
lower extremities	0.3/0.6	10/25	0.1
kidney/gall-bladder	1.2	80	0.1
angiography	0.3/0.6	10/25	0.16/0.5

The 0.3/0.6 mm X-ray tube will also do for fluoroscopy. As the value of  $b_x$  equals 2.3, the smaller focal spot will give a better object resolution.

### 5.1.2. Moving objects

The medical technique data are reviewed in table 5.1.14. The techniques are numbered for easy reference. The  $Q_p$ ,  $U_p$  and  $f_{rp}$  values have been borrowed from the Philips' exposure tables except the data for heart imaging (11, 12, 13) which were provided by MSD employees. The ranges of object velocities have been borrowed from literature (Berger, 1961, 1963; Stieve, 1965). A reasonable mean velocity (Berger, 1961, 1963) for heart and lung imaging is 50 mm/s.

**TABLE 5.1.14: Moving object imaging data**

no.	med. techn.	v [mm/s]	fr <sub>p</sub> [mm]	U <sub>p</sub> [kV]	Q <sub>p</sub> [mAs]		
					universal screens + grid	image int. (6")	
1	stomach, low U <sub>p</sub>	} 5–35	} 700–800	80–85	15–30	4.5 2	
2	stomach, high U <sub>p</sub>			125–150	1.5–5		
3	colon	1–10	700–900	85–100	15–80		
5	gall-bladder*	1–5	700–1000	60	65–100		
6	oesophagus	} 15–80	800	80	12		
7	bronchography		700–900	75–90	10–15		
8	larynx		700–900	65	20–30		
9	lung, low U <sub>p</sub>	} 10–150	} 1500	55–70	13–20		
10	lung, high U <sub>p</sub>			150	25–7		
11	heart, 70 mm	} 50–400	} 800	} 80	34		
12	heart, cine						
13	heart, AOT						

\* In contrast with the former assumption of a stationary gall-bladder (table 5.1.5), small movements may also be present. The optimum focal-spot sizes for both situations (table 5.1.5, and fig. 5.1.5) correspond well, so that both the minimum permissible exposure time (0.1 s) and the velocity seem reasonable.

All the techniques mentioned can in principle be carried out on a universal or general-purpose stand, like the Diagnost 120. This stand was, however, primarily conceived for techniques 1 to 8, and to a lesser extent for lung imaging (9 and 10).



For this reason, and because of the quite different conclusions which will be drawn for heart-imaging (11, 12, 13), we shall refer to techniques 1 to 10 as 'general-purpose techniques', 'general-purpose imaging' or the like.

The fr distance used for the Diagnost 120 is 900 mm, which is the shortest feasible distance for general-purpose stands. As mentioned in sec. 3.2.3, a short distance favours the object resolution. It is preferable, however, to make a lung radiograph at a distance of 1500 mm to obtain roughly equal distortion for structures at different depths. The influence of this larger distance will be mentioned later. The object-receptor distance is assumed to be 150 mm. A grid is used.

One can imagine a favourable effect going with geometric magnification if the grid is not used. The effect of the reduced Q-value may outweigh the detrimental effect, if any, of the magnification. An or distance of 360 mm will also be used therefore, with a corresponding reduction in the Q-value by a factor of 2. A factor of 4 is expected from the removal of the grid, but the reduction of the scattered radiation intensity due to geometric magnification leads to an increase by a factor of 2 (sec. 4.1). This and other possibilities will be analysed in sec. 5.2.5 in relation to the effect of scattered radiation.

Firstly the  $\eta_{x,m}$  values will be calculated to get an idea of the balance factors affecting the MTF quality. Secondly, optimum focal-spot sizes are calculated. This is done for the universal, high-definition and fast screens/film combinations, and for the 9", 5" and 6" image intensifier systems. The data of tables 5.1 and 5.1.14 serve as starting points.

#### 5.1.2.1 Influence of geometric magnification

The ranges of  $\eta_{x,m}$  values are given in fig. 5.1.3 for the grid and the no-grid situation. Ranges are involved because of the range of parameter values like  $v$  and  $Q$ . The largest  $\eta_{x,m}$  value corresponds to the smallest  $v$  and the smallest product of  $U_p$  and  $Q_p$ . The  $\eta_{x,m}$  values are of course larger for the more unsharp and more sensitive receptors, and if no grid is used.

#### Screens/film systems

As the value of  $\eta_{x,m}$  is generally smaller than 0.5, no geometric magnification should be applied. This holds especially for AOT heart imaging. Even though fast screens are used, the velocity of the heart is so high that very small values of  $\eta_{x,m}$  result.

The insensitive high-definition screens lead also to small  $\eta_{x,m}$  values. The optimum focal-spot sizes are correspondingly larger (and so is the dose to the patient). The value of  $\eta_{x,m}$  is small for screens in general. This indicates a dominance of the shadow image MTF, which means that the additional deterioration of the move-

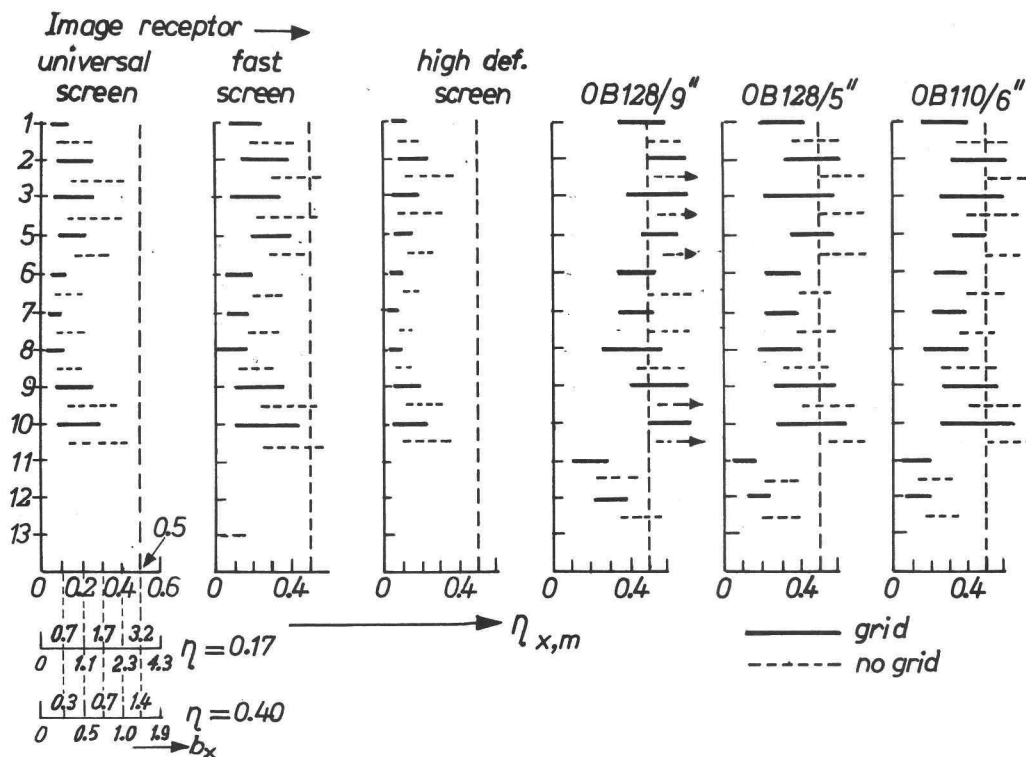


Fig. 5.1.3.

$\eta_{x,m}$  and  $b_x$  values for moving objects; — grid, - - - no grid.

ment MTF with a high definition screen will give worse system MTFs. This is illustrated in fig. 5.1.4, which gives the  $MTF_x$  for a typical lowest and highest velocity situation for different receptors. The high-definition screen gives the worst results, especially for the highest velocity. Its use will therefore not be considered any more.

In lung imaging, the larger fr value leads to even smaller  $\eta_{x,m}$  values, so that the conclusions remain valid.

#### Image intensifiers

For heart imaging, the same conclusions as for the screens/film systems hold. The velocity of parts of the heart is so large that geometric magnification is not useful, even for the mean velocity.

For general-purpose imaging with the intensifiers, the  $\eta_{x,m}$  values lead to the following conclusions. If no grid is used, then  $\eta_{x,m}$  is generally about 0.5 or larger, so that geometric magnification will have advantages. If a grid is used, then  $\eta_{x,m}$

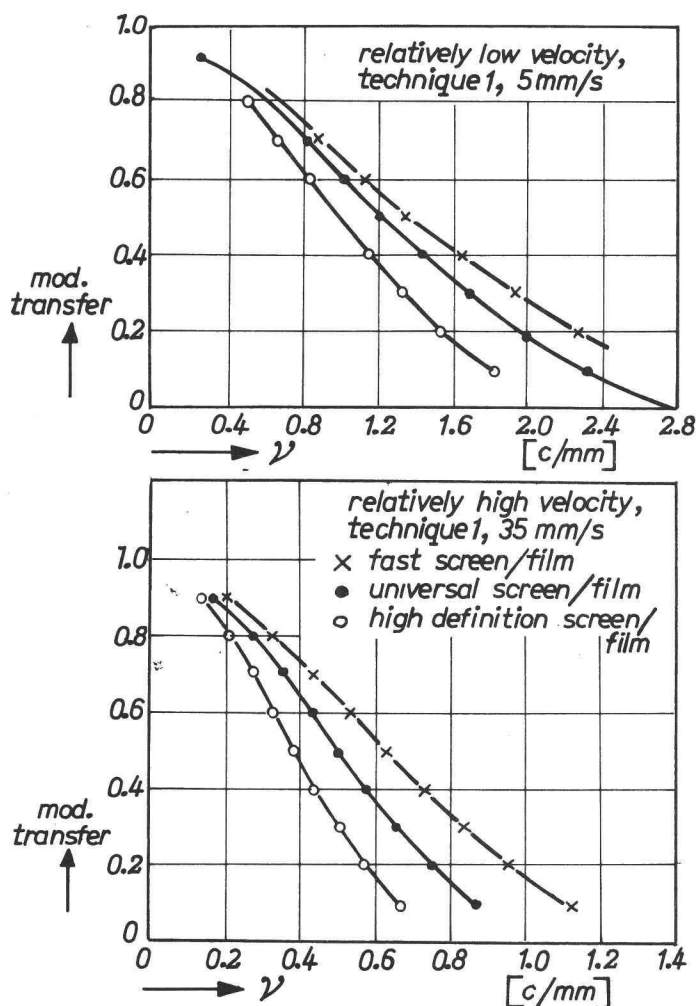


Fig. 5.1.4.  
MTF for a typical low and high velocity situation; different screens/film systems.

ranges between 0.2 and 0.7 for the sensitive 9" image intensifier, which means that geometric magnification is sometimes useful. For the 5" and 6" intensifiers,  $\eta_{x,m}$  is generally smaller than 0.5, so no magnification should be applied.

### 5.1.2.2 Focal-spot choice

The choice of the focal spot is difficult, because every technique involves a range of optimum sizes. These are indicated in fig. 5.1.5 for the five plausible imaging systems (see sec. 5.2.5), i.e. no deliberate magnification ( $\eta = 0.17$ ) and use of a

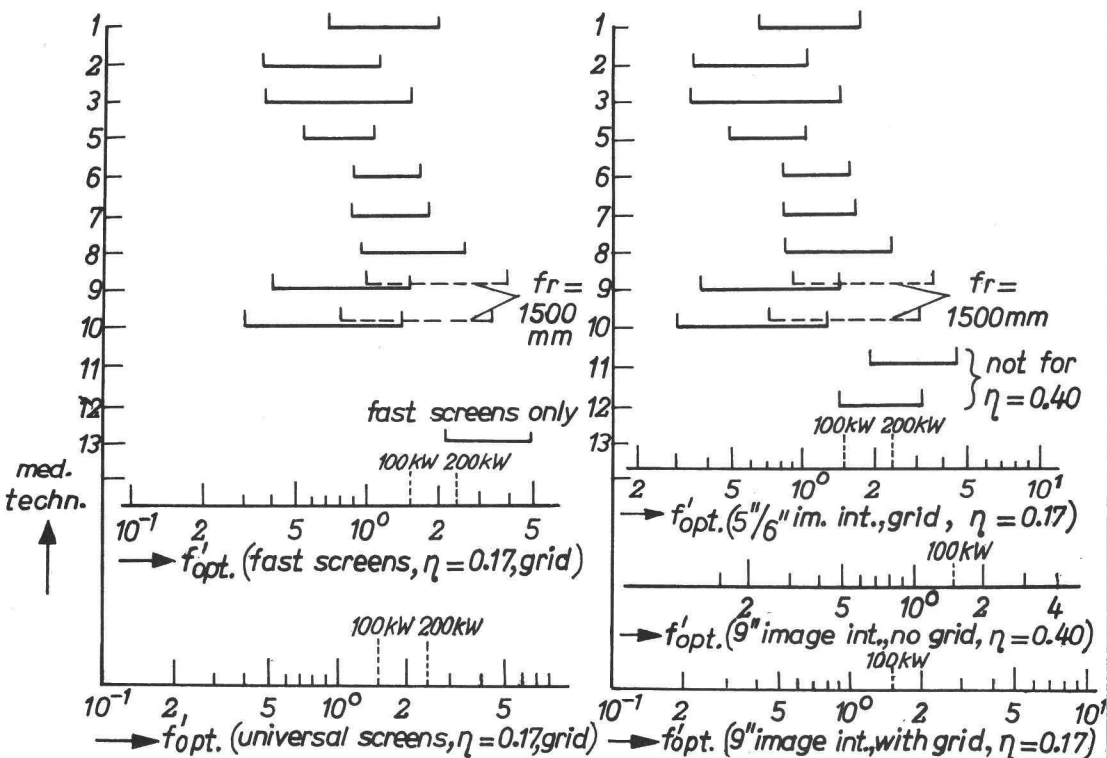


Fig. 5.1.5.

Optimum focal-spot sizes [mm] for moving object imaging.

grid for the screens and the image intensifiers (the 5" and 6" systems are given together because their optimum focal-spot sizes do not differ substantially), and magnification ( $\eta = 0.4$ ) without grid for the 9" image intensifier (heart imaging excluded). The optimum size is of course smaller for the more sensitive receptors and if geometric magnification is applied.

The importance of the choice of the focal-spot size is reflected in the value of  $b_x$  (see sec. 3.2.4.2). If  $b_x$  is smaller than unity, then the shadow image MTF dominates, and therefore the choice is critical. The values of  $b_x$  in relation to the  $\eta_{x,m}$  values can also be deduced from fig. 5.1.3, for  $\eta = 0.17$  and  $\eta = 0.40$ . The following situations are considered. Situations a) up to and including e) refer to general-purpose systems, whereas situation f) corresponds to heart imaging.

- a) Universal screens/film,  $\eta = 0.17$ : The value of  $b_x$  is generally smaller than 2, and values smaller than unity often occur. The choice of the focal spot is thus critical. Since only double focus tubes are available, a 0.6/1.5 mm combination (30/100 kW) is a reasonable choice for the whole range.

- b) Fast screens,  $\eta = 0.17$ :  $b_x$  is larger than for universal screens, although values smaller than unity are not rare. A 0.6/1.5 mm focus combination may suit even better.
- c) 5"/6" image intensifier,  $\eta = 0.17$ : The value of  $b_x$  is of the order of unity or larger (2–4). Consequently the focal-spot choice is less critical and a 0.6 or a 1.0 mm focal spot can be used.
- d) 9" image intensifier,  $\eta = 0.17$ :  $b_x$  is generally larger than 2, and therefore the choice is not critical. A 0.6 mm focal spot will do.
- e) 9" image intensifier,  $\eta = 0.40$ : geometric magnification is sometimes useful.  $b_x$  is smaller than for situation d. According to fig. 5.1.5 a 0.3 mm or a 0.15/0.4 mm focal spot is wanted.
- f) Heart imaging,  $\eta = 0.17$ :  $b_x$  is small. If fast screens/film are used, then 200 kW is required for the medium velocity of the heart ( $\approx 2.4$  mm focal-spot size). A 100 kW (1.5 mm) focus suffices for the 5"/6" image intensifier systems, whereas 60 kW ( $\approx 1$  mm focus) is adequate for a 9" image intensifier. With these latter intensifiers, even the fastest object of the heart can be optimally imaged with a 200 kW X-ray tube.

For lung imaging at a focal spot-to-image receptor distance of 1500 mm, larger focal-spot sizes are required. These are also indicated in fig. 5.1.5. A 150 kW X-ray tube is required for imaging with screens, when the low voltage technique (9) is used. 100 kW would do for the high-voltage technique. This loadability is also needed for 5"/6" intensifier systems. For the 9" intensifier, a lower loadability ( $\approx 80$  kW) suffices.

The optimum focal-spot size is proportional to  $fr^{6/5}$ , whereas the short-time loadability is proportional to  $f^{3/2}$ . The loadability is therefore proportional to  $fr^{9/5}$ . As a consequence, a small focal spot-to-image receptor distance not only favours the object resolution, but allows the use of a favourably less powerful X-ray generator.

A weighing of the focal spot choice with the visual system will be carried out in sec. 5.2.3.

### 5.1.2.3 Influence of the image receptor

A small value of  $b_x$  indicates that the shadow image MTF is dominant. In other words, the image receptor sensitivity is then too low in relation to its intrinsic resolution. This holds for the screens/film systems, so that the application of the more sensitive rare-earth screens will give better results. This is illustrated in fig. 5.1.6, which gives the system MTF for the different screens, for the high velocity situation, technique 1 (stomach, low  $U_p$ );  $b_x$  equals  $\approx 0.4$ . Further the low velocity situation, technique 10 is considered;  $b_x$  equals  $\approx 2$ . These two situations reasonably encompass the  $\eta_{x,m}$  range for universal screens (fig. 5.1.3).

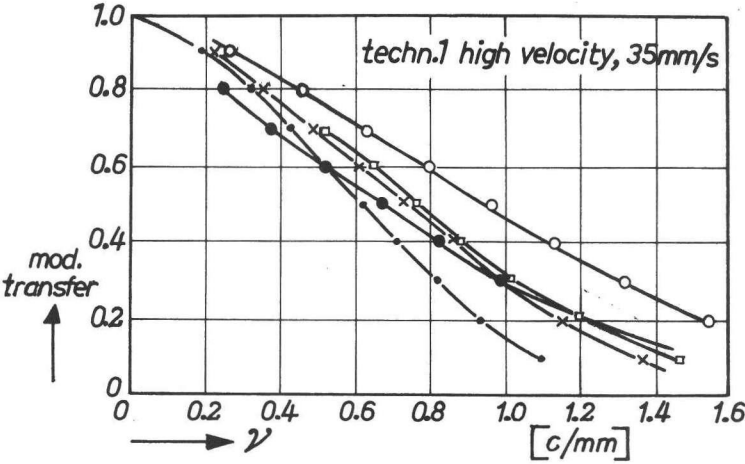


Fig. 5.1.6a

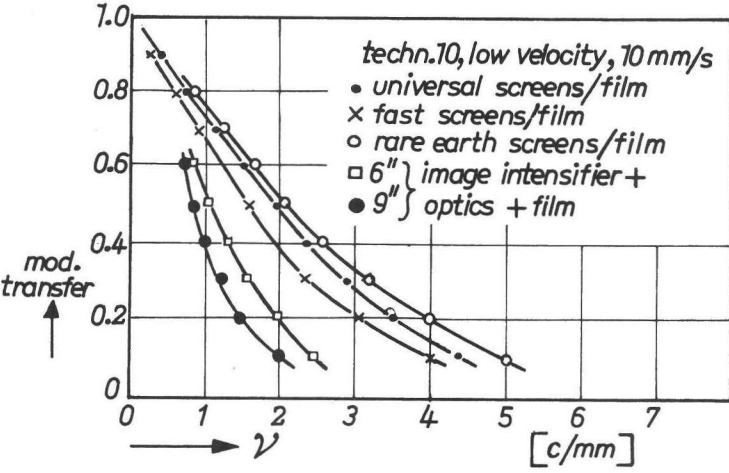


Fig. 5.1.6b

Fig. 5.1.6a/b.

$MTF_x$  as a function of the image receptor choice.

The more sensitive receptors give a better  $MTF_x$  for the smallest  $b_x$  situation, i.e. in high velocity stomach imaging. The 9" and 6" image intensifiers give results which are comparable with the fast screens receptor. Apparently, the effect of the reduced intrinsic resolution is compensated by the effect of the increased sensitivity.

If the shadow image MTF is not dominant, the rare-earth screens give only a slightly better  $MTF_x$ . The fast screens and the image intensifiers give a substantially worse  $MTF_x$  in this situation.

A trend to sharper image intensifiers would considerably influence the object resolution in those techniques where the shadow image MTF is not initially dominant. As can be seen in fig. 5.1.3, ( $b_x > 1$ , hence  $\eta_{x,m} > \approx 0.3$ ) this is the case in many techniques, with the exception of heart imaging.

### 5.1.3 Focal-spot intensity distribution

#### 5.1.3.1 Stationary objects

In sec. 3.4.2 the critical value of unity for  $b_x$  was introduced. Generally,  $b_x$  is larger than unity (fig. 5.1.2), hence a considerable smoothing of the focal-spot intensity distribution takes place. In fact, large values of  $b_x$  occur. A few exceptions exist, however, i.e. techniques 90 (ribs), 41 (sternum lat.), 62 and 63 (wrist obl. and lat.), 65 (hand obl.), 78 and 79 (foot) and 26 and 27 (cerebral angiography). For techniques 26 and 27 geometric magnification is deliberately chosen, whereas for techniques 90 and 41 magnification is inevitable due to the patient thickness. The magnification leads to a potentially larger influence of the shadow image MTF. Since techniques 62, 63, 65, 78 and 79 are carried out without intensifying screens, a high tube load is needed, which means that the focal spot has to be large.

There are however only a limited number of exceptions, so generally speaking the focal-spot intensity distribution has little effect. If geometric magnification is applied, the influence may be substantial.

#### 5.1.3.2 Moving objects

In sec. 3.4.1 the  $\eta_{eq}$  concept was developed. If  $\eta$  is larger than  $\eta_{eq}$ , then the influence of the focal-spot intensity distribution is relatively large. Conversely, if  $\eta$  is smaller than  $\eta_{eq}$ , the line-spread function corresponding to the shadow image MTF is smaller than the receptor LSF.

The  $\eta_{eq}$  values can easily be calculated on the basis of the  $\eta_{x,m}$  values assessed in sec. 5.1.2.1 (eq. 3.4.4). The ratio of  $\eta_{eq}$  and  $\eta$  is given in fig. 5.1.7a and fig. 5.1.7b per medical technique for the  $\eta = 0.17$  situation, with grid. The geometric magnification situation ( $\eta = 0.40$ ) without grid is given for the 9" image intensifier system in fig. 5.1.7c. The critical value of  $\eta_{eq}/\eta$  equal to unity is also indicated.

The same six situations as in sec. 5.1.2.2 will be considered.

- a) Universal screens/film,  $\eta = 0.17$ : Since the value of  $\eta_{eq}/\eta$  is smaller than unity, the influence of the focal-spot intensity distribution is relatively large. Consequently a falling intensity distribution will have advantages.
- b) Fast screens/film,  $\eta = 0.17$ : Since  $\eta_{eq}$  is smaller than  $\eta$  a falling intensity distribution is of advantage.

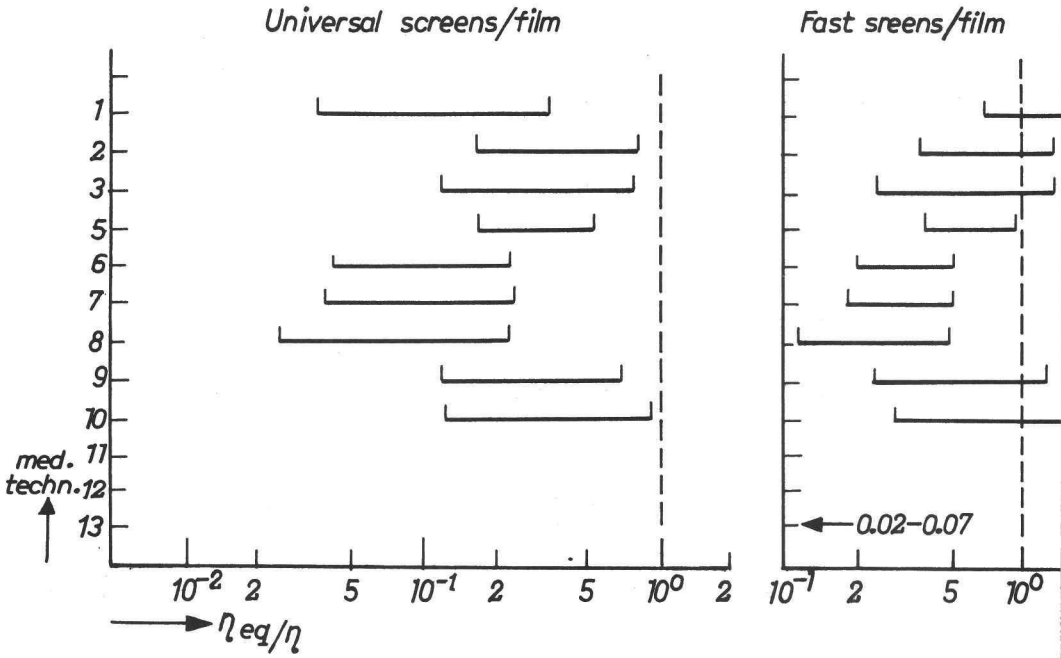


Fig. 5.1.7a.

$\eta_{eq}/\eta$  ratio per medical technique;  $\eta = 0.17$ , grid, intensifying screens.

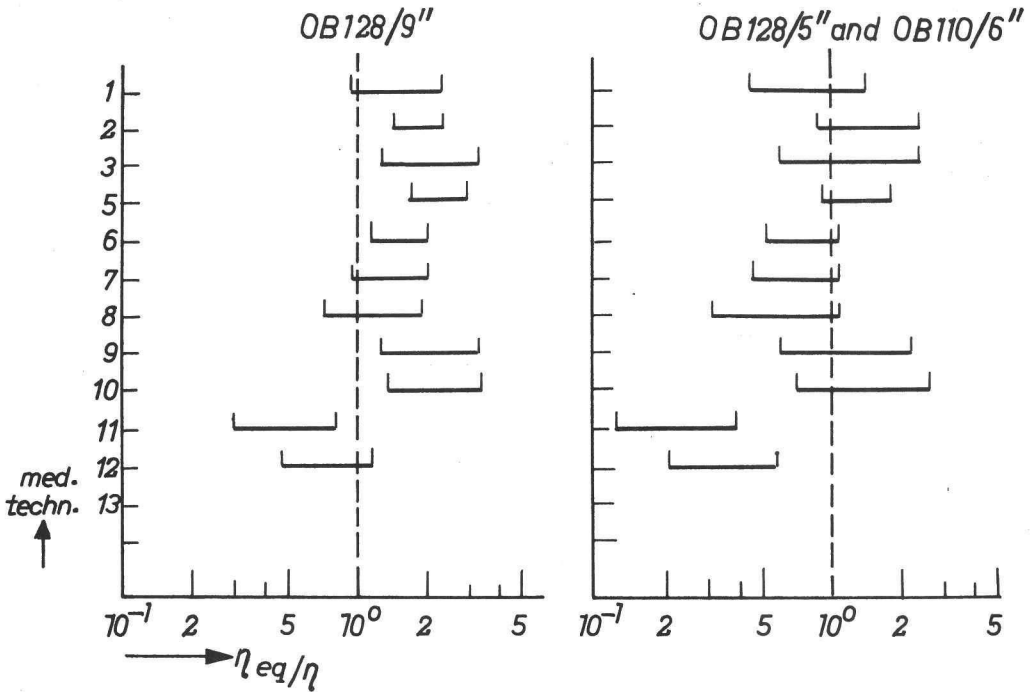


Fig. 5.1.7b.

$\eta_{eq}/\eta$  ratio per medical technique;  $\eta = 0.17$ , grid, image intensifier.



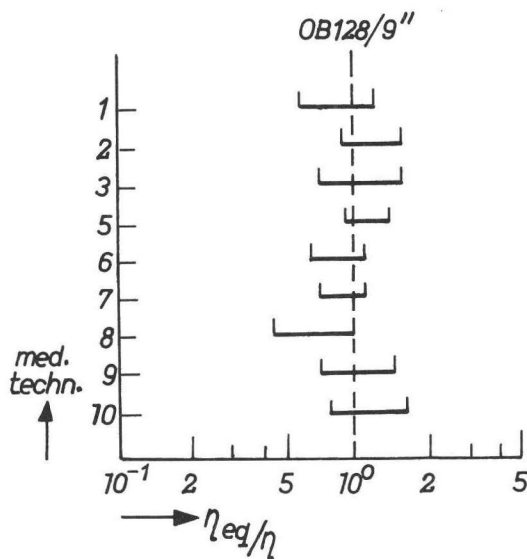


Fig. 5.1.7c.

$\eta_{eq}/\eta$  ratio per medical technique;  $\eta = 0.40$ , no grid, image intensifier.

- c) 5"/6" image intensifier,  $\eta = 0.17$ :  $\eta_{eq}$  being roughly equal to  $\eta$ , a Gaussian distribution suffices.
- d) 9" image intensifier,  $\eta = 0.17$ :  $\eta_{eq}$  being larger than  $\eta$ , the influence of the distribution is small. Any distribution will do, except for the highest velocity situations.
- e) 9" image intensifier,  $\eta = 0.40$ : The same conclusion as for situation c) can be drawn, so that a Gaussian distribution is of advantage.
- f) Heart imaging: Since  $\eta_{eq}$  for every receptor is substantially smaller than  $\eta$ , a falling intensity distribution will give better results.

### 5.1.3.3 Discussion

#### Stationary objects

Although the influence of the intensity distribution was assessed to be small, the recommended improvement of the intrinsic resolution of image receptors would imply that the distribution has a potentially larger influence.

#### Moving objects

The movement MTF is also involved. This may influence the conclusions in two ways. Firstly, the required optimum short-time loadability may not be feasible, because more than 200 kW is required. In this situation, the movement MTF will dominate, so that the intensity distribution will be smoothed considerably (fig. 3.4.5). This occurs only for AOT heart imaging and for lung imaging, high velocity,

at the larger  $f_r$  distance of 1500 mm (fig. 5.1.5). Secondly, a forced choice of a focal-spot size must be made, whereas actually a range of optimum sizes is required. For objects that move faster than in accordance with the chosen focal-spot size, considerable smoothing takes place. But slower moving objects will also be present, for which less smoothing occurs. The worst case corresponds to the imaging of the stationary objects present. The corresponding  $\eta_{x,st}$  and  $b_x$  values have been calculated for the focal-spot sizes and  $\eta$  values proposed. As expected, the 100 kW focus for application with the universal screens/film combination corresponds to a small value of  $b_x$  (0.72), so that the influence of the focal-spot intensity distribution is considerable. For the smaller focal spots (0.6 mm for universal screens, 0.6/1.0 mm for the 5"/6" image intensifier, 0.3/0.6 mm for the 9" intensifier) and other receptors, the minimum value of  $b_x$  is 1.4, which means that there is still an influence of the distribution. We must conclude that an optimum distribution for the imaging of moving objects may lead to unfavourable imaging of stationary objects.

If more sensitive screens are used, this will imply less distortion of the shadow image. The potential influence of the intensity distribution will then be smaller. A more sensitive screen also implies a favourably smaller patient dose. An example is the application of rare-earth intensifying screens with a higher sensitivity than universal screens (a factor of 4 has been claimed), but with a comparable MTF. Calculations indicate that the corresponding  $\eta_{eq}$  values are comparable to those for the fast screens. The conclusion may be drawn, therefore, that the focus-intensity distribution is likely to have only a moderate influence.

## 5.2 Visual resolution

The model of the visual system is coupled to that of the X-ray system so as to allow the visual resolution to be studied. The 'visual resolution' is inversely proportional to the threshold contrast of isolated objects. Consequently, the visual resolution is proportional to the maximum contrast gradient of the final image made by the visual system, taking both the unsharpness and the size of the objects into account (see fig. 2.2.11). The threshold contrast is further governed by the noise, in terms of the X-ray exposure or exposure rate at the entrance of the image receptor, and the noise-equivalent aperture.

Three classes of objects are considered: edges, bars and disks. These objects resemble medical objects like ribs, blood-vessels and micro-calcifications. As essentially edges are imaged if a bar or disk is large in relation to the unsharpness of the imaging system, we will understand by 'bars' objects which are small in one dimension. 'Disks' are small in two dimensions. Hence a 'small bar' is a pleonasm in this respect. Medium-sized objects are not considered. They can of course also be handled with our model of the visual system. But the mathematics involved is much more complicated (the image intensity distribution must be calculated by means of

the Fourier theory), which rules out a convenient representation by nomograms. Since only stationary objects were observed, only frozen pictures can be considered for moving objects. Moving disks are *not* considered by reason of the inherent anisotropy.

In sec. 5.2.1 the relation between the object and the visual resolution will be studied. The results of this investigation will be applied to stationary object imaging in sec. 5.2.2, and to the moving object situation in sec. 5.2.3.

Finally, the influence of the contrast is studied in sec. 5.2.4 with respect to the X-ray beam quality, and in sec. 5.2.5 with respect to the scattered radiation.

The imaging of the X-ray system is not described in the object plane, because this does not correspond to the practical viewing situation. On the contrary, the image receptor input plane has been chosen as the reference plane.

### 5.2.1 *The relation between object resolution and visual resolution*

Nomograms and equations are derived to describe the relative threshold contrast as a function of:

- (i) the position of the object,
- (ii) the focal spot-to-image receptor distance,
- (iii) the focal-spot size,
- (iv) the image receptor choice,
- (v) the viewing conditions.

If more than one parameter varies at a time, the appropriate nomograms must be applied sequentially. The object processing is described by the model of the visual system, and so is the influence of the viewing conditions. The relative influence of the graininess of different image receptors cannot be described.

Consequently, five situations can be discerned:

- (i) The fluoroscopic situation, which implies a dominant dynamic noisy background. A full description of the threshold contrast dependencies is available.
- (ii) The structureless background situation. A full description is available as the background does not contain effective noise. The scope of this situation may be larger than expected, as Pfeiler and Linke (1972) suggest that 'the quantum noise does not disturb in screens/film systems, except for the very sensitive systems'.
- (iii) The static-noise background (radiography, pulsed fluoroscopy and still cine pictures).

A full description is available if the static noise is not altered. We can therefore analyse the influence of the shadow image MTF (position of the object, focal spot-to-image receptor distance, focal-spot size) and the magnification factors (viewing distance, optical and image receptor magnification).

- (iv) The masking effect of the static noise is altered for a given image receptor. This can be done by changing the gamma of the imaging system, or by changing the tube load per image in pulsed fluoroscopy and still cine pictures. It has been concluded from literature that the masking effect of the noise is proportional to the  $\gamma$  (but the same holds for the contrast of the object, so the influence of the  $\gamma$  is zero), and inversely proportional to the square root of the tube load. A complete description is thus provided.
- (v) The static noise is altered by choosing another image receptor. The ultimate threshold contrast cannot be predicted; only the potential gain or loss in visual resolution as related to the object processing can be described.

### 5.2.1.1 Coupling of the visual system to the X-ray system

A complete medical X-ray system is illustrated in figure 5.2.1. It consists of an X-ray source, a moving or stationary object to be imaged, an image receptor, and finally an observer who perceives the image output plane. This is done on-line in the case of fluoroscopy, and off-line in the case of (cine) radiography. The image receptor is drawn with a separate input and output plane, which is the case if an image intensifier is used. The input and output plane practically coincide for screens/film combinations. The output plane contains the final image. It can also be a projected cine image.

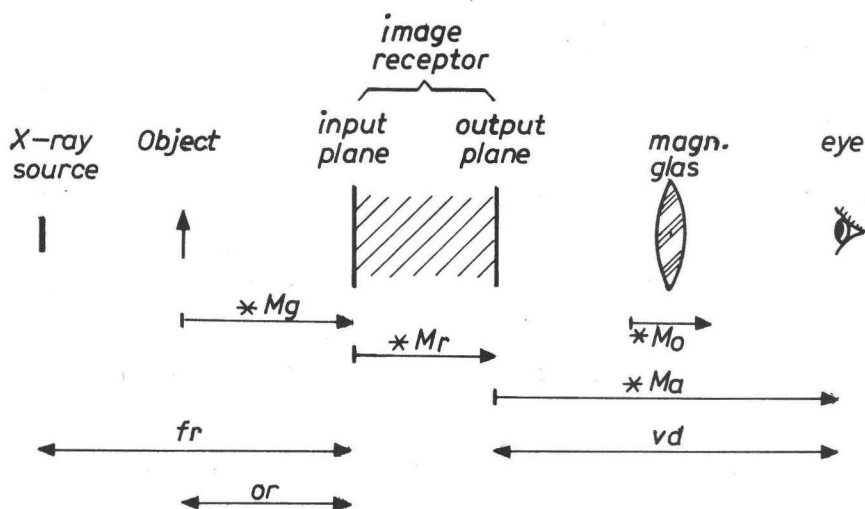


Fig. 5.2.1.  
X-ray system and magnification factors.

### Modulation transfer function

The visual system imaging can also be described by an MTF, so that a complete description of the X-ray system is possible. The reference plane must be an image plane, as this corresponds to the practical viewing conditions. In perception research the visual system would be the reference, but this is impractical for X-ray experts. Therefore the image receptor entrance is chosen as the reference plane; it will be called 'image receptor plane'. The corresponding MTF of the visual system is given by

$$MTF_v(\nu) = e^{-\frac{\beta}{M_r \cdot M_o \cdot M_a} \cdot \nu} \quad (5.2.1)$$

where (fig. 5.2.1)  $M_r$  is the magnification factor of the image receptor and  $M_o$  is the optical magnification factor. This is normally defined for the 'standard' viewing distance of 250 mm, but we shall relate it to the viewing distance used, i.e. for radiography/fluorography to a distance of 500 mm.  $M_a$  is the angular magnification factor to convert the spatial frequency  $\nu$  in periods per millimetre. Hence for  $M_a$  (unit degree/mm) we can write

$$M_a = \arctg(1/vd) \quad (5.2.2)$$

where  $vd$  denotes the viewing distance. If the counterpart of  $\beta$  is denoted by  $\beta'$  (unit mm) then  $MTF_v$  is given by

$$MTF_v(\nu) = e^{-\beta' \nu} \quad (5.3.2)$$

with  $\nu$  in periods per millimetre.

As the image receptor MTF can also be approximated by an exponential function, we can write for  $MTF_r$ :

$$MTF_r(\nu) = e^{-\frac{0.693}{\nu_{rec}} \cdot \nu} \quad (5.2.4)$$

The image receptor and the visual system together act as the *detector* of the image. The corresponding MTF, denoted by  $MTF_d$ , is given by (eqs. 5.2.3 and 5.2.4).

$$MTF_d(\nu) = e^{-\left(\beta' + \frac{0.693}{\nu_{rec}}\right) \cdot \nu} \quad (5.2.5)$$

Mathematically speaking, this detector MTF can be considered as a new image receptor MTF, which means that all the calculations and nomograms for the object

resolution (ch. 3) can be used. Nevertheless a detailed analysis of the visual resolution is justifiable, because (i) not the object plane but the image plane must be considered, and (ii) the effects of size and noise are not contained in the MTF description.

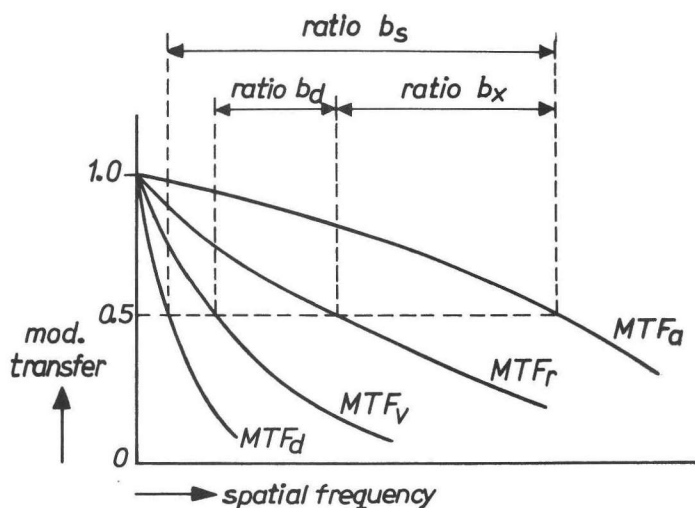


Fig. 5.2.2.

Definition of  $b_x$ ,  $b_d$  and  $b_s$

The balance between the factors which constitute  $MTF_d$  is denoted by  $b_d$  (fig. 5.2.2). The value of  $b_d$  is equal to the ratio between  $\nu_{rec}$  and  $\nu_{v,z=0.5}$ , a measure of the intrinsic resolution of the visual system. The new parameter  $\nu_{d,z=0.5}$ , i.e. the spatial frequency which is transferred by the image detector with modulation transfer 0.5, characterizes its intrinsic resolution. The relevant values of  $b_d$ ,  $\nu_{v,z=0.5}$  and  $\nu_{d,z=0.5}$  are given in table 5.2.1 for a number of image receptors and practical viewing conditions, as follows:

- Large-size films and 70 mm films are viewed at a distance of 500 mm. A magnifying glass for which  $M_O$  equals 5 can be used.
- The 35 mm cine films are projected with ten-fold magnification. The viewing distance is 1000 mm. Only stil pictures will be considered, or objects which did not move during the run.
- The viewing distance in the case of fluoroscopy is 2000 mm, i.e. corresponding to seven times the picture height.

The value of  $b_d$  is generally much larger than unity, unless optical magnification is applied.

TABLE 5.2.1: Image receptor and visual system data

image receptor	$M_R$	$\nu_{rec}$ [c/mm]	$\nu_d$ [mm]	$\nu_{v,z=0.5}$ [c/mm] and $b_d$						$\nu_{d,z=0.5}$ [c/mm]		
				$M_O = 1$		$M_O = 5$		$M_O = 10$		$M_O = 1$	$M_O = 5$	$M_O = 10$
					$b_d$		$b_d$		$b_d$			
film	1.000	20.00	500	0.159	126.0	0.794	26.0			0.157	0.762	
univers. } screens fast        + high def. } film	1.000	1.83	500	0.159	11.5	0.794	2.3			0.146	0.554	
	1.000	1.39	500	0.159	8.8	0.794	1.8			0.143	0.505	
	1.000	1.94	500	0.159	12.2	0.794	2.4			0.147	0.563	
9" } image 6.5" } intensif. + 6" } optics + 5" } 70 mm film	0.307	0.66	500	0.049	13.5	0.244	2.7			0.045	0.178	
	0.425	0.70	500	0.068	10.3	0.337	2.2			0.062	0.228	
	0.465	0.91	500	0.074	12.3	0.369	2.7			0.068	0.263	
	0.553	0.75	500	0.088	8.5	0.439	1.7			0.079	0.277	
9" } image 6.5" } intensif. + 6" } optics + 35 mm 5" } cine film	0.154	0.66	1000					0.122	5.4			0.103
	0.212	0.70	1000					0.168	4.2			0.136
	0.232	0.91	1000					0.184	4.4			0.153
	0.276	0.75	1000					0.219	3.4			0.170
6" image int. + TV system	1.820	0.50	2000	0.072	7.0					0.063		

The system MTF,  $MTF_s$ , is given by the product of the three MTFs:

$$MTF_s(\nu) = MTF_a(\nu) \cdot MTF_r(\nu) \cdot MTF_v(\nu) \quad (5.2.6)$$

or by

$$MTF_s(\nu) = MTF_a(\nu) \cdot MTF_d(\nu) \quad (5.2.7)$$

The system MTF can be written in a normalized way by using the counterparts of the  $\eta_{x,m}$  and  $\eta_{x,st}$  values, i.e. the newly defined parameters  $\eta_{s,m}$  and  $\eta_{s,st}$ . The appropriate image receptor is the image detector. The object positions  $\eta_{s,m}$  and  $\eta_{s,st}$  correspond to the equality of the detector and shadow image MTF. Instead of the balance factor  $b_x$ , the balance factor  $b_s$  (fig. 5.2.2) is defined. It describes the divergence of  $MTF_a$  and  $MTF_d$  if  $\eta \neq \eta_s$ .

The values of  $\eta_{s,m}$  and  $\eta_{s,st}$  are given by equations 3.2.43 and 3.3.9. The value of  $b_s$  is conversely given by equations 3.2.46 and 3.3.15. The corresponding figures (3.2.12, 3.2.27, 3.2.28, 3.3.1, 3.3.11 and 3.3.12) can be used, because the balance factors are insensitive to the reference plane position. The normalized shape of the system MTFs in the image receptor input plane is given by

$$e^{-\nu} \cdot \left| \frac{\sin \left( \pi \cdot \frac{0.603}{0.693} \cdot \frac{\eta}{\eta_{s,st}} \cdot \frac{1-\eta_{s,st}}{1-\eta} \cdot \nu \right)}{\pi \cdot \frac{0.603}{0.693} \cdot \frac{\eta}{\eta_{s,st}} \cdot \frac{1-\eta_{s,st}}{1-\eta} \cdot \nu} \right| \quad (5.2.8)$$

for stationary objects, and

$$e^{-\nu} \cdot \left| \frac{\sin \left( \pi \cdot \frac{0.442}{0.693} \cdot \left( \frac{\eta}{\eta_{s,m}} \right)^{3/5} \cdot \frac{1-\eta_{s,m}}{1-\eta} \cdot \nu \right)}{\pi \cdot \frac{0.442}{0.693} \cdot \left( \frac{\eta}{\eta_{s,m}} \right)^{3/5} \cdot \frac{1-\eta_{s,m}}{1-\eta} \cdot \nu} \right|^2 \quad (5.2.9)$$

for moving object imaging with the optimum focal-spot size.

The value of the expression in  $\eta$  and  $\eta_s$  in equations 5.2.8 and 5.2.9 increases for larger  $\eta$ . In other words, the system MTF in the image receptor plane is worse the further the object is shifted away from the receptor.

A convenient description of the system MTF will be chosen for a particular investigation, i.e. either

- (i) a description based on the intrinsic image receptor resolution  $\nu_{rec}$ ,  $b_x$  and  $b_d$  (the value of  $b_x$  is found on the basis of  $\eta$  and  $\eta_{x,m}$  or  $\eta_{x,st}$ ), or



- (ii) a description based on the intrinsic resolution of the image detector  $\nu_{d,z=0.5}$ ,  $b_s$  and  $\eta_s$ . This is particularly suited to an investigation of the influence of the object position.

#### Noise

The noise-equivalent aperture in the case of dynamic noise is given by

$$A_{eq} = [ 2\pi \int_0^{\infty} \nu \text{MTF}_d^2(\nu) d\nu ]^{-1} \quad (5.2.10)$$

so for  $C_T$  we have:

$$C_T \sim \nu_{d,z=0.5} = \frac{\nu_{v,z=0.5} \cdot \nu_{rec}}{\nu_{v,z=0.5} + \nu_{rec}} \quad (5.2.11)$$

Eq. 5.2.11 can be written in terms of  $b_d$ . If the effective visual system MTF is varied by for instance varying the viewing distance, then a convenient expression is

$$C_T \sim \nu_{rec} \cdot \frac{1}{1 + b_d} \quad (5.2.12)$$

Thus an increasing value of  $b_d$ , corresponding to e.g. an increase of the viewing distance, indicates a decrease of the threshold contrast; the visual system tends to dominate.

If the image receptor MTF is varied, eq. 5.2.11 becomes

$$C_T \sim \nu_{v,z=0.5} \cdot \frac{b_d}{1 + b_d} \quad (5.2.13)$$

Thus, if the image receptor resolution is improved, its noise integration properties will be reduced. The influence is smaller the larger the value of  $b_d$ : the visual system MTF dominates in that case.

#### 5.2.1.2 Point, line and edge spread function imaging

With respect to the dimensions of the objects we distinguish three classes of images. Point spread functions (PSF) are made if the anatomical structure is small in relation to the resolution of the system, in all directions. A line spread function (LSF) is made if the structure is small in one direction only. An edge spread function (ESF) is made if an edge is imaged, i.e. a step function of which the two plateaus are broad. The imaging of small disk-like structures (ulcers, calcifications)

leads to PSF imaging, while narrow bars (e.g. blood-vessels, stomach-wall structures) give rise to LSF imaging. If the width of the bar or the disk is large (e.g. gall-stones) then the imaging is also governed by edge spread functions.

The maximum object width for PSF and LSF imaging and the minimum width for ESF imaging depend on the system MTF. As far as the visual system is concerned, the maximum width is about 6' for disks (fig. 2.4.2.3) and about 3' for bars (fig. 2.4.2.4). The minimum size for edge spread function imaging to occur is correspondingly 40' for disks and 20' for bars. The corresponding critical object sizes are given in table 5.2.2. Screens/film combinations and film, and 6" image intensifier imaging are considered. A geometric magnification of unity or of two is applied. The viewing conditions are as listed in table 5.2.1. If the magnification factors are chosen larger, then smaller object sizes are involved. The conclusions for PSF imaging remain valid, of course, but the object for ESF imaging

**TABLE 5.2.2: Critical object sizes for PSF, LSF and ESF imaging**

image receptor	$M_r$	$M_g$	$M_o$	vd [mm]	largest width [mm] for which LSF/ PSF imaging occurs		smallest width [mm] for which ESF imaging occurs	
					LSF (bar)	PSF (disk)	ESF (bar)	ESF (disk)
(screens)/film	1.000	1	1	500	0.5	0.9	2.9	5.8
	1.000	1	5	500	0.1	0.2	>0.6	1.2
	1.000	2	1	500	0.2	0.4	1.5	3.0
	1.000	2	5	500	0.05	0.1	>0.3	> 0.6
6" image int. + 70 mm film	0.465	1	1	500	1.0	1.9	6.2	12.5
	0.465	1	5	500	0.2	0.4	1.2	2.5
	0.465	2	1	500	0.4	0.9	3.1	6.2
	0.465	2	5	500	0.1	0.2	>0.6	1.2
6" image int. + 35 mm cine film	0.232	1	10	1000	0.4	0.8	2.6	5.3
	0.232	2	10	1000	0.2	0.4	1.3	2.6
6" image int. + TV system	1.820	1	1	2000	1.0	1.9	6.2	12.5
	1.820	2	1	2000	0.5	1.0	3.1	6.2

would be so small that the X-ray system becomes the limiting factor (e.g. screens/film,  $M_g = 2$ ,  $M_o = 5$ , bar imaging). In these situations the  $MTF_x$  should also be taken into account to be sure of edge imaging. As an indication, the symbol  $>$  is introduced. We can conclude that blood-vessels with a diameter of  $200\ \mu\text{m}$  can often be considered as small, and that e.g. gall-stones of 5 to 10 mm will generally give rise to edge spread function imaging.

### 5.2.1.3 Estimation of the maximum contrast gradient

As mentioned in the introduction, the maximum contrast gradient governs the visibility of objects. In principle, this gradient must be calculated by taking the system MTF and the object properties into account. This is however a laborious affair, especially for the two-dimensional geometries. The complexity of the problem is greatly reduced by taking only the limiting situations into account, i.e. either very small or large objects are considered. The gradient can further conveniently be estimated in terms of the spatial frequency of a grating whose modulation transfer by the system equals 0.25, the  $\nu_{s,z=0.25}$  frequency.

#### Moving and stationary edges

From the work on the correlation between the MTF quality and the LSF/ESF quality (sections 3.2.2.2 and 3.3.2.2) it is concluded that the system spatial frequency for a modulation transfer 0.25,  $\nu_{s,z=0.25}$ , is approximately proportional to the maximum gradient of edges, if the system MTF is built up out of  $\sin(x)/x$  shaped and exponentially shaped MTFs. This holds for every value of practical balance factors  $b_s$ . From figs. 3.2.22, 3.2.24, 3.3.8 and 3.3.10 it can be inferred that the relation holds in any case when  $0.05 < b_s < 100$ .

#### Stationary bars

If LSF images are made, then the maximum gradient is proportional to  $\nu_{s,z=0.25}$  squared, as in addition the width of the LSF is inversely proportional to  $\nu_{s,z=0.25}$ . This is illustrated in fig. 5.2.3, where the maximum gradient is given as a function of the width of a bar, for the  $MTF = e^{-0.5\nu}$  and a 5% worse MTF,  $MTF = e^{-0.475\nu}$ . The change in the gradient is indeed 10% for the smaller bars ( $\Delta < 3'$ , which value is used in sec. 5.2.1.2 as the maximum size for LSF imaging), and only 5% for the larger bars ( $\Delta > 20'$ ).

As the contrast gradient is also proportional to the width of the bar (proportional to the 'energy' of the signal), we may write:

$$C_T \sim \frac{1}{\nu_{s,z=0.25}^2 \cdot \Delta} \quad (5.2.14)$$

This relationship is not valid however for all combinations of MTFs. The shadow image MTF corresponds to the more or less homogeneous focal-spot intensity distribution of the X-ray source. Hence, if the  $MTF_a$  dominates, then the imaging

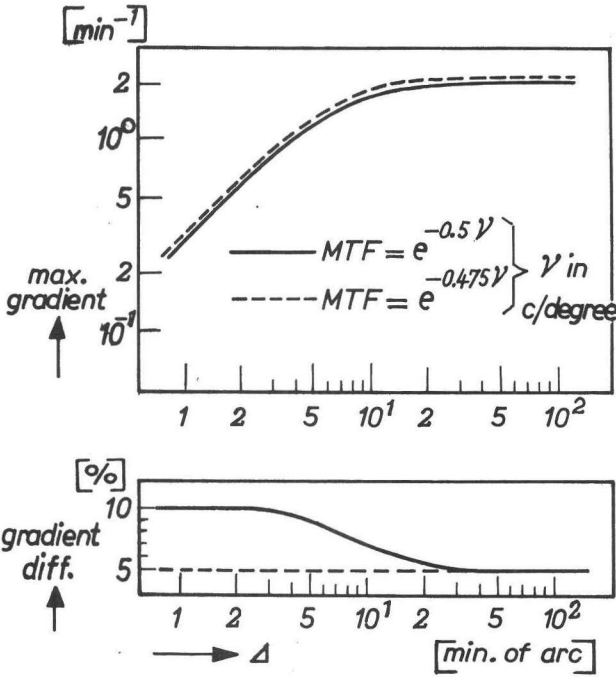


Fig. 5.2.3.  
Maximum contrast gradient of the bar image and the change in gradient, for two MTFs.

resembles edge spread function imaging and the given relationship is no longer valid. This is illustrated by fig. 5.2.4a, where the maximum contrast gradient is given as a function of  $\nu_{s,z}=0.25$ , with  $b_s$  as parameter. For  $b_s > \approx 0.5$ , the deviation from the prediction is smaller than 10%. The requirement for  $b_x$  is less stringent as its value is based upon the the image receptor MTF, which is often much better than the image detector MTF. For  $b_x$  we can write

$$b_x \geq \frac{\text{min. value of } b_s}{1 + b_d} = \frac{0.5}{1 + b_d} \tag{5.2.15}$$

Moving bars

The shadow image for the optimum focus condition corresponds to a triangular intensity distribution, so that a resemblance with edge spread function imaging as for stationary objects will never occur. Exponential and  $(\sin(x)/x)^2$  MTFs are therefore combined and the predicted contrast gradient behaviour is indeed approximately governed by the  $\nu_{s,z}=0.25$  value. In fig. 5.2.4b it is shown that the maximum contrast gradient is predicted within 10% by the  $\nu_{s,z}=0.25$  value squared. For small values of  $b_s$  the triangular distribution dominates, whereas for large values

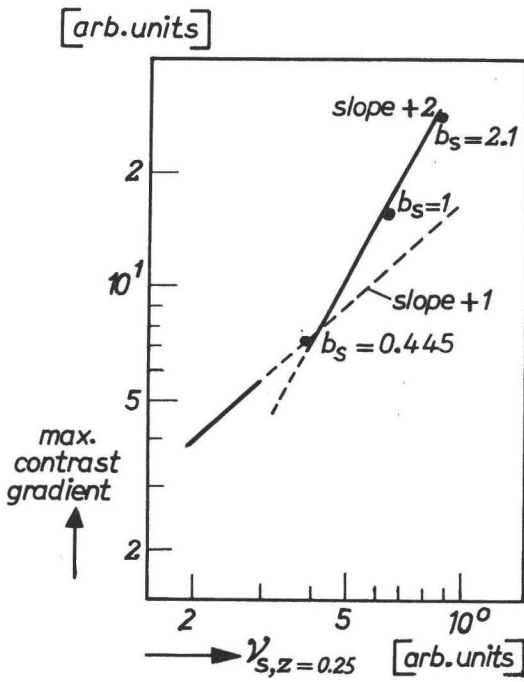


Fig. 5.2.4a.

Relation between  $\nu_{s,z=0.25}$  and the maximum contrast gradient, stationary bars

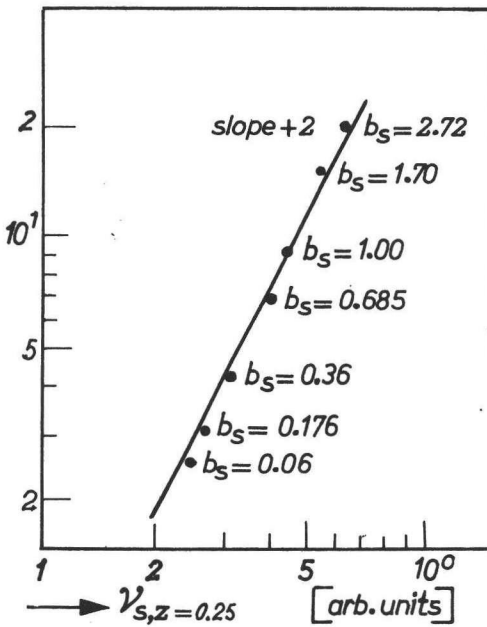


Fig. 5.2.4b.

Relation between  $\nu_{s,z=0.25}$  and the maximum contrast gradient, moving bars.

the exponentially shaped MTF governs the imaging. Consequently, the relationship as given by equation 5.2.14 is equally valid.

### Stationary disks

For PSF imaging, the maximum contrast gradient is proportional to  $\nu_{s,z=0.25}$  to the power of three. The same reasoning as for bars holds, but now two dimensions play a role. For convenience, the same range of  $b_s$  for the validity of this relationship is assumed as for stationary bars, as (i) the same problems concerning the shape of the MTFs exist, and (ii) the value of  $b_s$  is generally larger than unity (because the visual system MTF generally dominates). The risk of making serious mistakes is therefore small.

The contrast gradient is also proportional to the surface of the disk, so we may write

$$C_T \sim \frac{1}{\nu_{s,z=0.25}^3 \cdot \Delta^2} \quad (5.2.16)$$

#### 5.2.1.4 Variation of the position of the object

If the position of the object between the X-ray source and the receptor is varied, then (i) the unsharpness varies, (ii) the width of bars and disks varies proportionally to  $1/(1-\eta)$ , and (iii) no variation in the noise occurs, as the noise is governed by image detector properties (sensitivity, graininess). For the maximum gradient, the estimates of sec. 5.2.1.3 will be used. The  $\nu_{s,z=0.25}$  value is calculated with the aid of eqs. 5.2.8 and 5.2.9. The  $\eta_{s,st}$  and  $\eta_{s,m}$  values serve as the characterizing numbers. Firstly, nomograms will be developed. A mathematical formulation is given in the next section.

##### 5.2.1.4.1 *Nomograms*

#### Edges

The inverse threshold contrast is given in fig. 5.2.5 as a function of  $\eta$ , with  $\eta_{s,st}$  as parameter, for stationary edges. In fig. 5.2.6, the curves for moving edges are depicted.  $C_T$  is always worse for larger values of  $\eta$ , as (i) the size of the edge is not affected, and (ii) the shadow image MTF is worse for larger  $\eta$ . The influence of  $\eta$  is small if the image detector MTF dominates, i.e. if  $\eta_s$  is large. The reduction is smaller for moving objects as the focal-spot size is chosen smaller for larger  $\eta$  (eq. 3.2.31).

#### Bars

The effect of unsharpness is counteracted by the corresponding change of the size of the bar in the image receptor plane. Hence (fig. 5.2.7a, stationary objects, fig. 5.2.7b, moving objects), for large values of  $\eta_s$  ( $\eta_s > 0.8$ ) a large value of  $\eta$  is of advantage. Further, for  $\eta_s \approx 0.6-0.8$ , an optimum value of  $\eta$  of about 0.3-0.6

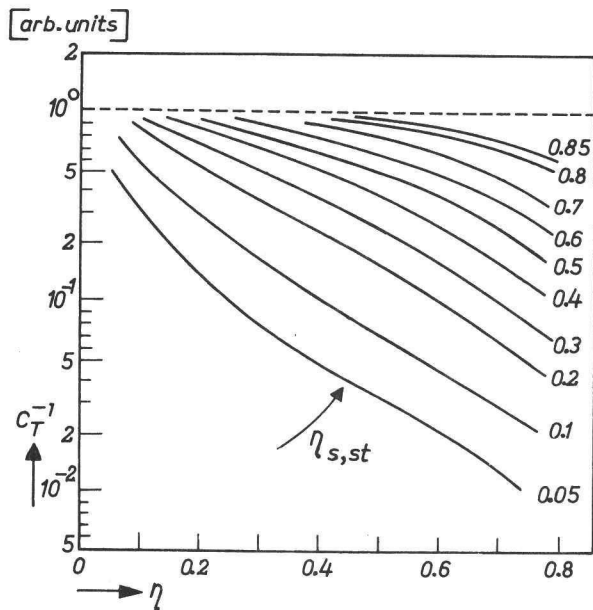


Fig. 5.2.5.

Threshold contrast of a stationary edge as a function of its position,  $\eta_{s,st}$  as parameter.

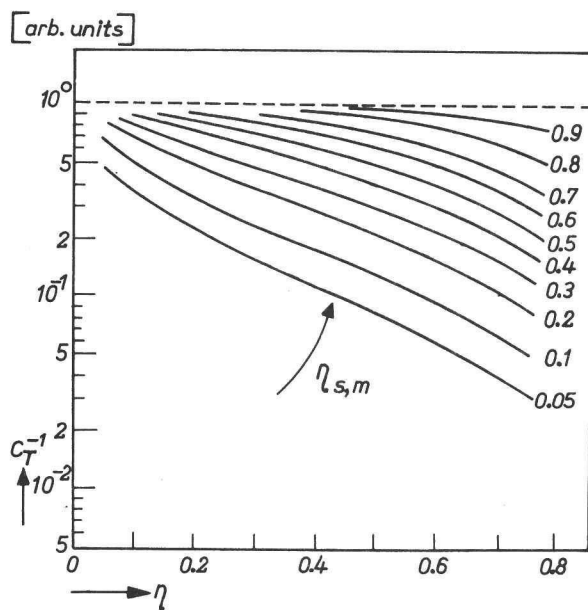


Fig. 5.2.6.

Threshold contrast of a moving edge as a function of its position,  $\eta_{s,m}$  as parameter

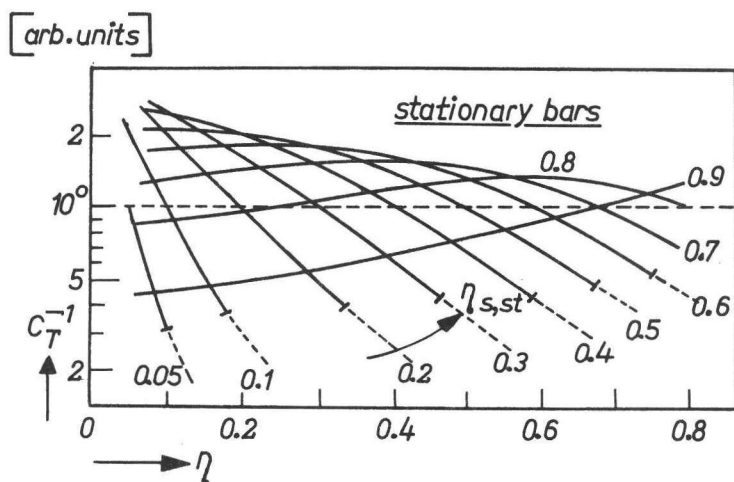


Fig. 5.2.7a

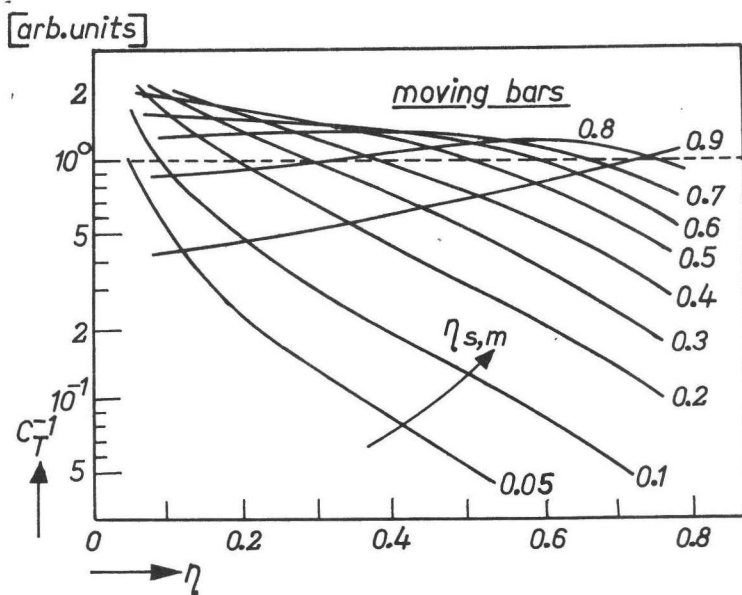


Fig. 5.2.7b.

Fig. 5.2.7a/b.

Threshold contrast of a bar as a function of its position,  $\eta_s$  as parameter.



exists. The optimum is of course smoother for moving objects. The dotted parts of the curves for stationary objects correspond to non-valid values of  $b_s$ .

### Stationary disks

The size effect, and also the unsharpness effect, are more pronounced for disks. Hence for  $\eta_{s,st}$  values as low as 0.5 (fig. 5.2.8) an optimum choice of  $\eta$  is possible. For  $\eta_{s,st} > 0.8$  the advantages in going to larger  $\eta$  are considerable.

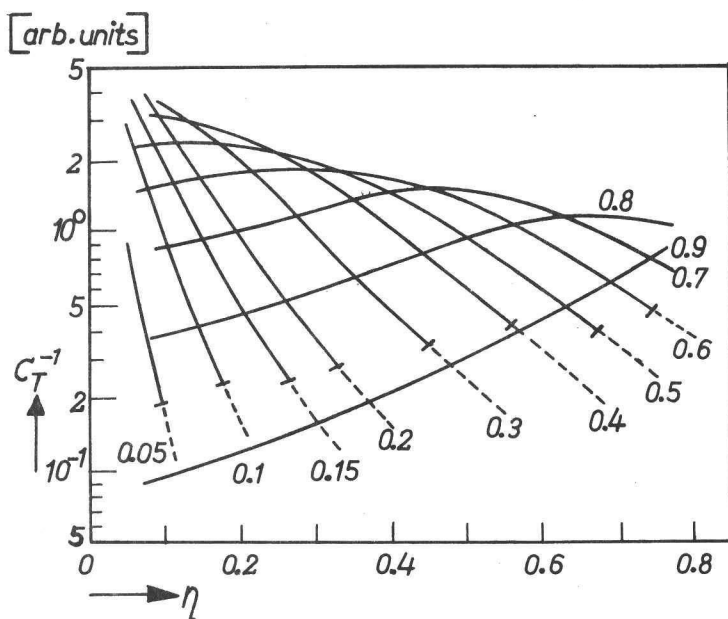


Fig. 5.2.8.

Threshold contrast of a stationary disk as a function of its position,  $\eta_{s,st}$  as parameter.

5.2.1.4.2 *Mathematical formulation.* The graphical presentation of the influence of the position of the object can be analytically understood by the investigation of  $\Delta C_T^{-1}/C_T^{-1}$ , the relative change in the inverse threshold contrast, if  $\eta$  changes by a small amount  $\Delta\eta$ .

### Influence of the MTF quality

$\Delta C_T^{-1}/C_T^{-1}$  is proportional to the change of the maximum contrast gradient of the image as governed by the MTF of the system. In sec. 5.2.1.3 we deduced that the maximum contrast gradient is proportional to  $\nu_{s,z}=0.25$ , and that the proportionality factor with respect to  $\Delta C_T^{-1}/C_T^{-1}$  is unity for edges, two for bars and three for disks. The proportionality factor will be denoted by  $p$ .

To describe  $\Delta CT^{-1}$  further, the relation between  $\nu_{s,z=0.25}$  and the object position is needed. The absolute value of  $\nu_{s,z=0.25}$  is completely defined by one of the two constituent MTFs, i.e.  $MTF_a$  or  $MTF_d$ , and their balance factor  $b_s$ . We can also state that the variation of  $\nu_{s,z=0.25}$  is completely described by the variation of  $b_s$  as induced by  $MTF_a$ , the  $MTF_d$  being fixed. Consequently, the  $\nu_{s,z=0.25}$  value is depicted in fig. 5.2.9 as a function of  $b_s$  for moving and stationary edges (one curve is given, as the difference is small). The proportionality factor between the relative change of  $b_s$  and that of the  $\nu_{s,z=0.25}$  value is governed by the gradient,  $\gamma$ , of the mentioned curve on log-log scales. This factor  $\gamma$  is also given in fig. 5.2.9. We infer that, as expected, for large values of  $b_s$ , i.e. for a relatively good  $MTF_a$ , changes in  $MTF_a$  will have a small effect: the  $\gamma$  is small. The  $\gamma$  approaches unity for small values of  $b_s$ .

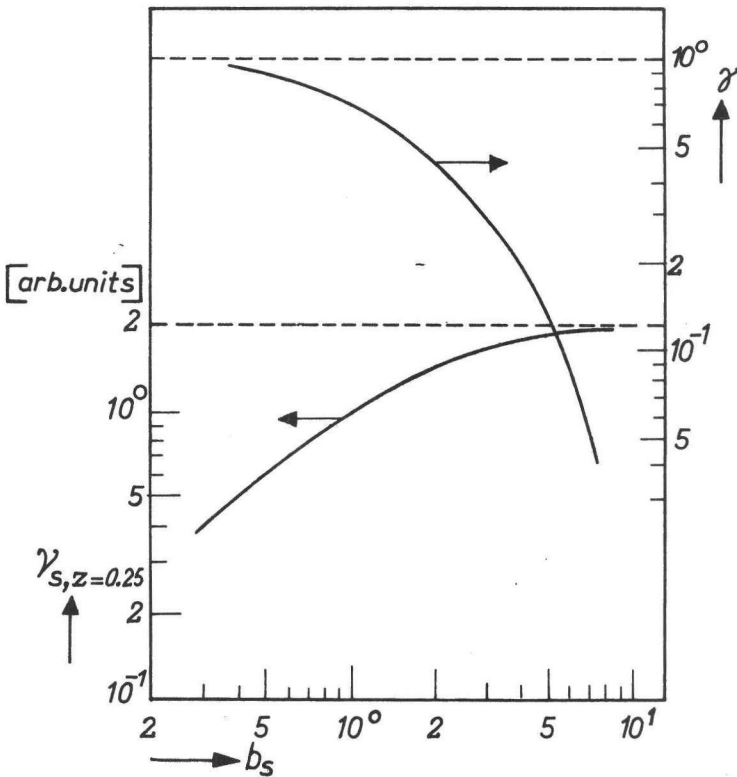


Fig. 5.2.9.

Measure of MTFs quality and the change in the quality, as a function of  $b_s$ .

Thus the change in MTF quality is indicated by the change in  $b_s$ , which is induced by the change in geometric magnification, and the change, if any, in the focal-spot size. For the influence of the focal-spot size, two situations must be considered:

- (i) Stationary objects: as an anti-scatter grid is often used, the influence of scattered radiation is small. Consequently, the exposure time, and hence the focal-spot size, are practically invariant with the position of the object. The  $MTF_a$  quality in the object plane is therefore inversely proportional to  $\eta$ .
- (ii) Moving objects: as the optimum focal-spot size is inversely proportional to  $\eta^{2/5}$ , a smaller  $\eta$  corresponds to a larger focal spot. The  $MTF_a$  quality in the object plane is inversely proportional to  $\eta^{3/5}$ .

The  $MTF_a$  quality change in the image receptor plane can further be calculated by taking the geometric magnification,  $1/(1-\eta)$  or  $1/(1-\eta-\Delta\eta)$ , into account.

#### Influence of the size of the object

For edges, no size effects occur. For bars and disks, the geometric magnification plays a role. The threshold contrast, then, is inversely proportional to  $(1-\eta)/(1-\eta-\Delta\eta)$  or  $(1-\eta)/(1-\eta-\Delta\eta)$  squared.

The fractional change of the inverse threshold contrast is expressed by the following equation, in which the value of  $p$ ,  $q$  and  $r$  will be chosen in correspondence with the application:

$$\frac{\Delta C_T^{-1}}{C_T^{-1}} = p \gamma \left\{ \left( \frac{\eta + \Delta\eta}{\eta} \right)^q \cdot \frac{1-\eta-\Delta\eta}{1-\eta} - 1 \right\} + \left\{ \left( \frac{1-\eta}{1-\eta-\Delta\eta} \right)^r - 1 \right\} \quad (5.2.17)$$

The derivation of this expression is simple but laborious, and is therefore omitted here. The parameter  $q$  corresponds to the focus size effect,  $r$  corresponds to the size effect proper and  $p$  governs the relation with the maximum contrast gradient for different objects. This equation will also be used for the analysis of the influence of the focus-to-image receptor distance.

#### Stationary edges

$p = 1$ ,  $q = -1$ ;  $r = 0$ . The value of  $\Delta C_T^{-1}$  is proportional to

$$-\Delta\eta \cdot \frac{\gamma}{\eta(1-\eta)} \quad (5.2.18)$$

hence  $\Delta\eta$  should be negative, and  $\eta$  must be made as small as possible. If  $\gamma$  is small, i.e. if the  $MTF_a$  is relatively good, the influence of any change in  $\eta$  is indeed small (fig. 5.2.5, large value of  $\eta_{s,st}$ ).

#### Moving edges

$p = 1$ ;  $q = -\frac{3}{5}$ ;  $r = 0$ .  $\Delta C_T^{-1}$  is proportional to

$$-\Delta\eta \cdot \frac{\gamma(2\eta + 3)}{5\eta(1-\eta)} \quad (5.2.19)$$

As  $2\eta + 3 > 0$ ,  $\Delta\eta$  should be negative, and  $\eta$  must be as small as possible (compare fig. 5.2.6).

#### Stationary bars

$p = 2$ ;  $q = -1$ ;  $r = 1$ . The approximation of  $\Delta C_T^{-1}/C_T^{-1}$  is

$$\Delta\eta \cdot \frac{\eta - 2\gamma}{\eta(1-\eta)} \quad (5.2.20)$$

If  $\eta < 2\gamma$ , then  $\Delta\eta$  should be negative and  $\eta$  should be chosen smaller. The value of  $\gamma$ , however, will also be smaller as  $b_s$  increases. As  $\gamma$  decreases faster,  $\eta$  will tend to be larger than  $2\gamma$ . But then the  $\eta$  value must be chosen larger. As a consequence, the optimum situation will be such that  $\eta = 2\gamma$ . (Compare the maxima in fig. 5.2.7a. If  $\eta_{s,st} = \eta = 0.7$ , then  $b_s = 1$  and  $\gamma = 0.68 \rightarrow \eta < 2\gamma \rightarrow \eta$  must indeed be chosen smaller.)

#### Moving bars

$p = 2$ ;  $q = -\frac{3}{5}$ ;  $r = 1$ . The approximate value of  $\Delta C_T^{-1}/C_T^{-1}$  is given by

$$\Delta\eta \cdot \frac{-6\gamma + \eta(5 - 4\gamma)}{5\eta(1 - \eta)} \quad (5.2.21)$$

If  $\eta > 6\gamma / (5 - 4\gamma)$  then  $\Delta\eta$  must be positive, hence  $\eta$  must be increased. But the value of  $\gamma$  increases also ( $6\gamma / (5 - 4\gamma)$  equals 6 for  $\gamma = 1$ ), and if  $\eta < 6\gamma / (5 - 4\gamma)$  then  $\eta$  should be decreased. As a consequence,  $\eta = 6\gamma / (5 - 4\gamma)$  is the optimum value (compare in fig. 5.2.7b the situation for  $\eta_{s,m} = 0.8$ . If  $\eta = \eta_{s,m}$ ,  $b_s = 1$ , and  $\gamma = 0.68 \rightarrow 6\gamma / (5 - 4\gamma) > 1$ , so that  $\eta$  should indeed be smaller).

#### Stationary disks

$p = 3$ ;  $q = -1$ ;  $r = 2$ . The  $\Delta C_T^{-1}/C_T^{-1}$  value is approximated by

$$\Delta\eta \cdot \frac{2\eta - 3\gamma}{\eta(1 - \eta)} \quad (5.2.22)$$

hence the optimum value of  $\eta$  equals  $3\gamma/2$ . If  $\eta < 3\gamma/2$ , then  $\eta$  should be made smaller.

#### 5.2.1.5 Variation of the focal spot-to-image receptor distance

If this distance, denoted by  $f_r$ , is varied, then three different situations can be distinguished regarding the focal spot choice:

(i); Moving objects: the optimum size must be chosen, hence the  $MTF_a$  quality in

the object plane varies in inverse proportion to  $fr^{1/5}$  (eq. 3.2.30), or proportionally to  $\eta^{1/5}$ .

- (ii) Stationary objects, fixed exposure time: the required electrical energy per exposure is proportional to  $fr^2$ , the loadability of rotating anode tubes is proportional to the 1.5 power of the focal-spot size, and therefore the  $MTF_a$  quality in the object plane is proportional to  $\eta^{1/3}$ .
- (iii) Stationary objects, fixed focus size: this is of interest because for a given X-ray tube the  $fr$  distance can be varied. The resulting exposure time should not exceed certain limits, of course.  
The  $MTF_a$  quality in the object plane is inversely proportional to  $\eta$ .

Graphical representations of the effect of a change in the  $fr$  value cannot easily be given for cases (i) and (ii) as the  $\eta_s$  values and the value of  $b_s$  change in a complex way. For case (iii), the  $\eta_{s,st}$  value is unaffected, so figures 5.2.5, 5.2.7a and 5.2.8 apply. A change in the  $fr$  distance must then be translated into a change in the  $\eta$  value.

In the next sections, analytical expressions for the  $fr$  influence will be derived.

5.2.1.5.1. *Stationary objects, fixed focus.* The same reasoning as for a change in the object position applies, because the focus is fixed.

Edges

$\eta$  must be made small, hence  $fr$  must be as large as possible. The unsharpness will then diminish, and size effects do not play a role.

Bars

If  $\eta < 2\gamma$ ,  $fr$  should be made larger. The reverse is true if  $\eta > 2\gamma$ , hence  $\eta = 2\gamma$  represents the optimum situation.

Disks

If  $\eta < 3\gamma/2$ ,  $fr$  should be made larger.  $\eta = 3\gamma/2$  is the optimum situation.

5.2.1.5.2 *Stationary objects, fixed exposure time.* Equation 5.2.17 will be used.

Edges

$p = 1; q = -\frac{1}{3}; r = 0$ . The fractional change in  $CT^{-1}$  is approximated by

$$\Delta\eta \cdot \frac{\gamma(1-4\eta)}{3\eta(1-\eta)} \quad (5.2.23)$$

so that the optimum value of  $fr$  corresponds to  $\eta = 0.25$ . Hence the optimum  $fr$  distance is equal to four times the object-to-image receptor distance.

## Bars

$p = 2; q = \frac{1}{3}; r = 1$ .  $\Delta C_T^{-1}/C_T^{-1}$  is given by

$$\Delta\eta \cdot \frac{\gamma \{2\gamma + \eta (3 - 8\gamma)\}}{3\eta (1 - \eta)} \quad (5.2.24)$$

If  $\gamma \leq 0.375$ ,  $\Delta\eta$  should be positive, and therefore  $fr$  must be as small as possible. If  $\gamma > 0.375$ , then  $fr$  should be made smaller if  $\eta < -2\gamma/(3 - 8\gamma)$ , and larger if  $\eta > -2\gamma/(3 - 8\gamma)$ . The optimum  $fr$  distance corresponds to  $\eta$  equal to  $-2\gamma/(3 - 8\gamma)$ . If  $fr$  is chosen smaller, the expression between braces in eq. 5.2.24 becomes negative so that  $\Delta\eta$  should be negative. In other words,  $fr$  should be chosen larger. The negative sign of the braced expression is found by bearing in mind that  $\eta$  and  $\gamma$  equal unity for the smallest  $fr$  possible.

## Disks

$p = 3; q = \frac{1}{3}; r = 2$ . For  $\Delta C_T^{-1}/C_T^{-1}$  we write:

$$\Delta\eta \cdot \frac{\gamma + \eta (2 - 4\gamma)}{\eta (1 - \eta)} \quad (5.2.25)$$

The same reasoning applies as for bars, so that if  $\gamma \leq 0.5$  then  $\eta$  must be larger, and therefore  $fr$  should be as small as possible. If  $\gamma > 0.5$  and  $\eta < -\gamma/(2 - 4\gamma)$  then  $fr$  should be decreased. The optimum  $fr$  corresponds to  $\eta = -\gamma/(2 - 4\gamma)$ .

## 5.2.1.5.3 Moving objects, optimum focus size.

## Edges

$p = 1; q = \frac{1}{5}; r = 0$ . The fractional change in  $C_T^{-1}$  can be approximated by

$$\Delta\eta \cdot \frac{\gamma (1 - 6\eta)}{5\eta (1 - \eta)} \quad (5.2.26)$$

so that the optimum  $fr$  corresponds to  $\eta = 1/6$ . In words, the optimum  $fr$  distance is equal to six times the object-receptor distance.

## Bars

$p = 2; q = \frac{1}{5}; r = 1$ .  $\Delta C_T^{-1}$  is proportional to

$$\Delta\eta \cdot \frac{2\gamma + \eta (5 - 12\gamma)}{5\eta (1 - \eta)} \quad (5.2.27)$$

so that if  $\gamma \leq 5/12$ , then  $\eta$  should be increased, and therefore  $f_r$  should be made small. If  $\gamma > 5/12$  and  $\eta < 2\gamma/(12\gamma - 5)$  then  $f_r$  should also be made smaller. If  $\eta > 2\gamma/(12\gamma - 5)$  then  $f_r$  should be larger. The optimum value of  $f_r$  corresponds to  $\eta = 2\gamma/(12\gamma - 5)$ .

### 5.2.1.6 Variation of the focal-spot size

No noise nor size variation occurs. For moving objects the shadow image MTF is varied according to an optimum focus size. The inverse threshold contrast value is given in fig. 5.2.10, as a function of  $b_x$  with  $b_d$  as parameter. No separate data are given for moving objects, as the difference is small. The parameters  $b_x$  and  $b_d$  are chosen as  $b_x$  is directly influenced by the focal-spot choice, whereas  $b_d$  is not.

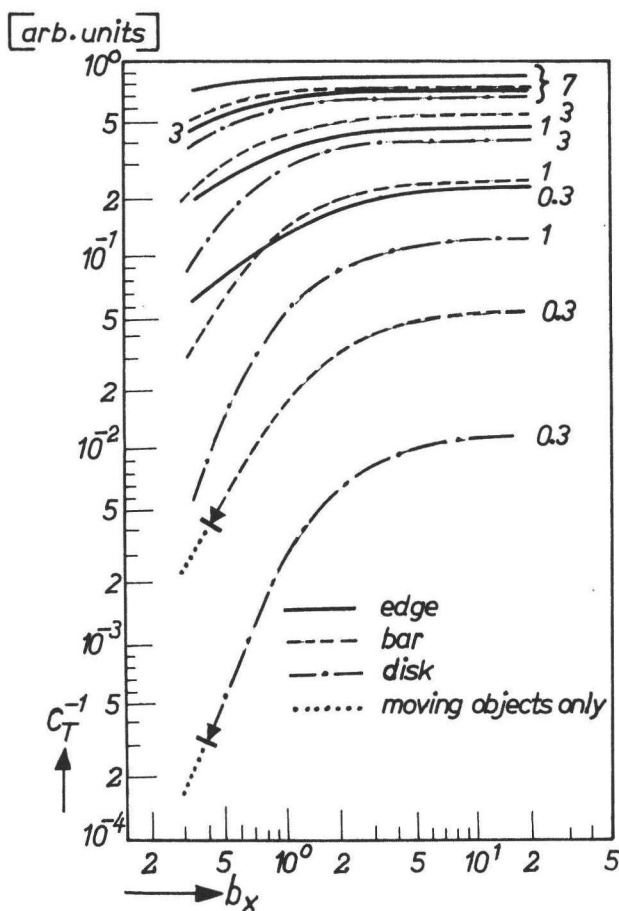


Fig. 5.2.10

Threshold contrast as a function of the shadow image unsharpness in terms of  $b_x$ ,  $b_d$  as parameter

All curves tend to an asymptote with zero slope for large values of  $b_x$ , because the shadow image unsharpness is then unimportant. A small value of  $b_x$  is detrimental in all situations, and the effect is of course (i) larger for disks and bars than for edges, (ii) smaller for larger values of  $b_d$ .

### 5.2.1.7 Variation of the visual system MTF in the image receptor input plane

This variation is governed by the variation of the magnification factors between the image receptor input plane and the visual system, i.e. by the change of the viewing distance and/or the optical and image receptor magnification. The variation is expressed in terms of the variation of the  $b_d$  value. As the value of  $b_x$  does not change, this parameter will be used as the reference parameter.

If the proposed variations are applied, then all three effects play a role, i.e. (i) the noise, if any, varies (eq. 5.2.12), (ii) the unsharpness changes, and (iii) the size of bars and disks varies. Fig. 5.2.11 gives the inverse threshold contrast in the noiseless/static noise situation, fig. 5.2.12 is appropriate to dominant dynamic X-ray noise. The curves are calculated for a variation of  $b_d$ , with  $b_x$  as parameter. The dotted parts of the curves are not valid for stationary objects. A smaller  $b_d$  value indicates a smaller viewing distance, or the application of a magnifying glass, or the use of a larger image intensifier magnification.

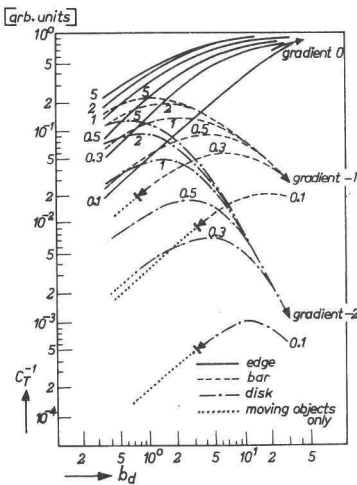


Fig. 5.2.11 Noiseless/static noise

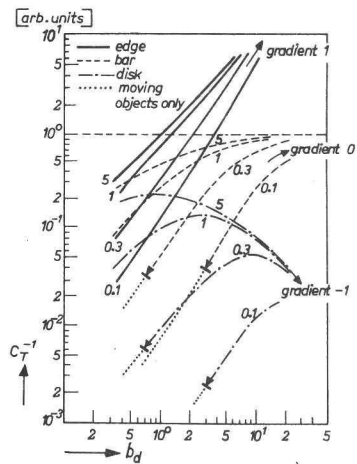


Fig. 5.2.12 Dominant dynamic X-ray noise

Fig. 5.2.11–5.2.12.

Threshold contrast as a function of the viewing distance and the image receptor and optical magnification, in terms of  $b_d$ ,  $b_x$  as parameter; different background as to the noise.



5.2.1.7.1 *Noiseless and static noisy systems.* Referring to fig. 5.2.11, the following can be said:

#### Edges

The  $\nu_{s,z=0.25}$  value increases with growing  $b_d$ , as the influence of the X-ray system unsharpness becomes smaller. Therefore the largest viewing distance is best.

#### Bars

As size effects and the effect of the unsharpness counteract each other, an optimum value of  $b_d$  (e.g. viewing distance) exists.

#### Disks

The same reasoning as for bars holds, but the optimum  $b_d$  value is smaller.

Generally, if  $b_d$  is large enough, unsharpness effects are absent and only the size effect remains. This corresponds to a gradient  $-2$ ,  $-1$  and  $0$  of the curves for disks, bars and edges.

5.2.1.7.2 *Dominant dynamic X-ray noise.* According to eq. 5.2.12, the larger the value of  $b_d$  the larger the noise integrating area. The curves of fig. 5.2.11 are changed accordingly in fig. 5.2.12 in that a stronger tendency for larger  $b_d$  value shows up.

#### Edges

A more pronounced positive effect of an ever increasing value of  $b_d$  is shown.

#### Bars

As the size effect is balanced by the effect of the different noise integrating area, these curves do not show an optimum. The largest  $b_d$  is best.

#### Disks

An optimum  $b_d$  still exists, but at a higher value of  $b_d$ .

Generally, if the visual system MTF is sufficiently dominant, i.e. if  $b_d$  is large enough, then only size and noise effects remain. The size effect is discussed in sec. 5.2.1.7.1, and the noise is integrated over an area which is proportional to the value of  $b_d$  squared. For sufficiently large values of  $b_d$ , the noise can no longer be regarded as dominant, and therefore a gradual transition to the noiseless situation (fig. 5.2.11) will occur.

### 5.2.1.8 Variation of the image receptor

The influence of the choice of the image receptor on the static noise has not been measured. We must therefore confine ourselves to systems where the static noise is

unimportant, i.e. to practically noise-free systems or to systems with a dominant dynamic noise.

The introduction of another image receptor may influence (i) the unsharpness (image receptor unsharpness, visual system unsharpness via the image receptor magnification,  $M_R$ , focal-spot change due to different sensitivity), (ii) the dynamic noise (absorption efficiency for X-rays, intensity amplification factor,  $M_I$  factor) and (iii) the size ( $M_R$ ). We will first investigate the influence of a variation of the image receptor unsharpness, all other parameters being constant.

5.2.1.8.1. *Variation of the unsharpness.* No size effects occur, but the unsharpness influences both the noise (eq. 5.2.13) and the contrast gradient.

The inverse threshold contrast is given (fig. 5.2.13a, without noise influence, fig. 5.2.13b with dominant dynamic X-ray noise) as a function of  $b_d$  with  $b_x \cdot b_d$  as parameter; this product is not affected by a choice of different  $b_d$  values.

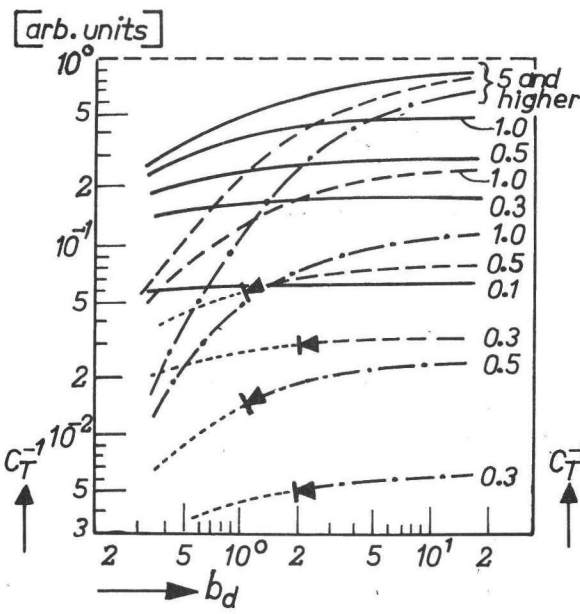


Fig. 5.2.13a  
Noiseless image

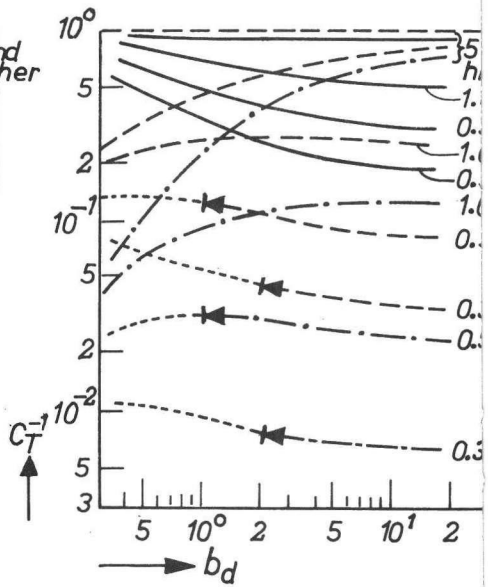


Fig. 5.2.13b  
Dominant dynamic X-ray noise

Fig. 5.2.13a/b.  
Threshold contrast as a function of the image receptor unsharpness in terms of  $b_d$ ,  $b_x \cdot b_d$  as parameter; ——— edge; - - - - bar; - . - . disk; . . . . moving objects only.

The dotted parts of the curves are not valid for stationary objects. No separate figures are given for moving objects as the difference is small.

### Noiseless image

If the shadow image MTF dominates, i.e. if  $b_x \cdot b_d < 1$ , then the effect of  $b_d$  variation is of course small. For large values of  $b_x \cdot b_d$ , the value of  $b_d$  should be large, although values larger than  $\approx 5$  give only a small improvement. The influence of  $b_d$  is more prominent for bars and disks, and a large value of  $b_d$  is of advantage.

### Dominant dynamic X-ray noise

The part of the curves for lower values of  $b_d$  is lifted as then a considerable noise integration takes place (for  $b_d = 0.3$ ,  $(1+b_d)/b_d = 4.3$ ). Hence if the shadow image MTF dominates ( $b_x \cdot b_d \ll 1$ ) the smallest value of  $b_d$  is advantageous. For large values of  $b_x \cdot b_d$  the effect of a  $b_d$  variation is small.

In practice  $b_d > 1$  (see table 5.2.1), so that the noise integration effect will be small.

**5.2.1.8.2 Comparison of different receptors.** For convenience we denote the parameter values of the second image receptor by an accent.

### Contrast

Three effects must be taken into account, i.e. (i) the effect of the receptor input field size on the scattered radiation intensity (sections 4.1.4 and 5.2.5), (ii) the contrast rendition (sections 4.2.3 and 5.2.4), and (iii) the low-frequency drop.

### Noiseless systems

Only the additional effect of the sensitivity and the magnification need be taken into account. The ultimate effect on the threshold contrast is approximated by the sum of the percentage changes of  $C_T^{-1}$  as caused by the different image unsharpness, the different focal spot and the size effect.

The starting point is the original combination of  $b_x$  and  $b_d$ . The influence of the image receptor unsharpness change is found by means of fig. 5.2.13a, and the application of a shift from the  $b_d$  to the  $b_d'$  value. The influence of the shadow image MTF variation is found with fig. 5.2.10. The new value of  $b_x$ ,  $b_x'$ , is larger by a factor

$$\left( \frac{s'}{s} \right)^p \quad (5.2.28)$$

where  $s$  denotes the sensitivity of the receptor in terms of the inverse of the required milliamperere-second product per image. The value of  $p$  is equal to  $2/3$  for stationary objects, prescribed exposure time (eq. 3.3.5), and equal to  $2/5$  for

moving objects (eq. 3.2.31). In other words either the minimum permissible focus size or the optimum size is chosen. In the case of stationary objects and a fixed focus size,  $p$  equals zero. The influence of a different image receptor magnification is taken into account by applying fig. 5.2.11.

#### Dynamic noise background

The unsharpness effect on the noise should also be taken into account, so instead of fig. 5.2.11, fig. 5.2.12 is used to investigate the influence of the image receptor magnification. In addition, the influence of the noise intensity must be investigated.

The threshold contrast is inversely proportional to the square root of the minimum quantum density in the chain. In practical systems, the absorption of the X-ray quanta governs the minimum density. Therefore the threshold contrast is, in addition, proportional to  $\sqrt{s/\sigma}$ , where  $\sigma$  denotes the quantum absorption efficiency of the receptor.

#### 5.2.1.9 Advantages of varying the viewing conditions

As discussed, different magnification factors must be taken into account, i.e. the geometric, image receptor, optical and the angular magnification factors. The first one and the latter two can relatively easily be varied. The application of geometric magnification can reduce the threshold contrast of disks and bars when the positive effect on their size outweighs the negative effect of the increased unsharpness in the image receptor plane. The object resolution, i.e. the intrinsic information available, may however be decreased. In this situation, variation of viewing conditions is preferred, because

- (i) the X-ray dose to the patient need not be higher;
- (ii) the X-ray system can be simple;
- (iii) the information retrieval is more flexible. The demands for the visualization of edges, bars and disks are conflicting; optical magnification can be adapted to each situation;
- (iv) the object resolution does not deteriorate.

If the  $\eta_{X,st}$  or  $\eta_{X,m}$  values are so large as to indicate an increase of the object resolution with geometric magnification, then this is the obvious way (apart from the dose to the patient).

#### 5.2.2 Application to stationary object imaging

The coupling of the visual system with the X-ray system will be carried out for stationary object imaging. Starting points are the practical viewing distance of 500 mm and no optical magnification. The  $b_X$  and  $\eta_{X,st}$  data have been analysed in sec. 5.1.1. In addition the  $b_d$  values for the universal screens/film system (11.5),

for film proper (126), for 9" image intensifier fluorography (13.5) and 6" image intensifier fluoroscopy (7.0;  $vd = 2000$  mm) are needed. They are borrowed from table 5.2.1.

The role of the magnification is investigated in sec. 5.2.2.1. The value of  $b_d \cdot b_x$  will be studied to determine the influence of the image receptor unsharpness (sec. 5.2.2.2). The influence of the focal spot is investigated (sec. 5.2.2.3) by means of the  $b_x$  and  $b_s$  values. Further, focal-spot sizes out of the range 0.15, 0.30, 0.60, 1.2 and 1.5 mm will be chosen on the basis of their influence on the threshold contrast. The influence of the focal spot-to-image receptor distance is analysed in sec. 5.2.3.4.

The role of the geometric magnification is analysed for the conditions of sec. 5.1, i.e. with or without a grid. The small magnification/grid combination vs. considerable magnification/no grid is analysed in sec. 5.2.5.

### 5.2.2.1 Magnification

#### Geometric magnification

The sole determinant is the  $\eta_{s,st}$  value. Typical values are given in fig. 5.2.14 for all the techniques concerned. They are generally larger than the critical value of 0.7, and often even larger than 0.9. This means that (i) the influence on the edge imaging is small (fig. 5.2.5), and (ii) the bar and disk imaging (fig. 5.2.7a, fig. 5.2.8) is favoured by geometric magnification.

#### Optical magnification

The preceding results can be understood by bearing in mind that apparently the X-ray system unsharpness is relatively small. This implies that optical magnification will also be useful. Indeed (fig. 5.2.11) the  $b_d$  values are large, and the  $b_x$  values (fig. 5.1.2) are generally much larger than unity. Consequently a magnification of up to 5 times is useful for radiography with screens or for fluorography. For radiography without screens even larger magnification factors will be useful.

In a few techniques the  $b_x$  value is of the order of unity (89, 39, 90, 40, 41, 61 – 65, 79, 81 – 84, 26, 27, mammography), so smaller factors are recommended. In technique 41, for instance,  $b_x$  equals 0.5 and  $b_d$  equals 11.5. Therefore the optimum magnification factor for disks is 2, whereas the initial viewing conditions are near the optimum for bars.

In fluoroscopy dynamic noise is dominant, so (fig. 5.2.12) optical magnification is only useful for disks. As  $b_x$  is about 2, and  $b_d$  equals 7, a reduction of the  $b_d$  value by a factor of about 3 is useful. This can be obtained by placing the monitor at about 600 mm instead of at 2000 mm.

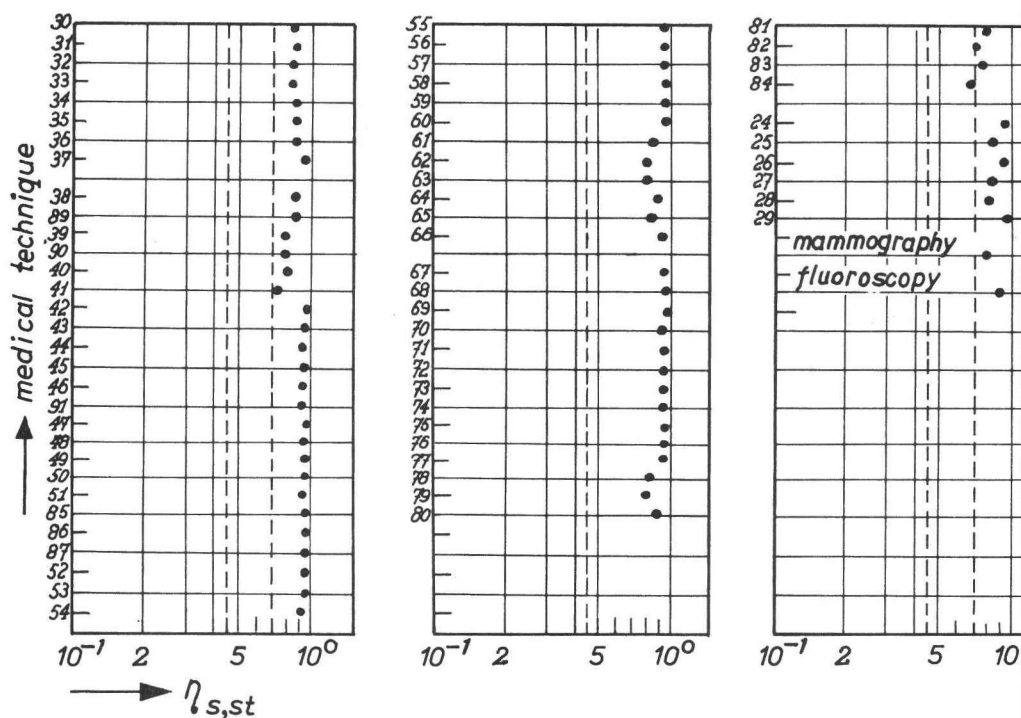


Fig. 5.2.14.

The  $\eta_{s,st}$  value for stationary object imaging.

### Conclusion

As the object resolution is generally smaller if geometric magnification is applied (sec. 5.1.1.2), optical magnification is preferred. The exceptions are techniques 85/86, 69 and image intensifier imaging. Further, a variation of the viewing conditions cannot easily be performed in fluoroscopy. Therefore a variable geometric magnification and/or image receptor magnification might nevertheless be useful.

#### 5.2.2.2 Image receptor

Since the  $b_x \cdot b_d$  values are generally larger than 5, the upper curves of fig. 5.2.13a and 5.2.13b apply. Further, as the  $b_d$  values without optical magnification are 7 or larger, it can be stated that the influence of the image receptor unsharpness will be small. If optical magnification is applied (say 5 times), then the MTF of the image receptor and the visual system are of the same order of magnitude (except for non-screen film) and so an unsharpness change will have some influence. This holds also for fluoroscopy of bars and disks, i.e. for objects in dominant dynamic noise.

### 5.2.2.3 Focal spot and focal-spot intensity distribution

As the value of  $b_d$  is 7 or larger, the upper curves of fig. 5.2.10 apply. The influence of the focal-spot choice is small unless  $b_x$  is small. Therefore this tendency is more pronounced if (i) geometric magnification is applied (techniques 26 and 27), (ii) optical magnification is applied, (iii) the focal-spot MTF tends to dominate (techniques 63, 78, 79, 90, 41, 81 – 84). Generally, however, the value of  $b_x$  (fig. 5.1.2) is much larger than unity, so the influence is small.

The influence of the choice of focal spot in a critical situation is supported by the results in table 5.2.3, which gives the  $\nu_{s,z=0.25}$  value – the measure of the visual resolution – for techniques 24 and 26. Cerebral angiography is analysed here for four combinations of geometric magnification (1.1 and 2 times) and optical magnification (1 and 5 times). The  $\nu_{s,z=0.25}$  value is calculated for three X-ray tube loadabilities, i.e. 25, 50 and 100 kW. The corresponding focal-spot sizes are 0.6, 1.0, and 1.5 mm nominal.

The spatial frequencies are normalized to the 50 kW situation.

TABLE 5.2.3 Visual resolution of cerebral angiography

P [kW]	$\nu_{s,z=0.25}$ (normalized)			
	techn. 24; $M_g = 1.1$		techn. 26; $M_g = 2$	
	$M_o = 1$	$M_o = 5$	$M_o = 1$	$M_o = 5$
25	1.00	1.08	1.00	1.33
50	1.00	1.00	1.00	1.00
100	0.99	0.85	0.98	0.49

As can be seen, the focal spot influence is larger for larger geometric and optical magnifications. This corresponds to the  $b_x$  and  $b_d$  values calculated for the 0.6 mm focus. For  $M_g = 1.1$ ,  $b_x$  equals 6, whereas for  $M_g = 2$  it equals 0.6. The  $b_d$  value (table 5.2.1) equals 11.5 for  $M_o = 1$ , and 2.3 for  $M_o = 5$ . The results in table 5.2.3 were calculated with a computer program. They can also be found approximately by means of fig. 5.2.10.

As regards the focal-spot intensity distribution, it was shown in sec. 3.4.2 that the  $b_x$  value is of importance as far as the object resolution is concerned. For the visual resolution the  $b_s$  value is crucial. Accordingly, if  $b_s$  is larger than unity, then the influence of the intensity distribution is small. The  $b_s$  values have been calculated and are given for the optimum focal-spot size in fig. 5.2.15. As the  $b_s$  value is always larger than 6, the influence of the distribution of the focal spot will be negligible, even if a larger than optimum spot were chosen.

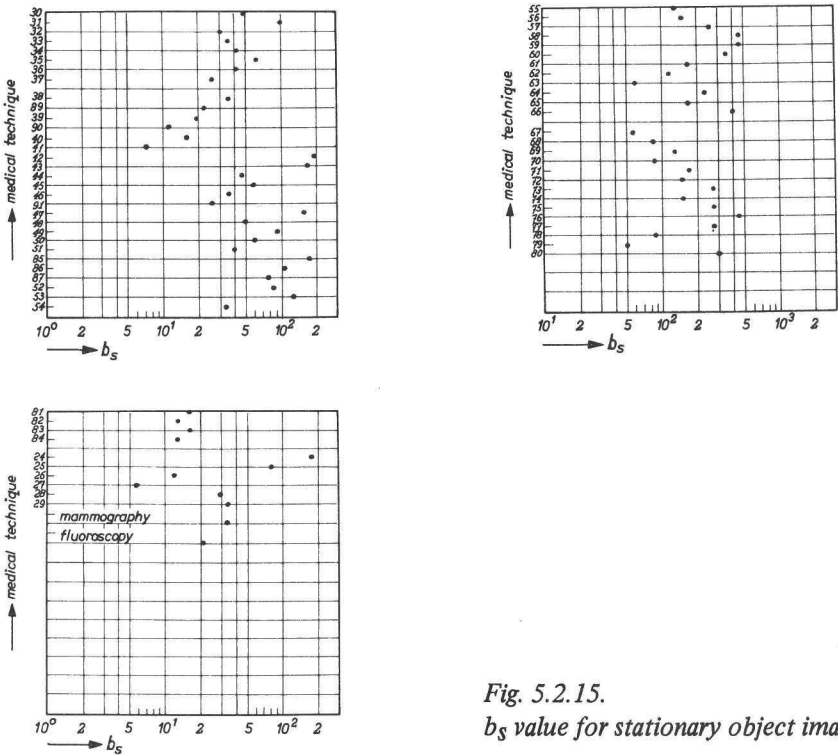


Fig. 5.2.15.  
 $b_s$  value for stationary object imaging

#### 5.2.2.4 Focal spot-to-image receptor distance

In sec. 3.3.3 it is argued that a smaller value favours the object resolution. In sec. 5.2.1.5 it is shown that the best visual resolution of edges is obtained if  $fr$  equals 4 times the  $or$  value. If bars and disks are imaged, then the size effects caused by the geometric magnification should also be taken into account. The optimum  $fr$  will thus be smaller than the optimum for edge imaging. In practice, it holds that  $fr > 4 \cdot or$ , so the resolution of the X-ray systems can be improved by choosing smaller distances, and by choosing the appropriate loadabilities. As far as edges are concerned, the influence of  $fr$  on the visual resolution is generally small, as (i) the focal-spot MTF changes in inverse proportion to the cube root of  $fr$ , and (ii) the influence of the focal-spot MTF as such is small. The ranges of  $fr$  for which the edge threshold contrast varies only a few percent are given in table 5.2.4.

A smaller  $fr$  distance is more important for the imaging of disks and bars, because of the effect of geometric magnification on their sizes. As regards the technical consequences, a smaller loadability of the X-ray tube and generator can be afforded, and therefore it is advisable to choose  $fr$  not larger than necessary.

We conclude that for a general-purpose X-ray system, the smallest  $fr$  distance can be



**TABLE 5.2.4: Range of fr-distances for small variations in the visual resolution of edges**

technique	range [mm]
skull	400–1000
trunk	600/800–1000
upper extremities	200–400/600
lower extremities	400–1000
kidney/gall-bladder	400–1000
angiography (no geometric magnification)	400–1000

600 mm as far as the edge visual resolution is concerned. This distance is already the smallest possible, because of the inevitable matter in the X-ray beam (beam-limiter, patient, table-top etc.). For dedicated systems the distance could be smaller, e.g. for the Craniodiagnost 400 mm would apply. If only upper extremities are to be radiographed, 200 mm would do. Sharper images are obtained, then, with a double focus X-ray tube of say 0.25 kW/1 kW.

### 5.2.2.5 Conclusion

#### X-ray tube/generator

We have found (sec. 5.1.1.2) that a three-focus tube can cope with all demands in the imaging of stationary objects. The same tube can also be used for fluoroscopy. If the X-ray generator could also be suited for a three-focus tube, then such a tube/generator combination could generally be applied. As regards the loadabilities, a 10 kW/ 25 kW/80 kW X-ray tube suffices for a focus-to-image receptor distance of 1000 mm. If a favourably smaller distance can be chosen, smaller loadabilities apply. If, for instance, the distance is reduced to 800 mm, a 6 kW/15 kW/50 kW tube would do. Dedicated systems could be made with high resolution and very small loadabilities if the focal spot-to-image receptor distance could be further reduced. If, for example, only upper extremities are to be radiographed, a distance of 200 mm is possible. The loadability of the tube is then about 0.25 kW/1 kW.

The focal-spot intensity distribution influence is negligible.

#### Patient support

A distance smaller than 1000 mm between the focus and image receptor favours both the object and the visual resolution (sec. 5.2.2.4) and implies smaller loadabilities.

Geometric magnification is not recommended, unless image intensifiers are used.

### Image receptor

It will be worth-while using sharper screens/film combinations. The present rare-earth technology makes such an improvement possible without lowering the sensitivity, so that the patient dose need not be increased. For a discussion on the concomitant noise and contrast conditions, see sec. 5.2.3.4.

### Viewing conditions

Up to 10 times magnification can be an improvement for a viewing distance of 500 mm. We have found optimum magnifications in the range of 2 to 10, so a zoom system is worth investigating.

If such magnification is applied, then the choice of the focal-spot size and of the image receptor becomes important.

## 5.2.3 *Application to moving object imaging*

### 5.2.3.1 Introduction

The complete range of object resolution situations has been investigated in sec. 5.1.2. A complete analysis for the visual resolution would be very time-consuming, and is therefore not provided. The trends can nevertheless be analysed by the following investigation of stomach and colon radiography, as performed with the Diagnost 90 universal stand. All practical image receptors are used, i.e. the universal and rare-earth screens, and a 5" and 9" image intensifier in combination with 70 mm film. The range of  $\eta_{x,m}$  values encompasses practical values as well. The rare-earth screens are also studied because they offer greater sensitivity (factor of 4) for the same intrinsic resolution. For moving objects such highly sensitive screens might be especially useful. For the same reason the loadability of the X-ray tube is of interest. Consequently, a 25, 50, 100 or 150 kW loadability of a standard tube is chosen. Further, two other types of tube may be used. One is the standard tube with the smallest anode angle adapted to the image-receptor size. A generally applicable value would be  $13.5^\circ$ . For the  $12^\circ$  anode angle the fr distance must be chosen larger for some film sizes. (The useful aperture of the X-ray tube is limited by the self-absorption by the anode. In practice, the minimum anode angle must be one degree larger than corresponds to the image-receptor size. The smaller the angle, the better the performance of the X-ray tube (eq. 3.2.7)). The other is a tube with the standard anode angle of  $12^\circ$ , but employing another technology. This so-called ceramic tube has a short-time loadability which is 1.5 times larger. Thus  $P = 150$  kW instead of 100 kW corresponds to a 1.5 mm nominal focal-spot size.

The  $\nu_{s,z=0.25}$  values were calculated for the relevant situations. The fr distance is 1000 mm (in sec. 5.1.2 a distance of 900 mm is used, but the effect of this difference is small), the or value is 150 mm, the viewing distance is 500 mm, and 1 or 5 times optical magnification can be used.

The medical techniques are summarized in table 5.2.5. The data are taken from tables 5.5.1 and 5.1.14, except the high-voltage  $Q_p$  value for colon radiography. Although this technique does not figure in the exposure table, the  $Q_p$  value can be deduced to be about one quarter of the low voltage value, as follows. According to the relevant p-factor (fig. 4.2.9), the low voltage  $Q_p$  value should be divided by 3, whereas for stomach radiography (a comparable situation) a reduction factor of 6 to 10 must be applied (techniques 1 and 2 in table 5.1.14).

**TABLE 5.2.5: Medical technique data for moving objects**

no.	description	image receptor	$U_p$ [kV]	$Q_p$ [mAs]	$f_{rp}$ [mm]	$v$ [mm/s]
1	stomach, low $U_p$	5" I.I./70 mm	80– 85	6.5– 13	700– 800	5–35
2a	stomach, high $U_p$	universal screens	125– 150	1.5– 5	700– 800	5–35
2b		rare-earth screens	125– 150	0.38– 1.2	700– 800	5–35
3	colon, low $U_p$	9" I.I./70 mm	85– 100	2– 11	700– 900	1–10
18a	colon, high $U_p$	universal screens	125	4– 20	700– 900	1–10
18b		rare-earth screens	125	1– 5	700– 900	1–10

The optimum focal-spot size, the corresponding loadability and the exposure time are given in table 5.2.6. The minimum and maximum focal-spot sizes are entered corresponding to the smallest and the largest  $c_{a,m}$  values.

**TABLE 5.2.6 Optimum exposure conditions for moving object imaging**

med. techn.	ca,m	X-ray tube								
		$\alpha = 13.5^\circ$			ceramic tube			standard		
		f <sub>opt</sub> [mm]	P [kW]	t [ms]	f <sub>opt</sub> [mm]	P [kW]	t [ms]	f <sub>opt</sub> [mm]	P [kW]	t [ms]
1	small	0.77	33	35	0.62	40	28	0.73	34	33
	large	2.20	160	14	1.80	200	11	2.10	166	13
2a	small	0.54	19	24	0.44	24	20	0.50	20	23
	large	1.80	117	11	1.40	135	9	1.70	121	11
2b	small	0.30	8	14	0.25	10	11	0.29	8	13
	large	1.00	48	6	0.82	61	5	0.96	51	6
3	small	0.25	6	57	0.20	7	46	0.24	6	54
	large	1.10	56	24	0.88	67	20	1.00	57	23
18a	small	0.32	9	73	0.26	11	59	0.31	9	69
	large	1.40	80	31	1.10	94	25	1.30	81	30
18b	small	0.19	4	42	0.15	5	34	0.18	4	40
	large	0.79	34	18	0.64	42	14	0.76	36	17

Up to 200 kW is required. The exposure time is generally not shorter than 10 ms. The optimum loadabilities are larger for the ceramic tube and smaller for the larger anode angle, by reason of their corresponding larger or smaller specific loadability.

### 5.2.3.2 Characteristic parameters

In the following the consequences of a choice of different X-ray tubes are analysed for the high ca,m value only, because the results for the low ca,m value hardly depend on this choice. The characteristic parameters for the 100 kW standard tube situation are entered in table 5.2.7. By means of these numbers, the influence of different parameter sets can be understood.

**TABLE 5.2.7: Characteristic parameters for moving object imaging with the 100 kW standard X-ray tube**

med. techn.	$M_O$	object resolution			visual resolution		
		$b_a$	$b_x$	$\eta_{x,m}$	$b_d$	$b_x \cdot b_d$	$\eta_{s,m}$
1	1	0.43	0.82	0.20	8.5	6.9	0.80
	5				1.7	1.4	0.50
2a	1	0.74	0.51	0.08	11.5	5.8	0.75
	5				2.3	1.2	0.33
2b	1	3.00	0.80	0.17	11.5	9.2	0.85
	5				2.3	1.8	0.50
3	1	2.80	2.20	0.41	13.5	30.0	0.95
	5				2.7	6.0	0.80
18a	1	1.40	0.70	0.12	11.5	8.0	0.80
	5				2.3	1.6	0.42
18b	1	5.50	0.82	0.22	11.5	9.4	0.90
	5				2.3	1.9	0.60

### 5.2.3.3 Choice of the X-ray tube

The normalized  $\nu_{s,z=0.25}$  values are given in table 5.2.8. The normalization is carried out in relation to the 100 kW standard tube situation. The 25, 50 and 100 kW loadabilities refer to different classes of X-ray systems. For the other tube types, only the 100 kW situation is considered.

**TABLE 5.2.8: Visual resolution ( $\nu_{s,z}=0.25$ ) for moving object imaging, relative to the 100 kW standard X-ray tube situation**

med. techn.	$M_0$	X-ray tube					
		$\alpha = 13.5^\circ$	ceramic	standard tube			
		100 kW			25 kW	50 kW	150 kW
1	1	1.00	1.00	1.00	0.79	0.93	1.01
	5	0.99	1.01	1.00	0.44	0.69	1.08
2a	1	0.99	1.01	1.00	0.76	0.92	1.00
	5	0.98	1.07	1.00	0.43	0.69	1.03
2b	1	1.00	1.00	1.00	0.99	1.00	1.01
	5	0.98	1.06	1.00	0.91	1.04	1.00
3	1	1.00	1.00	1.00	1.00	1.00	1.00
	5	0.99	1.01	1.00	0.98	1.00	1.02
18a	1	1.00	1.01	1.00	0.92	0.96	0.99
	5	0.97	1.06	1.00	0.64	0.89	0.94
18b	1	1.00	1.01	1.00	1.01	1.01	0.99
	5	0.98	1.07	1.00	1.06	1.09	0.91

#### Unaided eye ( $M_0 = 1$ )

The ceramic tube gives slightly better results, the larger anode-angle tube is slightly worse. A loadability of 100 kW is definitely needed for low-voltage image intensifier and universal screens imaging (1, 2a, 18a). This may explain why the old D100 system (fr is also 1000 mm), provided with a 50 kW tube, sometimes gave unsatisfactory results. If rare-earth screens were used, 50 kW loadability would also do.

#### Aided eye ( $M_0 = 5$ )

Differences in  $\nu_{s,z}=0.25$  are more prominent. A 100 kW loadability is sometimes needed (18a) but 50 kW (2b, 3, 18b) or 25 kW (3, 18b) would also do. A 150 kW tube may be useful (1).

The use of a ceramic tube will give perceptibly sharper results, whereas the influence of the slightly enlarged anode angle will hardly be perceived. The 2% contrast gradient decrease is adopted as the criterion — see sec. 2.4.4.3.

A compromise on the choice of X-ray tube would be a two-focus type, either

100 kW/35 kW or 100 kW/50 kW. The 150 kW focus is omitted because it seldom gives better results. The smaller loadability is a compromise for both types of screens. The ceramic tube type is recommended, because it may lead to perceptible gains in sharpness. The anode angle of  $13.5^\circ$  may be used.

An explanation of these findings can be given on the basis of fig. 5.2.10 and the characteristic numbers in table 5.2.7. The influence of the loadability choice is potentially large if the movement MTF is important, i.e. if  $b_a$  and  $b_x$  are small (techniques 1, 2a, 18a). If further the visual system MTF is not too bad, i.e. if  $b_d$  is about unity, then the visual resolution will indeed be influenced ( $M_O = 5$ ). The inherent influence of another type of tube via the corresponding changes in the  $c_{a,m}$  value is much smaller because only one factor (the focus MTF) is changed to a small extent.

#### 5.2.3.4 Magnification

##### Geometric magnification

The  $\eta_{x,m}$  value (table 5.2.7) is so small (fig. 3.2.29) that it prevents geometric magnification from being useful as far as the object resolution is concerned. It should therefore not be used, although the visual resolution of bars would be better for the unaided eye situation ( $\eta_{s,m} \geq 0.75$ ; table 5.2.7).

##### Optical magnification

The unaided eye situation is not optimal (table 5.2.7, fig. 5.2.11) as  $b_d$  is about 10 and  $b_x$  is between 0.5 and 2.2. An optical magnification of about 2 to 5 would therefore be useful for the imaging of bars. For edges no magnification should be applied.

#### 5.2.3.5 Image receptor

Generally, the influence of an intrinsic resolution variation is small because (table 5.2.7, fig. 5.2.13a) either the visual system MTF dominates ( $b_d$  is large for  $M_O=1$ ) or the other MTFs also play a role. This latter situation occurs if optical magnification is applied:  $b_d$  is smaller, but  $b_d \cdot b_x$  is also about 1 to 2. The very sensitive 9" I.I. colon fluorography technique (technique 3) is an exception in this respect. If optical magnification is applied, then the visual system MTF is not very dominant ( $b_d = 2.7$ ) and only the image receptor MTF counts ( $b_x = 2.2$ ). In this situation a sharper image intensifier would be of value. To this end the sensitivity may be smaller because the movement MTF is not dominant ( $b_a = 2.8$ ).

As regards the effects of different sensitivities, interesting conclusions can be drawn for the rare-earth screens. For the calculations, the MTF of the rare-earth screens was assumed to be the same as for the universal screens. Nevertheless a better visual resolution can be expected in terms of  $\nu_{s,z}=0.25$ , because their sensitivity is

assumed to be four times higher. For comparison the  $\nu_{s,z=0.25}$  values are given for the two optimum combinations of universal screens/100 kW tube and rare-earth screens/50 kW tube. The improvement is evident if optical magnification is applied.

**TABLE 5.2.9: Relative visual resolution  $\nu_{s,z=0.25}$  for universal and rare-earth intensifying screens**

med. techn.	$M_O = 1$		$M_O = 5$	
	universal, P = 100 kW	rare-earth, P = 50 kW	universal, P = 100 kW	rare-earth, P = 50 kW
8	1.00	1.03	1.00	1.26
18	1.00	1.02	1.00	1.15

The improvement is relatively small all the same, because other MTFs also play their role. If only the shadow image MTF were of importance, then the spatial frequency would be improved by a factor of 1.74 ( $=4^{2/5}$ , eq. 3.2.30).

To draw a conclusion about any improvement of the final image, the influence of the noise and of the contrast rendition must also be taken into account. As to the noise, its masking effect need not be higher because the improvement of the sensitivity is partially obtained by an increase of the X-ray absorption. Wagner and Weaver (1976) reported on a noise difference which 'is subtle and is within or near the limits of the reproducibility of the equipment' for a sensitivity increase of 2. But the situation is not clear, as can already be inferred from the large number of parameters and phenomena mentioned by Stevels (1975). As to the contrast rendition, we have measured (sec. 4.2, fig. 4.2.5) an 8% smaller iodine (or barium) contrast for rare-earth screens. This indicates that in these applications

- for  $M_O = 1$ , i.e. for the optimum imaging of edges (see sec. 5.2.3.4), the use of the BaFC1:Eu<sup>2+</sup> screens is not recommended, whereas
- for  $M_O = 5$ , i.e. for the optimum imaging of bars (sec. 5.2.3.4), the rare-earth screens will be of advantage.

### 5.2.3.6 Conclusion

#### X-ray tube

The visual consequences for a few representative techniques have been analysed. The X-ray tube proposed in this section (100/35 kW or 100/50 kW) on the basis of the visual resolution fits reasonably well the recommendations on the focal-spot choice in sec. 5.1.2.2.

Ceramic technology will have its advantages. The influence of the anode angle is small.

The proposed loadabilities can be chosen smaller if a smaller focal spot-to-image receptor distance is chosen. This favours the object resolution and also the visual



resolution. The same reasoning holds as for stationary object imaging (sec. 5.2.2.4; this result is confirmed by the remark on the imaging of bars in sec. 5.2.3.4). The smallest feasible distance is about 900 mm, which is the optimum value for edge imaging (sec. 5.2.1.5.3). The influence of the  $f_r$  value on the visual resolution for edges is small, provided that the corresponding optimum loadabilities are chosen.

#### Focal-spot intensity distribution

Its influence can quickly be assessed by means of the relevant  $\eta_{eq}$  value, i.e. if the visual system MTF is also taken into account. The correlation between  $\eta_{x,m}$  or  $\eta_{s,m}$  and  $\eta_{eq}$  is given in fig. 3.4.10.

For the unaided eye situation,  $\eta_{s,m}$  (table 5.2.7) is 0.75 or larger, so  $\eta_{eq}$  is 0.5 or larger. As  $\eta$  equals 0.15, the influence of the intensity distribution will be negligible. If  $M_O = 5$ , then  $\eta_{s,m}$  ranges from 0.33 (technique 2a) to 0.8 (technique 3). Therefore  $\eta_{eq}$  is between about 0.17 and 0.6. Consequently, a Gaussian-shaped intensity distribution will have advantages (see sec. 3.4.1.3). A falling intensity distribution is not needed for the techniques considered.

#### Image receptor

Unlike stationary object imaging, the shadow image MTF is important, so that more sensitive intensifying screens will be of advantage. Rare-earth technology can be used for this purpose.

The reverse is true for the highly sensitive 9" image intensifier: a better intrinsic resolution will be of value.

#### Magnification

Geometric magnification is not recommended, except for many (especially 9") image intensifier techniques (see sec. 5.1.2.1). Optical magnification in the range of 2 to 5 can be useful.

### 5.2.4 *Influence of the X-ray beam quality*

#### 5.2.4.1 Introduction

The choice of the tube high voltage has an influence on the contrast of the object, the noise and the dose to the patient. The influence on the dose will be studied in sec. 5.2.6.

The contrast is smaller the higher the tube high voltage because the absorption contrast is smaller (fig. 4.2.5) and the scattered radiation intensity is greater (fig. 4.1.8). The scattered radiation will not be taken into account here because (i) the scattered radiation intensity as such is generally small since either an anti-scatter grid or geometric magnification will be applied (sec. 5.2.5) and (ii) the relative influence, if any, of the tube high voltage is small (fig. 4.1.8).

As regards the influence on the noise, it is generally argued that the noise will be more prominent at higher voltages because fewer photons are needed to produce a certain film density. Barnes (1976) however observed both psychophysically and physically very little voltage dependence for commonly used film/screens combinations. In going from  $U = 60$  kV to  $U = 120$  kV, typically only a 7 percent increase in the standard deviation of the density fluctuations was measured. The image receptors were a medium-speed and a sensitive combination,  $\text{CaWO}_4$  screens (duPont Cronex4/duPont Par Speed and Kodak RP/duPont Hi Plus). The X-ray generator was of the 6-pulse type with smoothing capacitors. Further, an extra 19 mm aluminium filter was applied to simulate the patient, so the X-ray beam quality resembled ours. The film was scanned with a 5' circular aperture. Since the corresponding spatial resolution was comparable with that of the eye-optics (see sec. 2.6.2.1, 'object variation'), a visually relevant noise was indeed measured. The voltage influence was larger for a rare-earth screen (Kodak RPR/Radelin Rarex B Mid Speed-Yttrium oxysulphide), i.e. 20% increase in going from 60 to 80 kV. But no influence could be measured for the shift from 80 to 120 kV. We conclude, therefore, that the influence on the noise is negligible for practical screens/film combinations. This is true in any case if the masking effect of the noise as such is small, as may be the case for less sensitive systems and for larger viewing distances (see sec. 2.5.2.1, table 2.5.3). The same independence of the noise on X-ray beam quality can be envisaged for 70 mm-fluorography: according to Beekmans (1978) and Rowley (1974) the exposure conditions are such that the quantum noise is effectively absent or is not disturbing. For fluoroscopy, where normally dominant dynamic X-ray noise is encountered, no such conclusions can be drawn. We decided therefore to leave out the investigation of fluoroscopy.

The contrast is smaller the higher the tube high voltage. But the unsharpness will also be smaller because smaller focal spots can be used by virtue of the reduced attenuation of the X-ray beam. Therefore an optimum high voltage exists at which the object or visual resolution is best. As the maximum contrast gradient is proportional to the ultimate contrast as well, the proportionality to  $C_0$  (fig. 2.2.11) must be introduced correspondingly. For the object resolution, then, the product  $\nu_{x,z=0.25} \cdot C_0$  must be maximized. For the visual resolution this scheme must be applied to the product  $(\nu_{s,z=0.25})^p \cdot C_0$ , where  $p$  equals 1 for edges, 2 for bars and 3 for disks.

In principle nomograms can be made for this optimization, because all relations are known. The contrast dependence is given by figures 4.2.6 and 4.2.7. The spatial frequency dependence can be deduced from fig. 5.2.9, which gives the change in  $\nu_{s,z=0.25}$  as a function of the change in  $b_s$ . This graph can also be used for deducing the  $\nu_{x,z=0.25}$  change by applying the  $b_x$  values. The change in the value of  $b_x$  and  $b_s$  corresponds to the change in the  $Q$  value as indicated in figs. 4.2.8 and 4.2.10. If the corresponding optimum focal-spot sizes are chosen, then the  $b_x$  or  $b_s$  value changes by a factor of  $Q^{2/3}$  for stationary objects (eq. 3.3.5) or by  $Q^{2/5}$  for moving objects (eq. 3.2.31). Nomograms are not

available, however, owing to lack of time. Instead we have chosen the pragmatic approach by investigating the influence of a shift from 70 kV to 110 kV. The lower voltage is generally used in iodine contrast radiography. The higher voltage gives favourably small exposure times, and corresponds to less dose to the patient.

For a mean thickness of 150 mm water the contrast is a factor of 1.57 smaller (sec. 4.2). A better  $\nu_{x,z=0.25}$  and  $\nu_{s,z=0.25}$  value will of course be obtained as well, and so it remains to be investigated whether the visibility of objects is improved or not. The decrease of the Q value amounts to a factor of about 6 (figs. 4.2.8 and 4.2.10) for both intensifying screens. The reduction in the  $b_x$  and  $b_s$  values equals 3.30 for stationary objects and 2.05 for moving objects. The change in the relevant spatial frequency depends on the initial value of  $b_x$  or  $b_s$ . The larger this value, the smaller the effect because then the shadow image MTF is less important. If  $b_x$  or  $b_s$  is small ( $< \approx 0.1$ ) then the  $\nu$  value is directly proportional to  $b$ . In this way fig. 5.2.16 is deduced from fig. 5.2.9. The maximum permissible initial  $b_x$  and  $b_s$  values are indicated in the figure for all situations. These values are summarized in table 5.2.10. For example the critical value for the visual resolution of disks is obtained by stating that the change in  $\nu_{s,z=0.25}$  to the power of three must be equal to or larger than the contrast change, i.e. larger than a factor of 1.57.

**TABLE 5.2.10: Maximum permissible initial  $b_x$  or  $b_s$  value for a high voltage shift from 70 kV to 110 kV**

	object resolution; $b_x$	visual resolution; $b_s$		
		edges	bars	disks
stationary objects	1.20	1.20	2.3	3.0
moving objects	0.76	0.76	1.8	

#### 5.2.4.2 Stationary objects

The relevant techniques are kidney and gall-bladder radiography (81 – 84, table 5.1.5) and cerebral and abdominal angiography (24 – 29, table 5.1.6).

As regards the object resolution, the value of  $b_x$  (fig. 5.1.2) is about unity for techniques 81 – 84 and 26, so that the influence of the voltage shift is small. An exception is technique 27, cerebral angiography with geometric magnification and a relatively short exposure time. The  $b_x$  equals 0.4, which means that a higher voltage is of advantage if the corresponding smaller optimum focal spot is chosen as well.

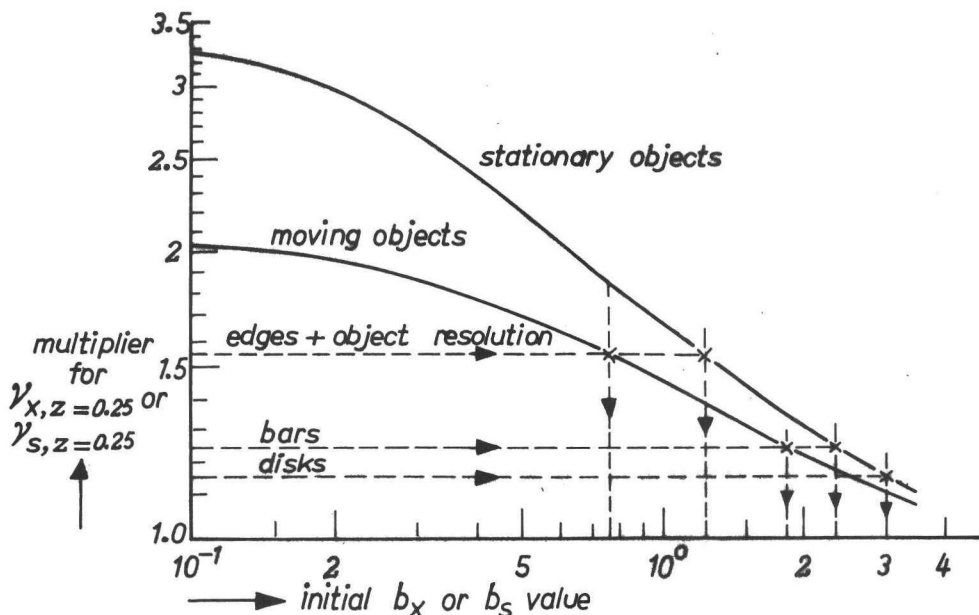


Fig. 5.2.16.

Relevance of high voltage shift from 70 to 110 kV (see further sec. 5.2.4).

For techniques 24 and 25 (cerebral angiography) and 28 and 29 (abdominal angiography with screens or the 9" intensifier) no voltage shift is recommended because  $b_x$  is larger than 2.

As regards the visual resolution, fig. 5.2.15 shows that  $b_s$  is generally larger than 10 for practical viewing conditions, i.e.  $vd = 500$  mm and no optical magnification. Consequently the voltage shift is not recommended. If 5 times optical magnification is applied, then a voltage shift may make sense for technique 27, for which the initial  $b_s$  equals 5.7.

#### 5.2.4.3 Moving objects

The techniques to be considered are given by table 5.1.14, with the exception of lung radiography (9 and 10). The relevant  $b_x$  value can be deduced from fig. 5.1.3 for the object relatively close to the image receptor ( $\eta = 0.17$ , with grid; geometric magnification is not recommended for these techniques). The critical value of  $b_x$  equals 0.76, which corresponds to a value of  $\eta_{x,m}$  equal to 0.12. This critical  $\eta_{x,m}$  value is also indicated in fig. 5.1.3. The conclusions are as follows:

- The change to a higher voltage is of advantage for the whole range of parameter values for stomach radiography (1, low  $U_p$ ; this implies that a shift to higher voltages, i.e. technique 2, indeed makes sense), for bronchography (7), for radiography of the oesophagus (6), for the larynx (8) and for the heart with the AOT (13).

- Only the imaging of the faster moving or the more absorbing objects benefits by the shift to a higher voltage for radiography of the colon (3) and of the gall-bladder (5), and for fluorography of the heart with 70 mm- (11) or cinefluorography (12). It must be mentioned that the advantage for cinefluorography is marginal,  $\eta_{x,m}$  being generally larger than 0.12. (We assume that the contrast rendition of the image intensifier is comparable with that of the screens measured. We may venture this assumption because the materials show more or less the same X-ray attenuation behaviour as a function of the quantum energy. Further, the use of the fairly broad X-ray spectrum will smooth out the difference, if any. An indication of this effect may be the invariance (fig. 4.1.7) of the relative scattered radiation intensity to the choice of the image receptor.)

As regards the visual resolution, a rough estimate of the  $b_s$  value for practical viewing conditions ( $vd = 500$  mm and  $M_O = 1$ ) can be made by bearing in mind that  $b_d$  is about 10 (table 5.2.1), and  $b_x$  is about unity. The  $b_s$  value is thus approximated by the  $b_d$  value. Consequently, a voltage shift is not recommended. If 5 times optical magnification is applied, then  $b_s$  is about 2, and a shift to higher voltages may make sense for the imaging of fast moving bars.

#### 5.2.4.4 Conclusion

A shift to higher voltages (70  $\rightarrow$  110 kV) is of potential interest if the object resolution improves. More information is then potentially available. This is the case for the imaging of many (faster) moving objects. Except for cerebral angiography with geometric magnification, it is not the case for stationary objects.

As regards the visual resolution, the beneficial effects of a voltage shift are absent if the unsharpness effects are small, i.e. if the viewing distance is 500 mm and if no optical magnification is applied. An optical magnification factor of 2 to 5 is of advantage for the imaging of moving bars (sec. 5.2.3.4). If a factor of 5 is applied, then the high voltage shift is of advantage for the faster moving bars.

### 5.2.5 *Influence of the scattered radiation*

#### 5.2.5.1 Introduction

The smaller the scattered radiation intensity, the larger the contrast. Therefore any measure aiming at a reduction of this intensity, i.e. the application of a grid and/or geometric magnification, may benefit the object and the visual resolution. The effects on the sharpness must also be taken into account in this analysis. The concept 'resolution' must consequently be understood as a combination of the contrast  $C_1$  (fig. 2.2.11) and the spatial frequency resolution  $\nu_{x,z=0.25}$  or  $\nu_{s,z=0.25}$ . Two situations will be considered, i.e.

- (i) Small magnification factor, with grid or without grid. The influence of the smaller Q value may outweigh the contrast reduction influence.

- (ii) Small magnification factor/grid vs. considerable geometric magnification/no grid.

The third combination, i.e. application of a grid with or without magnification, has already been discussed in sections 5.2.1 and 5.2.2. There are then hardly any contrast effects. The fourth combination, i.e. small magnification/no grid vs. considerable magnification/grid, does not make sense: the absence of the grid at small magnifications will lead to worse results (sections 5.2.5.2 and 5.2.5.3), whereas for large magnifications the contrast is hardly improved by a grid.

#### Mathematical formulation

The light intensity distribution  $C_l(r)$  (fig. 2.2.11) as seen by the film can be described as regards its contrast by means of the intensities of the scattered and primary radiation,  $I_s'$  and  $I_p$ , and by means of the extra absorption of the object, denoted by  $\Delta I_p$ . Apparently, we can write for  $C_l$  (i.e. the contrast of  $C_l(r)$  without the influence of the unsharpness)

$$C_l = \frac{\Delta I_p}{I_p + I_s'} \quad (5.2.29)$$

If the subscript 1 or 2 denotes the relevant situation, then the contrast ratio is given by

$$\frac{C_{l,1}}{C_{l,2}} = \frac{\Delta I_{p,1}}{I_{p,1} + I_{s',1}} / \frac{\Delta I_{p,2}}{I_{p,2} + I_{s',2}} \quad (5.2.30)$$

which is equal to

$$\frac{C_{l,1}}{C_{l,2}} = \left( \frac{\Delta I_{p,1}}{I_{p,1}} / \frac{\Delta I_{p,2}}{I_{p,2}} \right) \cdot \frac{1 + a_2}{1 + a_1} \quad (5.2.31)$$

The fractional reduction of the primary beam,  $\Delta I_p/I_p$ , will hardly depend on the situations concerned (for instance the presence of a grid hardly influences the contrast, see fig. 4.2.2), so we can write for the contrast ratio

$$\frac{C_{l,1}}{C_{l,2}} \approx \frac{1 + a_2}{1 + a_1} \quad (5.2.32)$$

#### 5.2.5.2 Moving objects

The relevant 'a' and  $C_l$  values depend on the conditions chosen. To be in line with the analysis given in sections 5.1, 5.2.2 and 5.2.3, the minimum  $\eta$  value is 0.17 for a

patient thickness equivalent to 150 mm water. The maximum value is 0.4. The X-ray field area is  $14.3 \times 14.3 \text{ cm}^2$  – this corresponds to a  $24 \times 24 \text{ cm}^2$  film or to 9" image intensifier imaging at the larger  $\eta$  value. A universal grid like the one used in sec. 4.1 can be applied.

The 'a' values are given in table 5.2.11. The fig. 4.1.16 is used for the no-grid situation. The relevant smaller  $\eta$  is then about 0.1 according to the local definition in sec. 4.1: the skin-to-image receptor distance is relevant, which is about 75 mm for the patient thickness concerned, with the object situated in the centre of the patient. The relevant larger  $\eta$  is correspondingly 0.35. In this region the influence of  $\eta$  is small (see fig. 4.1.8). Fig. 4.1.15 is used for the grid situation for a field area of  $\approx 200 \text{ cm}^2$ . This figure is valid for a water thickness of 200 mm, but a correction is obtained by assuming the 'a' value to be proportional to the thickness (see fig. 4.1.16).

**TABLE 5.2.11: Relative scattered radiation intensities for moving object imaging**

	$a = I'_s/I_p$	
	$\eta = 0.17$	$\eta = 0.40$
no grid	1.4	0.55
grid	0.4	0.34

The relative contrasts compared to the grid/ $\eta = 0.17$  situation are given in table 5.2.12. The influence of geometric magnification with a grid is indeed small.

**TABLE 5.2.12: Relative contrast for moving object imaging**

	$C_{l,2}/C_{l,1}$	
	$\eta = 0.17$	$\eta = 0.40$
no grid	0.58	0.90
grid	1.00	0.96

The relative Q values are governed by the Bucky factor of the grid, which was about 4 (measured) for  $\eta = 0.17$ , and by the factor for geometric magnification without a grid (about 2, see fig. 4.1.8). The corresponding relative Q values are given in table 5.2.13. The value for the grid situation with geometric magnification is borrowed

from fig. 4.1.11. In fact, the uncertainty in the relative Q-values is allowed to be considerable because the unsharpness is not strongly influenced by a change in one such factor of the total chain.

**TABLE 5.2.13: Relative Q-values for moving object imaging**

	$Q_2/Q_1$	
	$\eta = 0.17$	$\eta = 0.40$
no grid	0.25	0.50
grid	1.00	1.17

*Influence of the grid, small geometric magnification factor*

As the geometric factors do not change, the analysis of the influence of the use of the grid is equivalent to that for the influence of the tube high voltage (sec. 5.2.4). The corresponding critical  $b_x$  value for the object resolution is about 0.4 for the contrast reduction factor 1.72 and the Q reduction factor of 4. As  $b_x$  is generally larger (fig. 5.1.3), a grid should always be used. The same holds for the visual resolution. The critical  $b_s$  value for edges is likewise very small, whereas the value for bars is equal to 1.35. The practical values of  $b_s$  are always larger, as can be seen from the  $b_d$  values of table 5.2.1.

*Small geometric magnification/grid vs. considerable magnification/no grid*

Since the geometric factors, the required energy per exposure and the contrast change simultaneously, an analysis is rather complex.

**Object resolution**

The change in  $\eta$  from 0.17 to 0.40 in combination with a reduction of the Q value by a factor of 2 indicates a change in the absorption image MTF (eq. 3.2.30) by a factor of 0.80 for the object plane. The image receptor MTF is improved in the same plane by a factor of 1.38 (i.e.  $M_{g,2}/M_{g,1}$ ). The absolute value of  $b_x$  therefore changes by a factor of 0.58. The resulting provisional decrease in the spatial frequency  $\nu_{x,z=0.25}$  can be deduced from fig. 5.2.9 and is given in fig. 5.2.17. The absolute value of the object resolution is then found by bearing in mind that the applied  $b_x$  value is related to the improved image receptor MTF in the object plane. The factor of improvement is 1.38, so that if the  $\nu_{x,z=0.25}$  reduction is smaller than  $1/1.38 = 0.725$ , an actual improvement of the object resolution takes place. We conclude from fig. 5.2.17 that  $b_x$  should then be larger than 1.3. The  $\nu_{x,z=0.25}$  must improve by a factor of 1.11 or larger to outweigh the effect of the decreased



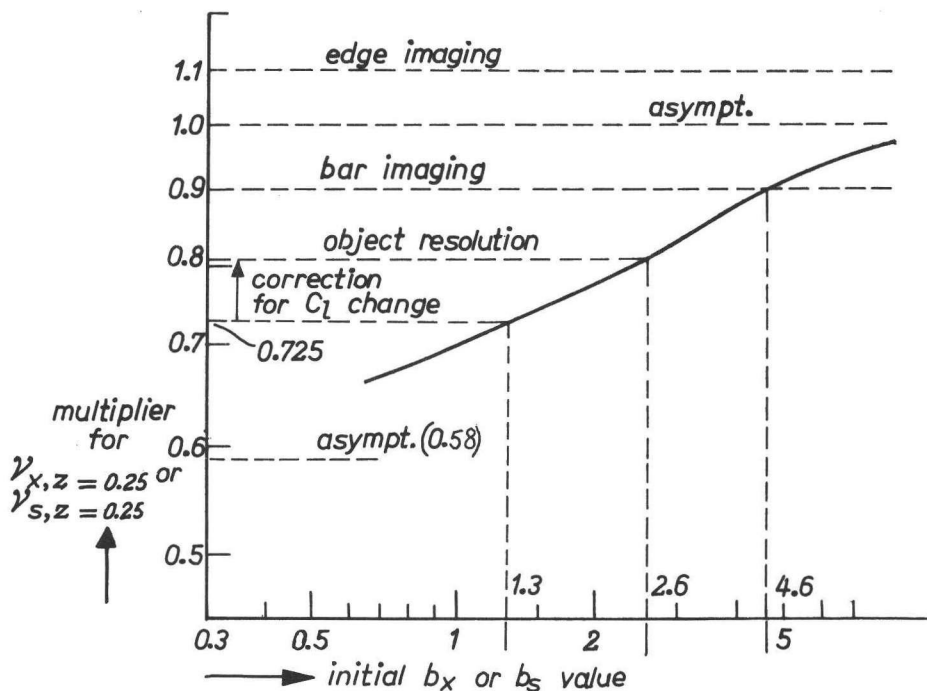


Fig. 5.2.17.

*Relevance of omission of the grid and simultaneous application of geometric magnification, moving objects (see further sec. 5.2.5.2).*

contrast. This correction factor for  $C_l$  change is also indicated in fig. 5.2.17. We therefore conclude that the initial  $b_x$  value should be larger than 2.6 for the proposed change to make sense. The corresponding initial  $\eta_{x,m}$  value is about 0.4. The  $\eta_{x,m}$  values (fig. 5.1.3) for intensifying screens imaging are generally smaller, especially for the high-velocity imaging, so that the proposed change is not recommended. For 9" image intensifier imaging  $\eta_{x,m}$  is generally larger for the low-velocity situation, so that in this case the change is recommended. For the high velocities the change has only a slight influence; small improvements and small deteriorations occur. There is still a general improvement for 5"/6" image intensifier fluorography of relatively slow-moving objects. For the high velocities worse results will be obtained. An exception is the imaging of the heart: the proposed change is never recommended, because  $\eta_{x,m}$  is small.

### Visual resolution

There are three important differences as compared with the object resolution. Firstly, the influence of the unsharpness of the X-ray system is smaller. Secondly the size effect for bar imaging will play a role. Thirdly, as the image receptor input plane is the reference plane, no image receptor MTF correction should be applied.

### Edge imaging

Since the critical  $b_s$  value is equal to the initial critical  $b_x$  value, i.e. 0.58, the drawn curve in fig. 5.2.17 is valid as to the reduction factor of  $\nu_{s,z=0.25}$ . The change of geometry under study leads to a smaller value of  $b_s$ , and therefore to a decrease of the  $\nu_{s,z=0.25}$  value. As the contrast will also be smaller, the proposed change is never recommended.

### Bar imaging

The product of  $(\nu_{s,z=0.25})^2 \cdot M_g \cdot C_1$  is crucial. The factor  $M_g$  governs the size effect.

If the effect of the unsharpness is negligible, i.e. if  $b_s$  is large, then only the product  $M_g \cdot C_1$  counts. As the ratio of the geometric magnification factors equals 1.38 and as the contrast is smaller by only a factor of 1.11, we conclude that the proposed change will be of advantage in this situation. The minimum initial value of  $b_s$  for the proposed change to make sense equals 4.6. The large  $b_d$  values of table 5.2.1 correspond to a large  $b_s$  value as well. This indicates a positive effect of the omission of the grid in combination with geometric magnification if no optical magnification is applied. If  $M_O$  equals 5, then this change is not recommended.

### 5.2.5.3 Stationary objects

In many situations there is less material in the X-ray beam (skull, extremities) than in moving object imaging, so both the influence on the contrast and the Q value per choice of geometric magnification factor and the use of a grid will be smaller. Fortunately the influence on both parameters is of the same sign, so that differences will be smoothed out. Consequently, the data for moving object imaging (table 5.2.12 and 5.2.13) will be used as an indication. We will further consider only those techniques for which a grid is used. The relevant smaller  $\eta$  values are then indeed of the order of magnitude of 0.17. (In the other techniques the scattered radiation intensity is smaller, i.e. in techniques 37, 46, 91, 55 – 66, 70 – 80). We expect the influences of the contrast changes to be more important, as the influence of the shadow image MTF is small (see sec. 5.1.1).

#### *Influence of the grid, small geometric magnification factor*

The same analysis as for moving objects (sec. 5.2.5.2) and for the influence of the tube high voltage (sec. 5.2.4.1) is applied. The relevant  $b_x$  or  $b_s$  change corresponds to the change in the Q value to the power of 2/3 (eq. 3.3.5), i.e.  $b_x$  and  $b_s$  are larger by a factor of 2.52. The corresponding critical  $b_x$  value for the object resolution equals 0.8. As  $b_x$  is generally larger (see fig. 5.1.2), the omission of the grid is not recommended. Technique 41 (sternum lat.) is the only exception. However, geometric magnification is inevitably applied here, so this technique is outside the scope of this section.

As for the visual resolution, the critical  $b_s$  value equals 0.8 for edges, 1.8 for bars and 2.9 for disks. The  $b_s$  values (fig. 5.2.15) are always much larger, so that the presence of the grid is recommended.

*Small geometric magnification/grid vs. considerable magnification/no grid*

The same kind of analysis as for moving objects must be applied. The corresponding graph is given in fig. 5.2.18.

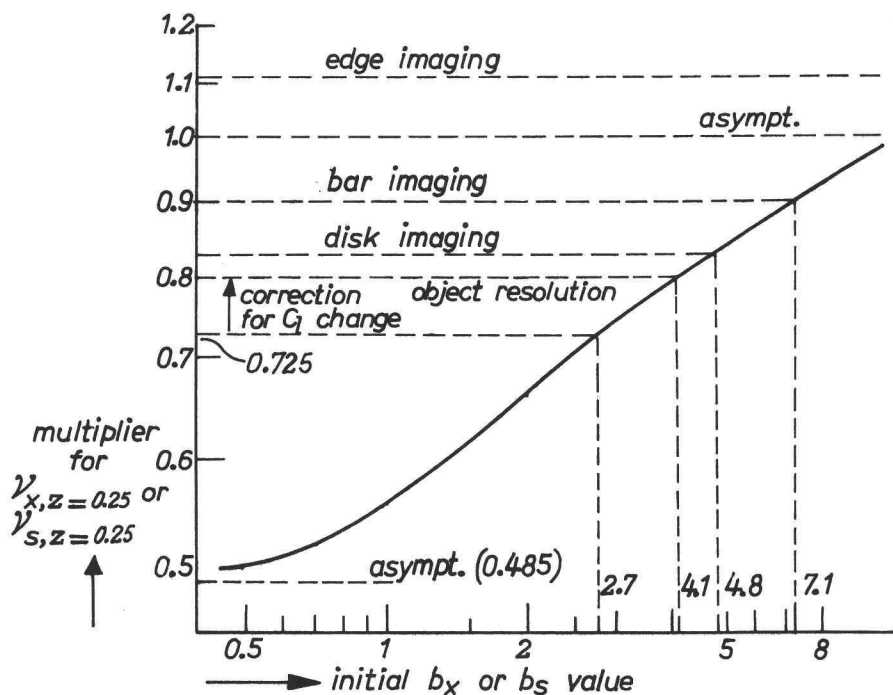


Fig. 5.2.18.

*Relevance of omission of the grid and simultaneous application of geometric magnification, stationary objects (see further sec. 5.2.5.3).*

**Object resolution**

The change from  $\eta = 0.17$  to  $\eta = 0.40$  and the reduction of the  $Q$  value by a factor of 2 imply a change in the absorption image MTF quality (eq. 3.3.5 and 3.2.12) by a factor of 0.67 (i.e. a factor  $2^{2/3} = 1.58$  as to  $Q$ , and  $0.4/0.17 = 2.35$  as to  $\eta$ ). The influence of the geometric magnification on the object resolution is greater than for moving objects because the focus size is not adapted to the object-to-image receptor distance. As the image receptor MTF is improved by a factor of 1.38, the absolute value of  $b_x$  changes by a factor of 0.485. The provisional corresponding decrease in

$\nu_{x,z=0.25}$  is given in fig. 5.2.18. The correction for the improvement in the image receptor MTF by a factor of 1.38 must also be applied, which means that the  $\nu_{x,z=0.25}$  improves if  $b_x > 2.7$ .

If the contrast is also taken into account, then  $b_x$  should be larger than 4.1. This is indeed the case for a limited number of techniques (fig. 5.1.2): 31, 35, 42, 43, 45, 47, 49, 50, 85 – 87, 52, 53, 67, 69, 24, 25. For the other techniques, especially kidney and gall-bladder radiography and fluoroscopy, the proposed change will deteriorate the object resolution.

#### Visual resolution

The same analysis as for moving objects is valid (see fig. 5.2.18). The initial  $b_s$  decreases by a factor equal to 0.485.

#### Edge imaging

The proposed change is never recommended as both the spatial frequency  $\nu_{s,z=0.25}$  and the contrast would be worse.

#### Bar and disk imaging

The initial  $b_s$  value should be larger than 7.1 for bars and larger than 4.8 for disks. This is generally the case (fig. 5.2.15) if no optical magnification is applied, and therefore the proposed change is recommended. If  $M_O$  equals 5, then the  $b_s$  value for a large number of techniques will be too small for this recommendation to be given.

#### 5.2.5.4 Conclusion

A grid is recommended if the object is close to the image receptor. Both the object and the visual resolution would deteriorate if a grid were not used.

Such straightforward recommendations cannot be given if the grid is omitted, provided that geometric magnification is applied additionally. These changes are recommended if the object resolution improves, as more information can then potentially be extracted from the image. This holds for low-velocity object imaging with the 9" and the 5"/6" image intensifiers, and for some stationary objects. For moving object imaging with intensifying screens this is not the case, either for high-velocity objects imaging in general or for heart imaging in particular.

If the object resolution deteriorates, better visual resolution is still possible by virtue of the size effect. But the choice should then be to apply optical magnification, the more so because the visual resolution for edges will always be worse. If an optical magnification of 5 times is applied, the object should indeed be close to the image receptor.

## 5.2.6 *The dose administered to the patient*

### 5.2.6.1 Introduction

In considerations on the dose to the patient an attempt is made to evaluate the risk of radiation exposure in relation to the beneficial effects of the examination, i.e. the chance of and the effect of a correct diagnosis.

According to Oosterkamp (1976), genetic effects in human beings have not been observed, nor do acute somatic effects occur when proper radiological procedures are used. Generally only late somatic effects are therefore taken into account. It has been concluded (Oosterkamp, 1976) that there is generally a considerable benefit surplus, so considerations on the dose are of secondary importance. This may be less true for mass surveys, where many healthy subjects are irradiated.

For the examination of a patient the possibility of a correct diagnosis is of prime importance. Nevertheless, since there is always a risk involved, dose considerations should not be ignored. Consequently three important areas will be considered, i.e. fluoroscopy, the application of geometric magnification and the change to a higher tube voltage. The optimization of the focal-spot size and the intensity distribution need not be investigated, because there are no repercussions on the dose whatever.

As stated, in an examination of a patient the establishment of the diagnosis is of prime importance. Therefore the ICRP 26 recommendations (1977) state 'With certain medical exposures a very much higher level of risk may in fact be justified by the benefit derived . . .'. This agrees well with the remark of Rowley (1974), that the dose per image for cinefluorography ' . . . is close to accepted estimates of the limit below which the information content of the image decreases due to quantum noise'. The same has been measured by Beekmans (1978), who studied 70 mm fluorography. In image intensifier imaging the dose per image can be adjusted within large ranges, to minimize the hindrance of X-ray noise.

In a study of mass surveys (Oosterkamp, 1976), an estimate is given of the ratio between lives saved and lives lost; the ratio is equal to 10 for stomach surveys and 100 – 200 for mass chest surveys.

There is however uncertainty, which is partially caused by the fact that refined statistical methods have to be conceived to track the negative effects of irradiation. (This, incidentally, is in itself an indication of the insignificance of the effects!) There is further the uncertainty as to the dose – risk relationship for small doses and dose rates. In the above-mentioned study by Oosterkamp a linear relationship was applied. It may be, however, (Jacobi, 1976), that the risk is even less than proportional to the dose for the small doses involved, especially if the dose is fractionated.

### 5.2.6.2 Fluoroscopy

For practical exposure rates ( $30 - 120 \mu\text{R/s}$  at the input screen of the image intensifier), our measurements (fig. 2.5.1.2 and 2.5.1.3) showed that the X-ray noise dominates. The threshold contrast is thus inversely proportional to the square of the exposure rate; this is true under the conditions applied, i.e. the tube current was varied for a given tube high voltage. Under these conditions, considerably better images are indeed obtained with a higher exposure rate. Unfortunately, no conclusions can be drawn if the X-ray beam quality (tube high voltage) is changed as well. A lot of information is available (see sec. 5.2.6.4), but time was lacking to measure the effect on the dominant dynamic noise.

Of course, a better image — and hence a higher dose rate — may mean that less time is taken to arrive at a diagnosis, so that after all the dose may be less. One should further define an acceptable image quality, which may restrict the dose to the patient as well. The latter remark is equally valid for sections 5.2.6.3 and 5.2.6.4. Further work should take these aspects into account.

### 5.2.6.3 Geometric magnification

We have chosen to image a given section of the subject irrespective of the degree of geometric magnification. For this purpose the X-ray beam aperture is adjusted correspondingly. The irradiated area of the skin does not change much. It follows then (inverse-square law) that the dose is approximately proportional to  $1/(1-\eta)^2$ . The dose can further potentially be higher due to the loss of scattered radiation, which must be compensated by e.g. an increase of the exposure time. These adverse effects must be compared with the visual resolution, for which the geometric magnification can be of advantage in the observation of bars and disks. In the limit, i.e. for an ideally sharp system, their threshold contrast is inversely proportional to  $1/(1-\eta)$  and  $1/(1-\eta)^2$  respectively.

Two situations will be considered below: a variable focus-to-image receptor distance and a fixed distance.

#### Variation of the focus-to-image receptor distance

A smaller fr distance implies a higher dose, but better images can be obtained. In sections 3.2.3 and 3.3.3 it is argued that the object resolution improves if the corresponding smaller optimum X-ray source is chosen. The visual resolution will often improve as well (sections 5.2.2.4 and 5.2.3.6). This effect is more prominent if the size of the objects plays a role, i.e. in the case of bars and disks. For instance a stationary disk at  $\eta = 0.2$  for  $fr = 1000$  mm would need a 1.8 times smaller threshold absorption contrast if the fr distance were reduced to 500 mm. The dose would be higher by the same factor.

For many stationary objects the initial  $\eta$  value is much smaller, so that there are hardly any effects on the dose nor on the resolution. A favourably smaller X-ray tube loadability can be afforded, however, as has been argued in sec. 5.2.2.5.

#### Variation of the object-to-image receptor distance

This has been studied in sec. 5.2.5. Two comparisons have been made, namely small magnification factor ( $\eta = 0.17$ ) with grid vs. small magnification factor without grid, or vs. a larger magnification ( $\eta = 0.40$ ) without grid. The effective intensity of scattered radiation is involved.

If the object is close to the image receptor (small geometric magnification factor), then the omission of the grid implies a Q-value — hence a dose to the patient — which is four times as small (table 5.2.13). The image would be sharper as well. Nevertheless the detrimental effect on the contrast makes the presence of the grid necessary: the contrast would otherwise almost be halved (table 5.2.12, sections 5.2.5.2 and 5.2.5.3).

As regards the comparison between small magnification/with grid and considerable magnification/no grid (sections 5.2.5.2 and 5.2.5.3), there are hardly any effects on the dose: the proportionality to  $1/(1-\eta)^2$  implies an increase by a factor of 2.1, but the required Q-value (table 5.2.13) will be halved.

#### 5.2.6.4 Beam quality

As in sec. 5.2.4, the analysis will be carried out for a shift of the tube high voltage from 70 to 110 kV. The choice of the fixed additional filter of 2 mm Al corresponds to practical conditions.

For the dose — and also for the object resolution — an interesting multiplicity of effects must be taken into account, viz. (i) the effect on the Q-value per exposure, (ii) the influence on the exposure rate, (iii) the ratio between the volume dose and the skin dose, (iv) the effect on the contrast and (v) the effect on the resolution.

re i : In sec. 4.2.4 it is argued that

$$Q \sim \frac{1}{U^{2.5}} \quad (5.2.33)$$

re ii : From the work of McCullough and Cameron (1970) we deduce that the influence on the exposure rate in air as a function of the tube current is given by

$$\dot{X} \text{ per mA} \sim U^{2.4} \quad (5.2.34)$$

For X-rays we can assume that the skin dose rate is proportional to this exposure rate.

- re iii : The ratio between the skin dose and the volume dose must be taken into account, because the ratio changes considerably with the beam quality. According to Zieler (1961) the ratio is proportional to  $U$  for a phantom which corresponds reasonably well with our geometry.
- re iv : According to table 4.2.1 and eq. 4.2.1, the object contrast  $C_O$  is given by

$$C_O \sim \frac{1}{U} \quad (5.2.35)$$

Only the primary radiation intensity is involved in  $C_O$ . Ultimately, the influence of the scattered radiation must also be taken into account, so as to obtain the primary light image contrast  $C_I$ . We conclude that for  $C_I$  the same dependence as for  $C_O$  holds, because the relative intensity of the scattered radiation does not strongly depend on the X-ray beam quality (sec. 5.2.4).

- re v : The influence on the resolution has been studied in sec. 5.2.4.

The ratio between the image contrast and the skin dose is apparently proportional to  $U^{0.1}$ ; in relation to the volume dose the ratio is proportional to  $U^{1.1}$ . Thus the dose decreases faster than the contrast. This is an additional advantage if a better resolution is obtained as well (i.e. for the object resolution of (faster) moving objects and for cerebral angiography when geometric magnification is also applied), but it should not dictate the decision if the resolution deteriorates (e.g. the visual resolution for normal viewing without visual aids) — see sections 5.2.4.2 and 5.2.4.3.



## Appendix I

### THEORETICAL THRESHOLD CONTRAST CURVE FOR DISKS

This curve describes the inverse of the maximum contrast gradient of the image of disks, made by an unsharp optical system. Its unsharpness is described by an exponentially shaped MTF:

$$\text{MTF}(\nu) = e^{-\beta \nu} \quad (\text{I. 1})$$

where  $\beta$  is a parameter and  $\nu$  is the spatial frequency. If the disk is small compared with the FWHM of the PSF, then point spread function images are made. If the disk is large, then edge spread function imaging takes place.

According to Johnson (1973), the PSF and ESF intensity distributions according to the proposed MTF are respectively

$$I_p(r) = \frac{2\pi}{\beta^2} \cdot \frac{1}{\left(1 + \frac{4\pi^2}{\beta^2} \cdot r^2\right)^{3/2}} \quad (\text{I. 2})$$

and

$$I_l(x) = \frac{1}{2} + \frac{\arctg\left(\frac{2\pi}{\beta} \cdot x\right)}{\pi} \quad (\text{I. 3})$$

The total flux in the PSF and the step in the ESF equal unity. The FWHM of the PSF equals  $0.24 \beta$ .

We shall calculate the maximum contrast gradient for a disk with unit contrast. The inverse of this maximum gradient equals the predicted threshold contrast.

For the contrast gradient we can write

$$\frac{dI(r)}{dr} \sim 2\pi^2 \Delta \int_0^\infty \nu \cdot \text{MTF}(\nu) \cdot J_1(\pi\nu\Delta) \cdot J_1(2\pi\nu r) d\nu \quad (\text{I. 4})$$

The maximum gradient is found by calculating the gradient for the interesting range of distances  $r$ . An expression for the maximum gradient can easily be found when the shape of the image intensity distribution is known, i.e. if PSF or ESF imaging occurs. The *asymptotic* behaviour of the predicted  $C$ - $\Delta$  curve can therefore

easily be calculated. If the diameter is expressed in units of FWHM by the parameter  $\Psi$ , i.e.

$$\Psi = \frac{\Delta}{\text{FWHM}} \quad (\text{I. 5})$$

then the intensity distribution of the image of small disks reads (eq. I.2 corrected for flux):

$$I_p(r) = 0.0297 \pi^2 \Psi^2 \frac{1}{\left(1 + \frac{4\pi^2}{\beta^2} \cdot r^2\right)^{3/2}} \quad (\text{I. 6})$$

The maximum contrast gradient is found at  $r = \beta / 4\pi$ , and its value is given by

$$1.57 \frac{\Psi^2}{\beta} \quad (\text{I. 7})$$

For large disks no flux correction is needed, and the intensity distribution is given by equation I.3. The maximum gradient is situated at  $x = 0$ , and its value is given by

$$\left. \frac{d I_e(x)}{dx} \right|_{\max} = \frac{2}{\beta} \quad (\text{I. 8})$$

The intersection of the two asymptotes is situated at the equality of the gradients according to eqs. I.7 and I.8, so that  $\Psi = 1.13$ . The influence of  $\beta$  is of course eliminated by this procedure.

The validity of equation 2.2.1.5, i.e.

$$\beta = 3.62 \Delta_i \quad (\text{I. 9})$$

is now demonstrated by the fact that for this disk size  $\Delta_i$  it holds that  $\Psi = 1.13$ ; further  $\Psi = \Delta/\text{FWHM}$  and  $\text{FWHM} = 0.24 \beta$ .

## Appendix II

### NOISE-EQUIVALENT APERTURE

The value of the equivalent aperture is governed by the MTF of the imaging system, i.e.

$$A_{eq} = \frac{1}{2\pi} \cdot \frac{1}{\int_0^{\infty} \nu \cdot MTF^2(\nu) d\nu} \quad (II. 1)$$

The square of the noise-equivalent width,  $d_{eq}$ , is also used as the equivalent aperture (Franken et al., 1973d). The noise is then thought to be scanned by a slit with width  $d_{eq}$ . For  $d_{eq}$  we can write

$$d_{eq} = \frac{1}{2} \cdot \frac{1}{\int_0^{\infty} MTF^2(\nu) d\nu} \quad (II. 2)$$

In general  $A_{eq}$  is not equal to  $d_{eq}$  squared, however. This is illustrated by writing for the MTF the generalized form

$$MTF(\nu) = e^{-[\nu^\gamma]} \quad (II. 3)$$

The  $A_{eq}$  value is compared with  $d_{eq}$  squared in fig. II.1.

Correct results are fortuitously obtained if a Gaussian shaped MTF is considered, i.e. if  $\gamma = 2$ . Substantial deviations exist if  $\gamma = 1$ , that is if the MTF is exponentially shaped. This latter situation is more practical, as present image receptors tend to show such an MTF.

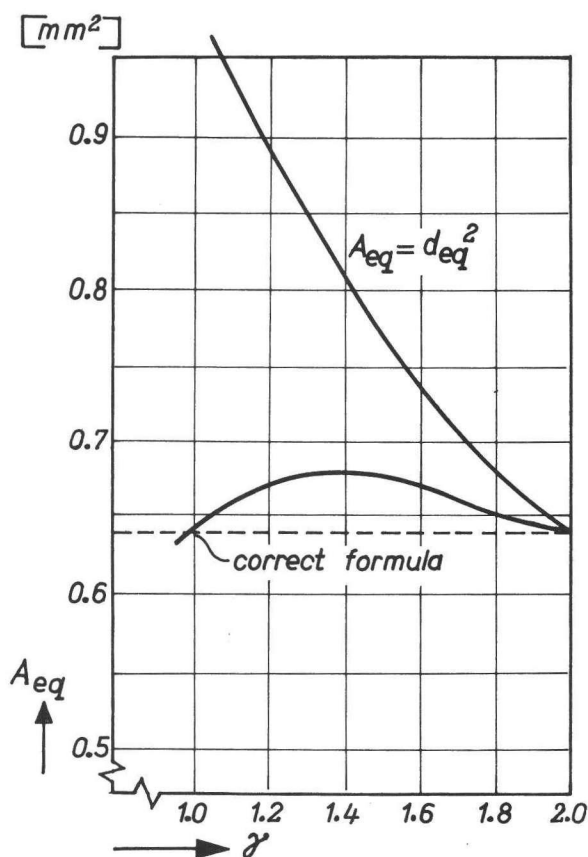


Fig. II.1.

Noise-equivalent aperture for two methods of calculation;  $MTF(\nu) = e^{-[\nu^\gamma]}$ .

## Appendix III

## LUMINANCE DISTRIBUTION MEASUREMENT ON THE MONITOR

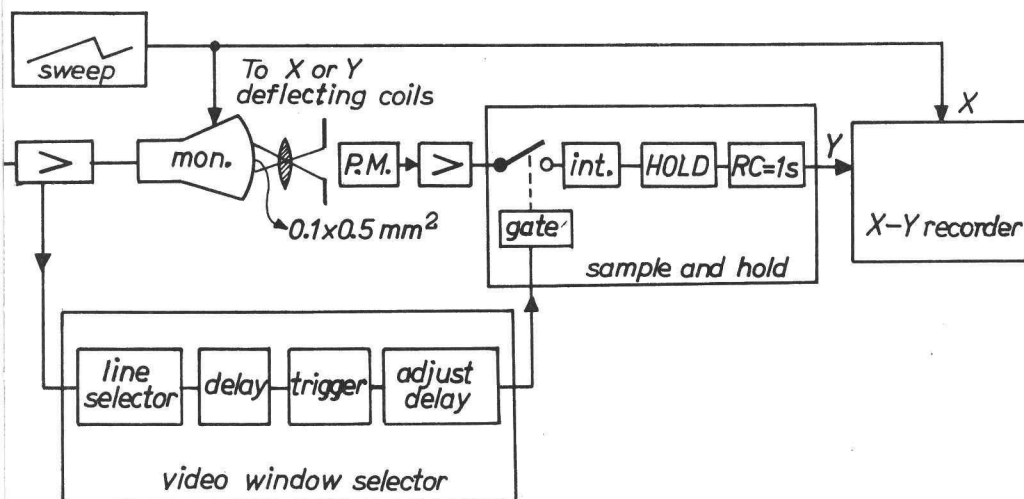


Fig. III.1.

*Intensity distribution measurement*

The apparatus is schematically shown in fig. III.1. By means of the lens and the diaphragm, the photomultiplier (type 153AVP) sees a small, long section of the monitor screen. The height of the section is 0.5 mm, i.e. one line is scanned. The width is smaller, 0.1 mm, so as to obtain the spatial resolution required. Every 40 ms the scanning beam of the monitor generates a light pulse, which is converted by the photomultiplier to an electrical signal.

The duration of the pulse is about  $20 \mu\text{s}$  (decay time included) so the duty cycle is very low. The corresponding poor signal-to-noise ratio is improved by a sample-and-hold-circuit (Brookdeal type 415). The signal is sampled and integrated when the pulse is present, and held at the measured value until the next pulse arrives. The gate is triggered via a video window selector (own make).

The screen is scanned by shifting the monitor image. This is achieved by applying a sawtooth voltage to the horizontal or vertical deflection coils. An image of the intensity distribution is obtained with an X-Y recorder (type PM8120) by feeding its X input with the deflecting voltage, and the Y input with the sample-and-hold output. This input is provided with a smoothing RC circuit with a time constant of 1 s.

As the contrast is a few per cent, small instabilities in the background luminance have a large effect on the measurements. During the scanning of the screen, the object is therefore switched on and off. A typical graph on the recorder is re-

produced in fig. III.2. The intensity distribution is now estimated by eye by assessing the step in luminance for each position. The irregular course of the signal is mainly due to instabilities, but also to irregularities in the screen and to the noise.

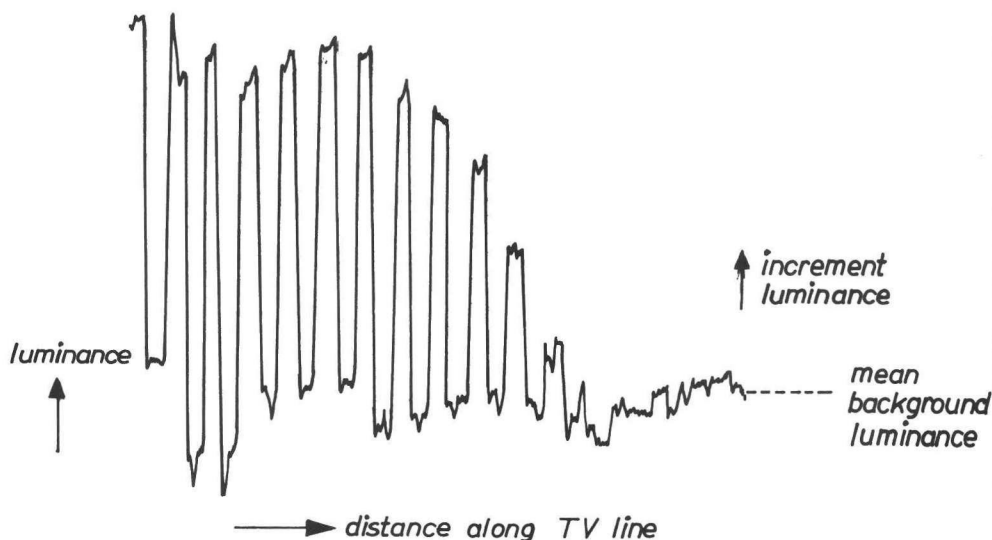


*Fig. III.2.*  
*X-Y plot of edge intensity distribution.*

There is good resemblance between the measured and calculated luminance intensity distribution (fig. III.3) for the proposed MTF (eq. 2.4.1.1).

We regard the TV system as isotropic as to its MTF because the vertical and the horizontal intensity distribution show only slightly different shapes. In general, this difference is not perceived.

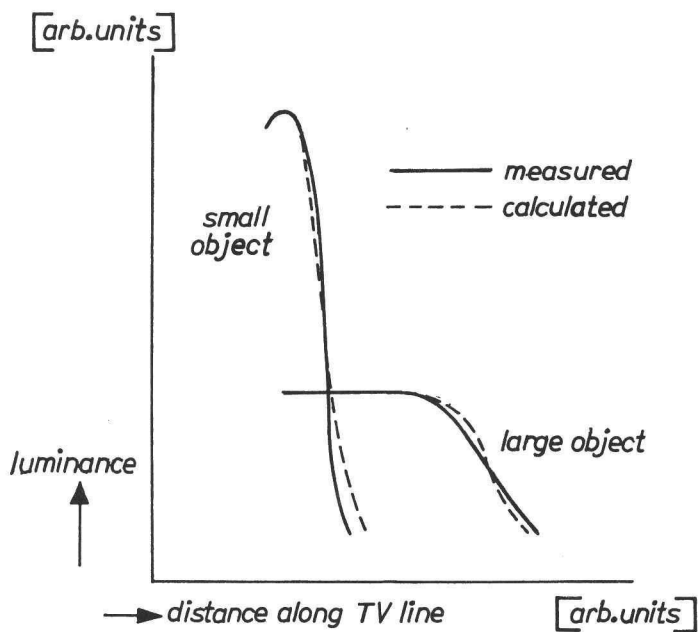


Fig. III.3.

Comparison between measured and calculated intensity distributions on the monitor screen.

## Appendix IV

## THE INFLUENCE OF SCATTERED RADIATION ON THE OPTIMUM MODULATION TRANSFER FUNCTION OF AN X-RAY SYSTEM

Generally, a larger object-to-image receptor distance implies a worse shadow image MTF. As the image receptor MTF in the object plane improves, however, a better object resolution is possible, provided that the initial shadow image MTF is not too dominant.

This trend in the object resolution is conveniently predicted on the basis of the  $\eta_{x,m}$  or  $\eta_{x,st}$  value. If  $\eta_{x,m}$  is smaller than about 0.5, then no geometric magnification should be applied. The same holds for  $\eta_{x,st}$  values smaller than about 0.45.

The mathematical formulations of  $\eta_{x,m}$  (eq. 3.2.43) and  $\eta_{x,st}$  (eq. 3.3.9) are based on a  $c_a$  value which does not depend on the geometric magnification factor. This is practically the case if a grid is used (see fig. 4.1.11). If no grid is used and if the reduction of the effective scattered radiation is obtained by virtue of the geometric magnification, then the Q value will be larger. This can mathematically be taken into account by means of the Bucky factor of the magnification:

$$Q|_{\eta} = B(\eta) \cdot Q|_{\eta \approx 0} \quad (\text{IV.1})$$

where  $Q|_{\eta \approx 0}$  is the Q value for small magnifications. The maximum Bucky factor is about 2.2 – 2.5 (see sec. 4.1), which is reached for  $\eta$  between 0.3 and 0.5.

In section 5.2.5 it was shown that the omission of the grid for small magnifications is not recommended. A practical shift will correspondingly be from small magnification/grid to considerable magnification/no grid. Actually, the Q value is then *reduced* by a factor of about 2 (see table 5.2.13).

We expect, therefore, that magnification is to be recommended for smaller  $\eta_{x,m}$  and  $\eta_{x,st}$  values. It turns out that the critical value for moving objects becomes 0.41 (sec. 5.2.5.2), a lower value indeed. The difference is slight, however, so the influence of a change in the Q value is relatively small. This can be understood by bearing in mind that the image receptor MTF also plays its role, and that the Q value is entered according to a 2/5 (moving objects, eq. 3.2.30) power law.

These ideas are supported by the calculation of  $\nu_{x,z=0.5}$  as a function of  $\eta_{x,m}$  with  $\eta$  as parameter. If no Q correction need be applied, eq. 3.2.43 can be used for  $\eta_{x,m}$ , yielding the full curves in fig. IV.1. It is once more shown that for small  $\eta_{x,m}$  the smallest  $\eta$  gives the best results. The reverse is true for large values of  $\eta_{x,m}$ . If now the Q value is corrected according to eq. IV.1, then the dashed curve is obtained. Only the curve for  $\eta = 0.3$  has been drawn. The Bucky factor is 2.5; this corresponds to fig. 4.1.5, i.e. no grid is applied. In the figure it is shown that the influence is indeed small.



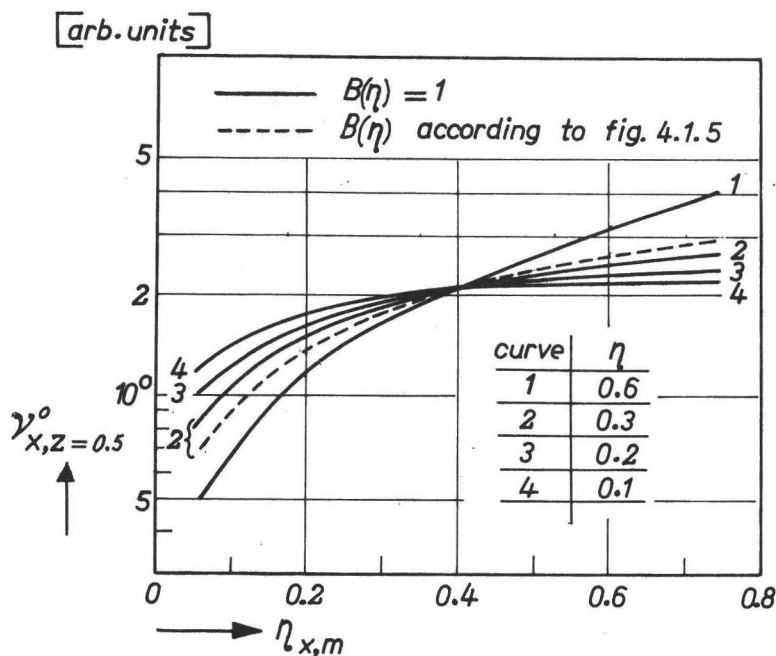


Fig. IV.1.

Influence of the  $Q$  correction on the modulation transfer quality of the X-ray system.

When the  $Q$  value depends on  $\eta$ , then the calculation of  $\eta_{x,m}$  is more intricate. The dependence of  $c_{a,m}$  in equation 3.2.43 is entered analogously to eq. IV.1 as follows

$$\frac{1 - \eta_{x,m}}{\eta_{x,m}^{3/5}} = \left( \frac{B|\eta_{x,m}}{B|\eta \approx 0} \right)^{2/5} \cdot \frac{(c_{a,m}|\eta \approx 0)^{2/5} \cdot \text{fr}^{4/5} \cdot \nu_{\text{rec}}}{0.442} \quad (\text{IV.2})$$

In principle any reference value of  $\eta$  can be chosen. To stay in line with sec. 4.1,  $\eta$  is chosen to be small, say 0.05.

## Appendix V:

## PHOTOMULTIPLIER AMPLIFIER/DIVIDER

## Introduction

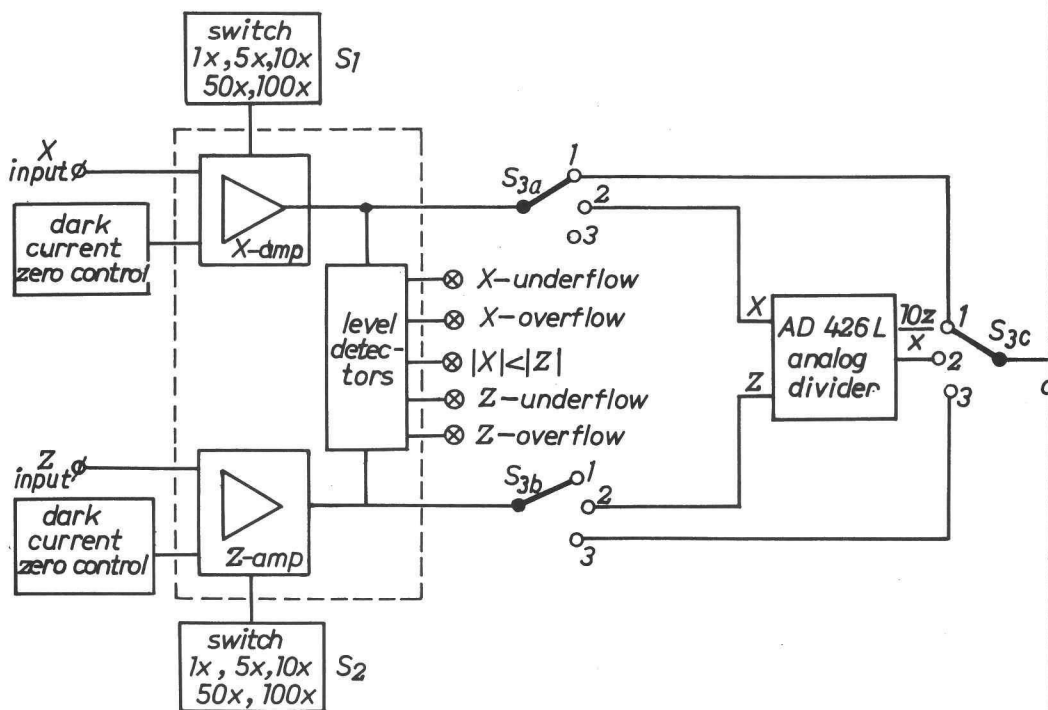


Fig. V.1.

Block diagram of PM amplifier/divider

With this apparatus, shown schematically in fig. V.1, systematic fluctuations in a photomultiplier (PM) signal are cancelled out by dividing this signal by a reference PM signal which is prone to the same fluctuations. In our set-up the two PMs measure the fluctuating intensity of the beam of a diagnostic X-ray tube. One PM signal is deliberately varied by placing unknown absorbers in that part of the beam. The other PM delivers the reference signal. The apparatus consists of two amplifiers, an analog divider and five level detectors. Signal offsets can be corrected.

## Signal amplifier

The input circuit (fig. V.2) consists of a  $1\text{ M}\Omega$  resistor to convert the PM output current into a voltage signal. This voltage is smoothed by a  $1\text{ }\mu\text{F}$  capacitor ( $\tau = 1\text{ s}$ )



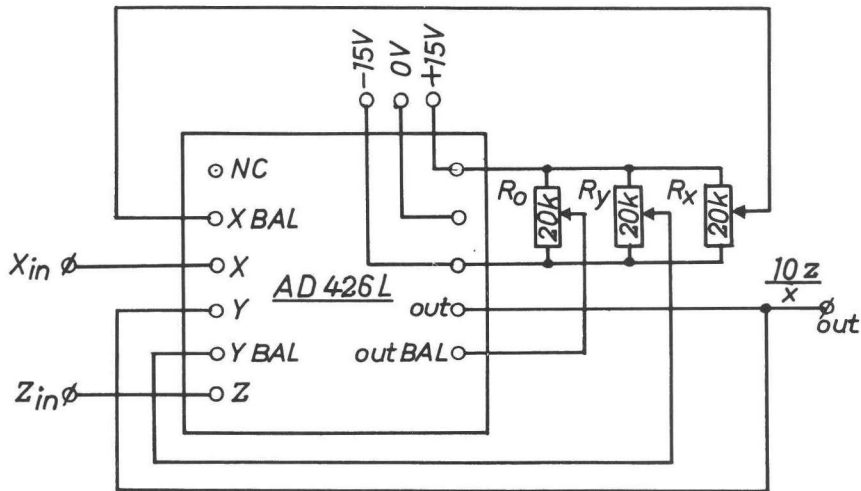


Fig. V.3.  
Analog divider.

**Output**

The output signal is fed to a DVM. Via switch S3 either the X, the Z or the divided result can be presented. The X and Z signals indicate absolute intensities. They serve also for checking the working of the PMs as to the long-term stability, the dark current and the linearity.

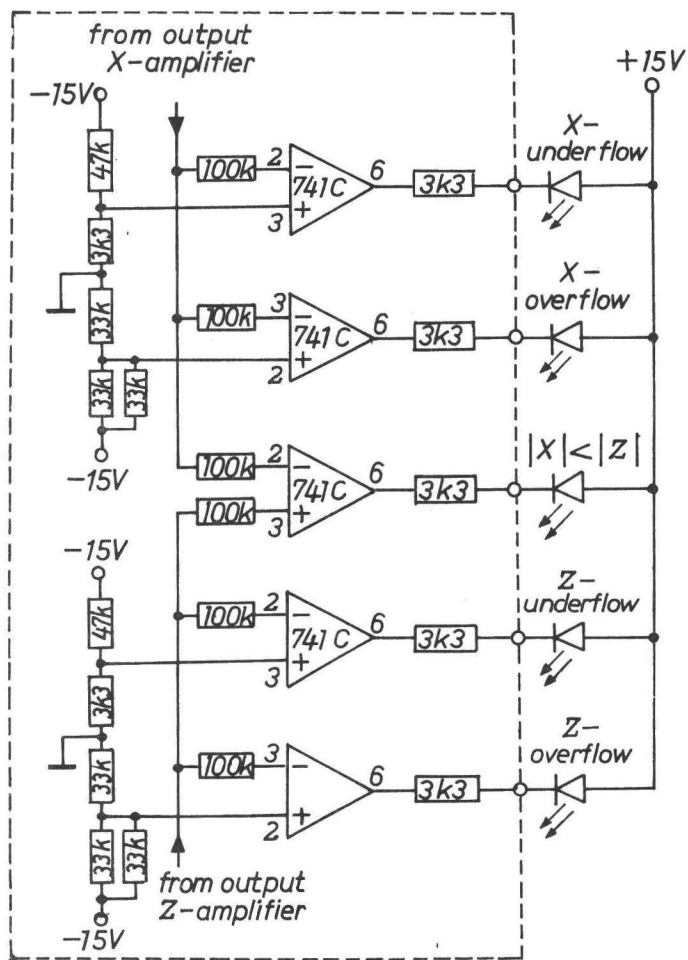


Fig. V.4.  
Level detectors.

## Appendix VI

### REMARKS ON COMPUTERIZED TOMOGRAPHY

#### Introduction

Recently, the computerized tomography (CT) technique has gained wide acceptance in the market for head and abdominal imaging. With such a system, the X-ray attenuation of a cross-section of the patient is measured in many directions. The intensity profiles for each direction serve as the input to a computer, which calculates the local linear attenuation coefficient in the section. These are presented as a matrix of say  $256 \times 256$  picture elements (pixels).

A drawback of conventional shadow imaging is thus circumvented, i.e. the effects of overlying structures are eliminated. They are of course also eliminated by conventional tomography, which blurs the non-interesting structures. But this results in low-contrast images, whereas in CT 1% attenuation coefficient differences are still recognizable, for objects with a width of a few mm. In addition, scattered radiation has little influence, because on the one hand the irradiated volume is small (for a patient thickness of 200 mm and 10 mm section thickness the ratio  $I_s'/I_p$  is less than 0.1 — fig. 4.1.13), and on the other hand the inherent elongated irradiated area implies less chance of scattered radiation detection.

In the following we will try to apply relevant perception theories. This will prove to be rather difficult because of the peculiarities of CT imaging. The spatially sampled character of the image also makes it difficult to describe the imaging technically. Results and suggestions will be compared with literature, which is generally not psychophysically oriented. Nevertheless a few results could be traced.

We will confine ourselves to the imaging of cylinders perpendicular to the slice.

In the limit they correspond to small lesions. The resulting images resemble disks, so the correlation with our visual research is favoured. Further, the analysis will be carried out for a given dose to the patient. The influence of the pixel width will be studied, as this strongly influences the noise and the contrast of the image.

#### Imaging characteristics

The spatial sampling by pixels implies that the conventional PSF does not exist. Firstly, the image of a small object does not depend on its position as long as it is situated within the pixel. Secondly, if the object is situated in more than one pixel, its image will correspondingly be smeared out. The resulting intensity distribution depends further on the particular position of the object. Thirdly, intensity sampling is applied as well.

The contrast scale can be expanded at will by the computer. This means that noise can always be made dominant. This is generally the case for the interesting attenuation coefficient differences of about 1% (Ommaya et al., 1976; McCullough et al., 1976.)

The noise is generally expressed in the standard deviation  $\sigma(\mu)$  of the reconstructed attenuation value. According to Brooks and DiChiro (1976), it is given by

$$\sigma(\mu) \sim \sqrt{\frac{1}{w^3 h}} \quad (\text{VI.1})$$

where  $w$  is the pixel width and  $h$  is the slice thickness, for a given patient skin dose. Thus the influence of the pixel width is considerable. The influence of  $h$  is in accordance with conventional expectations in terms of the number of quanta per measurement. Some spatial smoothing of the intensity profiles is applied to prevent artefacts. This results in a 'PSF' which extends over more than one pixel, but also some correlation of the noise is introduced. This has clearly been demonstrated by Boyd et al., (1976), who measured the standard deviation as a function of the sampling diameter (i.e. our measurements as described in sec. 2.5.1.3.1). Completely uncorrelated noise would result in a standard deviation which is inversely proportional to the square root of the sampling aperture; in fact, however, the standard deviation changes less rapidly.

### Technical resolution

It is generally stated that the best technical resolution will be obtained by a pixel width comparable to the object size. The image is further scanned with the same aperture, i.e. with the object cross-section. According to eq. VI.1 a larger pixel width corresponds to less noise, but the dilution of the contrast is more severe. A smaller pixel width also gives worse results because the measured contrast remains the same, but there will be more noise.

The slice width should equally be comparable with the object height. A larger or smaller slice width results in a worse contrast-to-noise ratio.

### Visual resolution

The choice of an optimum pixel width is much more difficult than for the technical resolution because a) the threshold contrast for a *range* of diameters is to be studied, b) the *visual size* of a pixel and of the final image is involved, c) the object position in relation to the pixel is of interest, and d) apart from these pure contrast considerations, a model for the effective, i.e. static noise is to be developed.

re. d : Such a model does not exist. We may argue, however, that the masking efficiency of the noise will be proportional to  $\sigma(\mu)$ , the standard deviation for one pixel, as follows. The normal range of pixel widths (for example one can choose with the Philips D300 body scanner 265 pixels for a 65 mm image, i.e. 0.24 mm/pixel) is comparable with the spatial resolution of screens/film systems, for which the same relationship for the noise can be found. By further stating, as before, that for a given type of noise the

shape of the C- $\Delta$  curve does not depend on the noise intensity, we can predict both the trend and the similarity of the C- $\Delta$  curves measured by Boyd et al. (1976). He found for three scanners similar C- $\Delta$  curves, where the smaller  $\sigma(\mu)$  value indeed corresponds to the smaller threshold contrast. (Contrary to our proposal he uses a 'noise-area function' (Albrecht, 1976) as a characterizer, i.e. the standard deviation for the aperture corresponding to the object dimension. This leads to inconsistent results in the sense that the noise-area function of two of the three scanners cross, whereas the C- $\Delta$  curves do not.)

re. c : To calculate the contrast corresponding to a disk with size  $\Delta$  and a pixel of width  $w$ , it was tacitly assumed that their centres coincide. In practice, however, other positions of the object are equally possible. This will lead to a smaller probability of the maximum possible contrast being obtained. This effect has only qualitatively – if ever – been taken into account in the literature.

Referring to fig. VI.1 and VI.2, five cases can be distinguished.

- $\Delta \leq w$  – the maximum contrast is obtained if the disk is completely retained in the pixel. For  $\Delta = w$  the probability of this situation arising is zero, and therefore the definition of the technical resolution cannot be used. In general, the probability, calculated by simple geometric considerations, can be written as

$$\left(1 - \frac{\Delta}{w}\right)^2 \quad (\text{VI.2})$$

As expected, the probability is unity for  $\Delta$  equal to zero.

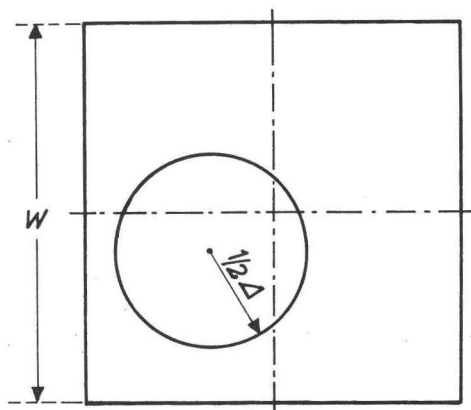


Fig. VI.1.

Pixel with object disk,  $\Delta \leq w$ .



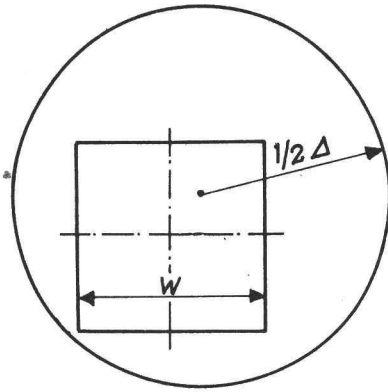


Fig. VI.2.

Pixel with object disk,  $\Delta \geq \sqrt{2} w$ .

- $w \leq \Delta \leq \sqrt{2} w$ : the maximum contrast only occurs if the centres coincide, so the probability is zero.
- $\sqrt{2} w \leq \Delta \leq 2\sqrt{1.25} w$ : the whole pixel is only contained in the disk if the centre of the disk is situated in the central region of the pixel (fig. VI.2). The probability is approximated by

$$\frac{1}{2} \left( \frac{\Delta}{w} \right)^2 - \sqrt{\left( \frac{\Delta}{w} \right)^2 - 1} \quad (\text{VI.3})$$

- $2\sqrt{1.25} w \leq \Delta \leq 2\sqrt{2} w$ : like the former case, the probability is approximated by

$$1 - \frac{1}{2} \left( \frac{\Delta}{w} \right)^2 + 4 \sqrt{\frac{1}{4} \left( \frac{\Delta}{w} \right)^2 - 1} \quad (\text{VI.4})$$

- $\Delta \geq 2\sqrt{2} w$ : the disk is so large that at least one pixel is always enclosed.

The figure VI.3 gives the corresponding probability of the maximum contrast as a function of  $\Delta/w$ . This is quite different from the conventional situation, where the probability is always unity (unless there is noise, of course; but noise was not involved up till now).

re. b : So far we have dealt with the influence of the object size and its position in relation to the pixel. The visual consequences, however, can be very different, because the visual size of the pixels and objects play a role. If, for example, the final image on the screen is small for the visual system,

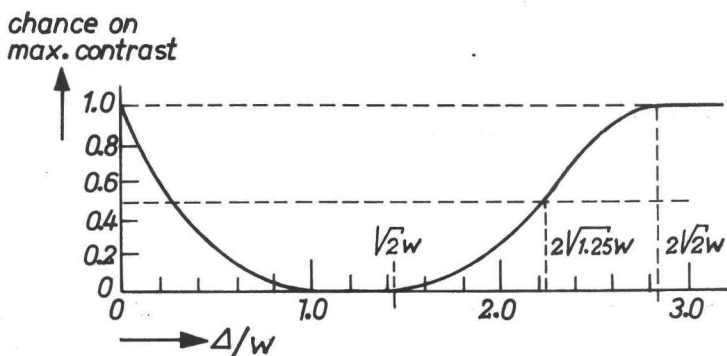


Fig. VI.3.

*Probability of the maximum contrast of the image of a disk in relation to the pixel width.*

then the spatially integrated signal is of prime importance; consequently the contrast distribution is not very important.

Practical data for the Philips D300 scanner indicate that either a 240 mm (minimum) or 480 mm (maximum) body section is depicted with 256 pixels per diameter of the 65 mm image. This implies 0.24 mm per pixel in the image, which will render the unsharpness relatively unimportant for the threshold contrast: The limit for a small disk is 6' (see sec. 5.2.1.2), which corresponds to either 3.3 or 6.6 mm in the body.

It can be concluded that the noise sets the limit of the detail dimension with the interesting linear attenuation coefficient difference of about 1%. Correspondingly, results reported in the literature (McCullough et al., 1976) indicate that the threshold disk width is over 4 times the pixel width (EMI head scanner, i.e.  $\approx 6$  mm in the body) to 14 times (Acta/Delta/EMI body scanners, i.e.  $\approx 19$  mm in the body). Therefore discretization effects hardly exist, and the probability of the maximum contrast occurring is close to unity. Perceptible objects with a higher contrast, e.g. in phantoms, may extend over fewer pixels. In this situation, discretization effects may interfere, causing a reduced probability of maximum contrast (fig. IV-3).

### The optimum pixel width and slice width

Both the optimum widths depend on the size of the object and the viewing conditions. This always implies a compromise. Three situations can be distinguished, based on the visual size of the disk.

- *The disk is large* for the visual system, i.e. its diameter in the image is about 40' or more (sec. 5.2.1.2). This corresponds to between 20 and 40 mm in the body, so that many pixels will be involved. In this situation a larger pixel width will be of advantage as (i) the contrast and the probability of this contrast remain the same (fig. VI.3), and (ii) the noise decreases considerably (eq. VI.1). This trend has indeed been measured by McCullough et al. (1976) for the Delta body scanner.
- *The disk is small* for the visual system and in relation to the pixel width. The probability of the maximum contrast is therefore close to unity. Further, since the ratio between the contrast and the noise is inversely proportional to  $w^{1/2}$ , a smaller pixel width is of advantage if the viewing angle is increased correspondingly. If this angle is not altered, the contrast effect is cancelled by the effect of the size, and a larger pixel width will be advantageous because the noise intensity would be smaller.
- *For disks with intermediate dimensions* the trend will be to increase the pixel width, with a weighting of the adverse effects of less probability of the maximum contrast.

As regards the optimum slice width, the difficult compromise must be found between an adapted width, corresponding to a high contrast, and a larger width, corresponding to less probability of missing the object and fewer slices to cover a certain thickness.

## Discussion

It has been mentioned that spatial smoothing of the data is carried out by the computer. In this way the noise intensity is reduced and discretization effects are less severe. The same can be said of the influence of the pixel width on the visibility of the object. On the other hand it can be concluded from the work of Schröder (1976) that *less* spatial smoothing corresponds to better visibility.

We concluded that for certain objects a larger pixel width may be of advantage. This does not favour, of course, the imaging of closely spaced objects.

The analysis of these two aspects — pixel width and smoothing — proves to be difficult even for a limited choice of technical parameters (we did not discuss, for instance, the influence of artefacts) and for relatively simple objects. As the real object, i.e. the human body, is complex, the reasoning given can be no more than a guide to pragmatic experiments.



## SUMMARY

The quality of images made by medical X-ray systems can only be properly described if the visual system is also taken into account.

In this thesis, therefore, the visual threshold contrast of edges, bars and disks has been chosen as the criterion. Since these objects resemble medical objects like tumour-mass outlines, blood vessels and micro-calcifications, a correlation with X-ray practice is possible. In addition, the chosen objects are so essential to imaging that the results of the visual research will be applicable to other disciplines as well. Only the conventional X-ray systems will be considered, which means that computerized tomography is excluded. However, because of its great importance, a brief analysis of computerized tomography is given in the appendix.

Considerable attention is paid to unsharpness and the minimization of its influence on the threshold contrast, to the influence of the noise on the threshold contrast, and to the contrast formation as such. The unsharpness is described in terms of the corresponding modulation transfer function (MTF). This description is allowed although the system is non-linear (film, TV monitor), because only small contrasts will be considered. The MTF quality criterion is based on the perception of the corresponding point-spread, line-spread and edge-spread images. It is shown that there is a positive correlation between this psychophysical quality and the spatial frequency for which the modulation transfer equals 0.25. This relation holds good for practical combinations of the exponentially and  $\sin(x)/x$  shaped MTFs, which normally describe the system MTF.

The problems inherent in an analysis in terms of functions are thus avoided. This enables a set of characteristic parameters to be developed, which combine the lucidity of the unsharpness concept with the exactness of the description by the modulation transfer function. As a result, nomograms and equations are given to estimate the influence of the typical X-ray system properties i.e. unsharpness, image contrast, X-ray noise and viewing conditions.

The characteristic parameters serve to describe the X-ray system in general terms and to estimate the relative importance of its components. An understanding of this relative influence is a great help in the development of new systems, and for the understanding of existing systems. The results of our analysis of existing systems are in good agreement with practical findings. This provides an additional proof of the validity of the modelling, as one may state that the parameter values will be near the optimum, after so many decades of X-ray application.

Finally, the consequences for the dose administered to the patient are analysed.

In chapter 1 an *introduction* is given.

Chapter 2 deals with the *visual resolution*. The threshold contrast of isolated objects is investigated as a function of their unsharpness and size and as a function of the background noise. The backgrounds used are dynamic noisy backgrounds as occur in TV fluoroscopy and cine fluorography, static noisy backgrounds as are found in radiography, and a structureless background.

Many good predictions are obtained with our model of the visual system, which is partially based on Blackwell's measurements (1946) on sharp disks. We propose that the visual system can be described as performing a spatial integration and a differentiation, thus enabling us to take into account both the unsharpness of the visual system and its high sensitivity to spatial or temporal modifications of the scene. The unsharpness of the visual system is described by an MTF as well, so that the imaging of the X-ray system can readily be extended. The aspect of differentiation is introduced by assuming that the threshold contrast is inversely proportional to the maximum contrast gradient of the resulting image. The eye movements and circuits in the retina may play a role in the differentiation. The reverse order of actions, i.e. integration after differentiation, is mathematically equivalent. This order may be a more plausible model in the light of physiology and the results of for instance adaptation experiments.

As regards the noise we assume that its processing has no correlation with the object to be searched for. This leads to good predictions of the threshold contrast of objects in noise. Many correlation diagrams are conceivable and some have already been proposed. These schemes as well as our proposal may be fictitious, as the assumptions concerning the two processes are generally interrelated. Further we will show that very sensitive measurements are needed to distinguish between the properties of object- and noise processing.

The dynamic X-ray noise is varied in intensity, unsharpness and viewing distance. The influence of the unsharpness may be predicted on the basis of the noise equivalent aperture concept if the visual system MTF is also included. The effect of an intensity variation (X-ray exposure rate, gamma of the TV system) is predicted by any model based on the statistics of the number and the intensity of events in a certain area/time space. The masking effect is correctly predicted to be inversely proportional to the viewing distance.

Different static noises were not compared for their masking effect, so it is not possible to compare image receptors which differ in this respect. Many problems were nevertheless studied by analysing the influence of the viewing distance for a dominant static noise. It was found that the masking effect is invariant with the distance in practical situations; this independence cannot be reconciled with any model.

We confront our model with eight other models by assessing their predictive power for a large number of perceptual phenomena. It is concluded that no model possesses general validity and that often false predictions are given. This conclusion and the apparent abundance of models shows that the visual system is still incompletely understood. Our model partially fails in the prediction of the threshold contrast of disks in dynamic X-ray noise as a function of size. Furthermore the influence of the bar size is not correctly predicted. A pragmatic approach leads nevertheless to an operational model for assessing the quality of medical X-ray systems.

As stated, this model is based on the concept of threshold contrast. An analysis of practical X-ray systems reveals that the unsharpness often has relatively little effect

on the threshold contrast. A more sensitive criterion for the unsharpness would be the threshold increment-unsharpness, as has been found from a few pilot experiments. Calculations suggest that the proposed model of the visual system enables the threshold increment-unsharpness to be analysed as well. Many more experiments and much more modelling are needed to confirm this, however. Unlike the visibility of the object as such, the visibility of an unsharpness increment is rather insensitive to the contrast, the size of the object and the noise. Future work on the visual appreciation of images may therefore be based on the threshold contrast concept as far as the contrast formation and the size of the object is concerned (absorption contrast, influence of scattered radiation, magnification) and on the threshold increment-unsharpness as far as the unsharpness is concerned.

In chapter 3 an analysis is given of the *object resolution*, i.e. the MTF of the X-ray system proper in the object plane, for moving and stationary objects. As the object plane is the reference, the object resolution will be called the 'intrinsic' resolution of the X-ray system. The shadow image or absorption image MTF is governed by the properties of the X-ray source, the attenuation by the object, the sensitivity of the image receptor, and also by the movement, if any, of the object.

Firstly, the shadow image MTF is optimized by adaptation of the X-ray source to the movement of the object. As the relation between the size of the source and its loadability depends on its spatial intensity distribution, other distributions than the present 'camel back' distribution are also examined. Secondly the influence of the position of the object between the source and the image receptor is analysed. The object position governs the so-called geometric magnification factor. It is shown that the equality law may be used to minimize the combined effect of the blurring introduced by the X-ray source and the movement. This law does not apply to the effect of the object position, because of its typical influence on the various MTFs. Either the position is unimportant or the object should be shifted close to the source or to the receptor. Nomograms are obtained for the assessment of (i) the optimum source size, (ii) the influence of a non-optimum size, (iii) the source intensity distribution, (iv) the object position and (v) the choice of the image receptor.

Chapter 4 describes the *measurements of the contrast*. To take into account the X-ray spectral sensitivity of the image receptors, what is measured is the contrast of the light image as formed by the intensifying screen or image intensifier. As stated, only small contrasts are considered, and therefore the subsequent film can be assumed to be quasi-linear. Firstly, the scattered radiation intensity is analysed as a function of the object position. The X-ray beam aperture is adjusted so as to irradiate a fixed object area. The intensity of scattered radiation can be reduced by a factor of 2 to 4 by moving the object away from the receptor. The corresponding effects on the unsharpness and the contrast are evaluated in section 5.2.5. Secondly the influence is measured of the beam quality on the contrast corresponding to an iodine solution, which is a widely used contrast medium. The contrast turns out to be approximately inversely proportional to the high voltage on the

X-ray tube. A higher voltage may nevertheless be used to advantage because the unsharpness will also be smaller on account of the reduced attenuation caused by the object. This is analysed in section 5.2.4.

Chapter 5 presents *quantitative analyses* of X-ray systems.

Firstly the object resolution is studied. Secondly the visual system is included in the analyses and nomograms are developed for estimating the influence on the visual resolution of the choice of the X-ray source size, the image receptor and the viewing conditions (viewing distance and optical magnification factor).

Unlike the object resolution, the visual resolution must be described in an image plane, and size effects of bars and disks also play a role. These size effects may entail a better visual resolution if geometric magnification is applied, although the object resolution may deteriorate. One should preferably aim at the best object resolution so as to maximize the intrinsic information content of the image. In this situation, therefore, optical magnification would be chosen.

For quantitative analyses, the present state of the art and practical conditions are taken as the starting point. The resulting values for the characteristic parameters indicate trends only, because the parameters show a wide scatter. For a more restricted field of application, more exact information would be gained.

*Object resolution.* In the imaging of stationary objects the receptor unsharpness dominates, unless no-screen film is used. In the imaging of moving objects, however, the shadow image unsharpness tends to be dominant; this applies to heart imaging in general and when intensifying screens are used. The source unsharpness is expected to have less influence when image intensifiers are used. Consequently sharper screens are desired for stationary-object imaging, whereas more sensitive screens are favourable for moving-object imaging. Rare-earth technology may be appropriate for this purpose. Sharper image intensifiers are also advantageous, but little is gained for heart imaging.

Further the size of the source and its intensity distribution are not very important in the case of stationary-object imaging. A 10 kW/25 kW/80 kW source would suffice for most purposes. For moving objects the choice of the source is of greater interest. Loadabilities between 5 and 200 kW are required. If screens are used, and in the case of heart imaging, the most effective intensity distribution, i.e. the falling intensity distribution, is required instead of the present camel-back distribution. For image intensifier imaging a Gaussian distribution suffices.

The exceptions worth mentioning where stationary objects are concerned are kidney and gall-bladder imaging and cerebral angiography. The receptor and the shadow image unsharpness are then more or less balanced, because either the attenuation by the patient is rather high (kidney, gall-bladder), or geometric magnification is applied (angiography). Both effects indicate an increase in shadow image unsharpness.

*Visual resolution.* The influence of the system unsharpness on the visual resolution is generally small for normal viewing distances (500 mm) and when no optical



magnification is applied, unless rapidly moving objects are considered. The masking effect of the X-ray noise on the TV monitor is also practically independent of its unsharpness. Nevertheless unsharpness differences will often be perceived because the visual system is known from measurements to be highly sensitive to differences of suprathreshold objects.

The visual resolution may also be considerably influenced if optical viewing aids or geometric magnification are applied.

A Gaussian distribution usually suffices for the source intensity distribution.

*Magnification.* Geometric magnification is often recommended for the unsharp, sensitive 9" and some 5"/6" image intensifier techniques. With regard to optical magnification and the viewing distance, the demands for edge, bar and disk imaging are conflicting; there is further dependence on the noise (static or dynamic). Variable optical magnification is therefore desirable; up to 10 times magnification — and even reduction (for edges) — can be useful.

*Distance between X-ray source and image-receptor.* A small distance favours both the object- and the visual resolution; the influence on the latter can be considerable if small objects are involved, because of the resulting larger magnification factor. A smaller distance has the further advantage of requiring a smaller source-load-ability.

*Scattered radiation.* A grid should generally be used if the object is close to the image receptor. The grid can be omitted provided that at the same time the object is moved away from the image receptor. This application of geometric magnification, however, is only of interest in some low-velocity image intensifier techniques and in some stationary-object imaging applications.

*X-ray beam quality.* A shift to a higher X-ray tube voltage (from 70 to 110 kV) often improves the object resolution for the imaging of moving objects. This is in any case true for the faster moving or more strongly attenuating objects. For the imaging of stationary objects, however, the influence of the X-ray source unsharpness is generally relatively small and then the use of a higher tube voltage is not recommended: the detrimental effect on the contrast would outweigh the favourable effect of a smaller X-ray source. An exception is cerebral angiography if geometric magnification is also applied. In the latter technique the visual resolution may improve as well if optical magnification is used at the same time. The same applies to the imaging of the faster moving bars. In general, however, the higher voltage is not recommended for a normal viewing distance (500 mm), without optical magnification.

*Dose administered to the patient* The results reported in the literature indicate that the benefits greatly outweigh the risks involved, when proper radiological procedures are used. We may conclude therefore that the feasibility and reliability of the

diagnosis — which are partially governed by the object resolution and visual resolution — are usually more important considerations than the radiation hazard. In *fluoroscopy* dynamic noise is dominant, so considerably better images can be obtained at the expense of a higher dose administered to the patient. A higher dose is also involved if *geometric magnification* is applied by reducing the distance between the X-ray source and image receptor, a procedure which makes small objects more visible. If the magnification is achieved by a shift of the object with the associated omission of the antiscatter grid, then the dose is hardly affected. A higher tube voltage results generally in a smaller dose; a better image quality is only obtained for the applications mentioned under the heading *X-ray beam quality*.

## SAMENVATTING

De beeldkwaliteit van medische röntgensystemen kan alleen dan beschreven worden als de waarneming van het beeld eveneens in de beschouwing wordt betrokken. Als maatstaf is daarom gekozen het drempelcontrast van kantovergangen, balkjes en schijfjes. Een koppeling met het röntgensysteem is mogelijk daar er overeenkomst is respectievelijk met bijvoorbeeld de rand van grote objecten als tumoren en galstenen, met bloedvaten en beenbalkjes, en met microcalcificaties. De gekozen objecten zijn verder zo essentieel dat de resultaten van het visuele onderzoek ook voor andere afbeeldingssystemen toepasbaar zijn. Alleen de conventionele röntgensystemen zullen beschouwd worden. De computerized tomography (CT) zal toch — wegens het grote belang van deze techniek — in een appendix worden besproken.

Behandeld worden de beschrijving en het tot een minimum terugbrengen van de onscherpte, de invloed van de onscherpte en de ruis op het drempelcontrast, het röntgencontrast en de patient-dosis. De onscherpte wordt beschreven met behulp van de modulatie-overdrachts-functie (MTF, Modulation Transfer Function). Deze beschrijving is toegestaan daar slechts kleine contrasten beschouwd worden; de invloed van de niet-lineariteit van het röntgensysteem (film, TV-monitor) is dan gering.

Het blijkt dat de maatstaf voor MTF-kwaliteit kan worden gebaseerd op de perceptie van de corresponderende punt-spreid-functie (PSF, Point Spread Function), lijn-spreid-functie (LSF, Line Spread Function) en kant-responsie (ESF, Edge Spread Function). Er is goede correlatie tussen het drempelcontrast en de frequentie voor een modulatie-overdracht gelijk aan 0,25. Deze relatie is geldig voor combinaties van de typische röntgensysteem-MTFs (exponentieel en volgens een  $\sin(x)/x$  functie). De problemen die zich voordoen bij een analyse met behulp van functies zijn hiermee opgelost. Bijgevolg kan een aantal kengetallen worden ontwikkeld, waarmee de eenvoud van het begrip onscherpte gecombineerd wordt met de nauwkeurigheid van de MTF-beschrijving. Met deze kengetallen wordt het röntgensysteem in algemene termen beschreven. Belangrijker nog is dat ook snel een schatting van de invloed van elke component verkregen wordt. Dit is nuttig voor het begrip van de huidige systemen en voor de ontwikkeling van nieuwe systemen.

De analyse van de huidige systemen leidt tot resultaten die goed met de praktijk overeenstemmen. Daar men mag aannemen dat na zoveel jaren toepassing een redelijke keuze van parameterwaarden verkregen is, kan deze overeenstemming gezien worden als een aanwijzing voor de geldigheid van de systeembeschrijving.

De *introductie* wordt gegeven in hoofdstuk 1.

In hoofdstuk 2 wordt de *visuele resolutie* behandeld. Onderzocht wordt het drempelcontrast van stimuli als functie van de onscherpte en hun afmeting, en als functie van de ruis in de achtergrond. Als achtergrond worden toegepast dyna-

mische ruis als in TV-fluoroscopie en cine-fluorografie, statische ruis als in radio-grafie, en een homogene achtergrond.

Vele goede voorspellingen worden verkregen met ons model van het visuele systeem. Dit model is gebaseerd op metingen door Blackwell (1946) aan scherpe schijfjes. Aangenomen wordt dat het visuele systeem een spatiële integratie en een differentiatie uitvoert. Dus zowel de onscherpte van het visuele systeem als de grote gevoeligheid voor spatiële en temporele wijzigingen worden in de beschouwing betrokken. De onscherpte wordt eveneens met behulp van een MTF beschreven, zodat koppeling met het röntgensysteem eenvoudig mogelijk is. Het aspect differentiatie wordt ingevoerd door aan te nemen dat het drempelcontrast omgekeerd evenredig is met de maximale contrast-gradient van de afbeelding van de stimulus. Physiologisch gezien lijkt gradientdetectie mogelijk; oogbewegingen zouden hier eveneens een rol kunnen spelen. De omgekeerde volgorde, namelijk integratie na differentiatie, is mathematisch equivalent. Deze volgorde stemt wellicht meer met de werkelijkheid overeen, zoals wordt gesuggereerd door de physiologie van het visuele systeem en de resultaten van adaptie-experimenten.

Wat de ruis betreft nemen we aan dat het maskerende vermogen niet afhangt van de stimulus. Dit leidt tot vele goede voorspellingen van het drempelcontrast. Vele voorstellen zijn gedaan voor het verband tussen de ruis- en de stimulusverwerking door het visuele systeem. Deze relaties, zowel als onze veronderstelling van een afwezigheid van een relatie, kunnen fictief zijn. In de eerste plaats zijn de veronderstelling voor de beide processen afhankelijk van elkaar. In de tweede plaats zullen wij aantonen dat het moeilijk is om experimenteel scheiding aan te brengen tussen stimulus- en ruisverwerking.

De dynamische röntgenruis wordt gevarieerd naar intensiteit, onscherpte en kijkafstand. De invloed van de onscherpte kan worden voorspeld met behulp van de bijbehorende ruis-equivalente apertuur, mits de MTF van het visuele systeem meegenomen wordt. Het effect van intensiteitsvariatie (röntgenbundelintensiteit, gamma van het TV-systeem) wordt voorspeld door elk model gebaseerd op de statistiek van het aantal en de intensiteit van de te detecteren elementaire eenheden (bijv. photonen). Zo wordt eveneens juist voorspeld dat het maskerend effect van de dynamische ruis omgekeerd evenredig is met de kijkafstand.

In tegenstelling hiermee is er geen invloed van de kijkafstand voor dominerende statische ruis. Deze onafhankelijkheid kan niet verklaard worden. Verschillende statische ruis zoals behorend bij verschillende beeldontvangers, kon niet worden onderzocht.

Ons model wordt vergeleken met acht andere modellen met betrekking tot een groot aantal perceptie resultaten; geen enkel model voorspelt alle resultaten. Deze conclusie, en de talrijkheid van modellen, toont aan dat de werking van het visuele systeem nog niet goed begrepen wordt. Ons model geeft geen goede voorspelling

van het drempelcontrast van schijfjes als functie van de diameter, in dynamische ruis. Hetzelfde geldt voor balkjes, voor elke achtergrond. Niettemin is een pragmatische keuze van de MTF van het visuele systeem mogelijk, met behulp waarvan een schatting van de beeldkwaliteit van medische röntgensystemen verkregen wordt.

Als maatstaf voor de invloed van de onscherpte is het drempelcontrast gekozen. De analyse van een aantal bestaande röntgensystemen toont aan dat de onscherpte dikwijls weinig invloed heeft. Een gevoeliger criterium zal zijn de zichtbaarheid van de onscherpte als zodanig, zoals aangetoond aan de hand van oriënterende experimenten. Het resultaat van enkele berekeningen suggereert dat met ons model eveneens de drempelonscherpte voorspeld kan worden. Voor een definitieve uitspraak zijn echter veel meer experimenten nodig.

Anders dan de waarneembaarheid van het object is die van de onscherpte niet sterk afhankelijk van het contrast, de afmeting van het object en de ruis. In de toekomst zouden dus de parameters röntgencontrast, strooistralenintensiteit, vergrotingsfactoren en ruis in de eerste plaats op hun invloed op het drempelcontrast beoordeeld kunnen worden. Voor de onscherpte is dan de drempelonscherpte of de drempelonscherpte-toename van belang.

In hoofdstuk 3 wordt de *object-resolutie* geanalyseerd, voor bewegende en niet-bewegende objecten. De object-resolutie wordt beschreven met behulp van de MTF, zonder het visuele systeem daarbij te betrekken. Daar tevens het objectvlak het referentievlak is, noemen wij de object-resolutie ook "intrinsieke" resolutie van het röntgensysteem.

De schaduwbeeld-MTF hangt af van de röntgenbron, de bundelverzwakking door het object en de gevoeligheid van de beeldontvanger (voortaan gemakshalve "ontvanger" genoemd) en de eventuele beweging van het object. Deze MTF wordt geoptimaliseerd door de röntgenbron aan te passen aan de bewegingsonscherpte. In deze aanpassing speelt de belastbaarheid van de bron als functie van de afmeting een belangrijke rol. Daar deze belastbaarheid ook afhangt van de intensiteitsverdeling van de bron, is de invloed van andere dan de huidige "kameelrug"-verdeling eveneens onderzocht. In de tweede plaats wordt de invloed van de objectpositie tussen de bron en de ontvanger geanalyseerd. De objectpositie bepaalt de geometrische vergrotingsfactor.

De "gelijkmatigheidswet voor de onscherpten" blijkt te gelden voor de optimalisatie van de schaduwbeeld-MTF (röntgenbron en beweging). Deze wet geldt niet voor de keuze van de objectpositie, als gevolg van haar typische invloed op de schaduwbeeld-MTF en ontvanger-MTF. Of de positie is van weinig belang, óf het object moet zo dicht mogelijk bij de bron of de ontvanger geplaatst worden.

Nomogrammen worden gegeven voor (i) de bepaling van de optimale röntgenbron-

afmeting en voor de schatting van de invloed van (ii) een niet-optimale afmeting en (iii) van de bron-intensiteitsverdeling, (iv) van de objectpositie en (v) van de beeldontvanger.

De metingen aan het *contrast* worden beschreven in hoofdstuk 4. Gemeten wordt het contrast van het lichtbeeld gevormd door de ontvanger; hiermee wordt de afhankelijkheid van de ontvangergevoeligheid van de röntgenenergie in rekening gebracht. Zoals gesteld worden alleen kleine contrasten beschouwd, zodat voor deze metingen met de niet-lineariteit van de film geen rekening behoeft te worden gehouden.

Eerst wordt de intensiteit van de stroostralen gemeten als functie van de objectpositie. Het röntgendiafragma wordt steeds zo gekozen dat het aangestraalde objectoppervlak niet wijzigt. Door de afstand tussen het object en de ontvanger te vergroten kan de intensiteit van de stroostralen ter plaatse van de ontvanger met een factor twee tot vier verlaagd worden. De gevolgen voor het contrast en de onscherpte worden geanalyseerd in hoofdstuk 5.2.5.

Ten tweede wordt de invloed van de bundelkwaliteit op het contrast gemeten. Onderzocht is het contrast van de belangrijke jodiumhoudende contrastvloeistoffen. Het contrast blijkt bij benadering omgekeerd evenredig met de hoogspanning op de röntgenbuis te zijn. Toch kan een hogere spanning gunstig zijn, omdat ook de onscherpte kleiner is dank zij de geringere verzwakking van de bundel door de patient. De gezamenlijke invloed van deze effecten wordt onderzocht in hoofdstuk 5.2.4.

De *kwantitatieve analyse* van röntgensystemen wordt gegeven in hoofdstuk 5. Eerst wordt de object-resolutie beschouwd, daarna wordt de visuele resolutie geanalyseerd. Nomogrammen worden ontwikkeld om de invloed op de visuele resolutie te schatten van de röntgenbronaafmeting, de ontvanger, de positie van het object en de bekijkcondities (bekijkafstand — normale waarde ongeveer 500 mm —, en optische vergroting). In tegenstelling tot de object-resolutie moet de visuele resolutie in een afbeeldingsvlak beschreven worden. Verder speelt de afmeting van de objecten een belangrijke rol. Dit kan ertoe leiden dat door geometrische vergroting een betere visuele resolutie verkregen wordt, terwijl de object-resolutie afneemt. Daar men hiermee de intrinsieke resolutie van het röntgensysteem zou verlagen, verdient in dit geval optische vergroting of verkleining van de bekijkafstand de voorkeur.

Voor de kwantitatieve analyse is de huidige stand van de techniek als uitgangspunt gekozen. Een aantal systemen voor algemene toepassing is geanalyseerd. Het optimale röntgensysteem is een compromis, daar er steeds een spreiding van parameterwaarden is (bijv. voor de objectsnelheid). De hierna volgende conclusies zijn daarom niet meer dan indicaties. Voor speciale systemen, met een beperkt toepassingsgebied, kunnen nauwkeuriger aanwijzingen gegeven worden.

*Object-resolutie.* Voor de afbeelding van stationaire objecten overheerst de ontvan-  
geronscherpte tenzij film zonder versterkingsschermen wordt gebruikt. Voor  
bewegende objecten domineert echter de schaduwbeeldonscherpte. Dit is minder  
het geval als de gevoeliger beeldversterkers worden toegepast, behalve voor opna-  
men van het hart. Daarom zijn scherpere versterkingsschermen gewenst voor de  
afbeelding van stationaire objecten, terwijl gevoeliger schermen van belang zijn als  
het om bewegende objecten gaat. De fosforen op basis van zeldzame aarden kunnen  
hier een oplossing bieden. Scherpere beeldversterkers zijn eveneens van belang, de  
winst voor de afbeelding van het hart zal uiteraard gering zijn.

De afmeting en de intensiteitsverdeling van de röntgenbron zijn eveneens van min-  
der gewicht voor de afbeelding van stationaire objecten. Met een drie-focus, 10 kW/  
25 kW/80 kW röntgenbuis zouden bijna alle opnamen gemaakt kunnen worden.  
Voor bewegende objecten is de keuze van de röntgenbuis kritischer. Afhankelijk  
van de toepassing ligt de optimale belastbaarheid tussen 5 en 200 kW. De meest  
effectieve intensiteitsverdeling, de "vallende last"-verdeling, is gewenst als verster-  
kingsschermen worden gebruikt, en voor opnamen van het hart in het algemeen.  
Is de ontvanger een beeldversterker, dan is in het merendeel van de gevallen een  
Gauss-verdeling voldoende. Beide verdelingen leiden tot een betere schaduwbeeld-  
MTF dan die behorende bij de huidige "kameelrug"-verdeling.

Als uitzonderingen voor de conclusies wat betreft stationaire objecten moeten  
nier- en galblaasopnamen en cerebrale angiografie genoemd worden. De ontvan-  
ger- en schaduwbeeldonscherpte zijn hier van dezelfde orde van grootte, omdat  
ofwel de bundelverzwakking door de patient groot is (nier, galblaas), ofwel geo-  
metrische vergroting toegepast kan worden (angiografie). In beide gevallen is er een  
ongunstig effect op de schaduwbeeldonscherpte.

*Visuele resolutie.* De invloed van de object-resolutie op de visuele resolutie is in het  
algemeen klein, als geen optische hulpmiddelen worden gebruikt en de bekijkaf-  
stand 500 mm is. De invloed kan aanzienlijk zijn voor de opnamen van de sneller  
bewegende objecten. Het maskerende effect van de röntgenruis op de TV-monitor  
hangt nauwelijks van de onscherpte af. Toch zullen onscherpte verschillen van goed  
zichtbare stimuli vaak waargenomen worden, daar het visuele systeem hiervoor zeer  
gevoelig blijkt te zijn.

De visuele resolutie kan sterk afhankelijk zijn van de bekijkafstand en de optische  
vergroting.

Ten aanzien van de intensiteitsverdeling van de röntgenbron geldt, dat een Gauss-  
verdeling meestal voldoende is.

*Vergroting.* Geometrische vergroting is dikwijls aan te bevelen als de onscherpe en  
gevoelige beeldversterkers toegepast worden. Ten aanzien van de optische vergroting  
en de bekijkafstand geldt dat de eisen strijdig zijn voor de waarneming van respec-  
tiefelijk kantovergangen, balkjes en schijfjes; de eisen zijn bovendien nog afhanke-

lijk van de object-resolutie en de aard van de ruis (dynamisch of statisch). Een variabele optische vergroting en bekijkenafstand is daarom aan te bevelen: een tienvoudige vergroting en zelfs verkleining (voor kantovergangen) is gewenst.

*Afstand tussen de röntgenbron en de ontvanger.* Een kleinere afstand is gunstig voor zowel de object- als de visuele resolutie. De invloed op de visuele resolutie kan groot zijn dankzij de geometrische vergroting. Voor een kleinere afstand is bovendien een kleinere buisbelastbaarheid voldoende.

*Strooistralen.* Voor objecten dicht bij de ontvanger is een anti-strooistralenrooster in het algemeen aan te bevelen. Het rooster kan worden weggelaten, mits het object ook verder van de ontvanger verwijderd wordt. Deze toepassing van geometrische vergroting is echter slechts van voordeel voor enkele objecten met een relatief lage snelheid waarbij een beeldversterker wordt toegepast, en voor enkele stationaire objecten.

*Stralenkwaliteit.* De toepassing van 110 kV buisspanning in plaats van 70 kV leidt voor bewegende objecten vaak tot een betere object-resolutie, zeker als alleen de sneller bewegende of de sterker verzwakkende objecten beschouwd worden. Voor stationaire objecten is de invloed van de schaduwbeeldonscherpte in de regel gering. De hogere buisspanning wordt dan niet aanbevolen: het gunstige effect van de kleinere bronafmeting zou niet opwegen tegen het effect van het lagere contrast. Een uitzondering is cerebrale angiografie met geometrische vergroting. Ook de visuele resolutie zou nog toenemen, als ook optische vergroting zou worden toegepast. Hetzelfde geldt voor de afbeelding van sneller bewegende balkjes. In het algemeen echter leidt de hogere buisspanning tot een slechtere visuele resolutie, voor de normale bekijkenafstand, zonder optische vergroting.

*Patientdosis.* Volgens de literatuur wegen in het algemeen de voordelen van het röntgenonderzoek ruimschoots op tegen de eventuele nadelige effecten van de röntgenstralen, mits de juiste radiologische procedures worden gevolgd. Men stelt dan ook dat de betrouwbaarheid van de diagnose — die gedeeltelijk afhangt van de object- en de visuele resolutie — een belangrijker maatstaf is dan het stralingsrisico. In *fluoroscopie* heeft men te maken met dominerende dynamische röntgenruis; verhoging van de röntgenintensiteit leidt dus tot een aanzienlijk betere beeldkwaliteit maar ook tot een grotere dosis. Een grotere dosis wordt ook toegediend als *geometrische vergroting* wordt toegepast door de afstand tussen de röntgenbron en de ontvanger te verkleinen, een procedure die kleinere objecten waarneembaar zal maken. Als de geometrische vergroting verkregen wordt door het object te verplaatsen, waarbij dan het antistrooistralenrooster wordt weggelaten, dan wordt de dosis nauwelijks beïnvloed. Een *hogere buisspanning* leidt in het algemeen tot een lagere dosis; een betere beeldkwaliteit wordt echter alleen verkregen voor de gevallen genoemd in de vorige paragraaf.



## LIST OF REFERENCES

- Albrecht, C.  
Oosterkamp, W.J.      The evaluation of X-ray image-forming systems  
Medicamundi 8, 106–115 (1962)
- Albrecht, C.  
Proper, J.      Detail rendition in X-ray images: theory and experi-  
mental results  
Medicamundi 11, 44–48 (1965)
- Albrecht, C.      Private communication, X-ray Development Department  
of Philips (1976)
- Bagrash, F.M.      Size-selective adaptation: psychophysical evidence for  
size-tuning and the effects of stimulus contour and  
adapting flux  
Vision Res. 13, 575–598 (1973)
- Barnes, Gary T.      The dependence of radiographic mottle on beam quality  
Am.J. Roentgenol. 127, 819–824 (1976)
- Beekmans, A.A.G.      Private communication, X-ray Development Department  
of Philips (1978)
- Berger, Alfred      Zum Problem der Bewegungsunschärfe im Röntgenbild  
der Lunge und des Herzens  
Rö.-Bl. 14, 369–379 (1961)  
Rö.-Bl. 16, 122–137 (1963)
- Blackwell, H.Richard      Contrast thresholds of the human eye  
J. Opt. Soc. Am. 36, 624–643 (1946)
- Blakemore, C.  
Campbell, F.W.      On the existence of neurones in the human visual system  
selectively sensitive to the orientation and size of retinal  
images  
J. Physiol. 203, 237–260 (1969)
- Blondel, A.  
Rey, J.      Sur la perception des lumières brèves à la limite de leur  
portée  
J. Phys. Théorie Appl., série 5 vol. 1, 530–551 (1911)
- Bouman, M.A.  
Koenderink, J.J.      Psychophysical basis of coincidence mechanisms in the  
human visual system  
Reviews of Physiology 65, 126–172 (1972)

- Bouwers, A. Ueber die Technik der Momentaufnahmen  
*Acta Radiologica* **12**, 175–183 (1931)
- Bouwers, A. Ueber moderne Aufnahmetechnik  
*Fortschr. Röntgenstr.* **50**, 588–596 (1934)
- Bouwers, A.  
Oosterkamp, W.J. Die Unschärfe einer Röntgenaufnahme  
*Fortschr. Röntgenstr.* **54**, 87–91 (1936)
- Boyd, D.P.  
Korobkin, M.T.  
Moss, A. Engineering status of computerized-tomography scanning  
*Spie* **96**, Optical Instrumentation in Medicine V,  
303–312 (1976)
- Breitmeyer, B.  
Julesz, B. The role of on and off transients in determining the  
psychophysical spatial frequency response  
*Vision Res.* **15**, 411–415 (1975)
- Brooks, Rodney A.  
Di Chiro, Giovanni Statistical limitations in X-ray reconstruction  
tomography  
*Med. Phys.* **3**, 237–240 (1976)
- Bronkhorst, Willem Kontrast und Schärfe im Röntgenbild  
Georg Thieme Verlag, Leipzig (1927)
- Burger, G.C.E.  
v. Dijk, B. Ueber die physiologischen Grundlagen der Durch-  
leuchtung  
*Fortschr. Röntgenstr.* **54**, 492–504 (1936)
- Burger, G.C.E.  
Combée, B.  
van der Tuuk, J.H. X-ray fluoroscopy with enlarged image  
*Philips Techn. Rev.* **11**, 321–329 (1946)
- Büchner, H. Direkte Röntgenvergrößerung und normale Aufnahme  
*Fortschr. Röntgenstr.* **80**, 71–87 (1954)
- Campbell, F.W.  
Green, D.G. Optical and retinal factors affecting visual resolution  
*J. Physiol.* **181**, 576–593 (1965)
- Campbell, F.W.  
Robson, J.G. Application of Fourier analysis to the visibility of  
gratings  
*J. Physiol.* **197**, 551–566 (1968)
- Campbell, F.W.  
Carpenter, R.H.S.  
Levinson, J.S. Visibility of aperiodic patterns compared with that of  
sinusoidal gratings  
*J. Physiol.* **204**, 283–298 (1969)

- Chantraine, H. Ueber den Verstärkungsschirm bei Lungenaufnahmen  
Fortschr. Röntgenstr. 42, 108–115 (1930)
- Chantraine, H. Ueber die Bedeutung von Schärfe und Kontrast für die  
Mindestdicke von erkennbaren Einzelheiten  
Fortschr. Röntgenstr. 47, 437–447 (1933a)
- Chantraine, H. Ueber die Unschärfe des Verstärkungsschirmes  
Fortschr. Röntgenstr. 48, 613–621 (1933b)
- Chérigüé, E. Die 70-mm-Aufnahme vom Bildverstärker und ihre  
Zukunftsaussichten  
Rö.-Bl. 25, 275–291 (1972)
- Chesters, M. Susan  
Hay, George A. The influence of visual noise on visual threshold  
detection  
Private communication (1977a)
- Chesters, M. Susan  
Hay, George A. The relation between signal area and threshold-limiting  
noise  
Private communication (1977b)
- Cobb, P.W.  
Moss, F.K. The four variables of visual threshold  
J. Frank. Inst. 205, 831–847 (1928)
- Cohn, Theodore E.  
Lasley, David J. Spatial summation of foveal increments and  
decrements  
Vision Res. 15, 389–399 (1975)
- Coltman, John W. Scintillation limitations to resolving power in imaging  
devices  
J. Opt. Soc. Am. 44, 234–237 (1954a)
- Coltman, John W. The specification of imaging properties by response to a  
sine-wave input  
J. Opt. Soc. Am. 44, 468–471 (1954b)
- Coltman, J.W.  
Anderson, A.E. Noise limitations to resolving power in electronic  
imaging  
Proc. IRE 48, 858–865 (1960)
- Connor, J. Preston  
Ganoung, Robert E. An experimental determination of the visual thresholds  
at low values of illumination  
J. Opt. Soc. Am. 25, 287–294 (1935)
- Cornsweet, T.N. Visual Perception  
Academic Press, New York (1970)

- De Palma, J.J.  
Lowry, E.M. Sine-wave response of the visual system. II.  
Sine-wave and square-wave contrast sensitivity  
*J. Opt. Soc. Am.* **52**, 328–335 (1962)
- Ditchburn, R.W. Eye-movements in relation to retinal action  
*Optica Acta* **1**, 171–176 (1955)
- Ditchburn, R.W.  
Fender, D.H. The stabilised retinal image  
*Optica Acta* **2**, 128–133 (1955)
- Doi, Kunio  
Sayanagi, Kazuo Role of optical transfer functions for optimum magnifi-  
cation in enlargement radiography  
*Japan. J. appl. Phys.* **9**, 834–839 (1970)
- Dünisch, O.  
Pfeiler, M.  
Kuhn, H. Probleme und Aspekte der radiologischen  
Vergrößerungstechnik  
*Electromedica* **3/71**, 114–119 (1971)
- Elmer, Richard A. 70 mm filming: Factors affecting image sharpness.  
*Radiology* **89**, 420–425 (1967)
- Evers, E.  
Schober, H. Ueber den Einfluss der Fokusgrösse auf die Detail-  
erkennbarkeit kleinster Objekte  
*Rö.-Bl.* **8**, 68–79 (1955)
- Evers, E.  
Schober, H. Ueber den Einfluss der Fokusgrösse auf die Detail-  
erkennbarkeit kleinerer Objekte  
*Rö.-Bl.* **9**, 313–318 (1956)
- Enroth-Cugell, C.  
Robson, J.G. The contrast-sensitivity of the retinal ganglion cells of  
the cat  
*J. Physiol.* **187**, 517–552 (1966)
- Feddema, J.  
Botden, P.J.M. Magnification techniques, especially geometric enlarge-  
ment  
*Diagnostic Radiologic Instrumentation*; Robert D.  
Moseley Jr., John H. Rust, ed.,  
Charles C. Tomas, Springfield (1965)
- Feddema, J.  
Recourt, A.  
Monté, G.L.A. Evaluation of image quality in various methods for the  
recording of movement phenomena  
*Medicamundi* **14**, 150–154 (1969)

- Feddema, A.G. Private communication, X-ray Application Department of Philips (1976)
- Feleus, R. Bildqualität bei 70 mm-Bildverstärkeraufnahmen  
Vijverberg, G. Rö.—Bl. 23, 125–129 (1970)
- Fenner, E. Der elektronenoptische Röntgenbildverstärker und seine  
Stahnke, I. Kennwerte  
Rö.—Bl. 19, 540–547 (1966)
- Fenner, E. Das Auftreten von Pseudoschärfe in der Zentralpro-  
Friedel, R. jection von Röntgenstrahlen  
Schnitger, H. Fortschr. Röntgenstr. 116, 696–701 (1972)
- Foley-Fisher, J.A. Contrast, edge-gradient and target line width as factors  
in vernier acuity  
Optica Acta 24, 179–186 (1977)
- Franken, A. Private communication, Philips Research Laboratories  
v.d.Linden, P.W. (1973a)  
Scheren, W.J.L.
- Franken, A. Private communication, Philips Research Laboratories  
v.d.Linden, P. (1973b)  
Scheren, W.
- Franken, A.A.J. Private communication, Philips Research Laboratories  
v.d.Linden, P.W. (1973c)  
Scheren, W.J.
- Franken, A.A.J. Private communication, Philips Research Laboratories  
v.d.Linden, P.W. (1973d)  
Scheren, W.J.
- Franken, A.A.J. Private communication, X-ray Application Department  
Hellekamp, J.C. of Philips (1975)  
Marquerinck, J.E.
- Gajewski, H. Optimierung der Aufnahmebedingungen an Magen-  
Kuhn, H. Untersuchungsgeräten  
Rö.—Bl. 23, 298–309 (1970)
- Gajewski, H. Computer-aided optimization of radiographic conditions  
Kuhn, H. Acta radiol. Diagnosis 12, 506–512 (1972)
- Gelade, G.A. The pooling of excitation in threshold bar stimuli  
Poole, C.L. Vision Res. 14, 317–327 (1974)  
Beurle, R.L.

- Graham, C.H.  
Brown, R.H.  
Mote, F.A.      The relation of size of stimulus and intensity in the human eye: I. Intensity thresholds for white light  
*J. Exp. Psychol.* **24**, 555–573 (1939)
- Growney, Ronald      The function of contour in metacontrast  
*Vision Res.* **16**, 253–261 (1976)
- Haendle, J.  
Horbaschek, H.      Die hochauflösende Röntgenfernsehkette  
*Röntgenpraxis* **29**, 95–108 (1976)
- Hale, John  
Mishkin, Mark M.      Serial direct magnification cerebral angiography  
*Am. J. Roentgenol., Rad. Therapy & Nuclear Med.* **107**, 616–621 (1969)
- Harms, A.A.  
Zeilinger, A.      A new formulation of total unsharpness in radiography  
*Phys. Med. Biol.* **22**, 70–80 (1977)
- Hartline, H.K.      The nerve messages in the fibers of the visual pathway  
*J. Opt. Soc. Am.* **30**, 239–247 (1940)
- Hay, George A.      Private communication (1976)
- Hay, George A.  
Chesters, Susan M.      A model of visual threshold detection  
*J. theor. Biol.* **67**, 221–240 (1977)
- Heckenmueller, E.G.      Stabilisation of the retinal image: a review of method, effects and theory  
*Physiological Bulletin* **63**, 157–169 (1965)
- Hemmingsson, Anders  
Jung, Bo  
Lönnerholm, Torsten      Perception of simulated lesions in the lung  
*Acta radiol. Diagnosis* **16**, 494–502 (1975)
- Higgins, G.C.  
Jones, L.A.      The nature and evaluation of the sharpness of photographic images  
*J. SMPTE* **58**, 277–290 (1952)
- Hoekstra, J.  
van der Goot, D.J.  
van den Brink, G.  
van Bilsen, F.A.      The influence of the number of cycles upon the visual contrast threshold for spatial sine wave patterns  
*Vision Res.* **14**, 365–368 (1974)
- Hollander, Bentley A.  
Hilal, Sadek K.  
Seaman, William B.      Evaluation of a radiographic imaging system with a microfocal spot X-ray tube  
*Radiology* **103**, 667–674 (1972)

- Hondius Boldingh, W.      Grids to reduce scattered X-rays in medical radiographs  
Thesis, Eindhoven University of Technology (1964)
- Hubel, D.H.  
Wiesel, T.N.      Receptive fields, binocular interaction and functional  
architecture in the cat's visual cortex  
*J. Physiol.* **160**, 106–155 (1962)
- Jacobi, W.      Veränderungen und neue Erkenntnisse in der Abschätzung  
des somatischen Strahlenrisikos  
*Fortschr. Röntgenstr.* **124**, 489–492 (1976)
- Johnson, C.B.      Point-spread functions, line-spread functions, and edge-  
response functions associated with MTFs of the form  
 $\exp [-\omega/\omega_c]^n$   
*Applied Optics* **12**, 1031–1033 (1973)
- Jones, Loyd A.  
Higgins, George C.      Photographic granularity and graininess. III.  
*J. Opt. Soc. Am.* **37**, 217–263 (1947)
- Kelly, D.H.      Visual response to time-dependent stimuli. I. Amplitude  
sensitivity measurements  
*J. Opt. Soc. Am.* **51**, 422–429 (1961)
- Kelly, D.H.      Flickering patterns and lateral inhibition  
*J. Opt. Soc. Am.* **59**, 1361–1370 (1969)
- Kelly, D.H.      Visual contrast sensitivity  
*Optica Acta* **24**, 107–129 (1977)
- Kincaid, W.M.  
Blackwell, H.R.  
Kristofferson, A.B.      Neural formulation of the effects of target size and  
shape upon visual detection  
*J. Opt. Soc. Am.* **50**, 143–148 (1960)
- Klasens, H.A.      Measurement and calculation of unsharpness combina-  
tions in X-ray photography  
*Philips Res. Rep.* **1**, 241–249 (1946)
- Knibbe, G.      Private communication, X-ray Systems Engineering  
Department of Philips (1976)
- Kruithof, A.M.      Perception of contrasts when the contours of details are  
blurred  
*Philips Techn. Rev.* **11**, 333–339 (1950)

- Kühl, W. Considerations on image quality, especially in image intensifier systems  
*Medicamundi* 10, 108–111 (1964/65)
- Kühl, W. Information transfer with image intensifier systems  
*Diagnostic Radiologic Instrumentation*; Robert D. Moseley Jr., John H. Rust, ed., Charles C. Tomas, Springfield (1965)
- Kulikowski, J.J. Some stimulus parameters affecting spatial and temporal resolution of human vision  
*Vision Res.* 11, 83–93 (1971a)
- Kulikowski, J.J. Effect of eye-movements on the contrast sensitivity of spatio-temporal patterns  
*Vision Res.* 11, 261–273 (1971b)
- Kulikowski, J.J.  
Tolhurst, D.J. Psychophysical evidence for sustained and transient detectors in human vision  
*J. Physiol.* 232, 149–162 (1973)
- Kulikowski, J.J.  
King-Smith, P.E. Spatial arrangement of line, edge and grating detectors revealed by subthreshold summation  
*Vision Res.* 13, 1455–1478 (1973)
- Lale, P.G. The examination of internal tissues, using gamma-ray scatter with a possible extension to megavoltage radiography  
*Physics Med. Biol.* 4, 159–167 (1959)
- Langmuir, I.  
Westendorp, W.F. A study of light signals in aviation and navigation  
*Physics* 1, 273–316 (1931)
- Lamar, Edward S.  
Hecht, Selig  
Shlaer, Simon  
Hendly, Charles D. Size, shape and contrast in detection of targets by daylight vision. I. Data and analytical description  
*J. Opt. Soc. Am.* 37, 531–545 (1947)
- Lantz, B.  
Strid, K.-G. Contrast formation in fluoroscopic videodensitometry  
*Acta radiol. Diagnosis* 14, 625–637 (1973)
- v. Leunen, J.A.J.  
Pennings, J.C. Private communication, Elcoma Division of Philips (1973)



- Levinson, L. Nonlinear and spatial effects in the perception of flicker  
Doc. Ophthalmol. 18, 36–55 (1964)
- Marschall, D. Private communication, C.H.F. Müller GmbH (1973)  
Möller, A.
- Marschall, D. Private communication, C.H.F. Müller GmbH (1973)
- McCann, J.J. Visibility of continuous luminous gradients  
Savoy, R.L. Vision Res. 14, 917–927 (1974)  
Hall, jr., J.A.  
Scarpetti, J.J.
- McCullough, Edwin C. Performance evaluation and quality assurance of  
Payne, J. Thomas computed tomography scanners, with illustrations from  
Baker, Hillier L. the EMI, ACTA, and Delta scanners  
Hattery, Robert R. Radiology 120, 173–188 (1976)  
Sheedy, Patrick F.  
Stephens, David H.  
Gedgaudus, Eugene
- McCullough, Edwin C. Exposure rate from diagnostic X-ray units  
Cameron, John R. Brit. J. Rad. 43, 448–451 (1970)
- van Meeteren, A. Resolution and contrast sensitivity at low luminances  
Vos, J.J. Vision Res. 12, 825–833 (1972)
- van Meeteren, A. Visual aspects of image intensification  
Institute of Perception TNO, Soesterberg, The Netherlands (1973)
- van Meeteren, A. Calculations on the optical modulation transfer function  
of the human eye for white light  
Optica Acta 21, 395–412 (1974)
- Meiler, J. Die Zusammensetzung der verschiedenen Unschärfefaktoren zur Gesamtunschärfe im Röntgenbild  
Fortschr. Röntgenstr. 82, 107–117 (1955)
- Meiler, Joseph Ueber die Bildunschärfe bei der Lungenaufnahme  
Rö.-Bl. 16, 161–171 (1963)
- Middleton, W.E. Knowles Photometric discrimination with a diffuse boundary  
J. Opt. Soc. Am. 27, 112–116 (1937)

- Möller, A. Private communication, C.H.F. Müller GmbH (1973)
- Morgan, Russel H. An analysis of the physical factors controlling the diagnostic quality of roentgen images  
Am.J. Roentgenol. & Rad. Therapy **62**, 870–880 (1949)
- Morgan, Russel H. The frequency response characteristics of X-ray films and screens  
Bates, Lloyd M. Am. J. Roentgenol., Rad. Therapy & Nuclear Med. **92**, 426–440 (1964)  
Gopalarao, U.V.  
Marinaro, Alex
- Morgan, Russel H. Threshold visual perception and its relation to photon fluctuation and sine wave response  
Am. J. Roentgenol., Rad. Therapy & Nuclear Med. **93**, 982–997 (1965)
- Morgan, Russel H. Noise contrast in diagnostic radiologic systems  
Television in Diagnostic Radiology, Robert D. Moseley, Joh. H. Rust, ed., Aesculapius Publishing Company, Birmingham, USA (1969)
- Nachmias, J. Effect of exposure duration on visual contrast sensitivity with square-wave gratings  
J. Opt. Soc. Am. **57**, 421–427 (1967)
- Nachmias, J. Visual resolution of two-bar patterns and square-wave gratings  
J. Opt. Soc. Am. **58**, 9–13 (1968)
- Nemet, A. Blurring in radiography  
Cox, W.F. Brit. J. Rad. **19**, 257–271 (1946)  
Walker, C.B.
- Nemet, A. The contrast problem in high kilovoltage medical radiography  
Cox, W.F. Brit. J. Rad. **26**, 185–192 (1953)  
Hills, T.H.
- van Nes, F.L. Spatial modulation transfer in the human eye  
Bouman, M.A. J. Opt. Soc. Am. **57**, 401–406 (1967)
- Newell, R.R. Sharpness of shadows in radiography of the lungs  
Radiology **30**, 493–499 (1938)

- Newell, R.R.  
Garneau, R.      The threshold visibility of pulmonary shadows  
Radiology 56, 409–415 (1951)
- Nitka, H.      Die Messung der Zeichenschärfe von Verstärkerfolien  
Physikalische Zeitschrift 39, 436–439 (1938)
- O'Brien, Vivian      Contour perception, illusion and reality  
J. Opt. Soc. Am. 48, 112–119 (1958)
- Ommaya, A.K.  
Murray, G.  
Ambrose, J.  
Richardson, A.  
Hounsfield, G.      Computerized axial tomography: estimation of spatial  
and density resolution capacity  
Brit. J. Rad. 49, 604–611 (1976)
- Oosterkamp, W.J.      Problemen bij de constructie van technische röntgen-  
buizen  
Thesis (in Dutch), Delft University of Technology (1939)
- Oosterkamp, W.J.  
Albrecht, C.      Methods of evaluating the new instrumental systems for  
diagnostic radiology  
Medicamundi 5, 73–79 (1959)
- Oosterkamp, W.J.      Monochromatic X-rays for medical fluoroscopy and  
radiography?  
Medicamundi 7, 68–77 (1961)
- Oosterkamp, W.J.      New concepts and progress in instrumentation for cine-  
and video-radiology  
Medicamundi 19, 79–84 (1974)
- Oosterkamp, W.J.      Benefit/risk comparison in diagnostic radiology  
Medicamundi 21, 1–6 (1976)
- Papoulis, A.      Probability, Random Variables and Stochastic Processes  
McGraw-Hill, New York (1965)
- Papoulis, A.      Systems and Transforms with Applications in Optics  
McGraw-Hill, New York (1968)
- Patel, A.S.      Spatial resolution by the human visual system. The  
effect of mean retinal illuminance  
J. Opt. Soc. Am. 56, 689–694 (1966)

- Pfeiler, M.  
Linke, G.                      Bessere Indirektaufnahmen durch hochauflösende  
Röntgenbildverstärker  
Electromedica 4/72, 136–144 (1972)
- v.d. Plaats, G.J.              Prinzipien, Technik und medizinische Anwendungen  
der radiologischen Vergrößerungstechnik  
Fortschr. Röntgenstr. 77, 605–610 (1952)
- Pollehn, H.  
Roehrig, H.                    Effect of noise on the modulation transfer function of  
the visual channel  
J. Opt. Soc. Am. 60, 824–848 (1970)
- Proper, J.                      Private communication, X-ray Development Department  
of Philips (1975)
- Rao, Gopala U.V.  
Bates, Lloyd M.                Effective dimensions of roentgen tube focal spots based  
on measurement of the modulation transfer function  
Acta radiol. Ther. Phys. Biol. 9, 362–368 (1970)
- Rao, Gopala U.V.  
Clark, Richard L.  
Gayler, Bob W.                Radiographic magnification: a critical, theoretical and  
practical analysis  
Part I: Applied Radiology, January/February, 37–40  
(1973)  
Part II: id. March/April, 25–33 (1973)
- Rao, Gopala U.V.  
Fatouros, Panos                The relation between resolution and speed of x-ray  
intensifying screens  
Med. Phys. 5, 205–208 (1978)
- Recommendations of the International Commission on Radiological Protection;  
ICRP Publication 26, Pergamon Press, Oxford/New York/Frankfurt (1977)
- Reichmann, Sven              Efficiency of intensifying screens  
Acta radiol. Diagnosis 15, 295–304 (1974)
- Riggs, Lorrin A.  
Armington, John C.  
Ratliff, Floyd                Motions of the retinal image during fixation  
J. Opt. Soc. Am. 44, 315–321 (1954)
- Robson, J.G.                    Spatial and temporal contrast-sensitivity functions of the  
visual system  
J. Opt. Soc. Am. 56, 1141–1142 (1966)

- Rose, A. The sensitivity performance of the eye on an absolute scale  
J. Opt. Soc. Am. 38, 196–208 (1948)
- Rosenbruch, K.-J. Die Kontrastempfindlichkeit des Auges als Beitrag zur Frage der Gütebewertung optischer Bilder  
Optik 16, 135–145 (1959)
- Rossmann, K.  
Seemann, H.E. Detail visibility in radiographs: theoretical study of the effects of X-ray absorption in the object on the edge unsharpness of radiographic images  
Am. J. Roentgenol., Rad. Therapy & Nuclear Med. 85, 336–371 (1961)
- Rowley, K.A. Patient exposure in cardiac catheterization and cine-fluorography using the Eclair 16 mm camera at speeds up to 200 frames per second  
Brit. J. Rad. 47, 169–178 (1974)
- Sachs, M.B.  
Nachmias, J.  
Robson, J.G. Spatial-frequency channels in human vision  
J. Opt. Soc. Am. 61, 1176–1186 (1971)
- Schade, O.H. A new system of measuring and specifying image definition  
Nat. Bur. Standards (U.S.), Circ. 526, April 29 (1954)
- Schade, sr., Otto H. An evaluation of photographic image quality and resolving power  
J. SMPTE 73, 81–119 (1964)
- Schober, H. Die klinische Bedeutung der Feinstfokusröhre  
Rö.-Bl. 6, 101–113 (1953)
- Schröder, J. Private communication, Philips Research Laboratories (1976)
- Seemann, Herman E. Secondary radiation as a function of certain geometrical variables  
Am. J. Roentgenol. & Rad. Therapy 39, 628–633 (1938)

- Shapley, Robert      Gaussian bars and rectangular bars: the influence of width and gradient on visibility  
Vision Res. 14, 1457–1462 (1974)
- Spiegler, P.  
Norman, A.      The total unsharpness in radiography  
Phys. Med. Biol. 18, 884–887 (1973)
- Stargardt, A.  
Angerstein, W.      Der optimale Abbildungsmaßstab bei der direkten Röntgenvergrößerung  
Fortschr. Röntgenstr. 123, 73–78 (1975)
- Stevens, A.L.N.      New phosphors for X-ray screens  
Medicamundi 20, 12–22 (1975)
- Steinman, Robert M.  
Haddad, Genevieve M.  
Skavenski, Alexander A.  
Wyman, Diane      Miniature eye movement  
Science 181, 810–819 (1973)
- Stieve, F.E.      Methoden und Ergebnisse moderner Durchleuchtungstechnik  
Rö.-Bl. 18, 457–471 (1965)
- Stieve, F.E.      Medizinisch notwendige Bildqualität im Verhältnis zur Strahlenbelastung  
Rö.-Bl. 20, 545–566 (1967)
- Stieve, F.E.      Das Aufnahmesystem vom Ausgangsschirm des Bildverstärkers  
Rö.-Bl. 25, 244–274 (1972)
- Sturm, Ralph E.  
Morgan, Russel H.      Screen intensification systems and their limitations  
Am. J. Roentgenol. & Rad. Therapy 62, 617–634 (1949)
- Ter-Pogossian, Michel      Monochromatic roentgen rays in contrast media roentgenography  
Acta Radiologica 45, 313–321 (1956)
- Thomas, James P.  
Rourke, Daniel L.  
Wilder, Dennis G.      Inhibitory effects of less intense stimuli upon the increment threshold for a narrow test line  
Vision Res. 8, 537–542 (1968)
- Thomas, J.P.      Model of the function of receptive fields in human vision  
Psychol. Rev. 77, 121–134 (1970)

- Timmer, F. Private communication, X-ray Development Department of Philips (1972)
- Timmer, F. Private communication, X-ray Development Department of Philips (1973)
- Tol, T.  
Oosterkamp, W.J.  
Proper, J. Limits of detail perceptibility in radiology particularly when using the image intensifier  
Philips Res. Rep. **10**, 141–157 (1955)
- Tolhurst, D.J. On the possible existence of edge detector neurones in the human visual system  
Vision Res. **12**, 797–804 (1972)
- Tolhurst, D.J. Separate channels for the analysis of the shape and the movement of a moving visual stimulus  
J. Physiol. **231**, 385–402 (1973)
- Tuddenham, William J. The visual physiology of roentgendiagnosis. A. Basic concepts  
Am. J. Roentgenol., Rad. Therapy & Nuclear Med. **78**, 116–123 (1957)
- v.d. Tuuk, J.H. The 'Rotalix' tube for X-ray diagnosis  
Philips Techn. Review **3**, 292–298 (1938)
- Tynan, P.  
Sekuler, R. Perceived spatial frequency varies with stimulus duration  
J. Opt. Soc. Am. **64**, 1251–1255 (1974)
- de Vries, H.L. The quantum character of light and its bearing upon threshold of vision, the differential sensitivity and visual acuity of the eye  
Physica **10**, 553–564 (1943)
- Wagner, Robert F.  
Weaver, Kenneth E.  
Denny, Earl W.  
Bostrom, Robert G. Toward a unified view of radiological imaging systems  
Medical Physics **1**, 11–24 (1974)
- Wagner, Robert F.  
Weaver, Kenneth E. Prospects for X-ray exposure reduction using rare earth intensifying screens  
Radiology **118**, 183–188 (1976)

- Warren S. Reid      Roentgenographic unsharpness of the shadow of a moving object  
Radiology 28, 450–456 (1937)
- Warren, S. Reid      Roentgenographic unsharpness of the shadow of a moving object. II.  
Radiology 34, 731–740 (1940)
- Werner, Heinz      Studies on contour: I. Qualitative analysis  
Am. J. Psychol. 47, 40–46 (1935)
- Westheimer, G.      Modulation thresholds for sinusoidal light distribution on the retina  
J. Physiol. 152, 67–74 (1960)
- Wilsey, R.W.      The physical foundations of chest roentgenography. Part III. The dependence of sharpness upon movement of lung tissues and size of focal spot  
Am. J. Roentgenol. & Rad. Therapy 30, 388–400 (1933)
- Yarbush, A.L.      Eye-movement and Vision  
Plenum Press, New York (1967)
- Zieler, E.      Untersuchungen zur Bestimmung der Integraldosis in der Röntgendiagnostik  
Fortschr. Röntgenstr. 94, 248–260 (1961)
- Zimmer, E.A.      Methodische Bemerkungen und Leitsätze zur direkten Röntgenvergrößerung  
Fortschr. Röntgenstr. 75, 292–302 (1952)
- Zuber, B.L.  
Stark, L.      Microsaccades and the velocity-amplitude relationship for saccadic eye movements  
Science 150, 1459–1460 (1965)



## LIST OF SYMBOLS

In medical X-ray systems many different image planes and components exist. To obtain a consistent and comprehensible set of parameters, many parameters are specified by a superscript and a subscript, as follows:

symbol<sup>a<sub>1</sub></sup><sub>a<sub>2</sub></sub>

The most important symbols are:

- b : balance factor
- c : characteristic parameter
- C : contrast
- ESF : edge spread function
- L : luminance
- M : magnification factor
- MTF : modulation transfer function
- u : unsharpness
- $\Delta L$  : luminance increment
- $\eta$  : object position
- $\nu$  : spatial frequency

The symbol a<sub>1</sub> denotes the reference plane. Its abbreviations and meanings are:

- f : focal-spot plane
- i : receptor output ('i' stands for 'image') plane
- o : object plane
- r : receptor input plane
- v : visual system plane

The symbol a<sub>2</sub> denotes the component. The following parameters can be used:

- a : shadow image
- d : image detector (visual system + image receptor)
- f : focal spot
- m : movement
- p : patient
- r : image receptor
- s : X-ray system + visual system
- v : visual system
- x : X-ray system (i.e. no visual system)

Sy 2

In the listing below, in principle only the name of the symbol proper will be given. If appropriate, the meaning for different  $a_1$  and  $a_2$  values will also be given.

An extra indication for a parameter situation is sometimes needed. This is given by adding a vertical dash and writing the condition to the right of it as follows:

symbol  $\overset{a_1}{a_2} | a_3$

For  $a_3$ , 'opt' denotes the optimum situation. The maximum value is denoted by 'max'.

Often the spatial frequency  $\nu$  corresponding to a particular modulation transfer  $z$  must be indicated. This is done by means of the symbol

$\overset{a_1}{\nu} \underset{a_2, z = a_4}$

where  $a_4$  is a number between zero and unity.

To distinguish moving object imaging from stationary object imaging, the abbreviations 'm' and 'st' are added behind the  $a_2$  position, as follows:

symbol  $\underset{a_2, m}{a_2}$  or symbol  $\underset{a_2, st}{a_2}$

Symbol	Meaning	Unit
$a$	relative intensity of scattered radiation ( $a = I_s'/I_p$ )	—
$A_{eq}$	noise-equivalent aperture	$mm^2$ , degree <sup>2</sup>
$b_a$	balance factor for $MTF_m$ and $MTF_f$ ( $b_a = \nu_{m,z=0.5}/\nu_{f,z=0.5}$ )	—
$b_d$	balance factor for $MTF_r$ and $MTF_v$ ( $b_d = \nu_{r,z=0.5}/\nu_{v,z=0.5}$ )	—
$b_f$	ratio between actual and optimum or initial focal-spot size	—
$b_s$	balance factor for $MTF_a$ and $MTF_d$ ( $b_s = \nu_{a,z=0.5}/\nu_{d,z=0.5}$ )	—

Symbol	Meaning	Unit
$b_x$	balance factor for $MTF_a$ and $MTF_r$ ( $b_x = \nu_{a,z=0.5}/\nu_{r,z=0.5}$ )	—
B	Bucky factor	—
$c_{a,m}$ $c_{a,st}$	{ absorption image characteristic parameter ( $c_a = c_p/c_f$ )	$mm^{1/2}$ $mm^{-1/2}$
$c_f$	X-ray tube characteristic parameter	$kW \cdot mm^{-3/2}$
$c_{p,m}$ $c_{p,st}$	{ patient characteristic parameter	$kW \cdot mm^{-1}$ $kW \cdot mm^{-2}$
$c_{s,m}$ $c_{s,st}$	{ total system characteristic parameter	— —
$c_{th}$	anode material characteristic parameter	$kW \cdot s \cdot mm^{-2}$
$c_{x,m}$ $c_{x,st}$	{ X-ray system characteristic parameter	— —
C	contrast	—
$C_a$	shadow-image or absorption contrast	—
$C_1$	contrast of the primary light image made by the image receptor input screen; influence of scattered radiation included	—
$C_l(x)$ , $C_l(r)$	primary light-image contrast distribution	—
$C_o$	object contrast; see $C_l$ , however without the scattered radiation influence; corresponds to $C_a$ , convoluted with the spectral response of the image receptor input screen	—
$C_s(x)$ , $C_s(r)$	visual system output contrast distribution	—
$C_T$	visual threshold contrast	—

# Sy 4

Symbol	Meaning	Unit
$C_X(x)$ , $C_X(r)$	X-ray system output contrast distribution	—
d	1. short side of a rectangular aperture 2. thickness of an object in the direction of the X-ray beam	mm, degree mm
$d_{eq}$	noise-equivalent width	mm, degree
D	film density	—
ESF	edge spread function	—
f	effective focal-spot size	mm
$f'$	nominal focal-spot size	mm
$f_{opt}$	optimum focal-spot size, effective value	mm
$f'_{opt}$	optimum focal-spot size, nominal value	mm
$f(z)$	scaling factor	—
$f_r$	focal spot-to-image receptor distance	mm
$f_{rp}$	$f_r$ for the patient reference data	mm
FSF	flicker sensitivity function	—
FWHM	full width at half maximum (e.g. of PSF or LSF)	mm, degree
h	1. parameter of the visual system MTF 2. slice thickness in CT imaging	— mm
$i_b$	beam current	mA
$i_n$	noise current	mA
$i_s$	signal current	mA
$I(r)$	intensity distribution	—

Symbol	Meaning	Unit
$I_p$	luminance of the image receptor response corresponding to the primary X-ray radiation, no geometric magnification	$\text{cd}\cdot\text{m}^{-2}$
$I'_p$	like $I_p$ , but geometric magnification applied	$\text{cd}\cdot\text{m}^{-2}$
$I_s$	like $I_p$ , but corresponding to the scattered X-ray radiation	$\text{cd}\cdot\text{m}^{-2}$
$I'_s$	like $I_s$ , but geometric magnification applied	$\text{cd}\cdot\text{m}^{-2}$
$J_0(x)$ , $J_1(x)$	Bessel functions	
$K$	contrast improvement factor	—
$l$	length of bar	mm, degree
$L$	(background) luminance	$\text{cd}\cdot\text{m}^{-2}$
$L_{\text{amb}}$	luminance of ambient surfaces	$\text{cd}\cdot\text{m}^{-2}$
$L_{\text{mon}}$	monitor luminance	$\text{cd}\cdot\text{m}^{-2}$
$L_s(r)$	visual system output luminance distribution	$\text{cd}\cdot\text{m}^{-2}$
LSF	line spread function	—
$M$	magnification factor	—
$M_a$	angular magnification factor	$\text{degree}\cdot\text{mm}^{-1}$
$M_g$	geometric magnification factor ( $M_g = 1/(1 - \eta)$ )	—
$M_o$	optical magnification factor	—
$M_r$	image receptor magnification factor	—
MTF	modulation transfer function	—

Symbol	Meaning	Unit
$MTF_a$	absorption image MTF ( $MTF_a = MTF_f$ for static objects, and $MTF_f \cdot MTF_m$ for moving objects)	—
$MTF_d$	image detector MTF ( $MTF_d = MTF_r \cdot MTF_v$ )	—
$MTF_f$	focal-spot MTF	—
$MTF_m$	movement MTF	—
$MTF_r$	image receptor MTF	—
$MTF_s$	total system MTF ( $MTF_s = MTF_x \cdot MTF_v$ )	—
$MTF_v$	visual system MTF	—
$MTF_x$	X-ray system MTF ( $MTF_x = MTF_a \cdot MTF_r$ )	—
$n$	1. frequency of rotation of the anode 2. number of photons	$c \cdot s^{-1}$ —
or	object-to-image receptor distance	mm
os	object to skin distance	mm
OTF	optical transfer function	—
p	tube high voltage p-factor (sec. 4.2.4)	—
P	short-time (0.1 s) X-ray tube loadability	kW
$P_{opt}$	optimum value of P	kW
PSF	point spread function	—
Q	product of X-ray tube current and exposure time	$mA \cdot s$
$Q_p$	Q for patient reference data	$mA \cdot s$
r	radius	mm, degree
$\bar{r}$	mean focal track radius	mm

Symbol	Meaning	Unit
R	spatial frequency which corresponds to the modulation transfer of 1 per cent	$\text{c}\cdot\text{mm}^{-1}$ , $\text{c}\cdot\text{degree}^{-1}$
s	1. optical source width or diameter 2. relative sensitivity of an image receptor	degree —
SGSF	spatial grating sensitivity function	—
t	(exposure) time	s
$t_i$	integration time of the visual system	s
$t_p$	permissible exposure time for the imaging of stationary objects	s
u	unsharpness	mm
$u_f$	unsharpness in the object plane due to the X-ray focal spot	mm
$u_m$	translation of the object	mm
$u_r$	unsharpness in the image receptor input plane due to the X-ray focal spot	mm
$u_t$	total unsharpness of the X-ray system	mm
U	X-ray tube high voltage	kV
$U_p$	U for the patient reference data	kV
v	object velocity	$\text{mm}\cdot\text{s}^{-1}$
$v_d$	drift velocity of a grating	$\text{c}\cdot\text{s}^{-1}$
$v_v$	angular velocity of the eye	$\text{degree}\cdot\text{s}^{-1}$
vd	viewing distance	mm
$V_L$	lamp voltage	V
w	pixel width in CT imaging	mm

Symbol	Meaning	Unit
$x$	abscissa value	mm, degree
$\dot{X}$	X-ray exposure rate	$\mu R \cdot s^{-1}$
$z$	modulation transfer ratio	—
$\alpha$	anode angle	degree
$\beta$ $\beta^*$	$\left\{ \begin{array}{l} \text{parameter of the visual system} \\ \text{MTF} \end{array} \right.$	degree mm
$\gamma$	1. gamma (according to the general definition $I_{out} = I_{in}\gamma$ ) 2. parameter of the visual system MTF (eq. 2.2.1.1) 3. weight for the influence of a $b_s$ or $b_x$ variation on the $MTF_s$ or $MTF_x$ quality (sec. 5.2.1.4.2)	— — —
$\gamma_c$	gamma for the intensifying-screen image contrast as a function of the tube high voltage ( $C_0 \sim U^{\gamma_c}$ )	—
$\gamma_x$	gamma of the fluoroscopic system ( $L_{mon} = \dot{X}\gamma_x$ )	—
$\Delta$	object size (diameter of disk, width of bar or blood-vessel)	mm, degree
$\Delta_i$	width of disk or bar at the intersection of the asymptotes of the C- $\Delta$ curve	mm, degree
$\Delta I_p$	variation of $I_p$	$cd \cdot m^{-2}$
$\Delta L$	luminance variation	$cd \cdot m^{-2}$
$\Delta u$	unsharpness variation	mm, degree
$\Delta \eta$	variation of $\eta$	—
$\Delta \nu$	variation of $\nu_{x,z=0.25}^0$	$c \cdot mm^{-1}$ , $c \cdot degree^{-1}$



Symbol	Meaning	Unit
$\eta$	position of the object ( $\eta = \text{or/fr}$ )	—
$\eta_{\text{eq}}$	object position for the equality of the image receptor and shadow image LSF; moving objects only	—
$\eta_{\text{s,m}}$ $\eta_{\text{s,st}}$	{ object position for equality of MTF <sub>a</sub> and MTF <sub>d</sub>	— —
$\eta_{\text{x,m}}$ $\eta_{\text{x,st}}$	{ object position for equality of MTF <sub>a</sub> and MTF <sub>r</sub>	— —
$\mu$	linear attenuation coefficient	$\text{mm}^{-1}$
$\nu$	spatial frequency	$\text{c} \cdot \text{mm}^{-1}$ , $\text{c} \cdot \text{degree}^{-1}$
$\nu_{a_1}$ $\nu_{a_2,z}$	spatial frequency in $a_1$ plane for which the MTF of component $a_2$ has the value $z$	$\text{c} \cdot \text{mm}^{-1}$ , $\text{c} \cdot \text{degree}^{-1}$
$\nu_{\text{opt}}$ $\nu_{a,z \text{opt}}$	optimum shadow image MTF spatial frequency	$\text{c} \cdot \text{mm}^{-1}$ , $\text{c} \cdot \text{degree}^{-1}$
$\nu_{\text{rec}}$	intrinsic resolution of the image receptor ( $\nu_{\text{rec}} = \nu_{f,z=0.5}$ )	$\text{c} \cdot \text{mm}^{-1}$
$\nu_{d,z=0.5}^{\text{r}}$	intrinsic resolution of the image detector (i.e. image receptor + visual system). For convenience the superscript 'r' is omitted in the text	$\text{c} \cdot \text{mm}^{-1}$
$\nu_{s,z=0.25}^{\text{r}}$	characteristic frequency for the visual resolution. For convenience the superscript 'r' is omitted in the text	$\text{c} \cdot \text{mm}^{-1}$
$\nu_{v,z=0.5}$	characteristic frequency for the visual system MTF	$\text{c} \cdot \text{mm}^{-1}$ , $\text{c} \cdot \text{degree}^{-1}$
$\nu_{x,z=0.25}^{\text{o}}$	characteristic frequency for the object resolution. For convenience the superscript 'o' is omitted in the text	$\text{c} \cdot \text{mm}^{-1}$

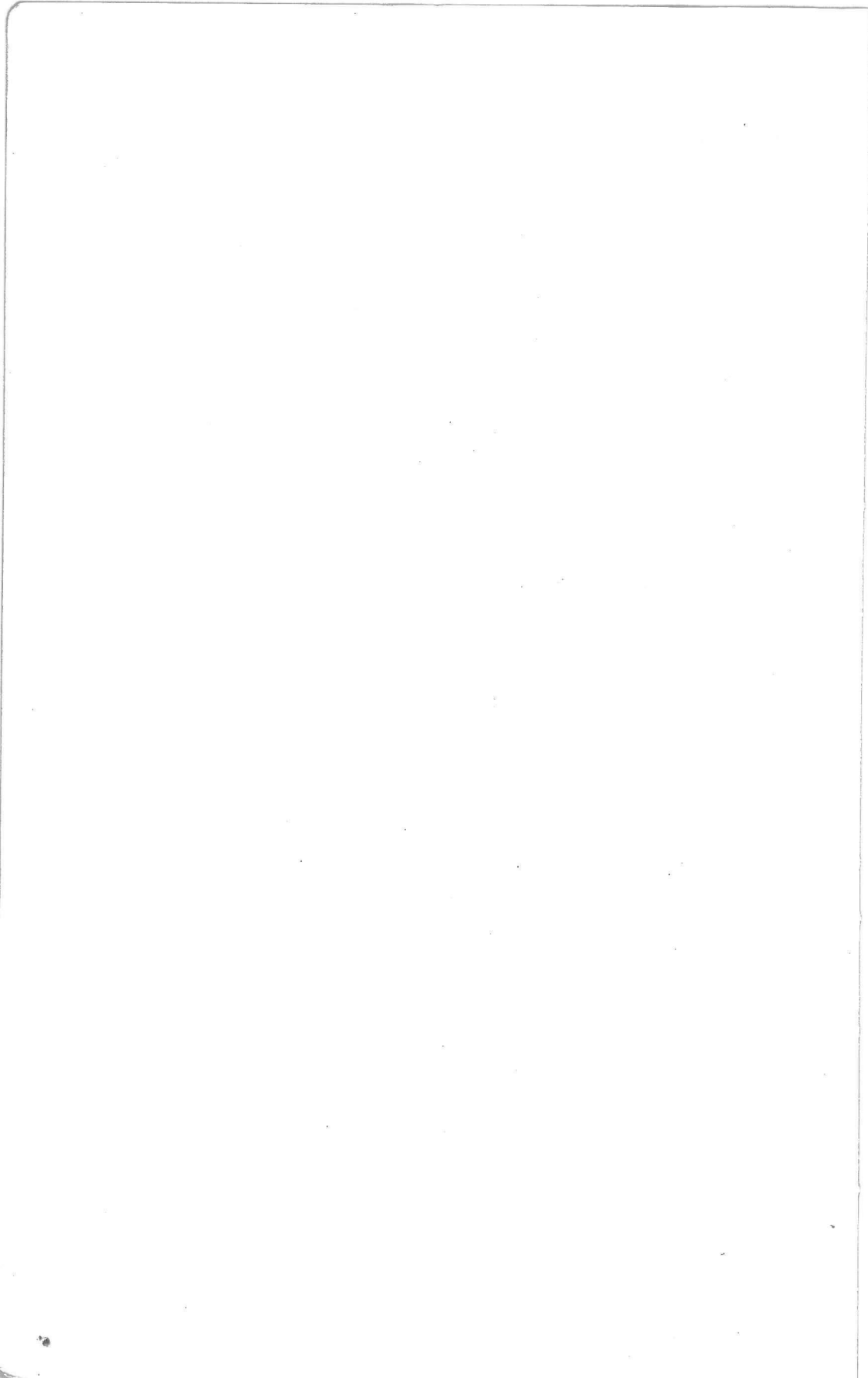
Sy 10

Symbol	Meaning	Unit
$\sigma$	X-ray absorption efficiency of the image receptor	—
$\sigma(\mu)$	standard deviation of the CT-reconstructed attenuation value	$\text{mm}^{-1}$
$\Sigma$	selectivity for the reduction of the scattered radiation intensity	—
$\tau$	RC time constant	s
$\varphi(\nu)$	phase transfer function	—
$\Psi$	diameter of a disk in units of the FWHM of the PSF of the imaging system	—

## CURRICULUM VITAE

- Nov. 1946      born in Den Helder, the Netherlands
- July 1964      certificate of Secondary School
- Jan. 1970      ir-degree in applied physics of the Delft University of Technology;  
thesis work in reactorphysics under the guidance of prof.dr. J.J.Went  
and dr. ir. H. van Dam
- 1970 – 1971    military service
- Sept. 1971     research and development scientist with N.V. Philips' Gloeilampen-  
fabrieken at Eindhoven, the Netherlands
- 1971 – 1973    systems engineer at the X-ray department of the Medical Systems  
Division, in the group of mr. G. Smeenk
- 1973 – 1977    medical X-ray and visual perception research at the Natuurkundig  
Laboratorium, under the guidance of prof. dr. J. Volger and dr. ir.  
W.J. Oosterkamp; the thesis is based on this work.
- 1978 –          research on medical applications of ultrasound at the Laboratoires  
d'Electronique et de Physique appliquée, Paris.

Married in 1968, three children.



**STELLINGEN**  
**bij het proefschrift van**  
**P.J. 't Hoen**

1. In de medische röntgenliteratuur is men niet steeds even consciëntieus. Zo is de integratietijd van het visuele systeem van 0.2 seconde (ontleend aan Rose, 1948) slecht onderbouwd; dit kan ook gezegd worden van de criteria voor de kwaliteit van de modulatieoverdrachtsfunctie van het medisch röntgensysteem.

A. Rose, J. Opt. Soc. Am. **38**, 196-208 (1948)

2. De beschrijvingen van afbeeldingssystemen met de frequentieresponsie en de impulsresponsie zijn mathematisch gelijkwaardig; op praktische gronden verdient de impulsresponsie echter vaak de voorkeur.
3. De bewering (Wagner et al., 1974) dat de benadering van de modulatieoverdrachtsfunctie van een medisch röntgensysteem door een Gauss-functie geoorloofd is, is onjuist.

Robert F. Wagner et al., Medical Physics **1**, 11-24 (1974)

4. Het verband tussen de objectresolutie en de geometrische vergroting van een medisch röntgensysteem wordt in de eerste plaats bepaald door de typische invloed van de vergroting op de modulatieoverdrachtsfunctie in het objectvlak van het schaduwbeeld en de beeldontvanger; de vorm van deze functies is van minder belang.
5. Het is niet uitgesloten dat er een koppeling bestaat tussen de signaal- en de ruisverwerking door het visuele systeem; bijzondere aandacht bij de keuze van de experimenten en extra behoedzaamheid bij de interpretatie van de resultaten is daarom geboden.
6. Een vroege invoering in het onderwijs van de zakrekenmachine kan nadelige gevolgen hebben.
7. De beeldverwerking door het visuele systeem is adaptief, wordt beïnvloed door psychische en fysiologische factoren, en hangt af van vele parameters; in het bijzonder in perceptieonderzoek is daarom de nauwkeurige afgrenzing van het geldigheidsgebied van onderzoekresultaten en hun interpretatie van belang.
8. De frequentie van medische ultrageluid- en röntgencongressen is te hoog, gezien het innovatietempo in deze gebieden.
9. De toepassing van drie aanpassingslagen voor een ultrageluidstransducent is niet zinvol, daar al met één of twee lagen een goede responsie verkregen kan worden.

10. In tegenstelling tot de gangbare mening is het niet vanzelfsprekend dat de vertragingstijden van de elementen van een focuserend array voor echografie gebaseerd zijn op het midden van de elementen.
11. De beeldvorming in echografie is paradoxaal: alleen inhomogeniteiten worden afgebeeld, deze verstoren echter ook de voortplanting van ultrageluid en daarmee de afbeelding van dieper liggend weefsel.
12. Een tussenstap op de weg naar een meer duurzame en bedrijfszekere auto zou de keuzemogelijkheid van meer "extra's" in die zin kunnen zijn.

